A study of the formation damage associated with the injection of oil and solids into fractured and non-fractured rock

Emad Solaman Al-Homadhi
(B.Sc., M.Sc.)

This Thesis is Submitted for the Degree of
Doctor of Philosophy
at
The Department of Petroleum Engineering
Heriot-Watt University
Edinburgh, UK
May 1998

DECLARATION

I hereby declare that the work presented in this thesis was carried out by myself at the Department of Petroleum Engineering, Heriot-Watt University, Edinburgh, U.K., except where due acknowledgement is made, and has not been submitted for any other degree.

Candidate

Emad Solaman Al-Homadhi

Supervisor

Dr. James M. Somerville

Date

May 1998

DEDICATION

I dedicate this thesis to my parents.

wife Asma and my two daughters Huda and Sarah.

and my brothers Abdulaziz Al-Othman and Abdulah Al-Hussayen.

TABLE OF CONTENTS

Chapter four

Computer simulation

ACKNOWLEDGEMENTS

I wish to express my appreciation to all those who contributed directly or indirectly in the completion of this study. I would like to thank Dr. James Somerville for his supervision, encouragement and co-operation. Thanks are due to Katriona Petrie for her valuable help and to Simon Whyte, Walter Crawford, Charles McLeod and George Pratt for their help in preparing the experimental slabs and maintaining the injection rig.

Thanks are also due to Min Jin for his useful help and to Lorraine Boak , Marile Marullier , Ian Littlehales , and Dr. Myles Jordon for their co-operation during the experimental work.

I would like to express my gratitude to the head department presented by Professor B. G. D. Smart for providing me with all what I needed.

The author would like to express his thanks to King Saud University for sponsoring him through this study.

ABSTRACT

Produced water injection is an important perspective in oil field management, particularly in relation to reducing oil emissions to the environment. Injectivity decline in oil fields is not yet understood and basic models and design practice not yet established. For example it has been observed that injectivity loss during produced water injection in field operations was not matched with associated linear core flooding tests. One consideration is thermal induced fractures alter the geometry of the wellbore and enhance injectivity. This thesis is focused on this aspect.

As the fractured systems exhibit different flow behaviour to linear core flooding and as there was no published experimental studies on this subject, it was necessary to study the fractured system and the effect of the flow area geometry on the matrix permeability damage extent caused by the injection of produced oily water.

New fractured sandstone slab models were designed, developed and executed to simulate the actual flow of produced water through induced fractures. The matrix damage extent in the fracture system was compared with the matrix damage in the linear core injection system. The flow and the pressure patterns within the fracture injection system were investigated by using the finite element program FLOTRAN.

For fracture injection, and due to the geometry, oil dispersions and particle suspensions caused a very small reduction in matrix permeability compared with the linear injection.
When a filter cake accumulated on the fracture face and started to block the fracture, a thin and long channel (connecting the inlet and the outlet of the fracture) started to form.
Computer simulation showed that for a radial flow model with a single fracture and a near fracture face skin, the reduction in the injectivity is minimal even at both large damaged zone extent and very low damaged zone permeability.

A simple model to calculate the injectivity reduction was developed by using the dimensional analysis method with the help of the experimental results, with two constants which depend on the injected fluid composition and the geometry of the injection system.
The fracture injection results indicated a gradual pore blocking or a permeable internal filter cake mechanism for all the tested particle suspensions. A linear injection model was modified in two ways: the slop of the injectivity versus time relationship in the first modification represents the degree of permeability alteration due to oil and particle mean size and concentration. The slope in the second modification represents the degree of permeability alteration due to the area difference between the fracture and the linear injection experiments as well as the alteration due to oil droplets and/or solid particle.

The geometry skin factor due to the geometry difference between the radial and the fracture injection and the skin factor due to the difference in matrix damage extent between the two systems were measured and calculated.

In this study a new data base was established which describe, evaluate and model the matrix damage mechanism in the fracture injection system caused by the injection of produced oily water along an open fracture.

NOMENCLATURE

a : fracture relative capacity or cross section area of the collector.

a_1, a_2,..., a_N : degrees of freedom.

A1 to A3 and B1 to B3: side outlets of the fractured slab.

A_F : fracture face area.

A_L : linear injection flow area.

A_r : rock area, cm^2.

A_s : flow inlet area.

b : fracture aperture (inch or mm).

b' : constant.

b_s : fracture damaged zone width.

$c(t,x)$: drop-volume concentration profiles.

C : dimensional analysis constant or permeability inverse.

C_1, C_2 and C_3 : filtration coefficients.

C_d :drag coefficient.

C_e : effluent particle concentration.

C_i : influent or initial concentration.

C_n : the number concentration of suspended particles.

C_o : droplets concentration (mg/l).

C_p : particle or droplet concentration.

C_s : particles concentration (mg/l)

C_{si} : initial particles concentration (mg/l).

C_{so} : equivalent concentration of solids and oil (mg/l).

C_v and C_w : filtration constants.

CFD : computational fluid dynamics.

CFR : cake to filter ratio.

CR : Concentration ratio.

d : dimensional analysis exponent.

d_g : average grain size of the rock (μm).

d_p or d_s : average particle size (μm).

D : hydraulic diameter.

Do : droplets mean diameter (μm).

D_{pore} : matrix pore throat diameter (μm).

D :pore size (cm)

D_p : particle or droplet mean diameter.

Ds : particles mean diameter (μm).

dN : the change in the number of particles trapped at the surface of the core with time.

DP : pressure drop.

DPi : initial pressure drop.

e : fracture roughness (inch or mm).

f : friction factor or plugging pathways fraction.

f_d : concentration of particles of critical size d.

F_g : gravity force.

F_i : force of Inertia.

F_i (i=1,2,...,N) : interior and boundary load terms.

F_L : lifting force.

F_p : pressure force.

F_y or F_d : drag force or viscous force acting on a particle.

f(v) : coefficient accounting for the effect of fluid velocity on filtration coefficient.

f_x : load term in the x-axis direction.

F_x : tangential force acting on a particle.

F_y : normal drag force.

f_y : load term in the y-axis direction.

h : fracture height (ft).

h_c or e : external cake thickness (inch).

HIT : half injectivity time (hours).

I : fracture inlet.

I_{ci} : depth of the impaired zone.

I_F : core depth.

II : injectivity index or injectivity inverse

J_r : particles jamming ratio.

J_r^* : critical value of particles jamming ratio.

K : loss coefficient.

K_c : permeability of the external cake (md).

K_{ci} : impaired zone permeability.

K_d : damaged matrix permeability (md).

K_f : fracture permeability.

K_F effective brine permeability.

K_{Fd} : damaged matrix permeability in the fracture injection system (md).

K_{Fi} : initial matrix permeability in the fracture system (md).

K_i : initial matrix permeability (md).

K_{ij} (i,j=1,2,...N) : integration functions.

K_m : initial matrix permeability (md).

K_o : clean bed permeability (md).

K_p and K_{np} : permeability of pluggable and nonpluggable pathways.

K_{pi}, K_{npi}, and $\in$: phenomenological constants.

$\overline{K}_r(t)$: permeability reduction rate with time t.

$\overline{K}_r(x_f)$: permeability reduction rate with distance x_f.

K_{Rd} : damaged matrix permeability in the radial injection system (md).

K_{Ri} : initial matrix permeability in the radial system (md).

K_S : skin permeability.

K_v : fluid permeability through invaded zone.

K_w : fluid permeability through filter cake.

K(x,t) : the change in permeability with distance and time.

K^* : permeability of damaged porous medium at time t^*.

L : average length of flow path, cm.

L_m : flow path length.

$L_{1/2}$: half invasion depth.

LFI : long fracture injection (fracture length = 40 cm).

LI : linear injection.

Mdr or MSR : mean diameter or size ratio (μm).

n : volumetric concentration of deposition particles.

n(x,t) : the change the number of particles with distance and time.

n* : number of trapped particles at transition time.

N_{PV} : number of pore volume injected.

N_{Re} : Reynold's number.

O : fracture outlet.

P : pressure distribution in the reservoir.

P_d : pressure distribution in the skin.

P_f : pressure inside fracture.

P_e : reservoir pressure at r_e.

P_I : inlet pressure (bar).

P_{init} : reservoir pressure (psig)

P_{inj} : bottom-hole injection pressure at time t (psig).

P_L : pressure at the end of the fracture.

P_o : outlet pressure along the fracture (bar).

p_F : pore fluid pressure (psi).

P_x : pressure at a distance x (along the fracture) from the wellbore axis.

PDS1 : pressure drop from fracture face to side outlets A1 and B1 (bar).

PDS2 : pressure drop from fracture face to side outlets A2 and B2 (bar).

PDS3 : pressure drop from fracture face to side outlets A3 and B3 (bar).

PDF : pressure drop along the fracture (bar).

PR : permeability ratio.

PS : side outlet pressure (bar).

pv : pore volume, cm^3.

PWRI : produced water injection.

ΔP : pressure drop (psi).

ΔPd : pressure drop due to the difference in matrix damage extent between the radial and the fracture systems (bar).

ΔP_{dF} : pressure drop due to matrix damage in the fracture injection system (bar).

ΔP_{dL} : pressure drop due to matrix damage in the linear injection system (bar).

ΔP_{dR} : pressure drop due to matrix damage in the radial injection system (bar).

ΔP_{Ds} : additional dimensionless pressure drop caused by the skin damage.

$\Delta P_{e,0}$: dimensionless pressure drop at drainage radius.

ΔP_{Fi} : initial pressure drop in fractured system (bar).

ΔP_{Gf} : pressure drop difference between radial and fracture system due to geometry effect (bar).

ΔP_{Gr} : pressure drop difference between radial and linear system due to geometry effect (bar).

Δp_i : initial pressure drop (atm).

ΔP_L : initial pressure drop in linear system (bar).

$\Delta P_{L,x}$: dimensionless pressure drop.

ΔP_{Ri} : initial pressure drop in radial system (bar).

ΔPv : pressure drop through invaded zone (psi).

ΔPw : pressure drop through filter cake (psi).

$\Delta P_{w,0}$: dimensionless pressure drop at wellbore radius.

q_f : undamaged production rate (bbl/day).

q_F : initial side flow rate in the case of fracture system.

q_{fd} : damaged production rate (bbl/day).

q_j : flow rate at the jth time step (bbl/day).

q_N : flow rate during the current step in the ramp-up (bbl/day).

q_o : injection flow rate at the injection surface.

q_R : flow rate in radial injection system.

q_s or q_F : side flow rate in the case of fracture system (cm^3/s).

Q : flow rate, cm^3/min.

Q_o : fracture outlet flow rate (ml/s) or initial injection flow rate.

Q_s : total side outlets flow rate (ml/s).

r_e : drainage radius (ft).

r_{eD} : dimensionless drainage radius.

r_o : outer radius of the radial injection system.

r_w : wellbore radius (inch).

r_{wD} : dimensionless wellbore radius.

R : resistance of the matrix to flow (1/m2) or the radius of particle.

R1 : leading radius of the drop (μm).

R2 : trailing radius of the drop (μm).

R_c :resistance of the reservoir fluid zone (1/m2).

Rd : additional resistance due to the external and/or internal matrix plugging (1/m2).

Ri : initial resistance of the matrix (1/m2).

R_m : filter medium resistance.

R_v : resistance of the invaded zone (1/m2).

R_w or R_c :resistance of the filter cake (1/m2).

R_x and R_y : distributed resistance terms.

R(x;a) : residual.

RI : radial injection.

s_{fs} or S : skin factor.

S : compaction function of the filter cake.

S_d : skin due to the difference in matrix damage extent between the radial and the fracture system.

S_{Fd} : damage skin due to matrix damage in fracture system.

S_{Gr} : geometry skin due the difference in geometry between the radial and the linear system.

S_{Gf} : geometry skin due the difference in geometry between the radial and the fracture system.

S_{Rd} : damage skin due to matrix damage in radial system.

SFI : short fracture injection (fracture length = 20 cm).

SFV1 : the side flow velocity at A1 or B1 (ml/s).

SFV2 : the side flow velocity at A2 or B2 (ml/s).

SFV3 : the side flow velocity at A3 or B3 (ml/s).

SWI : sea water injection.

t : injection time (sec)

t* : transition time (sec).

t^*_D : dimensionless transition time.

t_{Dxf} and T_{Dxf} : dimensionless production time through fracture.

T : tortuosity or shifted time variable.

Ts: solids concentration in flow stream, g/cm^3.

T_x : torque acting to remove particle from cake surface.

T_y : restraining torque.

TE : particle trapping Efficiency.

u_c : critical volume flux density.

u_p and u_{np} : flux density of fluid flowing through pluggable and nonpluggable pathways.

U or v or u : flow velocity (cm/s).

U(x,a) :approximate solution.

U_v : leak-off fluid velocity through filter cake.

U_w : leak-off fluid velocity through invaded zone.

um or μm : represents micrometer unit.

V^* : critical cumulative volume injected.

V_f : flow velocity at the fracture inlet (cm/s).

v_F : flow velocity through matrix in fracture system (cm/s).

v_p : fluid velocity through perforation.

v_R : flow velocity at the inflow face in the radial system (cm/s).

V_s : side flow velocity in the fractured injection slab.

V_l : flow velocity through linear injection slab.

V(t) : cumulative flux injection per unit area of the flow face (m3/m2).

Vx : flow velocity in the x-direction (cm/s).

Vy : flow velocity in the y-direction (cm/s).

V_Y : filtrate flux.

w : fracture width (mm).

w_d or W_d : average depth of skin.

W : fracture face width (ft)

W_c : filter cake weight per unit area (gm/cm^2).

W_e : eroded equivalent filter cake weight per unit area (gm/cm^2).

WHP : well head pressure.

x: : axial distance or the distance into the porous medium.

x_f : distance along the fracture.

$\tilde{x}$: reduced axial distance.

SYMBOLS

α : cake deposit constant or fractional injectivity index.

α^* : the number of particles required to block the entry pore through.

$\alpha(t)$: injectivity decline with time.

$\frac{1}{\alpha_{Rd}}$: injectivity inverse for the radial systems.

$\frac{1}{\alpha_{Fd}}$: injectivity inverse for the fracture systems.

ß : surface deposition constant or damage factor or flow restriction parameter.

$ß_W$: formation volume factor for the injected water (bbl/STB)

γ : specific gravity of the particle.

γ_w : shear rate.

δ or δ_F: damage factor.

λ_v : volume filter coefficient, 1/s.

τ_w : shear stress.

μ or μ_F : fluid viscosity (cp).

μ_e : effective viscosity.

μ_w : injected water viscosity.

$Ø_d$: damaged matrix porosity.

$Ø_c$: external cake porosity.

$Ø_{ci}$: porosity of the impaired zone.

$Ø_i$: matrix porosity.

$Ø_i^{(e)}(x,y)$: shape functions of element (e).

$\phi_i and \phi_f$: initial and final porous medium porosity.

$Ø_o$: initial undamaged porosity.

$Ø_o(x), Ø_1(x), Ø_2(x),....., Ø_N(x)$: trial functions.

$Ø(x,t)$: the change in porosity with distance and time.

ρ_{os} : particle and droplet equivalent density (gm/cm^3).

ρ_o : oil droplets density

ρ_s : solid particles density.

ρ_l or ρ_f : density of injected fluid.

σ : interfacial tension (dynes/cm) or volume of fines deposited per unit original pore volume.

σ_E : effective stress (psi).

σ_T : total stress (psi).

$\sigma(t,x)$: transient drop-volume retention.

σ_p and σ_{np} : volume fraction of fines.

Φ : volume fraction of solids in suspension.

Ω : the fraction of retained particles trapped at pore throats.

ε_o : clean bed porosity.

ν : ratio of volume of filter cake, cm3,to volume of filtrate, cm3.

υ_l : the leak-off velocity (cm/s).

$\wedge_{SI}$: reduced filtration coefficient.

List of Figures

Chapter one

Chapter two

Chapter three

Chapter four

Chapter five

Chapter six

List of plates

List of Tables

Chapter three

Chapter four

Chapter five

Chapter six

INTRODUCTION

The cumulative volume of produced water can exceed by ten times the volume of hydrocarbon production in some fields. This water contains dispersed and suspended impurities such as crude oil droplets and mineral material particles. The discharge of this polluted water into the environment will cause serious problems. The solution is to treat this water to remove these impurities or to reinject it into the formation. Produced water from the separators contains typically 40 -1200 ppm oil droplets of less than 20μm and 1-50 ppm solids of less than 10μm [36].

The separation of all oil droplets and filtering all of the solid particles is extremely expensive and impossible. The best solution is to reinject it into the formation. The injection of unfiltered produced oily water to the formation may lead to a significant amount of injectivity reduction, so the optimum water quality must be measured so that injectivity reduction can be minimised.

Attempts to predict permeability alteration and to measure the optimum water quality were made by several researchers (22, 35, 62, 71, 72, 90, 109) but they mainly concentrated on solid particle invasion, and there is very little published data on the formation damage resulting from produced oily water re-injection which is even more complicated than solid particles invasion mechanism. All the permeability alteration studies were conducted for linear core flooding.

It has been reported (19, 79, 89, 102, 104) that the results of linear core flood experiments injection of synthetic produced oily water did not match with the situation of injection of produced oily water in real injection wells, where it was found that injectivity loss was not as large as expected. This is thought to be a result of thermally induced fractures that alter the geometry of the wellbore and hence the mechanisms of formation damage (permeability alteration) associated with it [50, 52, 104].

As the fractured systems exhibit different flow behaviour than liner core flooding, it becomes necessary to study the fractured system and the effect of the flow area geometry on the matrix permeability damage extent. There is no published experimental studies on the subject of produced oily water injection through a fractured system.

The aim of this work was to study the permeability alteration associated with the flow of simulated produced oily water (with various oil droplet and solid particle concentrations) along the fracture and through the fracture faces. A fractured slab model was designed and injected with various solid particles and oil droplet sizes and concentrations to identify the factors associated with formation damage caused by produced oily water. One of the objectives was to relate the matrix damage in the fracture injection to the matrix damage in the linear core injection by conducting a detailed comparison study between the two systems.
In spite of the complexity of the fracture flow mechanism, a model of permeability decline was devised for this fracture geometry (similar to that devised for linear core floods) based on simple and practical laws.

The thesis consists of six chapters. Chapter one outlines the plugging mechanisms related to the capture of solid particles or oil droplets within the rock matrix pores. Also this chapter reviews some of the matrix damage experimental work carried out by many researchers and different matrix damage models are presented. Then a review study on fractures is presented including a comparison between the process of hydraulic fracturing and water injection fracturing.

Chapter two outlines the experimental equipment including the experimental rig, the construction and the testing of the fractured slab model and the preparation of the simulated oily water. Also the experimental procedures and the measured and calculated variables are defined in this chapter.

Chapter three presents the experimental work which is started by studying fluid flow distribution of fluids along and through the fracture face and the effect of different variables on this distribution. Then the damaging effect of solid particle suspensions, the damaging effect of oil emulsions and the combined damaging effect of particles and oil droplets on the matrix permeability of the fractured slab were examined. Also a comparison study, concerning the damaging extent in the matrix permeability caused by the injection of the simulated oily water, between the linear and the fracture systems was carried out. The effect of rock matrix heterogeneity and the filter cake accumulation on the fracture face and its erosion process were also investigated in this chapter.

Chapter four outlines the basic concepts of the finite element method and the finite element programming procedures including building the model, applying boundary conditions, obtaining the results and reviewing the results. The finite element program FLOTRAN was used in this study. As the variation of pressure and fluid velocities within the fracture and within the rock matrix in the experiments were unknown, the main aim of this chapter was to obtain the variation of pressure and flow velocity with distance by building a simulated fracture model having the same dimensions and boundary conditions as in the experiments. For comparison a linear injection model was built and tested in this chapter. Once the small scale models of the fracture flow had been tested, the Finite Element program was used to scale up the flow to examine the effect of flow from a wellbore into a fracture with or without a nearby damaged zone.

Chapter five discusses the use of dimensional analysis to produce a simple practical equation to describe the matrix damage with time in the fracture system. The produced model contains two constants the dimensional constant C and the exponent d, which were evaluated (by using the experimental results) for different simulated produced waters depending on particles mean size and concentration and oil droplets mean size and concentration. Then an attempt was made to find C and d values which were used to predict the effect of the brine content on the injectivity decline in real field fracture injection operations. These values were used to predict the change in pressure drop with time for two field cases.

Chapter six outlines the main differences between the injection along fracture and the linear or the radial injection and the effect of these differences between the two systems on the matrix damage extent when dirty brine was injected. The objective in this chapter was to compare the experimental results generated by this thesis with the predictions of formation damage models reported in the literature. The linear injection formation damage models were applied on the linear and the fracture injection experiments to investigate the change of injectivity with time as matrix damage took place and to measure the difference in the injectivity (due to matrix damage) between the two injection systems. The geometric skins to convert from linear to radial system and to convert from radial to fracture system were defined and calculated. Also the skin

to account for the difference in the matrix damage extent between the radial and fracture systems was defined then measured and calculated.

These chapters are followed by the final conclusions and the recommended future work.

At the end of the thesis there are three appendices:

Appendix I contains the experimental data.

Appendix II contains the Ansys/Flotran finite element simulation computer programs.

Appendix III contains the Malvern master sizer particles and droplets size distribution samples.

Appendix V contains the injection rig and the tesing cell.

CHAPTER ONE

LITERATURE REVIEW OF MATRIX DAMAGE

1.1 Introduction

This chapter outlines the plugging mechanisms related to the capture of solid particles or oil droplets within the rock matrix pores. These mechanisms were defined by many researchers in different ways. They defined the factors that affect the particle and the droplet retention within the matrix pores. These factors included the rock matrix properties and the injected fluid properties. Some of them theoretically explained the stages of the pore blocking process depending on their observations.

Also this chapter reviews some of the matrix damage experimental work carried out by many researchers, these experiments studied the matrix blocking caused by particle suspension injection, oil emulsion injection and by the injection of fluid containing oil and solids. Also some of the micro (small scale) model experimental observations were included in this chapter.

Different matrix damage models are presented in this chapter including static and dynamic filtration models, fracturing fluid leak of models and pore filling and blocking models.
To understand the flow through fractures, a review study on fractures is presented to achieve this goal. This study includes the effect of fractures on flow pattern within the formation, fracture initiation by injection process, fracture detection during injection, comparing the process of hydraulic fracturing with fractures induced by the injection of dirty water.

The models of production through fractures and the models of formation damage due to injection through fractures are also reviewed. At the end of the chapter the forces acting on solid particle flowing along filtration surface were defined and explained.

1.2 Plugging Mechanisms

HERZIG et al. (1979) defines the different mechanisms involved in particle filtration and stated that deep filtration is the result of several mechanisms such as the contacting of particles with the retention sites, the fixing of particles on sites and the breaking away of previously retained particles.

They concluded that the problem to be solved consists in relating the clogging rate (the number of retained particles per unit of time and per unit of volume of porous medium) to the various factors which define the system, namely:

The carrier fluid (flow rate, viscosity, density).

The suspension of particles (concentration, size, and shape of particles).

The porous medium filter (porosity, diameter of pores, size and shape of grains, retention).

Furthermore, the important problem of the pressure drop of the fluid through the bed has to be studied as well as its change with the clogging.

They described the different elementary mechanisms as:

1.Retention sites (Fig.1.1):

a) Surface sites: the particle stops and is retained on the surface of a porous bed grain.Crevice sites: the particle becomes wedged between the convex surfaces of two grains.

b) Constriction sites: the particle cannot penetrate into a pore of a smaller size than its own.

c) Cavern sites: the particle is retained in a sheltered area (small pocket formed by several grains.

2. Retention forces:

a) Axial pressure of the fluid: the fluid pressure may hold an immobilised particle against the opening at a constriction.

b) Friction forces: a particle wedged in a crevice may have been slightly deformed when stopped, and may remain in place by friction.

c) Surface forces: includes the Van der Waals forces, which are always attractive, and the electrical forces which are either attractive or repulsive according to the physicochemical conditions of the suspension.

d) Chemical forces: in the case of colloidal particles or in other particular cases, actual chemical bonding may occur.

3. Capture processes:

a) Sedimentation: if the particles have a density different from that of the liquid, they are subjected to gravity and their velocity no longer is that of the fluid.

b) Inertia: owing to their apparent weight, the particles cannot follow the same trajectories as the fluid, they deviate from the streamlines (when the direction of the trajectories change suddenly) and can be brought into contact with the bed grains.

c) Hydrodynamic effects: the nonuniform shear field and the nonsphericity of particles causes a lateral migration of suspended particles which may be brought into contact in this way with retention sites.

d) Direct interception: even with exactly the same density as the fluid, the particles would not be able, owing to their size, to follow the smallest tortousities of the stream lines of the carrier fluid and they will thus collide with the walls of the convergent areas of the pores.

e) Diffusion by Brownian motion: the particles diffuse and can reach areas which are not normally irrigated by the suspension, and they are retained there.

SELMECZI (1971) defines the various forces which contribute to the capture and retention of suspended particles in deep-bed filtration as:

1. Capture processes:

a) Screening: When two or more particles arrive at a restriction simultaneously, their combined diameter and coordination is an important factore in the capture mechanisim. Every particle that is caught in a restriction will further reduce the passageway, which in turn will result in the screening of progressively smaller particles. This could lead to the change from in-depth to cake filtration.

b) Sedimentation: Suspended particles are subject to gravitational forces and tend to settle out of the fluid at a velocity which can be calculated by Stokes law. Moving fluid has a velocity considerably greater than the settling velocity of the particle.

2. Retention forces: A particle making simultaneous contact with two or more filter grains may become wedged in this position. But it has to make contact with sufficient energy to be deformed and thus retained by the filter medium. Similarly, random motion of the suspended particles within the tortuous paths between the grains of the filter will cause direct contact between the particles. Flocculation and agglomeration of the particles may increase particle size to the point where sedimentation and screening mechanisms become significant.

A particle held against only two grains may be considered to be in a very delicate balance, and thus in a temporary location only.

He concuded that the random movement of suspended particles in a tortuous flow path is mainly responsible for transporting the particles either directly to the grains or close enough to the grain surface for other forces to become effective.

DONALDSON et al. (1977)stated that the path of fluid flow within a geologic porous system is a tortuous one which is subject to frequent sudden changes in direction and velocity. Suspended particles with densities greater than the density of the carrier fluid will not follow the stream lines as the fluid suddenly changes direction of flow and will impinge on the walls of the pore due to forces inherent in gravity and inertia, particles thus deposited will tend to form domes.

SPIELMAN (1977) studied the capture of small suspended particles from fluids in laminar flow on a collector. This capture is characterised by the simultaneous action of forces of fluid-mechanical origin along with forces of other origin that act between the particle and collector. These combined forces govern the particle trajectories which in turn determine whether a particle will be transported to and retained at the surface of a collector that is fixed in the flow. He defined the capture mechanisms in the classical theory and the modernistion of this theory:

First the Classical capture mechanisms:

a) Brownian diffusion: submicron particles undergo Brownian motion, which promotes their deposition during flow past a collector.

b) Interception: capture by interception assumes that the centre of a small nondiffusing spherical particle follows exactly an undisturbed fluid streamline near a large collector until the particle and collector touch, whereupon the particle is retained by contact adhesion. Interception ignores increased hydrodynamic resistance between particle and collector which results from forced drainage of the viscous fluid from the narrowing gap during approach, but also ignores the finite reach of strong attraction arising through universal intermolecular forces. These opposing effects tend to cancel one another (Fig.1.2).

c) Inertial impaction: Owing to inertia, sufficiently massive particles are unable to follow curvilinear fluid motion and tend to continue along a straight path as the carrier fluid curves around the collector. This gives rise to enhanced collection on the approach side. Impaction efficiency predictably increases with increasing particle size and fluid velocity.

d) Gravitational deposition: due to the difference between particle and fluid density.

Second the modernisation of capture mechanisms for liquid systems:

The classical analysis for capture by interception assumes that the centre of a small particle follows exactly an undisturbed fluid streamline near a larger collector until contact occurs and

adhesion retains the particle. However, a particle in close proximity to a collector must necessarily deviate from the undisturbed streamline. This is because the continuum description of fluid motion with no slip at both the collector and particle surface produces infinitesimally slow drainage of fluid from the gap between them as they approach under a finite force. With the assumption that the fluid is a viscous continuum, the anomalous conclusion is reached that contact cannot occur. The anomaly disappears, however, owing to the action of attractive Van der Waals forces that increase very rapidly as the particle approaches the collector and become strong enough to overcome the otherwise slow drainage.

DAVIDSON (1979) discussed the invasion mechanism and gave some remarks on the constant injection flow rate case and the constant injection pressure case:

He stated that the rate of impairment and depth of penetration are determined by the forces acting on the particle as it moves through the rock. Surface and gravitational forces cause particles to be separated from the fluid and deposited in pores, thus increasing the resistance to flow. The deposition process can be retarded by a force generated by the pore velocity. Two possibilities exist with respect to the final change in pore dimensions (Fig.1.3).

a) An equilibrium state is reached with no net deposition. Although the initial fluid velocity is not large enough to prevent deposition, the narrowing of pores could cause the fluid velocity to increase to the level at which an equilibrium state can form.

b) Deposition continues until the pore is narrowed to two or three particle diameters, at which time the pore is bridged and an internal filter cake begins to form.

The final stage of pore plugging is related not only to the initial pore velocity and relative particle and pore sizes, but to the change in pore velocity with deposition, which for core test is controlled by constraints of constant flow rate or pressure drop.

He concluded that for the injection at constant rate, particles that are filtered out reduce the cross-section of pores, but due to the maintenance of flow rate, the fluid velocity in the pores increases. The opportunity to form a nonretaining bed increases with deposition. However, in the formation the enormous velocity contrasts produced by areal spreading of fluid insures that there will be some radial location where insufficient velocity exists to prevent pore bridging.

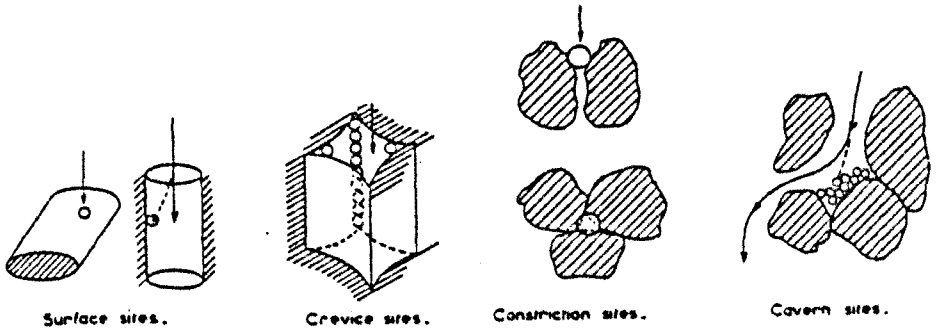

Fig.1.1: Retention sites (Herzic *et al.* 1979)

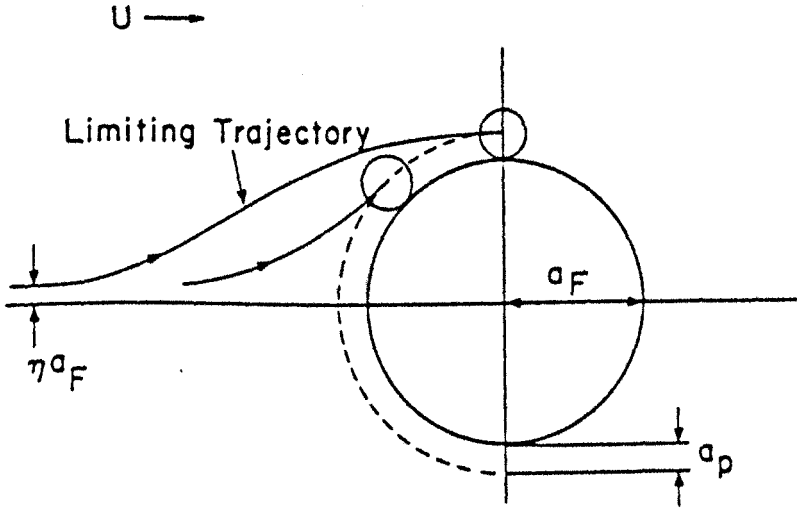

Fig.1.2: Trajectories for classical interception by a cylinder (Spielman 1977)

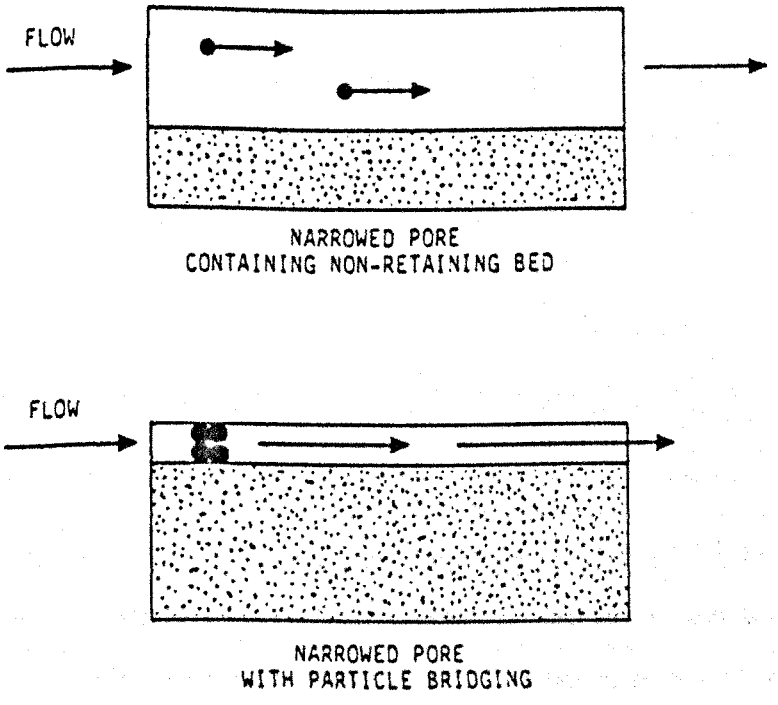

Fig.1.3: Final states of pore plugging (Davidson 1979)

But in the case of constant pressure drop, the impairment obtained by the depositing solids reduces the flow rate and, thus, the pore velocity. Internal pore bridging will occur unless the initial velocity at the start of the test is high enough to prevent particle deposition from starting.

TANG (1982) explained the effect of the free, emulsified and dissolved oil on the blocking mechanisms within the rock matrix as follows:
Produced water from a free water knock-out tank contains free oil, emulsified oil and dissolved oil. Free oil will cause a reduction in relative permeability to water. The emulsified oil, existing as 1to 15 micron oil droplets, can seal off pore throats if the sizes of the pore throats also fall into that range (Fig.1.4). This emulsion blocking effect is usually more serious than the reduction in relative permeability from free oil. Once trapped in the pores, these oil droplets can only be mobilised by a huge pressure drop described by the following equation:

$$\Delta p = 2\sigma(\frac{1}{R_1} - \frac{1}{R_2})$$

Where σ: is the interfacial tension

R_1: is the leading radius of the drop

R_2: is the trailing radius of the drop

Dissolved oil passes through the core readily without any plugging. Free oil can be emulsified at high shear rates while emulsified oil can coalesce to form free oil when the shear rate is reduced to zero or in the presence of emulsion breakers. Oil can also agglomerate with suspended inorganic solids present in the produced water, forming large globules which can plug the inlet face.

SOO et al. (1984) stated that as the emulsion drops are captured in pores by straining and interception with the possibility of straining being the dominant mechanism (Fig.1.5), and as the strained drops may re-entrain into the flowing stream once the local pressure drop increases enough to overcome capillary restraining forces (as the liquid drops are deformable), conventional deep bed filtration theory developed for undeformable solid suspensions is not strictly applicable for dispersed liquid droplet flow.

EYLANDER (1988) differentiated between the external and the internal filter cakes plots as is explained below:

To analyse the filtration phenomena that occur, either externally on the core-plug injection face or internally within the plug, the traditional filtration equation derived from Darcy's law and a mass balance of solids are rearranged in the form: $(dt/dV)\,\Delta p = m\,V + b$

Where m and b are measures for the permeability / porosity of the filter cake and the effective brine premeability of the porous medium, respectively.

The values of m and b are calculated from the linear plots of $(dt / dv)\,\Delta p$ versus cumulative injected volume, V.

If the external filter cake is formed, two phases may be distinguished during the filtration process: phase one, a limited irreversible loss of plug permeability attributed to impairment from pore filling at a shallow invasion depth, and phase two, formation of an external filter cake, resulting in a further but reversible permeability loss (Fig.1.6).

The resultant effective brine permeability is determined by knowing the extrapolation of phase two part of the filtration curve ' b'. The filter cake properties are calculated from the slope of the phase two part of the curve ' m '.

If the internal filter cake is formed, two phases can again be distinguished: phase one, impairment by deeply invading solid caused by internal pore throat blocking, resulting in an irreversible loss of plug permeability, and phase two, reversible impairment caused by pore throat bridging under dynamic conditions with pore throat bridging larger than that of pore throat blocking seen in phase one (Fig.1.7). Phase two of the filtration curve is extrapolated through a displaced origin (to the end of phase one) to get the intercept 'b', and the slope of phase two is 'm'. Then the effective brine permeability and filter cake properties can be calculated.

He concluded that in coreflood tests, use can be made of various injection sequences in combination with analysis of influent and effluent streams to judge the type of impairment behaviour. For example, where reduced permeability of the plug results from external filter cake formation, flow reversal will be instrumental in virtually completely restoring the original brine permeability; analysis will indicate a "burst of solids" being produced just after flow reversal has been initiated. If the observed permeability loss is the result of internal fines

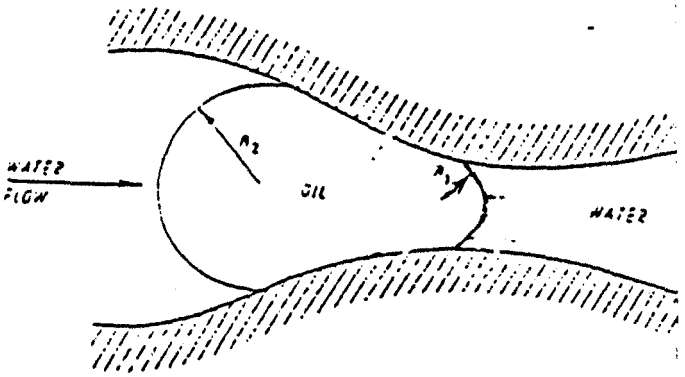

Fig.1.4: An oil droplet entering a pore throat (Tang 1982)

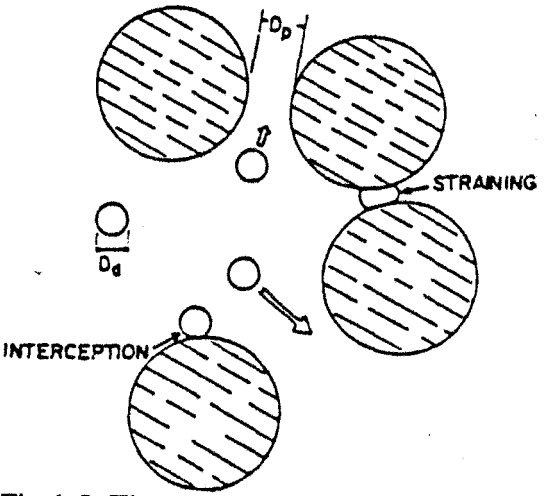

Fig.1.5: The mechanism of emulsion flow in porous media (Soo *et al.* 1984)

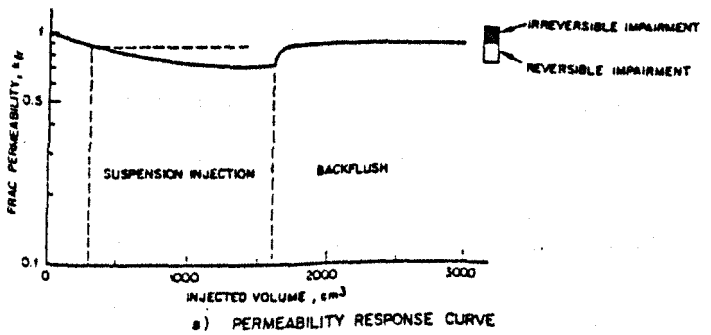

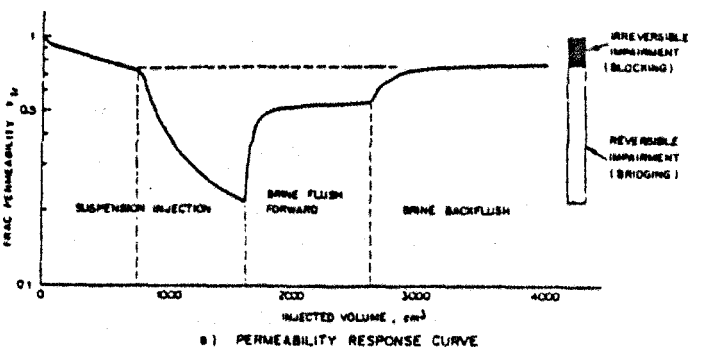

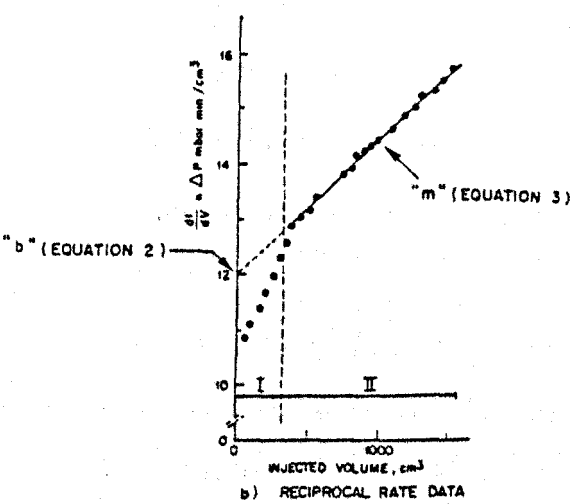

Fig.1.6: External filter-cake formation (Eylander 1988)

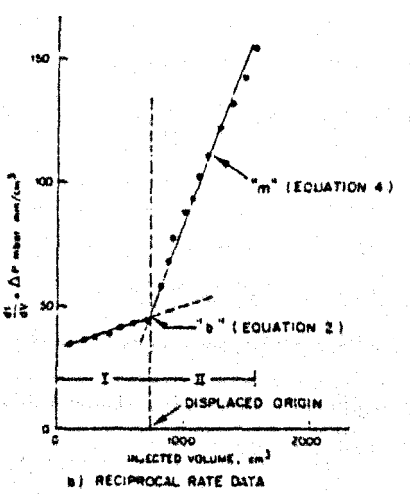

Fig.1.7:Internal filter-cake formation (Eylander 1988)

migration, flow reversal can momentarily release the plugging solids, but they subsequently become lodged elsewhere. A sharp permeability enhancement is then observed that rapidly falls to or near the original (impaired) level.

BENNION et al. (1994) stated that almost all problems associated with impaired injectivity can ultimately be related back to problems associated with water quality. Potential damage mechanisms which can be associated with water injection processes include:

1. Mechanically induced damage (Fig.1.8):

a) Solids injection:

Smaller particles invade deeper into the formation and can potentially form an internal filter cake which is generally more damaging due to its relative inaccessibility which reduces the efficiency of conventional mechanical or chemical stimulation treatments. At higher inflow velocity (>10 cm/min.) the more classical rules of sizing and invasion appear to hold. At lower injection velocities (< 2 cm /min.) more damage becomes apparent in the formation of the internal filter cake with respect to smaller particulate sizes.

b) Velocity induced damage (fine migration):

Loosely attached and mobile clays and detrital rock fragments, if dislodged into the flowing fluid stream by high injection water velocities may move to pore throat locations where they may plug and cause reduction in injectivity.

2. Injection water - formation rock interaction:

a) Clay swelling.

b) Clay Deflocculation.

c) Formation Dissolution.

d) Chemical Adsorption / Wettability Alteration.

3. Relative permeability effects (Fig.1.9):

Oil entrainment in injection water and subsequent entrapment is a major source of potential impaired injectivity in situations with the case of no or sub-irreducible oil saturation is present. This is due to the fact that a sufficiently high saturation of hydrocarbon liquid must be entrapped in the porous media around an injector to ensure that a continuous oil phase with finite relative permeability and mobility is obtained. Prior to this time, the hydrocarbon liquid is

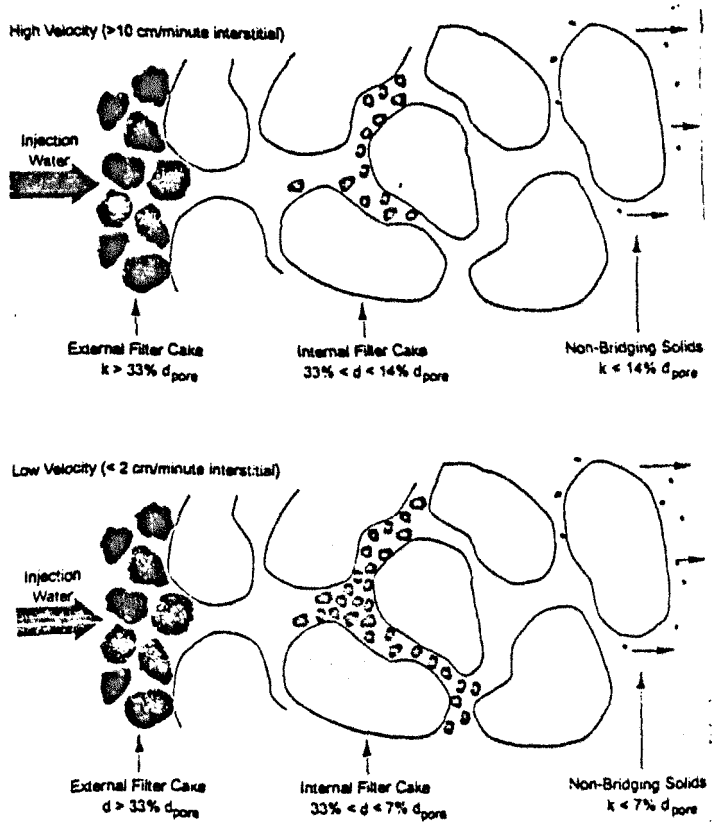

Fig.1.8: Mechanism of suspended solids entrainment (Bennion *et al.* 1994)

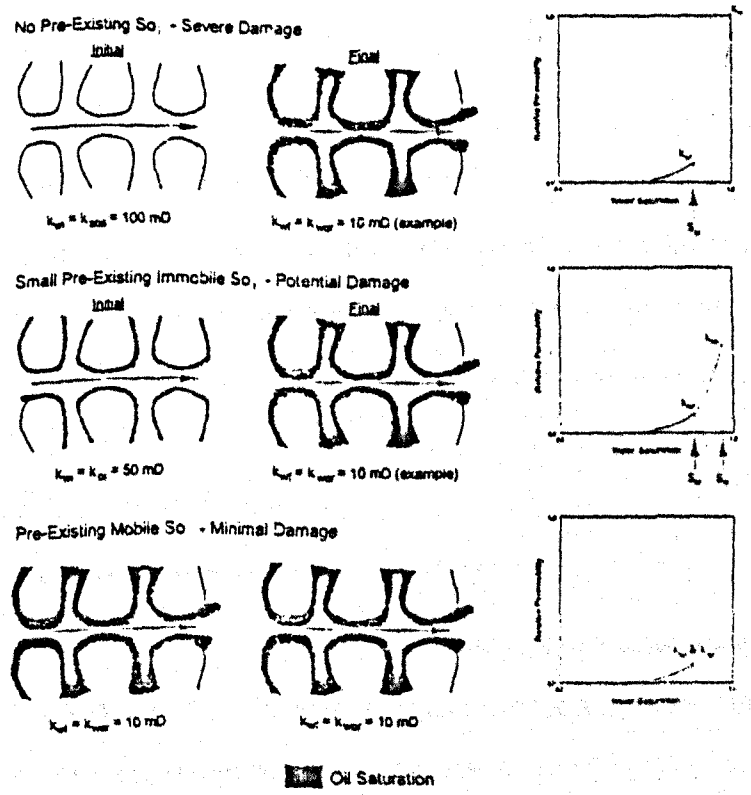

(Note: These drawings assume the injected oil is perfectly compatible and miscible with the in situ oil - if not, additional damage may be apparent.)

Fig.1.9: skim oil entrainment in different systems (Bennion *et al.* 1994).

merely entrapped as an immobile saturation. Although this saturation is immobile, it may have a profoundly reducing effect on the relative permeability to water.

WYER (1975) mentioned the uncontrollable factors affecting the process of Produced Water treatment efficiency as:

a) Physical and chemical properties of the crude oil, including solubility.

b) Suspended solids concentration.

c) Fluctuation of flow rate.

d) Degree of emulsification .

e) Characteristics of the produced water and the bacterial activities.

1.3 Particle Invasion Experiments

DONALDSON et al. (1977) tested particle transport within Berea, Noxie and Cleveland sandstones having mean pore sizes of 10, 15 and 30 microns, respectively, by injection of 1% brine aqueous suspensions of ground quartz sand particles having mean particle sizes of 4, 6 and 7 μm. A constant flow rate of 2.78 ml/ min was used.

They concluded that particles initially are passing through the larger openings in the core, i.e., the ones with the largest flow. Gradually the particles are stopped by the irregularities within the pores by a combination of the effects from gravitational sedimentation, direct interception, and surface attraction. The largest particles appear to be removed quickly. Even with this efficient removal of large particles, the pressure does not increase significantly until a large volume (several pore volumes) of the suspension passes (Fig.1.10).

Since a cake is built up on the surface of the core during the experiment, it is possible that the pressure build is due to the cake rather than plugging of the pores.

There are a number of points on a pressure profile where the pressure decreases significantly. Along with this decrease in pressure there is an increase in the number of effluent particles. Particles in one or more of the pores dislodge simultaneously, resulting in a greater open area in the core and consequently a pressure drop.

When they reassembled several of the cores that had the cake removed from their surface into the core holder and placed back on the pumping system and a 1% brine solution was pumped through each core at the same rate as before, the resulting pressure at which the liquid flowed

had decreased dramatically, almost to the pressure at which the core had originally been subjected at the beginning of the experiment. The porosity of the cores was checked and there was almost no change. This suggested that the core itself was only partially plugged, but the cake material formed at the face of the core and restricted the flow of slurry. The slurry flow through the core can be restored by cleaning the surface of the core and removing the cake formed.

GRUESBECK et al. (1982) in their study of particle entrainment and redeposition, stated that there was a critical velocity, or flow rate, below which entrainment of fines did not occur and above which the rate of entrainment increased linearly with flow rate. Thus, for a given flow rate, there was around the wellbore a cylindrical region in which entrainment and redeposition can lead to permeability reduction.

In the synthetic system experiments, he used a 2% KCl solution as the carrier fluid with a suspension of CaCo4 particles having a mean diameter of 0.8 μm. Packed columns of unconsolidated sand having grain size ranging from 840 to 2000 μm were used as the flowing medium.

They concluded that as the smaller path ways are blocked flow is diverted to larger pathways and more fine particles reach the effluent but eventually the pressure differential across the column, and hence any blocked pathway, is so great that some plugs are broken. This results in a spurt of fines in the effluent, but then new deposits grow.

In the finer sand, with mean diameters of 177 to 210 μm, the deposits tend to concentrate near the inlet end of the column and the mean permeability of the column tends to go to zero. In the coarser sand, with mean diameter of 250 to 297 μm, on the other hand, deposits tend to be more uniform and an equilibrium permeability is achieved. In the coarser sand there are many non-plugging pathways but in the finer sand nearly all pathways are plugging pathways.

Generally he observed that more deposition results (for a given pore volume throughput) under constant pressure conditions than for constant rate conditions.

For the case of the field core experiments, they concluded that the naturally occurring fines in a consolidated core would be entrained by a moving clean fluid from surface-type deposits and redeposited as plug-type deposits. And for the flow rate of 0.0367 cm^3/sec, the permeability was not changing but at each of the higher rates the permeability was continuously declining.

TODD et al. (1979) gave an example of how sea water flooding, having particle concentration of 1ppm and particle size from around 20 μm downwards, would significantly reduce the permeability of very high permeability (2D) north sea sandstone cores. This reduction can be seen in Fig.1.11 and the corresponding influent and effluent analysis is presented in Fig.1.12.

TODD et al. (1984) used aluminium oxide particles in a size range 3-5 μm at a concentration of 5ppm in his experiments. Core flooding with this suspension of high permeability core (2012 md) shows almost complete external filter cake damage (Fig.1.13), even for a core with the largest mean pore throat diameter (29.5 μm). A less permeable core (562 md), though still with a comparatively large mean diameter exhibited internal cake formation and half the damage obtained with the high permeability core (Fig.1.14). Todd's results serve to illustrate that mean pore size is not a simple criterion for explaining the damage to the cores.

SCOTT (1984) experimentally tested the effect of water quality on permeability damage by using two sandstone cores having different characteristics. He stated that for an injection well with an injection rate of 20,000 BWPD over a 100 ft interval and a 7" wellbore, 109 BWPD pass through each square foot of the wellbore surface. If the injection well is not open hole but cased and perforated then the rate per square foot is even higher. Assuming 4 shots per foot with a perforation depth of 8" and diameter of 1" gives 278 BWPD per square foot.
In order for this quantity of water to be injected day after day the water must be clean enough to prevent rapid blocking of the pores within the rock matrix, and hence a rapid decline in the water injection capability at a particular pressure.
He used 1 inch diameter cores .The fluid was a suspension of aluminium oxide powder (3-5 μm particles) in distilled water and a flow rate of 1.8 ml/s. Solids concentration of 5 ppm and 1 ppm were used. The original liquid permeability of Newbiggin sandstone was 1304 md compared to that of 319 md for the Clashach sandstone.
The results shows that:
a) For a particle concentration of 5 ppm, the Newbiggin core exceeded maximum possible injection pressure after only 17.6 hours while the Clashach took 24 hours. This served to indicate that permeability alone was not a good guide to estimating the effect of suspended solids on permeability reduction.

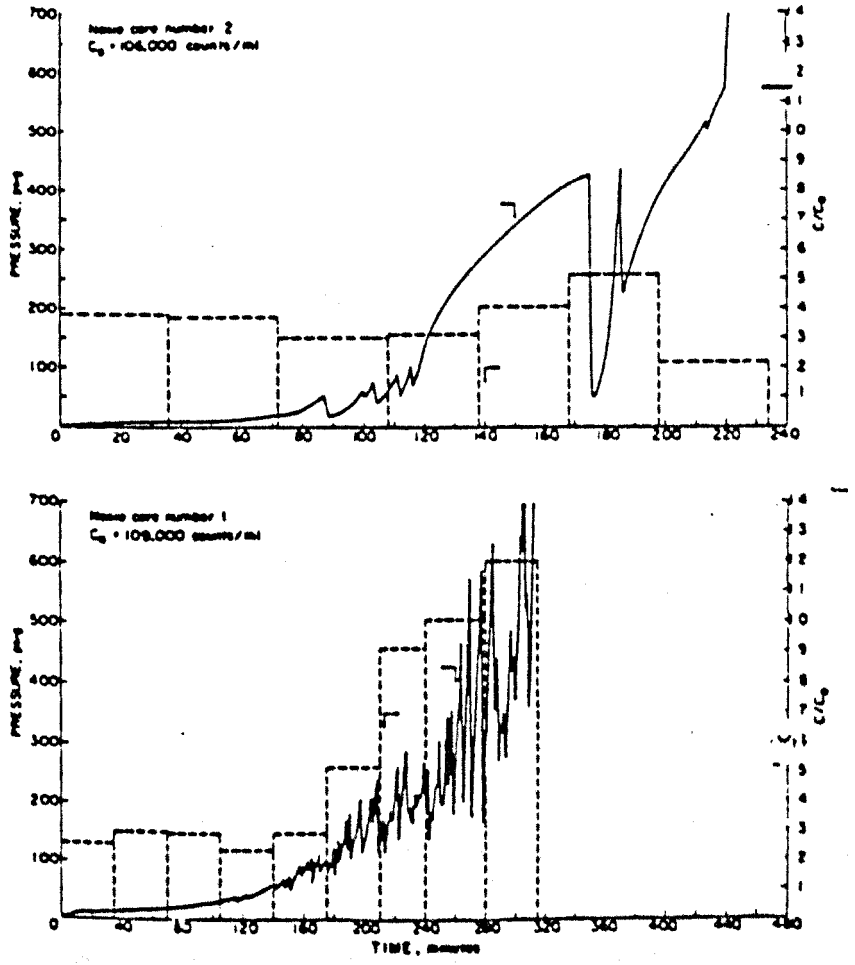

Fig.1.10: Pressure and effluent particle concentration versus time for noxie cores (Donaldson *et al.* 1977)

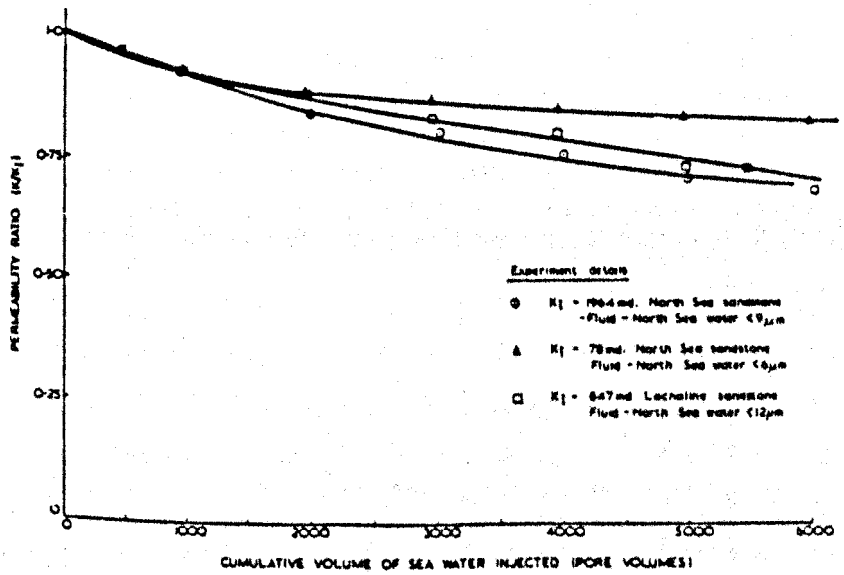

Fig.1.11: Permeability reduction in sandstone system resulting from injected North sea water (Todd *et al.* 1979).

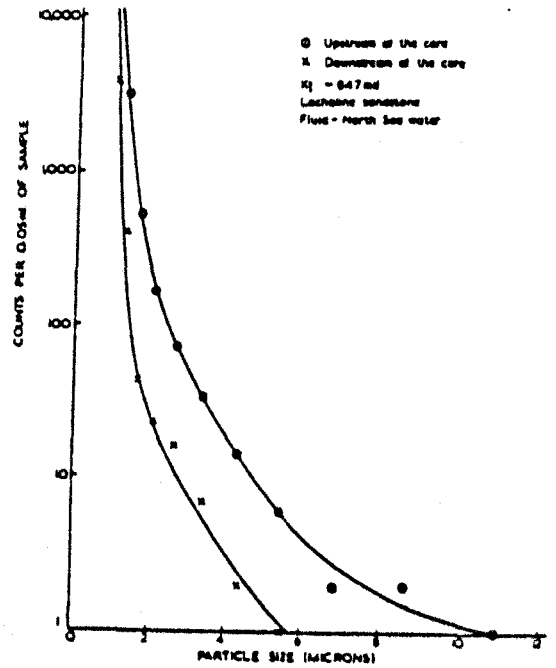

Fig.1.12: Particle size analysis of sea water before and after core (Todd *et al.* 1979).

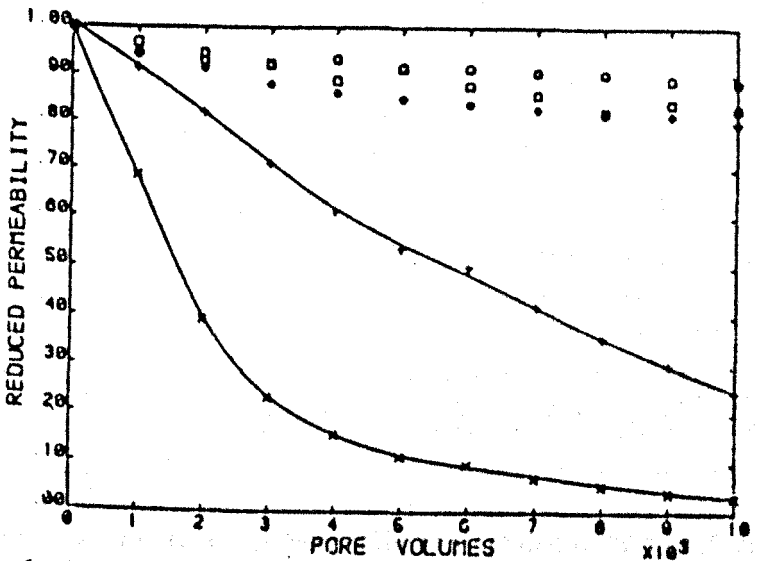

Fig.1.13: Permeability damage obtained by suspended solids injection typical of external filter cake formation (Todd *et al.* 1984).

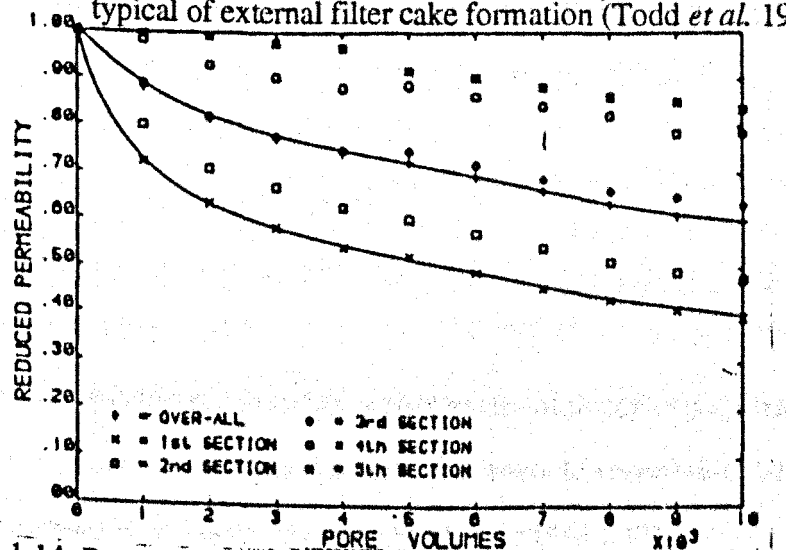

Fig.1.14: Permeability damage obtained by suspended solids injection typical of internal filter cake formation (Todd *et al.* 1984).

Examination of the capillary pressure curves for both rock types showed the Newbiggin to have a greater spread over the range of pore sizes. The Clashach had the majority of its pores concentrated in a very narrow band of pore diameters. The medium pore size for the Clashach was 22.5 μm as opposed to 18 μm for the Newbiggin. The Clashach had 77% of its pores with diameter greater than 15 um while the newbiggin had only 58.5% greater than this diameter.

b) With a particle concentration of 1 ppm initially the results were similar with the injection pressure continuing to rise but a lot more slowly. However, a maximum pressure appeared to be reached after approximately 55 hours and after this time the pressure rose and fell periodically but never regained this maximum value. This phenomenon appeared to be similar to the 'particle breakthrough' observed by Donaldson and Baker. In all cases, the effluent samples had lower counts in the majority of the channels as time progressed. Particles in all size ranges showed significant retention.

Another important point that he mentioned is that if subsequent 1 ppm experiments show no signs of external filter cake build up, it then becomes important to discover the depth of impairment so as to have a damage zone thickness for use in injectivity computation. This points towards longer cores and core holders. If an external cake is formed, long cores are unnecessary as the filter cake controls the injection pressure, the effect of internal plugging being negligible in comparison.

ERSHAGHI et al. (1986) studied the injectivity loss due to the injection of different particle size suspensions:

Cubical blocks were used with a 1/4" hole drilled at the centre of each block resembling the injection well. Particle suspensions at a concentration of 250 mg/l were prepared using graded dust consisting silica alumina and iron oxide (three groups of sizes 0-3 μm, 0-5 μm, and 0-10 μm) suspended in 0.2 μm filtered 2% Kcl solution.

After analysing the results, he concluded that:

a) For the low permeability sandstone blocks, the greatest reduction of injectivity index occurs during the flow of 0-3 μm particle size suspension (Fig.1.15). The medium size particles 0-5 μm shows a similar initial rapid drop but higher values of injectivity are retained at comparative injection time (Fig.1.16). The results for large size particle suspension 0-10 μm show an overall slower reduction of injectivity index with time (Fig.1.17).

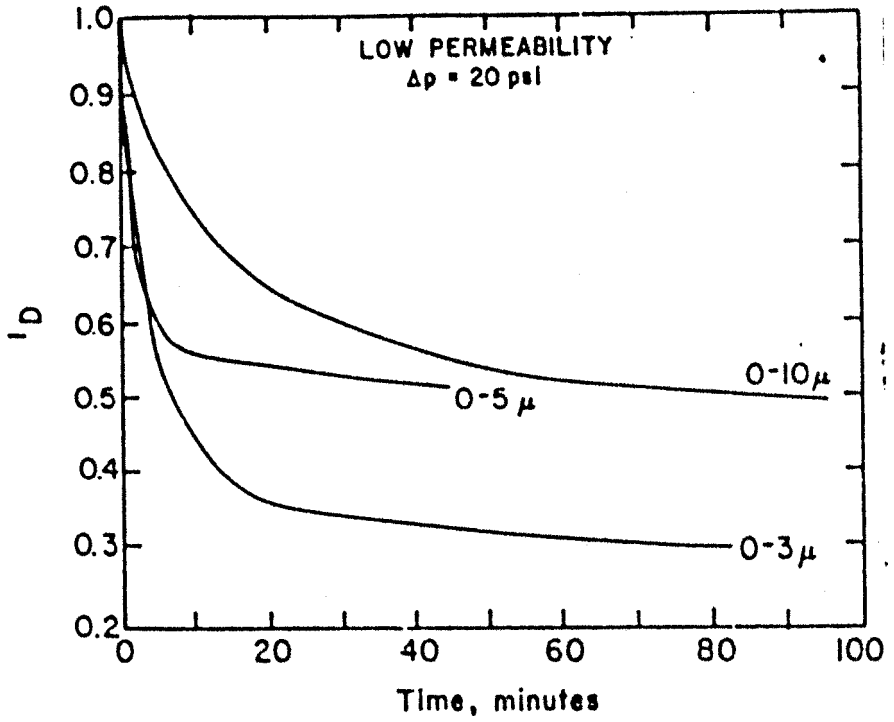

Fig.1.15: Injectivity losses measured for a low permeability block (Ershaghi *et al.* 1986).

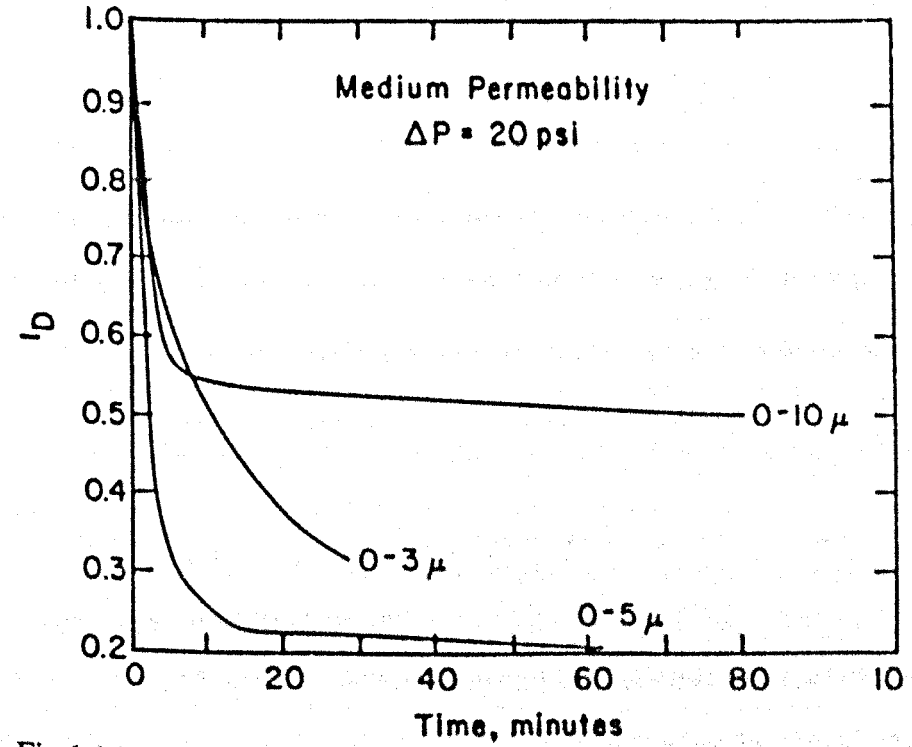

Fig.1.16: Injectivity losses measured for a medium permeability block (Ershaghi *et al.* 1986).

Since the mean pore size of low permeability cores is about 8 μm, indications are that the suspensions with a particle size range of 0-3 μm penetrate the rock and result in substantial permeability losses. The large size particles seem to be filtered out at the input face causing a gradual loss of injectivity. The nature of the cake buildups can be characterised by a continuous flow of fluid. The medium size particles maintain an injectivity index initially similar to the small size particles and later approach that of the large size particles. This can be interpreted as initial injectivity reduction because of particle invasion followed by the gradual buildup of a filter cake.

b) With medium permeability cores, the small size particles 0-3 μm manage to travel through the system and the overall injectivity loss is much less severe than what was observed for low permeability cores. The medium size particle seem to get trapped in the system and they show the worst performance. The large size particles initially show evidence of fine invasion and later on because of cake buildup, the injectivity loss reaches a plateau of about 50% of the initial.

c) Moving to even larger pore sizes, for high permeability cores where a mean pore size of 18 μm was measured, the small and the medium size particles seem to be able to invade the system causing in-situ permeability reduction. The performance for large size particles is no better as the chances for cake buildup is reduced and because of greater difficulty of these larger particles to pass through the system lower values of injectivity ratios are observed.

d) For the low and medium permeability blocks where the large size of particles (0-10 μm) had caused cake buildup, high differential pressure resulted in worsening of the half lives (the time required at constant pressure for the injection rate to decrease to half its initial value). This is mainly a sandface effect where the compacted cakes present additional flow resistance to passage of injected fluid.

Under higher differential pressures, particles which had invaded the system seem to be forced out resulting in improved injectivity ratios.

e) If filters on the injected fluid are used before the injectivity ratio has reached a low plateau value, the placement of filters extends the injectivity half-life. After the rocks have experienced their low plateau injectivity ratio, the filter placement has only minor improvement effect. They can, however, prevent further degradation of injectivity ratio.

VETTER et al. (1987) examined the factors affecting particle invasion and the related degree of damage.

They used a SEM technique in determining the particle concentration distribution for the core in which 0.05 micron particles in suspension were injected. This distribution was represented by the ratio of chromium(particles) to silicon (core material) concentration. One observation is that the submicron particles entered substantial depths and got trapped at various locations in the core. However, the concentration of the trapped particles decreased rapidly with depth.

They concluded that:

a) Above about 120 pore volumes of injection, both the 1 micron and the 7 micron particles practically plugged the cores, whereas the 0.05 micron particles caused the permeability to drop by about 60%. The bridging phenomenon is more evident for 0.05 micron particles. For the 7 micron particles there does not seem to be any bridging phenomenon, thus indicating that the decrease in permeability by large particles is mainly due to cake build-up (Fig.1.18 and 1.19).

b) For 0.05 micron chrome oxide particles, it is not evident whether the flow rate has any direct relation with the permeability impairment only the lower injection rates seem to damage the core much rapidly.

Contrary to the behaviour observed for chrome oxide particles, the blended cerium oxide particles are found to break through Berea sandstone cores at all flow rates between 2 and 10 ml/min (Fig.1.20). In general for submicron particles, the higher the flow rate, the less severe is the damage to the core plug.

c) The injection of the suspensions containing 250 mg/l and 500mg/l of less than 0.05 micron cerium oxide particles caused a rapid reduction in permeability equal to 50% after 40 PV. On the other hand, with a concentration of 90 mg/l of the same particles suspension, the permeability decreases by only 10% (Fig.1.21).

Then they used a blended cerium oxide suspension to flood (a)two plugs mounted in series within the same holder and (b)two core plugs mounted in two holders in series. These experiments may simulate the flow of particles across a fracture (one core holder) or a filter (two core holders).

a) Filtration (two core holders):

The particles, once breaking through the first core, should be able to go through the second core without any further deposition. However, they found a relatively thick cake at the inlet

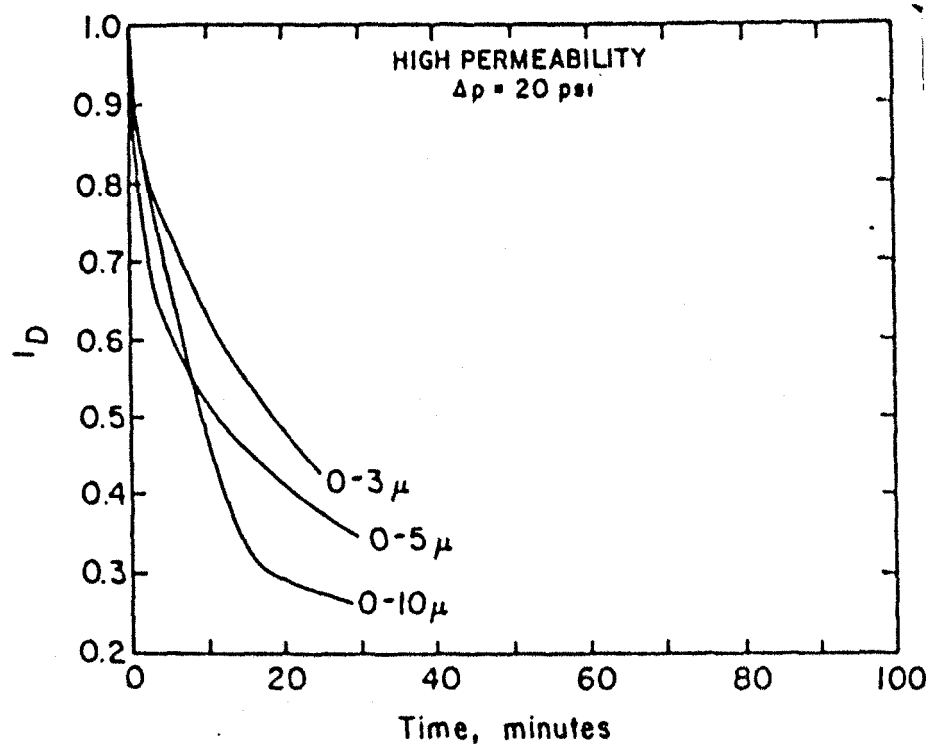

Fig.1.17: Injectivity losses measured for a high permeability block (Ershaghi *et al.* 1986).

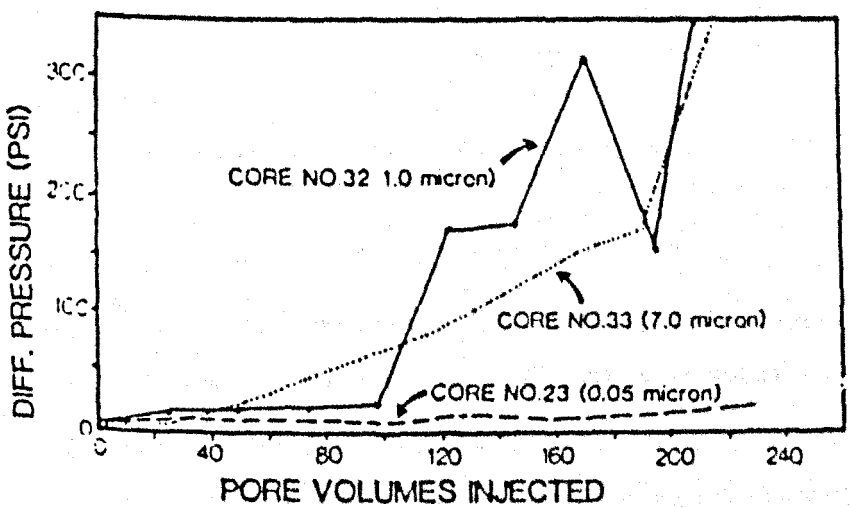

Fig.1.18: Core pressure history (chromium oxide particle injection) (Vetter *et al.* 1987).

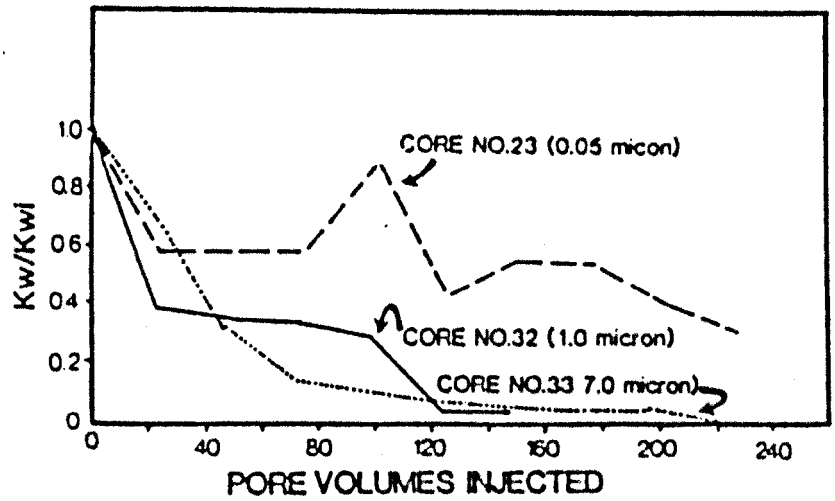

Fig.1.19: Core damage history (chromium oxide particle injection) (Vetter *et al.* 1987)

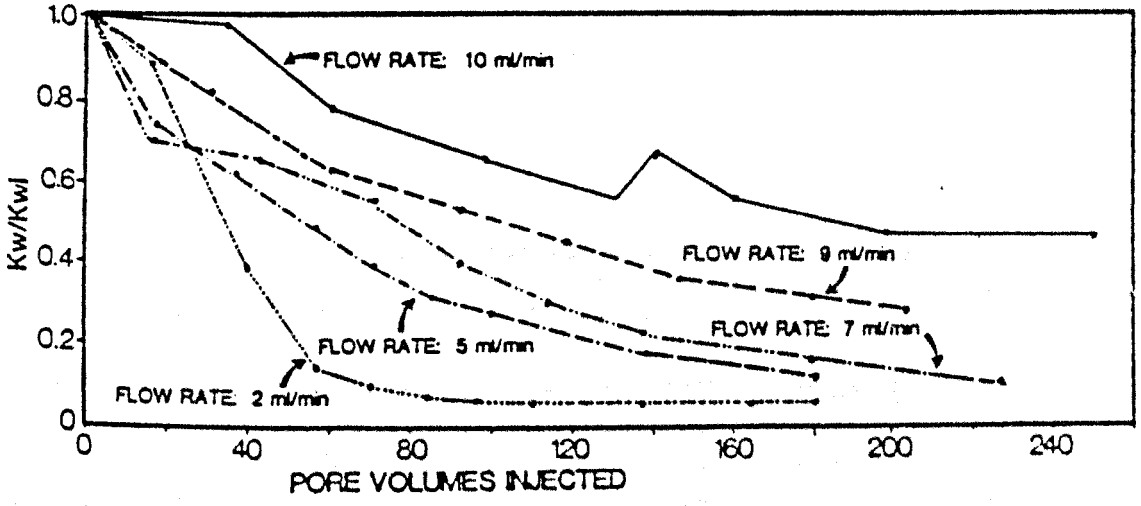

Fig.1.20: Core damage history effect of flow rate (cerium oxide particles : > 0.05 micron) (Vetter *et al.* 1987).

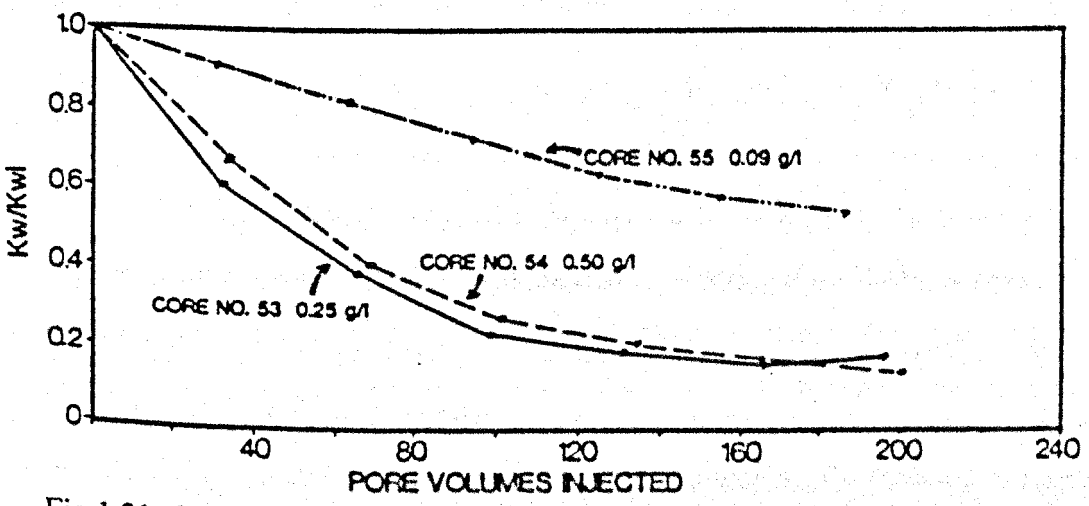

Fig.1.21: Core damage history effect of concentration (cerium oxide particles : > 0.05 micron) (Vetter *et al.* 1987).

face of the second core as well as deposition inside the second core. So if an injected brine is filtered down to the lowest particle size, particles will still be deposited in the rock matrix if its permeability is on the order of 100 and even 200md.

b) Fractures (one core holder):

He found a significant cake at the inlet face of the second plug. The particles breaking through the second plug didn't seem to have any different characteristics than those breaking through a single core plug. The results of this experiment suggest that the same cakes would occur at fractures within the formation.

TODD et al. (1988) presented a study of permeability decline for broken-face cores, with a permeability range of 250-1000 md, using injected water suspensions of 1-15 ppm with a size range of 0-3 μm, at flow rates representative of north sea injection wells. The duration of the tests have been up to 150 hours, equivalent to 40,000-60,000 core pore volumes.

The results indicated that in-depth invasion occurs for broken-face plugs compared to external filter cakes which often occur with sawn face plugs. In using a cut-faced core, the permeability of the inlet and outlet faces may not be representative of the permeability of the core.

The core material was clashach sandstone and the flow rate from 0.45cm/sec to 1.8cm/sec with an experimental duration up to 6 days.

They concluded that:

a) Within this range of size and concentration in a broken-faced core of 250 md, the permeability impairment was distributed along the core.The damage permeability zone extends up to the end of the core even with 15ppm concentration of 0-3 μm alumina.The SEM pictures taken after the experiment qualitatively shows the similarity of the permeability decline obtained from pressure monitoring. The permeability decline follows a definite trend in all the sections of the core and all of them eventually level off with increased injection time. These results suggest that the phenomena of entrainment and redeposition takes place when a critical pore velocity is achieved giving a stable permeability.

b) The plot of the ratio of permeability of the core to its initial permeability versus log of gross velocity of fluid at the inlet face have been found to be linear for different pore volumes of fluid injected. The relationship obtained from this plot can be used to predict the damaged permeability in a similar material at any new velocity of flow, provided the flow is maintained

within the laminar region and no fracture is initiated during the injection. It is observed that the permeability impairment due to solid particle invasion is not only a function of pore volume injected, but it also depends on the gross velocity. At higher flow velocity, the process of entrainment increases and, therefore, the overall permeability remains higher (Fig.1.22).

c) Test with 10ppm and 15ppm of less than 3 μm alumina particles using 1darcy and 250 md cores indicate that an external filter cake had not been formed. The results show an overall permeability decline as a function of particle concentration at constant flow rate of 0.9cm/sec. Also there is an exponential relationship between permeability variation and particle concentration (Fig.1.23).

PAUTZ et al. (1989) conducted a study to evaluate the 1/3 - 1/7 plugging ratio rule by using synthetic, cottage Grove sandstone and Berea sandstone cores.

When an external filter cake is formed, the permeability will be controlled by the permeability of the filter cake. As pressure is increased, permeability will be reduced because the filter cake compresses (Fig.1.24a). For the bridging particles, as the pressure is increased, some of the bridges can break and result in increasing permeability (Fig.1.24b).

As particle size is reduced further, relative to the pore diameter, particles are expected to invade the media completely and collect only in dead ends or low points in the flow channels (Fig.1.24c).

The cores (used in these tests) were invaded by 1.3, 2.5 and 5.4 μm latex bead suspensions at a concentration of 25 ppm at a constant injection rate of 1 ml/min and various injection pressures.

Results of the corefloods are classified by the ratio of invading particle size to the square root of permeability to evaluate the rule-of-thumb concept as applied in the field (Fig. 1.25).

They concluded that the 1/3 ratio tests resulted in 75% reduction in permeability (Fig.1.26). Permeability reduction at the 1/5 ratio appears to reach an equilibrium that is consistent with a successful waterflood operation (Fig.1.27). The 1/9 ratio corefloods exhibited little permeability reduction (Fig.1.28). Since angular and multisized invading particles would do more damage than the 2.5 μm latex beads used in these experiments, the application of the 1/5 or 1/7 ratio rule has some risk.

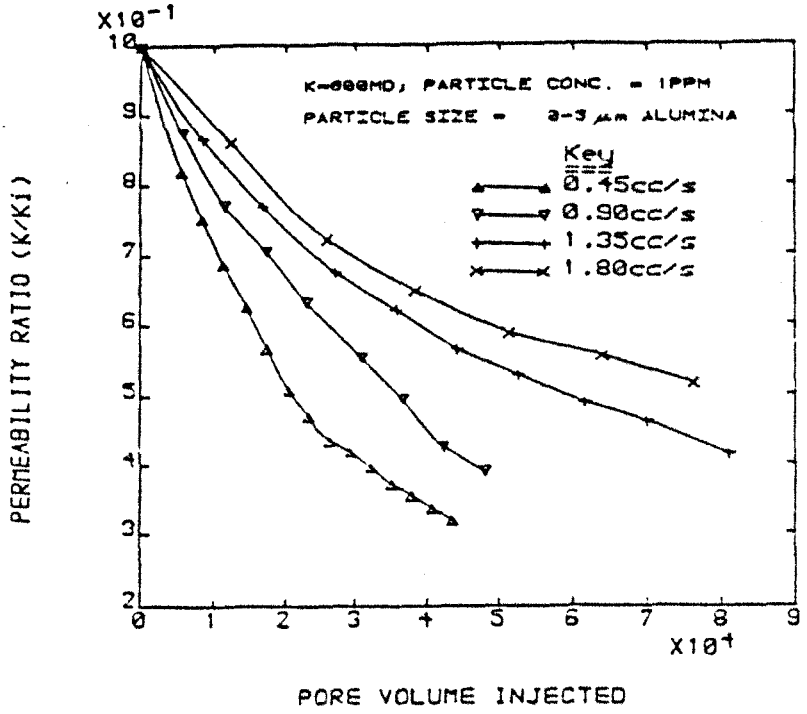

Fig.1.22: Permeability damage as a function of flow rate and pore volume injected (Todd *et al.* 1988).

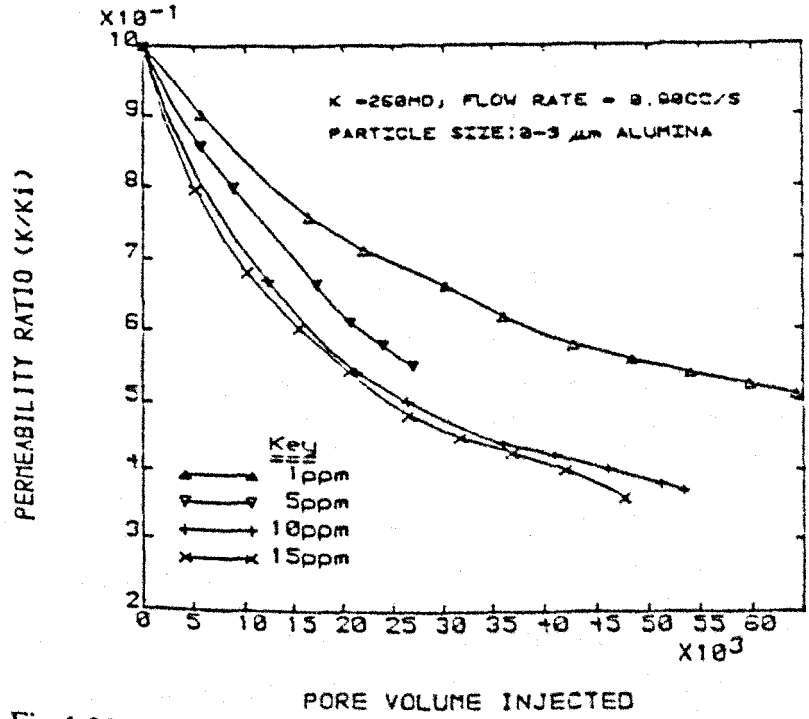

Fig.1.23: Permeability damage as a function of particle concentration and pore volume injected (Todd *et al.* 1988).

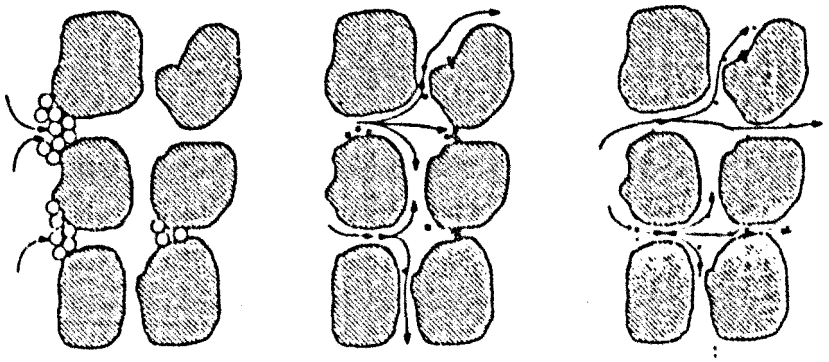

1a. - Cake formation. 1b. - Bridging. 1c. - Invasion and caverning.

Fig.1.24: Impairment mechanisms of particles flowing through porous media (Pautz *et al.* 1989)

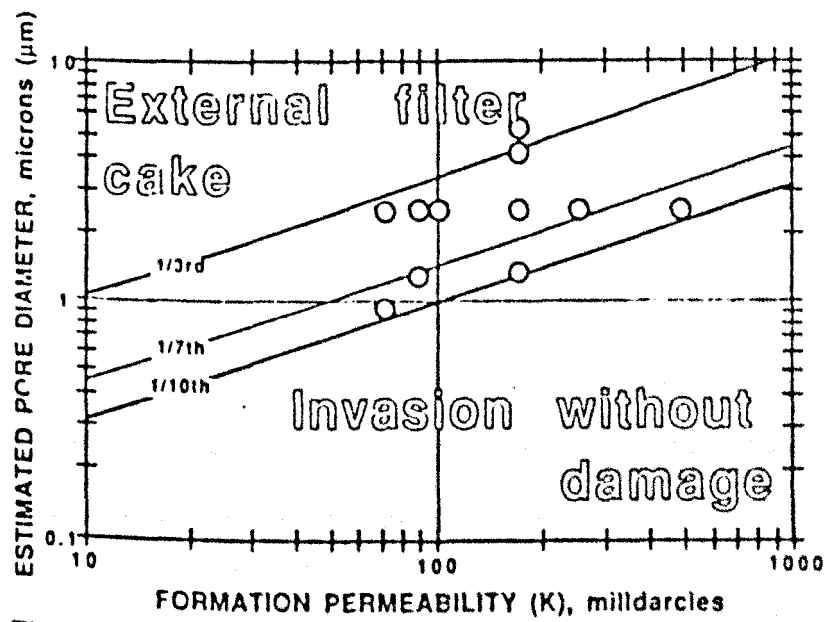

Fig.1.25: Relative relation of coreflood experiments to rules of thumb (Pautz *et al.* 1989).

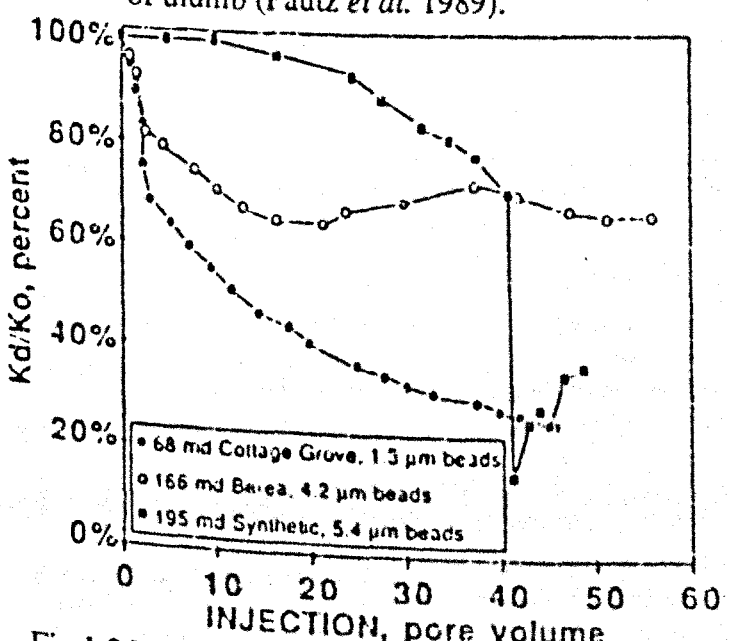

Fig.1.26: Permeability reduction for the 1/3 ratio corefloods (Pautz *et al.* 1989).

ARCIA et al. (1992) used formation sandstone cores from Ceuta Field (Venezuela) to study the pressure drop and the associated particle production due to particle injection.

The sandstone formation cores (mean pore size of 11μm) have a permeability of 25 to 1000 md. These cores were invaded by a quartz particle (7 μm mean diameter) suspended in a 2% NaCl solution.

For all the cores the differential pressure continuously increased with pore volume injected suggesting plugging due to a particle retention effect (Fig.1.29). The pulsing characteristic of the differential pressure data is an indication of the occasional breaking of the particle bridges . For the same reason there is a pulsation observed in the cumulative particle production data. The rate of particle production is initially high and decreases gradually.

VAN VELZEN et al. (1992) studied the effect of flow velocity of particle suspension on injectivity impairment.

Latex particles were used with a particle to pore size ratio of 0.08 to 0.37 and a concentration of 1.7 to 2.1ppm concentration through Bentheimer sandstone cores.

The results show that the rate of impairment decreases with increasing flow velocity and is very sensitive to velocity changes at low velocity levels (Fig.1.30). The effective half-life of an injector is considerably longer at the higher injection rate.

For inflow velocity above 10cm/min, the generally accepted "1/3 - 1/7 rule" giving the particle/pore size ratio for internal-cake formation is confirmed. Smaller particles seem to contribute more to formation damage at low inflow velocity (<2cm/min) (fig.1.31).

ELERI et al. (1992) conducted two sets of experiments, one under constant injection flow rate and a another under constant injection pressure differential.

They stated that in the constant flow rate process, since the flow rate is maintained ,the fluid velocity will continue to increase with increasing particle deposition until an equilibrium state is reached when the net deposition will become zero. As for the constant pressure drop process, the deposition of solid particles will reduce the flow rate and thereby the fluid velocity. Internal pore bridging will occur unless the initial velocity at the start of the test is high enough to prevent that. The constant flow rate tests were carried out with three flow rates (3, 5 and 10 ml/min) and spherical latex particles suspension of 0.5-2, 0.5-3 and 0.5-5 μm in a

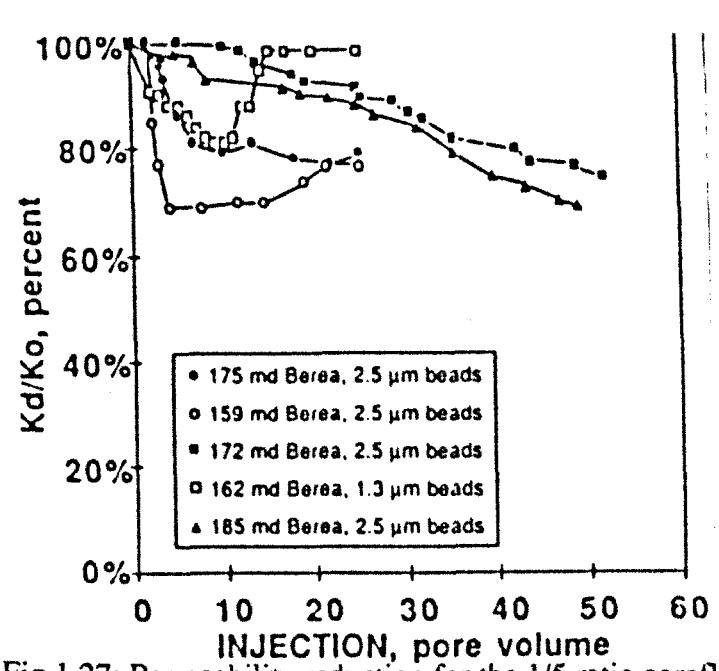

Fig.1.27: Permeability reduction for the 1/5 ratio corefloods (Pautz *et al.* 1989).

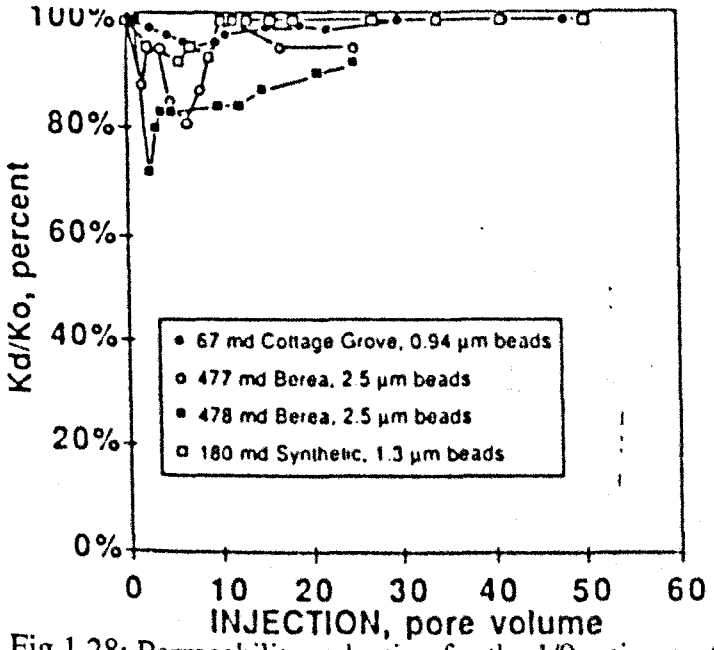

Fig.1.28: Permeability reduction for the 1/9 ratio corefloods (Pautz *et al.* 1989).

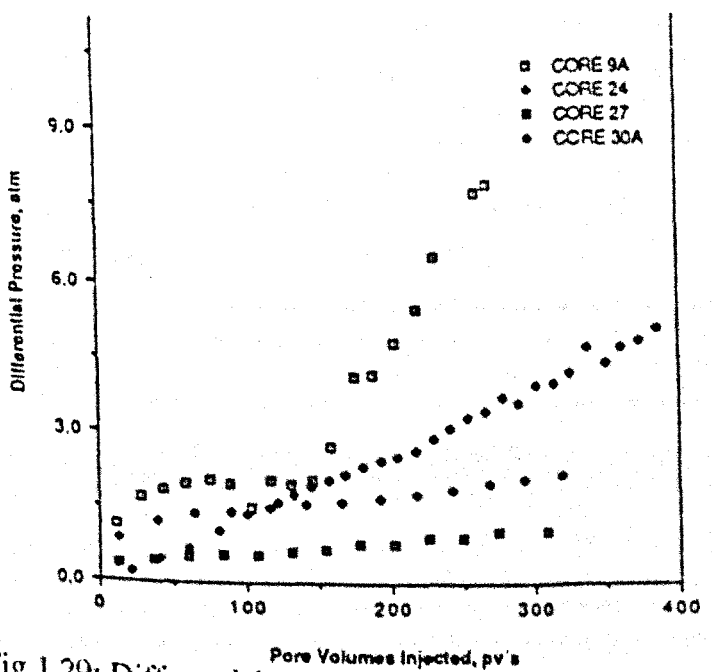

Fig.1.29: Differential pressure response (Arcia *et al.* 1992).

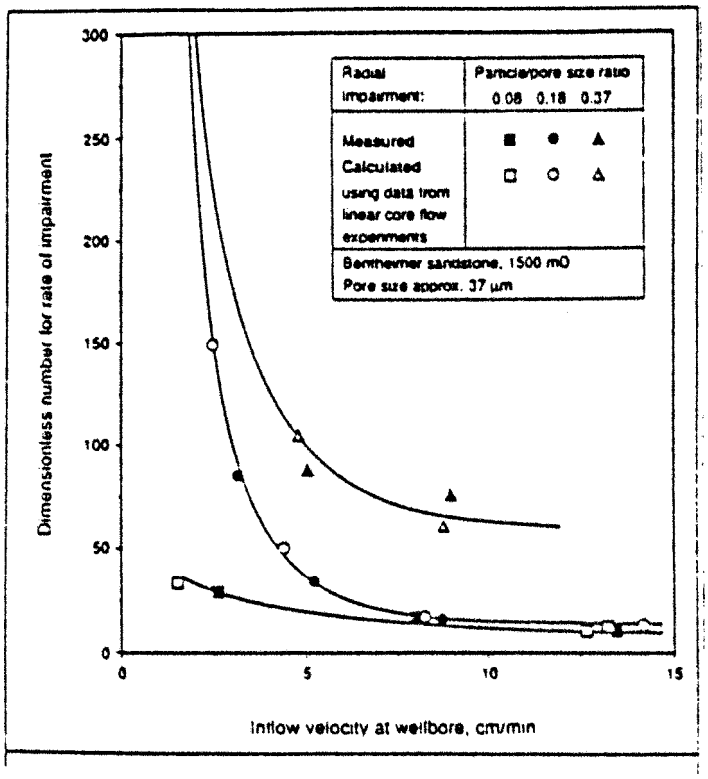

Fig.1.30: Rate of impairment as a function of inflow velocity (Van Velzen *et al.* 1992)

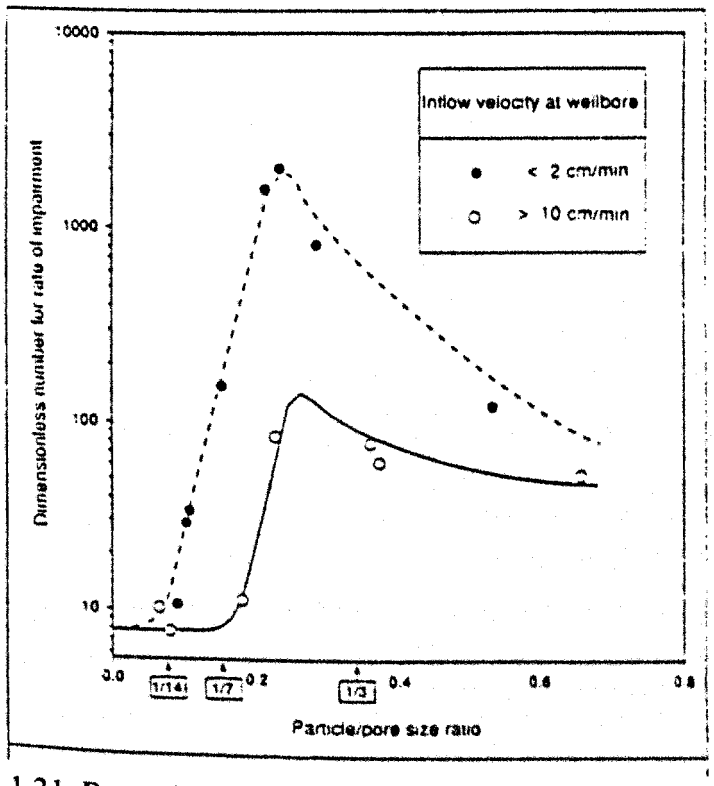

Fig.1.31: Rate of impairment as a function of particle/pore size ratio (Van Velzen *et al.* 1992).

concentration of 50-200 ppm. Berea sandstone cores were used in three different permeabilities (100, 250 and 500 md).

The constant flow rate tests show a sharp decline in permeability for low permeability cores no matter what was the particle size or flow rate with a sharp pressure rise. For high permeability cores, all particle sizes used seemed to invade the core causing a very gentle permeability reduction with a very low pressure increase (Fig.1.32). It appears that the injection particles were flushing through the high permeability cores (Fig.1.33). The higher the flow rate the less severe is the final state of plugging, and the higher the particle concentration, the more the damage to the core.

For the constant pressure drop tests two cores have a porosity of 0.19 and 0.2 with two different permeabilities (250 and 500 md) were used. The injected suspension contains 0.5-3 μm particles in a concentration of 100 ppm. A constant differential pressure of 40 psi was used.

The results of these test show that the high permeability cores give a weak response for the backflushing (Fig.1.34).The low effluent particle count especially at the early stages of the injection may mean that these particles were being deposited inside the surface of the pores (Fig.1.35). This deposition will result in the bridging of pores.

The plot of the cumulative filtrate volume against the square root of time for these cores shows two distinct portions, the initial convex portion when particle bridging dominated and the straight line portion when the cumulative filtrate volume is proportional to the square root of time. The slope and the intercept were used to calculate the different filter cake properties.

They concluded that the variation in permeability produced significantly different results, therefore the routine practice of using membrane filters to characterise or predict reservoir qualities of injection water can be misleading.

KHATIB (1994) studied the effect of filter cake properties on its permeability and began his study with the important role of the filter cake. He stated that the effect of penetrated particles on formation permeability may be dominant only at the early stages of injection. Once the cake is established and reaches a characteristic thickness, these effects are generally negligible compared to those of filter cake properties.

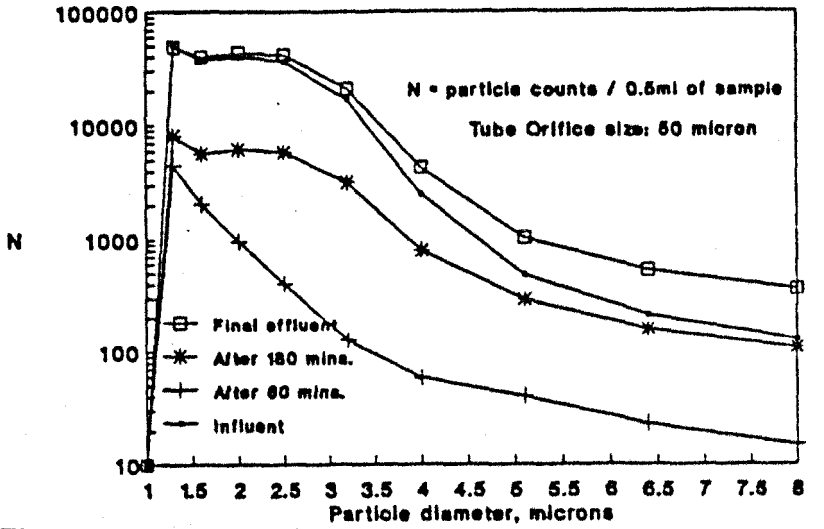

Fig.1.32: Core pressure profile; effect of rock permeability (Eleri *et al.* 1992)

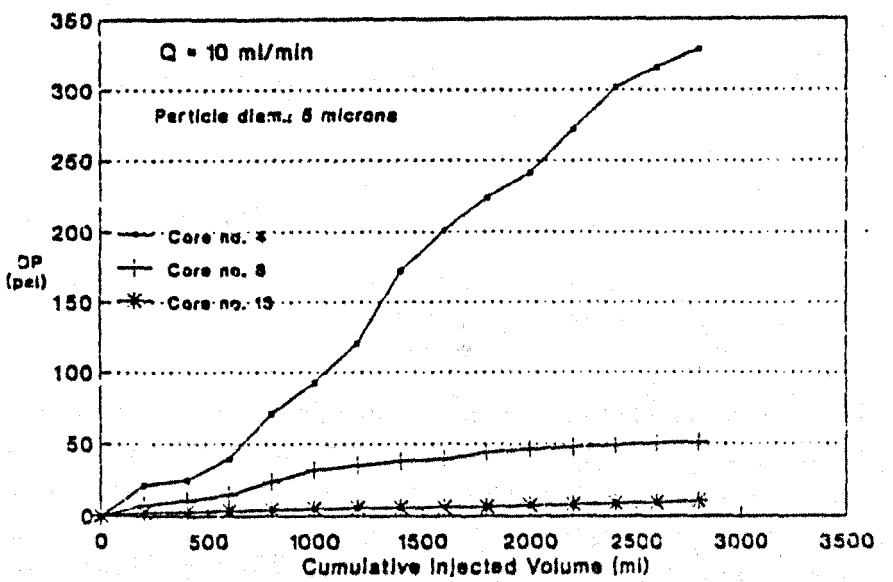

Fig.1.33: Particle size distribution analysis (Eleri *et al.* 1992).

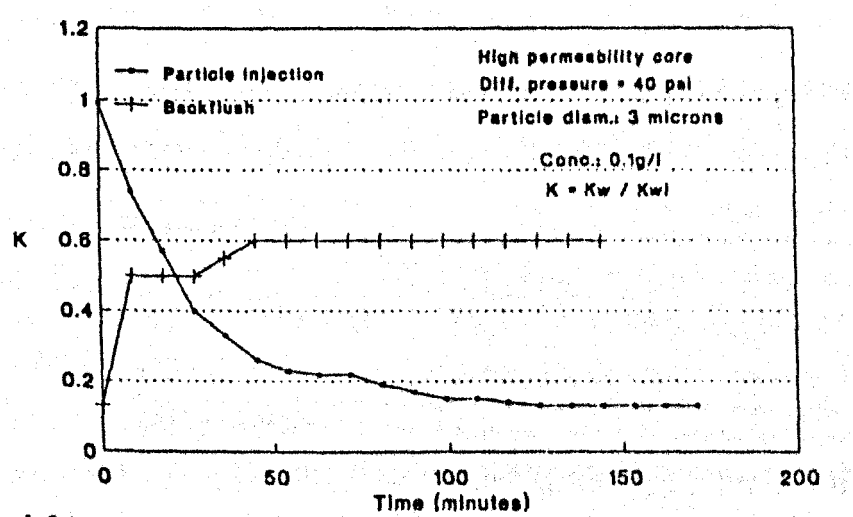

Fig.1.34: Permeability damage at constant diffrential pressure (Eleri *et al.* 1992).

He used Barite particles (average particle size of 5 μm in a concentration of 79ppm) suspended in a buffered 2% KCl brine. While the suspension was being stirred, a known volume was transferred to the cell and another to a filter for determining the solids concentration. The suspension was then compressed to various cake thicknesses.The cake thickness was measured using a caliper. At each stage of compression 2% KCl brine was injected to the cell at constant rate to determine the average permeability of the cake. The total porosity was calculated from the measurement of the cake thickness and solid concentration.

He concluded that:

a) Initially the permeability was reduced about 3 orders of magnitude with a decrease in cake porosity to 0.80, then it was reduced at a lower rate with further reduction in cake porosity.

b) When the particles were suspended for several days in 1% oil brine to coat the solids with oil and then the permeability and porosity of their thin cakes were determined. The results suggest that the cake permeability can be reduced as much as 50% when the solids are coated with oil (Fig.1.36). So the presence of oil should be minimised in injection water when solids contamination is expected.

PANG et al. (1994) collected water quality core flow test data available in the literature and analysed them.

They replotted these data as the inverse of the injectivity ($q/\Delta p$) decline versus pore volume injected and four types of curves were observed.

a) Type 1: Straight line:

This type of curve is observed when incompressible external filter cake (Fig.1.37) or pure internal filter cake (Fig.1.38) are formed.

b) Type 2: Curves with increasing slope:

These are obtained in cases where compressible external filter cake (Fig.1.39) or internal filter cake (Fig.1.40) are formed.

c) Type 3: Curves with decreasing slope:

In some experiments with no external filter cake formation the slope of the injectivity inverse vs. t plot decreases with time (Fig.1.41). These experiments often have a smaller injection particle size and a deeper particle invasion depth.

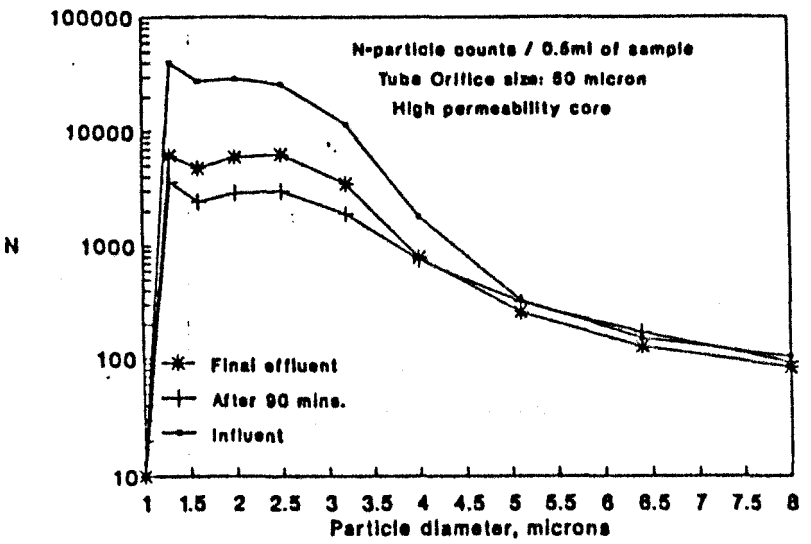

Fig.1.35: Particle size distribution analysis (Eleri *et al.* 1992).

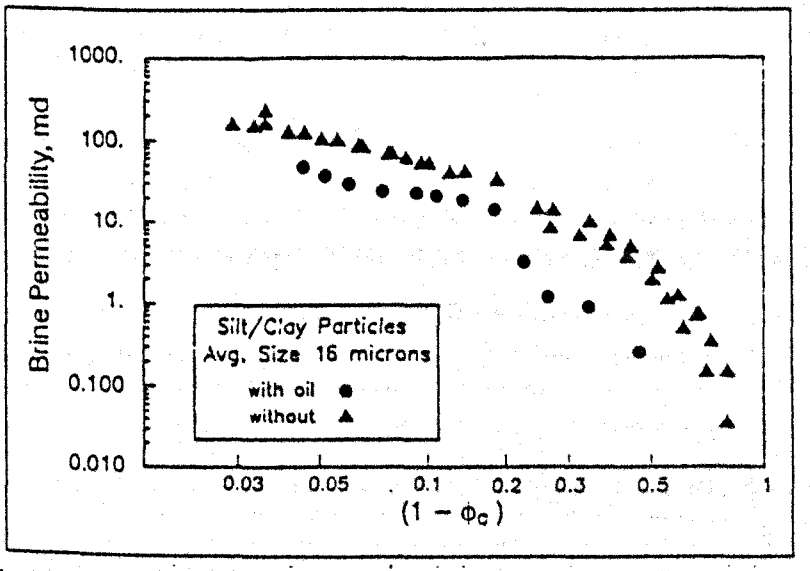

Fig.1.36: Effect of oil-coated solids on brine permeability (Khatib 1994).

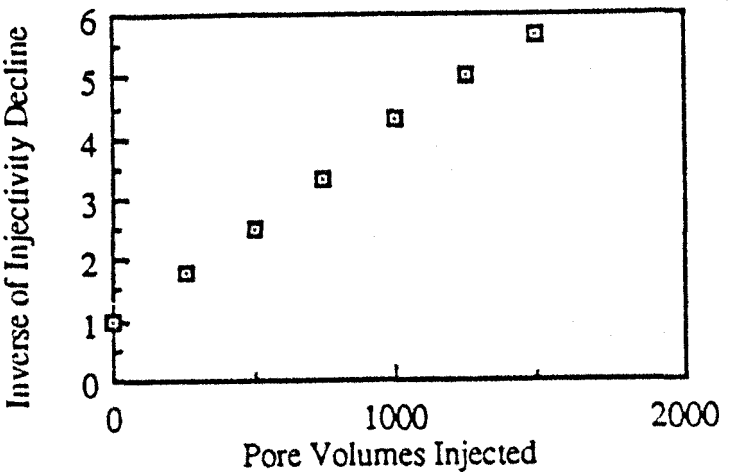

Fig.1.37: An example data set for Type Curve 1 (Pang *et al.* 1994)

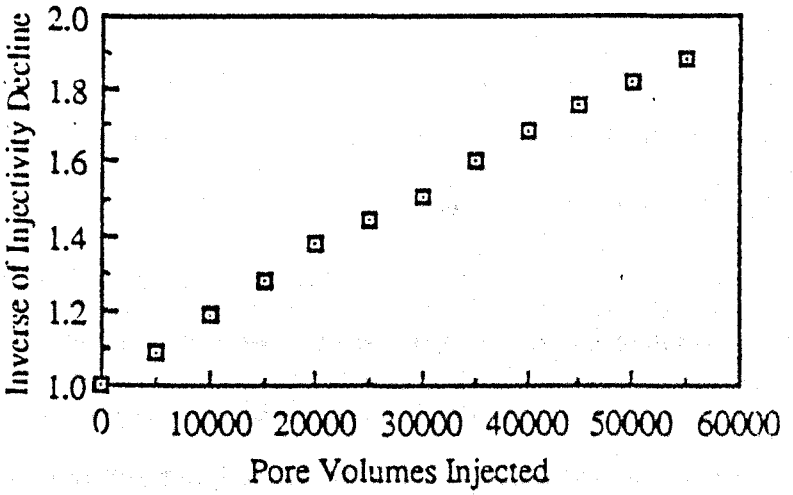

Fig.1.38: An example data set for Type Curve 1 (Pang *et al.* 1994)

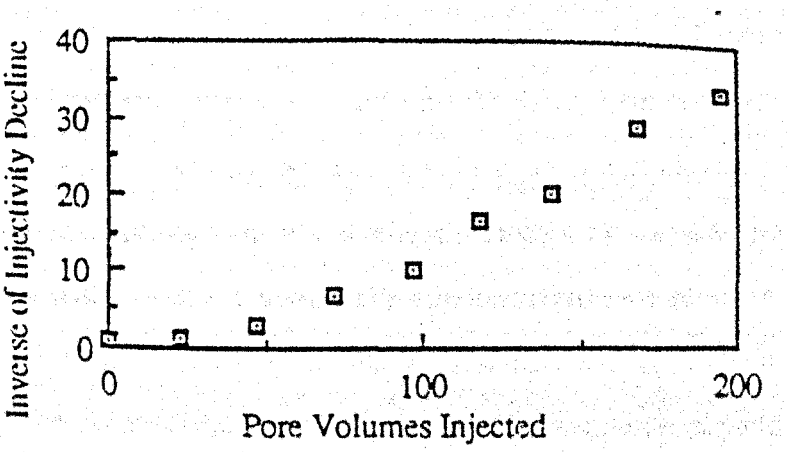

Fig.1.39: An example data set for Type Curve 2 (Pang *et al.* 1994)

d) Type 4: S shaped curves:

S shaped curves and other more complicated shapes of curves are obtained when several internal filtration mechanisms operate simultaneously (Fig.1.42). It is evident that internal filtration curves will depend on the mechanism of capture of particles. This complex dependence makes it difficult to generalise and predict the shape of internal filtration curves.

Retention can occur by two mechanisms (60):

The first one is a deposition on the upstream side of grains or collectors which is induced by normal hydrodynamic forces exerted on the particle when its distance is reduced to that of surface interactions.

The second one occurs in pore restrictions when several particles arrive at the same time in position of forming a multiparticle bridge.

ROQUE et al. (1995), based on these two theoretical approachs, conducted some experiments to study the process of formation damage caused by the injection of particles of known diameters into fontainebleau sandstone of well known pore size at different flow rates. The results show that retention occurs effectively according to the two mechanisms proposed by *Chauveteau* and is very strongly flow rate and particle size dependent. In addition, the formation damage process usually displays four steps.

They carried out the following experiments at constant flow rate:

Experiment (1): The injected particle suspension was mechanically stirred several millimetres from the inlet of the rock sample so as to minimise the effect of an external cake and develop phenomena inherent to the internal plugging of the porous medium. Likewise, the ratio between the mean diameter of the pore throats (16.4 µm) and the mean diameter of the particles (0.8 µm at a concentration of 4 mg/l)) was deliberately quite large so as to limit exclusion phenomena that might mask the mechanisms. The initial matrix permeability was 400 md and the flow velocity was held constant at 0.33 cm/min. The obtained results are given in Figure 1.43.

Experiment (2): Mechanical stirring at the inlet to the sample was maintained for the same reasons as previously, but this time the injection was performed with particles three times larger (2.35 µm) and at a three times faster flow velocity (1 cm/min). The test was continued until an external cake was obtained.

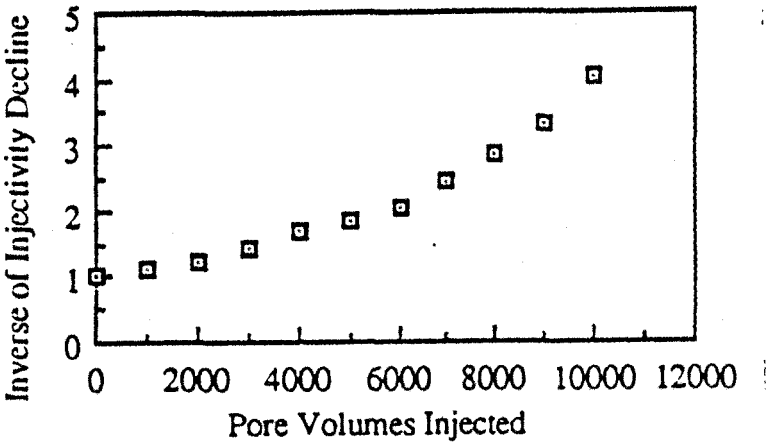

Fig.1.40: An example data set for Type Curve 2 (Pang *et al.* 1994).

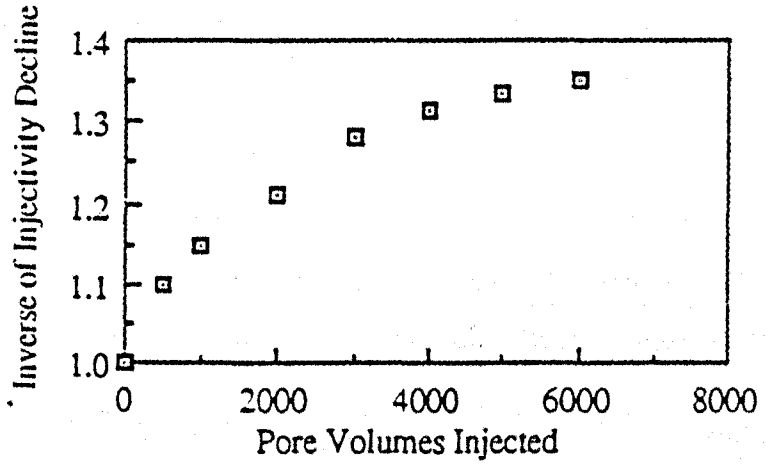

Fig.1.41: An example data set for Type Curve 3 (Pang *et al.* 1994)

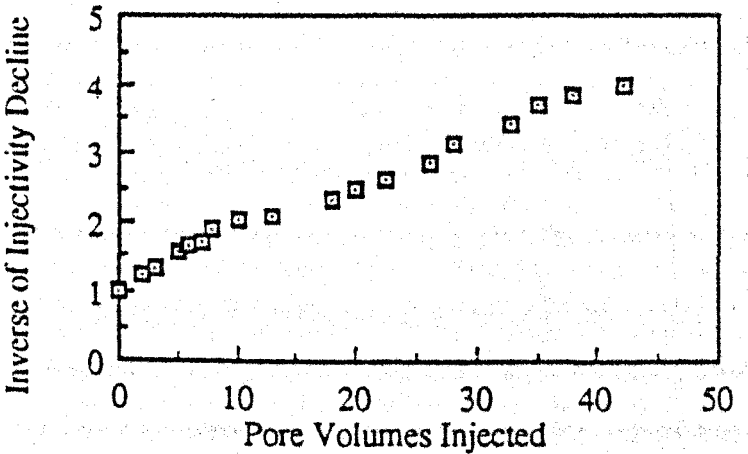

Fig.1.42: An example data set for Type Curve 4 (Pang *et al.* 1994)

The initial matrix permeability was 3000 md (17.4 μm pore throat diameter) and the particle concentration was 20 mg/l. The obtained results are given in Figure 1.44.

Experiment (3):

Here, there is no mechanical stirring at the inlet to the porous medium so as not to modify natural plugging phenomena and to observe the duration of the different phases and their possible concomitance under particle-concentration and fluid flow rate conditions favourable to rapid plugging.

They observed four dominant plugging systems in the plugging curves $K_w/K_{wi}=F(pv)$

a) Phase (1): the dominant system was the particle deposition on the upstream side of grains. During this phase, having a relatively long duration(150pv injected) in the specific experiment (1), the deposition of the particles in the porous medium does not cause any change in permeability. The very small particle concentration in the effluent (2 to 4 % for the Exp.(1)) show that the porous medium retains almost all the particles during this phase. The coupling of constant permeability and intensive retention of the injected particles suggests a particle deposition on the surface of the grains in the zone where the hydrodynamic forces cannot entrain the particles rapidly through the channels in the porous medium (Fig.1.45a).

The deposition probability on a rock grain for a concentration ratio (C/C_i) of 2% will be equal to less than 1%, which is a relatively high probability, and only 1/1000th of the pore volume is occupied by particles.

b) Phase (2): The dominant system is the monoparticle or multiparticle bridging.

When most of the deposition sites on the surface of the grains are saturated, the concentration of free particles circulating in the porous medium increases abruptly (up to 70% of the initial concentration) starting from 200 pv in the experimental case 1. The probability of pore throats being blocked by particles then increases very quickly. This results in an instantaneous drop in permeability. This is followed by a slow decrease in the particle concentration in the effluent, which can be interpreted as a larger and larger number of bridged pores (Fig.1.45b). The decrease in permeability nonetheless remains moderate. This phase may be interpreted by the complex multiparticle bridging of the pore, thus progressively reduce the possibilities of fluid circulation.

The prograssiveness of this bridging phenomenon causes the in-depth plugging of the porous medium since particles can cover a long distance without becoming entrapped.

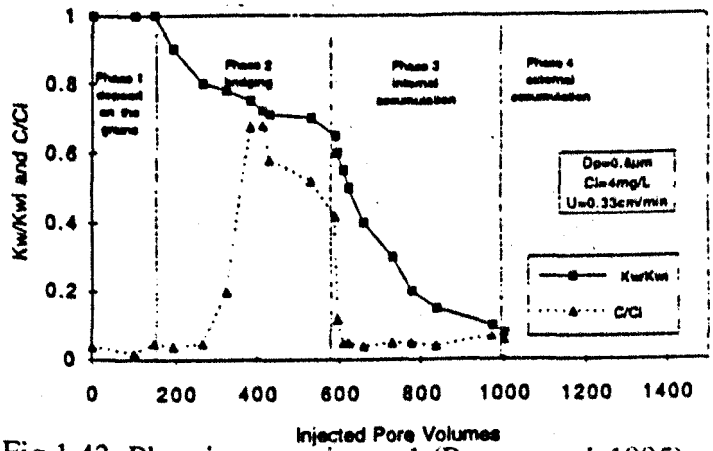

Fig.1.43: Plugging experiment 1 (Roque *et al.* 1995).

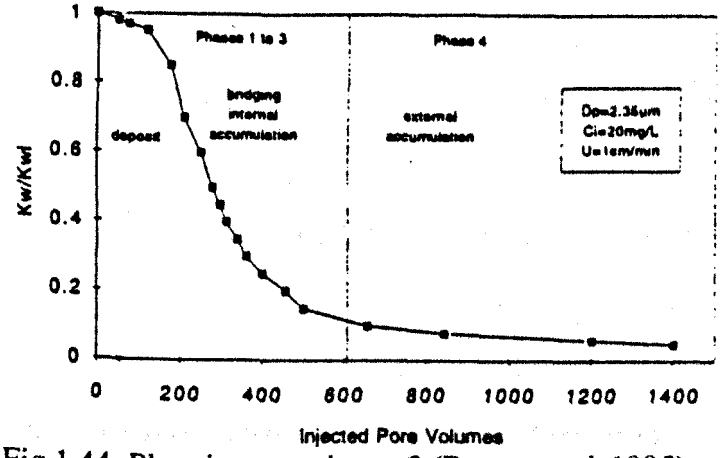

Fig.1.44: Plugging experiment 2 (Roque *et al.* 1995).

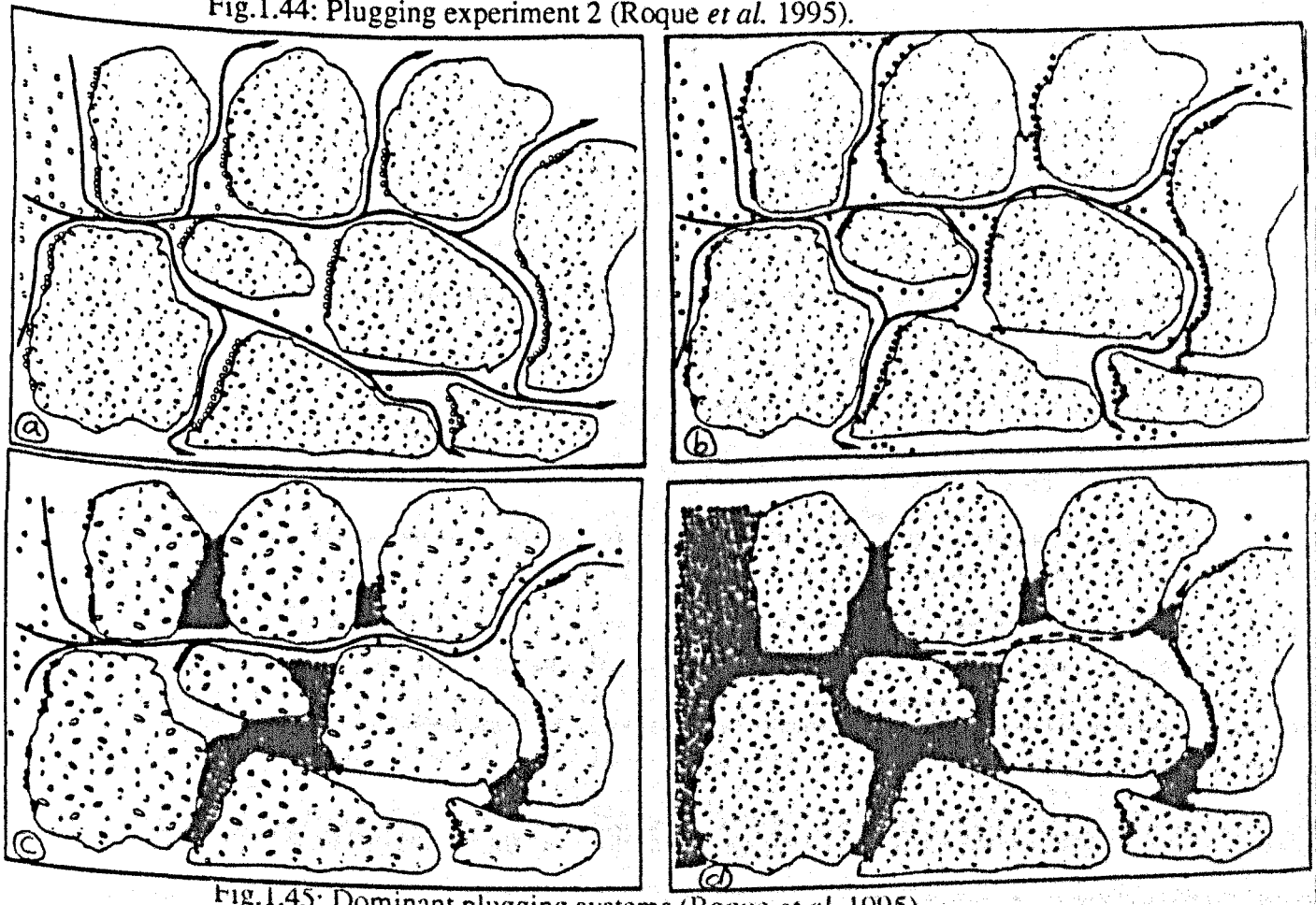

Fig.1.45: Dominant plugging systems (Roque *et al.* 1995).

For Experiments 2 and 3 during which particles three times larger were injected at a relatively low range of fluid flow rates, particle retention in the porous medium was almost total (less than 1% of the particles detected in the effluent no matter what plugging phase is considered). Maximum particle concentration in the effluent corresponds to the transition between deposition and bridging phases. The bridging that occurs after deposition consumes few particles and leaves a great many channels free for fluid circulation. When C/C_i reaches 60%, the probability of pore bridging will be 0.1% which is very small. This could explain the possibility of forming bridges at depth in the porous medium (particles can cover a long distance without becoming entrapped).

c) Phase (3): The dominant system is the internal accumulation of particles for formation of an internal cake.

This shows a rapid decrease in permeability and an abrupt and almost total drop in the free particle concentration in circulation. This phase may then be interpreted by an intensive accumulation of particles at the level of pores already plugged up by bridging (Fig.1.45c). Then, since fluid circulation is more and more difficult, particle accumulation continues in the zone of the porous medium closer and closer from the inlet face. The particle concentration of the effluent at the outlet then depends solely on the interconnected unbridgeable pore fraction.

d) Phase (4): The dominant system is the external accumulation of particles or formation of an external cake:

There is intensive accumulation of particles in the zone near the inlet face of core sample and, as soon as the particles can no longer penetrate, they accumulate on the outside by filling up the entire void space (Fig.1.45d). An external cake is then formed by progressive accumulation, which requires a very large volume of particles to appreciably reduce the mean apparent permeability. When a cake has been formed, this phase is characterised by a very slow decrease in permeability.

They concluded that these different phases may be perfectly overlapping to the point of becoming concomitant. Phases 2 and 3 often seem undifferentiated, which means that bridging and internal accumulation are often simultaneous phenomena. Only the influence of the external cake, whose properties govern the permeability of the system, may be assessed at the end of injection.

The effect of particle velocity on the kinetics of plugging can be seen in Figures 1.46 - 1.48.

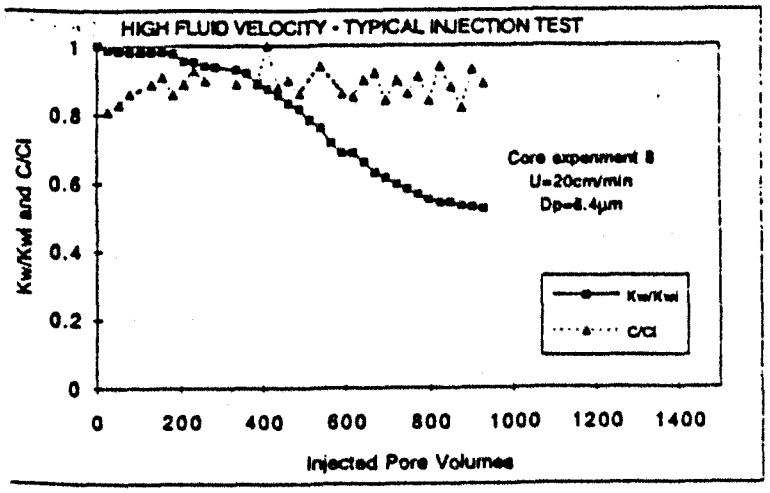

Fig.1.46: High fluid velocity -Typical injection test (6.4 µm particles) (Roque *et al.* 1995).

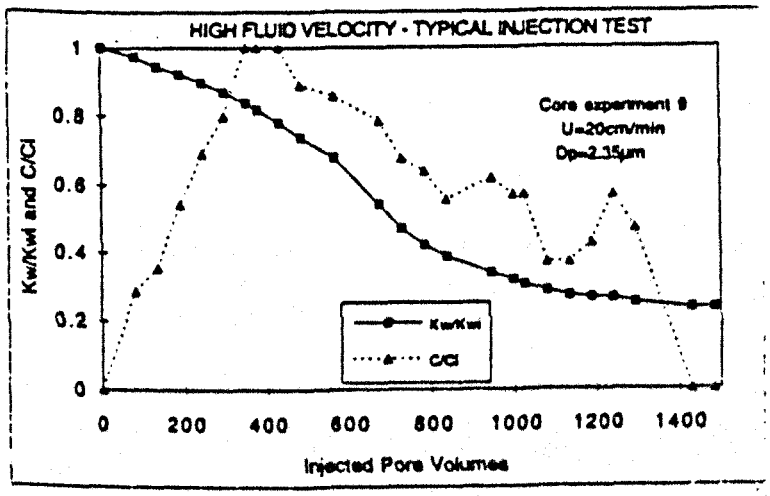

Fig.1.47: High fluid velocity -Typical injection test (2.35 µm particles) (Roque *et al.* 1995).

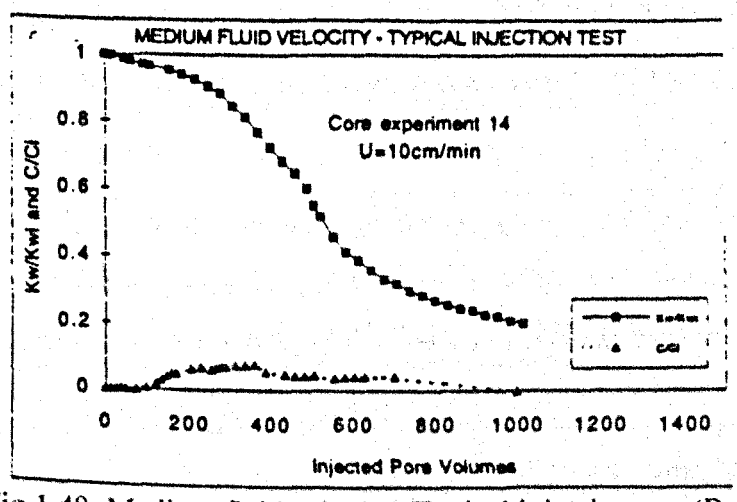

Fig.1.48: Medium fluid velocity -Typical injection test (Roque *et al.* 1995).

1.4 Droplets Invasion Experiments

TANG (1982) studied the permeability damage caused by the injection of oily water into reservoir core samples. The tests were performed at simulated bottom hole conditions using actual produced water with intermittent coinjection of 600 ppm of oil.

He concluded that the injection of both filtered (0.45 micron filter) and unfiltered produced water containing only 14.2ppm suspended solids and 15 ppm of dissolved oil did not cause any short-term plugging. Since oil cannot be successfully dispersed in water without surfactant, a water and oil co-injection technique was used. When produced water and 600 ppm oil were co-injected, oil flowing into the cores caused severe permeability reduction. The core acted like a filter in removing the suspended solids and oil droplets from the injection water. Solids gradually accumulated at the core inlet face. Oil entering the core is trapped and immobilised until residual oil saturation is reached.

For the low permeability core, the reduction in relative permeability to water due to increase in oil saturation is the main damage mechanism. The contribution of emulsion blocking damage becomes more significant as the permeability of the core increases. The permeability can be restored to a certain degree by flushing the core with water at high pressure.

SOO et al. (1984) studied how stable oil-in-water emulsions are transported in porous media. They used an average droplet diameters of 2, 3, 5, 7, and 10 micron flowing in a 0.32 porosity quartz sandpacks of permeability of 0.57 and 1.15 μm^2 with mean pore throat diameters of 17.3 and 29.5 micron, and at a superficial velocity of 0.07 mm/s. Oil content was 0.5 volume%. Drop-size distributions of the emulsions are controlled by blender speed. Fine Ottawa sand of known grain-size distribution is packed into a stainless steel cylinder and it is cleaned by repeated washing with dilute acid and base to establish a strongly water-wet surface. They concluded that:

a) For the 1.15 μm^2 permeability cores and drop size ranges from 2 to 6 micron (Fig.1.49), the core permeability falls over many injected fluid pore volumes and eventually levels off. Oil droplets do not appear in the effluent immediately at one pore volume. Rather, they are delayed, and after elution, their concentration slowly rises over several injected emulsion pore volumes until it reaches the inlet value of 0.5 vol %. At the time for which the droplets approach their inlet concentration, the permeability stops changing. Drops eluting early are generally smaller

than the injected distribution; as time proceeds the effluent droplets shift to larger diameters until, eventually, the inlet and the outlet drop-size distribution are matched.

b) Figure 1.50 demonstrates that the drops, once captured, do not reenter the flow stream, at least at the flow velocity of this work. Hence, steady flow is not a dynamic balance between drop capture and re-entainment.

c) The physical interpretation for a steady state was proposed as follows:

Initially, drops are preferentially captured in small size pores. As emulsion injection proceeds, more and more small pores become blocked. Flow is diverted mostly to the large size pores and drop capture rate decreases. When the drop capture sites in the large pores are filled steady state is reached. As the drop size increases, the effluent concentration data show that overall emulsion retention increases. This is because capture probability is higher for the larger drops. For emulsions of small mean drop diameters and consequent narrower size distribution (2 μm), the emulsion drops are delayed, but they emerge with essentially their inlet size distribution. Presumably, the capture probabilities are not significantly different between the largest and smallest drops in these smaller drop-size emulsion.

d) For the effect of the 3.3 micron drop-size emulsion on the two different permeability sandpacks, the low permeability sandpack exhibits later emulsion breakthrough indicating higher drop retention, which gives larger permeability reduction at steady state. For injecting 3.1 and 3.4 micron drop-size emulsion with oil-phase viscosities of 1.5 and 23 mPa.s, respectively, into the 1.15 μm^2 sandpack, both effluent concentration and transient permeability histories do not vary significantly as the oil-phase viscosity increases by 15 times.

HOFMAN et al. (1991) in their study on 1% oil emulsified in water with droplet size distribution between 1 and 8 μm injected into 40-60 μm glass beads porous core with a porosity of 0.375. They concluded that emulsions with low interfacial tension reduced the permeability during passage through it much more efficiently. This can be explained by the self-reinforcing effect of easy adjustment of a droplet to the shape of the solid wall near a constriction, and easy coagulation followed by coalescence.

TURNBULL et al. (1993) studied the damage effect of sea water injection and Produced Water injection. Sawn face cores of 1.5" diameter and 3" length with a permeability of 170 -1100 md

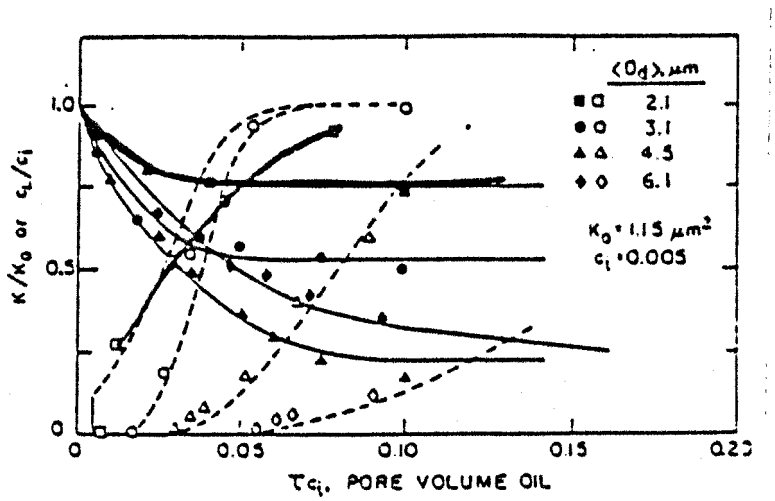

Fig.1.49: Experimental permeability reduction (filled symbols) and breakthrough concentration histories (open symbols) (Soo *et al.* 1984).

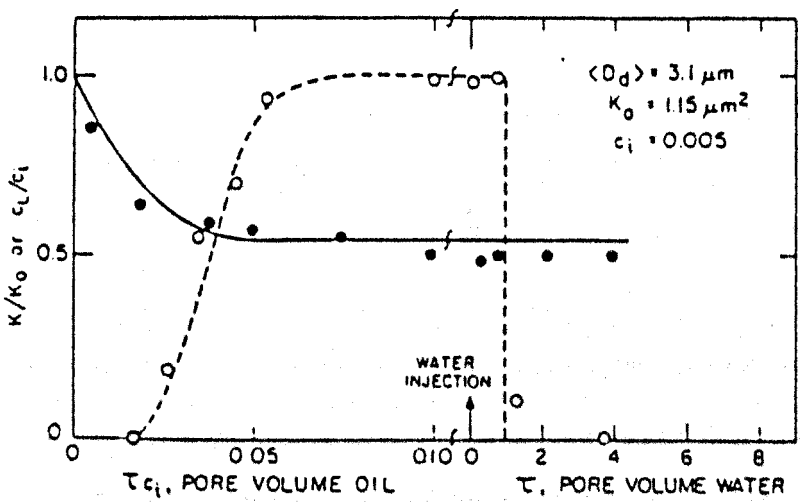

Fig.1.50: Experimental permeability reduction of a 20 pore volune pulse (Soo *et al.* 1984).

were used. An injection pressure of 400 psi was applied. The oil concentration was fixed at 100ppm and the mean droplet size range from 9 - 21 micron with 15 micron being used for the majority of the tests conducted.

They shows that:

a) Relative to the test with seawater the simulated produced water is more damaging. Taking the worst case, he suggested that simulated produced water is twice as damaging as seawater. The trends of produced water injection after seawater injection were also investigated. These trends showed a further severe decline in permeability (Fig.1.51a).

b) When seawater is injected following the produced water, there is only slight improvements in injectivity being noted. It was observed that an improved injectivity may then be followed by a slight decline which again stabilises (Fig.1.51b).

1.5 Particles and Droplets Invasion Experiments

SOO et al. (1985) investigated the flow behaviour of stabilised dispersions of liquid and solid particles in porous media under conditions where the two types of suspension have, as closely as possible, identical physical and chemical characteristics. Suspensions of 0.5 vol % oil were injected continuously into a quartz sandpack of initial permeability of 1.15 μm^2 at constant superficial velocity of 0.07 mm/s. The mean pore throat size of the sand pack was 29.5 micron with initial porosity of 0.34. The drops consist of a neutrally buoyant mixture of mineral oil and carbon tetrachloride with a volume mean droplet size of 2.2 micron. The solid particles are spherical polystyrene latexes with mean particle size of 2.2 micron.

Three major distinctions arise between the oil-in-water emulsion and the solid latex suspension (Fig.1.52).

1) The amount of flow restriction, as gauged by the permeability reduction, is much larger for the solid particles.

2) In the initial injection stage (less than 3 pore volumes injected) elution of the solid and liquid particles parallel each other, but after about three pore volumes of injection the outlet concentration of the solid particles begins to decrease.

3) Both the pressure drop and effluent concentration data for the emulsion reveal that a steady state is attained. Conversely, the solid suspension is unable to reach a steady state.

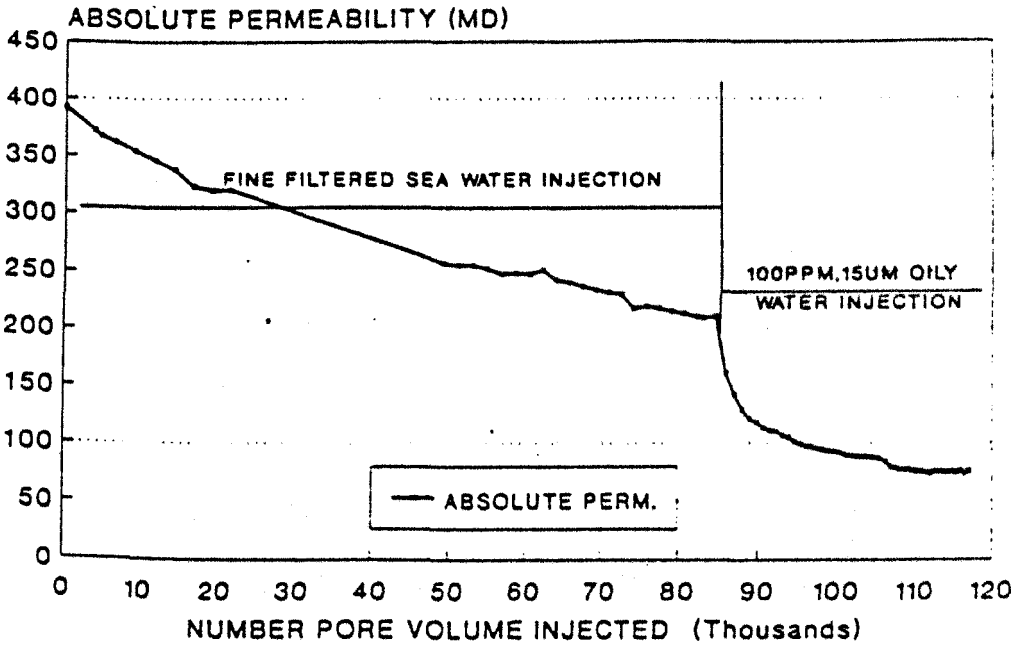

Fig.1.51a: Permeability reduction due to SW injection followed by PW injection (Turmbull *et al.* 1993).

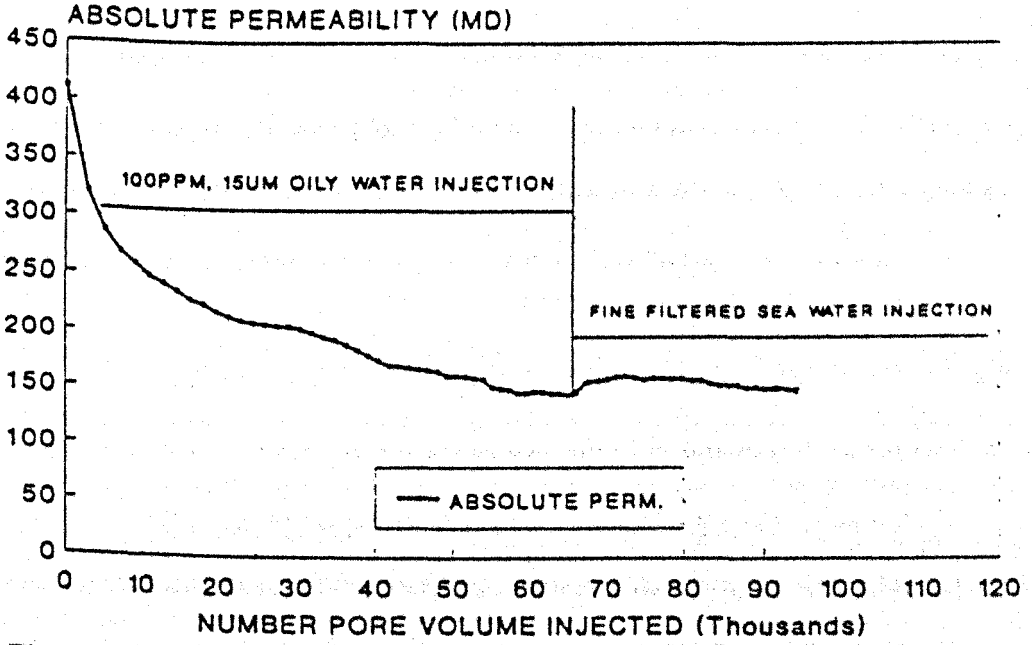

Fig.1.51b: Permeability reduction due to PW injection followed by SW injection (Turmbull *et al.* 1993).

They explaned the transient and the steady flow behaviour of the emulsion in Fig.1.52 as:

a) Droplets are strained out in the smaller pores of the packed bed, which are about the same size as the particles. Flow then diverts to the larger pores where interception capture prevails. Eventually, interception capture ceases when a maximum number of capture sites are filled. A maximum interception amount arises primarily because the flowing stabilised liquid droplets are not captured on top of droplets already adhering to the sand grains. If the large pore channels form interconnected paths through the medium, then steady state is established with all emulsion flow occurring in those channels. Steady state is possible only if the droplet-to-pore size ratio is below some critical value.

b) Based on a photomicroscopic observations, they hypothesized that dendrite formation was the origin of the latex particle flow behaviour reported in Fig. 1.52. Dendritic protuberances should cause considerable flow resistance and highly efficient capture. When dendrites growing from opposite pore walls collide, complete blockage may occur (this may not take place at high flow velocities). These observations explain the larger permeability reduction of the latex suspension, the decreasing concentration of latex particles eluting from the sandpack, and the lack of a steady state.

They concluded that liquid droplets can establish steady flow because they are unable to be captured on top of each other. Conversely, solid particles exhibit continual plugging because they build dendritic structures. Solid suspensions can be expected to exhibit well-bore damage and small penetration distance. In contrast, liquid suspensions, after satisfying the maximum number of capture sites , may exhibit significant penetration distances without catastrophic permeability loss.

HSI et al. (1990) used a specially designed portable core flow station which was installed in the produced water treatment facility at prudhoe Bay field to allow direct evaluation of permeability damage tendencies of produced water under simulated injection well bottomhole temperature and high pressure conditions. Oil containing reservoir core plugs were used to more closely approximate relative permeability effects. They started with some useful remarks concerning oil-solids-surfactant system:

a) If sufficient oil droplets are present in the produced water, they can be filtered out at the core face to increase oil saturation. Due to brine/ oil relative permeability effect, this small increase in

oil saturation can significantly reduce effective brine permeability.

b) Finely suspended solids can accumulate at the oil/water interface and help to stabilise oil-in-water reverse emulsions.These stabilised oil droplets are difficult to separate and can be carried all the way into the injection water stream to cause injectivity decline. Low interfacial tension surfactants can help to further reduce oil droplets size to minimise their permeability damage tendencies. In addition it can dissolve oil residues accumulated on the formation face and reduce oil saturation in the near wellbore region to increase water injectivity.

They conducted an on site core flow tests under reservoir temperature and 4000 psi overburden pressure conditions. Formation cores having a permeability of 170 md and a porosity of 0.3 were used. These cores have a mean pore size of 6.4 to 13.1 μm. The raw formation water contains 194 ppm oil and 3.1 ppm in average. Solids and oil particles size in the range of less than 7 μm.

To establish residual oil saturation, all test plugs were flooded initially with fine filtered produced water and then by stock tank oil. The initial effective brine permeability at residual oil saturation was measured using fine filtered produced water.Then test plugs were flooded with raw produced water and the permeability damage rate was calculated.

The results of the tests show that :

- Core permeability starts to decline as the injection water switched from fine filtered produced water to unfiltered produced water (Fig.1.53).Permeability damage rate in the presence of residual oil saturation is slower than in a 100% brine saturated core (Fig.1.54).
- Most of the permeability damage was found to occur within the first 0.5 inch from the injection face. This observed permeability damage is primarily due to suspended solids. Oil droplets and organic debris dispersed in the produced water also contribute to a lesser degree to permeability damage. Lower permeability cores are damaged at a higher rate than higher permeability cores.
- Some surfactants were found effective in initially restoring water injectivity. However, it fails in the subsequent treatment because it is effective in displacing residual oil but not in removing solids. Also injecting surfactant solutions at the levels required to improve injectivity will be prohibitively expensive.

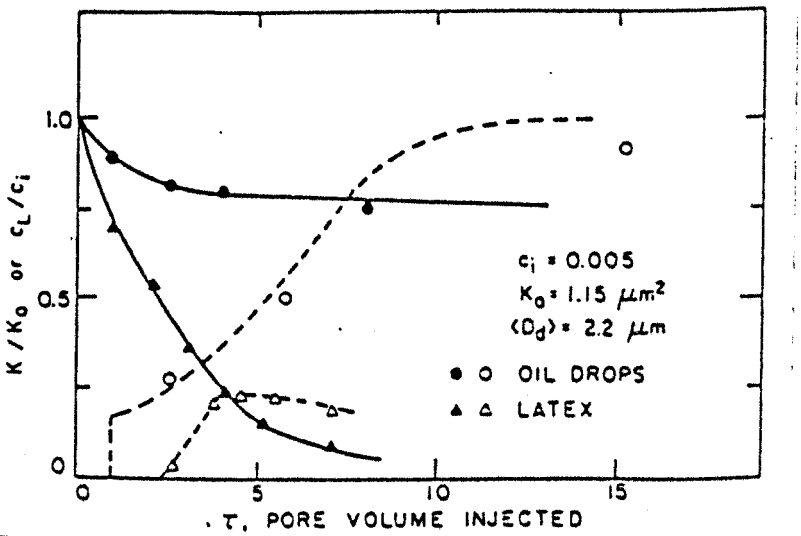

Fig.1.52: Histories for an oil in water emulsion O, and a latex suspension Δ (Soo *et al.* 1985).

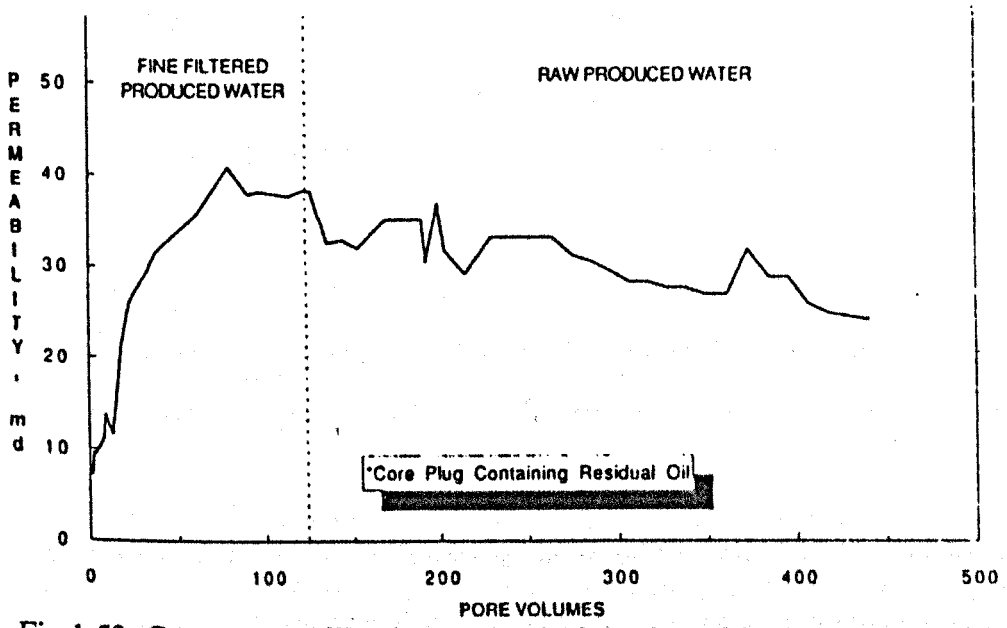

Fig.1.53: Core permeability damage by the injection of Prudhoe Bay produced water (Hsi *et al.* 1990).

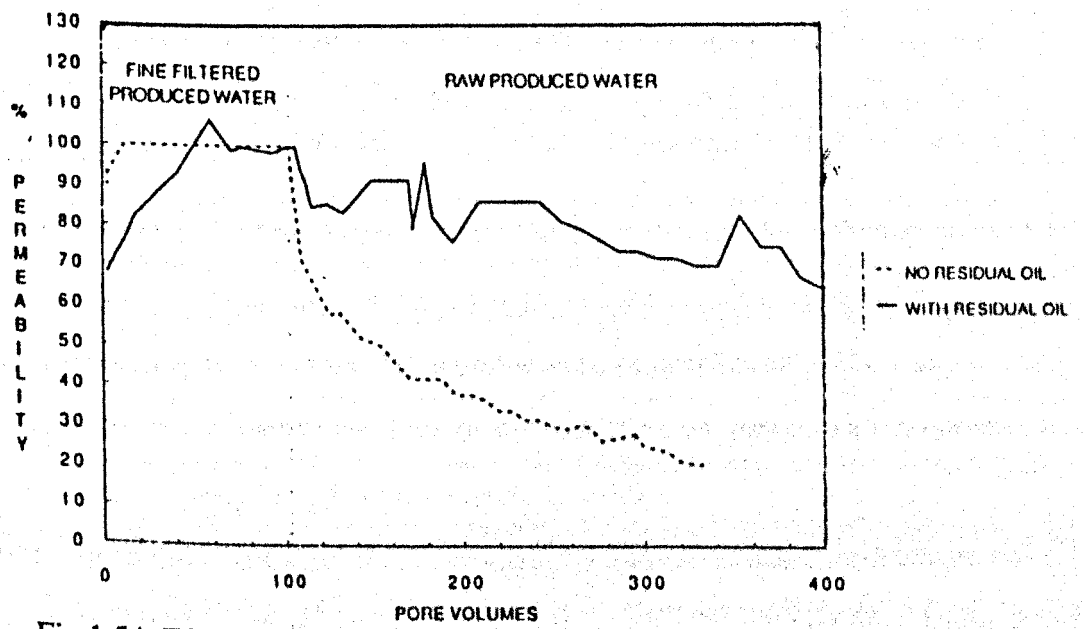

Fig.1.54: Effect of residual oil saturation on the permeability damage rate by produced water (Hsi *et al.* 1990).

- The treatment of core plug with mud acid can restore much of the damaged water injectivity, but at the expense of weakening the formation integrity which will lead to other potential problems.

They concluded that water injectivity can be improved by either improving the current produced water quality or by repeated acid stimulation. However the target water injection rate can also be met by continuously injecting above formation fracturing pressure gradient .

ZHANG (1994) used broken-faced Clashach sandstone with a porosity in the range 14-15% and a permeability in the range 150-300 md to identify the factors associated with formation damage caused by produced oily water injection. Experiments were carried out with a simulated produced oil water containing 40 to 500 ppm crude oil (3 - 7 μm mean diameter) at 1 to 50 ppm alumina solid particles (3 and 9 μm mean diameter) dispersed in 5% NaCl brine. The injection flow rate was 0.22 to 0.9 cm^3/s. Pressure tappings were arranged at the inlet face and at 5,12.5, 32 and 56.5 mm from inlet face respectively.

At first the damage caused by oil droplets alone was investigated ,then the damage caused by oil droplets and solid particles was examined.

They concluded that:

a) Oil droplets capture occurs only on the porous medium surface when its size is smaller than pore diameter and restricted by pore if its size is larger than the size of pore diameter.

b) The deformation of oil droplets caused by the shear rate in a porous medium when the droplet moves in a pore space or can be caused by a pore throat with a smaller diameter than the droplet. Since oil droplets can deform, they may pass through pore restrictions quite depth in the porous medium.

c) Permeability decline is not linked closely to oil concentration ,but it is linked to oil droplet size. Generally, a dispersion having a relatively high oil concentration but small droplets size reduced the permeability less than the dispersion with large droplets size (Fig.1.55).

d) When solid particles are transported through a porous medium, particles are retained not only by the pores but also by the previously retained particles.

e) On introducing alumina particles into the simulated produced oil water the pressure drop increased compared with the drop in case of oily water only. The permeability declined faster as the particle concentration and size increased (Fig.1.56).

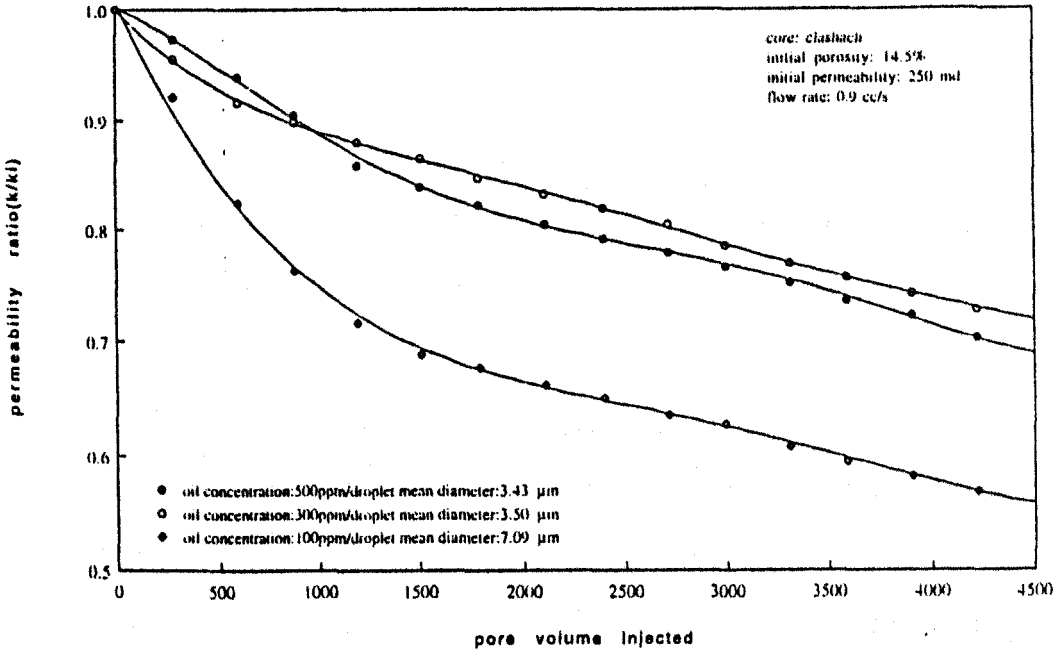

Fig.1.55: Effect of oil concentration and droplet size permeability decline (Zhang 1994).

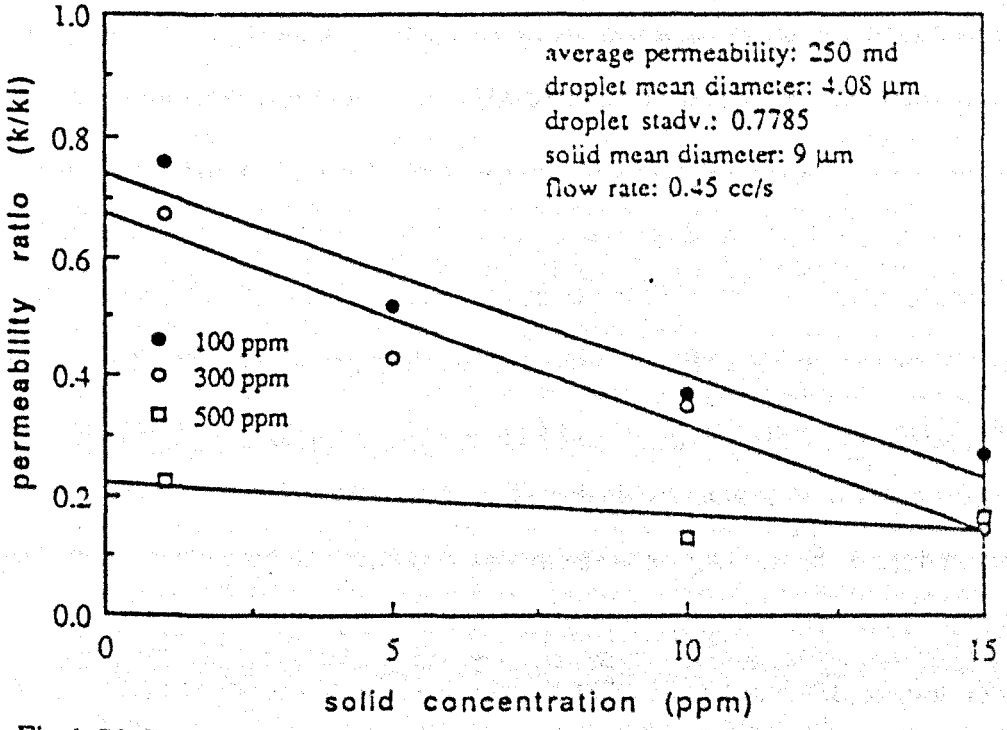

Fig.1.56: Effect of concentration of oil and solid on permeability decline (Zhang 1994).

f) When solid particles plugged or bridged the pore throats, it provided positions for following oil droplets to further plug the pore throat. Therefore, a significant permeability decline will take place. So the increase of oil droplets and particles concentration will increase the chance of meeting at pore restrictions and plug the pore throat. Also the injection of oily water containing very small solid particles will cause obvious permeability damage (Fig.1.57).

g) Large size particles will have larger mass than the smaller size, so the centrifugal inertial force and sedimentation force would tend to remove these large mass particles from the flow stream in a tortuous pore space. The invading distance of these particles moving in the porous medium under high flow rate would be shorter than that of these particles having smaller size and mass.

h) If there is an external cake, there will be a marked difference in pressure over the whole core compared to that over the individual sections. The presence of a internal filter cake produces less difference in pressure differential between internal sections of the core and the whole core.

i) Dispersions of oil and solid particles (particle mean diameter of < 3 μm and particle to pore mean diameter ratio is less than 1/8) may contribute a higher permeability damage than larger sizes of solid particles (at the same oil concentration and similar droplet size). This can be seen clearly in figure 1.58.

HSI et al. (1994) evaluated the effect of the presence of an additional damaging or enhancing factors on the plot of cumulative fluid loss versus square root of time. They stated that in addition to the problem of bacterial growth, bacteria can produce a confluent biofilm. Oil and solid particles present in injected water can cause permeability decline, and also can be trapped by the developing bacterial biofilm to cause more injectivity decline. A side stream of the Prudhoe Bay Field produced water being injected was allowed to flow through reservoir core plugs kept in high temperature -high pressure core holders to study the damage potential of suspended solids, oil droplets and bacterial growth. Two high pressure in-line filters were switched in and out of the flow stream to modify produced water qualities and a high pressure metering pump was used to inject additional biocide solution to ensure a total kill of bacteria. The test was conducted at 165°F and at pore pressure of 2370 psi and under a pressure drop of 20-50 psi.

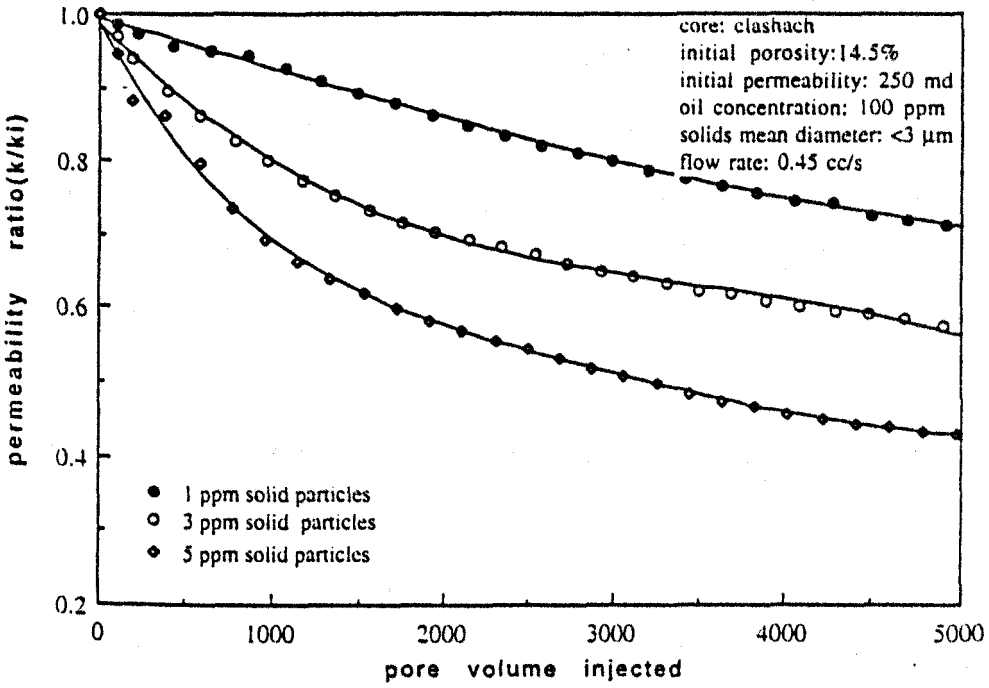

Fig.1.57: Effect of solid concentration on permeability alteration (Zhang 1994).

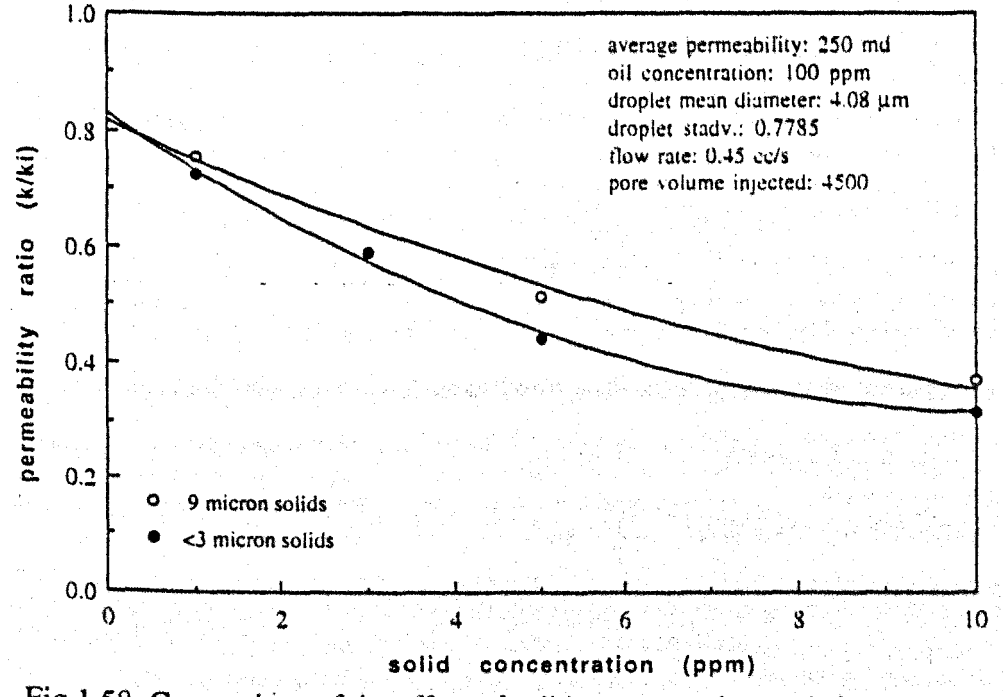

Fig.1.58: Comparison of the effect of solid concentration and size on permeability decline (Zhang 1994).

The test results shows that if core permeability damage is caused by internal and external filter cake buildups without the interference of bacterial growth or filter cake erosion, permeability damage rates should be directly proportional to the amount of fluid passing through the core plug (a plot of the injection throughput versus square root of time should yield a straight line). However, if the permeability damage is caused by additional damage mechanisms (bacterial growth and biofilm buildup in the core), cumulative fluid throughput will become slower with time and the plotted curve will deviate toward the time axis (Fig.1.59). On the other hand, if the filter cake are being eroded, the curve will deviate toward the fluid throughput axis.
They concluded that field injectivity losses in produced water injection, when observed at all, occured over periods of weeks to months, inconsistent with results of the core flood study. Also field observations are consistent with growing thermal fractures that dominate injectivity.

1.6 Micromodels Experiments

Micromodels are a very small scale tests used to closely observe the plugging process in action by using a magnifying video camera. They consists of one or two layers of artificial or natural grain.

DONALDSON et al. (1971) by using a microscopic model observed that displacement and recovery efficiency were good for water-wet systems and poor for the oil-wet systems. The model was composed of two layers of sand sandwiched between two flat microscopic specimen slides (Fig.1.60).

MUECKE (1978) stated that the result of core flooding experiments are difficult to interpret because of the complex relationships between the various factors that control fine movement. So micromodel experimental techniques that would allow direct visual observation of fines movement in the pore spaces while different fluids are flowing was needed. He built a micromodel which consisted of a monolayer of 200 μm (70/80 mesh) Pyrex glass chips centred between two flat Pyrex glass plates. 2 to 15 μm diameter calcium carbonate particles were used because these particles could dissolved easily with HCl after each experiment without damaging the model itself.

The results of this model helped to explain why sand production from weakly consolidated reservoir often follows the onset of water production. Before water production, when only oil is flowing, the connate-water film holds the water-wet fines in place (Fig.1.61). However, when both water and oil are flowing, large amounts of fines are carried toward the wellbore (they flow because the wetting phase become continuous) (Fig.1.62). Eventually, these either are produced to the surface or they bridge at pore restrictions near the wellbore.
He also found that pulsating flow may cause less plugging than continuous flow because pulsating can break some particle bridges.

SOO et al. (1984) in their model, oil-in-water emulsion with drop size ranging from 1 to 50 micron were injected into a micromodel of Ottawa sand sandwiched between two glass plates. The gap between the glass plates is 0.16 cm. With appropriate sand grain-size distributions, water permeability as low as 4 μm^2 (approximately a 50 micron average pore-entry size) can be attained.

After a series of tests, it was found that emulsions of acidic crude oil dispersed in caustic solution provide high visibility under a microscope. Therefore, in the micromodel work the emulsions are made by blending crude oil alone with an NaOH solution. The emulsion was pumped at superficial velocities of between 0.02 to 0.12 mm/s.
They observed that:
a) The behaviour of the emulsion of large 20 micron drop-size was obvious: they simply lodged in the pores. Drops following behind were then diverted to other nearby pores. When the flow rate, and hence the pressure drop, was increased abruptly, drops which were lodged slip through the pores to flow downstream. They do not adhere to the surface of the sand grains. For the smaller drops, a different type of flow behaviour was seen.
b) Though the drops were considerably smaller than the average pore diameter, many were collected in the porous medium. Most of them were retained in the pockets or crevices formed by the sand grains. After several of the small drops capture in a pocket, enough flow restriction occurs so that following drops flow through adjacent larger pores. Some of the smaller drops are also retained on the surface of the sand grains. Usually these drops re-enter the flow immediately after apparent contact, but a few, after sliding along the surface for a while, adhere permanently to the surface. Eventually, the sand grains become almost coated with small drops

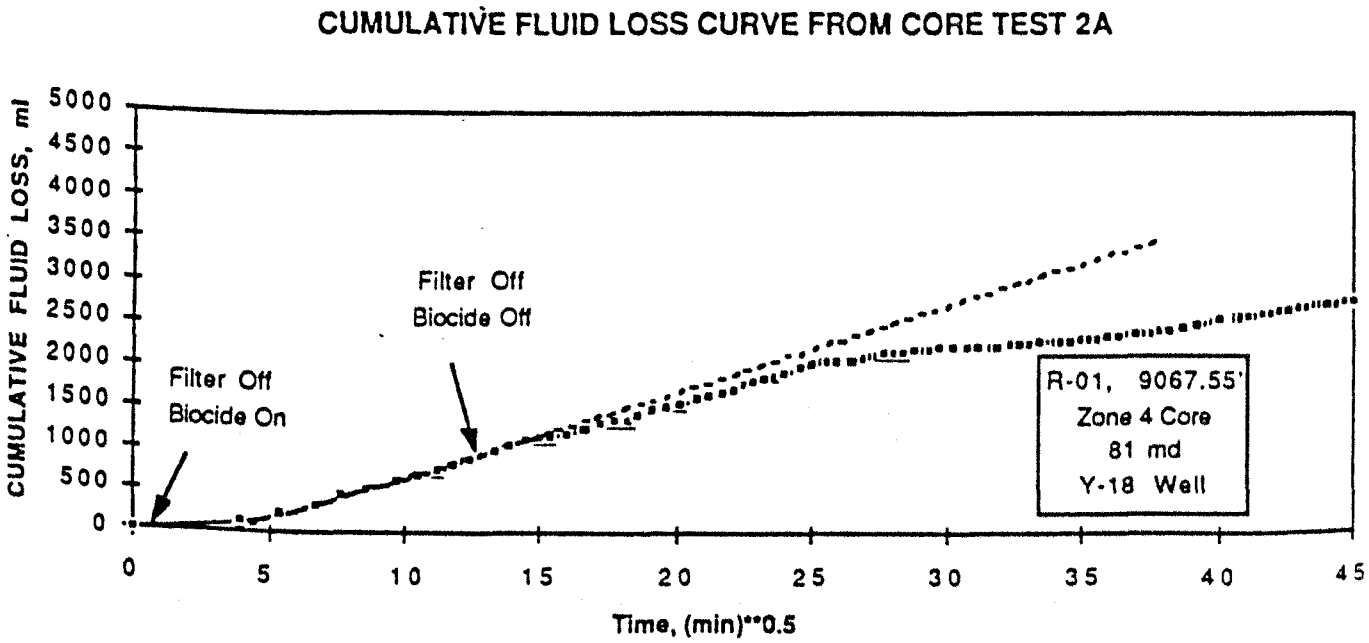

Fig.1.59: Response after termination of biocide injection (Hsi *et al.* 1994).

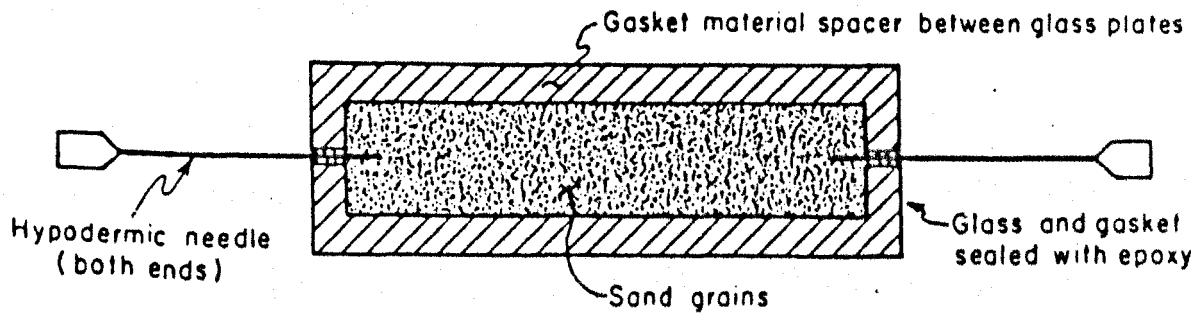

Fig.1.60: Micro model, Complete assembly (Donaldson *et al.* 1971).

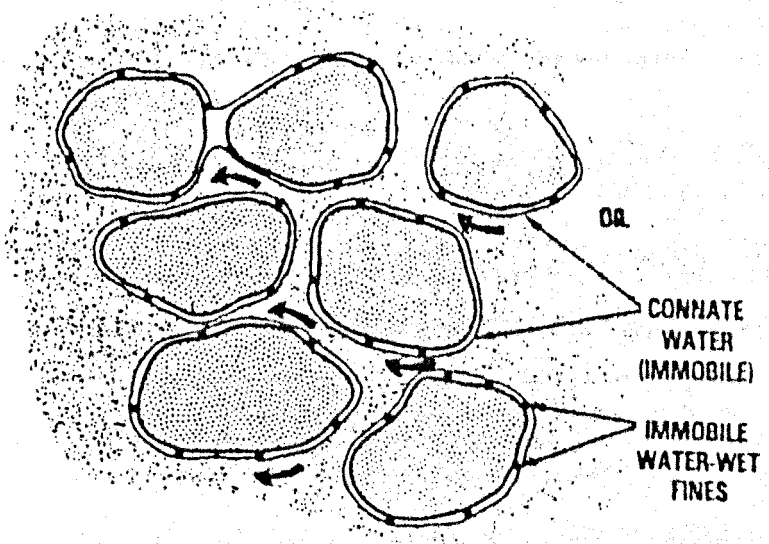

Fig.1.61:Water-wet fines are immobile when the water phase is immobile (Muecke 1978).

with the result that the available volume for flow in the sandpack decreases. A steady state is reached where all capture sites are occupied, and where local flow diverts to contiguous large channels.

They concluded that there are two factors which determine the overall permeability reduction, the volume of drops retained and how effective those drops are in restricting the flow. As the drop size of the emulsion increases, the drop retention increases. However, at identical volume retention, smaller sized drops are more effective in restricting flow.

CHAMOUN et al. (1988) used a glass flow cell which consisted of a microscope slide overlying a flat glass plate, being held together with epoxy and separated by a paper gasket for channelling the fluid flow. The cell dimensions were 1.5" in width and 3" in length with a spacing of 200 μm between the microscope slide and the glass surface. A flow system was designed to pump fluid through the flow cell. Three different sizes of polystyrene particles were used: 10, 20, and 40 μm with a specific density of 1.05 g/cm^3. Also three glass microsphere sizes were used: 10, 15,and 30 μm with a specific density of 2.5 g/cm^3.
After the flow system had been completely flushed, particles of the desired size were injected with a syringe. The particles were allowed to settle for a specified length of time, typically 24 hours. At the end of the deposition time, the initial particle concentration per unit area of the flow cell was measured and then the flow was initiated. At each flow rate, surface concentration of particles were measured by point counting. The flow was increased incrementally until the maximum allowable flow rate of the flow cell was reached (0.6 cm^3/sec, which corresponded to an average velocity of 8 cm/sec).
They defined a critical velocity Vc at which a measurable release of particles is observed, above this critical velocity the release of particles is continuous. Based on this definition Vc is a function of particle size (The larger the particle,the smaller is Vc). This is can be seen in Figure 1.63.

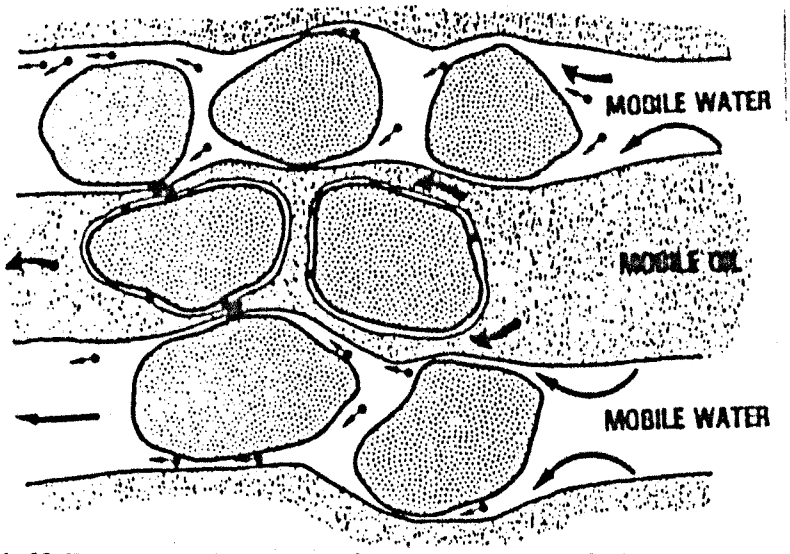

Fig.1.62:Water-wet fines not bridged at pore restrictions are mobile when both water and oil are flowing (Muecke 1978).

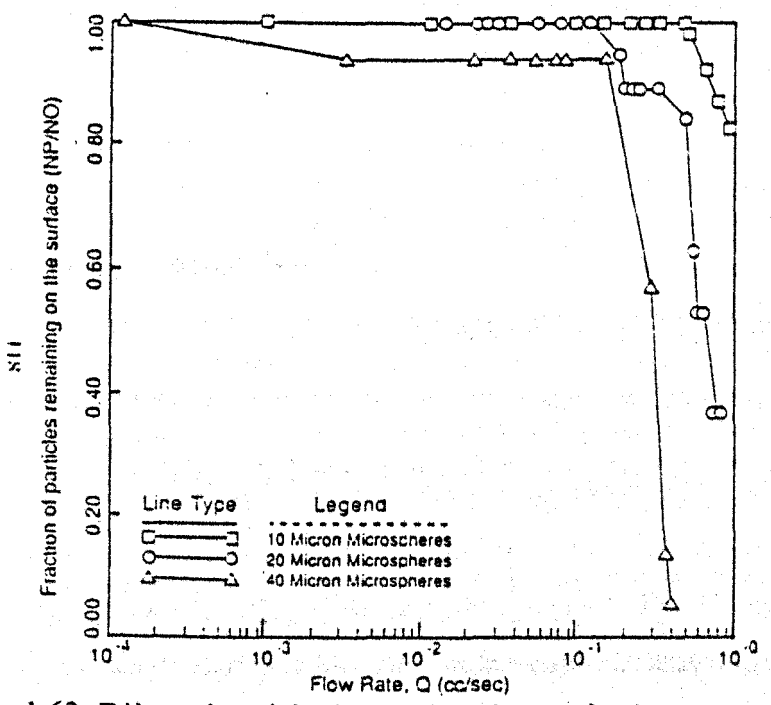

Fig.1.63: Effect of particle size on the release of polystyrene particle from a glass surface (Chamoun *et al.* 1988).

They noticed that the particle composition had an effect on the release velocity (Fig.1.64) and the release velocity is lowered by increasing the solution pH.

ZHANG (1994) designed a micromodel to observe the movement of oil droplets within porous medium and recorded it on a video tape.

He came out with the following observations:

a) Even though the droplets size was smaller than the diameter of pore throats, they did not simply flow through the model. They were retarded by the restrictions of the narrow pore throats and trapped in recirculation eddies, wedged in crevices or some times attached to the pore walls due to hydrodynamic forces.

b) The droplets attached to the pore walls may reduce effective pore diameter and help to restrict other droplets moving through the pore throat; the pore throats were gradually plugged and the flow was diverted to larger pores.

c) When the neighbouring pore throats were bridged gradually, the local pressure drop was increased. Due to oil droplets being deformable, bridges can be broken once the local pressure drop increased enough to overcome capillary restraining forces. These droplets may reform bridges in other pores at a deeper position.

1.7 Matrix Damage Models

In fracture injection fluid flows along a fracture (parallel to the fracture face) at high velocity while filtration takes place through the fracture face. In linear core injection the flow of fluid is perpendicular to the core inlet face with normal injection velocity.

In the case of linear core injection, researchers predicted a severe permeability damage. But in some actual field cases, there was no reduction in injectivity. The reason for that was the presence of induced fractures due to the injection of cold water into hot formation which reduced the fracturing gradient needed for fracturing the formation. It was suggested that due to the huge injection surface area of the fracture the permeability impairment was very low compared to linear core injection as the volume of the injected water is distributed on a very large area.

1.7.1 Factors involved in the flow along a fracture:

The large area of the fracture face is the main factor. The flow velocity through the rock matrix perpendicular to the fracture face will be much lower than the flow velocity through a laboratory core face.

The high flow velocity along the fracture will reduce the viscosity of the suspension (due to shear force)which increases the flow rate of the suspension leak-off into the rock matrix.

The movement of the solid particles and the forces that acts on them inside a fracture is not the same forces acting in the case of linear core injection. In the case of linear core injection all the forces act in the same direction which pushes the particle into the rock matrix. But in the case of injection along a fracture the forces do not act in the same direction. One forces the particle into the fracture face and the other forces it along the fracture. This difference in force distribution will result in different responses from the particles: the particles that may cause only bridging (inefficient sealing), and do not cause plugging, are removed from the fracture surface by the fluid motion.

The high shear rate of the flow in the fracture will erode any cumulative external cake which in turn increases the chance of maintaining high injectivity for longer time.

The aim of this section (section 1.7)was to review the relevant models and their use in explaining permeability impairment.

This goal was reached by studying:

1. Pore blocking in linear core injection.
2. Static drilling mud filtration.
3. Dynamic drilling mud filtration.
4. Fracturing fluid leak-off into the invaded zone in the hydraulic fracturing process.

Most of the damage models depend on one or two of the following principle laws:

1) Darcy's law:

$$U = \frac{K\Delta P}{\mu L}$$

Or

$$U = \frac{\Delta P}{\mu R}$$

Where R is the resistance of the matrix to flow = L/K

And

$$R = R_i + R_d$$

Where R_i is the initial resistance of the matrix.

R_d is the additional resistance due to the external and/or internal plugging.

At the start of the injection $R_d = 0$ and $R = R_i$. Due to the presence of solid particles and oil droplets Rd starts to increase as an indication of matrix plugging.

2) The build-up of the skin layer on any region of the inflow face depends on the cumulative flux of injected water through that region of the face.

$$Rd(t) = C\frac{V(t)}{Ki}$$

Where V(t) is cumulative flux injection per unit area of the flow face at time t (m^3/m^2).

K is matrix permeability (m^2).

C is determined from core flood experiment, and depends on the injected water quality and the formation properties.

1.7.2 The classical theory of static fluid leak-off:

This theory suggested that the leak-off velocity U is inversely proportional to the square root of the leak-off time t (34).

It was assumed that the flow of filtrate though the invaded zone is considered to occur under conditions that the fluid and rock are incompressible and the flow is piston-like darcy displacement with 100% saturation fluid filtrate of constant viscosity into an evacuated porous medium:

$$U_v = \frac{C_v}{\sqrt{t}} = \sqrt{\frac{K_F \phi \Delta P_v}{2\mu_F t}}$$

When the leak-off is mainly controlled by the filter cake:

$$U_w = \frac{C_w}{\sqrt{t}} = \sqrt{\frac{K_w \alpha \Delta P_w}{2\mu_F}}$$

Where: α is cake deposit constant (α volume passed will deposit unit volume of cake)

In the laboratory test when water in the core has been completely replaced and only the fluid filtrate is flowing through the core, the total pressure drop will be the some of ΔPv (pressure drop through invaded zone) plus ΔPw (pressure drop through filter cake) and:

$$U = \frac{C}{\sqrt{t}}$$

where:

$$C = \frac{C_v^2 C_w^2}{C_v^2 + C_w^2}$$

For the case of low concentration of solids and oil there is no filter cake build up and only the first equation will be applied.

$$U_v = \frac{C_v}{\sqrt{t}} = \sqrt{\frac{K_F \phi \Delta P}{2\mu_F t}}$$

1.7.3 Dynamic Filtration and Fracturing fluid leak-off Models

Dynamic filtration is the filtration of fluid passing parallel to a porous surface.

WILLIAMS (1939) in his study used cylindrical porous filters (consist of a siliceous synthetic material) contained in a steel holder. The permeability was determined to be 1.3 darcys. The evaluation of filtration constants for each mud sample run was carried out in simple brass filter, using filter paper as a filter medium.

In this dynamic filtration test, he found that the steady-state filtration rate (dv/dt) varied linearly with the square root of the rate of axial mud flow Q, and with the square root of the m value of the mud as determined by routine evaluation:

$$\frac{dV}{dt} \alpha \sqrt{Qm}$$

$$m = \frac{2P^{1-S}}{\mu v R(1-S)}$$

Where P: pressure drop across cake,atm.

μ: Viscosity of filtrate, cp.

v: ratio of volume of filter cake, cm^3,to volume of filtrate, cm^3.

R: a function of the resistivity of the cake (reciprocal permeability).

S: a compaction function of the cake.

WILLIAMS (1970) in his study of simulating dynamic flow along a fracture, constructed a flow system so that fluid containing additive could be circulated through a channel parallel to a core and he derived the following equation for the case of a zone invaded by fluid filtrate in dynamic filtration:

$$U = 0.00148 \sqrt{\frac{K_F \Delta P \phi}{\mu_F t}}$$

PEDEN (1983) stated that in a dynamic filtration test on a synthetic mixed silicate cores, the absence of material capable of externally bridging the core will result in the fluid loss being controlled by the viscosity of the filtrate (in this case the bentonite suspension). This viscosity will depend upon the amount of shear to which the fluid has been subjected and will obviously give rise to lower viscosities at higher annular velocities. He indicated that dynamic fluid loss Q increases with increasing annular velocity.

The relationship can be approximated by: $$C(V_a)^n = \frac{\Delta P}{\mu R}$$

Where v is the annular velocity

n is an exponent which will in general depend upon the fluid rheology, particle size and distribution, cake compaction and compressibility.

where $R = R_i + R_d$

R_i is the initial matrix resistance.

R_d= the resistance of the internal plugging (in the case of no external cake)

R_d= the resistance of the internal and the external plugging (if the external cake is formed).

PENNY et al. (1985) examined dynamic flow of suspensions of various fluid -loss additives parallel to formation cores surface under a variety of conditions. They stated that dynamic leak-off data can be analysed with a plot of log (volume/area) versus log (time) where the slope n is the exponent of the time and the intercept m is the leak-off rate: $$V = mt^n$$

They concluded that :

n is equal to 0.5 at low flow velocity along a fracture and the dynamic test approaches the static filtration test.

As flow velocity along a fracture increases n start to increase to a maximum value of 1.0.

Depending on the experimental conditions, the measured n can have different values.

POULSEN (1988) derived more generalised relationships for fluid loss and velocity along a hydruic fracture with some assumptions:

1. Fluid loss is linear and perpendicular to the fracture face.
2. The fluid leaking off obeys Darcy's Law.
3. The fluid leaking off is incompressible.
4. The reservoir is infinite perpendicular to the fracture face.

The last assumption implies that the fracture is vertical.

The apparent flow velocity is equal to the total pressure drop divided by the total resistance.

$$v = \frac{\Delta P_T}{R_T} = \frac{\Delta P_T}{R_W + R_v + R_C}$$

Where: R_W is the resistance of the filter cake.

R_v is the resistance of the invaded zone.

R_C is the resistance of the reservoir fluid zone.

By substitution of these three resistivities into the above equation.

$$v = \frac{dV}{dt} = \frac{2}{V}\left(\frac{2\alpha_C \Delta P_T}{1+\sqrt{1+4(\alpha_C / \alpha_{wv})^2 \Delta P_T}}\right)^2$$

where α is the fluid loss cofficient and V is the fluid loss volume per unit area.

Separating variables and integrating gives:

$$V = 2\left[\int_0^t \left(\frac{2\alpha_C \Delta P_T}{1+\sqrt{1+4(\alpha_C / \alpha_{wv})^2 \Delta P_T}}\right)^2 dt\right]^{1/2}$$

Where $$\alpha_{wv}^2 = \frac{\alpha_w^2 \alpha_v^2}{\alpha_w^2 + \alpha_v^2}$$

If no filter cake forms then: $\alpha_{wv} = \alpha_v$.

PENG et al. (1992) derived an equation for water based drilling fluid static and dynamic filtration based on the following assumptions:

1. The weight of eroded solids from the cake is proportional to the duration of circulation, the filter cake area, and the shear stress on the filter cake surface if the mud is circulating.
2. Filter cake build-up is a continual process of deposition and erosion, and these actions occur simultaneously.
3. Flow through the filter cake is laminar, which implies that darcy's law applies.
4. The filter cake is incompressible.
5. The filter cake medium resistance is constant through-out the whole filtration process.

The weight of cumulative deposited equivalent filter cake is given by:

$$W = W_c + W_e$$

where: W_c is the filter cake weight per unit area.

W_e is the eroded equivalent filter cake weight per unit area.

Applying darcy's law:

$$q = \frac{\Delta p}{\mu(R_C + R_M)}$$

Where: R_m is filter medium resistance and R_c is the filter cake rsistance.

$$R_C = \alpha W_C$$

Where: α is tha specific cake resistance (has a relationship with permeability)

By combining the above equations and putting: $q = \frac{1}{A}\frac{dV}{dt}$

Then solving for t vs. V with boundry condition V = 0 when t = 0 and all other terms to be constant with time:

The result is $t = C_1 V - C_2\left(1 - e^{-C_3 V}\right)$

For static filtration (on Shear stress), the above equation is reduced to:

$$t = a_1 V + a_2 V^2$$

By fitting the static filtration equation to the static filtration data, the coefficients a_1 and a_2 can be obtained. Then the average specific cake resistance α and the effective filter medium resistance R_m can be calculated by knowing a_1 and a_2.

By fitting the dynamic filtration equation to the dynamic filtration data, the coefficients C_1, C_2 and C_3 can be obtained. Then α, R_m and K_r can be calculated by knowing C_1, C_2 and C_3.

YI (1992) For static leak-off he modified the flow equation for a power law fluid filtration into a rock matrix. The fluid in the formation is displaced by the filtrate under the assumption of a piston-like displacement. The permeability and the porosity in the invaded zone are denoted as K_d and $\emptyset_d$. In this stage, the fluid loss is controlled by the mobility of the filtrate and the reservoir fluid.

For Newtonian fluids (low concentration of solids and oil): $\Delta P_1 = \left(\frac{\mu}{K_d}\right) L v_l$

Where L is the core length and v_l is the leak-off velocity.

In the invaded zone an internal plugging will take place and then at time t_o an external filter cake begins to form at the surface of the fracture, in this case:

$$\Delta P_2 = \alpha_C v_l V_l$$

Where $$\alpha_c = \frac{C_S}{1 - C_S}\frac{1}{1 - \phi_C}\frac{1}{K_C}$$

Where V_l is the leak-off volume per unit area.

C_s is the volumetric concentration of plugging agents

$\emptyset_c$ is the porosity reduction in the damaged zone due to internal cake or the external filter cake porosity

K_c is the permeability of the damaged zone or the permeability of the external cake.

For the case of a dynamic test, α_c (filter cake factor) should be corrected to $\alpha_o{}'$:

Where $$\alpha_c{}' = \alpha_c \left(\frac{t}{t_o}\right)^{\beta_{c1}} \quad \text{if } t \leq t_o$$

and $$\alpha_c{}' = \alpha_c \left(\frac{t}{t_o}\right)^{\beta_{c2}} \quad \text{if } t > t_o$$

The constants can be determined from the leak-off test data.

The total pressure drop $\Delta P = \Delta P_1 + \Delta P_2$

And $\Delta P_2 = \Delta P - \Delta P_1$

Then $$\alpha_c{}' = FPF = \frac{\Delta P - \Delta P_1}{\upsilon_l{}^n V_l}$$

FPF is known as the filter cake parameter function which is function of pressure drop, leak-off volume, leak-off velocity and flow behaviour index.

The leak-off velocity υ_l can be obtained by differentiating the leak-off volume with respect to time. FPF can be calculated from the test data. On the other hand, from the above equation it is obvious that if FPF is plotted against time t under the logarithmic scale a double-straight line curve should be obtained. The slope of the first line equal to β_{c1}; the slope of the second line is β_{c2}; the intersection of the two lines is at t_o; and the y value at t_o is α_c.

The first line represents the formation of the internal filter cake, while the second line represents the build up of the external filter cake. The effect of the internal filter cake makes β_{c1} positive while the effect of shear velocity and diffusion of external cake make β_{c2} negative.

CHARLES et al. (1995) used the method of dimensional analysis to obtain relevant dimensionless groups of variables. They then used these groups to correlate dynamic fluid loss with the properties of the porous medium and other process variables.

They assumed a dimensional homogeneity exists between the following variables:

From the initial defining equation: $$\frac{V_l}{A} = \mu^a (\Delta P)^b K^c t^d \gamma^e$$

a final result equation is obtained: $$\frac{V_l}{AK^{1/2}} = const. \left(\frac{\mu\gamma}{\Delta P}\right)^a (t\gamma)^b$$

Because the number of dimensionless groups are always fewer than the number of variables, dimensional analysis always requires considerably fewer experiments to establish a correlation between dimensionless groups than between individual variables.

The literature cites many more variables which are said to influence fluid leakoff during hydraulic fracturing, but dimensional analysis can accept only those variables that can be assigned a quantifiable dimension.

1.7.4 Pore Filling and Blocking Models

GRUESBECK et al. (1982) at any cross section in a column they visualized any fluid pathway as having two continuing, parallel branches: one of small pore size in which plug-type deposits of fines may occur, and the other, of larger pore size, in which only surface nonplugging deposits occur. It is from such surface deposits that fines can be re-entrained by moving fluid and may redeposited as plug-type deposits to cause a net permeability reduction.

Surface Deposition and Entrainment: is the mean mechanisim for packed column dominated by nonplugging pathways.

a) Surface Deposition: For a suspension of very small fine particles flowing through a porous medium having large pores, one would not expect plugging deposits to occur.

For this case at each change in flow rate, effluent particle volume concentration (C_e) fluctuated briefly, but this was followed by a steady value indicating steady-state conditions within the sand column. This provided a direct means of determining the local law of deposition from a material balance on fines:

$$\frac{\partial}{\partial t}(\phi C + \phi_i \sigma) + u\frac{\partial C}{\partial x} = 0$$

Where: Ø is remaining porosity after deposition.

u is volume flux density (q/A).

σ is the volume of fines deposited per unit original pore volume.

Assuming that Ø and C are essentially constant with time (as ØC is the volume of fines in suspension), then, if it was assumed that the local rate of fines deposition, $\partial\sigma / \partial t$, is simply proportional to fines concentration, C, the above equation integrates to yield (for a column of length L):

$$\beta = \frac{u}{\phi_i L}\ln\frac{C_e}{C_i}$$

Where ß is the surface deposition constant. This constant can be calculated from the experimental data.

These calculations yield the same value 0.01 1/sec for each flow rate. Thus, ß is independent of flow rate, and a local law of: $\frac{\partial \sigma}{\partial t} = \beta C$ was established for surface-type deposition.

b) Entrainment: flowing a clean fluid through a dirty column.

For this case an essentially steady effluent concentration is established after an initial burst of fines effluent following each flow rate change. There is a critical flow velocity (u_c) for the fines to be produced. At a velocity lower than u_c no fines are produced from the column.

Again the material balance on fines for steady-state conditions was used. Integrating over the length of the column with C=0 at core inlet and C=C_e at core outlet, then:

$$\frac{\partial \sigma}{\partial t} = \begin{cases} \alpha\sigma(u - u_c) & u > u_c \\ 0 & u < u_c \end{cases}$$

With α a constant and u_c a critical volume flux density.

Plugging Deposition and Entrainment: Both plugging and surface deposition processes occur. As fines build plug-type deposits within some of the narrower pore openings, fluid flow is diverted to the remaining open fluid pathways. In this theory pore space is divided into plugging and nonplugging pathways. A fraction f of element made of plugging pathways and a fraction 1-f of nonpluggable pathways. The pore size distribution of the porous medium and the particle size distribution of fines determines the value of f.

Then, the total flux density: $u = fu_p + (1-f)u_{np}$

Where u_p and u_{np} are the flux density of fluid flowing through the pluggable and nonpluggable pathways respectively.

Also, the volume of deposits per unit bulk volume of porous medium:

$$\phi_i \sigma = \phi_i \left[f\sigma_p + (1-f)\sigma_{np} \right]$$

Where σ_p and σ_{np} are volume fraction of fines of the respective pore volumes, $f\phi_i$ and $(1-f)\phi_i$, filled by plugging and nonplugging deposits.

Then he constructed two local laws of entrainment and deposition to specify $\partial\sigma / \partial t$:

a) In the nonpluggable pathways: it is reasonable to assume entrainment and deposition as deduced from experiments with synthetic systems:

$$\frac{\partial \sigma_{np}}{\partial t} = -\alpha(u_{np} - u_c)\sigma_{np} + \beta C$$

Where the first term is set to zero for $u_{np} < u_c$. For a system of pure surface deposition type, f is set zero and quantities labelled np become total quantities.

b) In the pluggable pathways: a snow-ball effect is expected. As plug deposits increase, the rate of deposition should increase. Thus a law of the following form was postulated with Ω and ρ are constants:

$$\frac{\partial \sigma_p}{\partial t} = (\Omega + \rho \sigma_p) u_p C$$

To complete this theory, Darcy's law was used to describe the flow diversion phenomena in term of the permeability, $K_p(\sigma_p)$ and $K_{np}(\sigma_{np})$, in the parallel pluggable and nonpluggable parts of the porous medium.

Thus, the fraction of flow through pluggable pathways is:

$$\frac{u_p}{u} = \frac{K_p(\sigma_p)}{K_p(\sigma_p) + K_{np}(\sigma_{np})}$$

There is really no direct method of determining how permeability changes as deposits grow, but a reasonable guesses for the general form can be written as: $K_p \approx K_{pi} e^{-a\sigma_p^4}$

and $$K_{np} \approx \frac{K_{npi}}{1 + \in \sigma_{np}}$$

with a, K_{pi}, K_{npi}, and $\in$ are phenomenological constants to be specified.

SOO et al. (1984) evaluated the filter coefficient and the flow diversion parameter, which both control the processes of drop capture in the medium, from the emulsion concentration histories. Conversely, the flow restriction parameter, which characterizes how effective retained drops are in obstructing flow, was obtained from permeability data.

The transient drop-volume retention and drop-volume concentration profiles $\sigma(t,x)$ and $c(t,x)$ obey the following expression in a linear medium of length L:

$$\frac{\sigma(T,\tilde{x})}{\varepsilon_o} = \frac{1 - \exp(\alpha \wedge_{SI} c_i T)}{\alpha[1 - \exp(\wedge_{SI} \tilde{x}) - \exp(\alpha \wedge_{SI} c_i T]}$$

$$\frac{c(T,\tilde{x})}{c_i} = \frac{\sigma(T,\tilde{x})}{\sigma_i(T)}$$

Where : $\tilde{x} = x / L$ is a reduced axial distance.

$T = \tau - \tilde{x}$ is a shifted time variable with $\tau = ut / \varepsilon_o L$.

$\wedge_{SI} = \lambda_{SI} L$ is the reduced filter coefficient, made dimensionless by the length L.

The subscript i refers to the bed inlet and ε_o is the clean bed porosity, while α is the flow redistribution parameter. SI refer to straining and interception.

The transient permeability reduction depends on the local retention as:

$$\frac{K_o}{K(\tau)} = \int_o^1 [1 - \beta\sigma / \varepsilon_o]^{-1} d\tilde{x}$$

Where ß is the flow restriction parameter.

From the first and the second equation, the filtration parameters $\wedge_{sl}$ and α are seen to control droplet chromatography. Therefore, they best evaluated from experimental effluent concentration histories. In contrast, ß influences flow resistance. Therefore, it is best to be evaluated from experimental pressure-drop data.

A distinguishing feature of the filtration model is that graphs of c_L / c_i and K/Ko vs. the variable $c_i(\tau - 1)$ should be independent of inlet concentration. Results for injecting a 4 μm mean drop-size emulsion of c_i=0.006, 0.012 and 0.025 volume concentration into a 2 μm^2 permeability sandpack. Both c_L / c_i and K/Ko obey the filtration theory for the two most dilute suspensions (Fig.1.65 and 1.66). The c_i=0.025 emulsion deviates toward higher retention and larger permeability reduction, due to the nonlinear dependence of drop capture kinetics on concentration as the c_i become higher than 0.012. As Herzig (1970) stated that c_i=0.001 is the upper limit of linear capture kinetics for solid particulates, the present study proves the linearity for liquid droplets up until about c_i=0.012.

WOJTANOWICZ et al. (1987) presented a theory which provided a practical tool for identification of the prevailing mechanism of permeability impairment in linear core flow systems (laboratory flow tests) as shown in Figures 1.67 and 1.68. The general assumptions are as follows:

Constant rate filtration; linear geometry of flow; low solids concentration, so volume reduction due to particles capture can be ignored; homogeneous formation, cake incompressibility; laminar flow and regular pore geometry.

The three basic mechanisms of pore blocking are:

Gradual pore blocking: continuous capture of fines at the rock walls due to retention force (Fig.1.69). The permeability response to this type of blocking is:

$$\sqrt{K} = \sqrt{K_i} - \frac{f_c T_s}{L\rho} t$$

$$\sqrt{K} = \sqrt{K_i} - C_1 t$$

Where: $$f_c = (CFR)\frac{Q\rho}{(pv)T_s}$$

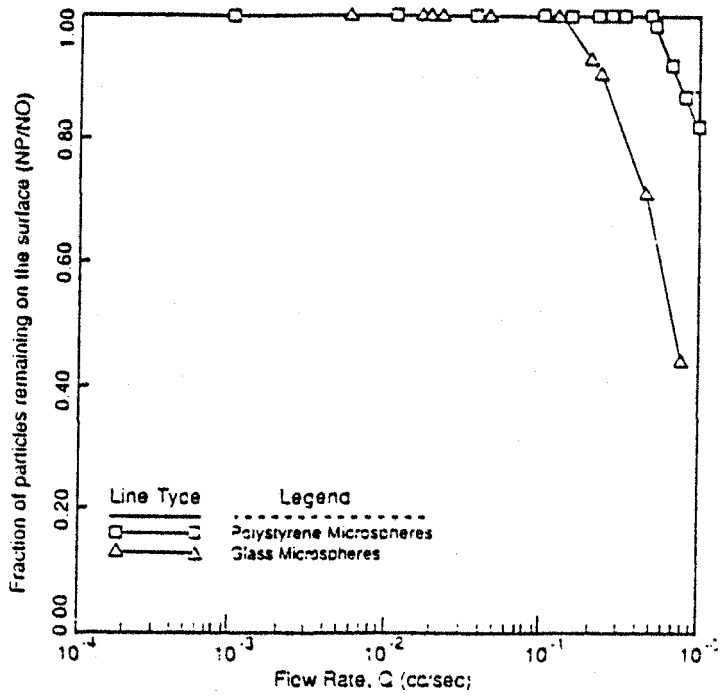

Fig.1.64: Effect of particle composition on release phenomena (Chamoun *et al.* 1988).

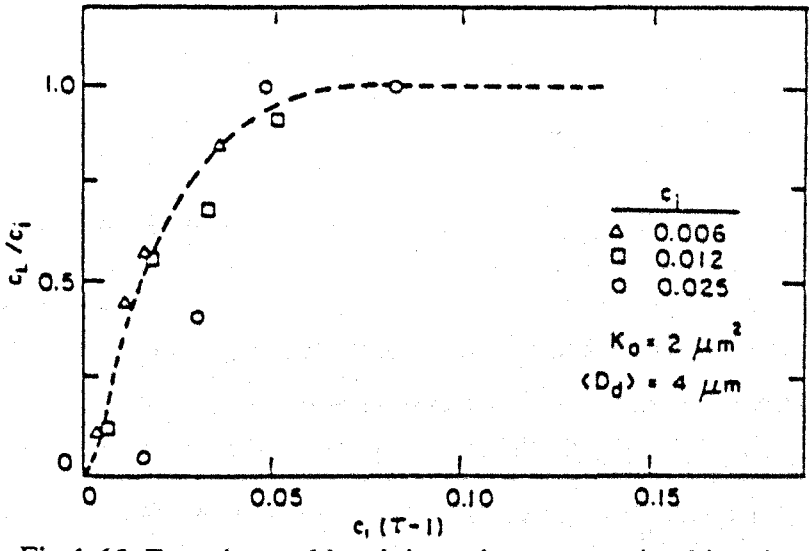

Fig.1.65: Experimental breakthrough concentration histories for varying injection concentrations (Soo *et al.* 1984).

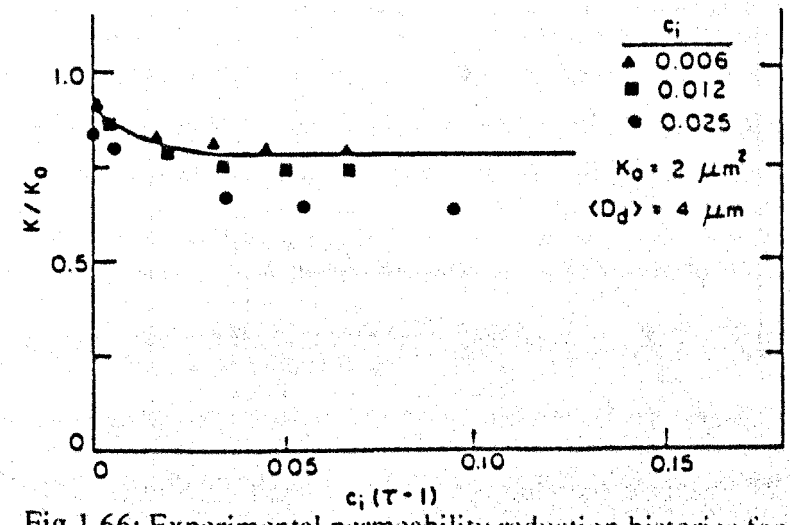

Fig.1.66: Experimental permeability reduction histories for varying injection concentrations (Soo *et al.* 1984).

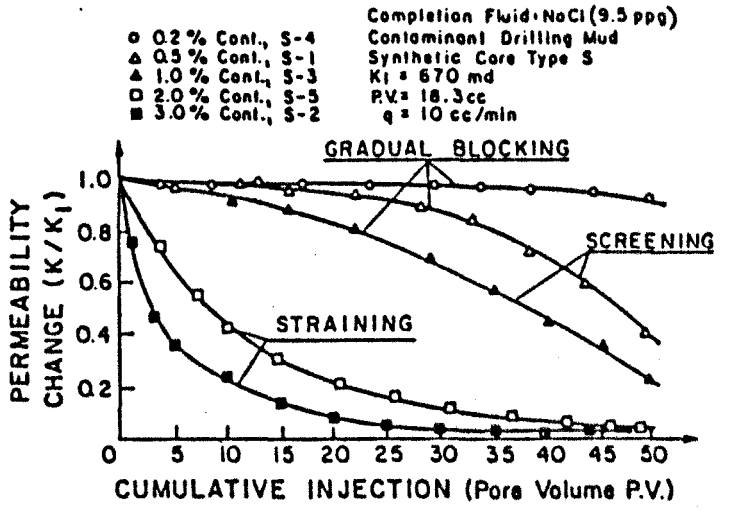

Fig.1.67: Manifestation of three particle capture mechanisms (Wojtanowicz *et al.* 1987)

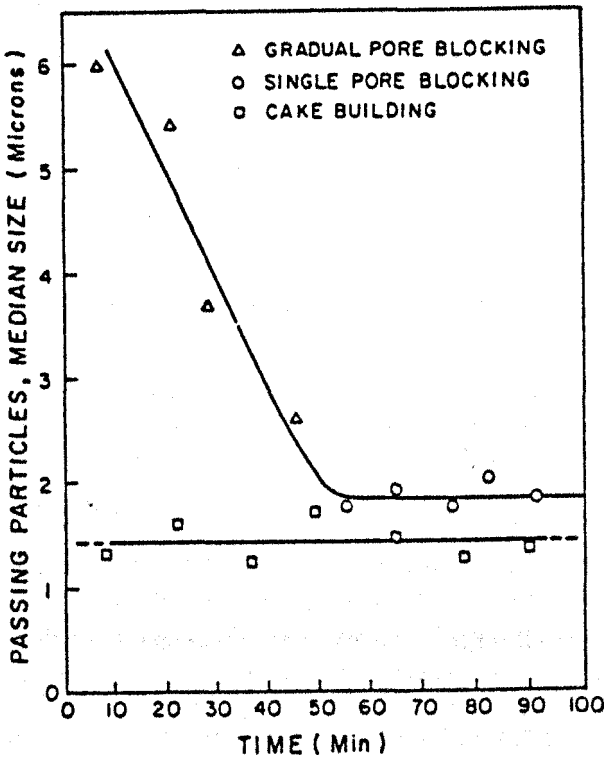

Fig.1.68: Relation of pore blocking mechanism and passing particle size (Wojtanowicz *et al.*1987)

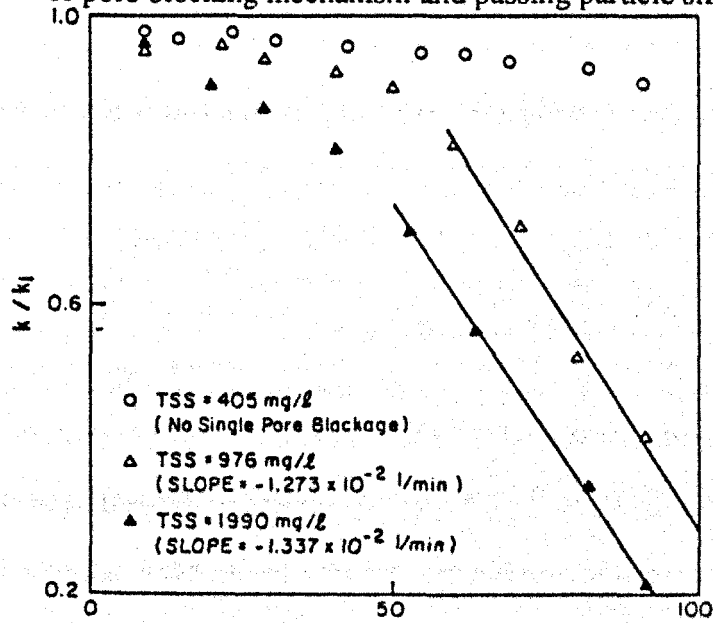

Fig.1.69: Diagnostic plot: particles invasion, gradual pore blockage (Wojtanowicz *et al.* 1987).

CFR: cake to filter ratio.

pv : pore volume, cm^3.

Ts : solids concentration in flow stream, g/cm^3.

L : average length of flow path, cm.

Q : flow rate, cm^3/min.

The last equation defines a straight line diagnostic plot of $\sqrt{K/Ki}$ versus t.

Single pore blocking (screening): occured when single particles of size close to the pore size (critical size) instantly blocked an individual pore, thus eliminating it from the flow system (Fig.1.70). The permeability response to this type of blocking is:

$$K = K_i - \frac{6QT_s f_d A^2}{\pi C^2 d^3 \rho} t$$

$$K = K_i - C_2 t$$

$$C = \sqrt{32\left(\frac{A}{D^2}\right)A_r T}$$

Where: f_d: is the concentration of particles of critical size d.

A : area of single pore, sq cm.

D : pore size, cm.

A_r: rock area, cm^2.

T : tortuosity.

Cake forming (straining):is associated with building up a filtration cake at or close to the formation face (Fig.1.71). The permeability response to this type of blocking is:

$$\frac{K_i}{K} = 1 + C_3 t$$

EYLANDER (1988) stated that a linear plot of reciprocal rate versus filtration volume implies that the discharge or fluid leak-off from the core plug is a parabolic function of time. To assess which factors have an impact on the parabolic behavior, he assumed that the injection is Newtonian and incompressible. Also the average cake porosity, $Ø_c$, is constant.

External Filter-cake Formation:

The total pressure drop can be equated to the sum of the pressure drop through the cake and the pressure drop through the filter medium:

$$\Delta p = \Delta p_c + \Delta p_m = \frac{\mu}{A}\left(\frac{e}{k_c} + \frac{L_m}{k_m}\right)\frac{dV}{dt}$$

Where e: is the cake thickness

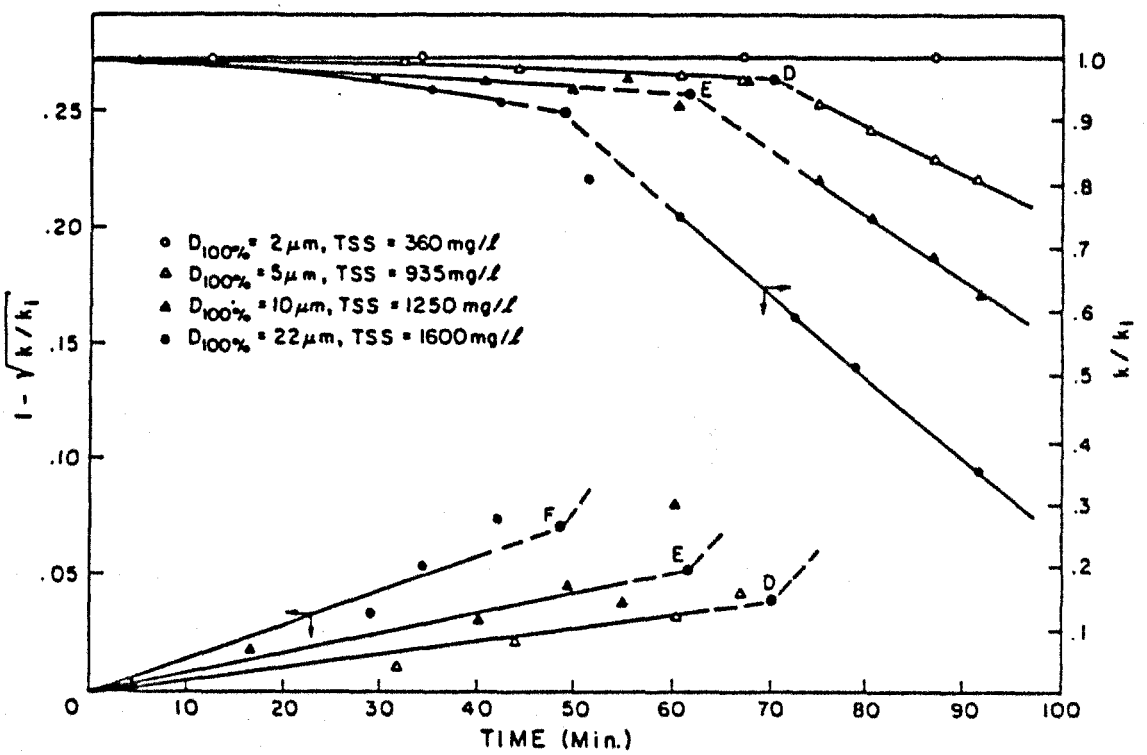

Fig.1.70: effect of solids size on permeability damage: transition from gradual pore blockage to single pore blockage (Wojtanowicz *et al.* 1987).

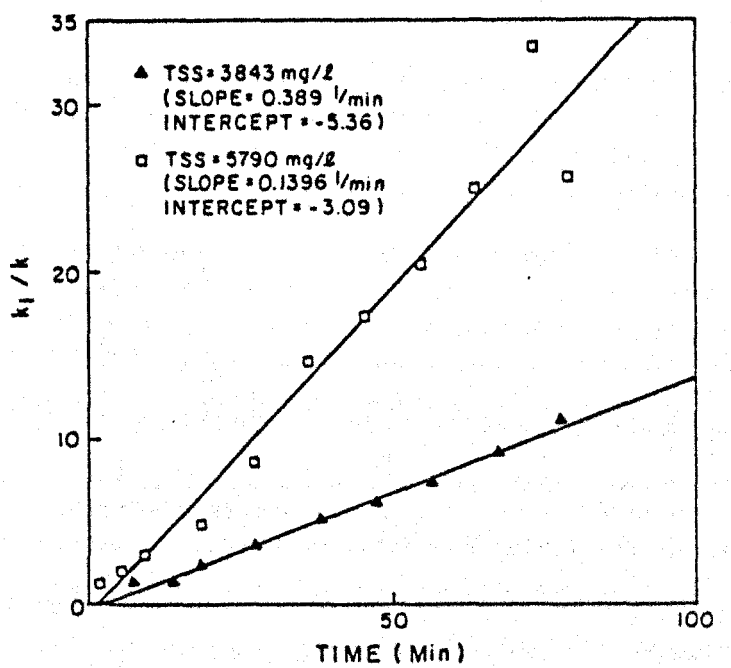

Fig.1.71: Diagnostic plot: foreign particales invasion, cake forming (Wojtanowicz *et al.* 1987).

The variable e and V are connected and the relation between them can be obtained by making a material balance between the solids in the injection water and in the cake:

$$Ae(1-W)(1-\phi_c)\rho_s = VW\rho_l + AeW\phi_c\rho_l$$

For injection water in general, W <<1

By subsituting: $$\frac{dt}{dV}\Delta p = mV + b$$

$$m = \frac{\mu\rho_l W}{A^2\rho_s(1-\phi_c)k_c}$$

Where:

$$b = \frac{\mu}{A}\frac{L_m}{k_m}$$

A plot of (dt/dV)Δp vs.V results in a straight line with intercept b and slope m. The filter cake permeability and porosity can be calculated from the slope m by knowing the specific surface area of the suspended solid from Coulter-Counter data.

Internal Filter-cake Formation:

For such dilute suspensions as injection water, we may assume that the volumes of injected water and filtrate in coreflood tests are the same.

The total pressure drop can be equated to the sum of the pressure drop through the porous medium affected by particle deposition and the pressure drop through porous medium not affected by particle deposition :

$$\Delta p = \frac{\mu}{A}\left(\frac{e}{k_d} + \frac{L_m - e}{k_m}\right)\frac{dV}{dt}$$

Assume W<< 1

$$e \cong \frac{V\rho_l W}{A\rho_s(1-\phi_c)\phi_m}$$

Where $\emptyset_c$ is for the internal cake.

By subsituting, then: $$\frac{dt}{dV}\Delta p = mV + b$$

$$m = \frac{\mu\rho_l W}{A^2\rho_s(1-\phi_c)\phi_m}\left(\frac{1}{\phi_m k_c} - \frac{1}{k_m}\right)$$

Where:

$$b = \frac{\mu}{A}\frac{L_m}{k_m}$$

The internal cake permeability and porosity can be derived from the slope m.

KUMAR (1988) developed a relationship between solid particles concentration C_s and instantaneous rock porosity $\emptyset_s$ which is based on the fact that during the invasion of suspension through a porous media at a constant flow rate, a part of solids from the suspension is retained in the matrix reducing its porosity.

$$\phi_S = \phi_i - \frac{(C_{Si} - C_S)\phi_i}{\rho_S - C_S}$$

Where: $\emptyset_i$ is the initial porosity.

C_{si} is the initial concentration.

ρ_S is the density of the solid particles.

Similarly, a relation between oil droplet concentration C_o and instantaneous rock porosity $\emptyset_o$ can be written as:

$$\phi_o = \phi_i - \frac{(C_{oi} - Ci)\phi_i}{\rho_o - C_o}$$

In these two relationships the size of the particles and the droplets was not considered.

The instantaneous rock porosity for the invasion of solid particles and oil droplets will be:

$$\phi = \phi_i - \frac{(C_{Si} - C_S)\phi_i}{\rho_s - C_s} - \frac{(C_{oi} - C_o)\phi_i}{\rho_S - C_o}$$

CIVAN et al. (1989) presented a relationship between the initial permeability and the damaged permeability as a function of altered porosity $\emptyset$ (due to solid particles and oil droplets invasion) and initial porosity $\emptyset i$:

$$K_d = K_i\left(\frac{\phi}{\phi_i}\right)^3$$

The above two models assumed that the reduction in matrix permeability due to only pore filling and there is no plugging or bridging of pore throat.

VAN VELZEN et al. (1992) developed a new model to describe wellbore impairment by internal cake formation during water injection.

$$\left(\frac{1}{\alpha} - 1\right)L = \frac{\delta_F C_O}{A\phi_m}\left[1 - \exp\left(-\frac{\lambda_v AL}{q_o}\right)\right]V$$

Where: α is fractional injectivity index.

δ_F is the damage factor.

C_o is volume fraction of solids in suspension at injection surface.

A is core cross-section area, m^2.

$\emptyset_m$ is fractional porosity of porous medium.

λ_v is volume filter coefficient, 1/s.

L is depth of porous medium, m.

q is initial rate of injection, m^3/s.

V is cumulative injected volume,m^3.

The damage factor, volume fraction of solids in suspension at injection surface, injection surface area, fractional porosity of porous medium, volume filter coefficient and initial rate of injection are constants. The depth of porous medium and cumulative injected volume are independent variables and $(1/\alpha - 1)L$ is the dependent variable.

$$\alpha = \frac{[q/(-\Delta P)]_{t=t}}{[q/(-\Delta P)]_{t=0}}$$

$$\delta_F = \left(\frac{K_i}{K_d} - 1\right)\frac{1}{(1-\phi_c)}$$

Where K_i is permeability of porous medium, m^2.

K_d is permeability of zone affected by particle deposition, m^2.

$\emptyset_c$ is fractional cake porosity.

The new model requires values for the damage factor and the volume filter coefficient as input parameters. Linear core flow experiments can be used to measure these parameters.

The damage factor can be determined as followes :

When $(1/\alpha - 1)L$, for the case of the maximum value of the depth of porous medium Lm, is plotted against cumulative injected volume, a straight line will be observed. This means that a linear relation exists between these two terms until particles begin to leave the core plug (Fig.1.72).

From the slope of the line, the damage factor can be calculated for a specified volume fraction of solids in suspension at the injection surface, cross-sectional area of the porous medium and fractional porosity of the porous medium.

The change in the slope after a critical value of the cumulative injected volume can be explained by a change in damage factor (the increase of slope is due to the formation of a second-phase internal filter cake).

The volume filter coefficient can be determined as followes:

When $(1/\alpha - 1)L$, for a given injected volume, is plotted as a function of the depth of the porous medium. This plot shows curved lines (one line for each constant injected volume) that, at increasing depth, $(1/\alpha - 1)L$ approaches a constant value which is $(1/\alpha - 1)L\max$ (Fig.1.73).

The value of the depth L ,where $\left(\frac{1}{\alpha} - 1\right)L = \frac{1}{2}\frac{\delta_F C_O}{A\phi_m}V$, is the so-called half invasion depth $\left(L_{1/2}\right)$. Substitution of the right-hand side of this equation in the main equation of the model results in an expression from which the volume filter coefficient can be calculated:

$$\lambda_v = \frac{q_O Ln(2)}{AL_{1/2}}$$

PANG et al. (1994) postulated that during some initial period an internal filter cake is formed. As more particles are trapped on the surface of the rock a point is reached where very few particles can invade the rock and an external filter cake begins to build. They refered to the time at which no more particles invade the rock, i.e., the time at which the initial layer of external filter cake is completely formed, as the transition time (t*). If the conditions under which particles will form internal and external filter cakes can be determined and the time required to form the initial layer of external filter cake (transition time), then the entire filtration process can be approximated by applying an internal cake filtration model before the transition time and an external cake filtration model after the transition time. Purely external filtration can be obtained in the limit $t^* \rightarrow 0$, and pure internal filtration can be obtained in the limit $t^* \rightarrow \infty$.

The transition time can be obtained as followes:

The trapping efficiency (TE) is defined as the fraction of suspended particles trapped by the porous medium. This is a local property and will increase with time. The number of trapped particles (n*) at which the TE is equal to 1 can be obtained. This n* corresponds to the transition time at which pure external cake build-up begins (very few particles go through into the porous medium thereafter).

The number of particles trapped at the surface of the core (dN) in the time interval dt (Fig.1.74) is given by: $dN = C_n V A TE(n) dt$

Where n is the average number of particles attached to each collector, C_n is the number concentration of suspended particles.

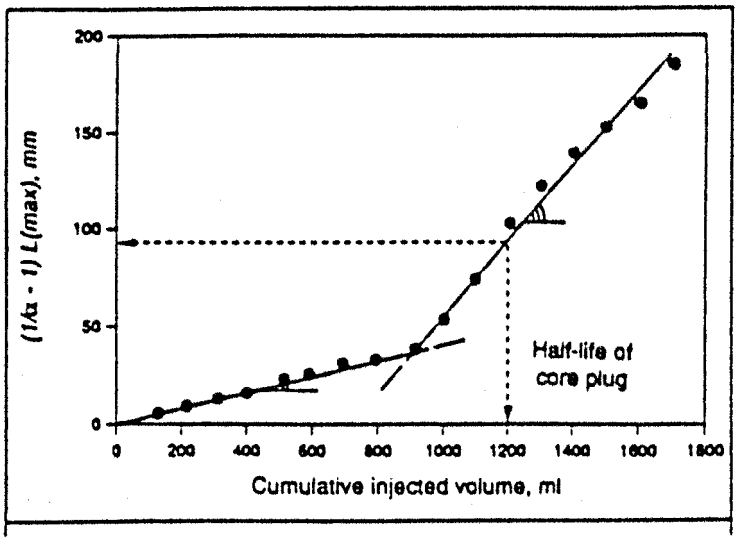

Fig.1.72: Determination of damage factor (Van Velzen *et al.* 1992).

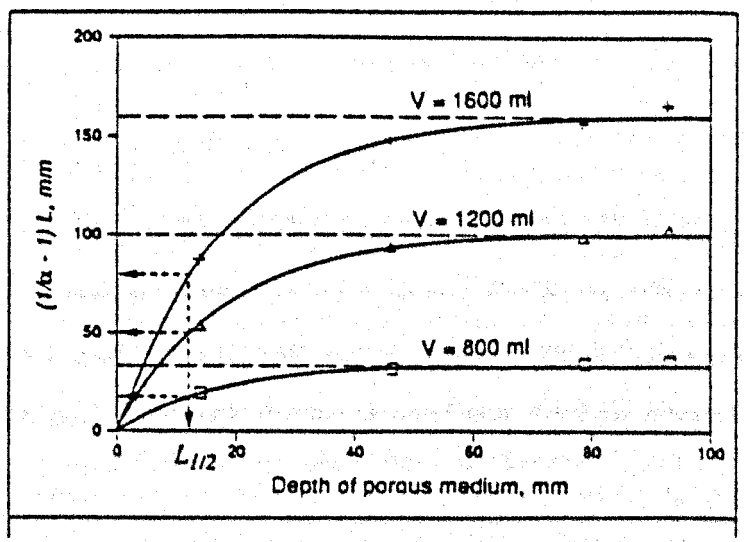

Fig.73: Determination of volume filter coefficient (Van Velzen *et al.* 1992).

If a is the cross section area of the collector:

Then dN=(A/a)dn

And the above equation becomes:

dn/dt =Cn V a TE(n), thus:

$$t^* = \frac{1}{C_n V a} F(n^*)$$

$$F(n^*) = \int_0^{n^*} \frac{dn}{TE(n)}$$

If t* is normalised with respect to the pore volumes injected:

$$t_D^* = \frac{AVt^*}{PV}$$

$$t_D^* = F(n^*)/\beta$$

$$\beta = C_n a PV / A$$

Where PV is the pore volume of the core = ALØ.

t^*_D is the dimensionless time (pore volume injected).

$$a = (2d_g)^2$$

$$C(ppm) = C_n \frac{1}{6} \pi d_P^3 10^{-6} \gamma$$

Where d_p is mean particle diameter.

d_g is mean grain diameter of the rock.

γ is the specific gravity of the particle.

By substitution :

$$\beta = 24 \phi C L d_g^2 / (\pi d_P^3)$$

Where C is in ppm, L in m, and dg and dp are in μm.

To obtain t*, the variation of the trapping efficiency (TE) as a function of the number of trapped particles n (Fig.1.75 and 1.76) must be calculated. This can be done using the Stokesian Dynamics computer code (Details of the simulation are provided by Vitthal and Sharma,1992). Based on the grain size of the rock and the injected particles size, a transition time (t*) is calculated.

An internal filtration model can be used to calculate the injectivity decline for $t < t^*$ and an external filtration model can be used for $t < t^*$. Then K_c and $Ø_c$ can be obtained by matching with the experiment data of the second section of the injectivity curve (external cake). ß and λ

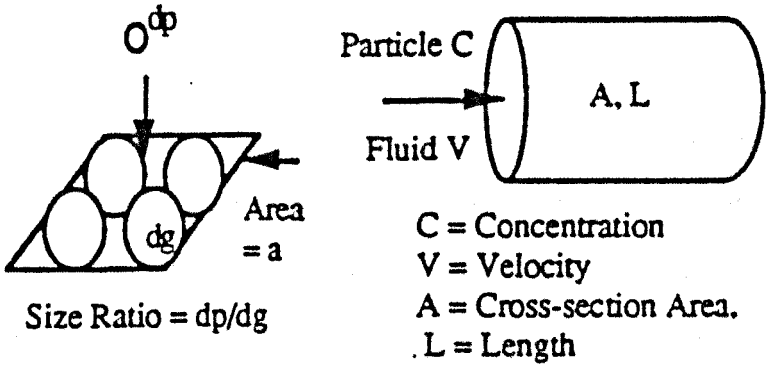

Fig.1.74: Schematic of collector and core (Peng *et al.* 1994).

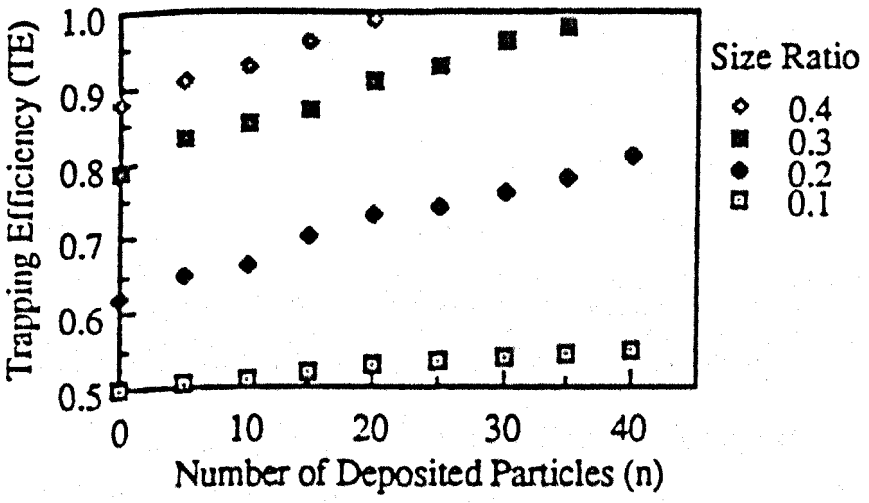

Fig.1.75: Trapping efficiency (Peng *et al.* 1994).

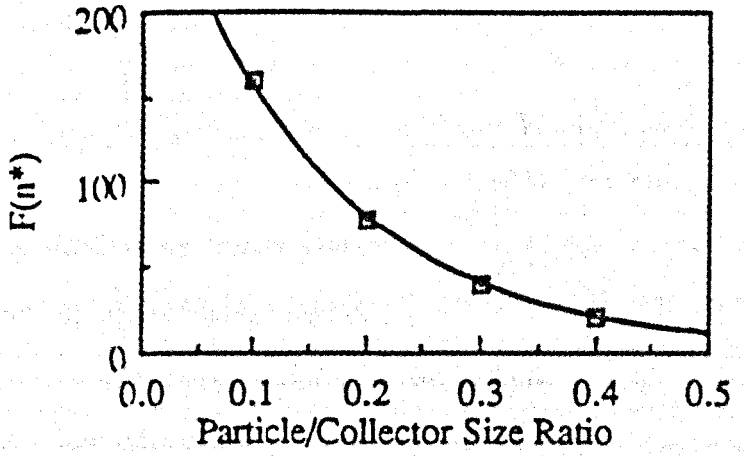

Fig.1.76: F(n*) versus size ratio (Peng *et al.* 1994).

can be obtained by matching with the experimental data of the first section of the injectivity curve (internal cake).

ZHANG (1994) developed an empirical model (using the same technique used by Eylander (1988)) for severe permeability impairment zone of a core plug, for external filter cake formation, and for the case of internal and external filter cake formation. His model depends on material balance. Since the concentration of oil droplets and solid particles in this study is low, which does not affect the rheological properties of the simulated produced oily water, it is assumed that the injection water is a Newtonian fluid and incompressible. The suspended solids are insoluble and exhibit no response to shear stress under the condition of laminar flow.

Due to different performance of solid particles and oil droplets in injected water stream, the treatment of solid particles and oil droplets is done separately. Based on the investigations, a concept of equivalent particle concentration is introduced in this study.

The equivalent concentration factor to oil droplet is set up, by which a certain concentration of oil may contribute the same permeability impairment as solid particles do at similar conditions in the experiments conducted. In this case, the permeability reduction contributed by oil droplets and solid particles both is taken into account simultaneously in the mathematical model.

A method of weight mean density of oil droplet and solid particles was used in this model:

$$\rho_{So} = \left(C_o\rho_o + C_S\rho_S\right) / \left(C_o + C_S\right)$$

The case of severe impairment was presented by Zhang as it is the common case at low solid particle concentration (1 - 20 ppm).

For the case of Severe Impairment Zone:

The material balance equation is: $I_{Ci} = \dfrac{VC_{So}\rho_1}{A_S\phi_{Ci}\left[(1-\phi_{Ci})\rho_{So} + C_{So}\phi_{Ci}(\rho_{So}-\rho_1)\right]}$

Where: I_{ci} is the depth of the impaired zone.

v is the total injected water volume.

C_{so} is equivalent concentration of solids and oil.

A_s is the flow inlet area.

$Ø_f$ is the porosity of the porous medium.

$Ø_{ci}$ is the porosity of the impaired zone.

ρ_1 is the density of the injected fluid.

ρ_{So} is the mean density of oil and solids.

This equation calculates I_{ci} at any certain cumulative injection volume.

Based on Darcy's law, the pressure drop equation for this case can by written as:

$$\Delta P = \frac{\mu}{A_S}\left(\frac{I_{Ci}}{K_{Ci}} + \frac{I_F - I_{Ci}}{K_F}\right)\frac{dV}{dt}$$

Where: I_f is the core depth.

K_f is effective brine permeability or the initial core permeability.

K_{ci} is the impaired zone permeability.

ROCHON et al. (1996) described the formation damage process using relatively few parameters. Particle size, concentration, flow rate, porosity, and permeability were identified as the most important variables involved.

Description of the analytical model:

a) Building-up the internal cake: the main assumption was that the number of particles moving on is much smaller than the number of particles which have already been deposited.

A mass balance equation can be written for linear flow.

$$\frac{Q}{A} * \frac{\partial C}{\partial x} + \frac{\partial n}{\partial t} = o$$

Where Q is injection rate at time t.

A is cross section area of the porous medium.

C is volumetric concentration of suspended particles.

n is volumetric concentration of deposition particles.

x is the distance into the porous medium as measured from the entry face.

Assumptions:

The concentration of particles in suspension is independent of time and decreases exponentially as a function of distance from the entry face (Fig.1.77). Also the constant concentration profile of particles in suspension depends on the real initial velocity within the pores (interstitial velocity $\frac{Q_o}{A\phi_o}$).

Then $$\left(\frac{\partial C}{\partial x}\right)_t = -\frac{\lambda A \phi_o}{Q_o} C$$

Where λ is the Filtration coefficient, 1/T.

Q_0 is initial injection flow rate.

$Ø_0$ is initial undamaged porosity.

Integration from the entry face to a depth x gives the concentration profile of suspended particles: $$C = C_O e^{-\frac{\lambda \phi_o}{Q_o} x}$$

Assumption:

Particle deposition corresponds to a decrease in porosity:

$$\frac{\partial n}{\partial t} = -\frac{\partial \phi}{\partial t}$$

By substitution of the last three equations in the first equation and integration with respect to time, porosity at a depth x at time t is calculated. Then replace the time-integral of injection rate by V (the cumulative volume injected):

$$\phi(x,V) = \phi_o \left[1 - \frac{\lambda C_o}{Q_o} e^{-\frac{\lambda \phi_o}{Q_o} x} V \right]$$

A linear relationship between the logarithm of permeability and porosity is assumed:

$$\frac{K}{K_o} = \exp\left[\beta'(\phi - \phi_o)\right]$$

Where ß' is the relationship coefficient.

The last two equations were combining. Then a change of scale operation was applied on the infinitesimal slice so as to obtain the average permeability over a distance L from the injection face. Flow across the slices corresponds to resistances in series:

$$\frac{K_o}{K} = \frac{1}{L} \int_0^L \exp\left[\frac{\lambda \beta' C_o \phi_o}{Q_o} e^{\frac{-\lambda \phi_o}{Q_o} x} V \right] dx$$

This equation is the ratio of initial permeability to average permeability after injection of a volume V.

b) Switching from internal damage to external cake:

The ratio of pore throat diameter to particle size is called the jamming ratio (J_r). Growth of the internal cake is accompanied by a decrease of jamming ratio at the entry face. There is a critical value J_r^* of the jamming ratio at the entry face , when the particles are stopped because the size of the pore throats decreases to a value sufficiently small to permit particle bridging or blocking. Another term is the cumulative volume injected when damage switches from internal damage to growth of the external cake when new particles can no longer enter but have to accumulate at the injection face. This term is called V*.

$$V^* = \frac{2Q_o L n \frac{J_r}{\alpha^*}}{\lambda \beta C_o \phi_o}$$

Where $\alpha^* = \frac{d_t^*}{d_p}$ and $J_r = \frac{d_t}{d_p}$

Qualitatively, α^* is the number of particles required to block the entry pore throat when the critical volume V* has been injected.

And d_p and J_t is particle and pore throat diameter respectivily.

c) Building-up the external cake at constant flow rate: the basic assumption is that once the external cake starts to form, no more particles enter the porous medium and the average permeability of the damaged porous medium has a value K* and remains constant while the external cake continues to build-up. The external cake thickness h_c increases with the arrival of new particles:

$$Q_o C_o = A(1-\phi_c)\frac{dh_c}{dt}$$

Integration gives the thickness of the cake as a function of the time (t - t*) since the external cake started to form:

$$h_c = \int_{t^*}^{t} \frac{Q_o C_o}{A(1-\phi_c)} dt = \frac{C_o}{A(1-\phi_C)}(V - V^*)$$

The overall resistance to flow corresponds to two resistances in series: due to damaged porous medium and due to the external cake.

$$L\left(\frac{1}{K} - \frac{1}{K^*}\right) = \frac{h_c}{K_c}$$

Combining the above two equations gives an expression for the change in overall permeability as a function of volume injected:

$$\frac{K_o}{K} - 1 = \frac{C_o K_o}{ALK_c(1-\phi_c)}(V - V^*) + \left(\frac{K_o}{K^*} - 1\right)$$

They used Fontainebleau sandstone cores with a porosity from 10 to 17 % and permeability from 230 to 1600 md. The solid particles were monosized beads of latex with particle sizes from 1.5 to 7.6 µm and a concentration from 2 to 14 ppm suspended in a 0.6g/l NaCl brine. The pH was adjusted to 8.5.

The plot of $\frac{K_o}{K} - 1$ as a function of cumulative injection show the three above stages. It starts with a near parabolic curve for the build-up of internal damage followed by a straight line for

the growth of the external cake. The critical volume V* when switching from internal cake to external cake is determined graphically (Fig.1.78 and 1.79).

Internal filtration coefficient λ and the constant ß' can be determined at constant injection rate:

a) By matching the experimental curve corresponding to the growth of the internal cake gives a correlation for λ (internal filtration coefficient) as well as ß' (the constant in the porosity / log permeability relationship). The switch from the formation of an internal to an external cake gives α^*. Finally, growth of the external cake gives the product $K_c(1-Ø_c)$.

b) By dimensional analysis: for the case of internal damage.

$$\lambda = \frac{Q_o}{AL\phi_o}(W_2)^{-0.50}(W_3)^{5.42}(W_4)^{-0.52}$$

$$\beta = (W_5)^{-0.44}(W_3)^{-2.26}$$

Where:

$$W_1 = \frac{Q_o}{AL\phi_o} \qquad W_2 = C_o \qquad W_3 = Ø_o \qquad W_4 = \frac{\pi(d_t)^2}{4A} \qquad W_5 = \frac{Q_o C_o \rho_S}{1.7*3\pi\mu d_p}$$

By dimensional analysis for the case of growth of an external cake:

$$K_c(1-\phi_c) = \frac{1}{10^{-11}}(W_6)^{0.94}(W_7)$$

Where: $W_6 = \frac{Q_o C_o \rho_S L}{A\mu}$ $\qquad W_7 = (d_p)^{0.2}(K^*)^{0.9}$

In this correlation $K_c(1-Ø_c)$ is in md and K* is in cm^2.

1.8 Fracture Review

1.8.1 Effect of fractures on flow pattern:

CRAWFORD et al. (1953) showed the effect of vertical and horizontal fractures on the sweep efficiency.

Sweep efficiency was obtained with the aid of a potentiometric model. The electrolyte reservoir was 20 inch wide by 30 inch long by approximately 0.5 inch deep. The electrolyte reservoir was built to correspond to a unit in a line-drive pattern. In using the model to represent a fracture system, a thin strip of copper was soldered to the well or wells and the length and orientation of the strip was made to conform to the vertical fracture under consideration.

They concluded that:

a) For the case of vertical fractures parallel to the direction of flood and when the flow is from the fractured to the unfractured well (Fig.1.80a):

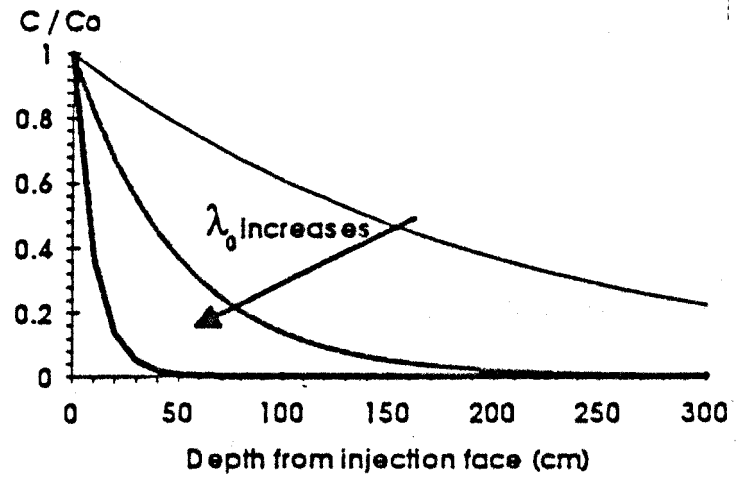

Fig.1.77: Normalized suspended particle concentration in porous medium (Rochon *et al.* 1996).

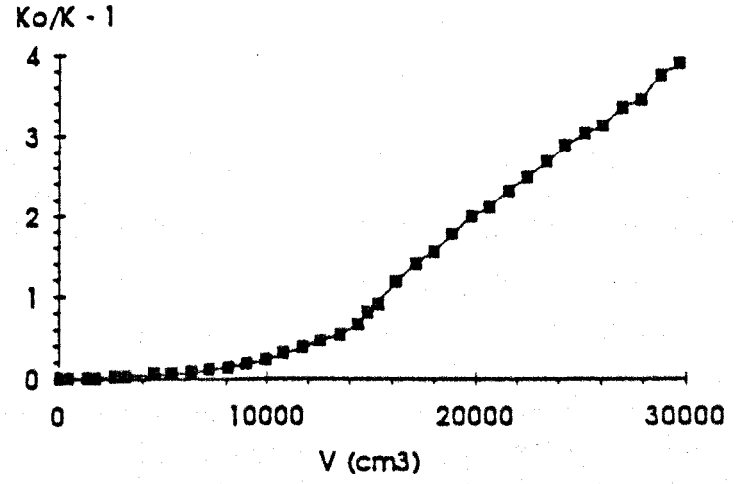

Fig.1.78: Typical curve at constant flow rate (Rochon *et al.* 1996).

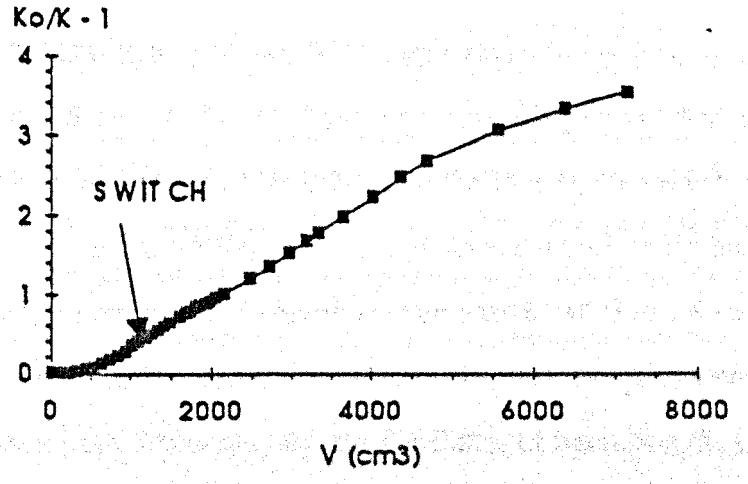

Fig.1.79: Typical curve at constant pressure gradient (Rochon *et al.* 1996).

The very long fractures produced a spearhead shape. As the fracture length was reduced, the shape of the flood fronts approached those of the unfractured system. The sweep efficiency is seen to decrease as the fracture length increases. If the fracture extends half the distance between wells, a sweep efficiency of only 28 per cent may be expected.

b) For the case of vertical fractures perpendicular to direction of flood and the flow is from the fractured to the unfractured well (Fig.1.80b):

As the length of the fracture increased the areal sweep efficiency increased. When equal and opposite parallel vertical fractures existed at each well, an areal sweep efficiency of 80 per cent was observed when the fracture's length were 23.5 per cent of the distance between adjacent input wells. For fractures extending half the distance between adjacent input wells, sweep efficiencies of near 90 per cent may be expected.

c) For two vertical fractures at right angles in one well, the presence of the fracture which is perpendicular to the flood enhanced the effect of the other fracture which is parallel to the flood.

d) For two systems of fractured injection and production wells and unfractured injection and production wells, fractured wells would take fluid 4.94 times the rate of the unfractured wells. Breakthrough will occur first between the two unfractured wells. When this occurs the invading fluid will have advanced only about half the distance between the unfractured wells (Fig.1.81).

1.8.2 Thermal fracture initiation:

WEINSTEIN (1974) studied the effect of increasing water viscosity in the near wellbore region (due to the injection of cold water) on injection pressure rating.

As a part of a pressure maintenance program, it had been proposed to inject 70° F surface water at the rate of 300,000 BPD into the 285° F formation.

For the unfractured system, ΔP increases with increasing rate and decreasing Kh (Fig.1.82). Injection temperature was varied from 70 to 285° F to evaluate the effect of heating the injected water. Results shows that ΔP has a strong dependence on injected water temperature. A small increase in temperature causes a significant decrease in ΔP (Fig.1.83). The pressure drop for an unfractured system and 70° F injection temperature would require a pressure rating in excess of the desired upper limit. Consequently, the feasibility of fracturing the formation was considered.

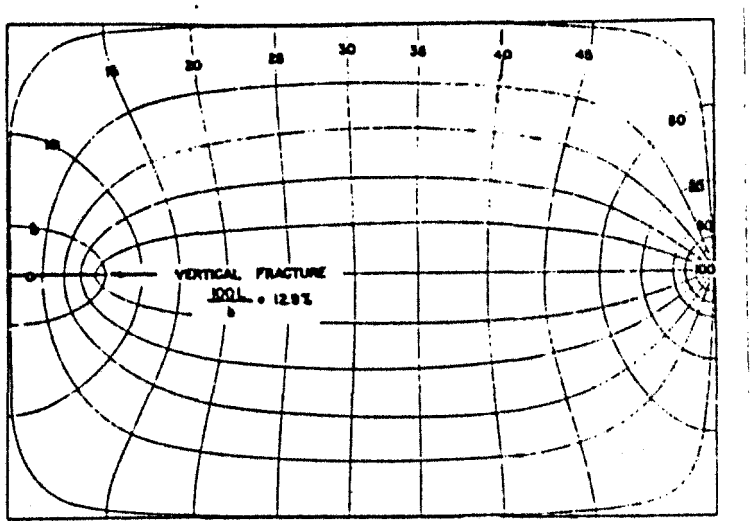

Fig.1.80a: Streamlines and isopotentials for a vertically fractured system fracture parallel to flow direction (Crawford *et al.* 1953).

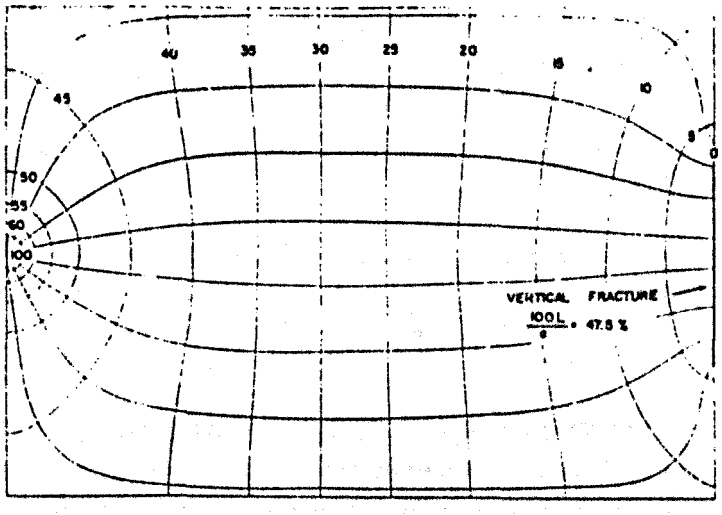

Fig.1.80b: Streamlines and isopotentials for a vertically fractured system fracture perpendicular to flow direction(Crawford *et al.* 1953)

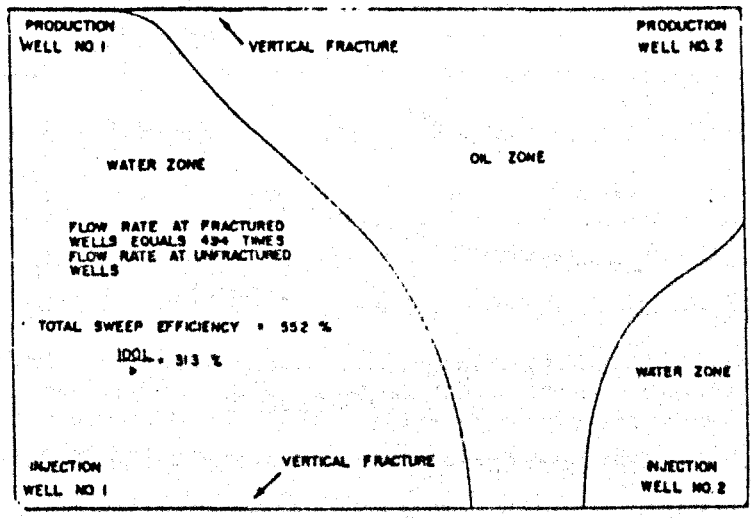

Fig.1.81: Flood fronts at breakthrough for a vertically fractured system (Crawford *et al.* 1953).

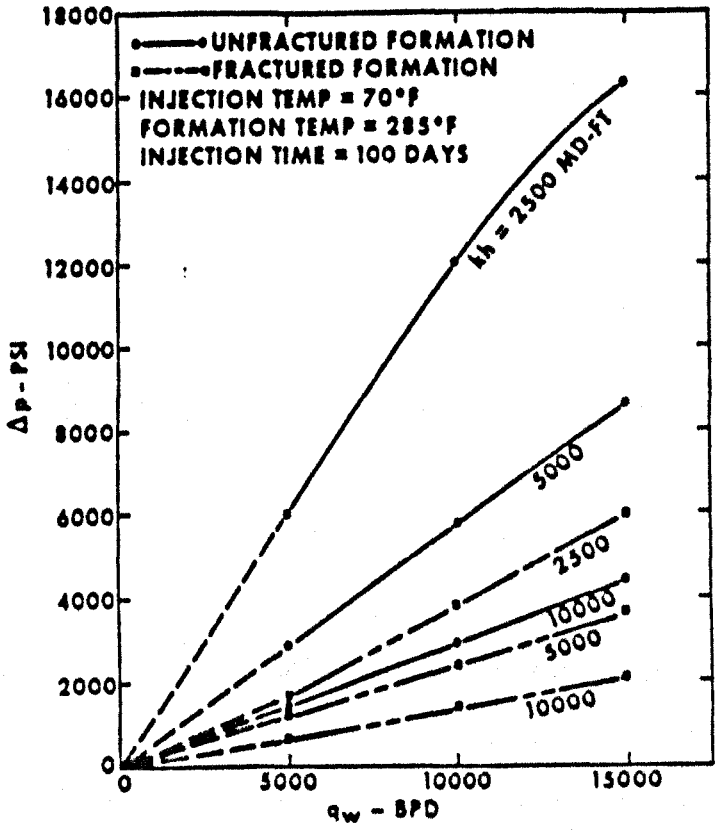

Fig.1.82: Effect of rate, kh and fracturing on pressure drop (Weinstein 1974).

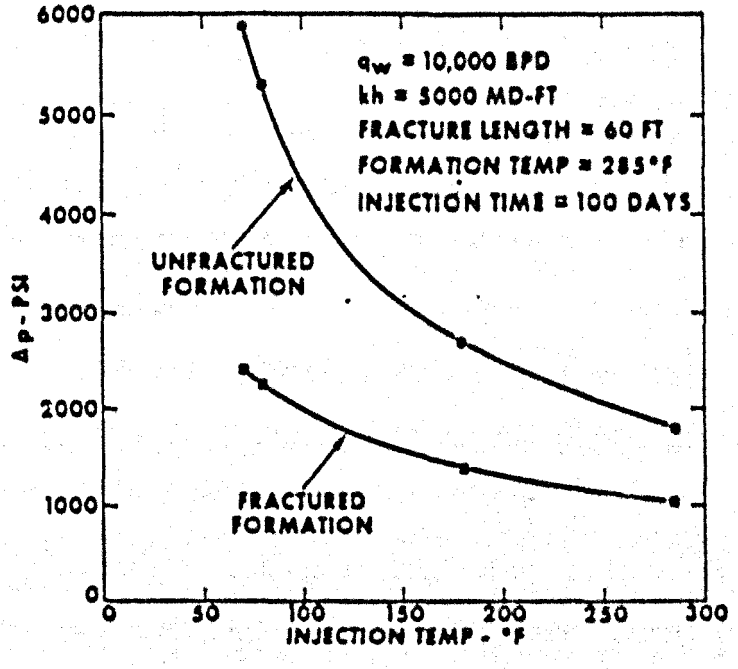

Fig.1.83: Effect of injection temperature and fracturing on pressure drop (Weinstein 1974)

He concluded that injecting cold water radially into a hot reservoir cools the formation in the vicinity of the wellbore. The increased water viscosity in this critical region creates a large pressure drop and would necessitate a higher pressure rating than may be desired.

MORALES et al. (1985) discussed a problem which refered to a 30 day filtered seawater injection into two perforated formations located in the west Coast of the Arabian Gulf. The injection test was conducted at three levels of constant tubing head pressure. The initial tubing head pressure of 990 psig was increased to an intermediate step of 1240 psig, and finally to a pressure of 1490 psig.

The formation transmissibility (kh / μ) value obtained for the initial stage of injection should remain unchanged unless there are variations in the reservoir conditions; for instance, a change in kh/μ could be caused by fracture initiation and/or fracture growth.

Data points after the tubing head pressure was raised to the second pressure level showed a kh/μ value of approximately twice as high as the kh/μ obtained during the initial pressure stage, and it further increased to four times the initial value at the final pressure stage (Fig.1.84). It is likely that an unexpected fracture caused these apparent higher transmissibilities. Fracture initiation would have occurred after approximately 360 hours of pumping, i.e. when the pressure was raised to the intermediate stage, followed thereafter by fracture propagation. The water temperature at the point of entry was approximately 51° F lower than the formation temperature. They concluded that the injection of cool water into a reservoir for relatively long periods of time can alter the in situ state of stress due to a decrease in reservoir temperature and an increase in pore pressure.

WRIGHT et al. (1990) explained the injected water temperature effect on rock tensile stress and stated that when rock around the wellbore is cooled by injection water, it tends to contract, shrinking away from the hot rock surrounding it. This sets up tensile stress in the cooled rock, and reduces the initial rock compressive stress. The thermo-elastic stress reduction may reach 20 psi per 1° C of cooling.

Fracture initiation at the wellbore is expected to occur at the point where stress reduction is greatest. Relatively high permeability streaks, which take more flow from the wellbore and are thus cooled more, are favoured for fracture initiation. Once the fracture is initiated, cooling in

its immediate vicinity is further promoted by higher injectivity and larger leak off area, so encouraging further fracture growth.

They concluded that low rate injection wells did not spontaneously thermally fracture in the same way as higher rate wells. This is because the injection water was heated more as it travelled downhole slowly and did not cool the formation sufficiently.

Continuous high pressure stimulation in low rate wells allowed fractures to be maintained at lower injection pressure subsequently. The higher injection rates during stimulation resulted in cold downhole temperature and adequate rock stress reductions.

SIMPSON et al. (1991) explained the thermal fracturing process as follows:

The effective stress of the formation is given by

$$\sigma_E = \sigma_T - p_F$$

Where σ_T = total stress

p_F = pore fluid pressure

Under initial stress-state conditions the total stress components are usually considerably greater than the pore fluid pressure, hence the resulting effective stresses are compressive.

In many fields, water is injected into a relatively warm formation. As the rock heat capacity is roughly twice that of the associated water, the thermal front moves at approximately one third of the speed of the water saturation front. Thus, for a typical north sea injector, where waterflooding gives a saturation front which is moving at around 2 feet per day, the thermal front will move at about 8 inches per day. The reduction in temperature of the cooled zone causes a reduction in total and effective stress.

Thermal stress reductions for consolidated sandstones are likely to be about 15 psi/1° F. Also injecting water increases the pore pressure and hence reduces the effective stresses (Fig.1.85).

They concluded that injecting cold water reduces the effective stresses and this may result in a switch from compressive to tensile stress. If this occurs fracture initiation or propagation of an existing fracture is likely to occur. As the switch from compressive to tensile stress will occur first in the direction of minimum stress, the fracture will open, and propagate outwards in the plane normal to that direction. Thus a vertical fracture in the plane of the maximum horizontal stress will be formed.

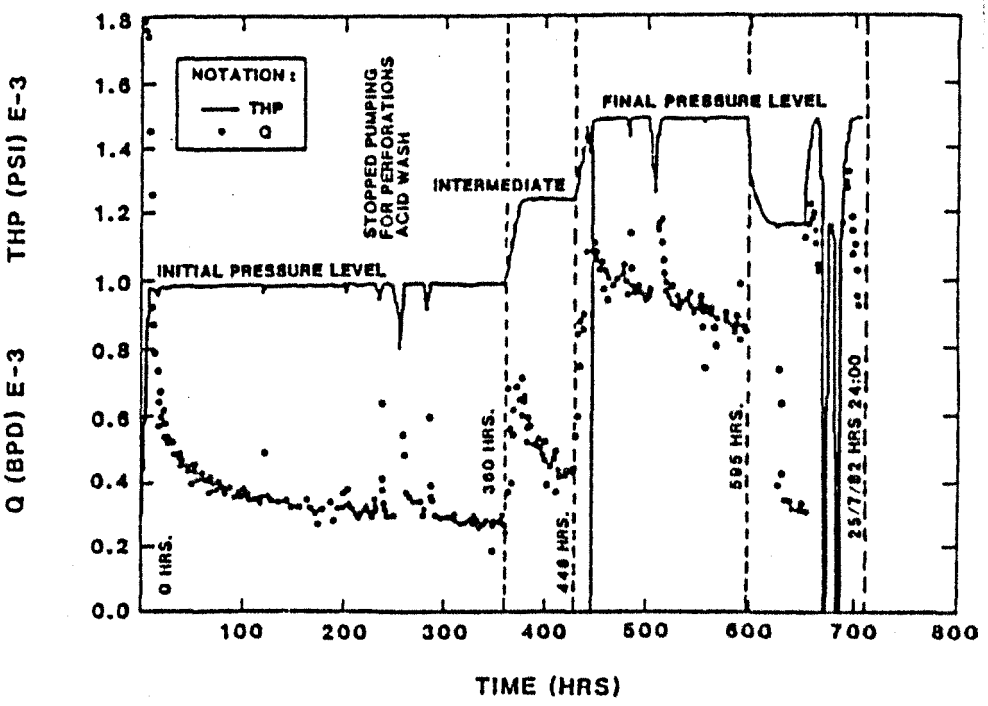

Fig.1.84: Sea water injection test history (Morales *et al.* 1985).

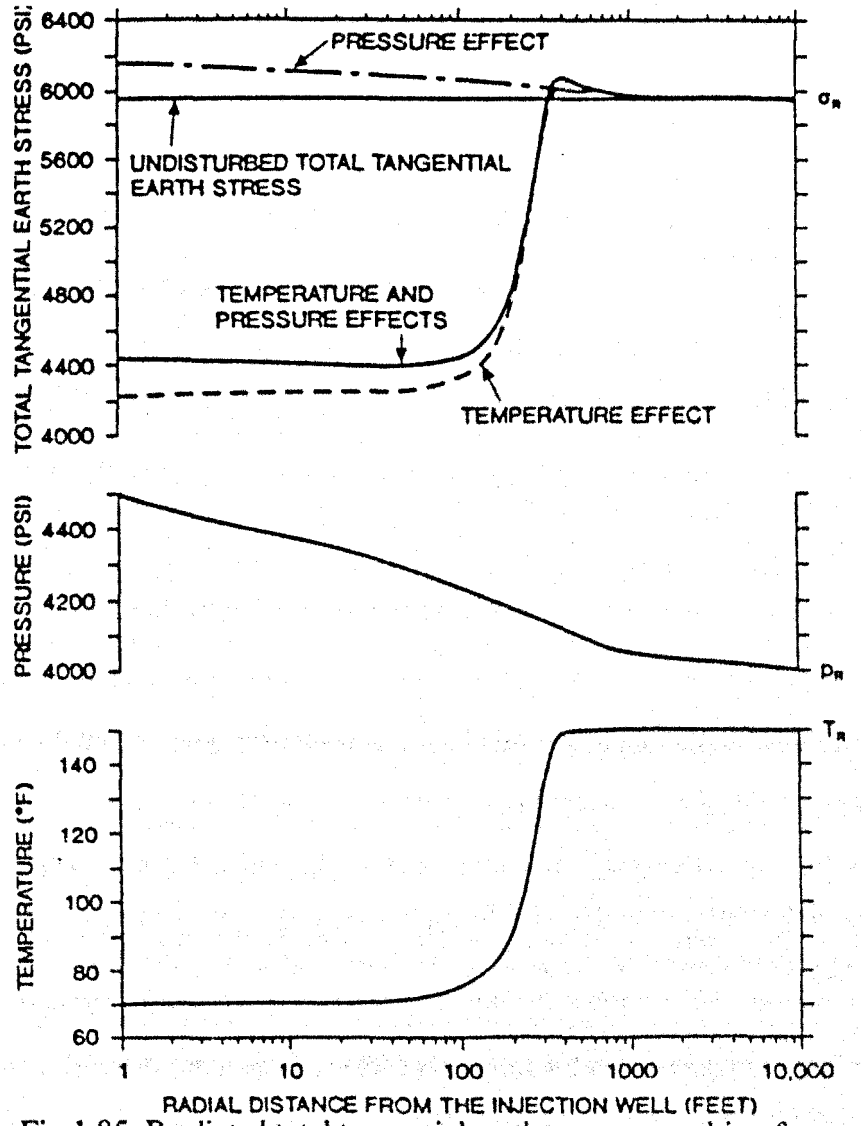

Fig.1.85: Predicted total tangential earth stresses resulting from temperature and pressure fields (Simpson *et al.* 1991).

CLIFFORD et al. (1991) gave a general information about how the conditions of the formation affect the fracture initiation within that formation starting with the fact that water injection wells commonly become fractured under standard operating conditions, without the need for a deliberate programme of hydraulic fracturing stimulation.

They stated that:

a) Depletion of pressure within a reservoir has the effect of reducing the rock stress, and for this reason it is easier for an injection well to fracture into a depleted formation than a highly pressured formation.

b) The likely effect of cooling on a naturally fractured system will be to increase the opening of existing cracks, rather than creating new fractures. The presence of fractures provides a much larger surface area for leak-off than a non-fractured wellbore. Furthermore, the fracture system is able under some circumstances to grow to expose new sandface and accommodate further downhole filtration.

MARTINS et al. (1994) discussed the flow and pressure behaviour of injection process of seawater and produced water at Prudhoe Bay field.

They stated that the pressure required to open an induced fracture depends both on the initial stresses in the rock and on stress changes induced by injection at different temperature and pressure. And the produced water has a higher pressure gradient (0.57 - 0.60 psi/ft) than sea water (0.53 - 0.54 psi/ft). This was linked to the higher well-head temperature of produced water (150°F) compared with that of sea water (80°F).

The results of the test showed that:

a) In Figure 1.86, each point represents the well-head pressure and corresponding rate for one day of injection. The well has been switched 6 times between sea water injection (SWI) and produced water injection (PWRI) over a 7 years. The points of SWI lie approximately on a straight line which intercepts the pressure axis at about 50 psi which is a good measure of the fracture-opening pressure.

The PWRI line show an intersection at 800 psi, and tend to converge to the SWi line as the injection rate increases.

b) It also appears that fractures are often likely to be shorter in length for PWRI in spite of the higher pressure.

c) In general, any injectivity which is lost on conversion from sea water to produced water is fully restored on conversion back to sea water, but this recovery takes 3 - 6 months to converge to a new steady value which is the time required for the temperature to be altered in a region around the well with a radius greater than fracture height and/or length (Fig.1.87).

d) In going from high to low water quality, the increase in WHP (well head pressure) compared with the Clean water was measured (at the same injection rate).

When oil concentration is increased from 0 to 400 ppm, at low solids loading, an additional 200 psi injection pressure is required to maintain the injection rate (20% loss of injectivity).

For less than 100 ppm oil, an increase in solids from 0-5 to 5-10 mg/l required only 30 psi additional pressure. At 400 ppm oil with the same increase in solids loading required an extra 100 psi. This supports the idea that oil causes solid particles to adhere, increasing the damage above the sum of the two components separately.

1.8.3 Fracture Detection

HOLZHAUSEN et al. (1987) explained the pressure analysis methods that can be applied to detect and evaluate fractures while injection is occurring.

Low-frequency techniques:

a) Pressure transient methods: can be applied to evaluate fracture size from measurements made while constant-rate water injection is taking place.

b) Continuous monitoring of well injectivity index: a sudden increase in the injectivity index may indicate fracture opening, although this information alone contains no information about fracture size.

The inverse of injectivity index can similarly be used in evaluating the onset of fracture growth.

High-frequency pressure analysis:

Well bore pressure oscillations occur when steady flow conditions are disturbed by, for example, valving at the wellhead. The sudden release of fluid causes a low-pressure wave to travel to the bottom of the well where it is then reflected upward. Upon returning to the wellhead, the wave is again reflected, this time downward. The process of propagation and reflection is thus repeated until the wave is fully damped by friction and by energy losses.

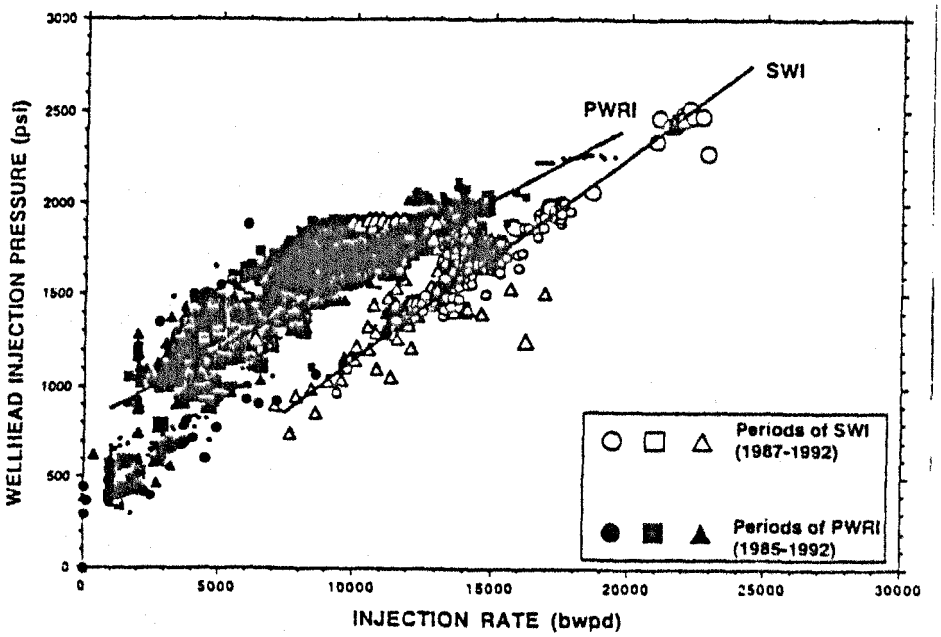

Fig.1.86: Performance plot (Martins *et al.* 1994).

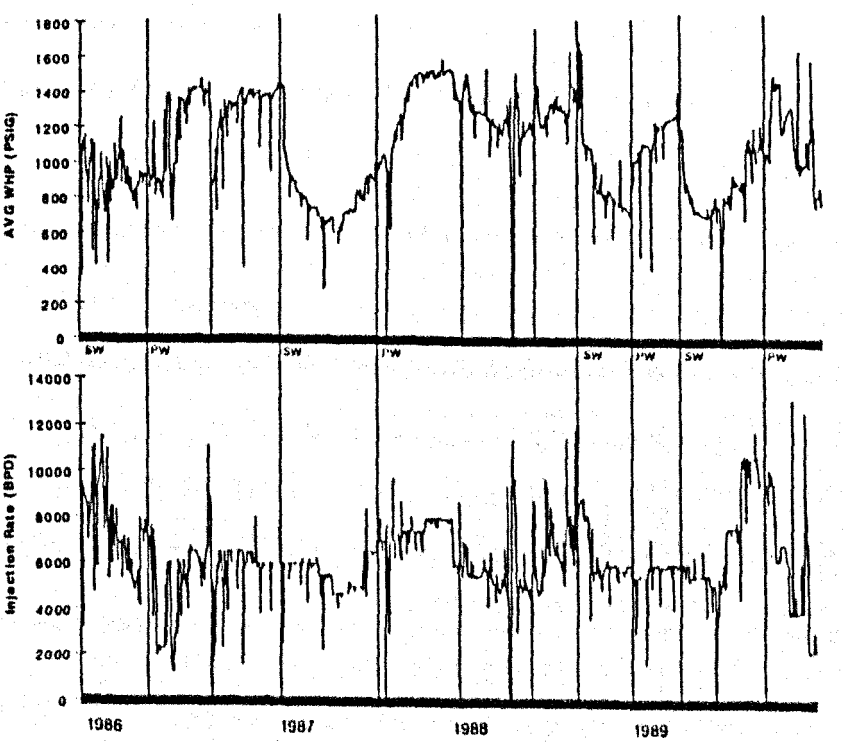

Fig.1.87: Trends WHP and injection during SWI - PWRI switching (Martins *et al.* 1994).

The resonant properties of the well can also be determined using forced oscillation which occurs when a well is excited with a continuous source, such as a reciprocating pump at the wellhead (Fig.1.88a).

This analysis is extremely effective at detecting the initiation of hydraulic fractures(or the opening of closed natural fractures) in previously unfractured wells (Fig.1.88b).

WILLIAMS et al. (1987) defined fracture gradient for thermal formation by using a new modified approach which involved plotting injection data with $1/II=\left[(p_{inj}-p_{init})/q_N\right]$ as the dependent variable and $sum=\sum_{j=1}^{N}\left\{\left[(q_j-q_{j-1})/q_N\right]*\log(t-t_{j-1})\right\}$ as the independent variable

The two terms can be shown to be related as $1/II=(162.6*\mu_w*B_w/kh)*(sum)+b'$

Where II : is the injectivity index

$ß_w$: is the formation volume factor for the injected water

P_{init}: is the reservoir pressure (psig)

P_{inj}: is the bottom-hole injection pressure at time t

q_i: is the flow rate at the jth time step

q_n: is theflow rate during the current step in the ramp-up

This is a typical slope-intercept equation of a straight line in which the slope is inversely proportional to the permeability-thickness product of the formation, and the intercept is related to the effective skin at the wellbore.

They explained that a change in the character of the line takes place when fracturing occurs and flow changes from radial to linear, and this change can pinpoint the formation breakpoint under the current injection conditions. It is important to note that use of this method requires detailed knowledge of the bottomhole pressure and the injection rate at discrete intervals within each step of the SRT (step-rate test).

When this technique was developed and applied for first time to the September 1984 SRT data of well S-6 (Prudhoe Bay oil field), a 0.5 psi/ft breakpoint was indicated (Fig.1.89). This was somewhat lower than the 0.54 psi/ft break supported originally by the traditional plot of injection pressure versus rate (Fig.1.90).

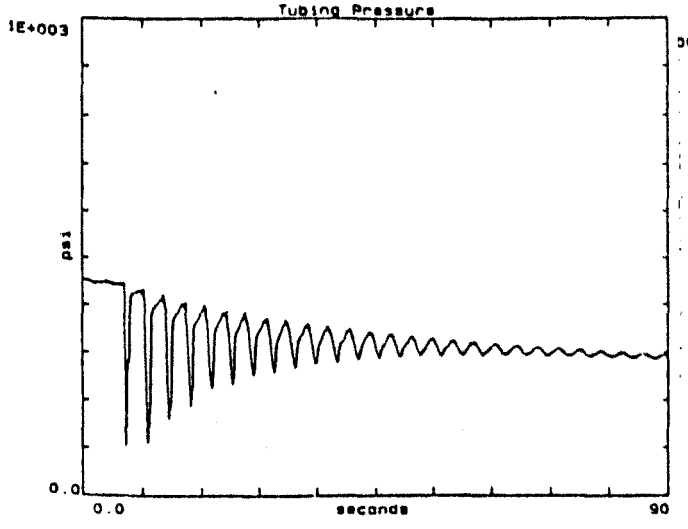

Fig.1.88a: Free oscillations of WHP before fracturing (Holzhausen *et al.* 1987)

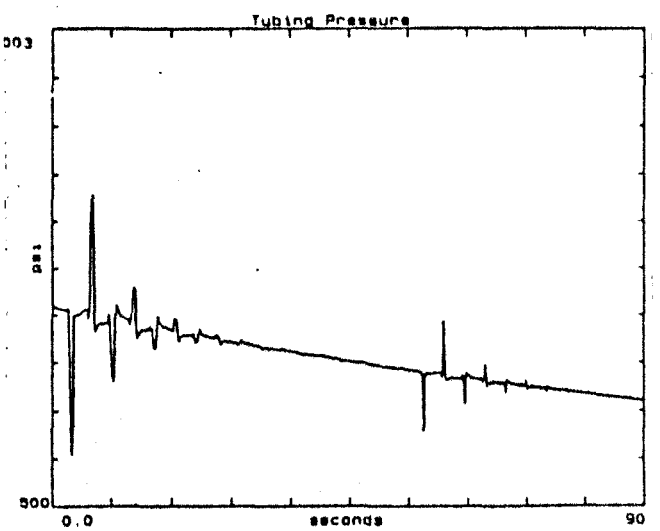

Fig.1.88b: Free oscillations measured at WH after fracturing (Holzhausen *et al.* 1987)

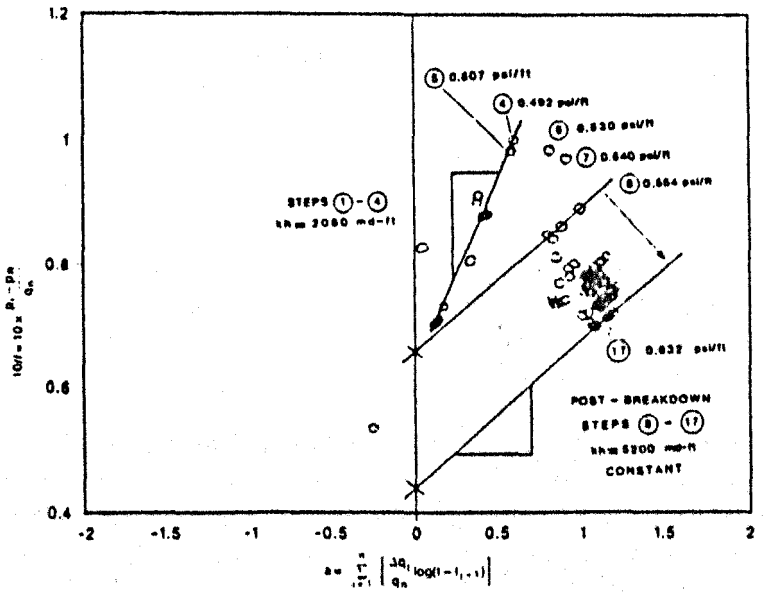

Fig.1.89: Oden-jones plot from the s-6 stop rate test (Williams *et al.* 1987).

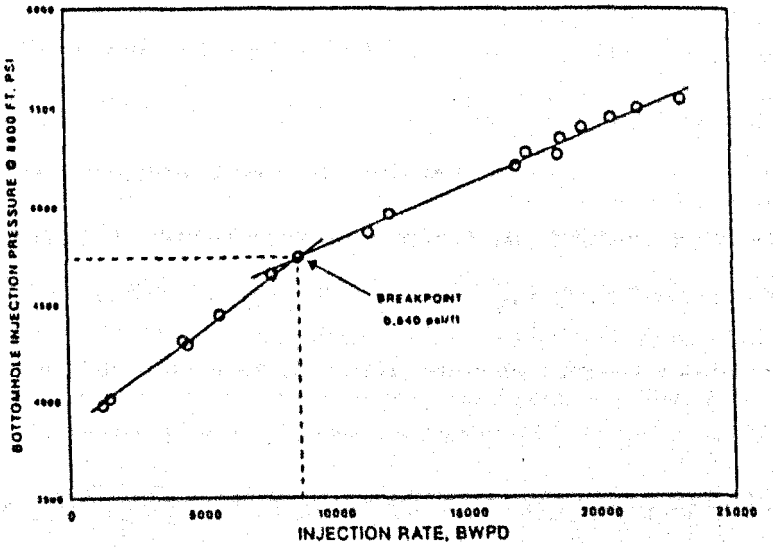

Fig.1.90:Bottom hole injection pressure versus rate for the s-6 SRT (Williams *et al.* 1987).

1.8.4 Comparison of Hydraulic fractures and water injection fractures

SETTARI et al. (1994) stated that waterflood induced fracturing has many similarities to, and some important differences from conventional fracturing (well stimulation). The two most important differences lie in the time scale and injected fluid viscosities of the fracturing operation.

They summaries the difference between the two as follows:

a) Waterflood fracturing is leak-off dominated process while stimulation fracturing is leak-off controlled process.

b) While the time scale of conventional fracturing is on the order of a day or less, waterflood fracturing propagates through the reservoir for a period of months or years.

c) The fluid efficiency (which is the ability of fluid to control leak-off through fracture face) is 20% or higher for stimulation treatments and can be very close to zero in waterflood fracturing.

d) As a result, the physics of waterflood fracturing is very complex, and consequently requires more rigorous models.

NEILSON (1984) stated that hydraulic fracture is expected to grow continually while pumping the fracturing fluid and the fracture will close when pumping stops, its length, width and height controlled by the volume and placement of the propant. On the other hand the waterflood induced hydraulic fracture is different as injection may continue for a long time, in the order of magnitude of years, and simulate this long time scale is difficult as the time in the hydraulic fracture simulation programmes is controlled by the total volume injected and the injection rate, both of which are numerically limited in size.

1.8.5 Fracture injection Field experience

GARON et al. (1988) described the change in reservoir temperature as a result of one year of water injection in Prudhoe Bay oil Field injection wells (Fig.1.91), and define the relevent reduction in stress caused by such change. Results are presented in Figures 1.92 and 1.93.

WRIGHT et al. (1990) stated that after several weeks of stable injection in Ula field water injection well, a very rapid improvement in the performance took place. The injection rate increased by 6000 bbl/d and the injection pressure decreased by 70 psi within a 15 minute.

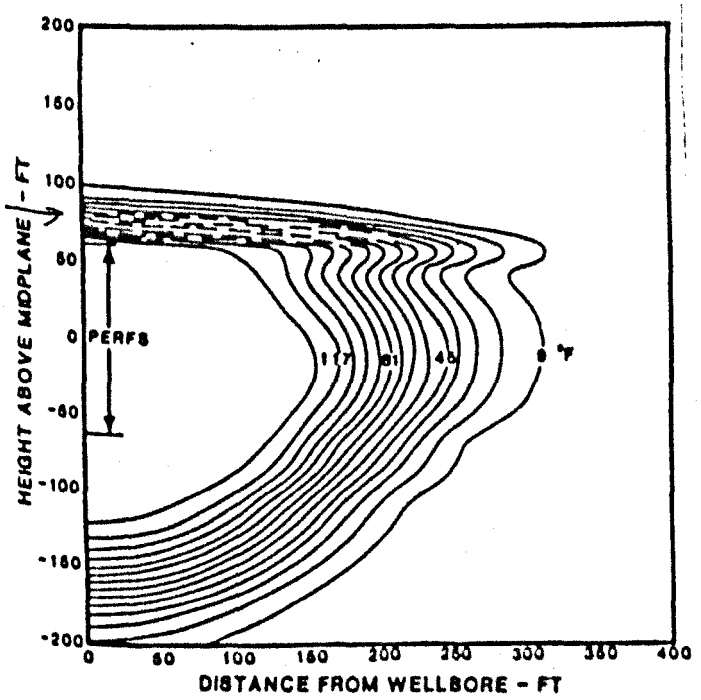

Fig.1.91: Cooling isotherme following one year of waterflooding without fracturing (Garon *et al.* 1988)

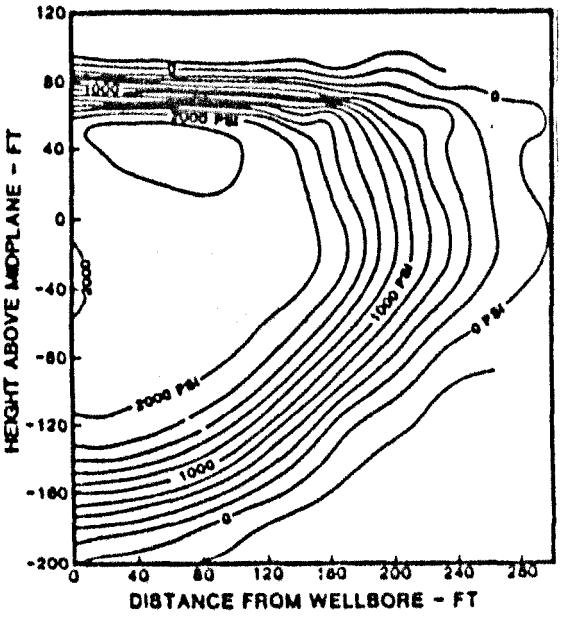

Fig.1.92: Stress change isobars after one year of waterflooding (Garon *et al.* 1988)

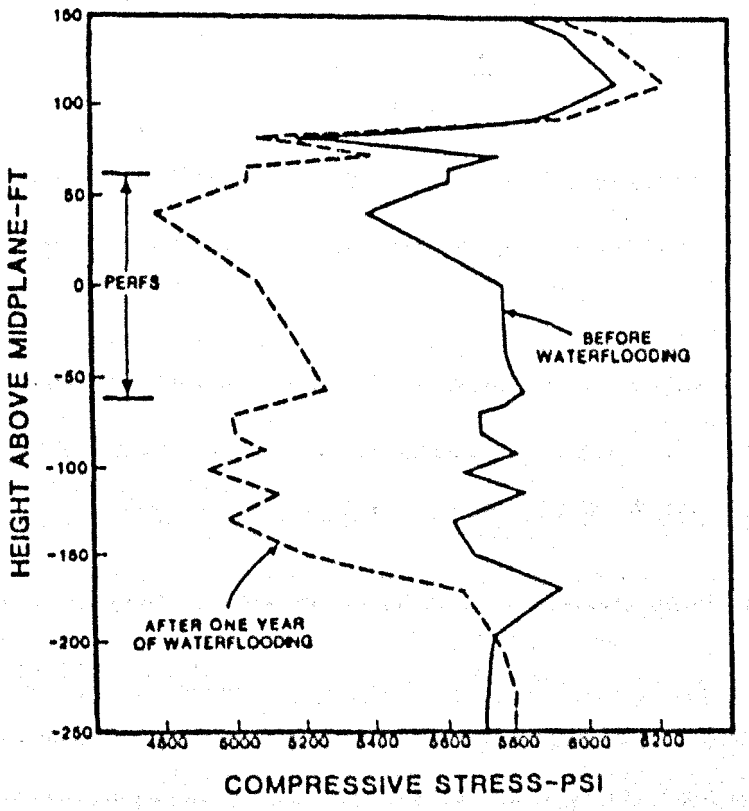

Fig.1.93: Vertical profiles of minimum horizontal stress before and after waterflooding (Garon *et al.* 1988).

During a second, slower, increase in performance, observed three days later, the injection rate built to 29000 bbl/d. However, the injection pressure remained at the same level as a week previously when the rate had been 18000 bbl/d. Both events correlated with drops in injection water temperature which had resulted from operational changes (Fig.1.94).

SIMPSON et al. (1991) observed no decline in well injectivity in the Forties field throughout a six week duration of a Produced Water injection trial. At the constant injection rate maintained by the mud pumps, no increase in wellhead injection pressure was recorded; this despite oil-in-water concentrations varying from 50-1200 ppm and suspended solids from 5-50 mg/l. Interpretation of the data indicates the presence of induced fractures.

1.8.6. Production Fracture Models

PRATS (1960) presented a fracture flow model. In this model he assumed that a horizontal oil producing a layer of constant thickness and of uniform porosity and permeability is bounded above and below by impermeable strata and that the reservoir liquid is incompressible. He also assumed that after the well is fractured, the cylindrical outer boundary is at a uniform potential, provided that it is not too near the fracture (Fig.1.95).

He stated that the effect of a fracture on the pressure distribution in the fracture itself and in an otherwise undamaged (no skin) reservoir indicated that the pressure distribution is a function of three parameters:

The first one is the ratio of the ability of the formation to carry fluids into the fracture to the ability of fracture to carry fluids into the well (relative capacity), and it is defined by:

$$a = \frac{\pi k 2L}{4k_f w}$$ where w is the fracture width.

The last two are the size of the wellbore and drainage radius (r_w and r_e) relative to the extent of the fracture from the well axis L.

The dimensionless pressure drop between the end of the fracture and any point in the fracture is essentially independent of the size of the reservoir, i.e. r_{eD}. however, this pressure drop is strongly dependent on the value of the relative capacity parameter a.

Figure 1.96 show the variation of this dimensionless pressure drop in the fracture with the dimensionless distance from the well. This pressure drop is given by:

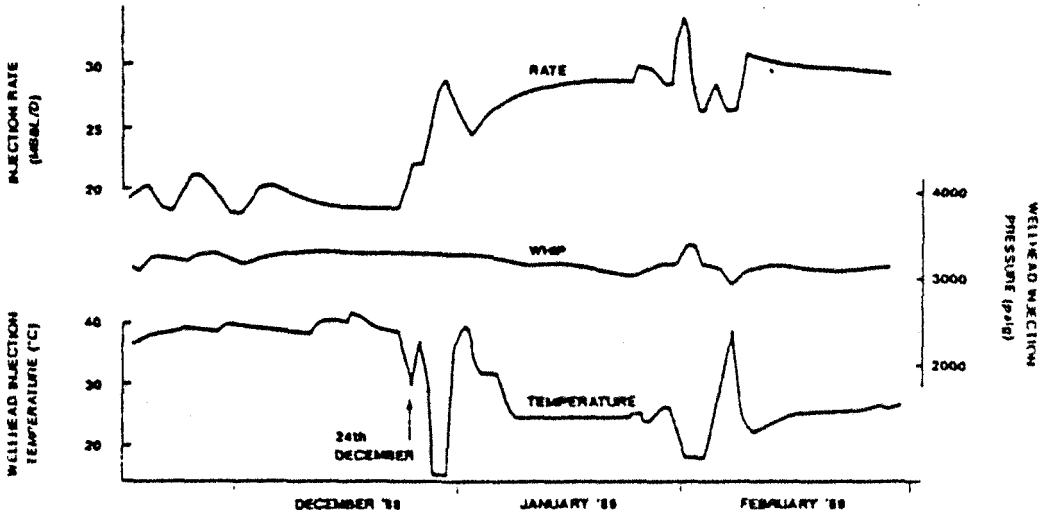

Fig.1.94: Performance of well A-40 during large temperature change (Wright *et al.* 1990).

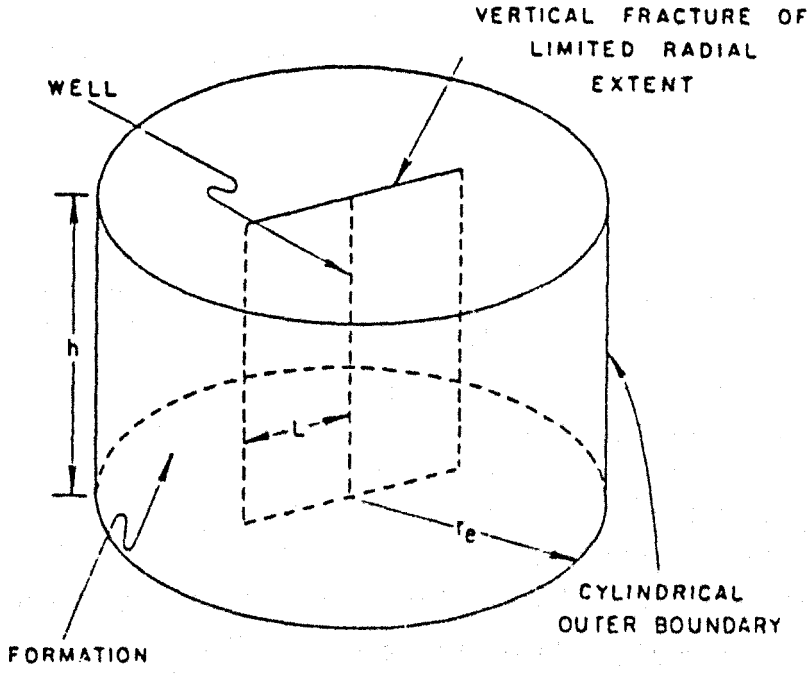

Fig.1.95: Schematic diagram of fractured system (Prats 1960).

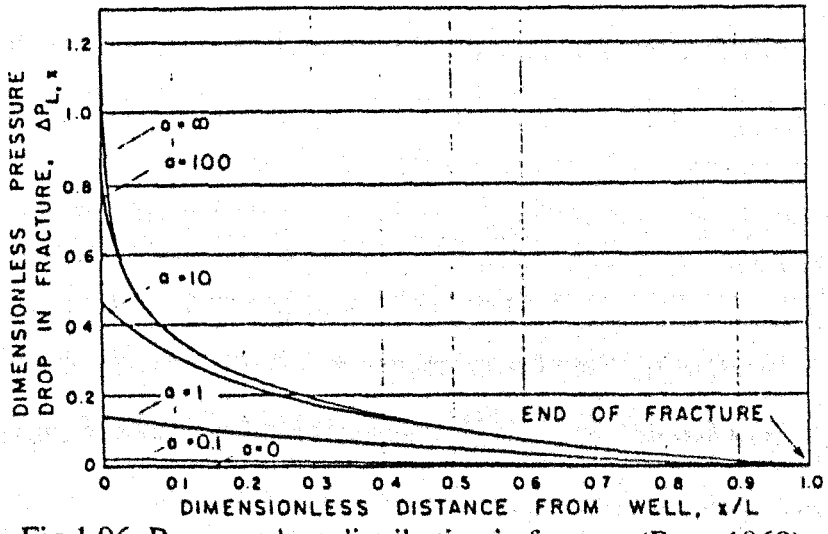

Fig.1.96: Pressure drop distribution in fracture (Prats 1960).

$$\Delta p_{L,x} = \frac{kh}{q\mu}(p_L - p_x)$$

Where (P_L-P_x) is the pressure drop between the end of the fracture at $x = L$ and any point in the fracture a distance x from the well axis.

He stated that the ratio of pressure drop in the fracture to that in the field is strongly dependent on the values of a and r_{eD} for a well of zero radius (Fig.1.97). This plot shows that the pressure drop in the fracture is negligible (less than 10 % of the pressure drop in the field) for values of $a \leq 0.1$ and for fracture lengths smaller than the field radius. Since most of fractures probably satisfy these conditions, it appears that pressure drop in clean fractures can be considered negligible in most cases.

He derived the improvement in production rate caused by fracture as:

$$\frac{q_f}{q} = \frac{\frac{1}{2\pi}\ln\frac{r_e}{r_w}}{\Delta p_{e,0}(a, r_{eD}) - \Delta p_{w,0}(a, r_{wD})}$$

The $\Delta p_{e,0}$ can be found from Fig.99

or
$$\frac{q_f}{q} = \frac{\ln\frac{r_e}{r_w}}{\ln\frac{r_e}{r_w'}}$$

Then he investigated the effect of skin presence around the fracture on the productivity as follows:

In a fractured well, the flow is distributed over the large surface area of the fracture, resulting in almost linear flow in the formation near the fracture and, consequently, small flow resistance. Thus, damage to the formation near the fracture may not change the total flow resistance appreciably.

The ratio of production rate after damage to undamage production rate is derived as follows: for the case of infinite fracture capacity ($a = 0$), the entire fracture is at a uniform pressure (P_f) equal to the well pressure. The damaged zone and the reservoir can be transformed into rectangular sections (Fig.1.98). The pressure distribution in ξ should be the same for all values of η; that is the pressure distribution is a function of ξ.

The pressure distribution in the skin of permeability Ks is: $p_d = b + c\xi$

And the pressure distribution in the reservoir is: $p = d + e\xi$

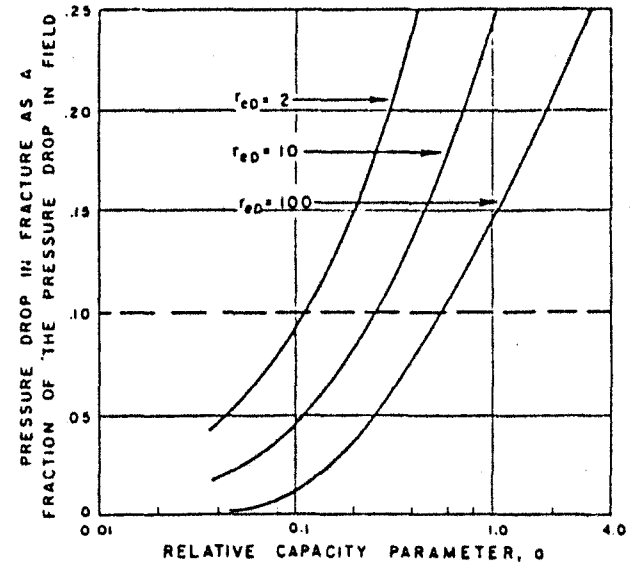

Fig.1.97: Pressure drop in fracture (Prats 1960).

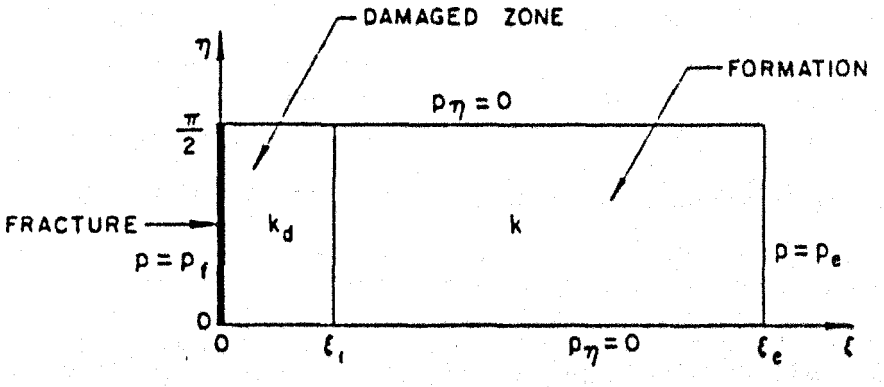

Fig.1.98: Damaged fractured reservoir in transformed plane (Prats 1960).

The constants b, c, d and e are to be determined from the boundary conditions:

$$p_d = p_f \quad \text{at} \quad \xi = 0 \quad \text{(the fracture)}$$

$$p = p_e \quad \text{at} \quad \xi = \xi_e \quad \text{(the outer boundary of the field)}$$

and the refraction conditions:

$$p_d = p$$

$$k_d \frac{dp_d}{d\xi} = k \frac{dp}{d\xi} \qquad \text{on } \xi = \xi_1 \text{ (the boundary between the skin and the formation)}$$

The quantity ξ_1 is related to the average depth of the skin by: $w_d = \frac{\pi}{4} L \xi_1$

The quantity ξ_e is related to the average field radius by: $\xi_e = \ln \frac{2r_e}{L}$

The application of the boundary, refraction and Darcy equation leads to a production rate after damage given by:

$$q_{fd} = \frac{2\pi kh}{\mu} \frac{(p_e - p_f)}{\ln \frac{2r_e}{L} + (\frac{k}{k_d} - 1)\frac{4w_d}{\pi L}}$$

Before the formation is damage, Kd = K, and the production rate is:

$$q_f = \frac{2\pi kh}{\mu} \frac{(p_e - p_f)}{\ln \frac{2r_e}{L}}$$

Thus, the ratio of damaged to undamaged production rate is given by:

$$\frac{q_{fd}}{q_f} = \frac{1}{1 + \frac{\frac{4w_d}{\pi L}(\frac{k}{k_d} - 1)}{\ln \frac{2r_e}{L}}}$$

For unfractured well surrounded by a damaged zone the ratio is given by:

$$\frac{q_d}{q} = \frac{1}{1 + (\frac{k}{k_d} - 1)\frac{\ln(1 + \frac{w_d}{r_w})}{\ln \frac{r_e}{r_w}}}$$

CINCO et al. (1981) considered a well intercepted by a fully penetrating vertical fracture. The well produces at constant flow rate a slightly compressible fluid from a homogeneous isotropic reservoir whose properties are independent of pressure. They presented an infinite conductivity fracture with fluid loss damage case.

For infinite conductivity fracture with a damaged zone of uniform width b_s and permeability K_s, pressure behaviour for an infinite conductivity fluid loss damaged fracture may be expressed as:

$$p_{wD} = f(t_{Dx_f}, s_{fs})$$

Where s_{fs} is a skin damage factor defined by:

$$s_{fs} = \frac{\pi b_s}{2x_f}\left(\frac{k}{k_s} - 1\right)$$

A log-log graph of p_{wD} versus t_{Dx_f} for this case shows that there is three flow periods.

a) The linear flow period; the solution is given by:

$$p_{wD}(t_{Dx_f}, s_{fs}) = \sqrt{\pi t_{Dx_f}} + s_{fs}$$

The larger the fluid loss damage skin factor, the longer the linear flow period.

b) The transition and the pseudoradial flow periods; the solution is given by:

$$p_{wD}(t_{Dx_f}, s_{fs}) = p_{wD}(t_{Dx_f}, (k_f b_f)_D = \infty) + \Delta p_{Ds}(s_{fs}, T_{Dx_f})$$

Where Δp_{Ds} is the additional dimensionless pressure drop caused by the skin damage.

When the pseudo-radial flow prevails the extra pressure drop becomes a function of s_{fs} only.

Figure 1.99 presents the stabilised flux distribution for different values of the fluid loss damage skin factor. The curves for small values of s_{fs} approach the infinite conductivity fracture case; however, as s_{fs} increase the flux distribution curves become more uniform approaching the uniform flux case.

Figure 1.100 shows a semilog graph of $p_{wD} - s_{fs}$ versus t_{Dx_f} for s_{fs} equal to 0.2 and 1. This figure clearly indicates, that the curves for fluid loss damaged fractures fall in between the infinite conductivity solution and the uniform flux solution; in such a way that curves become closer to the uniform flux solution as s_{fs} increases.

1.8.7 Fracture aperture and Permeability

Flow along a fracture is normally characterised by using the classical cubic equation for steady-state isothermal, laminar flow between two smooth parallel plates:

$$Q = 5.11*10^6\left[\frac{W\Delta p b^3}{L\mu}\right]$$

Where Q: is the flow rate (bbl/day)

w: is the width of fracture face (ft)

Δp: is the pressure differential (psi)

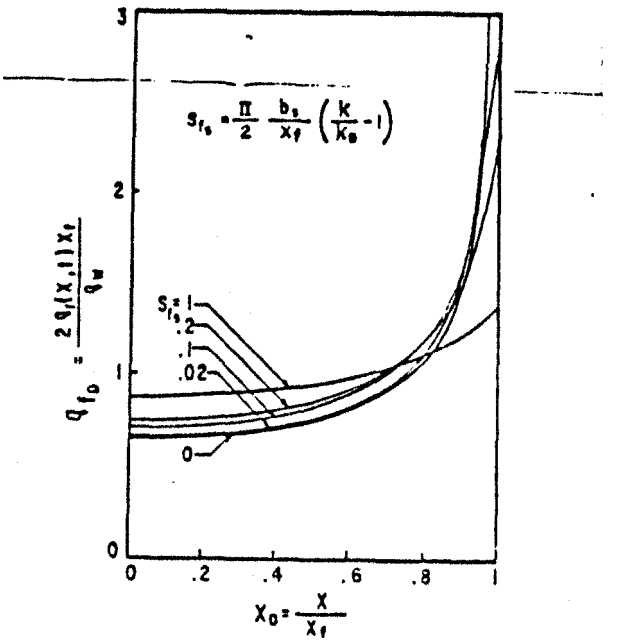

Fig.1.99: Stabilized flux distribution for a fluid loss damaged fracture (Cinco *et al.* 1981).

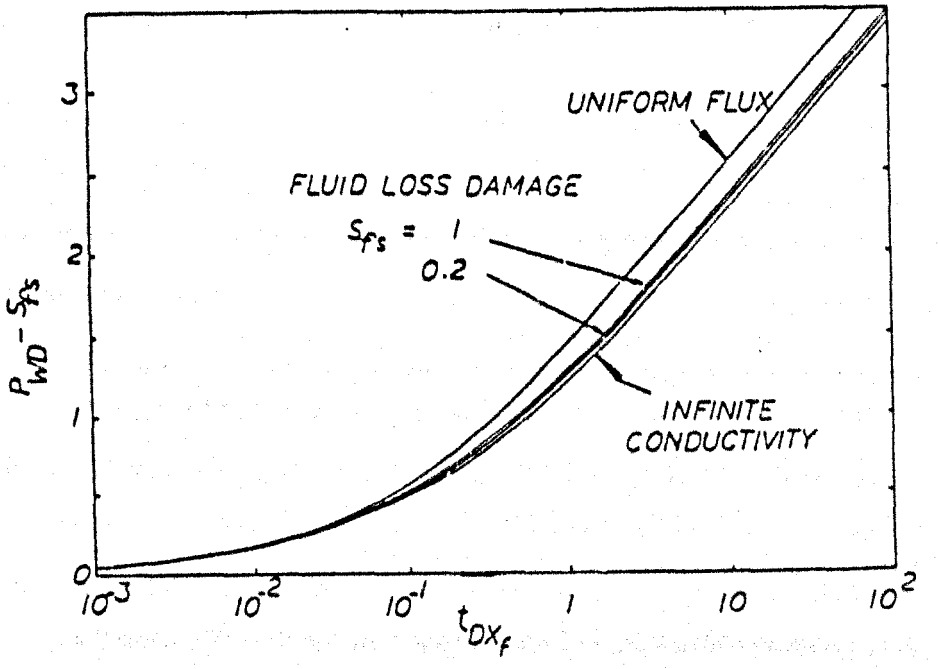

Fig.1.100: Comparison of fluid loss damaged fracture and undamaged fracture solutions (Cinco *et al.* 1981).

b: is the fracture aperture (in)

L: is the length of fracture (ft)

μ: is the fluid viscosity (cp)

JONES et al. (1988) explained that the rough surface does not always follow the above equation (Fig.1.101), so a new equation was developed which avoids the smooth plate assumption. The equation is derived from Bernoulli's equation for flow in pipes and is applied to natural fractures.

$$Q = 5.06*10^4 W\left[\frac{\Delta p b^3}{fL\rho}\right]^{0.5}$$

Where f : is the friction factor.

This equation is applicable for all single-phase open fracture laminar and turbulent flow calculations, provided the correct friction factor is used.

They stated that the effect of wall roughness on flow through fracture is dependent on the fracture aperture, If the aperture is large (0.0253 inch) compared to the surface roughness, that roughness will have little effect on flow and the flow will obey the cubic Law (Fig.1.102).

Friction factor must be determined experimentally for each individual type of rock fracture, until a relationship between surface roughness and fracture aperture is developed which will exclude rock type as a variable. Then the fracture aperture can be calculated by trial and error when flow rate and pressure drop are known.

They derived a simple equation for fracture permeability for smoth and rough surfaces by using Darcy's law as follows:

Darcy's law expresses fracture permeability as:

$$k = 10.65\frac{QL\mu}{Wb\Delta p}$$ Where k in darcy

Substituting for Q from a cubic law equation (for smooth parallel plate) for smooth surface fracture permeability can be calculated :

$$k = 5.44*10^7 b^3$$ Substituting for Q from rough surface equation, rough surface fracture permeability can be calculated if a correct friction factor is used:

$$k = 5.39*10^5 \mu\left[\frac{bL}{f\Delta p\rho}\right]^{0.5}$$

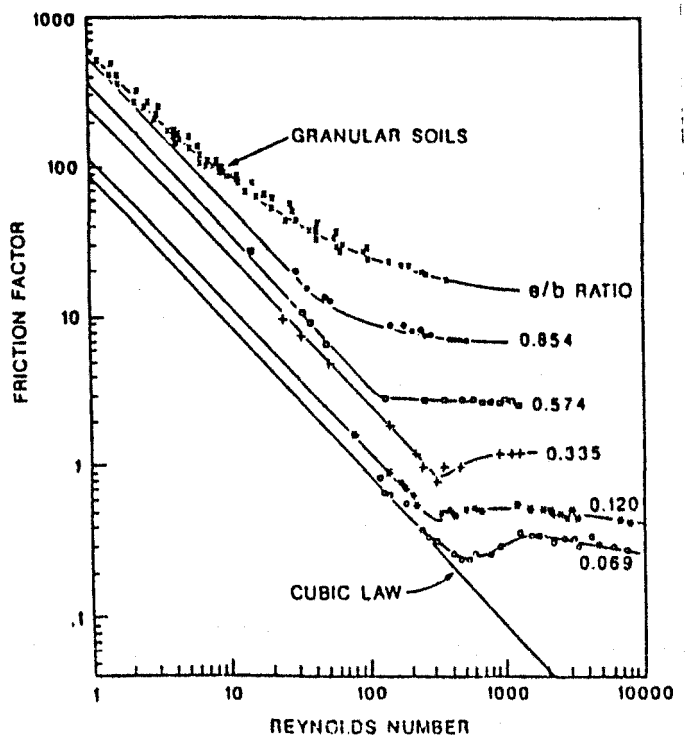

Fig.1.101: Effectof surface roughness / fracture aperture for artificial fracture (Jones *et al.* 1988).

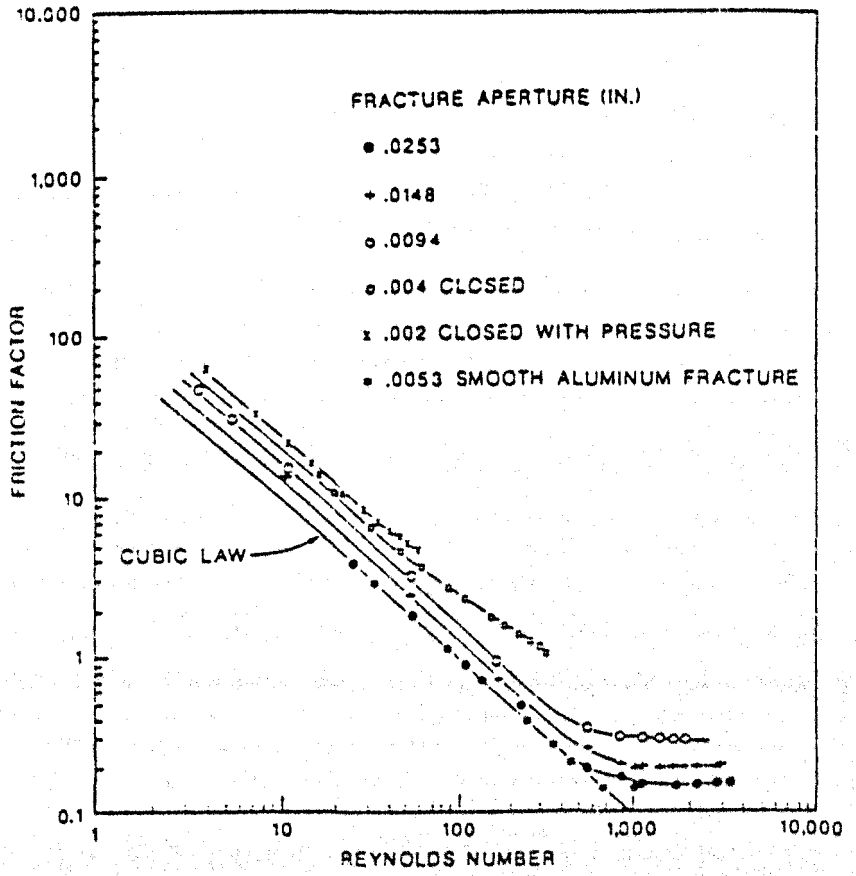

Fig.1.102: Effect of aperture for sandstone (Jones *et al.* 1988).

1.8.8 Damaged injection Fracture Models

PANG et al. (1985) presented some equations to model open hole and perforated completions as well as fractured wells. Methods for calculating filtration parameters were developed when core flow test data is not available.

Model equations for internal and external filter cake formation were given separately. They can be used separately to compute the Permeability Ratio or the injectivity decline for each impairment mechanism. They can also be used together to calculate the overall decrease in injectivity by using the transition time concept (t*).

Model for hydraulically fractured wells: For almost all cases, external filtration around the wellbore is not important because the fracture permeability is so large that the fluid is primarily directed into the fracture.

a) They stated that for the internal damage case : If the fracture conductivity is infinite, it is likely that particles will flow from the fracture into the formation and damage the formation. It can be assumed that the case is a near-fracture formation permeability reduction. So the equations for linear geometry can be used to predict permeability decline.

Flow area (A)= 2 h L and Flow velocity (v) = q / A

Where h: fracture higth.

L: fracture length.

Injectivity decline will be: $\alpha(t) = r_e \Big/ \left[\frac{r_e}{\bar{k}_r(x_f)} + (r_e - x_f) \right]$

Where: $x_f = Vt$ For $Vt < r_e$

$x_f = r_e$ For $Vt > r_e$

$$\frac{1}{\bar{k}_r(t)} = 1 + Mt$$

$$M = \delta f$$

$$\delta = \beta VC / x_f$$

$$f = 1 - \exp(-\lambda x_f / V)$$

Filtration parameters can be calculated, if no experimental data is available, by some empirical equations.

Filtration coefficient can be calculated by knowing particle/grain size ratio:

$$\lambda = f(v) * 14.481 \left[d_p / d_g \right]^{0.587}$$

Where: f(v) is the coefficient accounting for the effect of fluid velocity on filtration coefficient (can be obtained from literature (Gruesbeck[29])). F(v) = 1 for no velocity effect.

The retained particles n(x,t) can be retained at pore throats or in pore bodies. Particles retained in pore throats have much larger impact on permeability. So a defined value Ω was introduced, which is the fraction of retained particles trapped at pore throats (Fig.1.103). It is evident that as the injected particle size increases a larger fraction of retained particles will be lodged at pore throats and will contribute to permeability impairment. Particles much smaller than the pore throat size are likely to be retained in pore bodies and , therefore, contribute less to permeability impairment.

$$n(x,t) = \lambda C t \exp(-\lambda x / V)$$

Where: C is the injected solids concentration.

t is the injection time.

x is the distance inside the rock matrix.

V is the incident fluid velocity.

If the permeability is caused by pore throat blocking:

$$\frac{K(x,t)}{K_O} = \frac{1}{1+\delta n(x,t)}$$

$$\delta = \Omega\left((K_O/K_P)-1\right)$$

Where: Ko is the rock permeability.

δ is called damage factor.

Kp is the permeability of the plugged pore throats.

Also $$\delta = \Omega\left(\left(d_g^2/d_p^2\right)-1\right)$$

Where: d_g is the average grain size of the rock.

d_p is the average particle size.

If the injected particles are much smaller than the formation grain size, Ω —> 0, most particles will be retained in pore bodies:

$$\frac{K(x,t)}{K_O} = \frac{\phi^3(x,t)}{1-\phi^2(x,t)}\frac{1-\phi^2}{\phi^3}$$

Where: Ø(x,t)= Ø - (1 - Ω) n (x,t)

b) They stated that for the case of external damage: If the fracture conductivity/ aperture is relatively large and the formation permeability is relatively small, it is possible for particles to

accumulate at the rock face around the fracture. In this case also the equations for linear geometry can be used where $A = 2\,h\,L$ and $V = q / A$.

The total resistance will equal to the resistance of the rock plus the resistance of the cake:

$$\frac{L}{K} = \frac{h_C}{K_C} + \frac{L}{K_O}$$

$$h_C = \frac{Cqt}{A(1-\phi_C)}$$

where: L is the injection length.

K_c is the external cake permeability.

h_c is the external cake thickness.

$Ø_c$ is the external cake porosity.

Then
$$\frac{K}{K_O} = \frac{1}{\frac{K_O}{K_C}\frac{CV}{(1-\phi_C)L} + 1}$$

Filter cake properties can be obtained from direct measurement or empirical correlations. The cake porosity can be obtained if the particle volume in the filter cake is gravimetrically measured. The cake permeability can be obtained from tests if the cake thickness is measured. Empirical correlations such as the Blake-Cozeny can be used to obtain a permeability-porosity correlation for packed beds of particles:

$$K_P = \frac{d_P^2}{150}\frac{\phi^3}{1-\phi^2}$$

ROCHON et al. (1996) Stated that the performance of thermally induced fracture wells is a complex subject. so he limited his work to calculate the over all skin assuming infinite fracture conductivity.

Two sea water qualities were studied:

- A low solid content water with 0.5 ppm and a particle size of 0.5µm.
- A high solid content water with 14 ppm and a particle size of 3.0µm.

The laboratory results were applied to two types of injection wells:

- A well with thermally induced fractures (constant half length of 10 m).
- A well under normal darcy flow conditions into perforations(1" diameter, 12" penetration)

In the case of fractured well the skin is the sum of a geometric skin $-Ln\left[\frac{X_f}{2r_w}\right]$, and

a skin due to fracture face damage, permeability being reduced to K_d over a depth W_d.

The total skin factors:

$$S = \frac{\pi}{2}\frac{W_d}{X_f}\left(\frac{K_o}{K_d} - 1\right) - Ln\left[\frac{X_f}{2r_w}\right]$$

They concluded that

a) The internal damage has almost no influence with injection time until the external cake starts to build-up (Fig.1.104a and 1.104b).

b) For the low solid content and size an external cake starts to build-up after 9 years .

c) For the high solid content and 3μm size, it takes 2 years before switching between internal and external cake damage.

d) Assuming static filtration after these critical times (this is not quite true because of the shear flow component parallel to the fracture face), the fracture filling with a relatively permeable cake gives a slow increase in the injectivity.

e) It will take a shorter time to fill the fracture in the case of high content solids.

1.8.9. Forces acting on the solid particles flowing along filtration surface

JIAO et al. (1994) examined the forces of equilibrium that causes a particle to be released from a collection surface by sliding or rolling or stay attached to that collector:

An equilibrium cake thickness is achieved when the forces acting to hold colloidal particles on the cake surface are overcome by hydrodynamic shear forces that tend to entrain particles in the flow stream.

There are four forces acting on each particle: a hydrodynamic tangential force (shear stress) which is generated by the flowing suspension, a normal drag force which is generated by the filter flux, a hydrodynamic lift force, and surface forces. The lift force on a particle sitting on a flat surface in laminar flow is negligibly small. For colloid sizes less than 2 μm and a small density contrast, gravitational forces may be neglected. Surface forces between the colloids and the cake surface can be very large but are much shorter range than the hydrodynamic forces.

In his paper, two mechanisms of particle release, sliding and rolling, were evaluated. By performing a force balance on particles at the cake surface a cake growth model has been developed.

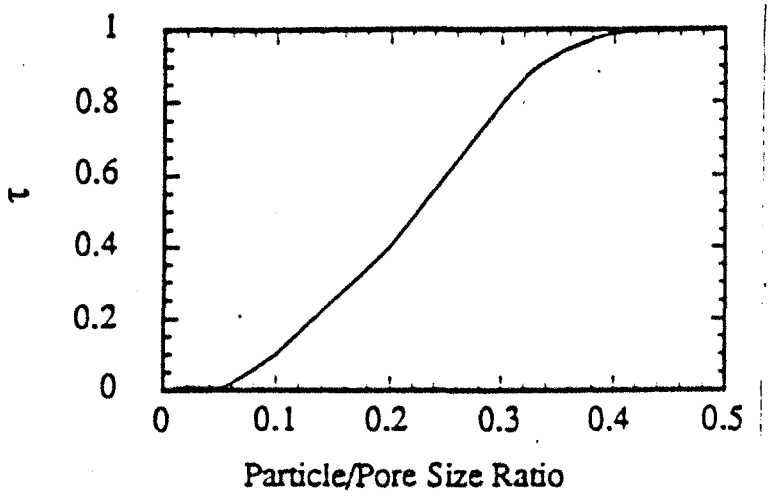

Fig.1.103: coefficient τ versus size ratio (Pang *et al.* 1995).

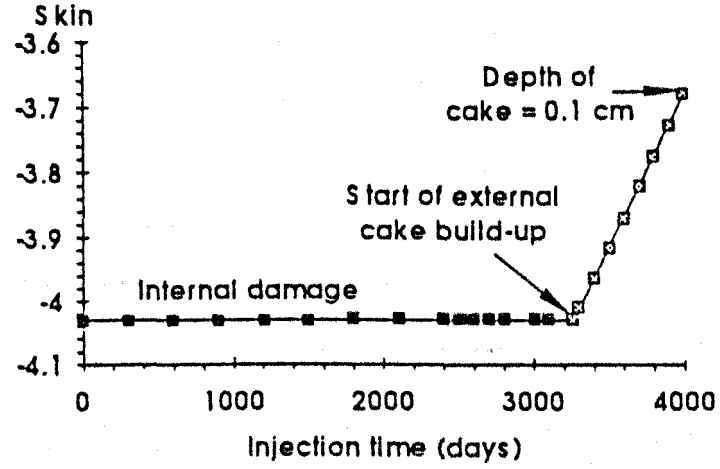

Fig.1.104a: Skin versus injection time for fractured reservoir (North sea conditions) (Rochon *et al.* 1996).

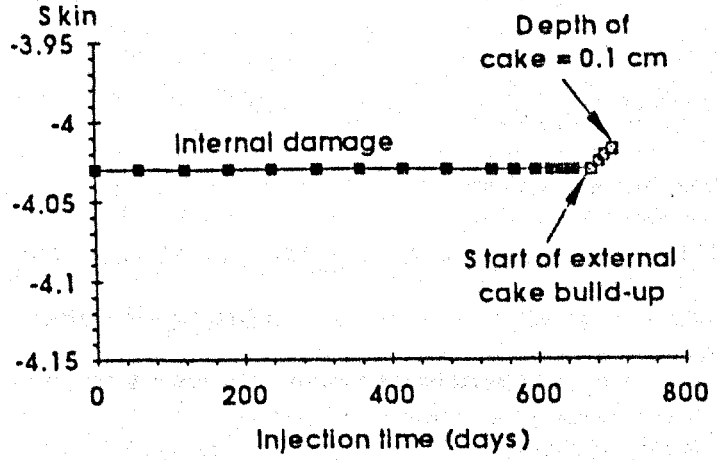

Fig.1.104b: Skin versus injection time for fractured reservoir (Gulnea Gulf conditions) (Rochon *et al.* 1996).

Stokes law can be used to calculate the normal drag force F_y. For small particles (1 to 5 μm) at low Reynolds number, the drag force can be calculated as:

$$F_y = \alpha\pi R^2 \frac{1}{2}\rho_S V_Y^2 \frac{24}{N_{Re}}$$

Where R is the radius of the particle.

V is the filtrate flux.

ρ_S is the density of particles.

α is a shape factor to account for the nonspherical shape of the particles.

$$V_Y = \frac{q}{(1-\Phi)A}$$

Where q is the instantaneous filtration rate.

A is the filter area.

Φ is the volume fraction of solids in suspension.

The force acting to remove the particle from the surface is a tangential force F_X, which can be obtained by integrating the shear stress over the particle surface.

$$F_X = \alpha 4\pi R^2 \tau_w$$

Where τ_w is shear stress at the cake surface.

For the case of particle release by sliding he stated that :

At any time during crossflow filtration, particles of a certain size R can be deposited if the tangential force and the normal drag force acting on the particles satisfy the inequality:

$$F_X \leq fF_Y$$

f is the coefficient of friction.

All particles with radii that satisfy the above inequality will be deposited on the cake surface. Larger particles will be entrained with the flowing suspension. As particles deposit and cake thickness increases, q decreases. This implies that smaller and smaller particles will be allowed to deposit on the cake surface. Eventually the filtration rate will be so small that small enough particles will not be available in the suspension and the cake will stop growing and a steady state will be reached (Fig.1.105).

For the case of particle release by rolling he stated that :

The hydrodynamic torque acting to remove the particle from the cake surface is obtained by:

$$T_X = R(\sin 60)F_X$$

This torque is balanced by a restraining torque given by:

$$T_y = R(\sin 30)F_Y$$

Particles (of a diameter R) for which $T_Y \leq T_X$ will not be deposited on the cake surface. At any given time the equality Ty=Tx will be satisfied for a certain R. All particles larger than This R will be removed from the cake surface. This occurs because the shear force tending to entrain the particles is proportional to the square of the particle radius and the normal drag force holding the particle on the cake surface is proportional to the first power of the particle radius.

NAVARRETE et al. (1994) Stated that the chances that a particle will reach the wall and stay there increase the larger the F_y/F_x ratio.

Where $$\frac{F_y}{F_x} = (\frac{\rho_s}{\rho_f})(\frac{3}{2}(\frac{q}{R\gamma_w}))^n$$

The ratio F_y/F_x increases:

1. the larger the leakoff flux toward the wall.
2. the smaller the particle size.
3. the smaller the shear rate.
4. the larger the ratio of particle-to-fluid density.

AHMED (1993) listed the forces acting on a sand particle transported through the wellbore annulus into the perforation (Fig.1.106).

a) The drag force (F_d):

The drag force tends to pull the particle in the direction of the flow in the perforation.

F_d = C_d* Surface area of particle* Dynamic pressure

$$F_d = C_d\pi(d_s)^2\rho_f V_p^2$$

Where: V_p is the fluid velocity through perforation.

ds is the grain diameter.

ρ_f is the fluid density.

Cd is the drag coefficient and is a function of Reynold's number (NRe).

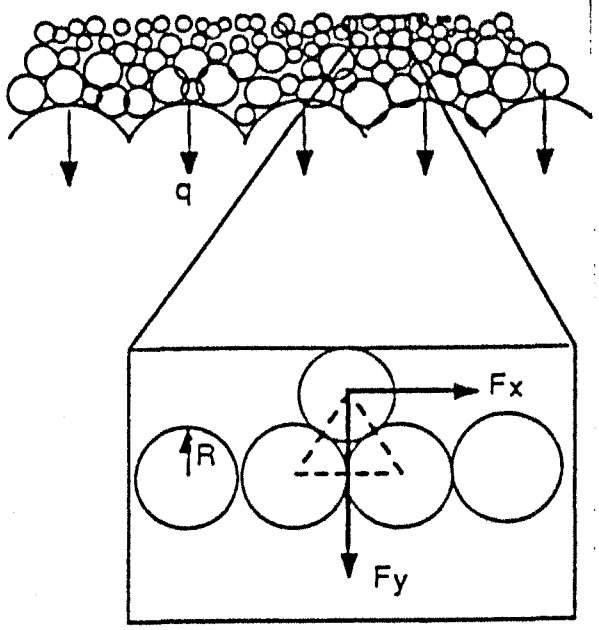

Fig.1.105: a schematic of the hydrodynamic forces acting on a particle at the filtercake surface (Jiao *et al.* 1994).

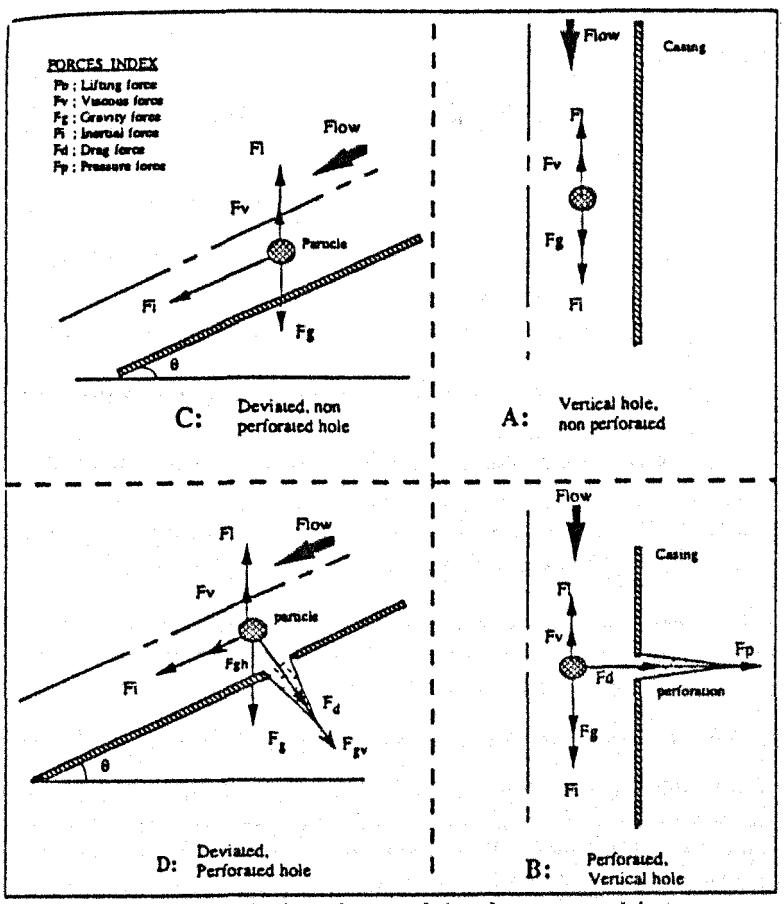

Fig.1.106: Types and directions of the forces working on a particle transporting into fluids in the wellbore (Ahmed 1993).

b) Force of Inertia (F_i):

Due to fluid acceleration. Causes the particle to resist to follow the fluid path into the perforation and tries to keep the particle moving in the same direction of fluid flow in the wellbore.

F_i = Mass of the particle * acceleration of the fluid in the wellbore

$$F_i = \frac{\pi}{6}\rho_s d_s^3 a$$

Where: ρ_s is the particle density.

c) Gravity force (F_g):

Which makes the particle settle downwards.

F_g = weight of particle = Mass of the particle * gravity factor

$$F_g = \frac{\pi}{6}\rho_s d_s^3 g$$

d) Lifting force (F_L):

Will lift or let the particle float into the fluid and acts opposite to the gravity force.

$$F_L = \frac{\pi}{6}\rho_f d_s^3 g$$

e) Viscous force (F_v):

Due to the shear stress of the viscous fluid on the surface area of the particle. This force tries to suspend the particle and to resist the settling rate of the particle.

F_v = shear stress * surface area of the particle

$$F_v = \pi d_s^2 \mu\gamma$$

f) Pressure force (F_p):

Due to the pressure gradient (or pressure drop).

F_p = area of perforation mouth * acting pressure drop (ΔP)

In all previous equations, the particle was assumed to be spherical in shape.

1.9 Conclusions

The following conclusions summarise the literature review results:

I- General conclusions regarding formation damage:

(1) Deep filtration is the result of several mechanisms such as the contacting of particles with the retention sites, the fixing of particles on sites and the breaking away of previously retained particles.

(2) The problem to be solved consists of relating the clogging rate to the various factors which define the system.

(3) The random movement of suspended particles in a tortuous flow path is mainly responsible for transporting the particles either directly to the grains or close enough to the grain surface for other forces to become effective.

(4) The final stage of pore plugging is related not only to the initial pore velocity and relative particle and pore sizes, but to the change in pore velocity as the pore spaces are blocked.

(5) As the oil droplets are deformable, conventional deep bed filtration theory developed for undeformable solid suspensions is not strictly applicable for dispersed oil droplets flow.

(6) The pressure drop during injection, along with an increase in the number of effluent particles, is an indication of particles being dislodged simultaneously.

II- For the linear injection of particle suspensions :

(1) Particle concentration of 1ppm and particle size from around 20 μm downwards, would significantly reduce the permeability of very high permeability sandstone cores.

(2) The ratio of mean pore size to mean particle size is not a simple criterion for explaining the damage to the cores.

(3) The submicron particles entered substantial invasion depths and were trapped at various locations in the core.

(4) There is an exponential relationship between permeability reduction and the particle concentration of the injected suspension.

(5) The rate of impairment decreased with increasing flow velocity and it is very sensitive to velocity changes at low velocity levels.

(6) The routine practice of using membrane filters to characterise or predict reservoir qualities of injection water can be misleading.

(7) The injectivity inverse versus pore volume injected plots showed four types of curves depending on the blocking mechanism.

III- For the linear injection of oil dispersions:

(1) Oil droplet capture occurs mostly on the porous medium surface when its size is smaller than the pore diameter and is restricted by the pore if its size is larger than the size of pore diameter. The small droplets can be retained in the pockets or crevices formed by the sand grains

(2) Matrix permeability decline is not linked closely to oil concentration, but it is linked to oil droplet size.

(3) When large droplets lodge in the pores, droplets following behind were then diverted to other nearby pores. When the flow rate, and hence the pressure drop, was increased abruptly, droplets which were lodged slip through the pores to flow downstream. They do not adhere to the surface of the sand grains.

(4) The droplets attached to the pore walls may reduce the effective pore diameter and help to restrict other droplets moving through the pore throat.

In general, solid suspensions were expected to exhibit well-bore damage and penetrate only a small distance into the formation. In contrast, oil droplets, after satisfying the maximum number of capture sites , may exhibit significant penetration distances without catastrophic permeability loss.

IV- For particle suspension plugging mechanism modelling:

(1) The rock matrix was modelled as having two continuing, parallel branches: one of small pore size in which plug-type deposits of fines may occur, and the other, of larger pore size, in which only surface nonplugging deposits occur. This assumption leads to the definition of the process of surface deposition and entrainment, and plugging deposition and entrainment [29].

(2) The particle blocking may be modelled as three separate mechanisms: gradual pore filling, pore throat blocking and filter cake formation. However all three mechanisms may occur simultaneously [103].

(3) The total pressure drop through a medium, when a particle suspension is injected, was modelled as the pressure drop over the damaged section plus the pressure drop over the undamaged section [24]. This required the invasion depth of particles to be experimentally measured.

(4) The matrix damage was modelled by introducing the concept of the damage factor and the volume filter coefficient which were assumed to be constants with time and can be measured experimentally [95]. These parameters are not constant with time.

(5) The particle invasion was modelled by introducing the transition time (the time at which no more particles invade the rock, i.e., the time at which the initial layer of external filter cake is completely formed). Based on the matrix grain size and the injected particle size, transition time can be calculated. Then the entire filtration process can be approximated by applying an internal cake filtration model before the transition time and an external cake filtration model after the transition time [60].

A similar model was developed which uses the critical jamming ratio at the entry face (ratio of pore throat to particle size) instead of the transition time [71].

The calculation of the transition time or the critical jamming ratio is a very complicated process requiring many assumptions.

(6) The invasion process has also been modelled by the relationship between solid particles concentration and instantaneous rock porosity $\emptyset_s$ which is based on the fact that part of solids from the suspension is retained in the matrix reducing its porosity [47]. The effect of the size of the particles was not considered in this model. A relationship between the initial permeability and the damaged permeability as a function of altered porosity was also developed in the literature [12].

The above two models (47, 12) assumed that the reduction in matrix permeability was due only to pore filling and there is no plugging or bridging of pore throat.

V- Droplets capture modelling: it was modelled by defining the filter coefficient and the flow diversion parameter, which both control the processes of droplet capture in the medium, from the emulsion influent and effluent concentration histories. Conversely, the flow restriction parameter, which characterises how effectively retained droplets are obstructing flow, was obtained from permeability reduction data [80]. This model depends completely on the experimental data and needs very accurate and careful monitoring of these data.

VI- Oil plus particles dispersion linear injection modelling: it was modelled depending on the concept of flow resistance in parallel (flow equal to the total pressure drop divided by the flow resistances) and on the concept of pore filling (the effect of particle size was not included). The equivalent concentration factor was introduced in this model. The equivalent concentration factor to oil droplet is set up, by which a certain concentration of oil may contribute the same permeability impairment as solid particles do at similar conditions in the experiments conducted. The permeability reduction contributed by oil droplets and solid particles were taken into account simultaneously in this mathematical model [108]. Again this model assumed that the reduction in matrix permeability is due to only pore filling and the plugging or bridging of pore throat was not taken in account.

VII- Some important facts drawn from literature:

(1) In the literature the filtrate loss velocity in hydraulic fracturing was simply modelled as the total pressure drop divided by the total flow resistance. As the two most important differences between the hydraulic fracture and the induced injection fracture lie in the time scale and the injected fluid viscosities of the fracturing operation, then the hydraulic fracture model could not be applied to the induced injection fracture process.

(2) In the literature it was assumed that the matrix damage in fractured systems is a near-fracture formation permeability reduction, so the linear geometry model equations were used to predict the permeability decline of the matrix near the fracture face.

The lack of the experimental work to simulate the matrix damage in a fracture injection system (caused by the produced oily water injection) and due to the importance of this subject, experimental programme to simulate the injection of produced water along a fractured slab is presented in this thesis. The last two assumptions were used in modelling and evaluating the matrix damaged extent in the fracture system. Also a dimensional analysis model to simulate the reduction in the injectivity with time was developed. An experimental comparison study of the matrix damage extent between the linear and the fracture systems was also performed.

CHAPTER TWO

EXPERIMENTAL PREPARATIONS

2.1 The objectives of experimental work

The objective of the experimental work was to asses the damage caused by flowing simulated produced oily water through a fractured sandstone slab and to compare the results of fracture injection and linear injection. A number of linear and fracture injection experiments were carried out for this purpose. The procedures of constructing the fracture slabs and preparing of the simulated produced water were explained in details in this chapter. The experimental procedures used in this study were explained and the measured and calculated variables were defined.
Each fractured slab experiment needed at lest five days to prepare and perform.

2.2 Experimental equipment

The fractured slab model can be seen in Figure 2.1. Fluid is allowed to enter the slab through the fracture inlet. Some of the fluid will travel along the fracture to reach the fracture outlet port and the rest will travel laterally through the fracture face into the rock matrix to be collected at six side outlets ports A1 to A3 and B1 to B3, three at each side.
Pressure transducers are mounted at the fracture inlet and oulet. The ports A1 to A3 and B1 to B3 were at atmospheric pressure. The volume of discharged liquid (at each port) over a time period and particle size distribution of the effluent (discharged fluid) samples was measured.

2.2.1 The Experimental Rig

The experimental rig was specially designed for the purpose of core flooding experiments. It consisted of :

(1) One glass tank with a capacity of 120 litres to store the oily water. Connected to this tank is a circulation pump to keep oil droplets and solid particles uniformly suspended in the brine during the experiment.

(2) Saturation tank connected to the flow line.

(3) A CO_2 cylinder connected to the flow line.

(4) Injection metering pump. It was a salt resistance pump with maximum injection pressure of 400 kPa and flow rate from 0 to 4.8 ml/s.

(5) A vacuum pump to evacuate the slab prior to saturation.

(6) Data logging system to log signals from pressure transducers to the computer. The inlet and the outlet pressure measured by the transducers were transformed into a set of pressure drop curves shown on the monitor.

A schematic of the experimental test rig is shown in Figure 2.2.

2.2.2 Construction and preparation of the fracture model

2.2.2.1 Slab Material:

The sandstone slabs used in the fractured slab models were prepared from Clashach sandstone which is a fairly homogeneous sandstone. It is an aeolian, quartz rich arenaceous sandstone with an average porosity of 14% and an average permeability of 300 mD. The sandstone is over 98% quartz and has a negligible clay content. It has a pore size range from 8 to 28 μm with an average of 18 μm[108].

2.2.2.2 Design of fracture technique:

The design of the fracture technique must ensure that a fracture is created in a similar manner to those created in the formation. Tensile fractures are induced around the wellbore therefore tensile fractures were required in the experimental rock samples.

A slab of rock 200x60x14 mm or 400x60x14 mm was cut from a bulk sample. Two grooves 0.5 mm in depth were cut along the length of the slab (on the top and bottom faces) in the middle .

A line load was then applied to the grooves by right angle section of aluminium held in a press. The compressive stresses applied at the grooves induced tensile stresses in the slab between the grooves and the slab fractured.The presence of grooves was essential to ensure a straight fracture. The fractured slabs were in two sizes:

Short slab with 200 mm length, 60 mm width and 14 mm height.

Long slab with 400 mm length, 60 mm width and 14 mm height.

For the linear injection slabs, the injection face of the slab was broken in the same way with dimensions of 30 mm length, 60 mm width and 14 mm height.

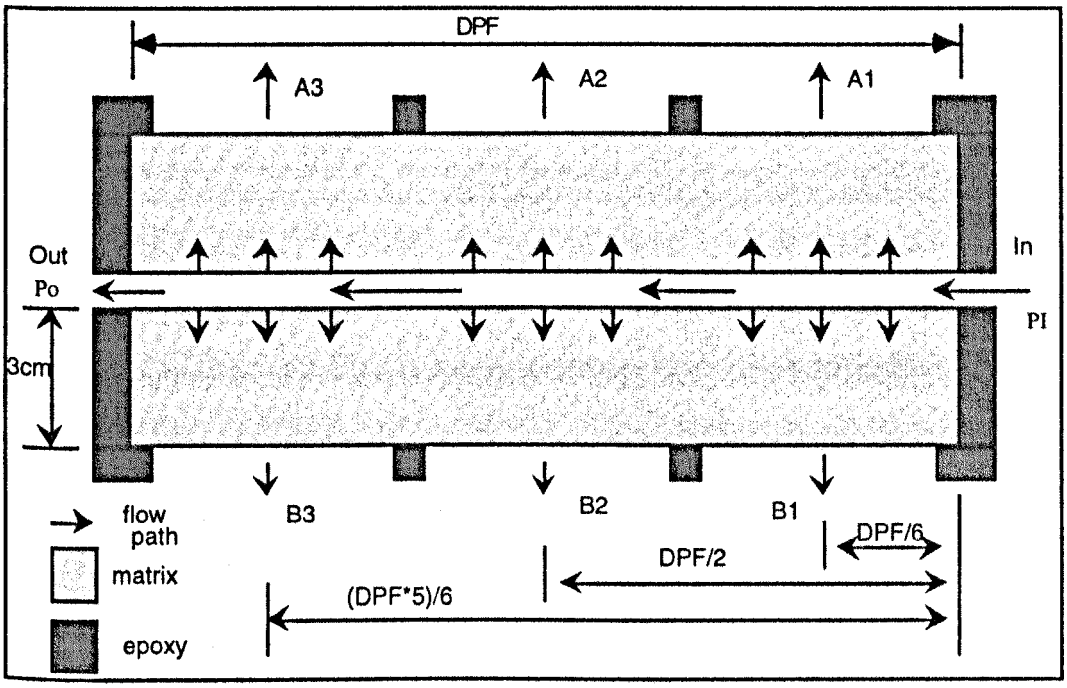

Fig.2.1: A complete flow diagram of the fracture.

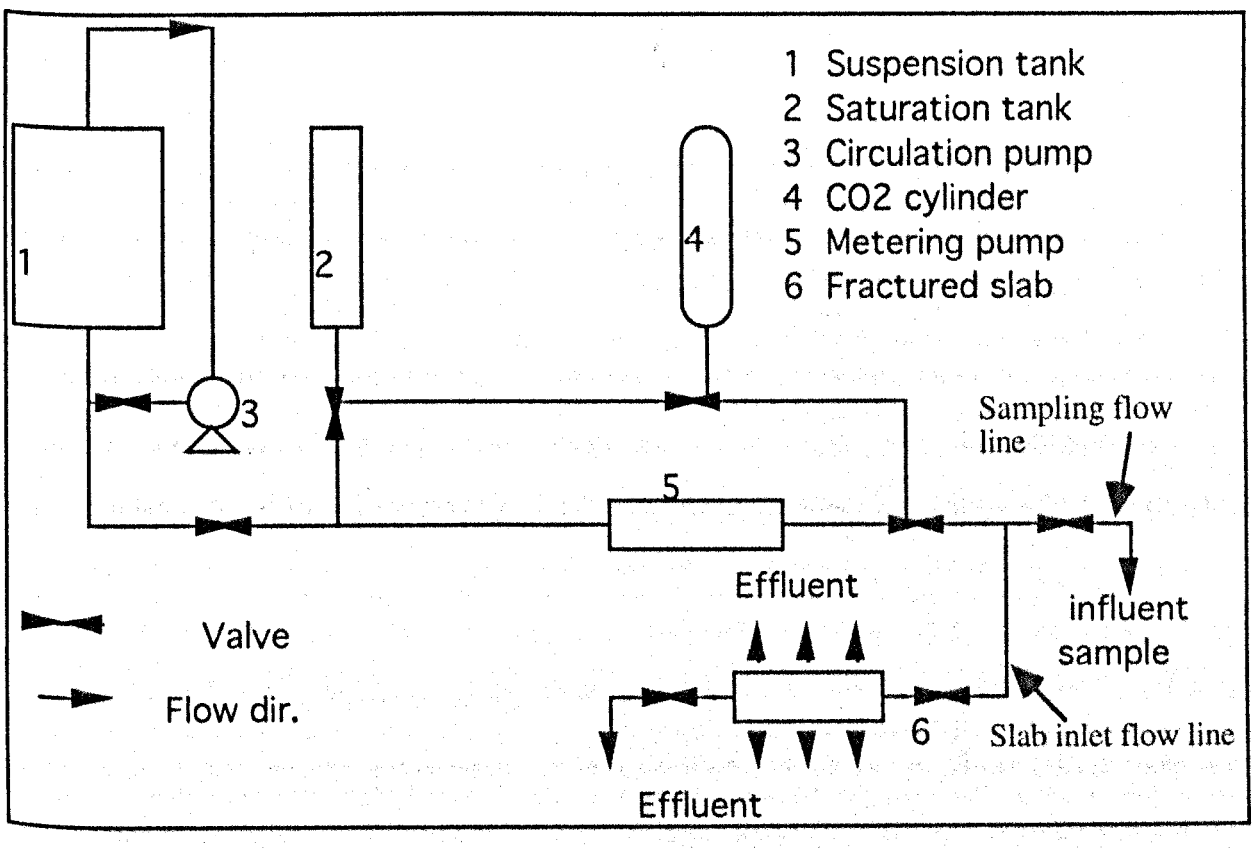

Fig.2.2:Schematic diagram of the experimental rig with the fractured cell is loaded in its place.

2.2.3 Resin encapsulation of the fractured slab model

After fracturing, the slab was placed in a constant temperature and humidity oven for 24 hours at 60°C to dry it out. Then the outside surfaces of the slab (excluding the fracture face) were coated with araldite resin in order to avoid any by-pass flow during the experiment. Guides were then placed along the fracture surface to hold it open. Nylon flow ports were glued in position at the fracture inlet and outlet and the whole slab was then fixed in position in a mould and encapsulated in epoxy resin prepared with the following ingredients:
39.7%wt resin; 39.7%wt marble flour; 19.8%wt hardner; 0.8%wt accelerator. The marble flour adds strength to the epoxy resin.

After 3 days at room temperature, the encapsulated slab was released from the mould and six equal area side outlets (slots) were machined in the epoxy resin. The rock face was sand blasted to ensure no traces of resin remained. The slab was then assembled in the flow rig by bolting on the side manifold (containing the flow ports); each port collected fluid from one side outlet area (Figs.2.3 and 2.4).

The linear injection slabs were also moulded with the same materials. The size of these slabs was 6 cm in width, 1.4 cm in higth and 3 cm in length.

2.2.4 Fractured slab vacuuming and saturation

Once the slab was loaded into the test rig, it was necessary to vacuum it for one and a half hours at -1 bar. Then carbon dioxide was allowed to enter the slab at a pressure of 2 bar to purge the cell of any residual gases. A second vacuum cycle was carried out for at least one and a half hours at -1 bar. This process was done to remove any air or gas in the pore space of the slab. The slab cell was then saturated with filtered 5% NaCl brine. The cell was left over night to saturate.

2.2.5 Testing of the fractured slab

At the start of each experiment two tests were run with 5% NaCl as the injection fluid to ensure the internal integrity of the slab and to ensure it was not internally damaged before the main experiment was run.

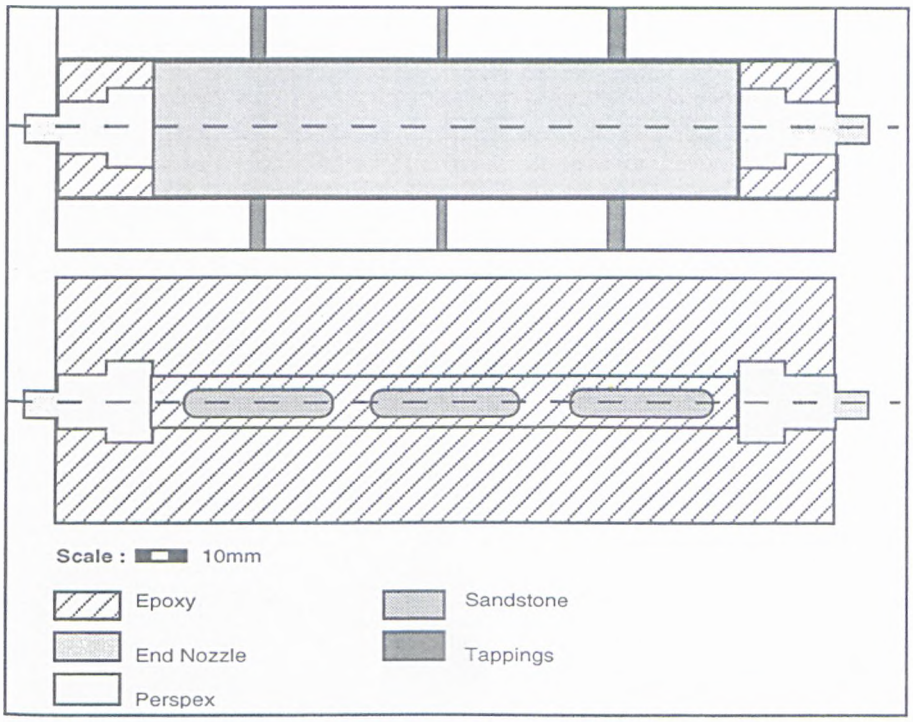

Fig.2.3. Plan View and 1st Elevation of the 20 cm long fractured slab model.

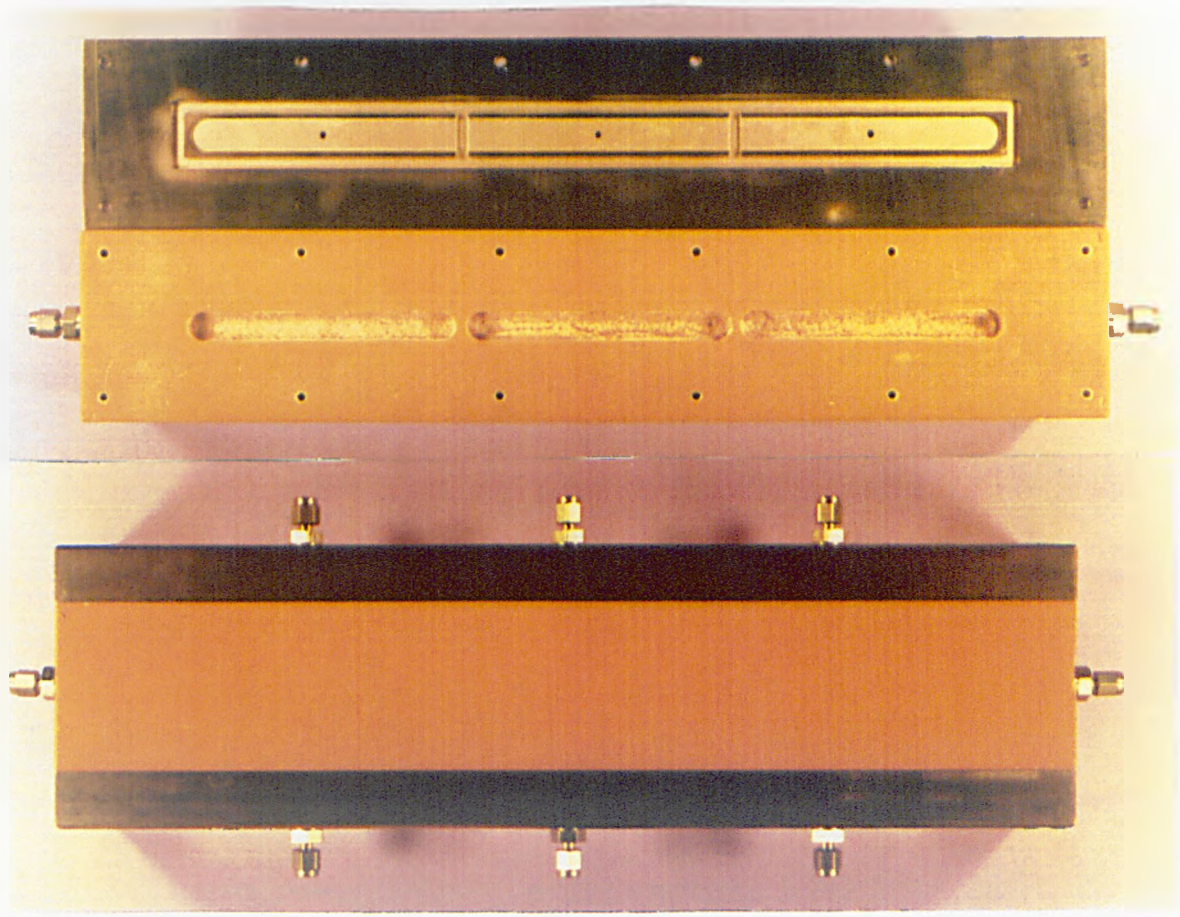

Fig.2.4 The long fractured slab model before and after bolting on the side manifolds.

Test 1 was run with fluid flow along the fracture only with no side ports open until a constant flow rate was established at constant pressure drop and this test was repeated several times at different inlet pressures. The pressure drop along the fracture was used to calculate fracture aperture and fracture permeability as can be seen later in section 2.6.

Test 2 was run with injection along the fracture with all side ports open and the initial permeability baseline through the slab matrix was measured

During the experiment the discharge point must be fixed in a stable position as changing the position will affect the flow distribution along the fracture and through the side outlets.

For the linear injection cells, a 5% NaCl Brine was allowed to flow though the slab. When steady state was reached, the initial Brine permeability of the slab was measured.

The slabs were ready then for the damage test experiments.

2.2.6 Preparation of the simulated produced oily water

Oil Dispersion:

Crude oil was emulsified into an oil-in-brine dispersion. A great deal of energy was required to overcome the interfacial tension between oil and brine when a dispersion was prepared. An emulsifying agent was added which had two functions:(1) to decrease the interfacial tension between the dispersed phase (the oil) and the continuous phase (the brine). (2) to stabilise the dispersed phase by forming a film around the oil droplets.

Thistle field crude oil with a density of 0.86 g/cm^3 and viscosity of 1.36 cp was used. The brine was prepared by adding 5 % by weight NaCl to distilled water and the mixture was filtered through 0.45 μm and 0.22 μm millipore filters. Synthetic surfactant Triton X-67 and Triton X-15 were used as the emulsifying agents.

Triton X-67 at a concentration of 0.15 g/cm^3 of crude oil was first melted at 40°C and then mixed with a predetermined volume of the Thistle crude oil. This mixture was poured into a beaker which contained 4 l of 5% NaCl solution. At the same time Triton X-15 at a concentration of 0.1 g/cm^3 of crude oil was added to the solution and stirred at constant speed.

The factors which governed the size distribution of oil droplets were the container dimensions, the stirring speed, the stirrer shape and stirring time. The mixing container dimensions, the stirer shape and the stirer speed were kept constant. So the main factor that governed the droplet

size distribution was the stirring time. The mixing beaker had a diameter of 18 cm and a mixing volume of 4000 cm^3.

An emulsion sample was taken each half hour to be tested by Malvern Master Sizer particle size analyser to check the droplet size distribution, then the sampling time was gradually reduced to 10 minutes. When the required droplet size distribution (an example of the size distribution can be seen in appendix III) was reached, the emulsion was diluted to the correct concentration.

Solid particles:

The solid particles (alumina particles) were diluted in a 1 *l* beaker and positioned in an ultra sonic bath to be dispersed more efficiently. A sample was taken from this dispersion to check the particle size distribution by Malvern Master Sizer.

The solid particles were added to the emulsion, after the emulsion was diluted to the final oil concentration, just prior to the damage test injection. This procedure was similar to what is happening in the real situation in the field (solid particles from the flow line were entering the flow stream as the produced water flow from the treating unites to the well head).

2.2.7 Rheological properties of simulated produced oily water:

Zhang (1994) investigated the rheological nature of 0 to 500 ppm oil emulsified in a 5%NaCl Brine and the following conclusions were obtained:

Newtonian behaviour was the general case.

The viscosity of the brine was measured as 1.1 cp.

The viscosity of the 40 ppm oil emulsion was 1.15.cp

The viscosity of the 100 - 200 ppm oil emulsion was equal to 1.2 cp

Yuhua[106] investigated the effect of adding solid particles to an oil-water emulsion on the viscosity of the emulsion. The general conclusion from his study was that the addition of solid particles at a very low concentration (volume fraction of solids of less than 0.014) does not have any obvious effect on the emulsion viscosity.

The solid particle concentration in this study was less than 100 ppm (volume fraction of less than 0.0001), so the effect of particle concentration on viscosity was neglected.

2.3 Experimental Procedures

When the tank was filled with the simulated produced water, the dispersion was stirred continuously to prevent particle precipitation.

The following procedure was followed

1. The slab inlet flow line was closed and the sampling flow line was opened. The injection metering pump was started and a sample the injected simulated produced water from the sample line was taken to measure of the influent specifications (the mean size, the size distribution and the obscuration) by using the Malvern Master Sizer. The Obscuration is a measurement of the degree of fluid clearness.
2. The sampling line was closed and the slab inlet line was opened allowing the simulated produced water to flow along the fracture and through fracture faces into the rock matrix.
3. After 10 min. the flow rates along the fracture and through the side outlets were measured. Also the inlet and the outlet pressure were recorded. Then effluent samples (from all the outlets) of the same volume (usually 75 ml) were taken to be analysed by the Malvern sizer to measure the size distribution and the suspension obscuration.
4. Step 3 was repeated every hour.
5. The injection should be continuous until the end of the day.
6. At the end of the day another influent sample from the sampling line was taken to be analysed.
7. The metering pump was switched off, the slab cell was disconnected and the slab cell inlet and all the slab cell outlets were closed.
8. The circulation pump was switched off, the injection tank was emptied and then the tank and the flow lines were cleaned several times by using detergent.
9. In the next day the tank was filled with a fresh simulated produced water with the same droplets and particles size distribution and concentration similar to the one which was used in the previous day.
10. Steps 1 to 8 were repeated but this time the first reading was taken after one hour.

The same experimental procedure was followed for the linear injection experiments. The pressure readings for the linear injection experiments and the size distribution of the effluent was taken at the same time intervals as in the fractured slab injection experiments.

2.4 The selected Flow rate:

All the experiments were carried out under a constant flow rate per unit area equal to 0.422 cm/s, which is equivelant to 2037 m^3/day or 12810 *bbl*/day injection through a 7 inch diameter well bore with formation thickness of 10 m.

For the linear injection, the slab face area was equal to 8.4 cm^2, therefore the flow rate was chosen to be 8.4 * 0.422 = 3.55 ml/s.

For the fracture injection, the fracture flow area was equal to 0.14 cm^2 and all the flow was injected through the fracture inlet, therefore the injection flow velocity was equal to 3.55/0.14 or 25.3 cm/s.

2.5. Post Test Techniques

The samples were cut open and photographs of the fracture faces taken to reveal any external mud cake that had formed. The fracture face surface was inspected by an optical microscope.

2.6 Measured And Calculated Variables

Pressure drop through side outlets was calculated (depending on the distance of the outlet from the fracture inlet) as follows:

Pressure drop from fracture face to side outlets A1 and B1 (PDS1) = $PI - \frac{PDF}{6} - PS$

Pressure drop from fracture face to side outlets A2 and B2 (PDS2) = $PI - \frac{PDF}{2} - PS$

Pressure drop from fracture face to side outlets A3 and B3 (PDS3) = $PI - \frac{PDF*5}{6} - PS$

Where PI is the inlet pressure.

Po is the outlet pressure along the fracture.

PS is side outlet pressure PS = 0.0 psig

PDF is pressure drop along the fracture = PI - Po

Analysing influent and effluent samples by Malvern master sizer gave the following quantities:

Particles Mean diameter (Ds) and particle size distribution

Droplets Mean diameter (Do) and droplet size distribution

Influent suspension Mean diameter and size distribution

Effluent suspension Mean diameter and size distribution for all outlet effluent volumes.

Influent suspension Obscuration

Effluent suspension Obscuration for all outlet effluent volumes.

The Obscuration is a measurement of the degree of fluid clearness. As the particle or droplet concentration of the fluid sample increases, the clearness of this fluid become lower and its Obscuration increases.

The collected samples for Malvern size analysis were all of constant volume; the instrument was calibrated and the same technique used for each measurement.

Since all the collected influent or effluent samples had the same volume and the Malvern was operated at a constant stirring speed all the time, then it was possible to use mean size ratio expression to measure the change in the mean size during the experiment time and to use the concentration ratio to measure the change in the concentration.

Mean size ratio (MSR) = Mean size of effluent sample / influent Mean size

Concentration ratio (CR) = Obscuration of effluent sample / influent Obscuration

Thus, the measured mean size and the obscuration was always related to the initial (influent) mean size and obscuration.

The obscuration was used instead of the volume percent because the volume percentage of the particles and droplets were very small (compared with the brine volume) which resulted in very similar readings each time.

Permeability Calculations:

The fluid was allowed to flow into the slab from a single inlet orifice connected to the fracture inlet opening, so the fluid will enter the fracture then flow in the axial direction through the fracture and in the lateral direction into the slab matrix.

a) The fracture aperture was calculated by using the following equation (after Jones et al):

$$Q = 5.06*10^4 W\left[\frac{\Delta p b^3}{fL\rho}\right]^{0.5}$$

Where Q: is the inlet flow rate (bbl/day)

W: is the width of fracture face (ft)

Δp: is the pressure drop along the fracture when the side outlets are closed (Test 1)

b: is the fracture aperture (in)

L: is the length of fracture (ft)

ρ: is the fluid density (lb/cu ft)

f: is friction factor and estimated (by using the data presented by Jones) to be equal to 0.6

b) The fracture permeability was calculated by using the following equation (after Jones):

$$k_f = 5.39*10^5 \mu \left[\frac{bL}{f\Delta p \rho} \right]^{0.5}$$

c) Matrix Permeability was calculated by Darcy's law :

$$k_m = \frac{Q\mu L}{A\Delta p}$$

Where ΔP : the pressure drop through middle side outlet (PDS2)

Q : the total side flow rate

A : the fracture face area

L : the length of the flow path from the fracture face to the side outlets (3 cm)

The permeability ratio (PR) was calculated by dividing the damaged permeability at a specific time by the initial permeability.

For the linear injection experiments (no fracture was present), the permeability was determined by using Darcy's law.

CHAPTER THREE

EXPERIMENTAL WORK AND RESULTS

3.1 Introduction

This experimental work is an attempt to study the flow of fluids along induced fracture.

The study started with the effect of pressure drop along a fracture, pressure drop through side outlets, matrix permeability and the impact of fracture width on the flow rate value along fracture outlet and through side outlets A1 to A3.

After studying the flow pattern of clean salt water through fractured slabs, the damaging effect of solid particle suspensions, the damaging effect of oil emulsions and the combined damaging effect of particles and oil droplets on the matrix permeability were examined. This was done for 20 and 40 cm long fractured slabs.

Linear injection experiments, with the same injected fluid composition as in the fractured slab experiments, were carried out so that a comparison study between the two injection systems can be made.

The change in effluent particle and/or droplet concentration and mean size along the fracture and through the three side outlets A1, A2 and A3 (Fig.2.1) with time were monitored for each experiment to see the effect of injection fluid composition on the degree of particle and/or oil droplet capture within the matrix.

The effect of rock matrix heterogeneity on the matrix blocking profile was investigated for two non-homogeneous fractured slabs, one was 20 cm long and the other was 40 cm long.

The filter cake accumulation on the fracture face and its erosion process was investigated carefully using different solid particle sizes.

In some of the experiments, a fluid leak in the fractured slab cell was noticed. So the results of these experiments were not reported in this study.

3.2 Flow distribution along fractures and through fracture faces

Clean brine was injected into the fractured slab through the fracture inlet (Fig.2.1). Some of the injected fluid flowed through the rock matrix (perpendicular to the fracture face) to reach the side outlets A1 to B3 and the rest flowed along the fracture to reach the fracture outlet. The flow through the matrix perpendicular to the fracture face at a certain location depends on how far is this location from the fracture inlet. The flow through the matrix to the outlets A1 and B1

was higher than the flow through outlets A2 and B2 as A1 and B1 were close to fracture inlet. The percentage of fluid flow at fracture outlet to the total inlet flow and the percentage of fluid flow through side outlets to the total inlet flow dependents on several interconnected factors. These factors are the pressure drop along the fracture, pressure drop through the side outlets, fracture aperture and rock matrix permeability.

At the beginning of each experiment a constant inlet flow rate test was carried out to test the integrity of the slab by flowing a 5%NaCl solution along the fracture while the side outlets A1 to B3 were closed. Then all the side outlets were opened and flow through all ports was started. The result of the fracture flow test was used to measure the fracture aperture by using the cubic law; the results of the second test was used to study the flow rate along the fractured slabs and through side outlets and to determine the rock matrix initial permeability.

The results of 10 experiments with long slabs (40 cm length) were used to study the flow distribution. The summary data is shown in Table 3.1.
The measured apertures of the fractures were between 0.3 and 0.54 mm.
The results of all the tests were combined to characterise, generally, the flow distribution in the cell.

3.2.1 The effect of the pressure drop along a fracture

Figure 3.1 shows the general relationship between the pressure drop along the fracture and the fluid flow along the fracture and through side outlets (where Q_o is the fracture outlet flow rate and Q_s is the total side outlets flow rate). For low values of pressure drop less than 0.25 atm the two values of the flow along the fracture and through side outlets are close together with no clear trend. As the pressure drop increased over this value, the total flow through side outlets starts to increase at the expense of the flow along the fracture.

Figure 3.2 shows the relationship of the flow distribution through the fracture face (or through side outlets) with the pressure along the fracture. Always the flow through A1 (the closest outlet to the fracture inlet) was higher than the flow through A2 and A2 flow was higher than A3 flow (with very few exceptions due to internal matrix heterogeneity).

At low pressure drops along the fracture, the flow rates through the three outlets were similar. As the pressure along the fracture increased the difference between the flow values through the three side outlets started to increase. This effect was equivalent to the effect of increasing fracture length (by increasing the fracture length, in fact the pressure drop along the fracture was increased).

3.2.2 The effect of the pressure drop through side outlets

For pressure drops less than 0.15 atm the flow along the fracture was higher than the total flow through side outlets. For higher values of pressure drop (as the pressure drop started to overcome the rock matrix resistance) the total flow through side outlets was higher than the flow along the fracture with clear difference (Fig.3.3).

The flow distribution through side outlets showed that at low pressure drops through side outlets (less than 0.2 atm), the flow rate through the three side outlets was similar. As the pressure drop increases the difference became greater until the pressure drop approached 0.35 atm. At this point the gap between the side flow rates started to decrease again (Fig.3.4) which may be due to the higher pressure drop redirecting fluid through the matrix at outlet A3 rather than flowing through the fracture outlet.

3.2.3 The effect of the matrix permeability

In the range of permeability for the slabs used, the flow through the side outlets was higher than the flow along the fracture and the difference between the two flows increased as the matrix permeability increased (Fig.3.5).

As the matrix permeability increased, the difference between the flow through the three side outlets increased (Fig.3.6).

3.2.4 The effect of Fracture aperture

The pressure drop along the fracture was highly affected by the fracture aperture. As the fracture aperture decreased, the pressure along the fracture increased (Fig.3.7). By reducing the fracture aperture from 0.5 mm to 0.4 mm the pressure drop along the fracture increased from 0.15 to 0.3 atm.

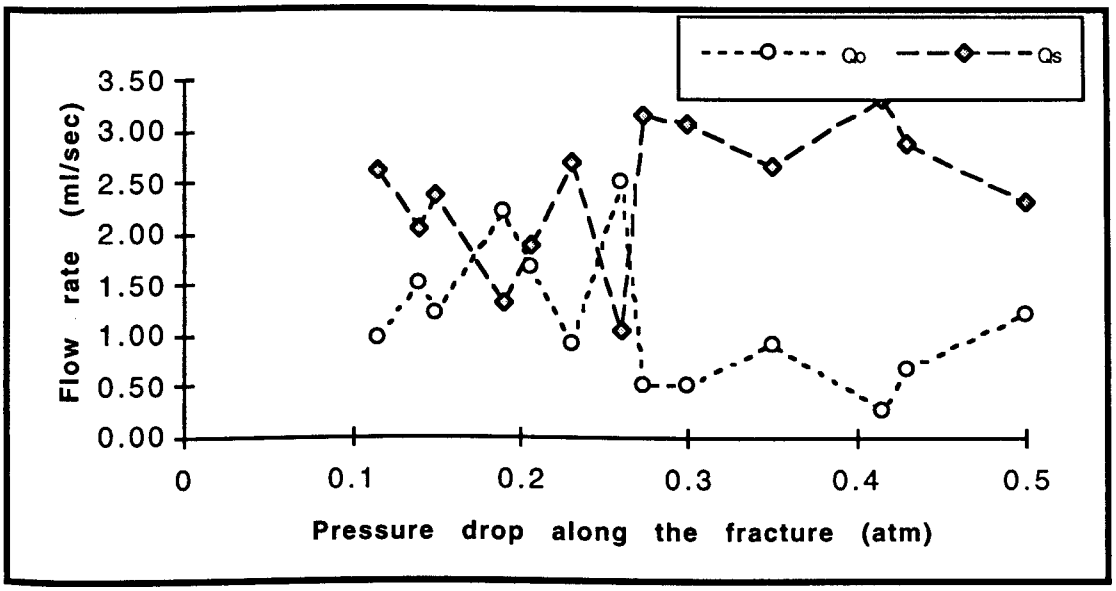

Fig.3.1: The change in flow rate along the fracture (Q_o) and through side outlets (Q_s) versus pressure drop along fracture.

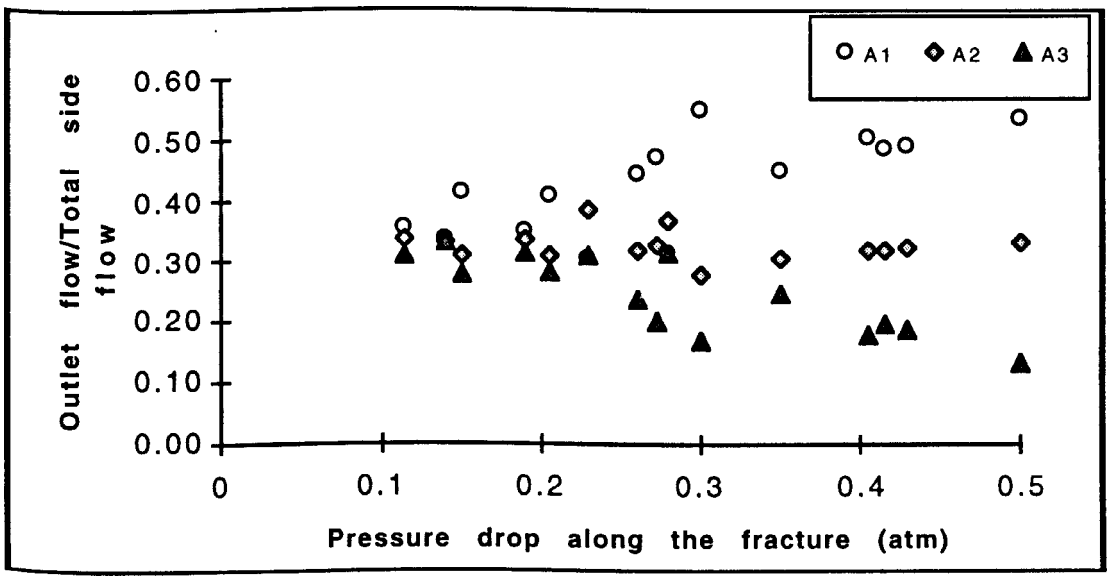

Fig.3.2: The side outlets (A1, A2, and A3) flow distribution versus pressure drop along fracture.

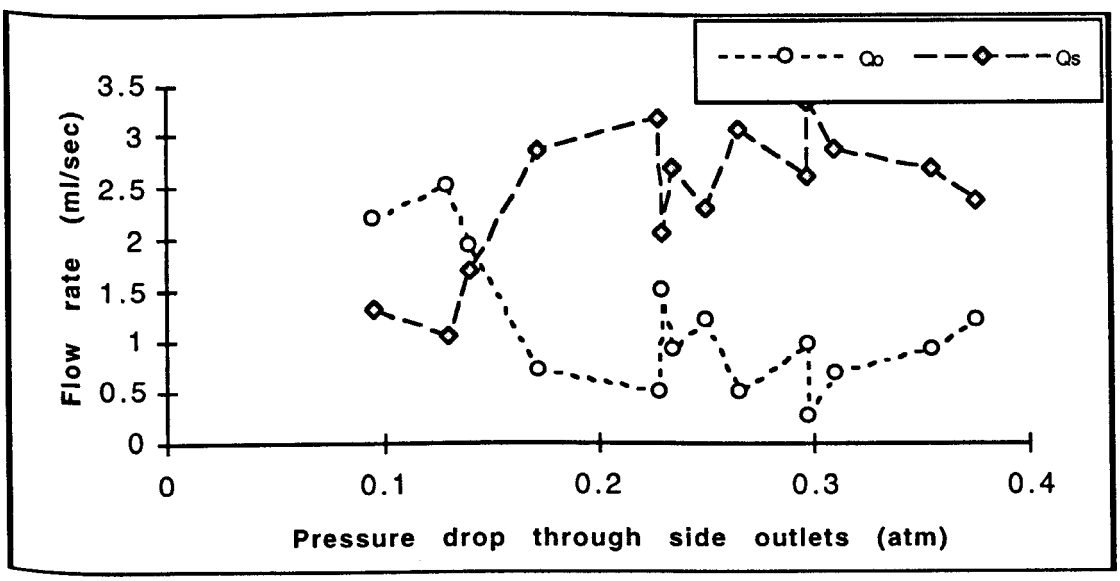

Fig.3.3: The flow rate along the fracture (Q_o) and through side outlets (Q_s) versus pressure drop through side outlets.

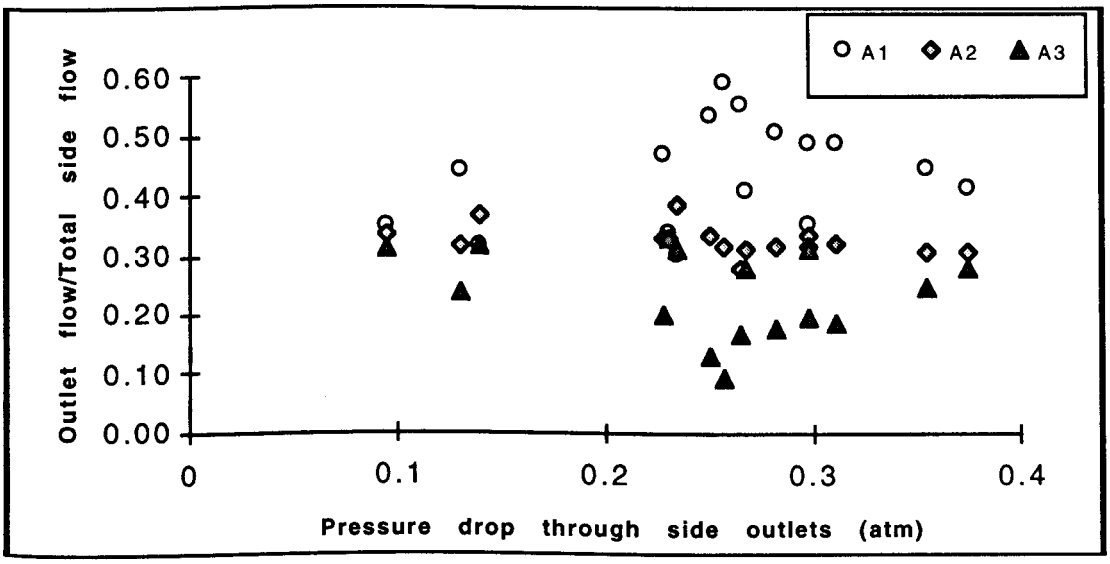

Fig.3.4: The change in side outlets (A1, A2, and A3) flow distribution versus pressure drop through side outlets.

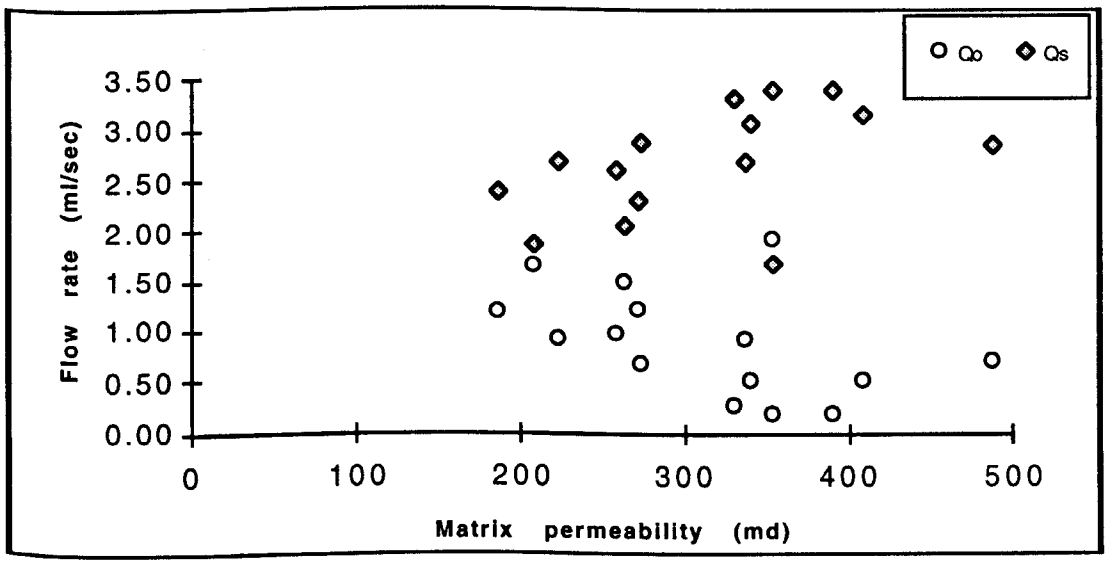

Fig.3.5: The flow rate along the fracture (Q_o) and through side outlets (Q_s) versus rock matrix permeability.

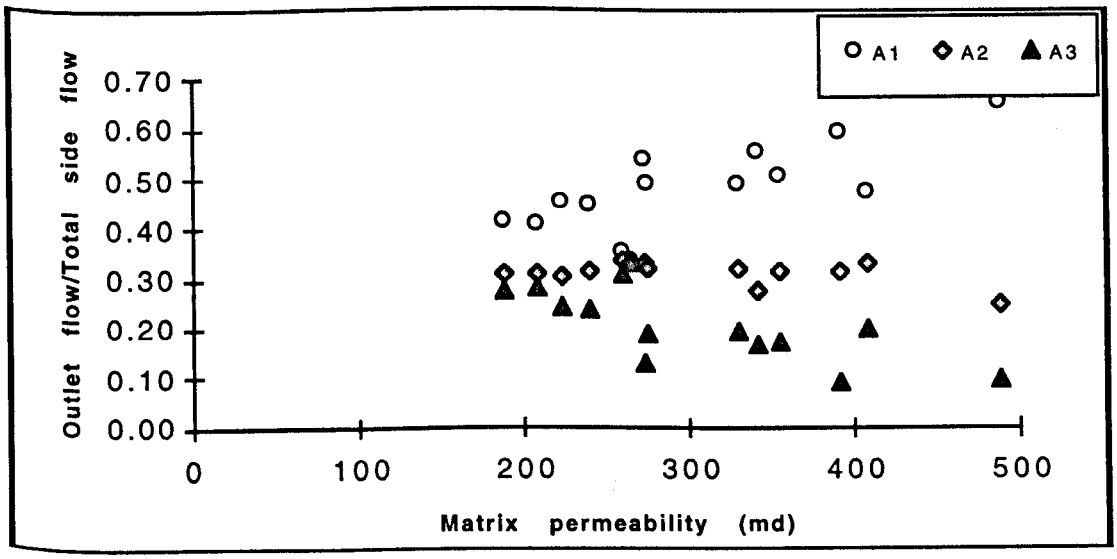

Fig.3.6: The change in side outlets (A1, A2, and A3) flow distribution versus rock matrix permeability.

As the pressure drop along fracture increased, the pressure drop through the side outlet decreased.

3.3. Matrix permeability alteration due to injection of simulated produced water along short fractures

20 cm long short fractured slabs were used to study the permeability alteration of the rock matrix due to:

(1) Oil droplets size and concentration effect.

(2) Solid particles size and concentration effect.

(3) Combined oil droplets and solid particles size and concentration.

The tests lasted between 9 to 12 hours with an inlet flow rate of 3.56 ml/s injected through the fracture inlet port. This is a high flow rate per unit flow area compared with the injection flow rate in the real field injection operations (the area of the slab inlet face equal to 9 cm^2, which gives a flow velocity of 4 cm/s). A complete description of the operating conditions of these experiments is presented in Table 3.2.

These tests were performed with the following:

Two different alumina particle size groups (Fig.3.8) with a particle concentration of 10 and 15 mg/l. The first group consisted of less than 6 μm particles with a mean size diameter of 2.1 μm and the second group was less than 20 μm particles with a mean size diameter of 4.7 μm (Table 3.3). Both sizes were used at both concentrations.

Two different oil droplet size groups (Fig.3.9) with an oil concentration of 100 and 200 mg/l were used. The first group was less than 10 μm droplets with a mean diameter of 3.6 μm and the second group was less than 16 μm droplets with a mean diameter of 6.2 μm (Table 3.4).

The pressure drop through the side outlets was adjusted at the start of each experiment to be higher than the pressure drop along the fracture as is the case in the real field fracture injection system. The results are presented as permeability ratio (the damaged matrix permeability divided by the initial matrix permeability) versus injection time.

3.3.1 The effect of oil droplet size and concentration

The emulsion of 100 mg/l and 3.5 μm droplet mean size caused no reduction in the matrix permeability even after 11 hours of injection (Fig.3.10).

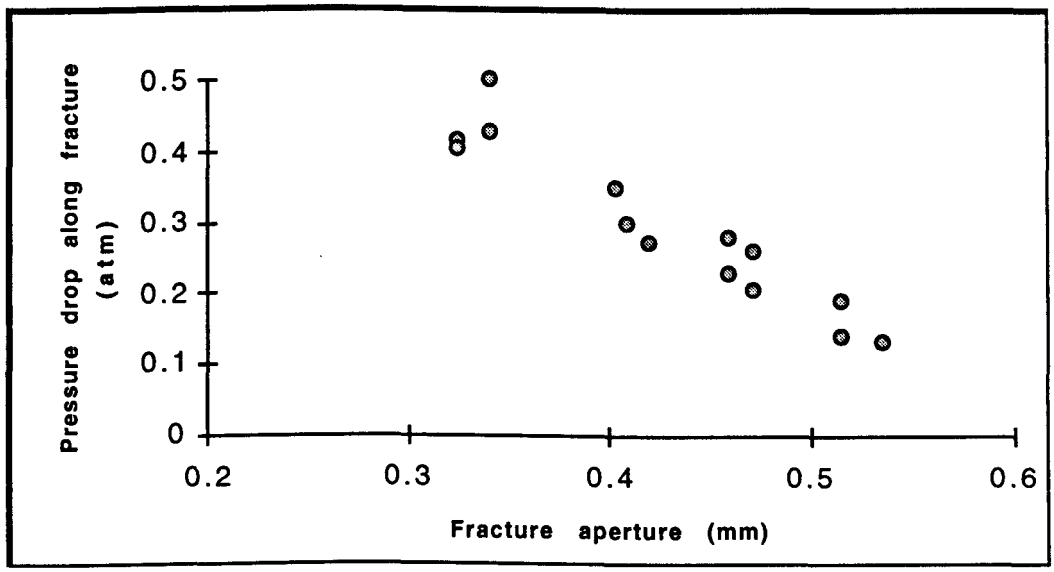

Fig.3.7: The pressure drop along the fracture versus fracture aperture.

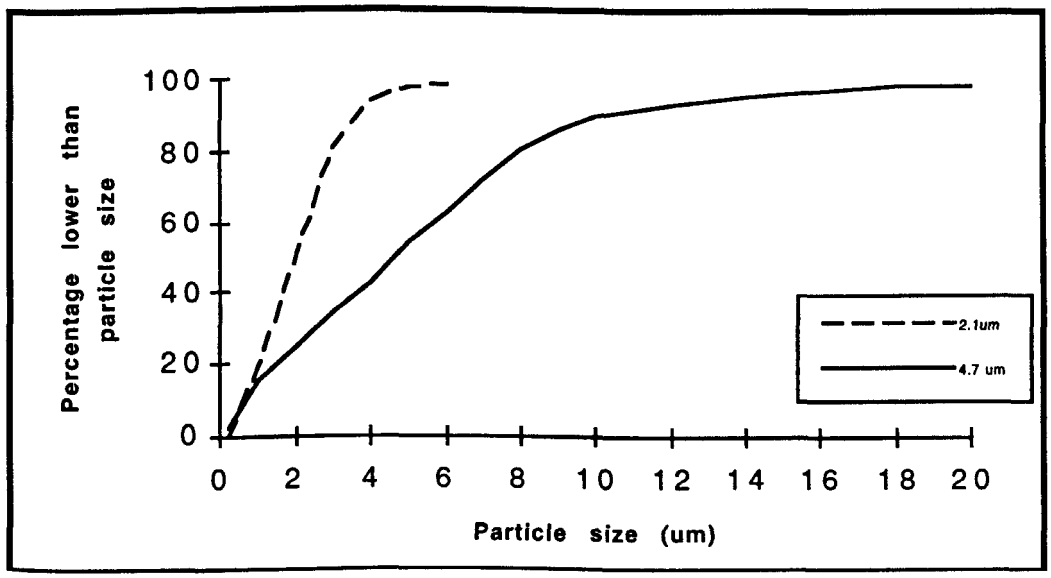

Fig.3.8: Particle size distribution of the two particle groups.

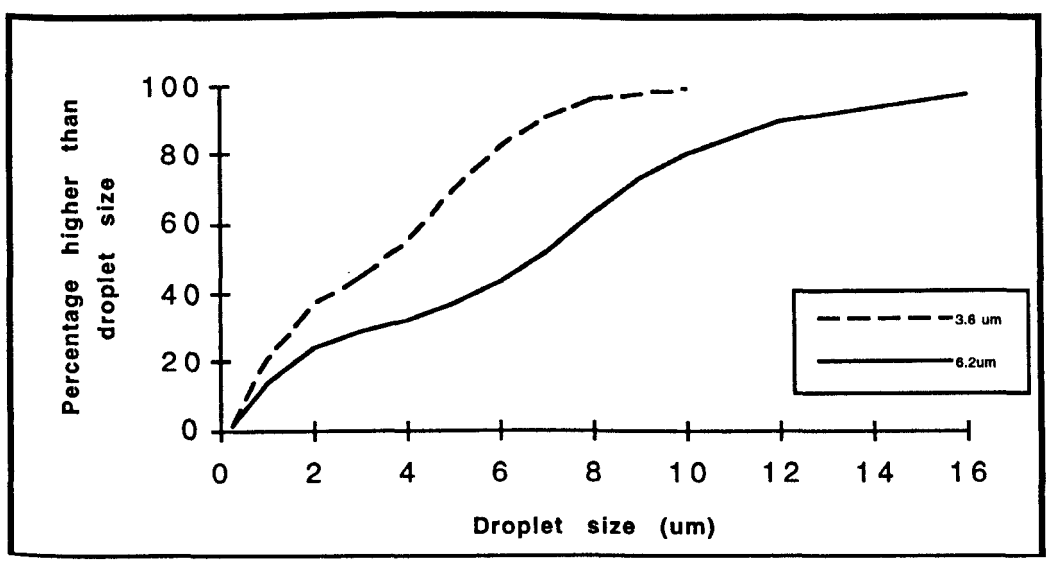

Fig.3.9: Droplet size distribution of the two droplet groups.

Increasing the droplet size from 3.5 μm (experiment no. 50) to 6 μm (experiment no. 51) at the same oil concentration of 100 mg/l resulted in a very small reduction in the matrix permeability of 2% after 11 hours of injection (Table 3.5).

Increasing the oil concentration from 100 mg/l to 200 mg/l (exp.52) at a constant droplet mean size around 3.6 μm has the same effect as increasing droplet mean size. The exception was with 200 mg/l concentration there was a more rapid reduction in permeability after 11 hours giving a 6% loss in matrix permeability after 11 hours of injection.

In general for fracture injection, emulsions of less than 200 mg/l oil concentration with a droplet mean size of less than 6 μm caused a very small reduction in matrix permeability after a very long injection time.

Some times there is an increase in the permeability ratio at the early time of injection. This may be due to the removal of the fines by the flowing oil which produced an increase in permeability. Or the increase in pressure drop (while permeability is constant) causes an increase in side flow rate, which intern increased the permeability ratio.

3.3.2 The effect of solid particle size and concentration

The suspension of the 10 mg/l solid concentration and 2.1 μm mean size particles (experiment no. 56) caused a reduction in permeability equal to 16% after 9 hours of fracture injection (Table.3.5).

Increasing the particle mean size diameter from 2.1 μm to 4.7 μm at the same particle concentration of 10 mg/l (experiment no.53) caused a greater reduction in the matrix permeability equal to 27%.

In general, increasing the particle concentration in the case of 2.1 μm particles had little further effect on the matrix permeability, whereas for the case of 4.7 μm particles, increasing particle concentration from 10 mg/l to 15 mg/l caused a further great reduction in the matrix permeability.

For the particle mean diameter of 2.1 μm, increasing the particle concentration from 10 mg/l to 15 mg/l (experiment no. 58) resulted in a reduction in the matrix permeability of 21% at the end of the experiment. For the 4.7 μm mean size particles, increasing the particle concentration from 10 mg/l to 15 mg/l (experiment no. 49) caused a much greater reduction in matrix permeability of 43 % at the end of the experiment.

Figure 3.11 shows the reduction in permeability ratio (damaged matrix permeability divided by the initial matrix permeability) with time for experiments 56, 53, 58 amd 49.

At 10 mg/l particle concentration, increasing the particle size from 2.1 μm to 4.7 μm had little effect on matrix permeability. Whereas at 15 mg/l particle concentration, increasing particle size from 2.1 μm to 4.7 μm causes a greater reduction in matrix permeability.
From the tests, increasing the concentration of the 4.7 μm particles is the main factor in matrix permeability reduction with time.

3.3.3 Combined effect of oil droplets and solid particles

At a constant oil concentration of 100 mg/l and a constant solids concentration of 10 mg/l, increasing the particle size from 2.1 μm (experiment no. 33) to 4.7 μm (experiment no. 46) increased the reduction in matrix permeability from 15% to 26% (after 11 hours of injection). Whereas at zero particle concentration and at 100 mg/l oil concentration, increasing droplet size from 3.5 μm (experiment no. 50) to 6 μm (experiment no. 51) increased the reduction in matrix permeability from 2% to only 8% . This shows the ability of particles to cause higher permeability damage than oil droplets in fracture injection (Fig.3.12 and Table 3.5).

At a constant mean particle size and concentration and constant mean droplet size, increasing oil concentration from 100 mg/l (experiments no. 25 and 54) to 200 mg/l (experiments no. 39 and 55) resulted in some reduction in matrix permeability in the first 8 hours but after that the two curves converge to read nearly the same value (Fig.3.13 and Table 3.5). This indicated that the oil concentration factor was very important in the first stages of fracture injection but its significance reduced as injection time proceeded.

At an oil concentration of 100 mg/l and droplet mean size of 3.5 μm, the permeability reduction caused by the 2.1 μm solid particles at 10 mg/l concentration (experiment no. 25) was almost identical to the reduction caused by the same particles at 15 mg/l concentration (experiment no. 40). This was also the case with the 4.7 μm particles (experiments no. 54 and 47) but with a slightly greater reduction in permeability ratio for the case of 15 mg/l particle concentration (Fig.3.14 and Table 3.5).

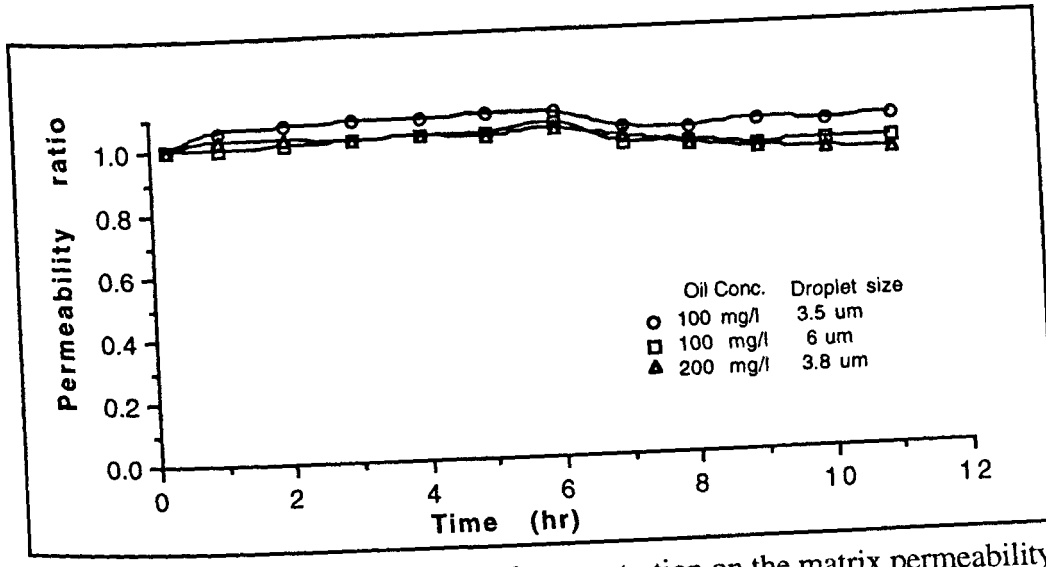

Fig.3.10: Effect of oil droplet size and concentration on the matrix permeability ratio (SFI exps. 50, 51, and 52).

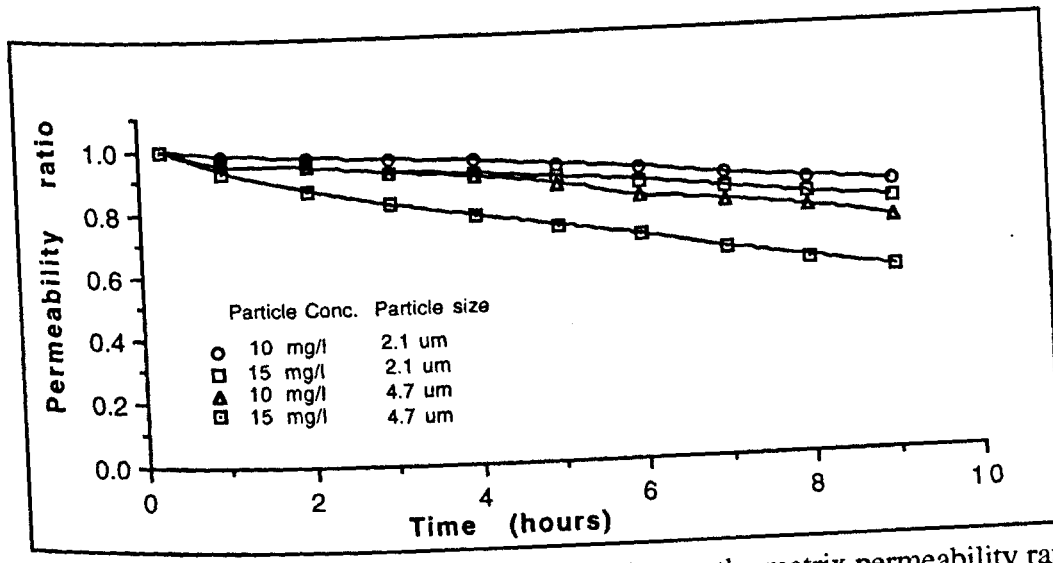

Fig.3.11: Effect of particle size and concentration on the matrix permeability ratio (SFI exps. 56, 58, 53, and 49).

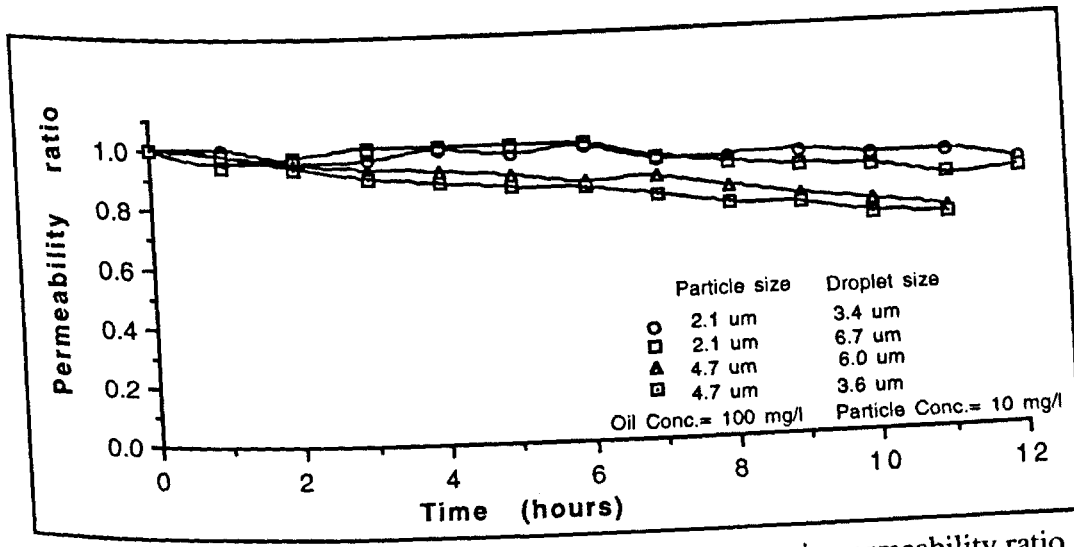

Fig.3.12: Effect of droplet size and particle size on the matrix permeability ratio (SFI exps. 25, 33, 46, and 54).

At constant particle mean size of 2.1 μm, increasing the particle concentration from 10 (exp. 56) to 15 mg/l (exp.58) decreased the final matrix permeability by 5% (matrix permeability ratio decreased from 0.84 to 0.79). The addition of oil at 100 mg/l concentration and at 3.6 μm droplet mean size to the 15 mg/l particle suspension (exp. 40) produced an increase in the final matrix permeability of 15% (matrix permeability ratio increased from 0.79 to 0.94). The same was recorded for the 4.7 μm mean size particles (experiments no. 53, 49 and 47).
So the presence of oil at a concentration of 100 mg/l and at 3.6 μm droplet mean size reduced the damage effect (on matrix permeability) caused by increasing the particle concentration from 10 to 15 mg/l.

At constant particle concentration of 10 mg/l, increasing the particle mean size from 2.1μm (exp. 56) to 4.7 μm (exp. 53) decreased the final matrix permeability by 11% (matrix permeability ratio was reduced from 0.84 to 0.73). The addition of oil at a concentration of 100 mg/l and 3.6 μm droplet mean size to the 4.7 μm mean size particle suspension (exp. 57) increased the final matrix permeability by 4% (the matrix permeability ratio was enhanced from 0.73 to 0.77). The same was recorded for the 15 mg/l particle concentration (experiments no. 58, 49 and 47) but with greater increase in the final matrix permeability when oil was added. Again the presence of oil at a concentration of 100 mg/l and at 3.6 μm droplet mean size reduced the damage effect (on matrix permeability) caused by increasing the particle mean size from 2.1 μm to 4.7 μm.

3.3.4 Comparison of the effects of solids, oil and solids plus oil dispersions

When only oil was added at a concentration of 100 mg/l and at a droplet mean size of 3.6 μm (experiment no. 50) without any particles, there was no reduction in matrix permeability after 9 hours of injection. When only the 2.1 μm particles were added with a concentration of 10 mg/l (experiment no. 56) without oil, matrix permeability decreased by 16% after 9 hours. It may be expected that the presence of the solid particles and the oil droplets together would result in further reduction in matrix permeability, however, when oil and solids were added together to the brine (experiment no. 25), the matrix permeability decreased only by 5% after 9 hours of injection compared with 16% in the case when only particles were added (Fig.3.15 and Table

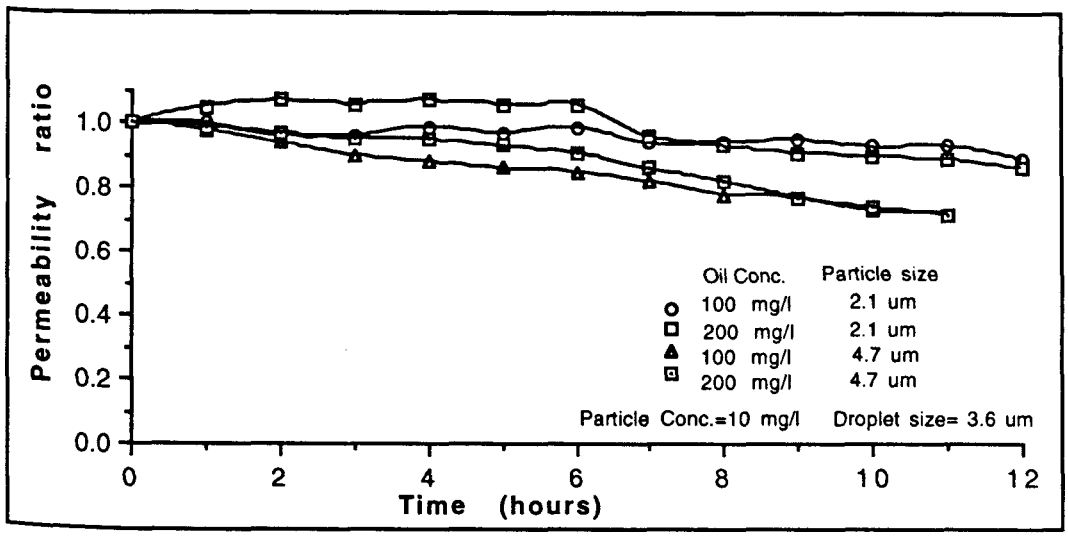

Fig.3.13: Effect of oil concentration and particle size on the matrix permeability ratio (SFI exps. 25, 39, 54, and 55)

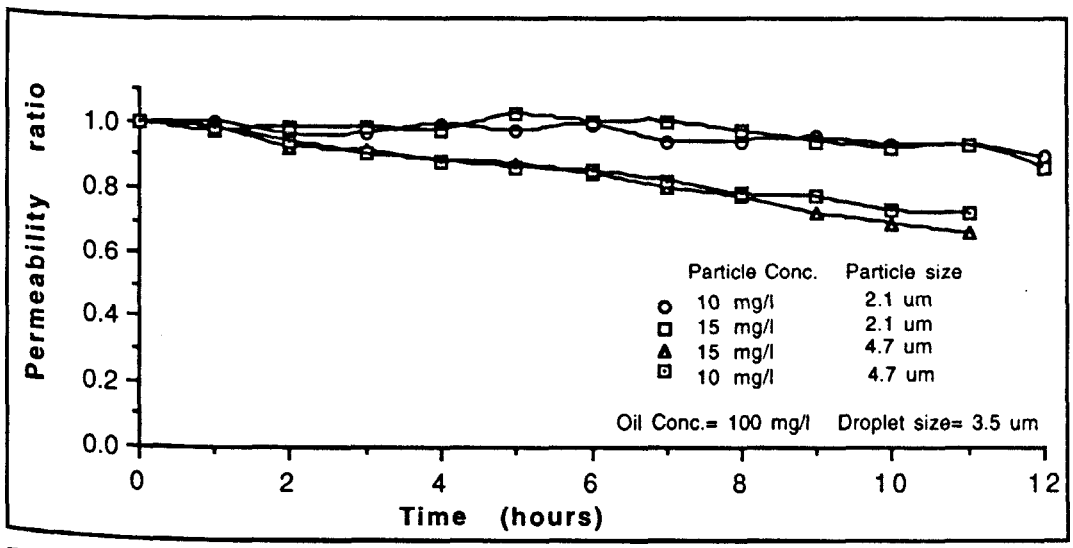

Fig.3.14: Effect of solids concentration and particle size on the matrix permeability ratio (SFI exps. 25, 40, 47, and 54).

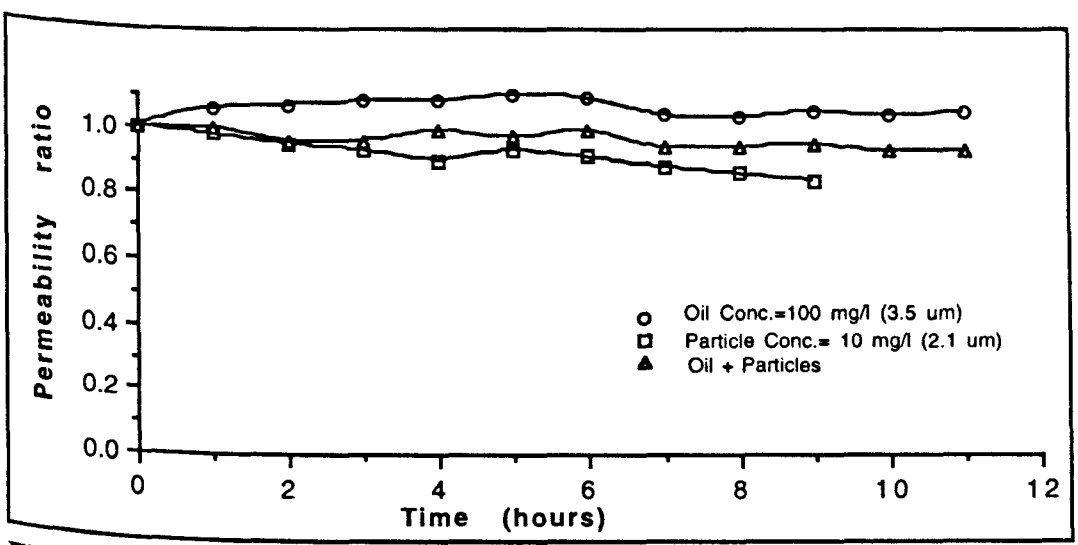

Fig.3.15: Comparison between the three effect of droplets alone, particles alone and the droplets and the particles together (SFI exps. 50, 56, and 25).

3.5). Similar results were obtained when the 2.1 μm particles were added at a concentration of 15 mg/l (Fig.3.16 and Table 3.5).

The experiments with the 4.7 μm particles gave similar results as in the case of the 2.1 μm particles (Figs.3.17 and 3.18).

These observations were made in all the experiments which were performed in this study.

Discussion:

The improvement of the final matrix permeability when oil droplets were present with the solid particles, compared with the case of the suspension of solid particles with out any oil droplets, may be due to some of the following factors:

Oil has the property of lubrication which reduces the friction between the solid particles and the rock matrix grains and reduces the contact between them.

The presence of oil in much higher concentration than the solids gives the oil droplets a control on most of the flow paths which reduces the total particle blocking probability due to the small number of paths available for particles. And as oil droplet has no permeability damage effect (as indicated from the experimental results), these two factors will lead to a lower reduction in matrix permeability.

No external filter cake was formed in any of these experiments as the external cake in the case of fracture injection will need a very long time to form.

3.4. Matrix permeability alteration due to linear injection of simulated produced water

Slabs of 6 cm width, 1.4 cm height and 3 cm length, were used to test the permeability damage produced by linear flow through the slab i.e. without the effect of the fracture. In this case all of the fluid is directed through the rock. The flow area was 8.5 cm^2 (which is 1.4 cm by 6 cm) and the flow rate was fixed at 3.55 ml/s. The droplet and particle mean sizes and oil and solids concentrations were similar to those used in the fracture injection. The operating conditions data for these experiments are given in Table 3.6.

The results show that the oil emulsion (without solids) of 100 mg/l oil with a droplet mean size of 3.6 μm (experiment no. 61) caused a 33% reduction in matrix permeability after only

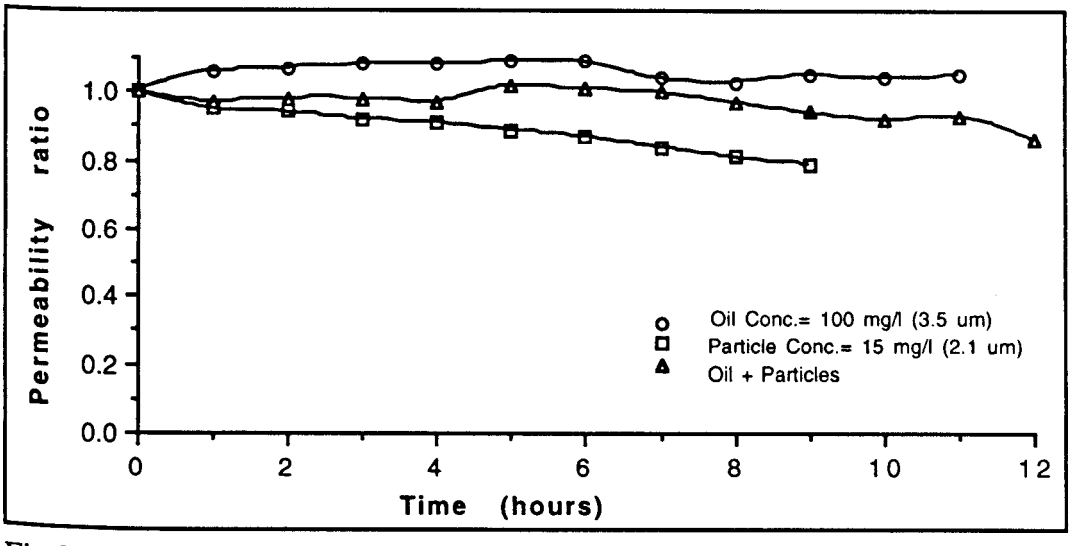

Fig.3.16: Comparison between the three effect of droplets alone, particles alone and the droplets and the particles together (SFI exps. 50, 58, and 40).

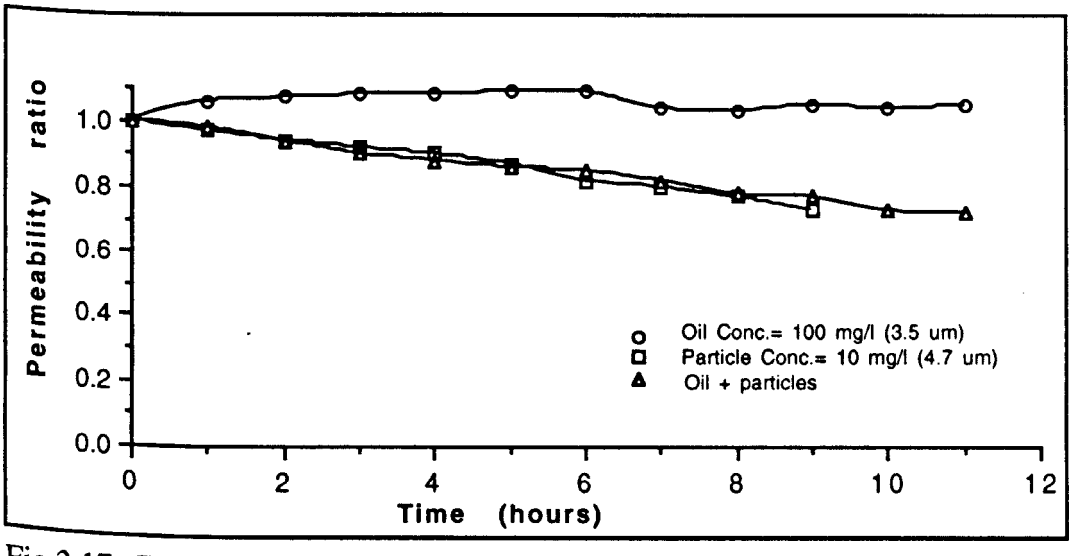

Fig.3.17: Comparison between the three effect of droplets alone, particles alone and the droplets and the particles together (SFI exps. 50, 53, and 54).

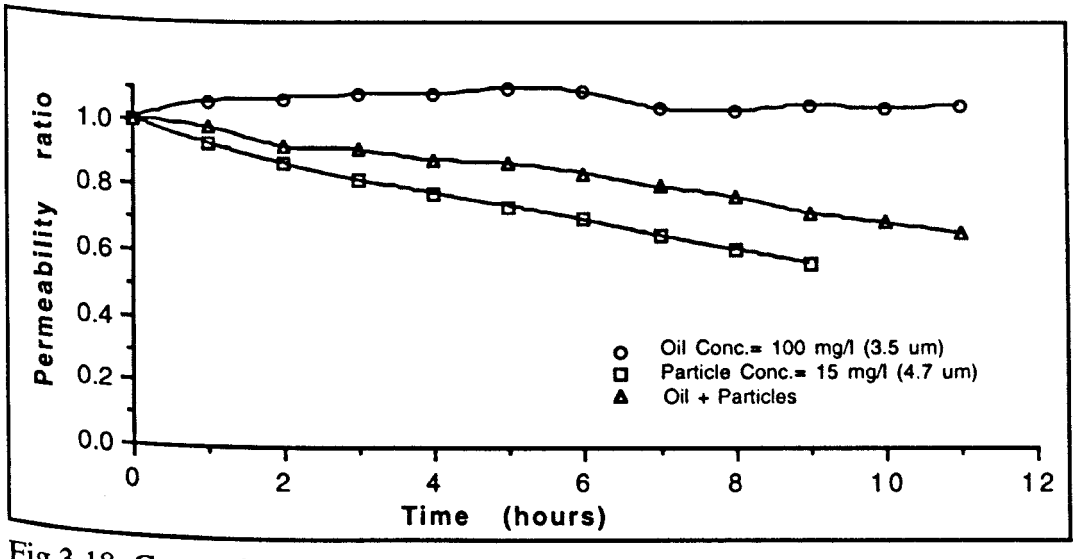

Fig.3.18: Comparison between the three effect of droplets alone, particles alone and the droplets and the particles together (SFI exps. 50, 49, and 47).

5 hours of injection. The particle suspension (without oil droplets) of 10 mg/l concentration with a particle mean size of 2.1 μm (experiment no. 59) caused a 57% reduction in the matrix permeability after only 5 hours of injection (Fig.3.19 and Table 3.7).

When oil droplets and solid particles were added together with the same sizes and concentrations as above (experiment no. 69), the reduction in matrix permeability was 37% after 5 hours of injection. The presence of oil at 100 mg/l improved the final matrix permeability by 20% (from 57% reduction when no oil was added to 37% reduction when oil was added).

When the concentration of the oil increased to 200 mg/l at the same particle concentration of 10 mg/l (experiment no. 74), the final matrix permeability decreased by 62% to its worst value (lower than the case of particles only with no added oil).
The presence of oil at low concentration (100mg/l) with the 2.1 μm solid particles improved the final matrix permeability; its presence in high concentration with the 2.1 μm solid particles reduced the final matrix permeability.

For the 4.7 μm particles suspension at 10 mg/l concentration with no oil (experiment no. 65), the matrix permeability decreased by 62% after 5 hours of injection.
When oil was present with the solid particles at a concentration of 100 mg/l (experiment no. 73) the matrix permeability decreased by 72% and when the oil concentration increased to 200 mg/l (experiment no. 72) this reduction became 77% after 5 hours of injection (Fig.3.20 and Table 3.7).

The improvement effect of the oil was repeated again when the concentration of the 2.1 μm particles was increases to 15 mg/l (Fig.3.21 and Table 3.7). The permeability ratio increased from 0.37 when no oil was added (experiment no. 60) to 0.62 when oil was added at a concentration of 100 mg/l (experiment no. 67).

When the concentration of the 4.7 μm particles increased to 15 mg/l (experiment no. 64), the matrix permeability decreased by 71% (Fig.3.22 and Table 3.7). The presence of oil at

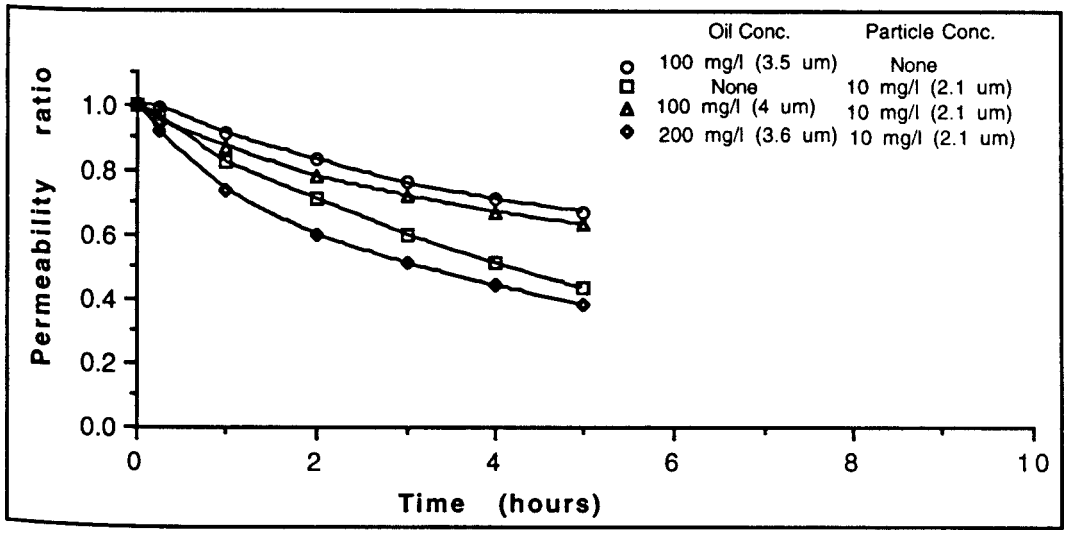

Fig.3.19: Comparison between the three effect of droplets alone, particles alone and the droplets and the particles together (LI exps. 61, 59 ,69, and 74).

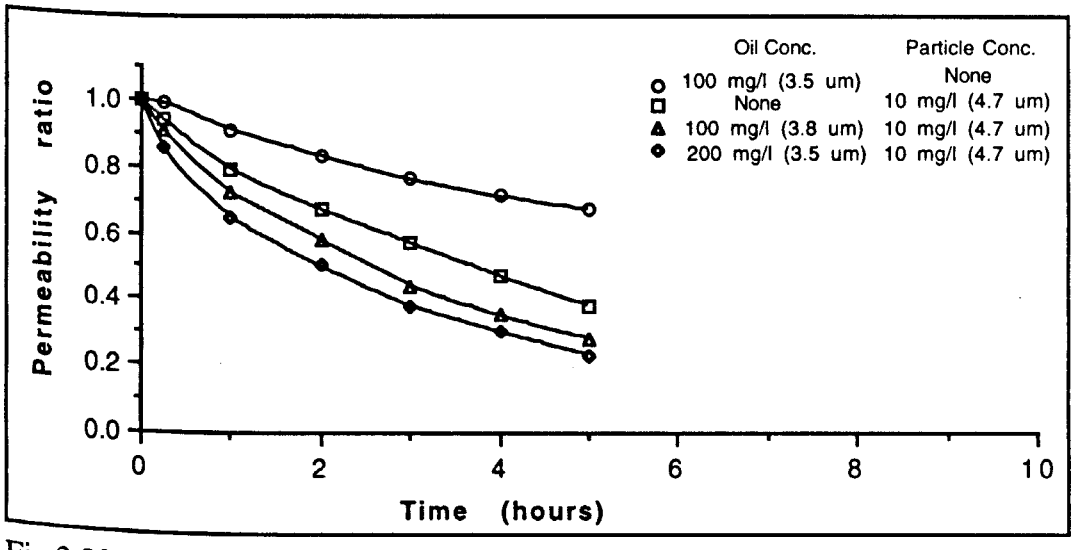

Fig.3.20: Comparison between the three effect of droplets alone, particles alone and the droplets and the particles together (LI exps. 61, 65, 73, and 72).

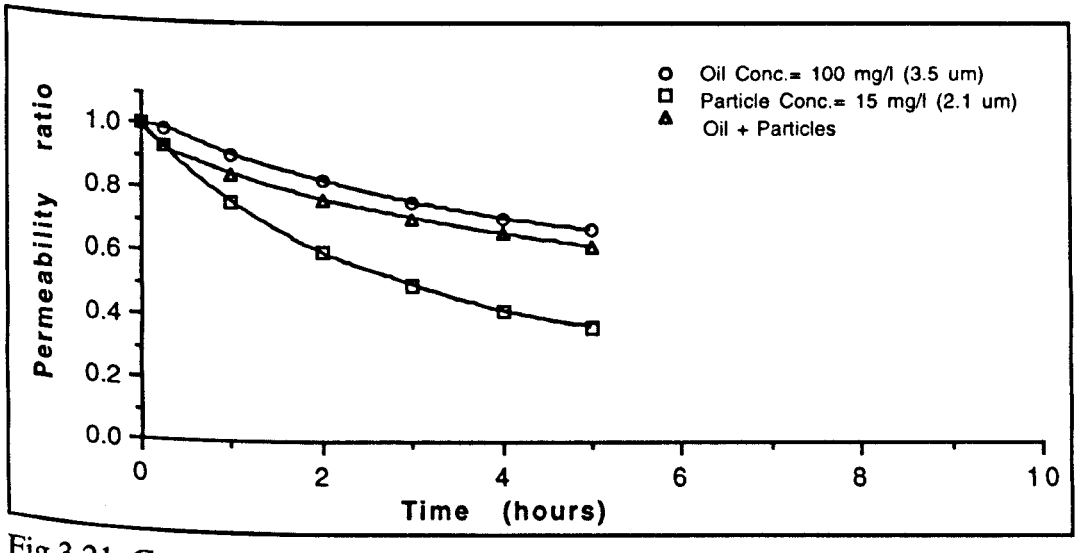

Fig.3.21: Comparison between the three effect of droplets alone, particles alone and the droplets and the particles together (LI exps. 61, 60, and 67).

a concentration of 100 mg/l with the solid particles (experiment no. 70) improved the final matrix permeability by only 7% (from 71% reduction in the matrix permeability to 64%).

No external filter cake was formed in any of the linear injection experiments as the injection time was too short for the external filter cake to be formed. The injection time was short because of the limitations of the prepared slab cell which can not be subjected to high pressure drop (linear injection through a small flow area cause a very high pressure drop), as rock matrix damage take place. This high pressure can cause a serious leak in the tested cell.

3.5. Matrix permeability alteration due to injection of simulated produced water along long fractures

The slabs used in this set of experiments were similar to those used in section 3.3. The length, however, was increased to 40 cm in order to allow more of the injected fluid to flow through rock matrix to reach the side outlets (instead of being collected at the fracture outlet as the case in the 20 cm short fracture) and to investigate the effect of increasing the fracture face area on the matrix damage process. As the fracture length increased, the pressure drop along the fracture also increased. Also the flow velocity along the fracture near the fracture outlet would be decreased as the fracture length increased. The experiments in this section were similar to the 20 cm fracture experiments in that they examined the effect of particles only, oil only and solids and oil combined.

The tests lasted between 14 to 22 hours with an inlet flow rate of 3.56 ml/s. A description of the operating conditions of these experiments is presented in Table 3.8.

The size distribution of the oil droplets and solid particles were identical to those used in previous sections.

The slab cell was cut open at the end of the experiment taking care not to disrupt the fracture face and the fracture face was observed by using a microscope. Observations indicated that there was no formation of external filter cake on the fracture face in all of these experiments. The pressure drop through side outlets was adjusted at the starting of each experiment to be higher than the pressure drop along the fracture as it is the case in field fracture injection.

3.5.1 Oil droplet size and concentration effect on matrix permeability

Oil emulsion of 200 mg/l oil concentration and 3.8 μm mean size droplets was injected along the fracture (experiment no. 75). The results indicated a slight reduction of 6% in matrix permeability after 16 hours of injection which is a similar performance to what was noticed in the case of short fracture (experiment no. 52). This result shows again that oil in a droplet mean size of 3.8 μm had a little damage effect on matrix permeability in fracture injection.

3.5.2 Solid particles size and concentration effect on matrix permeability

A suspension of particles (at different sizes and concentration) without any oil were injected along the fracture to measure the particles ability to reduce the matrix permeability. At a particle concentration of 10 mg/l, the matrix permeability decreased by 12% in the case of the 2.1 μm particles (experiment no. 77) and 18% in the case of 4.7 μm particles after 14 hours of injection (experiment no.79).

At a particle concentration of 15 mg/l, the matrix permeability decreased by 21% in the case of the 2.1 μm particles (experiment no. 76) and 24% in the case of 4.7 μm particles (experiment no. 80) after 14 hours of injection (Fig.3.23 and Table 3.9). For the 4.7 μm mean size particle suspensions, the recorded reduction in matrix permeability for the 40 cm fracture is much less than the recorded matrix permeability reduction for the 20 cm fracture. The recorded matrix permeability for the 4.7 μm mean size particle injection in the case of 40 cm fracture was much higher than expected.

3.5.3 Oil droplets and solid particles size and concentration combined effect

For the 200 mg/l oil emulsion, the matrix permeability decreased by only 6% after 16 hours of injection. The addition of the 2.1 μm particle suspension (at a concentration of 10 mg/l) to this emulsion (experiment no. 57) did not result in any additional reduction in matrix permeability during the first 12 hours of injection (Fig.3.24 and Table 3.9) then an extra additional 3% reduction in permeability was indicated after 16 hours of injection (a total of 9%).

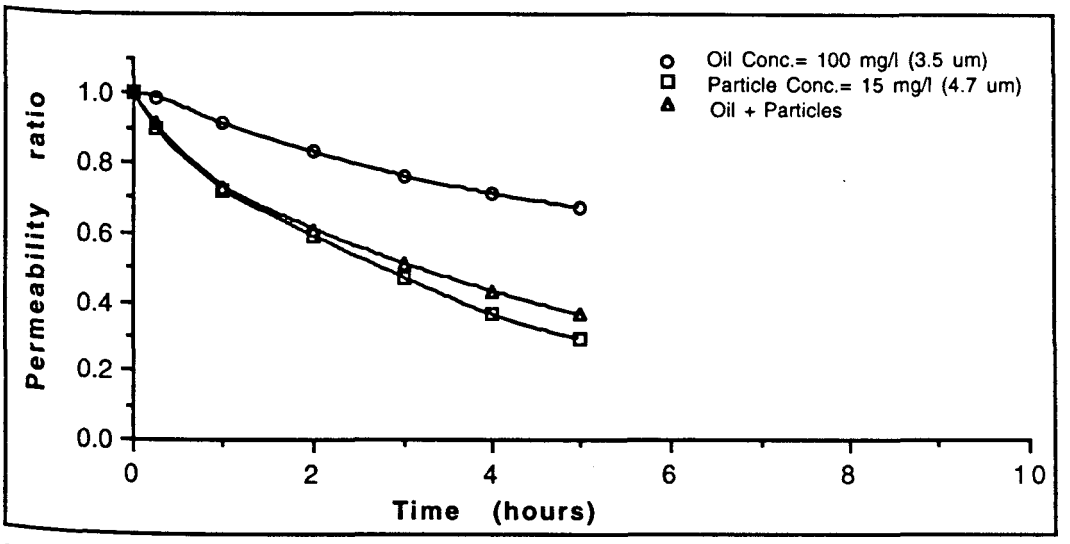

Fig.3.22: Comparison between the three effect of droplets alone, particles alone and the droplets and the particles together (LI exps. 61, 64, and 70).

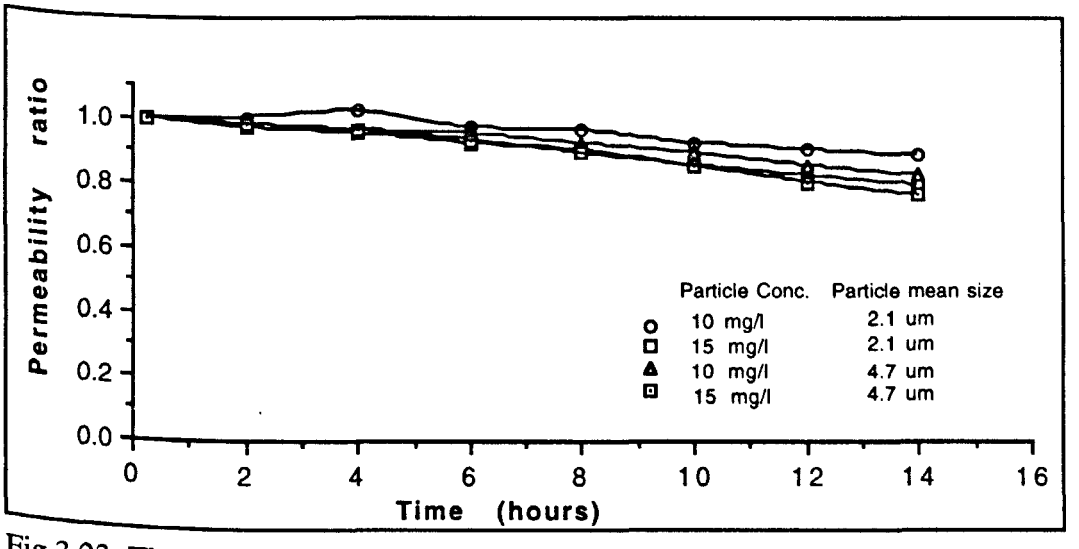

Fig.3.23: The Effect of particle mean size and concentration on matrix permeability ratio for the long fracture (exps. 77, 76, 79, and 80).

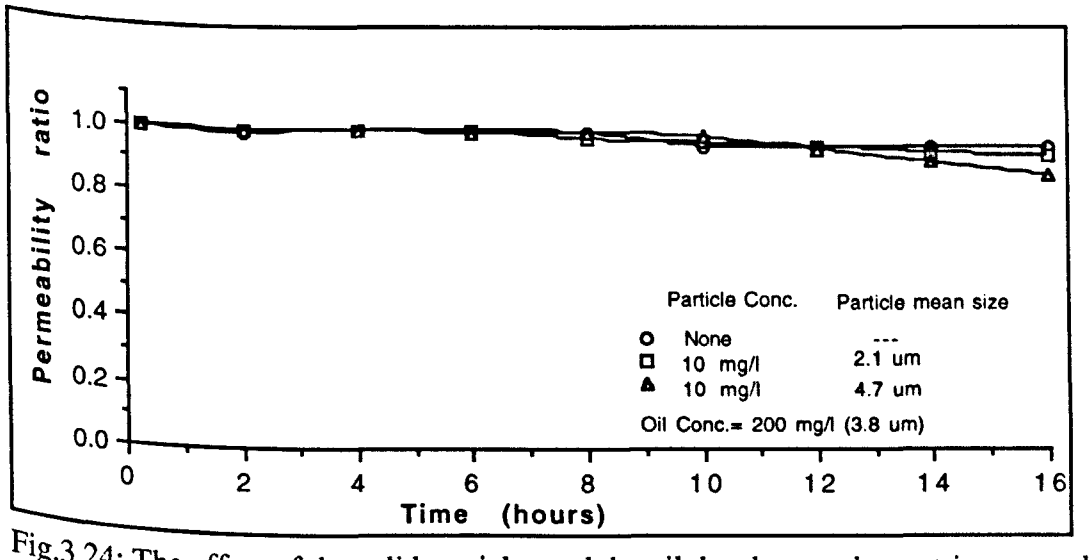

Fig.3.24: The effect of the solid particles and the oil droplets on the matrix permeability ratio for the long fracture (exps. 75, 57, and 42).

The addition of the 4.7 μm particles suspension (at a concentartion of 10 mg/l) to the same emulsion (experiment no.42) gave the same results as for the 2.1 μm particles in the first 12 hours and caused reduction in permeability at the end of the 16 hours of injection of 15 % (Fig.3.24 and Table 3.9).

The 2.1 μm particles suspension (without oil) at a concentration of 15 mg/l (experiment no. 76) reduced the matrix permeability by 21% after 14 hours of injection. By adding oil to this suspension at a concentration of 100 mg/l (experiment no. 81), the reduction in matrix permeability was 8%. This is an improvement of 13% in matrix permeability (Fig.3.25 and Table 3.9).

The 4.7 μm particles suspension (without oil) at a concentration of 15 mg/l (experiment no. 80) reduced the matrix permeability by 24% after 14 hours of injection. By adding oil to this suspension at a concentration of 100 mg/l (experiment no. 82), the reduction in matrix permeability was 16%. This is an improvement of 8% in matrix permeability.

The results show that the presence of oil with the particles effectively reduced the damaging effect of the solid particles (may be due to the lubrication effect of the oil droplets which reduces the friction between the solid particles and the rock grains surface).

3.6. Comparison of the linear and fracture injection results

The main difference between the fracture flow and linear flow experiments is the geometry of the sample. This, with a constant flow rate, means that the flow velocities through rock matrix are much lower in the fracture experiments than in the linear experiments. In the fracture injection experiments, the flow is distributed on a large area compared with the flow area in linear injection which made the injectivity (flow rate divided by pressure drop) in the fracture experiments much higher than the injectivity in linear experiments. The very low flow velocity through the rock matrix in the case of fracture injection will encourage the particle capture within the matrix pores near the fracture face while in the case of linear injection the high flow velocity flushed the particles deeper into the rock matrix.

In this section a comparison study is presented between the experimental linear injection results and the experimental results of the long fracture experiments.

The linear samples were cut from the fracture slabs, therefore the length of the linear injection slab was 3 cm (the same distance from the fracture face to the side outlets in the fracture experiments). The Fracture face area was 112 cm^2 which is nearly 13 times the area of the linear injection slab (8.5 to 9.0 cm^2). Due to this difference in flow area the injection pressure in the case of fracture injection was very low compared with the injection pressure in the case of linear injection. The flow velocity through the linear injection slab inlet face was around 0.4 cm /s, the velocity through the fracture face was typically between 0.02 and 0.03 cm/s. The initial permeability of the linear slab was chosen to be in the same range as the initial permeability of the fractured slab.

The experimental results were divided into three groups:

(1) Oil emulsion experiments.

(2) Particle suspension experiments.

(3) Simulated produced water experiments (containing oil and solids).

The comparison aspects were:

(1) Permeability ratio: the ratio of the damaged matrix permeability at any time to the initial matrix permeability

(2) Concentration ratio: the ratio of the effluent Obscuration to the influent obscuration.

(3) Mean diameter ratio: the ratio of the mean diameter of the effluent to the mean diameter of the influent.

(4) Flow velocity through rock matrix in linear injection, V_l, and the flow velocity through rock matrix perpendicular to the fracture face, V_s (Fig.3.26).

3.6.1 Oil emulsion experiments

The oil droplets had a mean diameter of 3.6 μm and at a concentration of 200 mg/l. The experimental data of the linear injection experiment is presented in Table 3.10 (experiment no. 62) and the data of the fractured injection experiment in Table 3.11 (experiment no. 75). The flow velocity through rock matrix in the linear injection was 0.43 cm/s whereas the flow velocity through rock matrix in the case of the fracture injection was 0.02 cm/s.

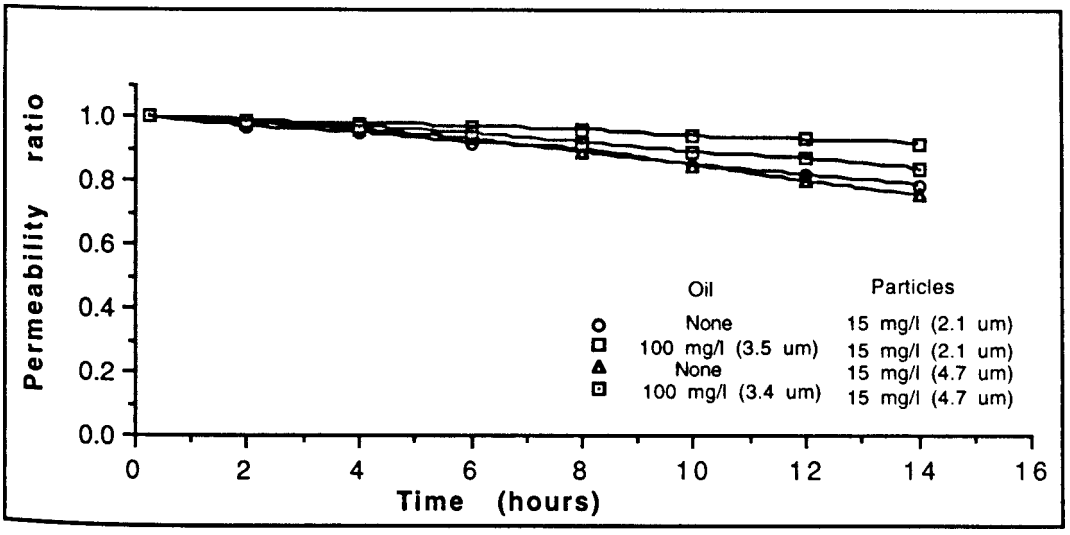

Fig.3.25: The effect of the solid particles and the oil droplets on the matrix permeability ratio for the long fracture (exps.76, 81, 80, and 82).

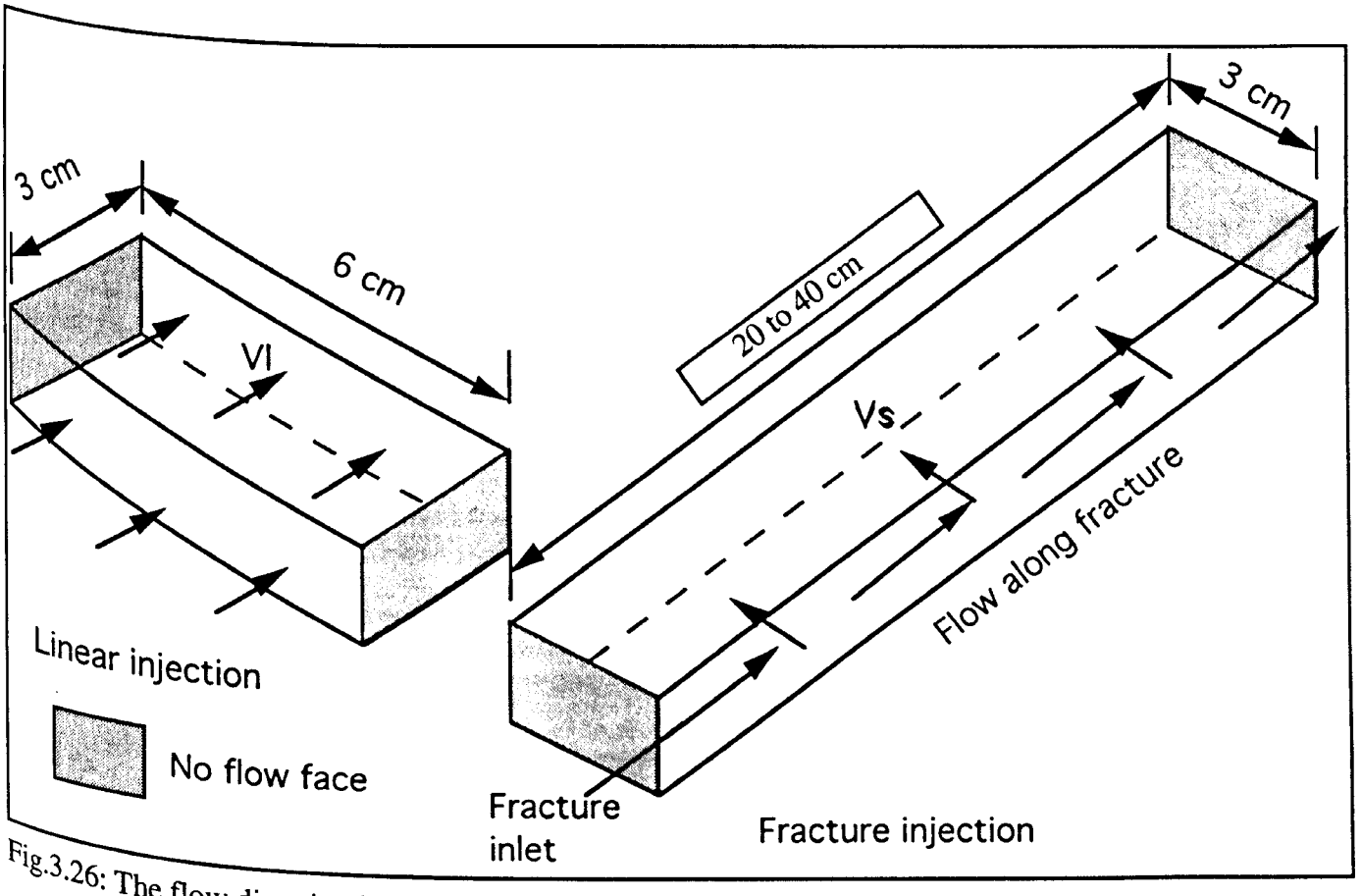

Fig.3.26: The flow direction in the linear and the fracture injection.

The matrix permeability in the linear injection decreased by 39% after only 5 hours of injection (7.8% reduction per hour). At the same duration there was negligible reduction in matrix permeability in the case of fracture injection (0.2% reduction per hour) and at the end of the test the matrix permeability decreased by only 6% after 14 hours of injection (Fig.3.27). The results of the permeability ratio are reflected by the mean diameter ratio (Mdr) and the concentration ratio (CR) results.

The two injection systems had an effluent mean dia ratio higher than 0.95 most of the times (Fig.3.28). At the first 4 hours the mean diameter ratio of the effluent of the linear injection was higher than that of the side effluent of the fracture injection by only 0.04 because of the higher flow velocity of the linear injection which tends to flush the droplets deeper into the matrix to reach the slab outlet. As the permeability damage was taking place at a higher rate in the case of linear injection, more large droplets were captured within the matrix and the mean diameter ratio of the linear injection effluent started to decrease after 3 hours of injection (Fig.3.28). The mean diameter ratio of the fracture injection ended at a value of 0.9 after 14 hours of injection which means that the large droplets were still managing to get through and reaching the side outlets after a long injection time.

The same indications can be seen in the concentration ratio (CR) plot (Fig.3.29). The CR of the linear injection effluent was 1.0 at the start of the experiment and decreased with time due to matrix permeability damage to a value lower than that of the fracture injection (after 3 hours of injection). The CR of the fracture injection started at a value of 0.86 and increased to 1.0 after 4 hours then starts to decrease to the end of the experiment. The fracture CR took some time (4 hours) before reaching the value of 1.0 whereas the CR of the linear injection reached the value of 1.0 at the start of the experiment due to the flushing effect of the high flow velocity. The CR of the fracture injection ended at a value of 0.84 after 14 hours which mean that 84% of the flowing oil through the matrix reached the side outlets and 16% was accumulated within the matrix (Fig.3.29).

The linear injection effluent properties (the mean diameter ratio and the concentration ratio) had nearly the same values of the fracture injection side effluent properties. But in spite of this the

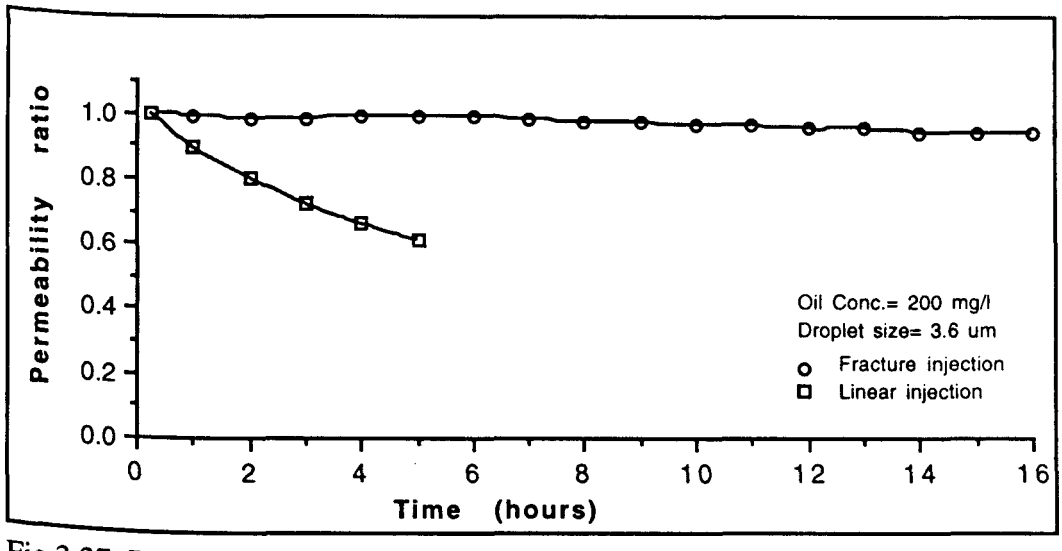

Fig.3.27: Permeability ratio change with time for the oil emulsion injection experiments (exps. 62 and 75).

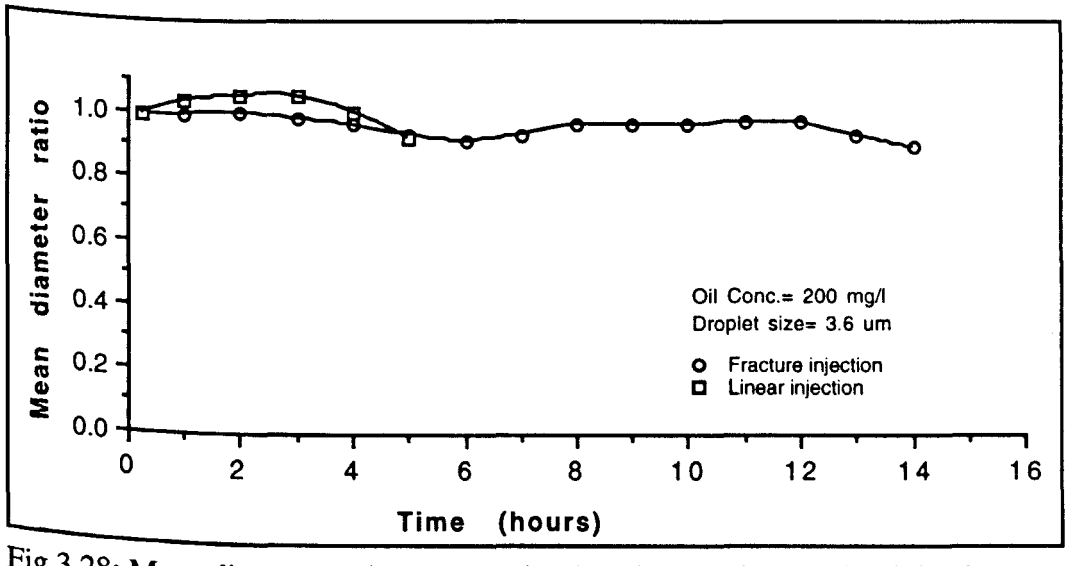

Fig.3.28: Mean diameter ratio change with time for the oil emulsion injection experiments (exps. 62 and 75).

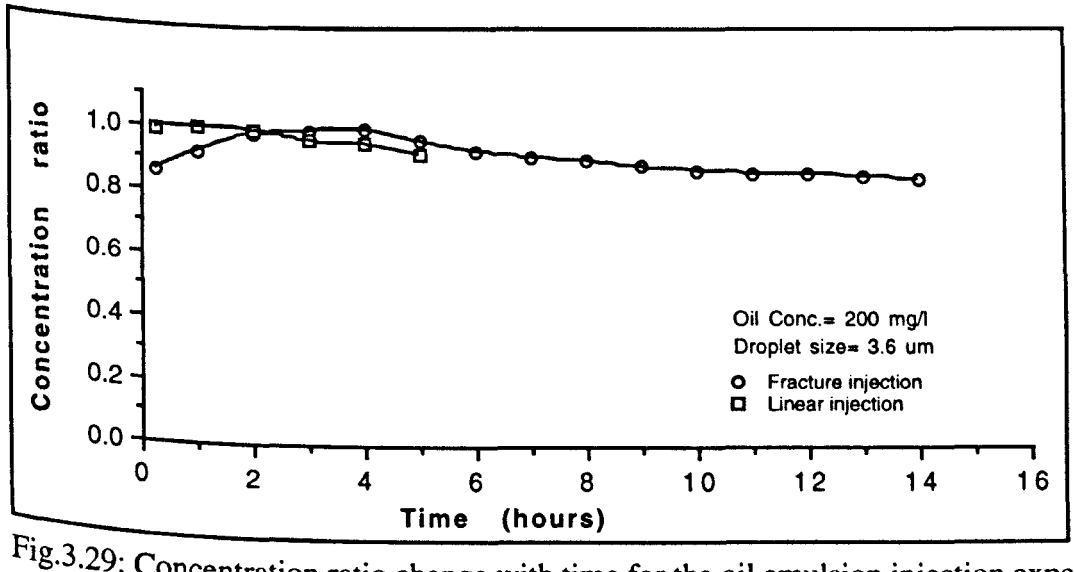

Fig.3.29: Concentration ratio change with time for the oil emulsion injection experiments (exps. 62 and 75)..

matrix permeability decreased in the case of linear injection by 39% after 5 hours whereas in the fracture injection case there was almost no reduction in the matrix permeability.
The explanation for these observations may be that the flow in the fracture injection is distributed on a much larger area which will reduce the damage effect of the injected emulsion. Similar results of mean dia ratio and concentration ratio for the linear injection and the fracture injection experiments (in spite of the difference in flow velocity) may indicate that oil droplets do not need a high driving flow (in the case of fracture injection) to pass through rock matrix.

3.6.2 Particle suspension experiments

The mean size of the particles were 2.1 μm and 4.7 μm with a concentration of 10 and 15 mg/l. The experimental data of the linear injection experiments are presented in Tables 3.12 - 3.15 (experiments no. 59, 60, 64 and 65) and the data of the fractured injection experiments in Tables 3.16 - 3.19 (experiments no. 76, 77, 79 and 80).
The flow velocity through rock matrix in the linear injection experiments was 0.41 cm/s whereas the flow velocity through rock matrix in the case of the fracture injection experiments was between 0.03 and 0.035 cm/s due to matrix permeability difference.

For linear injection the suspension of 2.1 μm particles at a concentration of 10 mg/l reduced the matrix permeability by 59% (11.8% reduction per hour) and at 15 mg/l reduced it by 65% (13% reduction per hour) after 5 hours of injection. At 5 hours of fracture injection there was almost no reduction in matrix permeability in the case of 10 mg/l concentration and a reduction of 6% for the case of the 15 mg/l particle concentration (1.2% reduction per hour). After 14 hours of fracture injection the matrix permeability decreased by 12% (0.86% reduction per hour) for the case of the 10 mg/l concentration and by 21% (1.5% reduction per hour) for the case of the 15mg/l concentration (Fig.3.30)

The linear injection of the 4.7 μm particle suspensions at a concentration of 10 mg/l (experiment no. 59) caused a reduction in matrix permeability of 62% (12.4% reduction per hour) and at a concentration of 15 mg/l the reduction was 71% (14.2% reduction per hour) after 5 hours of injection. At the same duration (5 hours), the fracture injection of the same particles at a

concentration of 10 mg/l caused only 4% reduction in matrix permeability and 5% (1% reduction per hour) when the concentration was 15 mg/l. At the end of the fracture injection experiment (14 hours of injection) the matrix permeability reduced by 18% (1.29% reduction per hour) for the 10 mg/l suspension and by 24% (1.71% reduction per hour) for the case of the 15 mg/l suspension (fig.3.31).

The distribution of the particles on the large fracture face area in the case of fracture injection resulted in a very low reduction rate in matrix permeability with time. On the other hand the passing of particles through a very small flow area in the case of linear injection resulted in a much higher reduction rate in matrix permeability with time. The difference between the two reduction rates is higher than would be expected compared with the flow area difference between the linear and fracture experiments.

At the first 5 hours of injection, the reduction rate in matrix permeability for linear injection of the 2.1 μm particle suspension (at a concentration of 10 mg/l) was higher than the reduction rate of the fracture injection of the same suspension by 59 times and this difference was reduced to 10.8 times when the particles concentration was increased to 15 mg/l. For the suspension of the 4.7 μm particles at a concentration of 10 mg/l the matrix permeability reduction rate in the linear injection was 15.5 times higher than the reduction rate in the fracture injection and this difference was reduced to 14.2 times higher when the particles concentration was increased to 15 mg/l.

By increasing the particle size and concentration, the ratio of the matrix permeability reduction rate of the linear injection to the matrix permeability reduction rate of the fracture injection was reduced.

The mean diameter ratio plot against time (Figs. 3.32 and 3.33) shows that the mean particle diameter of the effluent suspension in the linear injection was between almost the same mean particle diameter of the influent suspension and 0.75 of the mean particle diameter of the influent suspension (mean diameter ratio between 1.0 and 0.75). This indicated that particles in all sizes were passing through the matrix to reach the outlet.

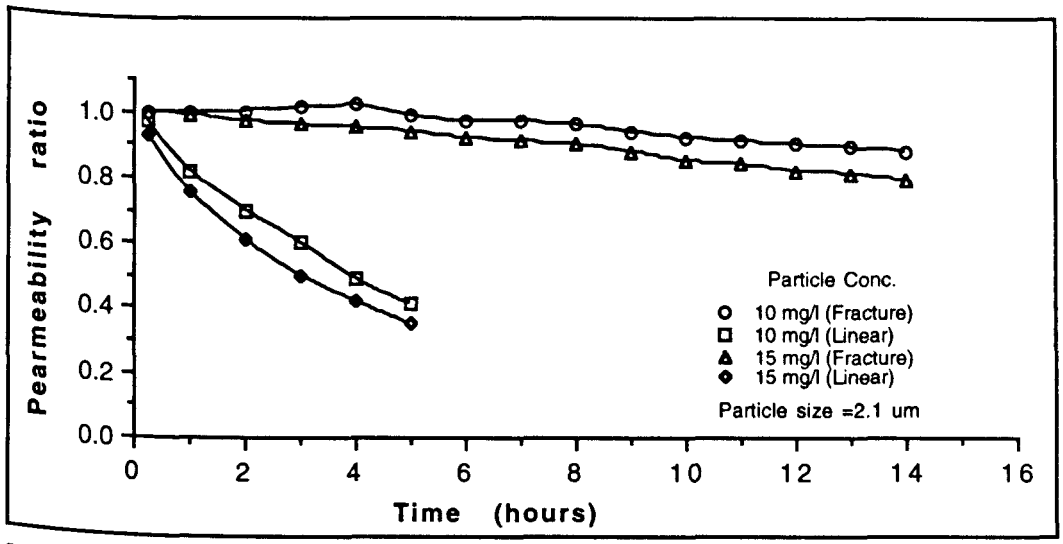

Fig.3.30: Permeability ratio change with time for the 2.1 μm particle suspension injection experiments (for LFI and LI exps. 77, 59, 76, and 60).

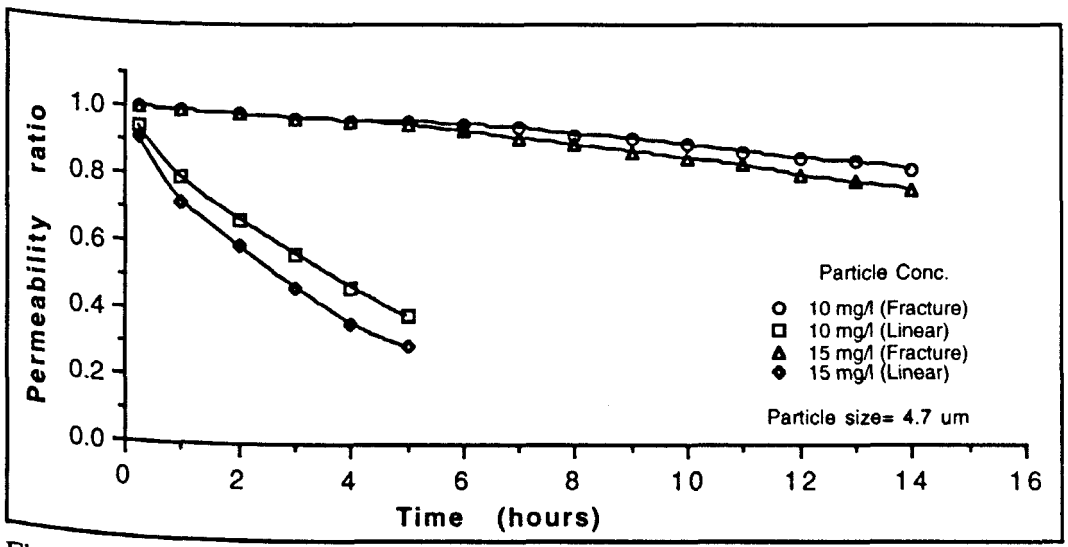

Fig.3.31: Permeability ratio change with time for the 4.7 μm particle suspension injection experiments (for LFI and LI exps. 79, 65, 80, and 64)

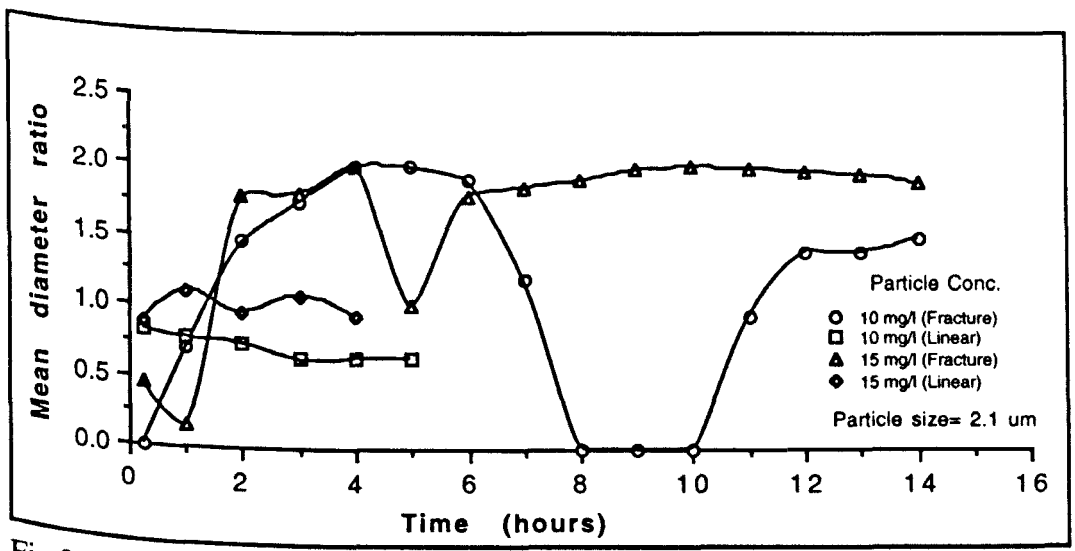

Fig.3.32: Effluent mean diameter ratio change with time for the 2.1 μm particle suspension injection experiments (for LFI and LI exps. 77, 59, 76, and 60)

In fracture injection, the side effluent of the 2.1 μm particles suspension mean diameter increased with time to reach a value higher than the particle mean diameter of the influent (mean diameter ratio of 1 to 2) and it remained at this range during most of the experiment. In the case of the 4.7 μm suspension, the side effluent mean diameter increased with time to reach a size equal to the mean diameter size of the influent (mean diameter ratio equal to 1.0).

In general the mean particle diameter of the side effluent in the case of the fracture injection most of the time is higher than 3 μm whatever the mean particle diameter of the influent suspension (2.1 μm or 4.7 μm particle suspensions). Whereas the mean particle diameter of the effluent in the case of linear injection is similar to or smaller than the mean particle diameter of the influent.

The concentration ratio of the side effluent in the case of fracture injection had a value between 0 and 0.3 whatever the injected suspension was (2.1 μm or 4.7 μm particle suspension). The concentration ratio of the 2.1 μm suspension effluent in the case of linear injection had a higher value at 0.4 to 0.6 and the 4.7 μm suspension effluent had a concentration ratio of 0.6 to 0.8 (Fig.3.34 and 3.35). The concentration ratio of the linear injection effluent was higher than the concentration ratio of the fracture injection side effluent. Presumably this was due to the high flow velocities in the linear experiments and due to the fact that injection pressure was higher in the case of linear injection than it was in the case of fracture injection.

From this it can be concluded that the particle invasion in the case of linear injection would be deep whereas the particle invasion in the case of fracture injection would be shallow.

3.6.3 Combined oil and solids experiments

The injection fluid contained solid particles of mean diameter 2.1 μm or 4.7 μm at a concentration of 10 and 15 mg/l and contained oil droplets of mean diameter of 3.6 μm at a concentration of 100 and 200 mg/l. The flow velocity through rock matrix in the case of linear injection was 0.36 to 0.42 cm/s and in the case of fracture injection was 0.025 to 0.03 cm/s. The experimental data of the linear injection experiments are presented in Tables 3.20 - 3.23 (experiments no. 67, 74, 70 and 72) and the data of the fractured injection experiments in Tables 3.24 - 3.27 (experiments no. 57, 81, 42 and 82).

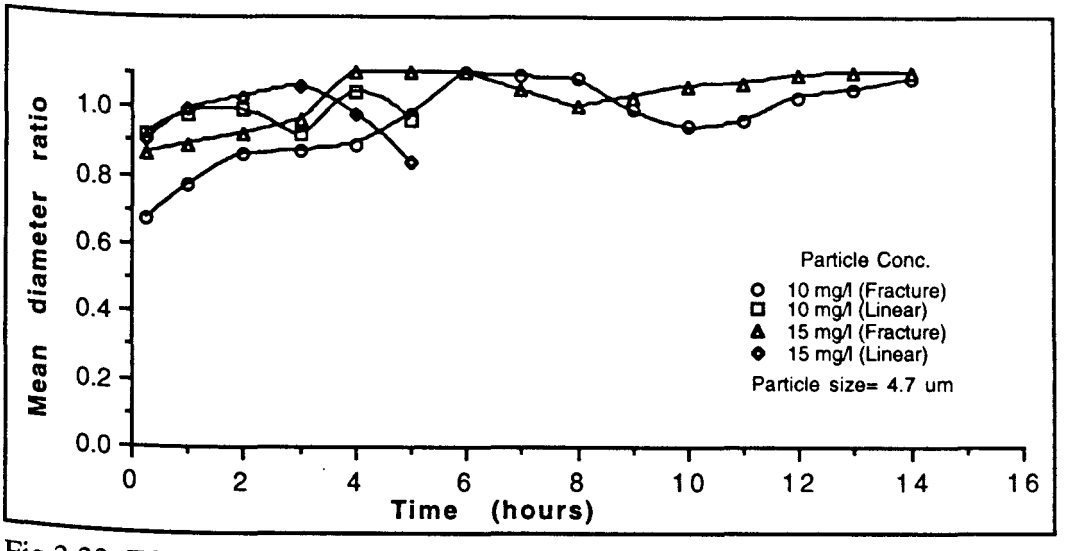

Fig.3.33: Effluent mean diameter ratio change with time for the 4.7 μm particle suspension injection experiments (for LFI and LI exps. 79, 65, 80, and 64)

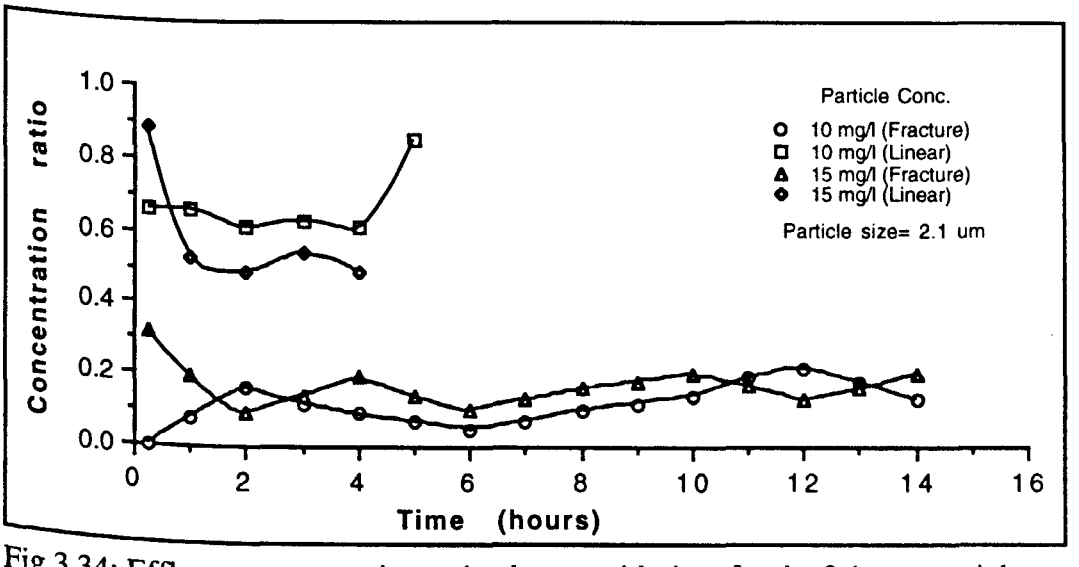

Fig.3.34: Effluent concentration ratio change with time for the 2.1 μm particle suspension injection experiments (for LFI and LI exps. 77, 59, 76, and 60)

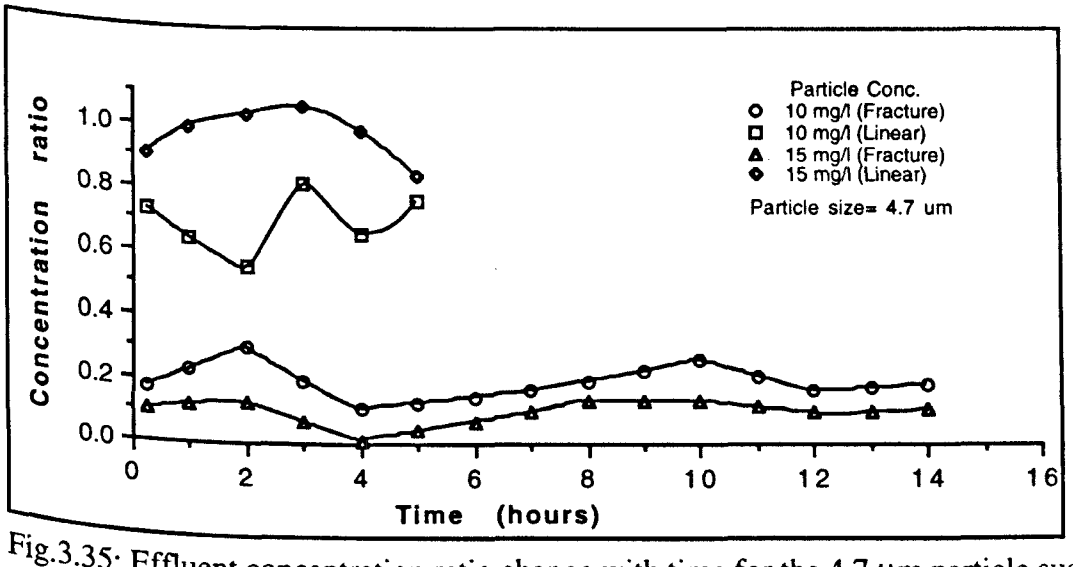

Fig.3.35: Effluent concentration ratio change with time for the 4.7 μm particle suspension injection experiments (for LFI and LI exps. 79, 65, 80, and 64)

The simulated produced water that contained 200 mg/l oil and 10 mg/l of 2.1 μm solid particles caused almost no reduction in matrix permeability after 5 hours in the case of fracture injection. In the case of linear injection, it caused a reduction of 62% (12.4% reduction per hour). After 14 hours of fracture injection the matrix permeability was reduced by 8% (0.57% reduction per hour) and after 22 hours it was reduced by 14% (0.64% reduction per hour). The difference in the matrix permeability reduction rates between the two injection systems was very high.

The simulated produced water that contained 100 mg/l oil and 15 mg/l of 2.1 μm solid particles caused a 3% reduction in matrix permeability after 5 hours of fracture injection and caused a 38% reduction in matrix permeability after 5 hours of linear injection. After 14 hours of fracture injection the reduction in matrix permeability was 8% (Fig.3.36).

By repeating the previous fracture injection experiments but with a particles of 4.7 μm mean diameter it was shown that the matrix permeability reduction result was similar to the previous results of the fracture injection of a simulated produced water that contained the 2.1 μm particles. But after 10 hours of injection the permeability ratio for the case of the 4.7 μm fluid injection continued to decrease at a rate higher than the reduction rate in the case of the 2.1 μm particles. Repeating the linear injection experiments with a particles of 4.7 μm mean diameter showed a higher reduction in matrix permeability than the 2.1 μm particles from the start of the experiment (Fig.3.37).

In the fracture injection process the reduction in matrix permeability was not sensitive to the variation in particle mean size and concentration or to the variation in droplet mean size and concentration if the injection time was short.
On the other hand, the matrix permeability reduction in the linear injection test was very sensitive to the variation in particle mean size and concentration.

For the case of simulated produced water that contained 2.1 μm particles, the mean diameter ratio of the side effluent in the fracture injection and the effluent in the linear injection had nearly the same values between 0.93 and 1.1. And for the case of simulated produced water that contained 4.7 μm particles, the mean diameter ratio values were between 0.88 and 1.05

(Fig.3.38 and 3.39). There was almost no difference between the influent particle mean diameter and the effluent particle mean diameter. As the oil droplets concentration in these experiments was far higher than the solid particles concentration, it was believed that the mean diameter ratio results represent the oil droplet mean diameter ratio more than they represented the particle mean diameter ratio.

The concentration ratio of the simulated produced water that contained the 2.1μm particles in the case of linear injection was close to 1 (very small quantities of oil and solids were left behind inside the pores of the rock matrix) during the 5 hour of injection whereas in the case of fracture injection the concentration ratio increased with time to reach its maximum value of 0.94 after 2 hours. It then started to decrease with time until the end of the experiment (larger quantities of oil and solids were left behind inside the pores of the rock matrix). In the case of the fracture injection, the reduction in the concentration ratio with time was higher when the simulated produced water contained 100 mg/l oil and 15 mg/l solids than when it contained 200 mg/l oil and 10 mg/l solids (Fig.3.40).
Similar results can be seen for the simulated produced water which contained a 4.7 μm mean diameter particles (Fig.3.41).

The small quantities of oil and solids remaining inside the rock matrix in the case of the linear injection had a great effect on the matrix permeability (caused a high reduction in matrix permeability) whereas the higher quantities remaining inside the rock matrix in the case of fracture injection had little effect on the matrix permeability (caused a very small reduction in matrix permeability).

As the oil droplet concentration in these experiments was far higher than the solid particles concentration, the concentration ratio results represented the oil droplet concentration ratio more than it represented the solid particles concentration ratio.

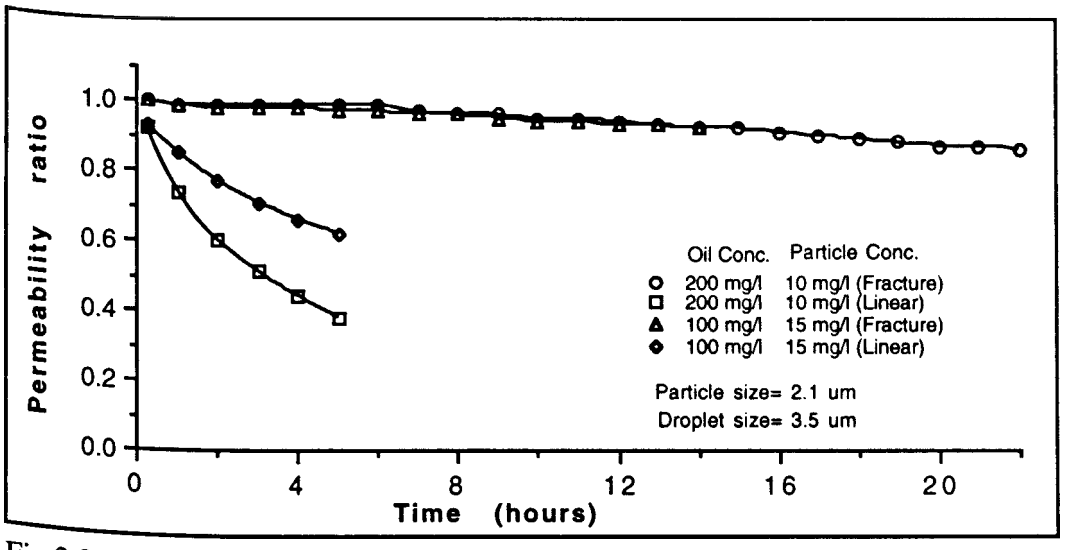

Fig.3.36: Permeability ratio change with time for the simulated produced water injection experiments (for LFI and LI exps. 57, 74, 81, and 67).

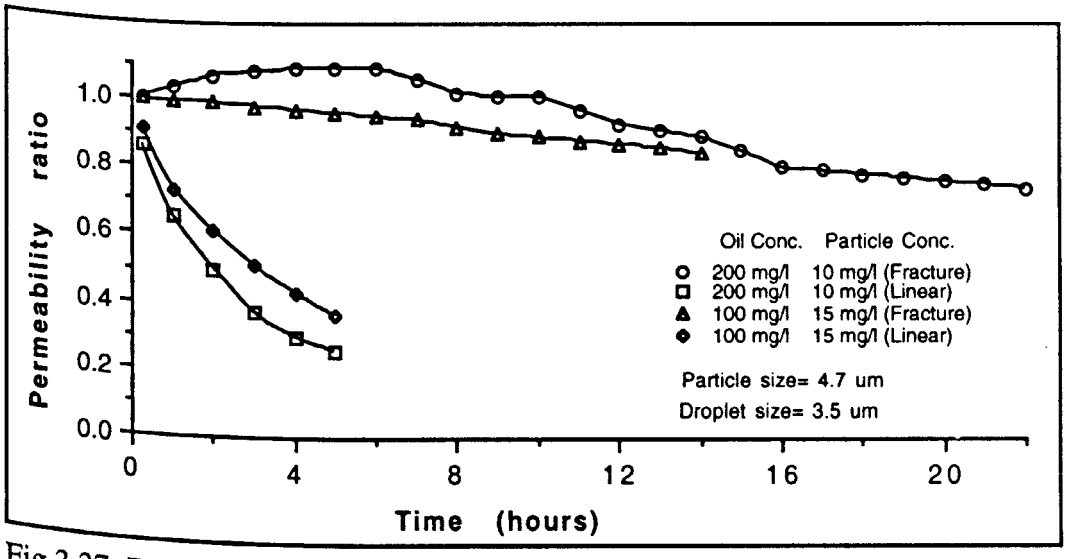

Fig.3.37: Permeability ratio change with time for the simulated produced water injection experiments (for LFI and LI exps. 42, 72, 82, and 70).

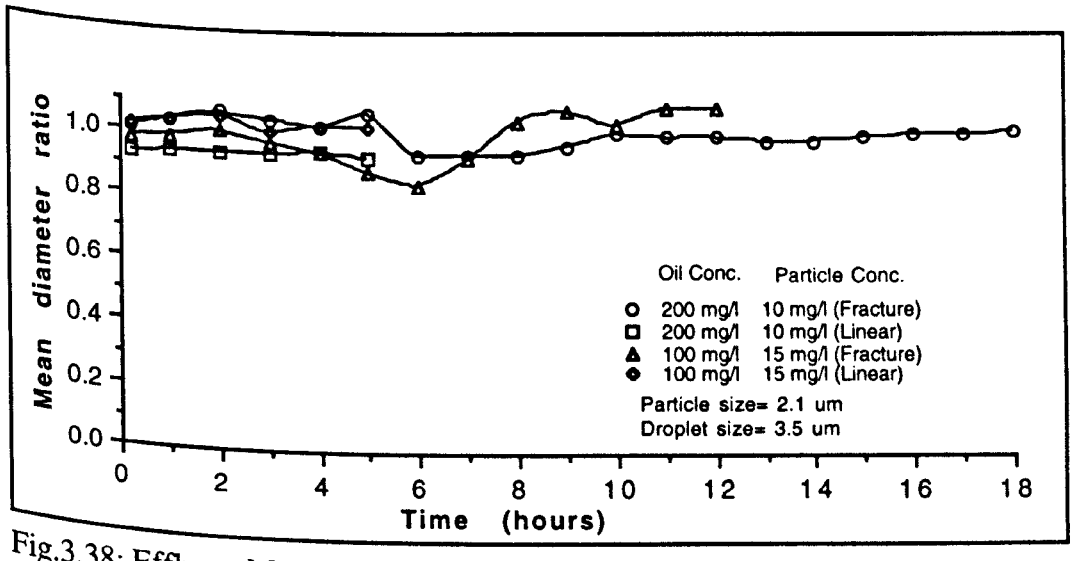

Fig.3.38: Effluent Mean diameter ratio change with time for the simulated produced water injection experiments (for LFI and LI exps. 57, 74, 81, and 67).

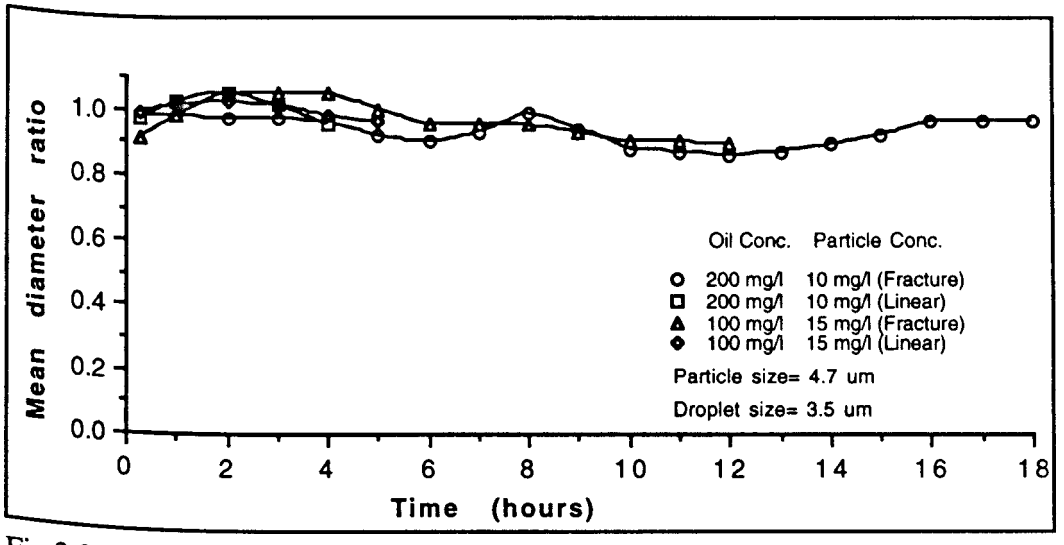

Fig.3.39: Effluent Mean diameter ratio change with time for the simulated produced water injection experiments (for LFI and LI exps. 42, 72, 82, and 70).

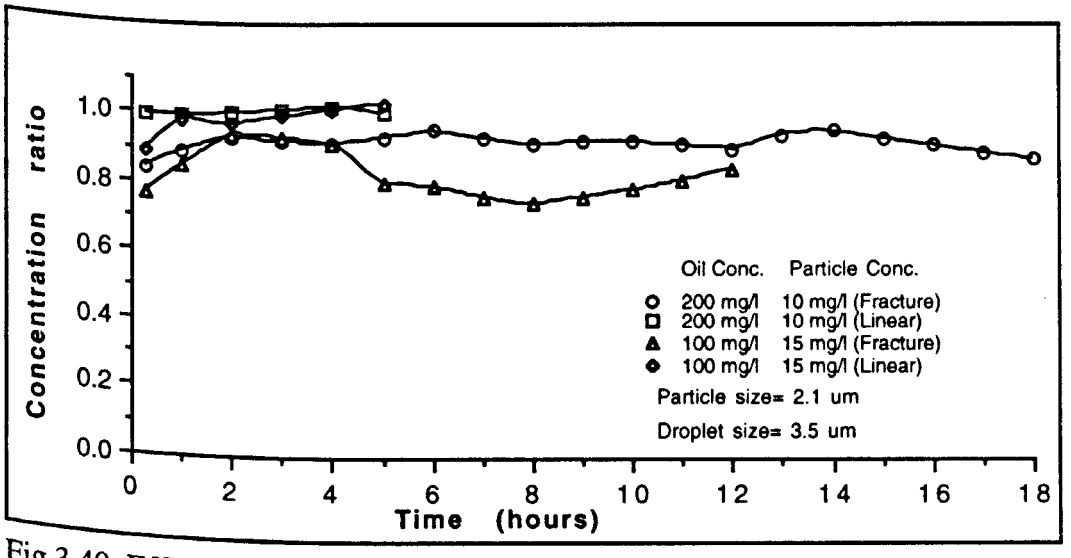

Fig.3.40: Effluent concentration ratio change with time for the simulated produced water injection experiments (for LFI and LI exps. 57, 74, 81, and 67).

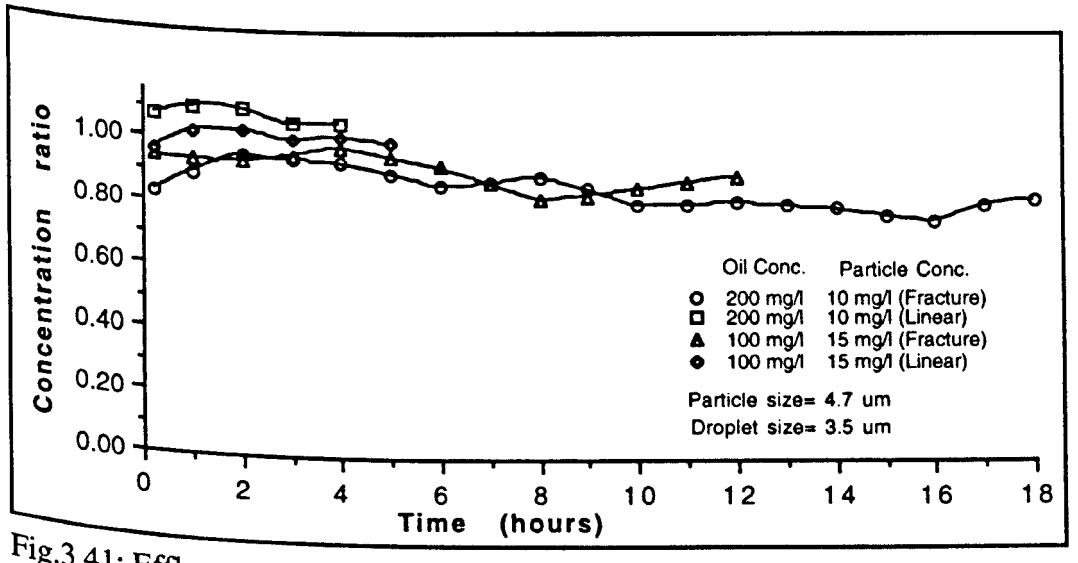

Fig.3.41: Effluent concentration ratio change with time for the simulated produced water injection experiments (for LFI and LI exps. 42, 72, 82, and 70).

3.7 The effluent along the fracture and through the side outlets:

The size and concentration measurements of the side outlet effluent and the fracture outlet effluent allowed the change in effluent properties to be tracked through time as the experiments continued.

The effluents of nine long fracture injection experiments were anaylsed and presented below. The fluid entered the fractured slab through the fracture inlet port. The fluid then flowed along the fracture and through the fracture face into the matrix to reach the side outlets. The side outlet effluent and the effluent along the fracture were analysed to measure the mean diameter ratio and concentration ratio of the particles and oil droplets. In this section a comparison study is presented between effluent properties of the different side outlets and the properties of the effluent along the fracture. The side effluent properties depended on many factors such as flow velocity and pressure drop. The pressure drop and the flow velocity were maximum at the nearest outlet to the fracture inlet which was A1 and B1; they were minimum at the outlets A3 and B3 which were farthest from the fracture inlet (Fig.2.1).

Due to these variations in flow velocity and pressure drop different effluent properties through side outlets are expected. Also the effluent properties along an open fracture would be expected to have similar properties as the influent fluid properties.

The mean diameter ratio (Mdr) and the concentration ratio (CR) data for the long fracture effluent is presented in Tables 3.28 and 3.29.

The study was divided into three parts depending on the injected fluid.

3.7.1 Oil emulsion with no solid particles

The emulsion consisted of a 3.8 μm oil droplets at concentration of 200 mg/l (experiment no. 75). The plots of mean diameter ratio and concentration ratio versus time showed that the effluent along the fracture had the same properties of the influent emulsion (Figs. 42 and 43). The side effluent of all the side outlets had a droplet mean size equal to the droplet mean size of the influent emulsion most of the time (Fig.3.42) and an oil concentration less than the influent concentration by only 5% (Fig.3.43).

The location of the side outlet had no effect on the droplet size or the oil concentration of its effluent. While oil flowed through the rock matrix to reach the side outlets, a small amount of droplets was captured within the matrix.

3.7.2 Solid particle suspension with no oil droplets

For the suspension that contained a 2.1 μm particles (experiment no. 77) at a concentration of 10 mg/l (Fig.3.44 and 3.45), the effluent along the fracture had the same particle mean size of the influent, and the particle concentration increase with time to reach the same influent particle concentration after 2 hours of injection. Then it started to decreases after 6 hours until the end of the experiment. The side effluent particle mean size fluctuated between nearly no particle (or less than 0.5 μm particles) and a size 2.5 times higher the influent particle mean size. The outlet A1 effluent had a mean size which was 1.5 times higher than the influent particle mean size most of the time whereas the outlet A3 had almost no particles most of the time.

The two outlets A1 and A3 effluent had particle concentrations lower than 25% of the influent particle concentration and the A1 outlet effluent had a particle concentration higher than the particle concentration of the outlet A3 at a later stage in the experiment.

For the suspension that contained 2.1 μm particles (experiment no.76) at concentration of 15 mg/l (Fig.3.46 and 3.47), the effluent along the fracture had the same particle mean size of the influent, and the particle concentration had the same influent particle concentration most of the time. The effluent particle mean size of the outlet A1 increased from 1μm (half the particle mean size of the influent) to 4 μm (double the particle mean size of the influent) and it stayed at this size until the end of the experiment. The effluent particle mean size of the outlet A3 fluctuated between nearly no particles (or less than 0.5 μm) and a size which was double the influent particle mean size all the way until the end of the experiment. The outlets A1 effluent had particle concentrations lower than 30% of the influent particle concentration and the outlet A3 effluent had a particle concentration lower than 10% of the influent particles concentration.

For the suspension that contained 4.7 μm (experiment no. 79) at a concentration of 10 mg/l (Fig.3.48 and 3.49), the particle mean size of the effluent along the fracture increased with time to reach a mean size equal to the influent particle mean size and the effluent particle concentration along the fracture decreased with time to a value lower than 50% of the influent particle concentration. The effluent of the outlet A1 had a particle mean size equal to the particle mean size of the influent suspension most of the time and a particle concentration between 10

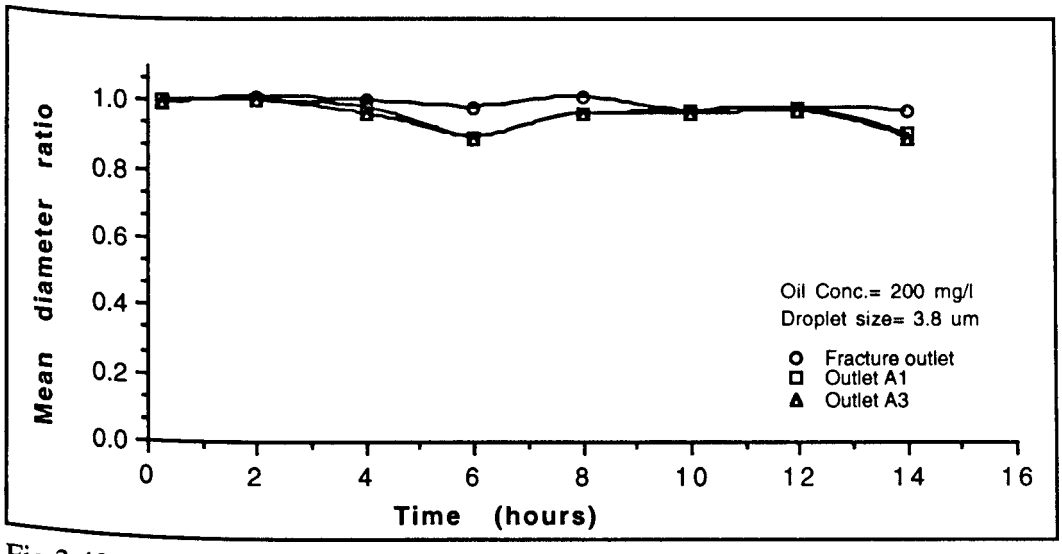

Fig.3.42: Effluent mean diameter ratio results for the fracture injection of an oil emulsion (exp. 75)

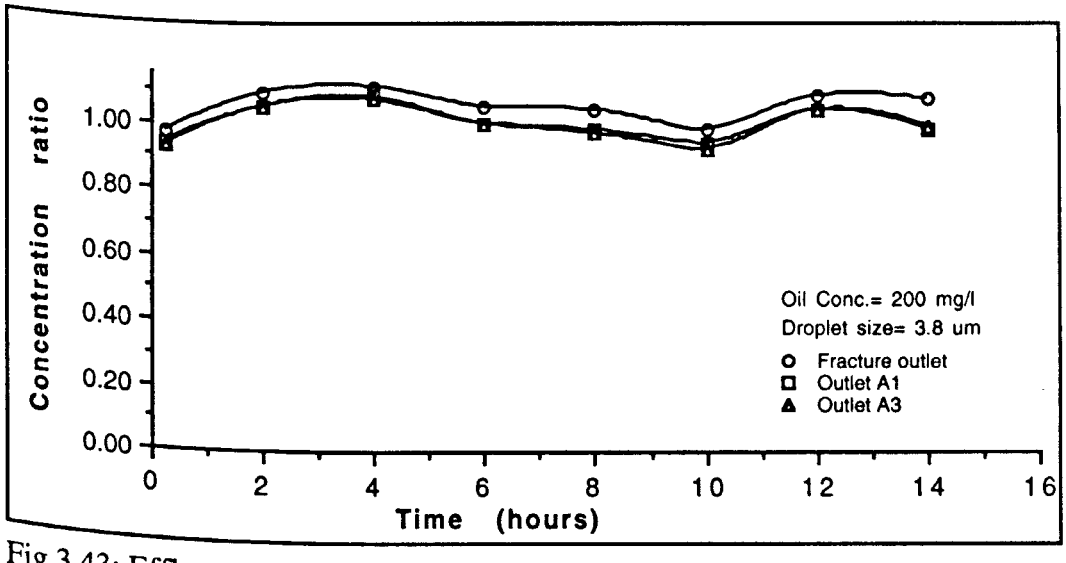

Fig.3.43: Effluent concentration ratio results for the fracture injection of an oil emulsion (exp.75).

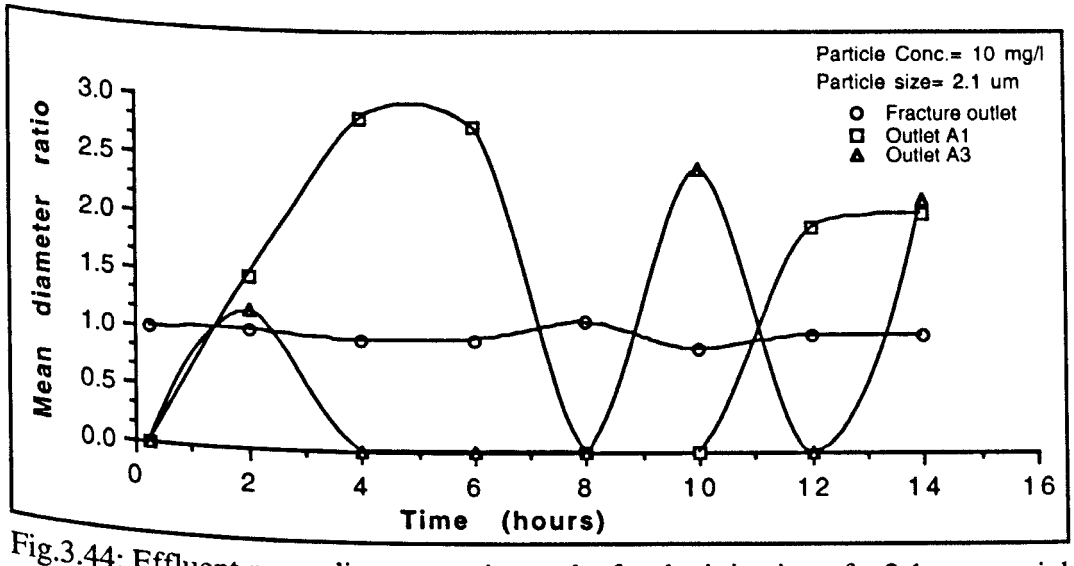

Fig.3.44: Effluent mean diameter ratio results for the injection of a 2.1 μm particle suspension at 10 mg/l concentration (exp. 77).

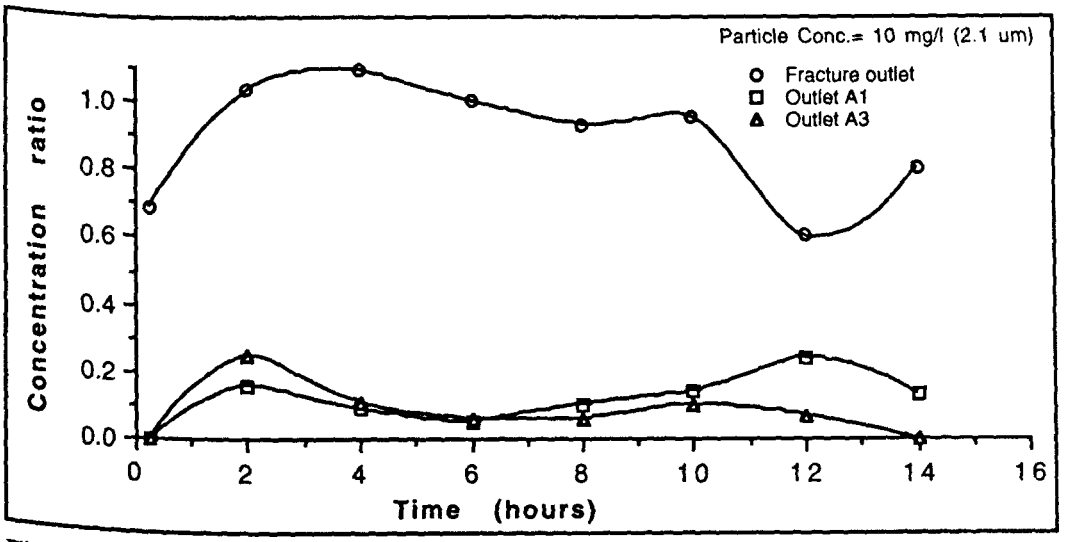

Fig.3.45:Effluent concentration ratio results for the injection of a 2.1 μm particle suspension at 10 mg/l concentration (exp. 77).

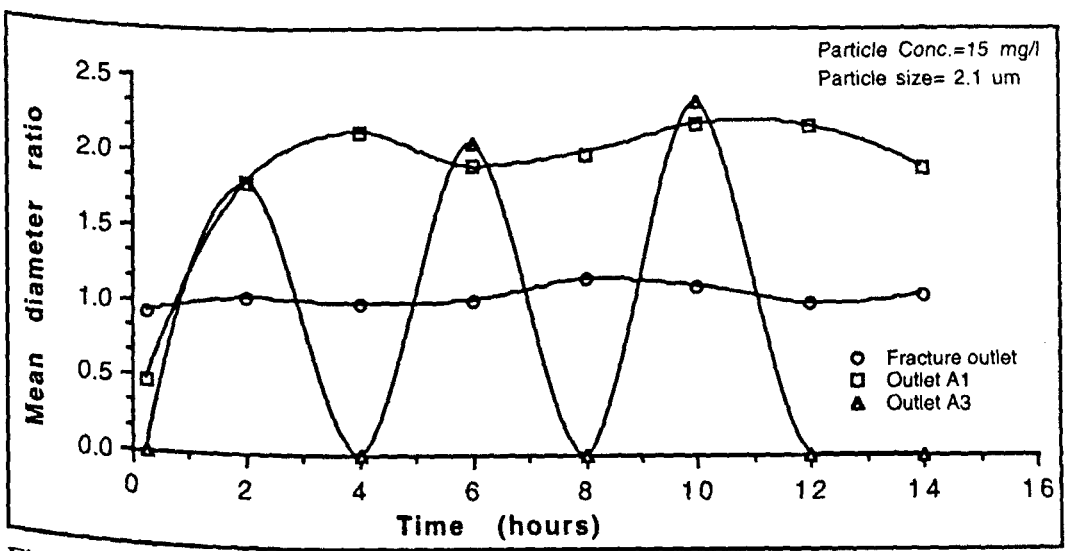

Fig.3.46: Effluent mean diameter ratio results for the injection of a 2.1 μm particle suspension at 15 mg/l concentration (exp. 76).

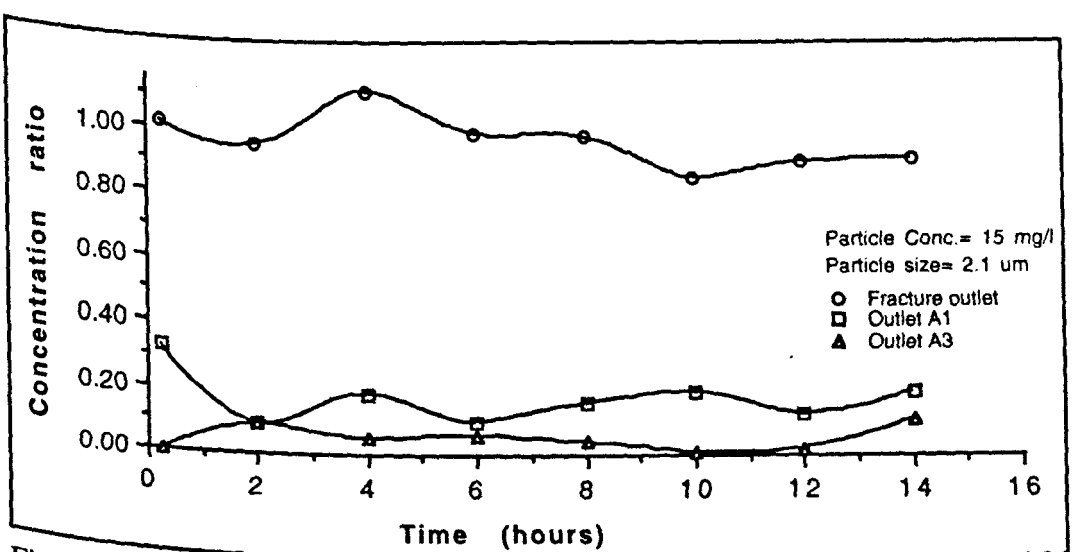

Fig.3.47: Effluent concentration ratio results for the injection of a 2.1 μm particle suspension at 15 mg/l concentration (exp. 76).

and 30% of the influent particle concentration. The outlet A3 had an average particle mean size of 2.5 μm (half the influent particle mean size) at 4 hours then the particle mean size dropped to nearly no particle (or less than 0.5 μm) with a particle concentration between 0 and 10% of the influent particle concentration.

For the suspension that contained 4.7 μm (experiment no. 80) at a concentration of 15 mg/l (Fig.3.50 and 3.51), the particle mean size of the effluent along the fracture had a particle mean size almost equal to the influent particle mean size, and the effluent particle concentration along the fracture was between 40 and 70% of the influent particle concentration. The side outlets A1 and A3 effluent had particle mean sizes slightly greater than the influent particle mean size, and a particle concentration of less than 15% of the influent particle concentration. The effluent particle concentration of the outlet A1 is higher than that of A3.

If the influent consisted of a particles of mean size equal to 2.1 μm, the particle mean size of the side effluent (effluent of A1 and A3) fluctuated between no particles in the effluent and particles of a size which is double the influent particle size. This fluctuation disappeared in the A1 effluent as the particle concentration of the influent increased from 10 to 15 mg/l, and the particle mean size of the outlet A1 was higher than 4 μm (double the particle mean size of the influent), but the fluctuation in the particle mean size was still seen in the A3 effluent.

As the influent particle concentration increased from 10 to15 mg/l, the difference between the effluent particle concentration of the outlets A1 and A3 increased and the effluent particle concentration along the fracture approached the particle concentration of the influent.

The capture of the 2.1 μm particles was higher at A3 than it was at A1, and the produced particle mean size for the side outlets was less than 0.5 μm or higher than the influent particle mean size, which indicated the capture of most of the meadium size particles.
As the concentration of the 2.1 μm particles in the influent increased, the particle concentration in the effluent along the fracture approches more the particle concentration of the influent fluid.

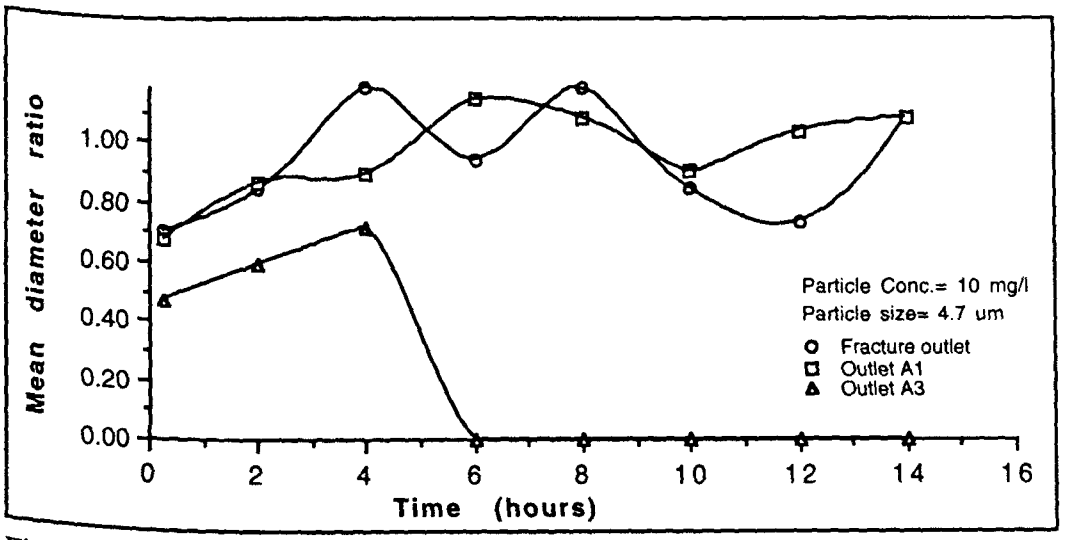

Fig.3.48: Effluent mean diameter ratio results for the injection of a 4.7 μm particle suspension at 10 mg/l concentration (exp. 79).

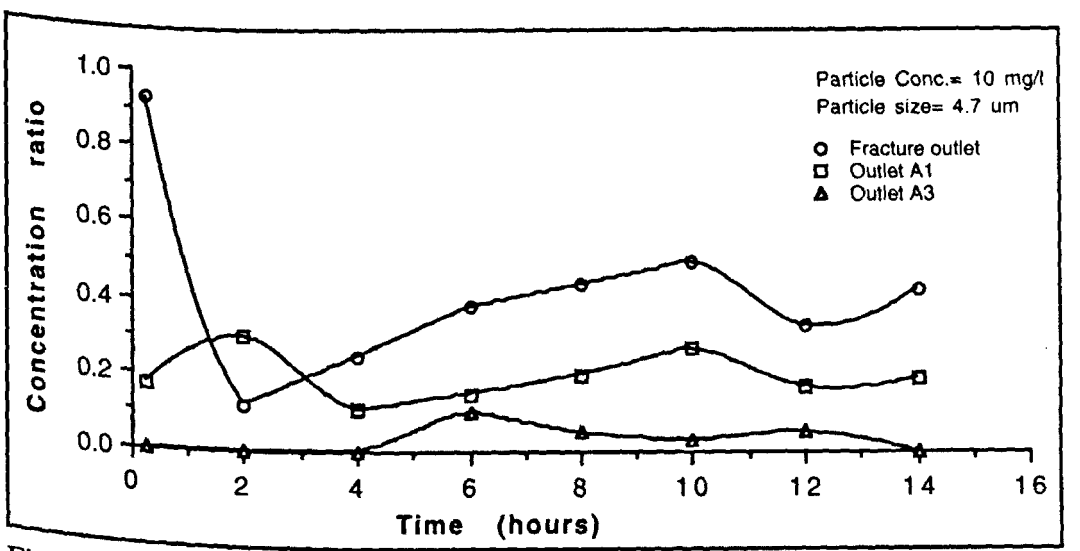

Fig.3.49: Effluent concentration ratio results for the injection of a 4.7 μm particle suspension at 10 mg/l concentration (exp. 79).

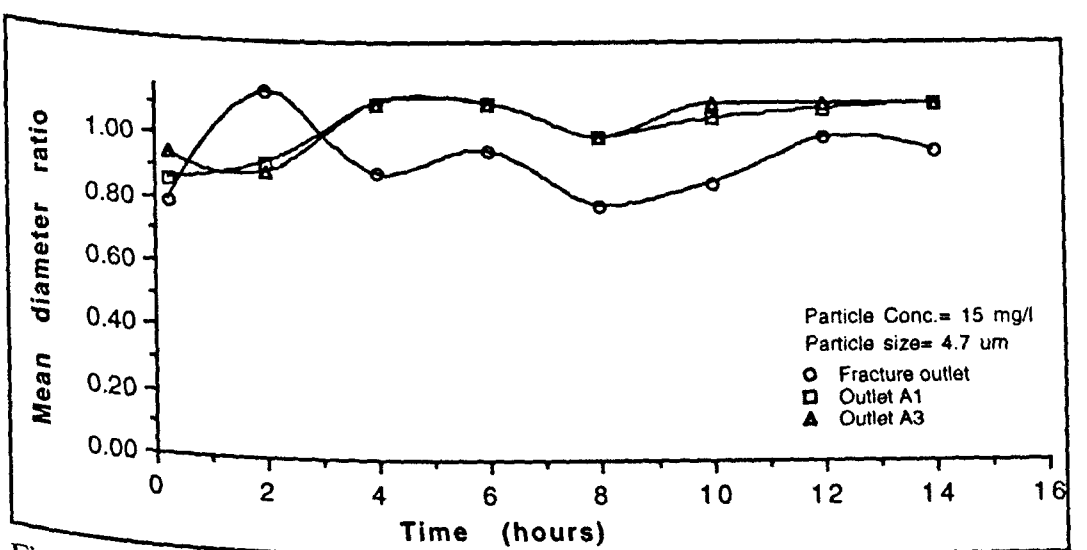

Fig.3.50: Effluent mean diameter ratio results for the injection of a 4.7 μm particle suspension at 15 mg/l concentration (exp. 80).

If the influent consisted of particles of mean size equal to 4.7 μm, the particle mean size of the port A1 was the same as the influent particle mean size but the A3 effluent had no particles after 4 hours. As the influent particle concentration increased from 10 to 15 mg/l, the particle mean size of the A3 effluent became equal to the mean size of the influent particle. For the injection of 4.7 μm particles, the particle concentration of the effluent along the fracture was much lower than the particle concentration of the effluent along the fracture in the case of the 2.1 μm particle injection. As the influent particle concentration increased the particle concentration of the effluent along the fracture increased and the particle concentration of the side effluent (through A1 and A3) decreased. Also the difference between the particle concentration in the A1 and A3 effluents decreased.

The concentration ratio at the side outlets A1 and A3 decreased as the particle concentration of the influent fluid increased from 10 to 15 mg/l, which indicated more capture of the 4.7 μm particles within the matrix. The reduction in CR at A1 was higher than it was at A3.

3.7.3 Simulated produced water

These experiments used four types of simulated produced water:

Particle mean size of 2.1 μm at a concentration of 10 mg/l and a droplet mean size of 3.5 μm at a concentration of 200 mg/l (experiment no.57).

Particle mean size of 2.1 μm at a concentration of 15 mg/l and a droplet mean size of 3.5 μm at a concentration of 100 mg/l (experiment no.81).

Particle mean size of 4.7 μm at a concentration of 10 mg/l and a droplet mean size of 3.5 μm at a concentration of 200 mg/l (experiment no.42).

Particle mean size of 4.7 μm at a concentration of 15 mg/l and a droplet mean size of 3.5 μm at a concentration of 100 mg/l (experiment no.82).

The effluent along the fracture and the effluent through the side outlets A1 and A3 had the same mean size all the time which was equal to the influent mean size when the injected fluid contained the 2.1 μm particles and less than the influent mean size by 4 to 10% when the injected fluid contained the 4.7 μm particles (Table 3.28).

For the case of the simulated produced water which contained the 2.1 μm particles at a concentration of 10 mg/l, the effluent along the fracture had nearly the same concentration as

the influent fluid. The side outlets A1 and A3 had an effluent concentration which was 5 to 10% lower than the influent concentration (Fig.3.52).

When the concentration of the 2.1 μm particles increased to 15 mg/l, the effluent concentration along the fracture became lower than the influent concentration by 7%. The side effluent concentration of the outlet A1 was decreased by 24% lower than the influent concentration and the effluent concentration of the A3 was lower than the effluent concentration of the A1 by 5 to 10 % (Fig.3.53).

Increasing the particle concentration increased the difference between the effluent concentration along the fracture and the effluent concentration through side outlets and also increases the difference between the effluent concentration of A1 and A3.

For the case of the simulated produced water which contained the 4.7 μm particles at a concentration of 10 mg/l, the effluent along the fracture and the effluent through side outlets A1 and A3 had a concentration between 10 and 20 % lower than the influent concentration (Fig.3.54) and the same results was obtained when the injected fluid contained a 15 mg/l of the 4.7 μm particles.

As the particle mean size of the influent increased from 2.1 μm to 4.7 μm (at the same particle concentration of 10 mg/l and the same oil concentration at 200 mg/l) the effluent concentration along the fracture and the effluent concentration through side outlets was reduced by 10 %.

As the oil concentration was much higher than the particle concentration, the mean diameter ratio and the concentration ratio results represented most of the time the mean diameter ratio and the concentration ratio of the oil droplets more than it represented the mean diameter ratio and the concentration ratio of the solid particles.

3.8. The effect of the rock matrix heterogeneity

In the linear core injection experiments the flow was directed through a very small flow area and only a small part of the formation was examined, which will not represent the heterogeneity

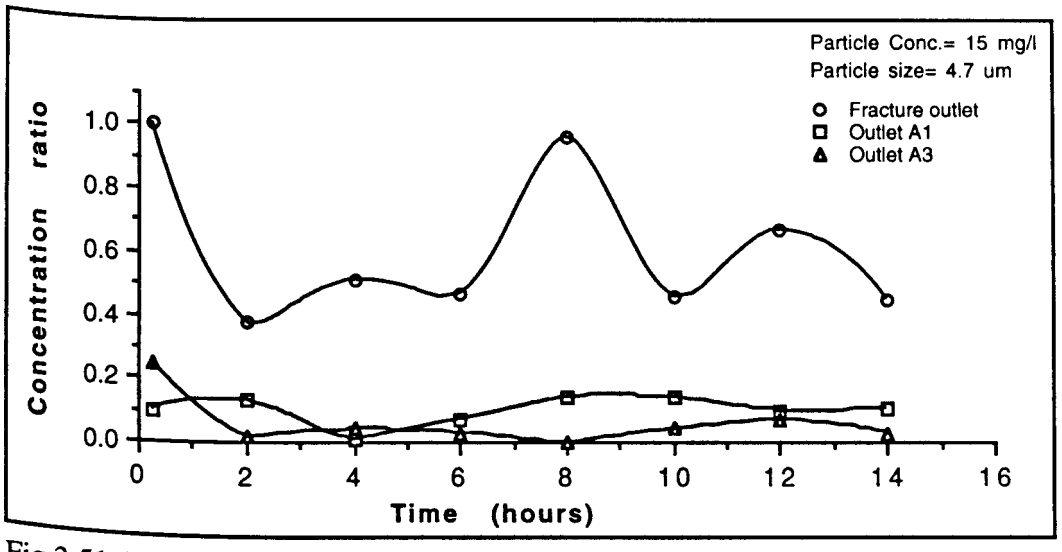

Fig.3.51: Effluent concentration ratio results for the injection of a 4.7 μm particle suspension at 15 mg/l concentration (exp. 80).

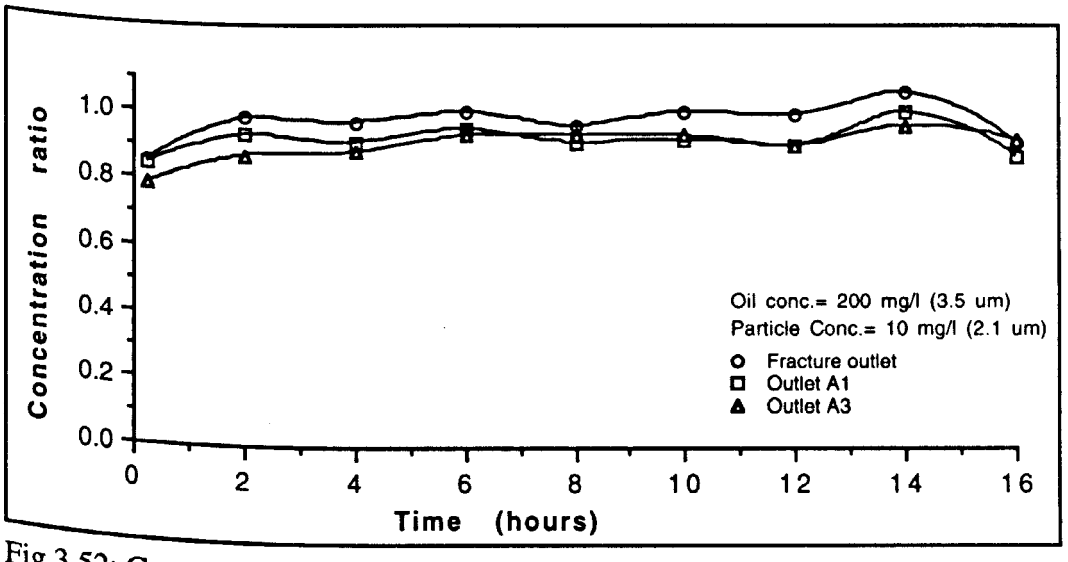

Fig.3.52: Concentration ratio results for the injection of a simulated produced water that contains 10 mg/l of 2.1 μm mean size particles and 200 mg/l oil (exp. 57).

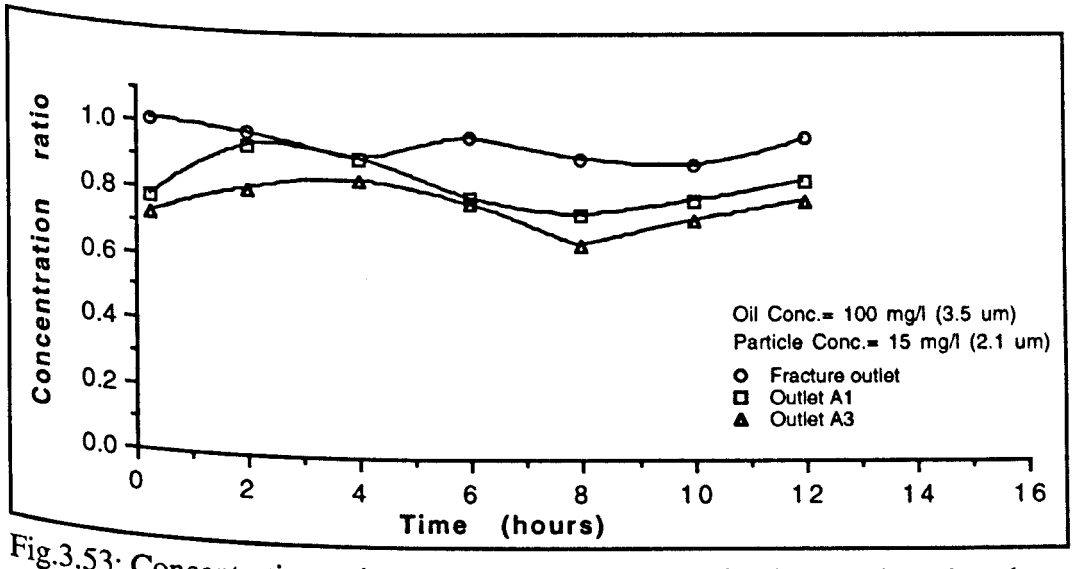

Fig.3.53: Concentration ratio results for the injection of a simulated produced water that contains 15 mg/l of a 2.1 μm mean size particles and 100 mg/l oil (exp. 81).

of the formation. In the case of fracture injection larger sections of the formation (which may represent the formation heterogeneity more than the small core) could be examined.

In fracture injection, the effect of formation heterogeneity on flow distribution through side outlets A1 to A3 (see fig.2.1) can be seen when the integrity of the fractured slabs was tested (section 3.1). In spite of the fact that outlet A1 is closer to the fracture inlet than A2 or A3, the flow rate through A3 some times was equal to the flow rate through A1, and the flow rate through A2 some times was higher than the flow rate through A1. These observations can be seen more clear as the pressure drop through the matrix increases. The flow distribution through the side outlets in the homogenous matrix was controlled by the distance of the outlet from the fracture inlet and the degree of matrix permeability damage at each outlet.

The following experiments were selected to represent the effect of matrix heterogeneity and matrix damage on flow distribution through side outlets. One experiment was performed by using a 40 cm long fractured slab and the other was performed by using a 20 cm long fractured slab. The complete data of these experiments is shown in Table 3.30.

In Experiment 17 a simulated produced water contained 6.5 μm mean size oil droplets at a concentration of 100 mg/l and 7.4 μm mean size solid particles at a concentration of 10 mg/l. The rock matrix was non homogenous as the initial permeability of matrix varied between 235 md at the first section of the slab at the outlet A1 and 295 md at the third section of the slab at the outlet A3.

The flow distribution was controlled by the distance from the fracture inlet and the degree of matrix damage. At the start of the injection, the flow rate through side outlets A1 and B1 was higher than the flow rate through side outlets A3 and B3 (Fig.3.55). This indicated that the fluid passing through outlets A1 and B1 was much larger than the fluid quantities passing through outlets A3 and B3 which resulted in a higher degree of damage through the side paths A1 and B1. As the permeability of the side paths A1 and B1 decreased the flow through the side outlets A1 and B1 decreased and the flow was directed more and more through the less damaged paths A3 and B3. Actually there was a successive increase and decrease in flow through all the side outlets (which was caused by a break of some blocked paths due to increase

in pressure drop but these paths started to be blocked again after some time), but the general indication was that the flow was increasing through outlets A3 and B3 and flow was decreasing through outlets A1 and B1. Therefore, as the damage was taking place in the matrix near to the fracture inlet, the flow was directed more and more along the fracture to cover a new, less damaged, fresh matrix with less resistance.

In Experiment 42 a simulated produced water containing a 3.4 μm mean size oil droplets at a concentration of 200 mg/l and 4.7 μm mean size solid particles at a concentration of 10 mg/l was used. The rock matrix was non homogenous as the initial permeability varied between 230 md at the first section of the slab at the outlets A1 and B1 and 320 md at the second section of the slab at the outlets A2 and B2. In spite of A1 and B1 being closer to the fracture inlet, at the start of the experiment the flow rate through A1 and B1 was lower than the flow rate through A2 and B2 because the permeability of the A2 and B2 paths was much higher (Fig.3.56). The outlets A2 and B2 accepted a higher quantity of fluid. But due to the less damaging nature of the particles used, it took a longer time before the damage started to affect the flow pattern and caused a reduction in flow rate in the A2 path. This reduction was compensated by an equal increase in flow rate through side path A1 which was less damaged and with a higher differential pressure (closest to the fracture inlet).

The reduction in flow rate through a certain side outlet due to matrix blocking may cause an increase in flow rate of a nearby side outlet which has less permeability impairment and higher differential pressure (instead of directing the flow along the fracture to cover a new less damaged fresh matrix).

In fracture injection, as the fracture length increased a wide range of matrix heterogeneity will lead to different degrees of matrix blocking from location to location. The random variation in matrix permeability will result in a random degree of matrix blocking which may not be dependent on the distance from the fracture inlet.

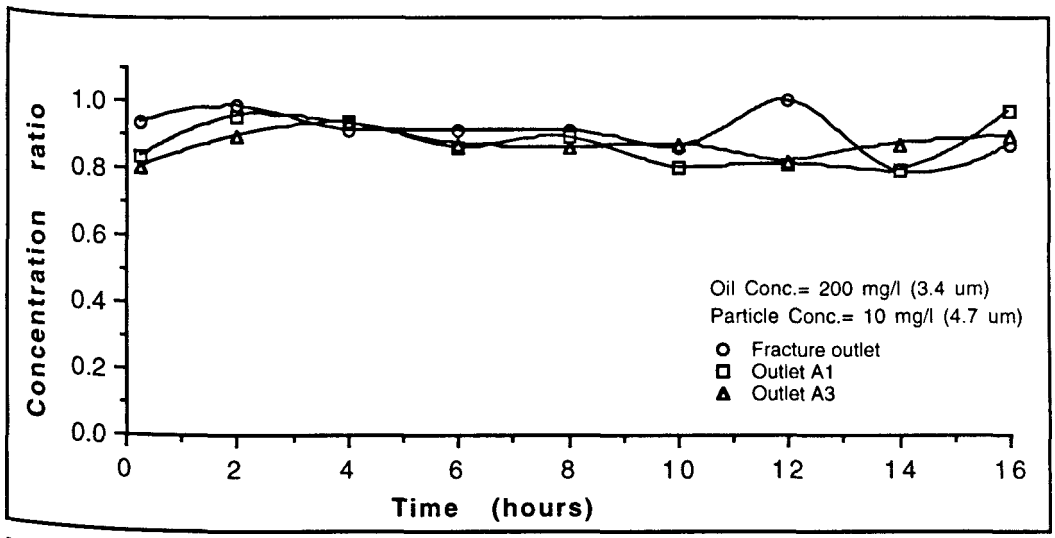

Fig.3.54: Concentration ratio results for the injection of a simulated produced water that contains 10 mg/l of a 4.7 μm mean size particles and 200 mg/l oil (exp. 42).

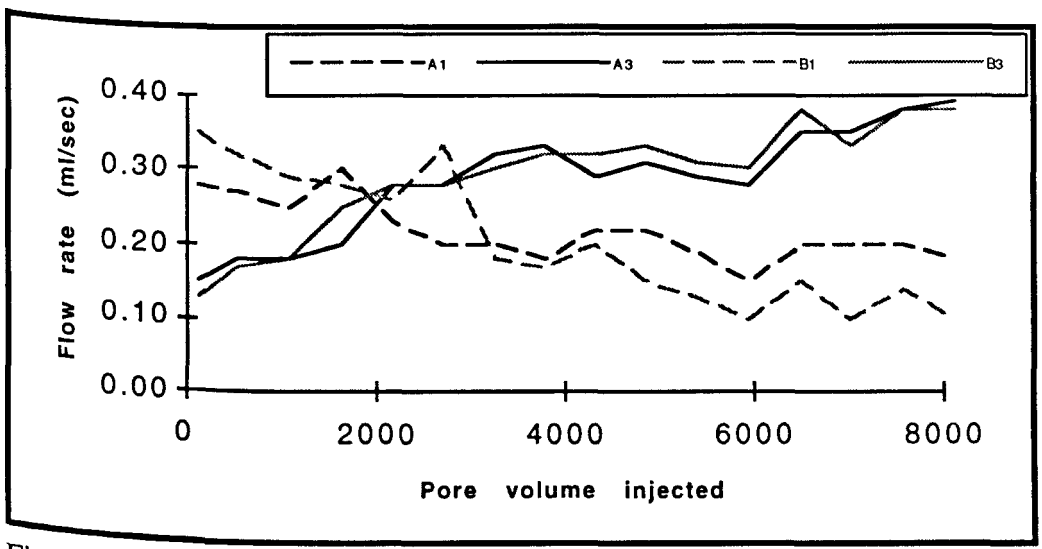

Fig.3.55: The change in flow distribution through side outlets for non homogenous short fractured slab (exp. 17).

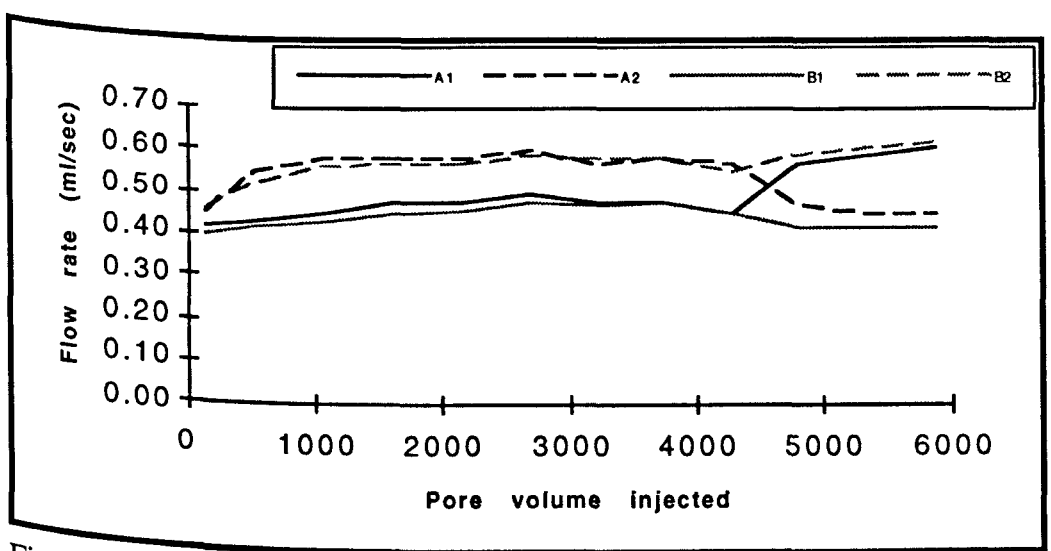

Fig.3.56: The change in flow distribution through side outlets for non homogenous long fractured slab (exp. 42).

3.9 Filter cake formation and erosion

This group of experiments were designed to study the formation of the internal filter cake inside the rock matrix behind the fracture face, the formation of the external filter cake on the fracture face and to study the flow behaviour along the fracture and through the rock matrix at this stage. The external filter cake starts to build up on the fracture face after a long time of contaminated water injection and for the cake to fill the fracture aperture it will take even more injection time. Rochon[71] stated that for quite clear North sea water an external cake started to build-up after almost 9 years and for the Guinea Gulf (much dirtier sea water) it takes 2 years before the switch between internal and external cake damage occurs. Assuming static filtration (the erosion effect caused by the velocity of flow along the fracture on the external cake was neglected) after that, the fracture will take 2 years to be filled for the North sea case and a half year for the Guinea Gulf case. For dynamic filtration (which is the case in the fracture injection) the accumulated external cake will be eroded due to the fluid shear along the fracture.

To observe experimentally the external cake formation along the fracture, it was important to decrease the time needed (due to time limitation) for the external cake to be formed and fill the fracture. To accelerate the process of the external cake formation and the process of filling the fracture with this cake, several steps were taken:

1. Suspensions which contained particle concentrations of 40 and 100 mg/l (which was much higher than the actual particle concentration recorded in field water injection schemes) were used.
2. The side pressure drop through the rock matrix perpendicular to the fracture face was increased to force the solid particles to accumulate on the fracture face. This was done by making the side pressure drop nearly 10 times greater than the pressure drop along the fracture.
3. Relatively low permeability fractured sandstone slabs (from 50 to 140 md) were used.

This group of experiments were undertaken with two particle concentrations of 40 and 100 mg/l. These particles were in three different mean size groups (2.0 μm , 4.7 μm and 9.4 μm). The particle size distribution of these three particle groups was measured by using Malvern master sizer and the results are shown in Figure 3.57. Fractured slabs of 20 cm long were used in these experiments.

The experimental conditions for this group of experiments were as follows:

Experiment no.	matrix perm. (md)	particle conc. (mg/l)	particle size (μm)	Fracture aperture (mm)
8	49	100	9.4	0.43
11	99	40	9.4	0.44
9	109	100	4.7	0.42
13	141	40	2.0	0.42

3.9.1 Large particle suspensions

Two experiments illustrate the effect of large particles: experiment 8 and 11.

Table 3.31 shows detailed information about experiment 8. The observations in this experiment confirmed the accumulation of a permeable external cake on the fracture face. The side flow rate through the fracture face increased with time and the flow along the fracture decreased as the filter cake started to build-up on the fracture face and resisted the flow along the fracture (as the available flow area along fracture is reduced) (Fig.3.58). As a result of this flow reduction along the fracture and flow increase through the fracture face, the pressure drop through side outlets increased. The concentration ratio plot against time confirmed the build-up of an external filter cake at this stage (Fig.3.59). In this plot it can be seen that the CR of the effluent along the fracture is less than 0.5 and CR of the effluent through side outlets is less than 0.05, so the rest of the particles must be accumulated as internal filter cake or as external filter cake on the fracture face until 3000 pore volume was injected. The increase in side flow and the decrease of flow along fracture with time confirm the belief of the external cake accumulation (as the internal cake presence will resist and decrease the side flow through rock matrix which is not the case here).

After 3000 pore volumes, the external cake nearly closed the fracture aperture and the CR of the effluent along the fracture reached a minimum value of 0.15. At this point the particle accumulation started to decrease as the flow path along the fracture become smaller and smaller (as the flow velocity became high enough to reduce the particle accumulation on the filter cake surface) then the CR of the effluent along the fracture started to increase to reach a value of 1.0 (zero particle precipitation on the filter cake surface) after 7500 pore volume was injected.

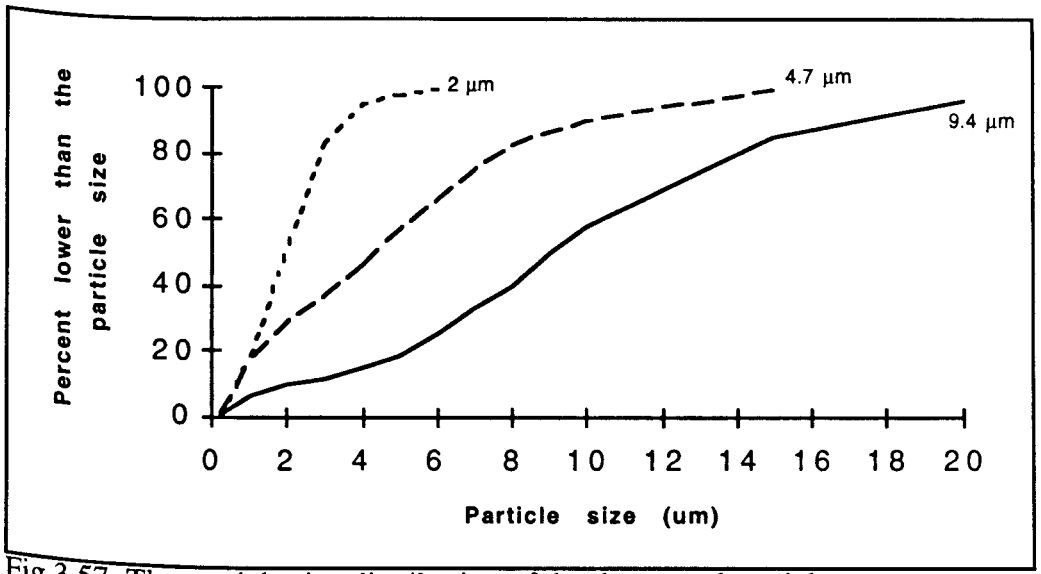

Fig.3.57: The particle size distribution of the three used particle groups.

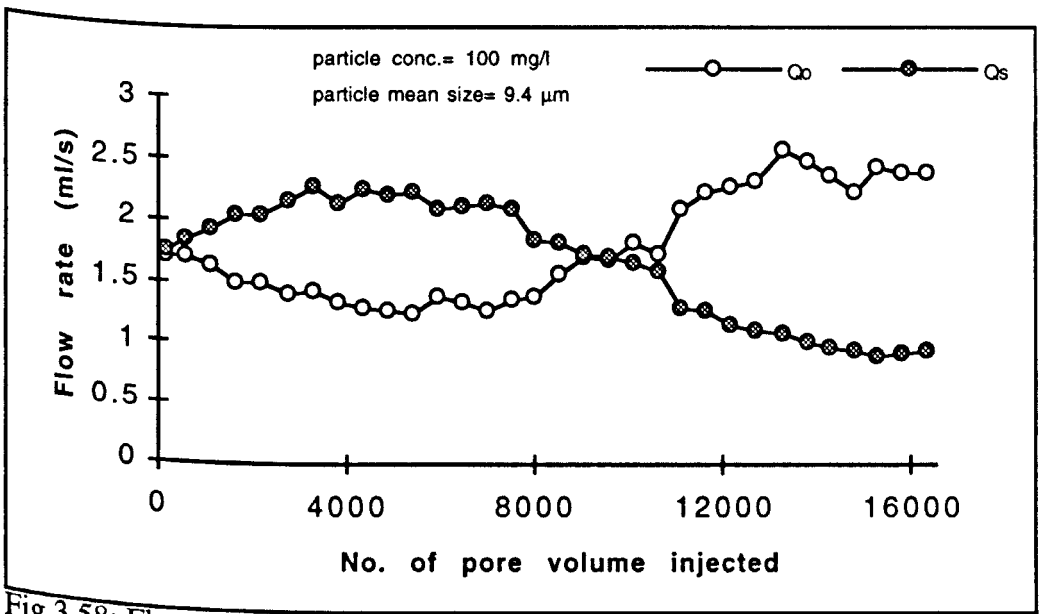

Fig.3.58: Flow along the fracture (Q_o) and the flow through side outlets (Q_s) for a 100 mg/l particle suspension injection with a 9.4 µm particle mean size (exp. 8).

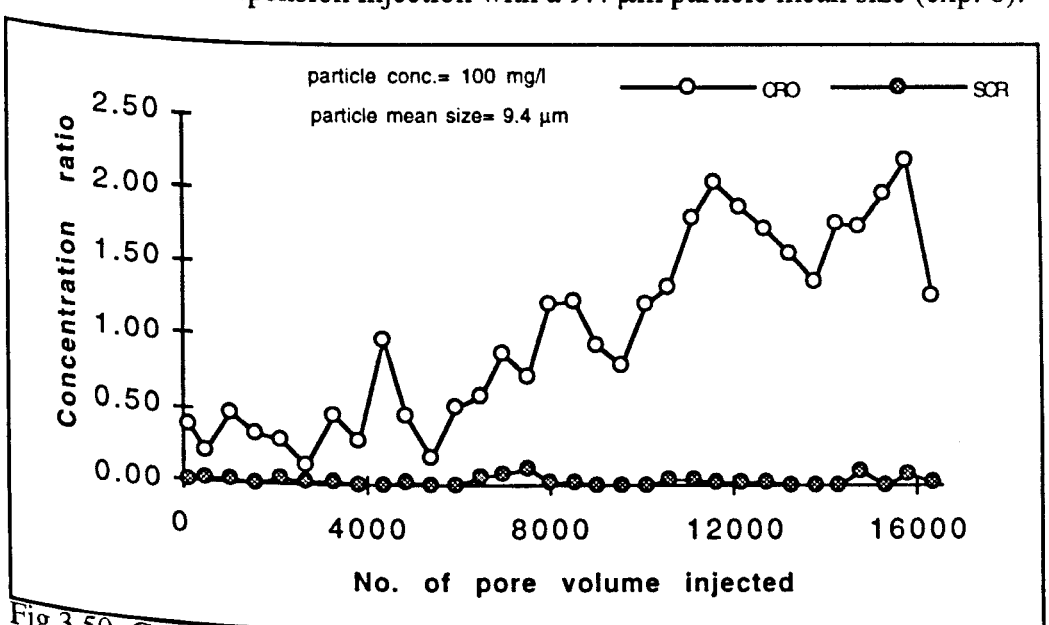

Fig.3.59: Concentration ratio of the effluent along the fracture (CRO) and the effluent through side outlets (SCR) for a 100 mg/l of 9.4 µm particle suspension injection (exp. 8).

As the permeability of the filter cake decreased, the flow was directed more and more along the fracture which caused the erosion of the filter cake as the flow forced its way along the fracture. This resulted in an increase in the CR of the effluent along the fracture to a value higher than 1.0 due to the erosion of the filter cake. As the flow increased along the fracture, more erosion of the filter cake took place as can be seen in the CR plot versus time (as a huge increase in particle concentration to a value which was double the influent particle concentration). The side flow rates decreased steadily indicating the build up of internal filter cake with time. The continuous increase in flow along the fracture caused a continuos increase in the pressure drop along the fracture (Fig.3.60).

The particle mean size ratio of the side effluent was less than 0.4 indicating that large particles were captured by the external cake and the particle mean size of the effluent along the fracture was nearly the same as the particle mean size of the influent (Fig.3.61).

When the slab was cut open along the fracture length, a very thick external filter cake all the way along the fracture was observed. Within the cake a thin and long channel (connecting the inlet and the outlet of the fracture) was seen (Plate 3.9.1)

The sample was then broken apart and two small chips of rock were then taken from the fracture face. On using a Scanning Electron Microscope, it was clear to see that the solid particles completely blocked the fracture face preventing any further invasion of particles into the rock matrix (Plate 3.9.2).

Table 3.32 shows a detailed summary of experiment 11.

Similar flow trends as in experiment 8 can be seen in experiment 11 with small differences. Due to the higher permeability of this slab and the lower particle concentration, the external cake started forming after a considerable number of pore volumes was injected. The absence of external cake at this stage caused some accumulation of internal plugging. This can be seen as a decrease in flow through side outlets at early injection time (Fig.3.62). The erosion of the filter cake started at an earlier time as indicated by the CR plot (Fig.3.63). When the slab was cut open, again a channel extended along the fracture was seen.

For both experiments some increase in CR of the effluent through side outlets when the external cake started to be eroded could be seen, indicating a re-exposure of some of the fracture face.

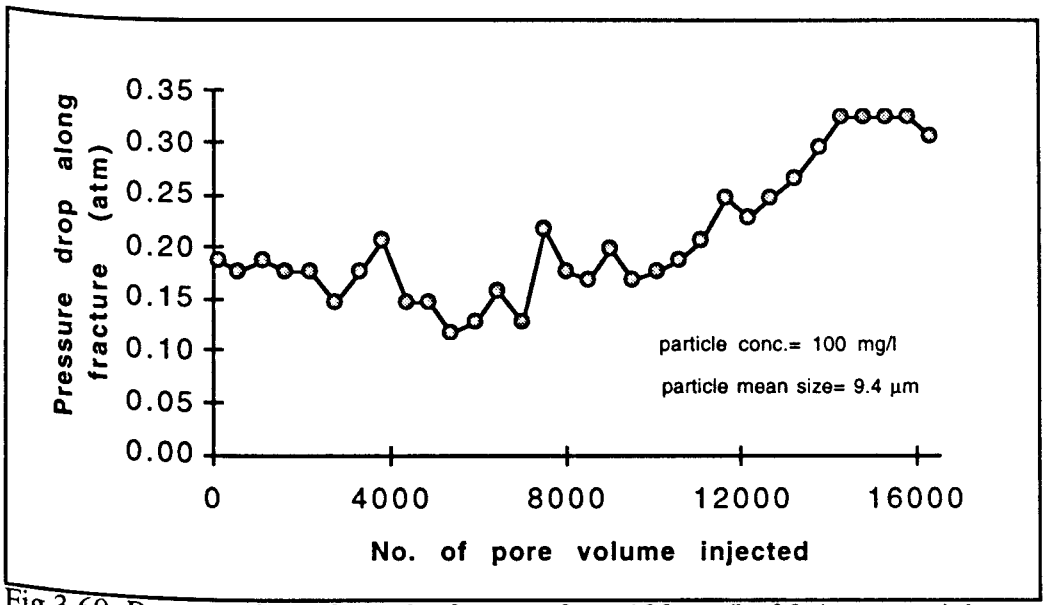

Fig.3.60: Pressure drop along the fracture for a 100 mg/l of 9.4 µm particle suspension injection (exp. 8).

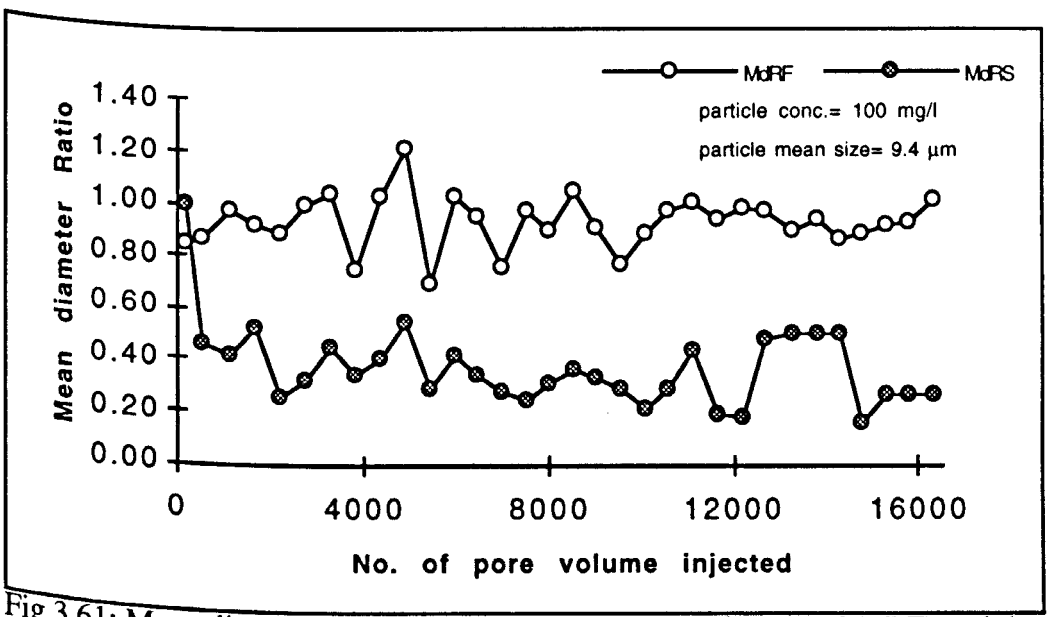

Fig.3.61: Mean diameter ratio of the effluent along the fracture (MdRF) and through the side outlets (MdRS) for a 100 mg/l of 9.4 µm particle suspension injection (exp. 8).

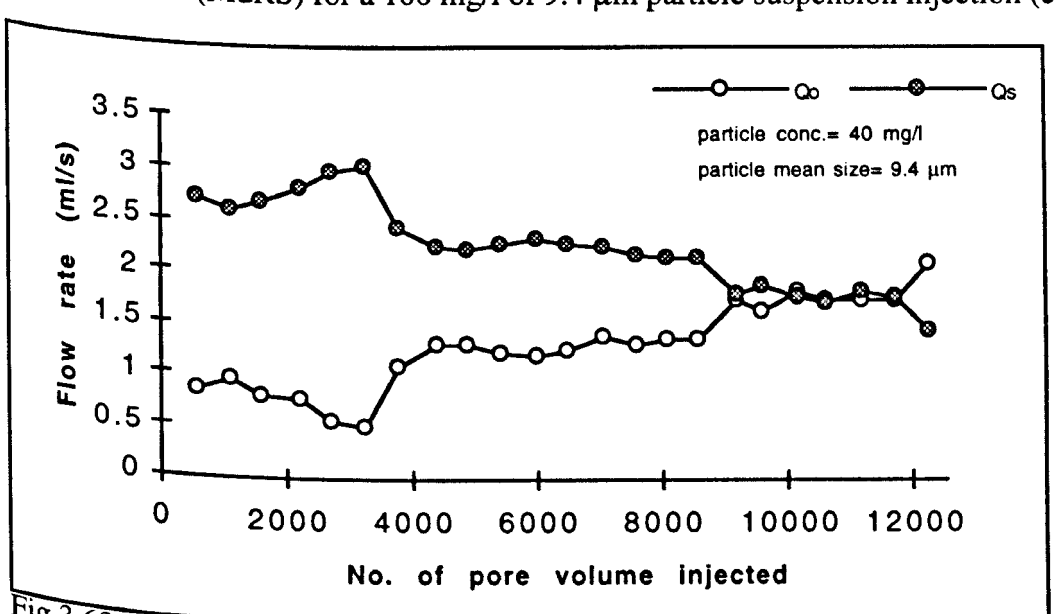

Fig.3.62: Flow along the fracture (Q_o) and the flow through side outlets (Q_s) for a 40 mg/l particle suspension injection with a 9.4 µm particle mean size (exp. 11).

Plate 3.9.1 Photograph of the fracture face when the fractured slab of Exp. 8 was cut open.

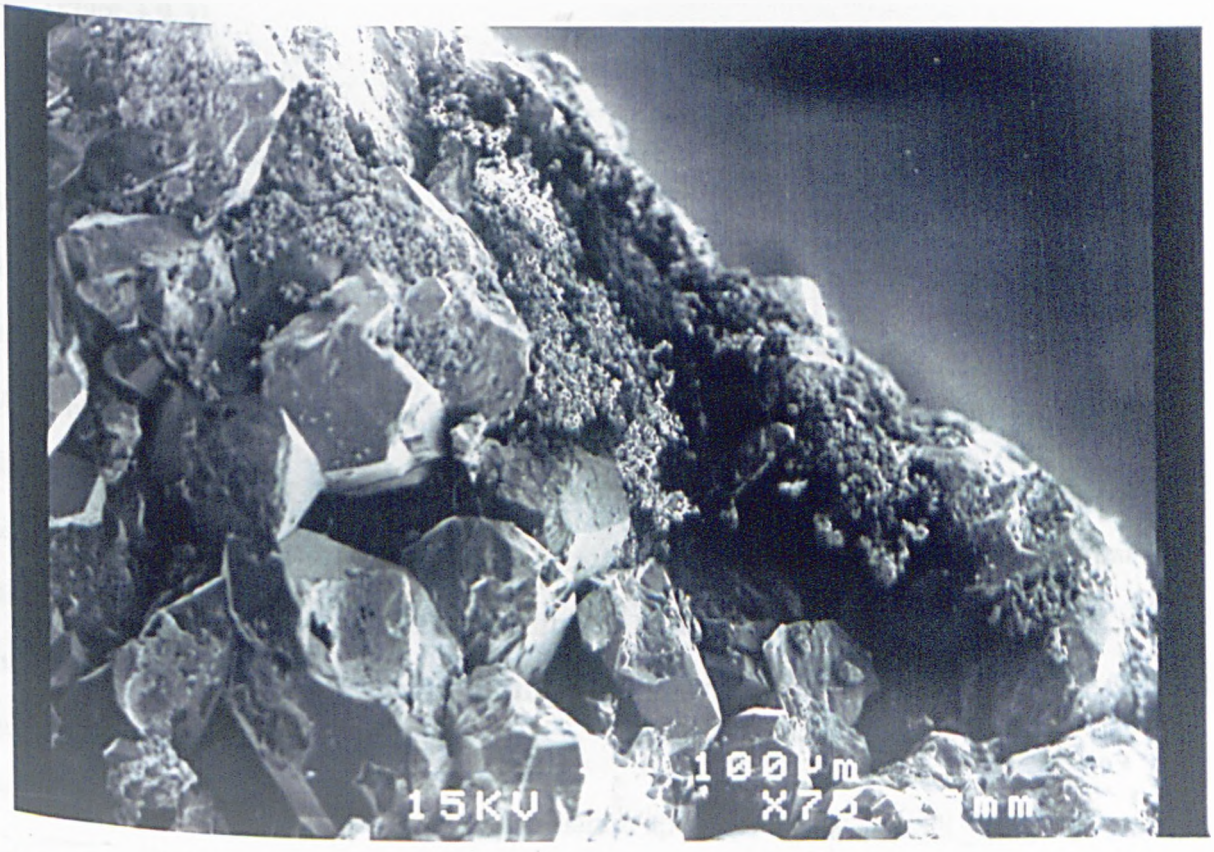

Plate 3.9.2 SEM image of the fracture face of the factured slab for Exp. 8.

This increase in the side effluent CR reached a value of 0.12 for experiment 8 and 0.23 for experiment 11.

3.9.2 Medium particle suspensions

Table 3.33 shows detailed information for experiment 9.

Again similar observations can be made for experiment 9. In this experiment 4.7 μm mean size particles were used (with 100 ppm concentration) which may have caused the formation of internal cake in the first stage and a less permeable external cake in the second stage. This can be seen as a continuous increase in the pressure drop through side outlets from 1.6 to 3.4 atm at the end of the experiment (Fig.3.64) which is far higher than the side pressure drop in the case of the two pervious experiments.

The filter cakes were very effective (even after the erosion of the external cake) in preventing particle production through the side outlets as the side effluent CR was almost zero at all times (Fig.3.65). A tortuous channel was seen when the slab was cut open. similar to that seen in experiment 8.

The Scanning Electron Microscope also confirmed the presence of internal and external filter cake (Plate 3.9.3).

3.9.3 Small particles suspension

Table 3.34 shows detailed information for experiment 13.

In this experiment particles of 2 μm mean size were used, these particles was expected to pass through the rock matrix to reach the side outlets with minimum capture.

At the beginning of the experiment, and due to high side pressure drop, all the flow was directed through the side outlets with zero flow at the outlet along the fracture. The CR of the side effluent was less than 0.4 (Fig.3.66). As the particles started to cause some internal blocking or filling, some of the flow was directed along the fracture (Fig.3.67). At the same time the CR of the effluent along the fracture increased to reach a value of 1.0 and the CR of the side effluent reached a very low value of 0.05.

When the external cake started to plug the fracture aperture, the flow along the fracture decreased to zero and this was the case with the CR of the effluent along the fracture. As the flow was directed through the side outlets, some of the particles accumulated in the filter cake

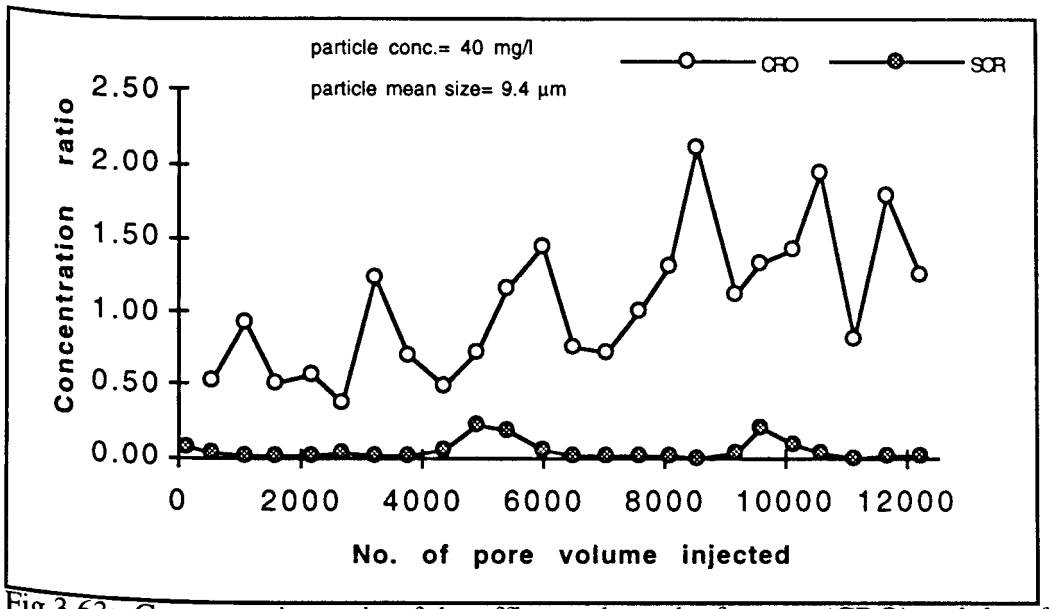

Fig.3.63: Concentration ratio of the effluent along the fracture (CRO) and the effluent through side outlets (SCR) for a 40 mg/l of 9.4 µm particle suspension injection (exp. 11).

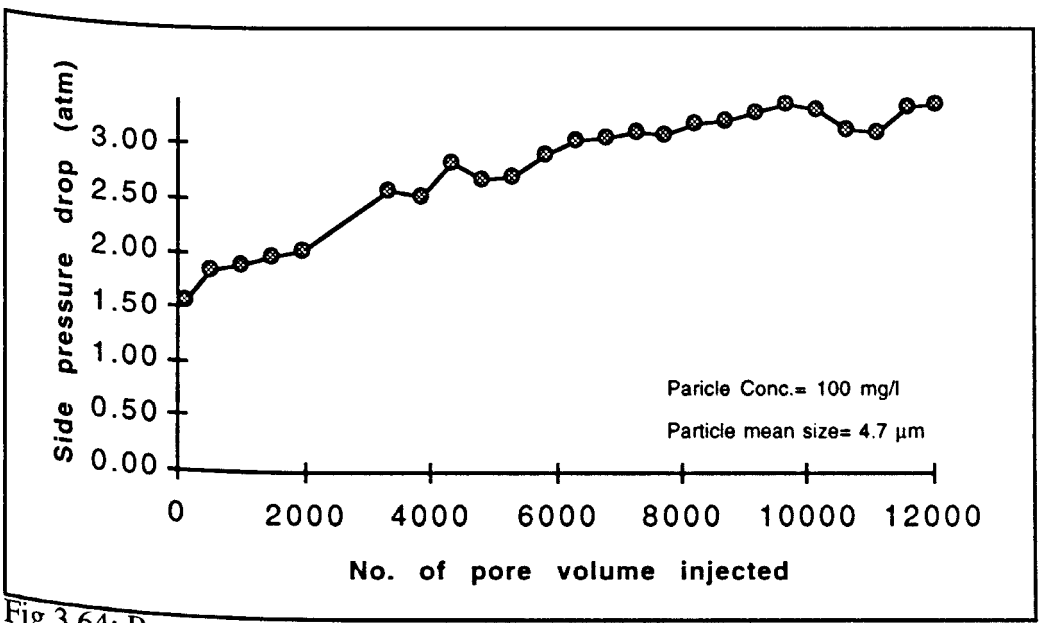

Fig.3.64: Pressure drop through side outlets for a 100 mg/l of 4.7 µm particle suspension injection (exp. 9).

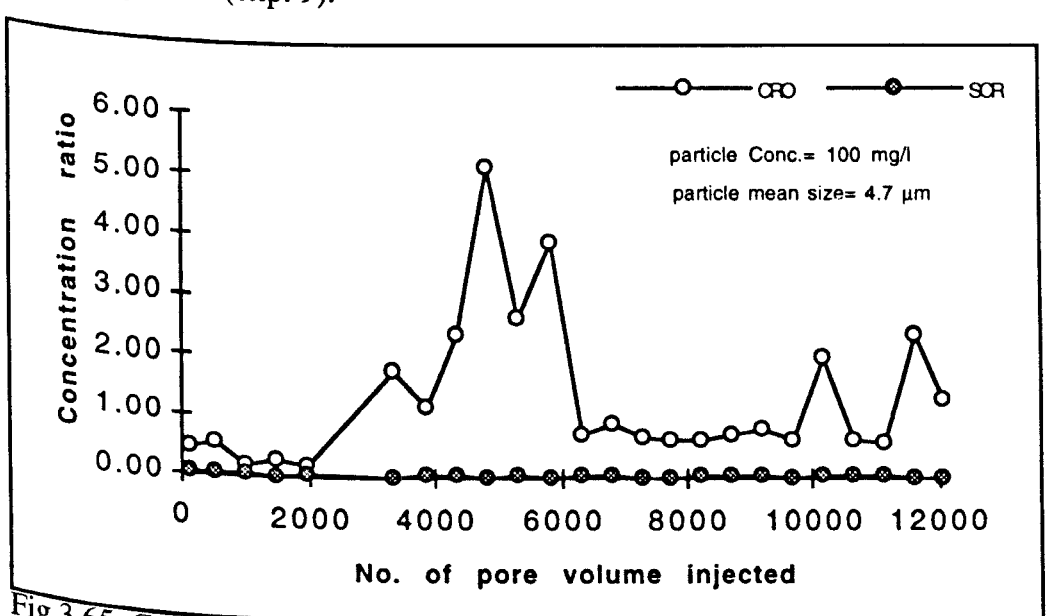

Fig.3.65: Concentration ratio of the effluent along the fracture (CRO) and the effluent through side outlets (SCR) for a 100 mg/l of 4.7 µm particle suspension injection (exp. 9).

and some passed through to reach the side outlets and the CR of the side effluent increased with time.

At 13000 pore volumes injected nearly all the particles were passing through the matrix to reach the side outlets and the CR of the side effluent reached a value of 1.0.

At some periods (as at 8000 pore volume injected) there was a peak in the CR of the effluent along the fracture due to a small break through in the flow along the fracture caused by a temporary resistance to the side flow through rock matrix.

The particle mean size in the side effluents or the effluent along the fracture was always equal to the particle mean size of the influent (Fig.3.68).

The point when the actual erosion of the external filter cake started was not reached. The observed process was only cake accumulation as the flow was not allowed to reach the fracture outlet due to the high side pressure drop.

When the slab was cut open a thin filter cake with a very smooth surface was seen, no channel was seen through the cake (Plate 3.9.4).

3.9.4 Rock matrix permeability alteration

Table 3.35 shows the permeability ratio (Kd / Ki) change with pore volume of fluid injected for experiment 8, 9, 11 and 13.

For a constant particle mean size of 9.4 μm, the increase of particle concentration reduced the permeability alteration of the rock matrix (Fig.3.69). For example by increasing the concentration from 40 ppm to 100 ppm, the permeability ratio at 8000 pore volumes injected increased from 0.62 to 1.0 (no reduction in Kd / Ki). This may be a result of the early formation of the external filter cake which prevented the matrix alteration. The external filter cake filters the fluid and thus cleaner fluid goes through the matrix, causing no damage. After 8000 pore volume injected, the measured CR value at the fracture outlet was high which may indicate external cake flushing allowing more fluid into the matrix which reduces the matrix permeability (from 8000 pore volume injected onwards).

For a constant particle concentration of 100 ppm, decreasing the particle mean size from 9.4 μm to 4.7 μm increased the permeability altration of the rock matrix by a large margin (Fig.3.70). For example the permeability ratio at 8000 volumes injected decreased from 1.0

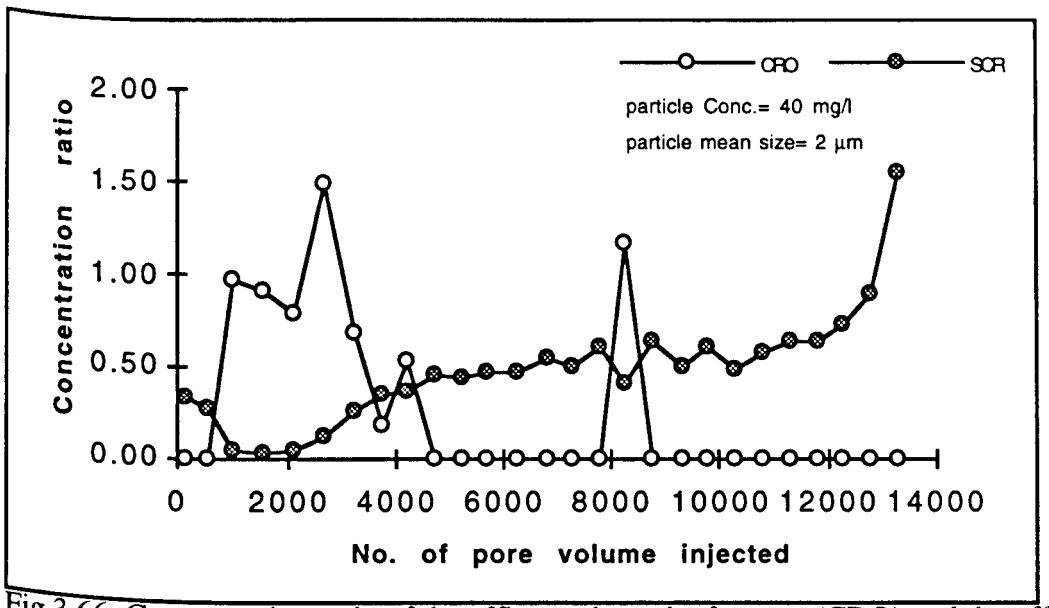

Fig.3.66: Concentration ratio of the effluent along the fracture (CRO) and the effluent through side outlets (SCR) for a 40 mg/l of 2 µm particle suspension injection (exp. 13).

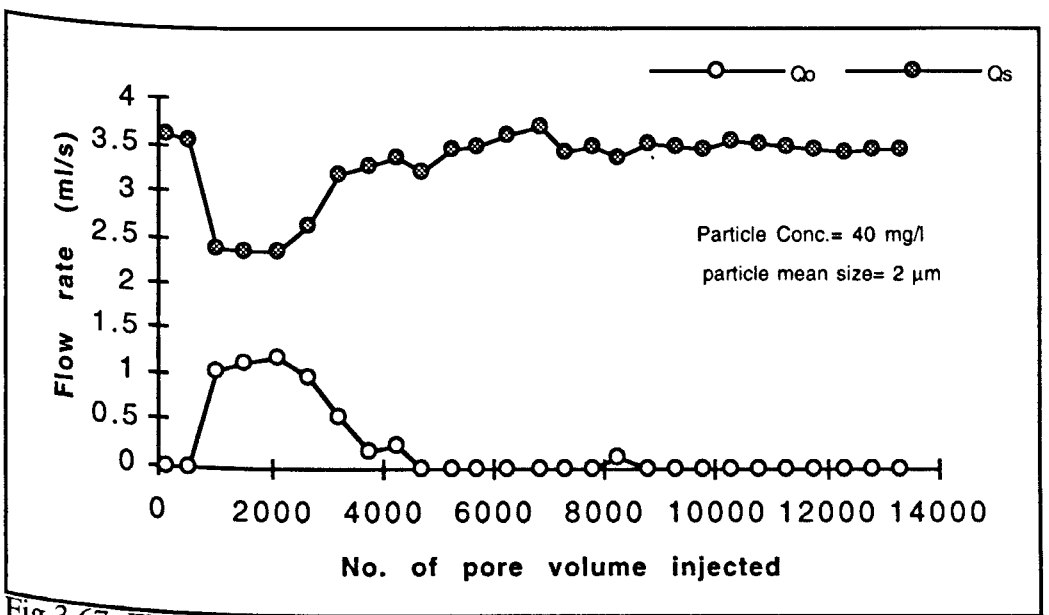

Fig.3.67: Flow along the fracture (Q_o) and the flow through side outlets (Q_s) for a 40 mg/l of 2 µm particle suspension injection (exp. 13).

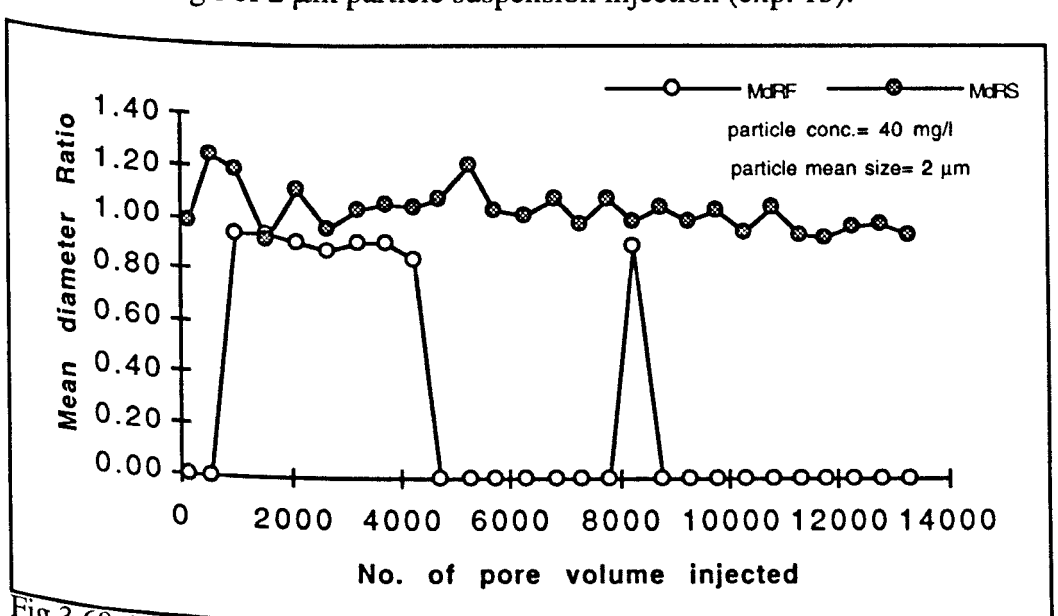

Fig.3.68: Mean diameter ratio of the effluent along the fracture (MdRF) and through the side outlets (MdRS) for a 40 mg/l of 2 µm particle suspension injection (exp. 13).

Plate 3.9.3 SEM image of the fracture face of the factured slab for Exp. 9.

Plate 3.9.4 Photograph of the fracture face when the fractured slab of Exp. 13 was cut open.

(no reduction in Kd / Ki) to 0.23. The 4.7 μm particles were 1/3 to 1/4 of the pore throat diameter, so they could invade the rock matrix and cause severe pore bridging and plugging which explained their high ability to reduce the matrix permeability.

The 9.4 μm particles were 1/2 of the pore throat diameter, so most of them would not be able to invade the matrix and they accumulated at the fracture face to form an external cake. When this cake was eroded the matrix will still have its initial permeability nearly intact.

For a constant particle concentration of 40 ppm, decreasing the particle mean size from 9.4 μm to 2 μm resulted in two different behaviours (Fig.3.71) depending on:

(a) The permeability of the external cake formed by the 9.4 μm particles

(b) The permeability of the external cake formed by the 2 μm particles and

(c) The matrix permeability after being invaded by the 2 μm particles.

The 2 μm particles had the ability to penetrate the external cake and the rock matrix without causing pore plugging (particle mean size / pore throat dia. ratio was equal to 1/10). So the 2 μm particles would alter the permeability less than the 9.4 μm particles as the injection proceeded. For example the permeability ratio at 8000 pore volumes injected increased from 0.63 to 0.92.

3.10 Conclusions of experimental work

The injection of a filtered salt water along the fracture showed that

(1) For low values of pressure drop along the fracture (less than 0.25 atm) the two values of the flow along the fracture and through side outlets are close together with no clear trend. As the pressure drop increases, the total flow through side outlets starts to increase at the expense of the flow along the fracture.

(2) The flow through A1 (the closest outlet to the fracture inlet) was higher than the flow through A2 and the flow through A2 was higher than A3 flow (with very few exceptions due to internal matrix heterogeneity).

(3) At low pressure drops along the fracture, the flow rates through the three outlets were similar. As the pressure along the fracture increases the deference between the flow rates through the three side outlets started to increase.

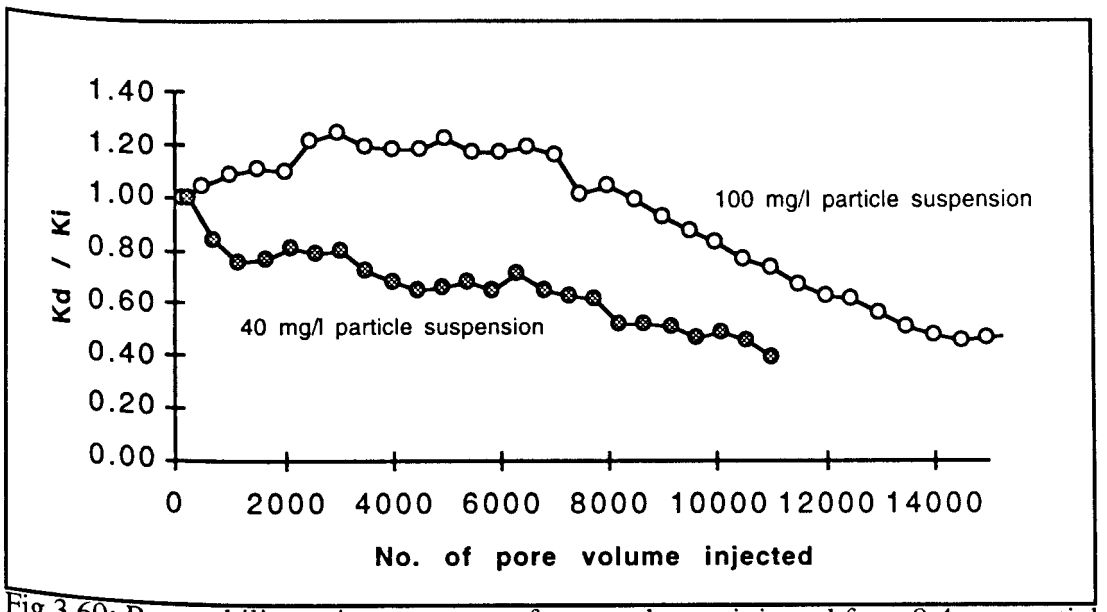

Fig.3.69: Permeability ratio versus no. of pore volumes injected for a 9.4 µm particle suspensions injection (exps. 8 and 11).

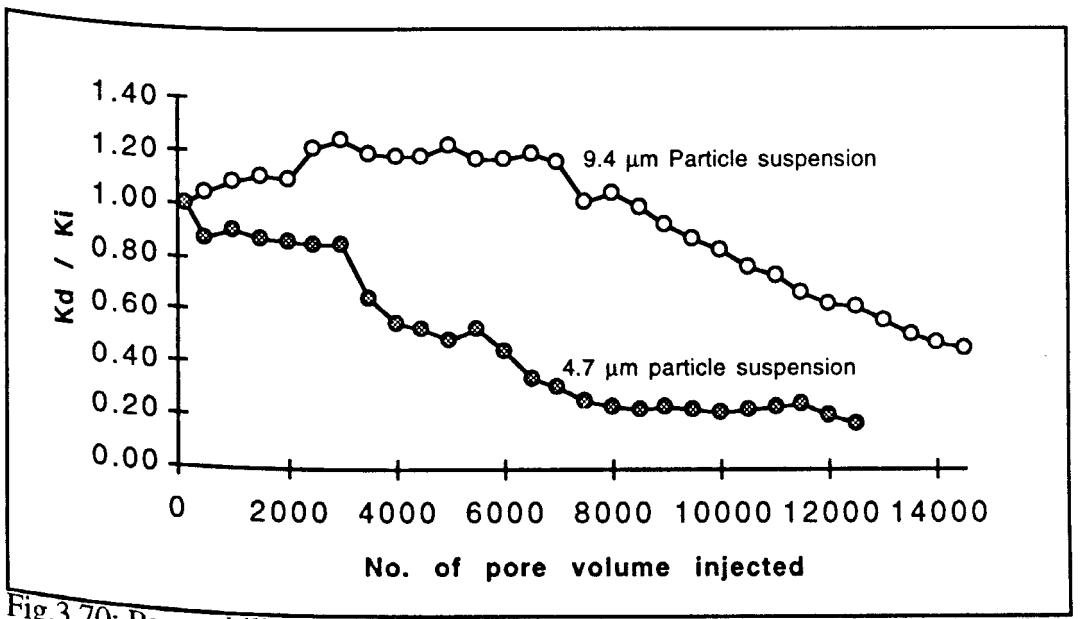

Fig.3.70: Permeability ratio versus no. of pore volumes injected for a 100 mg/l particle suspensions injection (exps. 8 and 9).

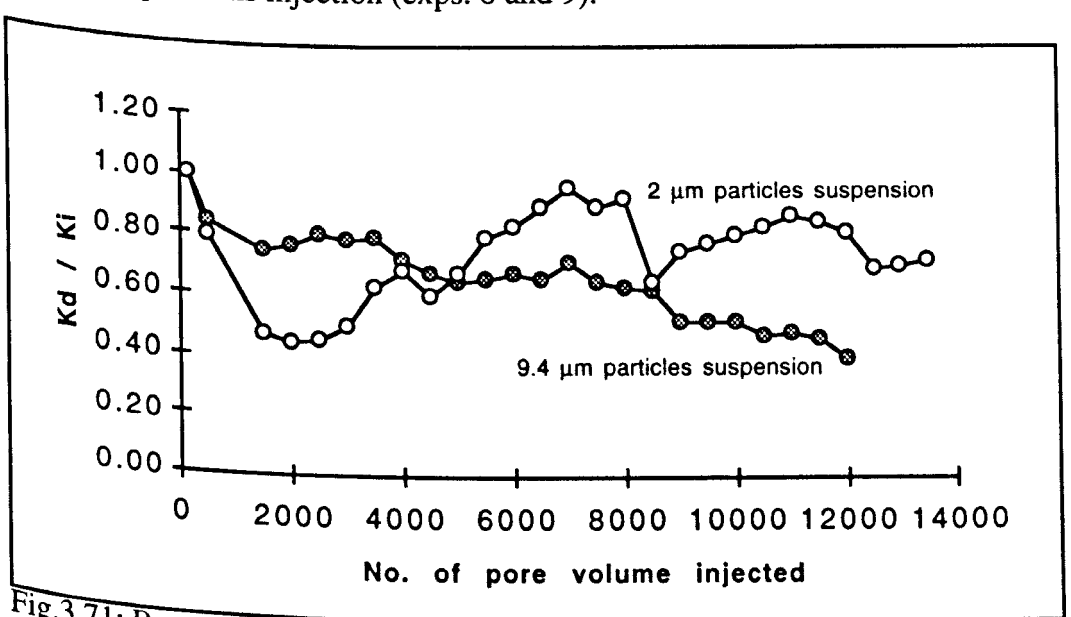

Fig.3.71: Permeability ratio versus no. of pore volumes injected for 40 mg/l particle suspensions injection (exps. 11 and 13).

(4) As the matrix permeability increased, the difference between the flow through the three side outlets increased.

(5) As the pressure drop along fracture increased, the pressure drop through side outlet decreased.

For the case of short fracture experiments:

(1) Dispersions of less than 200 mg/l oil concentration with a droplet mean size of less than 6 μm caused a very small reduction in matrix permeability (less than 6%) after 11 hours of injection.

(2) By increasing the particle concentration from 10 to 15 mg/l, the 4.7 μm particle suspension causes further reduction in matrix permeability which is three time higher than the further reduction caused by the 2.1 μm particle suspension injection.

(3) By increasing the particle mean size from 2.1 μm to 4.7 μm, the 15 mg/l particle suspension causes further reduction in matrix permeability which is two time higher than the further reduction caused by the 10 mg/l particle suspension injection.

(4) The solid particles had the ability to cause higher permeability damage than oil droplets.

(5) The presence of oil at a concentration of 100 mg/l and at 3.6 μm droplet mean size reduced the damage effect (on matrix permeability) caused by increasing the particle concentration from 10 to 15 mg/l or by increasing the particle mean size from 2.1 μm to 4.7 μm. This may be due to the lubrication property of the oil which may reduces the friction between the solid particles and the rock matrix grains and hence reduces the contact between them which may reduces the particle capture within the matrix pores.

(6) No external filter cake was formed in any of the short fracture experiments as the external cake in the case of fracture injection will need a very long time to form.

For the case of linear injection experiments:

(1) The addition of oil at a low concentration (100mg/l) to the 2.1 μm mean size particle suspensions improved the final matrix permeability; but its addition at high concentration (200 mg/l) to the 2.1 μm mean size particle suspensions reduced the final matrix permeability.

(2) No external filter cake was formed in any of the linear injection experiments.

For the case of long fracture experiments:

(1) Observations indicated that there was not any formation of external filter cake on the fracture face in all of these experiments.

(2) Oil with a droplet mean size of 3.8 μm and 200 mg/l concentration had little damage effect on the matrix permeability (which is only 6% reduction in matrix permeability) in fracture injection even after 16 hours of injection.

(3) When the fracture length increased from 20 to 40 cm, the reduction in matrix permeability for the case of particle suspensions injection decreased to the half and the improvement in matrix permeability damage (less matrix damage with time) for the case of 4.7 μm mean size particle suspensions injection was higher than the improvement rate of the case of 2.1 μm mean size particle suspensions injection.

(4) The addition of oil at a 100 mg/l concentration (with 3.6 μm mean size droplets) to the particle suspension reduces the damaging effect of the particle suspensions. This is more obvious in the case of the 2.1 μm mean size particle suspensions than in the case of the 4.7 μm mean size particle suspensions.

By comparing linear injection with fracture injection:

(1) The fracture face area was nearly 13 times the flow area of the linear injection slab. The initial injection pressure in the case of fracture injection was very low compared with the initial injection pressure in the case of linear injection. The flow velocity through the linear injection slab inlet face was around 0.4 cm/s, while the velocity through the fracture face was typically between 0.02 and 0.03 cm/s. The initial matrix permeability of the linear slab was chosen to be in the same range as the initial matrix permeability of the fractured slab.

(2) The injection of the 200 mg/l oil emulsion through linear slab causes 7.8% reduction in the matrix permeability per hour of injection, while it causes only 0.4% reduction in the matrix permeability per hour of injection when it was injected through the fractured slab.

The mean diameter ratio of the fracture injection ended at a value of 0.9 after 14 hours of injection which means that the large droplets were still managing to get through and reaching the side outlets (in spite of the very low flow velocity and pressure drop through rock matrix) after a long injection time.

The CR of the fracture injection ended at a value of 0.84 after 14 hours which means that 84% of the oil flowing through the matrix reached the side outlets and 16% was accumulated within the matrix

The linear injection effluent properties (the mean diameter ratio and the concentration ratio) had nearly the same values of the fracture injection side effluent properties.

The flow in the fracture injection is distributed on a much larger area which will ease the damage effect of the injected emulsion.

(3) For linear injection the 2.1 μm particle suspension causes 11.8 to 13% reduction in matrix permeability per hour of injection, while for fracture injection the reduction rate was 0.86 to 1.5% per hour of injection.

(4) For linear injection the 4.7 μm particle suspension causes 12.4 to 14.2% reduction in matrix permeability per hour of injection, while for fracture injection the reduction rate was 1.29 to 1.71% per hour of injection.

By increasing the particle size and concentration, the ratio of the matrix permeability reduction rate of the linear injection to the matrix permeability reduction rate of the fracture injection was reduced.

(5) The mean particle diameter of the effluent suspension in the linear injection was between 1 and 3/4 of the mean particle diameter of the influent suspension (mean diameter ratio between 1.0 and 0.75).

The mean particle diameter of the side effluent in the case of the fracture injection most of the time is higher than 3 μm what ever the mean particle diameter of the influent suspension (2.1 μm or 4.7 μm particle suspensions).

(6) The concentration ratio of the side effluent in the case of fracture injection had a value between 0 and 0.3 whatever the injected suspension was (2.1 μm or 4.7 μm particle suspension), while the concentration ratio of particle suspensions effluent in the case of linear injection was between 0.4 and 0.8. This is due to the difference in the driving force (flow velocity and pressure drop) between the two systems, which is higher in the case of linear injection than it is in the fracture injection.

Consequently, the particle invasion in the case of linear injection would be deep whereas the particle invasion in the case of fracture injection would be shallow and the stimulation process can effectively improve the long term injectivity in the case of fracture injection more than it could in the case of linear injection as the stimulation process is effective only at a short distance inside the rock matrix.

(7) When the injected fluid contains oil droplets and solid particles, the reduction in matrix permeability with time in the fracture injection process was not sensitive to the variation in particle mean size and concentration or to the variation in droplet mean size and concentration if the injection time was short. On the other hand, the matrix permeability reduction in the linear injection test was very sensitive to the variation in particle mean size and concentration.

(8) When the injected fluid contains oil droplets and solid particles, the mean diameter ratio of the side effluent in the fracture injection and the effluent in the linear injection had nearly the same values, and the concentration ratio of the side effluent in the fracture injection was less than that of the effluent in the linear injection by 5 to 15%.

As the oil droplet concentration was far higher than the solid particles concentration, it was believed that the mean diameter ratio results represent the oil droplet mean diameter ratio more than they represented the particle mean diameter ratio and the concentration ratio results represented the oil droplet concentration ratio more than it represented the solid particles concentration ratio.

Long fracture side outlets effluent showed that:

(1) When the 200 mg/l emulsion was injected along the 40 cm long fracture, the location of the side outlet had no effect on the droplet size or the oil concentration of its effluent.

(2) For the case of the 2.1 μm particle suspension, the outlet A1 effluent had a mean size which was 1.5 to 2.0 times higher than the influent particle mean size most of the time while the effluent particle mean size of the outlet A3 fluctuated between nearly no particles (or less than 0.5 μm) and a size which was 2.0 times higher than the influent particle mean size.

(3) For the case of the 4.7 μm particle suspension, the effluent of the outlet A1 had a particle mean size equal to the particle mean size of the influent suspension most of the time, while the outlet A3 had an average particle mean size half the influent particle mean size then dropped to nearly no particle (or less than 0.5 μm) in the effeluent. When the concentration increased to 15 mg/l, the side outlets A1 and A3 effluent had particle mean sizes slightly greater than the influent particle mean size.

(4) The particle concentration of the effluent of the outlet A1 was always equal or higher than the particle concentration of the outlet A3.

In spite of the fact that A1 is closer to the fracture inlet than A2 or A3, due to matrix heterogeneity the flow rate through A3 some times was equal to the flow rate through A1, and the flow rate through A2 some times was higher than the flow rate through A1.

The reduction in flow rate through a certain side outlet due to matrix blocking may cause an increase in flow rate of a nearby side outlet which has less permeability impairment and higher differential pressure (instead of directing the flow along the fracture to cover a new less damaged fresh matrix).

In fracture injection, as the fracture length increased a wide range of matrix heterogeneity will lead to different degrees of matrix blocking from location to location.

The random variation in matrix permeability will result in a random degree of matrix blocking which may not be dependent on the distance from the fracture inlet.

In the experiments which were designed to simulate the external filter cake accumulation on the fracture face and its erosion, when the slab was cut open along the fracture length, a very thick external filter cake all the way along the fracture was observed. Within the cake a thin and long channel (connecting the inlet and the outlet of the fracture) can be seen.

Experiment no.	fracture aperture (mm)	Inlet pressure (atm)	Pres. drop along frac. (atm)	Side pres. drop (atm)	Side flow rate (ml/s)	Flow rate along frac. (ml/s)	Matrix permeability (md)	A1 flow rate fraction	A2 flow rate fraction	A3 flow rate fraction
42	0.46	0.280	0.280	0.140	1.68	1.93	354	0.32	0.37	0.32
		0.350	0.230	0.235	2.69	0.92	337	0.30	0.39	0.31
45	0.54	0.130	0.130	0.065	1.81	1.80	820	0.64	0.25	0.11
		0.210	0.075	0.173	2.85	0.70	487	0.65	0.25	0.10
57	0.52	0.190	0.190	0.095	1.32	2.20	408	0.35	0.34	0.31
		0.300	0.140	0.230	2.06	1.50	264	0.34	0.33	0.33
		0.355	0.115	0.298	2.62	0.97	259	0.35	0.34	0.31
75	0.47	0.260	0.260	0.130	1.06	2.50	240	0.44	0.32	0.24
		0.370	0.206	0.267	1.68	1.87	208	0.41	0.31	0.28
		0.450	0.150	0.375	2.38	1.20	187	0.41	0.31	0.28
76	0.34	0.500	0.500	0.250	2.31	1.22	272	0.54	0.33	0.13
		0.525	0.429	0.311	2.89	0.67	274	0.49	0.32	0.19
77	0.40	0.530	0.350	0.355	2.68	0.92	223	0.45	0.31	0.24
79	0.32	0.505	0.415	0.298	3.44	0.22	330	0.49	0.32	0.19
		0.485	0.405	0.283	3.40	0.18	355	0.51	0.32	0.18
80	0.41	0.415	0.300	0.265	3.07	0.50	341	0.55	0.28	0.17
81	0.42	0.365	0.273	0.229	3.25	0.50	408	0.47	0.33	0.20
82	0.30	0.390	0.265	0.258	3.60	0.15	391	0.59	0.31	0.09

Table 3.1: Test 2 data (flow of clean brine while all outlets were open) of the ten long fracture carried out experiments.

Exp. no.	oil conc. (mg/l)	solids conc. (mg/l)	Droplets mean size (um)	Particles mean size (um)	Initial matrix perm. (md)	Fracture aperture (mm)
25	100	10	3.4	2.1	376	0.38
33	100	10	6.7	2.1	667	0.38
54	100	10	3.6	4.7	325	0.44
46	100	10	6.0	4.7	367	0.44
39	200	10	3.6	2.1	344	0.39
55	200	10	3.8	4.7	348	0.44
40	100	15	3.6	2.1	494	0.38
47	100	15	3.4	4.7	388	0.45
50	100	None	3.5		251	0.43
51	100	None	6.0		281	0.43
52	200	None	3.8		241	0.42
56	None	10		2.1	290	0.45
58	None	15		2.1	228	0.44
49	None	15		4.7	403	0.45
53	None	10		4.7	473	0.37

Table 3.2: Short slabs experiments operating conditions data.

Particle Dia.(μm)	2.1μm group % weight in size	4.7 μm group % weight in size
>0.2	100%	98%
>1	81%	85%
>2	49%	75%
>3	19%	66%
>4	6%	57%
>5	2%	46%
>6	1%	37%
>7		28%
>8		19%
>9		14%
>10		10%
>12		7%
>14		4.50%
>16		2.50%
>18		1.25%
>20		1%

Table 3.3: particle size distribution.

Droplet Dia.(μm)	3.6 μm group % weight in size	6.2μm group % weight in size
>0.2	99%	99%
>1	79%	86%
>2	63%	76%
>3	55%	71%
>4	45%	68%
>5	31%	63%
>6	18%	57%
>7	9%	48%
>8	4%	37%
>9	2%	27%
>10	1%	20%
>12		10%
>14		6%
>16		2%

Table 3.4: droplet size distribution.

Time (hr)	Exp.50	Exp.51	Exp.52	Exp.56	Exp.58	Exp.53	Exp.49	Exp.25	Exp.33	Exp.46	Exp.54	Exp.39	Exp.55	Exp.40	Exp.47
0.25	1.00	1.00	1.00	1.00	1.00	1.00	1.00	1.00	1.00	1.00	1.00	1.00	1.00	1.00	1.00
1	1.06	1.00	1.03	0.98	0.95	0.95	0.93	1.00	0.95	0.98	0.98	1.05	0.99	0.97	0.98
2	1.07	1.01	1.03	0.97	0.94	0.94	0.87	0.96	0.97	0.95	0.94	1.07	0.97	0.98	0.92
3	1.08	1.02	1.02	0.96	0.92	0.92	0.82	0.96	1.00	0.93	0.90	1.06	0.95	0.98	0.91
4	1.08	1.03	1.03	0.95	0.91	0.90	0.78	0.99	1.00	0.92	0.88	1.07	0.95	0.97	0.88
5	1.09	1.03	1.02	0.93	0.89	0.87	0.74	0.97	1.00	0.90	0.86	1.06	0.93	1.02	0.87
6	1.09	1.06	1.04	0.91	0.87	0.82	0.70	0.99	1.00	0.87	0.85	1.06	0.91	1.00	0.84
7	1.04	0.99	1.01	0.88	0.84	0.80	0.65	0.94	0.95	0.88	0.82	0.96	0.86	1.00	0.80
8	1.03	0.99	0.98	0.86	0.81	0.77	0.61	0.94	0.92	0.84	0.78	0.93	0.82	0.97	0.77
9	1.05	0.97	0.96	0.84	0.79	0.73	0.57	0.95	0.90	0.80	0.77	0.91	0.77	0.94	0.72
10	1.04	0.98	0.95					0.93	0.89	0.77	0.73	0.90	0.74	0.92	0.69
11	1.05	0.98	0.94					0.93	0.85	0.74	0.72	0.89	0.72	0.93	0.66
12								0.89	0.86			0.86		0.86	

Table 3.5: The permeability ratio results for the short fracture experiments.

Exp. no.	Oil conc. (mg/l)	solids conc. (mg/l)	Droplets mean size (um)	Particles mean size (um)	Initial matrix perm. (md)
66	100	10	6.2	2.1	538
69	100	10	4.0	2.1	355
74	200	10	3.6	2.1	310
67	100	15	3.6	2.1	557
71	100	10	6.2	4.7	340
70	100	15	3.6	4.7	500
73	100	10	3.8	4.7	339
72	200	10	3.5	4.7	360
68	200	10	3.5	3.4	500
65	None	10		4.7	493
64	None	15		4.7	488
59	None	10		2.1	240
60	None	15		2.1	248
61	100	None	3.5		234
63	100	None	6.0		269
62	200	None	3.5		230

Table 3.6: Linear injection experiments data.

Time (hr)	Exp.61	Exp.59	Exp.69	Exp.74	Exp.65	Exp.73	Exp.72	Exp.60	Exp.67	Exp.64	Exp.70
0	1.00	1.00	1.00	1.00	1.00	1.00	1.00	1.00	1.00	1.00	1.00
0.25	0.99	0.96	0.95	0.92	0.94	0.91	0.86	0.93	0.93	0.90	0.91
1	0.91	0.82	0.87	0.74	0.79	0.72	0.65	0.76	0.85	0.72	0.73
2	0.83	0.71	0.78	0.60	0.67	0.58	0.50	0.60	0.77	0.59	0.61
3	0.76	0.60	0.72	0.51	0.57	0.44	0.38	0.50	0.71	0.47	0.51
4	0.71	0.51	0.67	0.44	0.47	0.35	0.30	0.42	0.66	0.36	0.43
5	0.67	0.43	0.63	0.38	0.38	0.28	0.23	0.37	0.62	0.29	0.36

Table 3.7: The permeability ratio results for the linear injection experiments.

Exp. no.	Oil conc. (mg/l)	solids conc. (mg/l)	Droplets mean size (um)	Particles mean size (um)	Initial matrix perm. (md)	Fracture aperture (mm)
57	200	10	3.5	2.1	286	0.52
42	200	10	3.4	4.7	317	0.46
81	100	15	3.5	2.1	424	0.42
82	100	15	3.4	4.7	431	0.30
77	None	10		2.1	252	0.40
76	None	15		2.1	279	0.34
79	None	10		4.7	401	0.32
80	None	15		4.7	387	0.41
75	200	None	3.8		207	0.47

Table 3.8: Long fracture experiments data.

Time (hr)	Exp.77	Exp.76	Exp.79	Exp.80	Exp.75	Exp.57	Exp.42	Exp.81	Exp.82
0.25	1.00	1.00	1.00	1.00	1.00	1.00	1.00	1.00	1.00
2	1.00	0.97	0.98	0.98	0.98	0.99	0.99	0.98	0.99
4	1.02	0.95	0.96	0.96	0.99	0.99	0.99	0.98	0.97
6	0.97	0.92	0.95	0.93	0.99	0.99	0.98	0.97	0.95
8	0.96	0.90	0.92	0.89	0.98	0.96	0.98	0.96	0.92
10	0.92	0.85	0.89	0.85	0.94	0.95	0.97	0.94	0.89
12	0.90	0.82	0.85	0.80	0.94	0.94	0.93	0.93	0.87
14	0.88	0.79	0.82	0.76	0.94	0.92	0.89	0.92	0.84
16					0.94	0.91	0.85		

Table 3.9: The Permeability ratio results for the long fracture injection.

Time (hr)	Pres. Drop (atm)	Perm. ratio	Mean dia. ratio	Conc. ratio	Flow rate (ml/s)	Velocity (cm/s)
0.25	5.63	1.00	0.99	0.99	3.58	0.431
1	6.33	0.89	1.03	1.00	3.58	0.431
2	7.03	0.80	1.05	0.99	3.58	0.431
3	7.85	0.72	1.05	0.96	3.58	0.431
4	8.52	0.66	1.00	0.95	3.58	0.431
5	9.27	0.61	0.92	0.92	3.58	0.431

Table 3.10: The experimental data for the linear injection of oil emulsion (exp.62).

Time (hr)	Side pres. Drop (atm)	Pres Drop along Frac. (atm)	Permeability ratio	Mean dia. ratio	Conc. ratio	Side Flow Rate ml/s	Side velocity cm/s
0.25	0.320	0.162	1.00	0.99	0.86	2.16	0.019
2	0.334	0.151	0.98	1.00	0.98	2.21	0.020
4	0.335	0.150	0.99	0.96	1.00	2.24	0.020
6	0.340	0.141	0.99	0.91	0.93	2.28	0.020
8	0.343	0.143	0.98	0.96	0.90	2.28	0.020
10	0.343	0.153	0.97	0.96	0.87	2.17	0.019
12	0.352	0.145	0.96	0.97	0.86	2.23	0.020
14	0.357	0.142	0.94	0.89	0.84	2.28	0.020

Table 3.11: The experimental data for the fracture injection of oil emulsion (exp.75).

Time (hr)	Pres. drop (atm)	Perm. ratio	Mean dia ratio	Conc. ratio	Flow rate (ml/s)	Velocity (cm/s)
0.25	4.24	0.97	0.83	0.66	3.57	0.408
1	4.99	0.82	0.78	0.66	3.57	0.408
2	5.82	0.70	0.75	0.61	3.57	0.408
3	6.81	0.60	0.64	0.63	3.57	0.408
4	8.29	0.49	0.64	0.61	3.57	0.408
5	10.07	0.41	0.65	1.00	3.57	0.408

Table 3.12: The experimental data for the linear injection of 2.1 μm particles suspension at a concentration of 10 mg/l (exp.59).

Time (hr)	Pres. drop (atm)	Perm. ratio	Mean dia ratio	Conc. ratio	Flow rate (ml/sec)	Velocity (cm/sec)
0.25	4.94	0.93	0.89	0.88	3.57	0.408
1	6.06	0.76	1.11	0.33	3.57	0.408
2	7.57	0.61	0.97	0.49	3.57	0.408
3	9.14	0.50	1.09	0.54	3.57	0.408
4	10.86	0.42	0.94	0.49	3.57	0.408

Table 3.13: The experimental data for the linear injection of 2.1 μm particles suspension at a concentration of 15 mg/l (exp.60).

Time (hr)	Pres. drop (atm)	Perm. ratio	Mean dia ratio	Conc. ratio	Flow rate (ml/s)	Velocity (cm/s)
0.25	2.47	0.94	0.92	0.73	3.57	0.406
1	2.94	0.79	0.98	0.64	3.57	0.406
2	3.46	0.67	0.99	0.23	3.57	0.406
3	4.05	0.57	0.88	0.81	3.57	0.406
4	4.94	0.47	1.08	0.66	3.57	0.406
5	6.12	0.38	0.96	0.76	3.57	0.406

Table 3.14: The experimental data for the linear injection of 4.7 μm particles suspension at a concentration of 10 mg/l (exp.65).

Time (hr)	Pres. drop (atm)	Perm. ratio	Mean dia ratio	Conc. ratio	Flow rate (ml/s)	Velocity (cm/s)
0.25	2.41	0.91	0.90	0.69	3.57	0.406
1	3.01	0.72	0.99	0.24	3.57	0.406
2	3.70	0.59	1.03	0.72	3.57	0.406
3	4.69	0.47	1.06	0.71	3.57	0.406
4	6.02	0.36	0.98	0.75	3.57	0.406
5	7.60	0.29	0.84	0.53	3.57	0.406

Table 3.15: The experimental data for the linear injection of 4.7 μm particles suspension at a concentration of 15 mg/l (exp.64).

Time (hr)	Side pres. Drop (atm)	Pres Drop along Frac. (atm)	Permeability ratio	Mean dia. ratio	Conc. ratio	Side Flow Rate ml/s	Side velocity cm/s
0.25	0.333	0.321	1.00	0.00	0.00	2.74	0.028
2	0.339	0.319	1.00	1.47	0.16	2.8	0.029
4	0.345	0.318	1.02	2.00	0.09	2.89	0.029
6	0.353	0.321	0.97	1.90	0.05	2.83	0.029
8	0.364	0.315	0.96	0.00	0.10	2.89	0.029
10	0.372	0.312	0.92	0.00	0.14	2.82	0.029
12	0.379	0.309	0.90	1.40	0.22	2.82	0.029
14	0.386	0.304	0.88	1.50	0.13	2.8	0.029

Table 3.16: The experimental data for the fracture injection of 2.1 μm particles suspension at a concentration of 10 mg/l (exp.77).

Time (hr)	Side pres. Drop (atm)	Pres Drop along Frac. (atm)	Permeability ratio	Mean dia. ratio	Conc. ratio	Side Flow Rate ml/s	Side velocity cm/s
0.25	0.315	0.426	1.00	0.46	0.32	2.87	0.029
2	0.322	0.422	0.97	1.79	0.09	2.85	0.029
4	0.330	0.417	0.95	2.00	0.19	2.86	0.029
6	0.337	0.423	0.92	1.80	0.10	2.83	0.029
8	0.346	0.423	0.90	1.90	0.16	2.83	0.029
10	0.354	0.427	0.85	2.00	0.20	2.75	0.028
12	0.367	0.430	0.82	1.97	0.13	2.74	0.028
14	0.383	0.429	0.79	1.89	0.20	2.74	0.028

Table 3.17: The experimental data for the fracture injection of 2.1 μm particles suspension at a concentration of 15 mg/l (exp.76).

Time (hr)	Side pres. Drop (atm)	Pres Drop along Frac.	Permeability ratio	Mean dia. ratio	Conc. ratio	Side Flow Rate ml/s	Side velocity cm/s
0.25	0.264	0.449	1.00	0.67	0.17	3.46	0.035
2	0.269	0.449	0.98	0.86	0.30	3.46	0.035
4	0.274	0.449	0.96	0.89	0.11	3.46	0.035
6	0.278	0.451	0.95	1.10	0.15	3.47	0.035
8	0.288	0.451	0.92	1.08	0.20	3.46	0.035
10	0.297	0.453	0.89	0.94	0.27	3.45	0.035
12	0.308	0.460	0.85	1.03	0.17	3.44	0.035
14	0.321	0.464	0.82	1.08	0.19	3.44	0.035

Table 3.18: The experimental data for the fracture injection of 4.7 μm particles suspension at a concentration of 10 mg/l (exp.79).

Time (hr)	Side pres. Drop (atm)	Pres Drop along Frac. (atm)	Permeability ratio	Mean dia. ratio	Conc. ratio	Side Flow Rate ml/s	Side velocity cm/s
0.25	0.242	0.286	1.00	0.86	0.10	3.06	0.031
2	0.249	0.282	0.98	0.92	0.13	3.08	0.031
4	0.254	0.281	0.96	1.10	0.01	3.09	0.032
6	0.259	0.281	0.93	1.10	0.07	3.06	0.031
8	0.269	0.281	0.89	1.00	0.14	3.03	0.031
10	0.281	0.286	0.85	1.06	0.14	3.02	0.031
12	0.296	0.286	0.80	1.09	0.10	2.99	0.031
14	0.311	0.286	0.76	1.10	0.11	2.98	0.030

Table 3.19: The experimental data for the fracture injection of 4.7 μm particles suspension at a concentration of 15 mg/l (exp.80).

Time (hr)	Pres. drop (atm)	Perm. ratio	Mean dia ratio	Conc. ratio	Flow rate (ml/s)	Velocity (cm/s)
0.25	3.80	0.92	0.93	0.99	3.56	0.375
1	4.74	0.74	0.94	0.99	3.56	0.375
2	5.82	0.60	0.94	1.00	3.56	0.375
3	6.81	0.51	0.94	1.01	3.56	0.375
4	7.95	0.44	0.95	1.02	3.56	0.375
5	9.23	0.38	0.93	1.00	3.56	0.375

Table 3.20: The experimental data for the linear injection of a simulated produced water contains 200 mg/l of 3.6 μm oil droplets and 10 mg/l of 2.1 μm particles (exp.74).

Time (hr)	Pres. drop (atm)	Perm. ratio	Mean dia ratio	Conc. ratio	Flow rate (ml/s)	Velocity (cm/s)
0.25	2.17	0.93	1.02	0.89	3.57	0.403
1	2.38	0.85	1.04	0.99	3.57	0.403
2	2.64	0.77	1.06	0.97	3.57	0.403
3	2.85	0.71	0.99	0.99	3.57	0.403
4	3.07	0.66	1.03	1.01	3.57	0.403
5	3.27	0.62	1.03	1.03	3.57	0.403

Table 3.21: The experimental data for the linear injection of a simulated produced water contains 100 mg/l of 3.6 μm oil droplets and 15 mg/l of 2.1 μm particles (exp.67).

Time (hr)	Pres. drop (atm)	Perm. ratio	Mean dia ratio	Conc. ratio	Flow rate (ml/s)	Velocity (cm/s)
0.25	4.05	0.86	0.97	1.07	3.56	0.417
1	5.38	0.65	1.02	1.10	3.56	0.417
2	6.96	0.50	1.07	1.10	3.56	0.417
3	9.33	0.37	1.01	1.05	3.56	0.417
4	11.45	0.30	0.95	1.05	3.56	0.417

Table 3.22: The experimental data for the linear injection of a simulated produced water contains 200 mg/l of 3.5 μm oil droplets and 10 mg/l of 4.7 μm particles (exp.72).

Time (hr)	Pres. drop (atm)	Perm. ratio	Mean dia ratio	Conc. ratio	Flow rate (ml/s)	Velocity (cm/s)
0.25	2.47	0.91	0.99	0.96	3.57	0.361
1	3.06	0.73	1.01	1.02	3.57	0.361
2	3.67	0.61	1.02	1.03	3.57	0.361
3	4.39	0.51	1.01	0.95	3.57	0.361
4	5.22	0.43	0.98	1.01	3.57	0.361
5	6.24	0.36	0.96	0.99	3.57	0.361

Table 3.23: The experimental data for the linear injection of a simulated produced water contains 100 mg/l of 3.6 μm oil droplets and 15 mg/l of 4.7 μm particles (exp.70).

Time (hr)	Side pres. Drop (atm)	Pres Drop along Frac. (atm)	Permeability ratio	Mean dia. ratio	Conc. ratio	Side Flow Rate ml/s	Side velocity cm/s
0.25	0.266	0.111	1.00	1.01	0.84	2.48	0.022
2	0.279	0.104	0.99	1.07	0.93	2.59	0.023
4	0.288	0.095	0.99	1.03	0.91	2.66	0.024
6	0.296	0.089	0.99	0.94	0.95	2.74	0.024
8	0.306	0.089	0.96	0.94	0.91	2.74	0.024
10	0.318	0.094	0.95	1.01	0.92	2.82	0.025
12	0.328	0.094	0.94	1.00	0.90	2.88	0.025
14	0.338	0.094	0.92	0.99	0.94	2.91	0.026
16	0.348	0.094	0.91	1.01	0.93	2.95	0.026
18	0.358	0.094	0.89	1.02	0.89	2.97	0.026
20	0.368	0.094	0.87			3	0.027
22	0.378	0.094	0.86			3.05	0.027

Table 3.24: The experimental data for the fracture injection of a simulated produced water contains 200 mg/l of 3.5 μm oil droplets and 10 mg/l of 2.1 μm particles (exp.57).

Time (hr)	Side pres. Drop (atm)	Pres Drop along Frac. (atm)	Permeability ratio	Mean dia. ratio	Conc. ratio	Side Flow Rate ml/s	Side velocity cm/s
0.25	0.222	0.267	1.00	0.98	0.77	3.08	0.031
2	0.229	0.254	0.98	1.01	0.94	3.11	0.032
4	0.231	0.250	0.98	0.95	0.91	3.13	0.032
6	0.234	0.252	0.97	0.85	0.79	3.16	0.032
8	0.239	0.253	0.96	1.05	0.74	3.18	0.032
10	0.244	0.252	0.94	1.04	0.78	3.19	0.033
12	0.249	0.252	0.93	1.09	0.84	3.22	0.033
14	0.254	0.252	0.92			3.24	0.033

Table 3.25 The experimental data for the fracture injection of a simulated produced water contains 100 mg/l of 3.5 μm oil droplets and 15 mg/l of 2.1 μm particles (exp.81).

Time (hr)	Side pres. Drop (atm)	Pres Drop along Frac. (atm)	Permeability ratio	Mean dia. ratio	Conc. ratio	Side Flow Rate ml/s	Side velocity cm/s
0.25	0.26	0.23	1.00	0.98	0.83	2.71	0.028
2	0.27	0.21	1.07	0.97	0.95	3	0.031
4	0.28	0.20	1.09	0.96	0.93	3.18	0.032
6	0.29	0.19	1.09	0.90	0.86	3.26	0.033
8	0.31	0.20	1.02	0.99	0.89	3.22	0.033
10	0.33	0.20	1.01	0.88	0.80	3.4	0.035
12	0.35	0.20	0.93	0.86	0.81	3.33	0.034
14	0.37	0.20	0.89	0.89	0.79	3.36	0.034
16	0.38	0.20	0.80	0.96	0.75	3.19	0.033
18	0.40	0.20	0.78	0.96	0.82	3.25	0.033
20	0.42	0.20	0.76			3.34	0.034
22	0.44	0.20	0.74			3.4	0.035

Table 3.26: The experimental data for the fracture injection of a simulated produced water contains 200 mg/l of 3.4 μm oil droplets and 10 mg/l of 4.7 μm particles (exp.42).

Time (hr)	Side pres. Drop (atm)	Pres Drop along Frac. (atm)	Permeability ratio	Mean dia. ratio	Conc. ratio	Side Flow Rate ml/s	Side velocity cm/s
0.25	0.237	0.257	1.00	0.91	0.94	3.38	0.034
2	0.241	0.256	0.99	1.05	0.93	3.4	0.035
4	0.246	0.254	0.97	1.05	0.98	3.4	0.035
6	0.252	0.251	0.95	0.95	0.92	3.4	0.035
8	0.259	0.252	0.92	0.95	0.82	3.41	0.035
10	0.268	0.254	0.89	0.90	0.85	3.42	0.035
12	0.277	0.256	0.87	0.89	0.89	3.42	0.035
14	0.287	0.256	0.84			3.45	0.035

Table 3.27: The experimental data for the fracture injection of a simulated produced water contains 100 mg/l of 3.5 μm oil droplets and 15 mg/l of 4.7 μm particles (exp.82)

Exp. no.	Exp. 75	Influent: 200 mg/l oil (3.8 μm)		Exp. 77	Influent: 10 mg/l solids (2.1 μm)		Exp. 76	Influent: 15 mg/l solids (2.1 μm)	
Time (hr)	Fracture outlet effluent	outlet A1 effluent	outlet A3 effluent	Fracture outlet effluent	outlet A1 effluent	outlet A3 effluent	Fracture outlet effluent	outlet A1 effluent	outlet A3 effluent
0.25	0.99	1.00	0.99	0.99	0.00	0.00	0.93	0.46	0.00
2	1.01	1.00	1.00	1.02	1.47	1.18	1.03	1.79	1.79
4	1.00	0.98	0.96	0.95	2.86	0.00	1.00	2.13	0.00
6	0.98	0.89	0.89	0.96	2.78	0.00	1.02	1.90	2.06
8	1.01	0.96	0.96	1.11	0.00	0.00	1.16	1.99	0.00
10	0.97	0.97	0.96	0.87	0.00	2.42	1.12	2.18	2.33
12	0.98	0.98	0.97	1.00	1.92	0.00	1.00	2.17	0.00
14	0.97	0.90	0.89	1.01	2.05	2.16	1.06	1.89	0.00
16									
Exp no.	Exp. 79	Influent: 10 mg/l solids (4.7 μm)		Exp. 80	Influent: 15 mg/l solids (4.7 μm)		Exp. 57	Influent: 200 mg/l oil (3.5 um) and 10 mg/l solids (2.1 μm)	
Time (hr)	Fracture outlet effluent	outlet A1 effluent	outlet A3 effluent	Fracture outlet effluent	outlet A1 effluent	outlet A3 effluent	Fracture outlet effluent	outlet A1 effluent	outlet A3 effluent
0.25	0.70	0.67	0.47	0.79	0.86	0.94	1.00	1.01	1.02
2	0.84	0.86	0.59	1.14	0.92	0.89	1.05	1.07	1.09
4	1.18	0.89	0.71	0.89	1.11	1.11	1.00	1.03	1.02
6	0.94	1.14	0.00	0.96	1.11	1.11	1.06	0.94	0.97
8	1.18	1.08	0.00	0.79	1.00	1.00	0.92	0.94	0.94
10	0.84	0.90	0.00	0.86	1.06	1.11	1.01	1.01	1.04
12	0.73	1.03	0.00	1.00	1.09	1.11	1.02	1.00	1.03
14	1.08	1.08	0.00	0.96	1.11	1.11	0.92	0.99	0.99
16							1.04	1.02	1.02
Exp. no.	Exp. 81	Influent: 100 mg/l oil (3.5 μm) and 15 mg/l solids (2.1 um)		Exp. 42	Influent: 200 mg/l oil (3.4 um) and 10 mg/l solids (4.7 μm)		Exp. 82	Influent: 100 mg/l oil (3.5 um) and 15 mg/l solids (4.7 μm)	
Time (hr)	Fracture outlet effluent	outlet A1 effluent	outlet A3 effluent	Fracture outlet effluent	outlet A1 effluent	outlet A3 effluent	Fracture outlet effluent	outlet A1 effluent	outlet A3 effluent
0.25	0.94	0.98	1.03	0.94	0.98	0.99	0.96	0.91	0.98
2	0.94	1.01	1.07	1.03	0.97	0.99	1.06	1.05	1.08
4	0.75	0.95	0.94	0.97	0.96	0.97	1.07	1.05	1.08
6	0.94	0.83	0.85	0.85	0.87	0.89	0.97	0.95	1.00
8	1.01	1.12	1.12	0.97	0.99	0.99	0.98	0.95	0.96
10	0.94	1.04	1.12	0.88	0.88	0.88	0.93	0.90	0.94
12	0.97	1.13	1.17	0.86	0.86	0.87	0.91	0.89	0.92
14				0.85	0.89	0.92			
16				0.94	0.96	0.98			

Table 3.28: Mean diameter ratio versus time data for the long fracture effluent.

Exp. no.	Exp. 75	Influent: 200 mg/l oil (3.8 μm)		Exp. 77	Influent: 10 mg/l solids (2.1 μm)		Exp. 76	Influent: 15 mg/l solids (2.1 μm)	
Time (hr)	Fracture outlet effluent	outlet A1 effluent	outlet A3 effluent	Fracture outlet effluent	outlet A1 effluent	outlet A3 effluent	Fracture outlet effluent	outlet A1 effluent	outlet A3 effluent
0.25	0.97	0.94	0.93	0.69	0.00	0.00	1.01	0.32	0.00
2	1.09	1.05	1.05	1.03	0.16	0.25	0.95	0.09	0.09
4	1.11	1.08	1.07	1.09	0.09	0.11	1.12	0.19	0.05
6	1.05	1.00	1.00	1.00	0.05	0.06	0.99	0.10	0.06
8	1.04	0.98	0.97	0.93	0.10	0.06	0.98	0.16	0.04
10	0.98	0.94	0.92	0.95	0.14	0.10	0.85	0.20	0.01
12	1.08	1.04	1.04	0.60	0.24	0.07	0.90	0.13	0.02
14	1.07	0.98	0.99	0.80	0.13	0.00	0.91	0.20	0.11
16									
Exp no.	Exp. 79	Influent: 10 mg/l solids (4.7 μm)		Exp. 80	Influent: 15 mg/l solids (4.7 μm)		Exp. 57	Influent: 200 mg/l oil (3.5 um) and 10 mg/l solids (2.1 μm)	
Time (hr)	Fracture outlet effluent	outlet A1 effluent	outlet A3 effluent	Fracture outlet effluent	outlet A1 effluent	outlet A3 effluent	Fracture outlet effluent	outlet A1 effluent	outlet A3 effluent
0.25	0.93	0.17	0.00	1.00	0.10	0.25	0.85	0.84	0.78
2	0.12	0.30	0.00	0.38	0.13	0.02	0.98	0.93	0.87
4	0.25	0.11	0.00	0.51	0.01	0.04	0.97	0.91	0.88
6	0.38	0.15	0.10	0.47	0.07	0.03	1.00	0.95	0.93
8	0.44	0.20	0.05	0.96	0.14	0.00	0.96	0.91	0.93
10	0.50	0.27	0.03	0.46	0.14	0.04	1.00	0.92	0.93
12	0.33	0.17	0.05	0.67	0.10	0.07	0.99	0.90	0.90
14	0.43	0.19	0.00	0.45	0.11	0.03	1.06	1.00	0.96
16							0.91	0.87	0.92
Exp. no.	Exp. 81	Influent: 100 mg/l oil (3.5 um) and 15 mg/l solids (2.1 μm)		Exp. 42	Influent: 200 mg/l oil (3.4 um) and 10 mg/l solids (4.7 μm)		Exp. 82	Influent: 100 mg/l oil (3.5 um) and 15 mg/l solids (4.7 μm)	
Time (hr)	Fracture outlet effluent	outlet A1 effluent	outlet A3 effluent	Fracture outlet effluent	outlet A1 effluent	outlet A3 effluent	Fracture outlet effluent	outlet A1 effluent	outlet A3 effluent
0.25	1.01	0.77	0.72	0.93	0.83	0.80	0.99	0.94	0.75
2	0.98	0.94	0.81	0.98	0.95	0.89	0.92	0.93	0.94
4	0.91	0.91	0.84	0.91	0.93	0.93	0.98	0.98	0.94
6	0.97	0.79	0.77	0.91	0.86	0.87	0.95	0.92	0.88
8	0.91	0.74	0.65	0.91	0.89	0.86	0.88	0.82	0.72
10	0.89	0.78	0.72	0.86	0.80	0.87	0.81	0.85	0.79
12	0.97	0.84	0.78	1.00	0.81	0.82		0.89	
14				0.79	0.79	0.87			
16				0.87	0.97	0.89			

Table 3.29: Concentration ratio versus time data for the long fracture effluent.

Exp. no.	Oil conc. (mg/l)	Droplet Mean size (um)	Particle conc. (mg/l)	Particle Mean size (um)	Matrix homogeneity	Initial Permeability (md)	Fracture aperture b (mm)
17	100	6.5	10	7.4	non homogeneous	235- 295	0.34
42	200	3.4	10	4.7	non homogeneous	230 - 320	0.46

Table 3.30: The experimental data for the fractured non homogeneous rock slabs (exp.17 and 42).

no. of pore volumes injected	Pres. Drop along fracture (atm)	Pres. Drop through side outlets (atm)	Flow rate along fracture (ml/s)	Flow rate through side outlets (ml/s)	frac. effluent Concentration ratio	Side effluent concentration ratio	Fracture effluent mean dia. ratio	Side effluent mean dia. ratio
132	0.19	2.12	1.70	1.75	0.39	0.01	0.84	1.00
542	0.18	2.13	1.70	1.84	0.22	0.02	0.87	0.45
1085	0.19	2.16	1.62	1.93	0.49	0.03	0.97	0.41
1626	0.18	2.22	1.50	2.04	0.35	0.02	0.92	0.52
2169	0.18	2.25	1.50	2.05	0.32	0.04	0.89	0.25
2714	0.15	2.15	1.40	2.16	0.15	0.03	1.00	0.32
3280	0.18	2.21	1.43	2.27	0.49	0.03	1.04	0.45
3811	0.21	2.17	1.33	2.14	0.31	0.01	0.75	0.34
4351	0.15	2.30	1.28	2.25	0.99	0.01	1.03	0.41
4883	0.15	2.27	1.27	2.21	0.48	0.02	1.21	0.55
5411	0.12	2.19	1.23	2.22	0.20	0.00	0.70	0.29
5944	0.13	2.18	1.38	2.10	0.54	0.02	1.03	0.41
6471	0.16	2.20	1.32	2.12	0.62	0.07	0.96	0.34
6991	0.13	2.17	1.27	2.13	0.89	0.08	0.76	0.28
7516	0.22	2.17	1.35	2.08	0.75	0.12	0.97	0.25
8006	0.18	2.20	1.37	1.83	1.23	0.02	0.90	0.30
8525	0.17	2.12	1.57	1.82	1.26	0.03	1.05	0.36
9049	0.20	2.11	1.70	1.73	0.96	0.01	0.91	0.33
9567	0.17	2.23	1.68	1.70	0.82	0.00	0.77	0.29
10095	0.18	2.29	1.81	1.64	1.24	0.00	0.89	0.21
10601	0.19	2.31	1.72	1.59	1.35	0.05	0.98	0.29
11120	0.21	2.05	2.10	1.29	1.81	0.05	1.01	0.44
11653	0.25	2.08	2.23	1.25	2.05	0.02	0.95	0.19
12178	0.23	2.08	2.28	1.15	1.89	0.03	0.99	0.17
12701	0.25	2.10	2.33	1.09	1.75	0.02	0.97	0.48
13260	0.27	2.15	2.57	1.09	1.57	0.02	0.90	0.50
13793	0.30	2.16	2.47	1.01	1.38	0.01	0.94	0.50
14304	0.33	2.31	2.37	0.97	1.78	0.00	0.86	0.50
14790	0.33	2.38	2.23	0.94	1.76	0.09	0.88	0.16
15299	0.33	2.40	2.43	0.89	1.99	0.00	0.93	0.26
15807	0.33	2.40	2.40	0.92	2.21	0.09	0.93	0.26
16317	0.31	2.36	2.40	0.94	1.29	0.03	1.02	0.26

Table 3.31: The experimental data for the fracture injection of 9.4 μm particles suspension at a concentration of 100 mg/l (exp. 8)

no. of pore volumes injected	Pres. Drop along fracture (atm)	Pres. Drop through side outlets (atm)	Flow rate along fracture (ml/s)	Flow rate through side outlets (ml/s)	frac. effluent Concentration ratio	Side effluent concentration ratio	Fracture effluent mean dia. ratio	Side effluent mean dia. ratio
132	0.16	2.13				0.07		0.44
544	0.17	1.89	0.85	2.70	0.52	0.02	1.05	0.47
1086	0.19	2.04	0.97	2.59	0.93	0.02	1.02	0.34
1592	0.19	2.06	0.80	2.67	0.51	0.01	1.06	0.43
2183	0.20	2.06	0.77	2.82	0.57	0.02	1.14	0.83
2691	0.12	2.23	0.55	2.97	0.37	0.04	1.05	0.50
3229	0.12	2.26	0.50	3.03	1.24	0.01	1.12	0.60
3768	0.25	2.00	1.08	2.43	0.70	0.02	1.23	0.36
4368	0.15	1.95	1.30	2.24	0.49	0.04	0.90	0.37
4890	0.21	2.02	1.30	2.22	0.71	0.23	0.92	0.21
5383	0.22	2.05	1.22	2.28	1.16	0.19	1.22	0.21
5991	0.30	2.02	1.20	2.32	1.45	0.06	1.14	0.24
6490	0.27	2.06	1.25	2.27	0.75	0.01	0.73	0.42
7048	0.20	1.88	1.38	2.26	0.71	0.02	1.03	0.32
7580	0.30	1.97	1.32	2.18	1.00	0.00	1.13	0.48
8074	0.28	2.01	1.37	2.15	1.30	0.01	1.14	0.37
8572	0.26	2.06	1.35	2.15	2.10	0.00	1.13	0.42
9194	0.22	2.06	1.73	1.80	1.12	0.04	1.14	0.21
9597	0.28	2.13	1.62	1.87	1.32	0.21	1.23	0.11
10148	0.27	2.04	1.83	1.77	1.42	0.08	1.22	0.21
10612	0.33	2.17	1.75	1.71	1.95	0.02	1.08	0.36
11159	0.29	2.24	1.75	1.83	0.82	0.00	1.13	0.42
11696	0.33	2.29	1.75	1.77	1.78	0.02	1.18	0.32
12233	0.35	2.16	2.10	1.43	1.25	0.00	1.08	0.53

Table 3.32: The experimental data for the fracture injection of 9.4 μm particles suspension at a concentration of 40 mg/l (exp. 11).

no. of pore volumes injected	Pres. Drop along fracture (atm)	Pres. Drop through side outlets (atm)	Flow rate along fracture (ml/s)	Flow rate through side outlets (ml/s)	frac. effluent Concentration ratio	Side effluent concentration ratio	Fracture effluent mean dia. ratio	Side effluent mean dia. ratio
128	0.14	1.57	0.47	2.89	0.46	0.02	0.89	1.01
494	0.12	1.84	0.39	2.96	0.53	0.02	0.86	0.67
1005	0.11	1.90	0.25	3.15	0.15	0.01	1.18	0.96
1485	0.16	1.96	0.21	3.14	0.25	0.00	0.80	0.91
1963	0.15	2.04	0.13	3.19	0.16	0.01	0.93	0.73
3310	0.20	2.55	0.17	3.03	1.78	0.00	1.40	0.73
3842	0.20	2.50	0.70	2.56	1.18	0.01	0.85	0.51
4362	0.15	2.83	0.53	2.74	2.39	0.03	0.68	0.73
4842	0.17	2.68	0.67	2.43	5.13	0.00	0.95	0.49
5332	0.19	2.71	0.62	2.67	2.65	0.02	0.89	0.73
5834	0.21	2.90	0.93	2.36	3.92	0.00	1.01	0.87
6317	0.26	3.03	1.30	1.88	0.70	0.01	1.32	1.15
6806	0.27	3.06	1.50	1.70	0.89	0.01	1.48	1.26
7286	0.32	3.10	1.70	1.44	0.68	0.00	1.45	1.07
7755	0.33	3.08	1.75	1.32	0.63	0.00	1.42	1.13
8228	0.36	3.19	1.82	1.28	0.62	0.01	1.31	0.98
8701	0.35	3.22	1.78	1.34	0.72	0.03	1.35	0.96
9193	0.32	3.27	1.90	1.32	0.79	0.05	1.42	0.81
9663	0.38	3.36	1.81	1.28	0.65	0.00	1.41	0.67
10135	0.33	3.32	1.75	1.34	2.03	0.01	1.29	0.73
10627	0.36	3.14	1.85	1.37	0.61	0.01	1.41	0.89
11117	0.38	3.12	1.83	1.37	0.60	0.01	1.54	1.12
11593	0.44	3.34	1.92	1.20	2.40	0.00	1.28	0.68
12056	0.38	3.36	1.98	1.05	1.31	0.00	1.31	0.53

Table 3.33: The experimental data for the fracture injection of 4.7 μm particles suspension at a concentration of 100 mg/l (exp. 9).

no. of pore volumes injected	Pres. Drop along fracture (atm)	Pres. Drop through side outlets (atm)	Flow rate along fracture (ml/s)	Flow rate through side outlets (ml/s)	frac. effluent Concentration ratio	Side effluent concentration ratio	Fracture effluent mean dia. ratio	Side effluent mean dia. ratio
132	0.25	1.51	0.00	3.62	0.00	0.33	0.00	0.98
525	0.20	1.84	0.00	3.55	0.00	0.27	0.00	1.25
1015	0.23	2.15	1.03	2.41	0.97	0.03	0.95	1.19
1544	0.24	2.22	1.13	2.36	0.91	0.03	0.94	0.92
2108	0.24	2.20	1.18	2.38	0.78	0.04	0.92	1.12
2660	0.27	2.19	0.95	2.64	1.49	0.12	0.88	0.97
3230	0.31	2.11	0.53	3.2	0.69	0.25	0.92	1.03
3760	0.29	2.02	0.17	3.29	0.18	0.34	0.91	1.06
4236	0.29	2.00	0.23	3.36	0.53	0.36	0.85	1.06
4722	0.30	1.98	0.00	3.23	0.00	0.45	0.00	1.08
5254	0.30	1.81	0.00	3.46	0.00	0.44	0.00	1.21
5717	0.24	1.75	0.00	3.51	0.00	0.46	0.00	1.04
6264	0.25	1.67	0.00	3.61	0.00	0.47	0.00	1.02
6832	0.29	1.61	0.00	3.72	0.00	0.54	0.00	1.09
7300	0.25	1.59	0.00	3.44	0.00	0.50	0.00	0.99
7795	0.26	1.59	0.00	3.51	0.00	0.61	0.00	1.09
8252	0.16	1.70	0.11	3.37	1.16	0.40	0.90	1.00
8775	0.19	1.80	0.00	3.53	0.00	0.64	0.00	1.05
9304	0.19	1.87	0.00	3.5	0.00	0.49	0.00	0.99
9800	0.19	1.81	0.00	3.48	0.00	0.61	0.00	1.04
10300	0.19	1.77	0.00	3.55	0.00	0.49	0.00	0.96
10800	0.19	1.70	0.00	3.54	0.00	0.58	0.00	1.05
11300	0.20	1.72	0.00	3.51	0.00	0.63	0.00	0.94
11800	0.20	1.76	0.00	3.46	0.00	0.63	0.00	0.93
12300	0.18	1.90	0.00	3.44	0.00	0.72	0.00	0.97
12800	0.20	1.95	0.00	3.47	0.00	0.90	0.00	0.98
13300	0.22	2.01	0.00	3.48	0.00	1.54	0.00	0.94

Table 3.34: The experimental data for the fracture injection of 2 μm particles suspension at a concentration of 40 mg/l (exp. 13).

No. of pore volume injected	Kd/Ki for Exp.8	Kd/Ki for Exp.9	Kd/Ki for Exp.11	Kd/Ki for Exp.13
132	1.00	1.00	1.00	1.00
500	1.04	0.87	0.84	0.80
1000	1.08	0.90	0.75	0.47
1500	1.11	0.87	0.77	0.44
2000	1.10	0.86	0.81	0.45
2500	1.22	0.86	0.79	0.50
3000	1.24	0.85	0.79	0.63
3500	1.19	0.64	0.72	0.68
4000	1.19	0.55	0.68	0.60
4500	1.18	0.53	0.65	0.68
5000	1.23	0.49	0.66	0.79
5500	1.17	0.53	0.68	0.83
6000	1.17	0.44	0.65	0.90
6500	1.19	0.34	0.71	0.96
7000	1.16	0.30	0.65	0.90
7500	1.01	0.25	0.63	0.92
8000	1.04	0.23	0.62	0.65
8500	0.99	0.22	0.52	0.75
9000	0.93	0.23	0.52	0.78
9500	0.87	0.22	0.51	0.80
10000	0.83	0.21	0.47	0.84
10500	0.76	0.22	0.48	0.87
11000	0.73	0.24	0.46	0.85
11500	0.67	0.24	0.39	0.82
12000	0.63	0.19		0.69
12500	0.61	0.17		0.70
13000	0.57			0.72
13500	0.51			
14000	0.48			
14500	0.45			
15000	0.46			
15500	0.48			

Table 3.35: The permeability ratio change with pore volume injected for the experiments designed to simulate the filter cake accumulation and erosion (exp 8, 9, 11 and 13)

CHAPTER FOUR

COMPUTER SIMULATION

4.1 Introduction

The basic idea behind the finite element method (FEM) is to divide the structure, body, or region being analysed into a large number of finite elements. These elements may be one, two or three dimensional.

Consider a 2-D body of fluid and the pressure and flow velocity distribution within this body is needed under a certain specified boundary condition. Because there is an infinite number of points in this body, there is also an infinite number of pressure and velocity to be measured. The problem is therefore said to have an infinite number of degrees of freedom. When closed form analytical solutions exist, these solutions allow the computation of the pressure and velocity at any point in the body expressed as a mathematical solution of a function with certain variables. But irregular geometry precludes such a closed form solution, therefore an alternate approach is needed.

Instead of requiring that the pressure or velocity be determined at every point in the fluid body, in FEM this requirement was changed to determination of pressure and velocity at only a finite number of points. The irregular geometry (in the FEM) can be discretized into several triangular or rectangular elements, then the pressure and velocity are determined at the vertices (or nodes) of these triangular or rectangular elements. The curved boundaries are approximated by the straight sides of the triangles (Fig.4.1).

The FEM will provide the pressure and velocity (in this case) of the fluid only at the nodal points. Interpolation functions are used within each element to describe the variation of the variables as a function of the global coordinates [86].

4.2 Finite Element basic concepts

The Finite Element Method is a computer-aided mathematical technique for obtaining approximate numerical solution to the abstract equations of calculus that predict the response of physical systems subjected to external influences. Basically the analyst is looking for a numerical solution to the governing equation and loading conditions that characterise and determine the behaviour of the system.

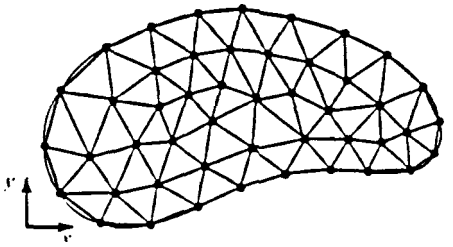

Fig.4.1:Irregularly shaped plate shown discretized into many triangular finite elements (after Stasa).

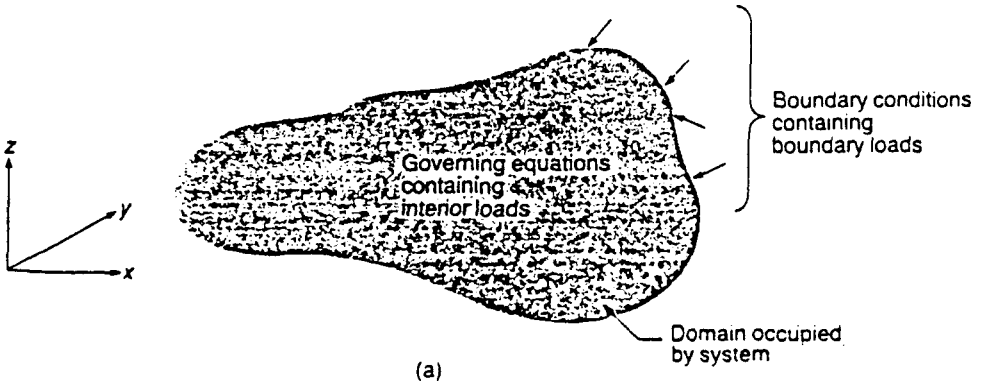

System: A flexible cable with tension T, hanging under its own weight ρg

Domain:	Interval $0 < x < 10$ along x-axis
Boundary of domain:	The two end points $x = 0$ and $x = 10$
Governing equation:	$\frac{d}{dx}\left(T\frac{dW}{dx}\right) = \rho g$ where W is the vertical displacement
Interior load:	ρg
Boundary conditions:	$W = 0$ at $x = 0$ $W = 0$ at $x = 10$

(b)

System: A sound source at frequency ω and intensity f radiating inside a closed room with (ideally) rigid ceiling, walls, and floor

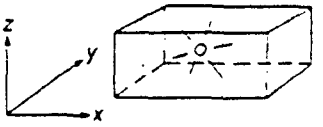

Domain:	Volume occupied by room
Boundary of domain:	The ceiling, walls, and floor
Governing equation:	$\frac{\partial^2 p}{\partial x^2} + \frac{\partial^2 p}{\partial y^2} + \frac{\partial^2 p}{\partial z^2} - \frac{\omega^2}{c^2} p = f$ where p is the acoustic pressure
Interior load:	f
Boundary conditions:	$\frac{\partial p}{\partial n} = 0$ on ceiling, walls, and floor (n is normal to surfaces)

(c)

Fig.4.2: Mathematical description of a physical problem (after Burnett).

The system is typically, but not necessarily, a physical object (Fig.4.2). The domain of the problem is the region of the space occupied by the system. The governing equation may be differential equation expressing a conservation or balance of some physical property such as mass, momentum, or energy. Loading conditions are externally originating forces, temperatures, currents, etc., that interact with the system, causing the state of the system to change. Loads acting in the interior of the domain (interior load) appear as part of the governing equation (such as the distributed resistance boundary which is used in the flow through rock matrix models to represent the permeability of the matrix). Loads acting on the boundary of the domain (boundary loads) appear in separate equation called boundary conditions (6).

The domain of the problem is divided into smaller regions called elements. The shape of the elements are intentionally made as simple as possible (such as triangles and quadrilaterals in the two dimensional domains and tetrahedral and hexahedral in three dimensional domain.

In each element the governing equation, usually in differential or variational (integral) form, are transformed into algebraic equations called the element equations, which are an approximation of the governing equations (6).

The FEM seeks an approximate solution which only approximately satisfies the governing equation and boundary conditions. The FEM obtains an approximate solution by using the classical trial solution procedure. Burnett (6) defined the procedure steps to obtain this solution:

Step 1: The trial solution is constructed in the form of a finite sum of functions:

For a one dimensional problem:

$$U(x;a) = \emptyset_o(x) + a_1\emptyset_1(x) + a_2\emptyset_2(x) + \ldots\ldots\ldots + a_N\emptyset_N(x) \qquad (4.1)$$

where U(x,a) is the approximate solution

$\emptyset_o(x)$, $\emptyset_1(x)$, $\emptyset_2(x)$,....., $\emptyset_N(x)$ are known functions called trial functions.

a_1, a_2,....., a_N are undetermined parameters called degrees of freedom.

Here x represents all the independent variables in the problem.

For a two dimensional problem:

$$U^{(e)}(x,y;a) = \sum a_i \emptyset_i^{(e)}(x,y) \qquad i = 1,2,\ldots,n \qquad (4.2)$$

where $\emptyset_i^{(e)}(x,y)$ are known functions called the shape functions of element (e) (depends on the shape of the element and function of both x and y).

Step 2: The construction of a trial solution consists of constructing expressions for each of the trial functions in terms of specific, known functions. From a practical standpoint it is important to use functions that are algebraically as simple as possible and also easy to work with.

For example:

For a one dimensional element the powers of x (polynomials) is the most suitable trial solution:

$$U(x;a) = a_1 + a_2 x + a_3 x^2 + a_4 x^3 + \ldots\ldots\ldots\ldots + a_N x^{N-1} \quad (4.3)$$

For a two dimensional triangular element (Fig.4.):

$$U^{(e)}(x,y;a) = \sum a_j \emptyset_i^{(e)}(x,y) \qquad j=1,2,3 \qquad (4.4)$$

$$\emptyset_i^{(e)}(x,y) = (b_j + c_j x + d_j y) / 2\Delta$$

where $b_j = x_k y_l - x_l y_k$

$c_j = y_k - y_l$

$d_j = x_l - x_k$

Δ is the area of element.

The subscripts j, k, l have the value 1, 2, 3 for $\emptyset_1^{(e)}(x,y)$ and are permuted cyclically for $\emptyset_2^{(e)}(x,y)$ and $\emptyset_3^{(e)}(x,y)$.

Step 3: All the terms in the governing equation are transferred to the left-hand side (LHS) so that zero is on the right-hand side (RHS), the left-hand side of the governing equation is called the residual R(x;a).

In the Galerkin approximate solution method (for example) the residual is multiplied by the trial function $\emptyset_i(x)$ associated with each a_i.

The Galerkin residual equations:

For one dimensional problem is $\int R(x;a)\, \emptyset_i(x)\, dx = 0 \quad i = 1,2,\ldots,n \qquad (4.5)$

For two dimensional problem is

$$\int^{(e)}\int R(x,y;a)\, \emptyset_i^{(e)}(x,y)\, dx\, dy = 0 \qquad i = 1,2,\ldots,n \qquad (4.6)$$

where $\int^{(e)}\int dx\, dy$ means integration over the area of element (e).

Step 4: The highest derivative term in these equations is integrated by parts.

Then the general form of the trial solution (Eqs.4.1 or 4.2) is substituted into the integral form of the residual equations (Eqs.4.5 or 4.6).

The result of the integration is arranged as follows:

$$\begin{bmatrix} K_{11} & K_{12} & \cdots\cdots & K_{1N} \\ K_{21} & K_{22} & \cdots\cdots & K_{2N} \\ \vdots & \vdots & & \vdots \\ \vdots & \vdots & & \vdots \\ K_{N1} & K_{N2} & \cdots\cdots & K_{NN} \end{bmatrix} \begin{Bmatrix} a_1 \\ a_2 \\ \vdots \\ \vdots \\ a_N \end{Bmatrix} = \begin{Bmatrix} F_1 \\ F_2 \\ \vdots \\ \vdots \\ F_N \end{Bmatrix} \qquad (4.7)$$

The terms F_i (i = 1, 2,....., N) are the interior and the boundary load terms. They are integration functions (function of trial or shape function and function of a and/or y)

The terms K_{ij} (i, j= 1, 2,....., N) are integration functions (function of trial or shape functions and function of x and/or y).

Step 5: Substitute the trial or shape functions (Eqs.4.1 and 4.2) into the system equations (Eqs.4.5). As the trial and shape functions are function of x and/or y, all the integrals are transformed to an algebraic form (which is function of x and/or y).

Specify numerical data for the problem, which are the coordinate of each node (x and/or y), nodes numbers and elements numbers.

As the nodes coordinates are specified, all the interior terms in the system equation (except the boundary conditions term) can be numerically evaluated by substituting the nodes x and/or y coordinates by their values.

Step 6: Apply the boundary conditions to the system equation.

The boundary terms which have no prescribed boundary value can be eliminated by doing some column and row operation and the matrix of coefficients is sparse; that is, most of the coefficients are zero.

The final form of the system equation for six elements 1-D domain is:

$$\begin{bmatrix} C_{11}^1 & C_{12}^1 & 0 & 0 & 0 & 0 & 0 \\ C_{21}^1 & C_{22}^1 + C_{22}^2 & C_{23}^2 & 0 & 0 & 0 & 0 \\ 0 & C_{32}^2 & C_{33}^2 + C_{33}^3 & C_{34}^3 & 0 & 0 & 0 \\ 0 & 0 & C_{43}^3 & C_{44}^3 + C_{44}^4 & C_{45}^4 & 0 & 0 \\ 0 & 0 & 0 & C_{54}^4 & C_{55}^4 + C_{55}^5 & C_{56}^5 & 0 \\ 0 & 0 & 0 & 0 & C_{65}^5 & C_{66}^5 + C_{66}^6 & C_{67}^6 \\ 0 & 0 & 0 & 0 & 0 & C_{76}^6 & C_{77}^6 \end{bmatrix} \begin{Bmatrix} a_1 \\ a_2 \\ a_3 \\ a_4 \\ a_5 \\ a_6 \\ a_7 \end{Bmatrix} = \begin{Bmatrix} b_1^1 \\ b_2^1 + b_2^2 \\ b_3^2 + b_3^3 \\ b_4^3 + b_4^4 \\ b_5^4 + b_5^5 \\ b_6^5 + b_6^6 \\ b_7^6 \end{Bmatrix}$$

where b and C are numerical values. The superscripts refer to the element number and the subscripts refer to the nodes. Each element has a sharing node with the neighbour element.

Step 7: Solve the system equations which is in this case seven equations with seven unknowns. The values of a_1, a_2, a_3,.....,a_6 are the nodal solution of the degree of freedom(Burnett).

4.3 Programming

The ANSYS (SWANSON ANALYSIS SYSTEMS INC.) program was used in this study. It is a computer program for finite element analysis and design. It is used to find out how a given design works under operating conditions, thus the proper design for a given operating conditions could be calculated.

The ANSYS program is a general purpose program which can be used for almost any type of finite element analysis. It is organised into two basic levels, the Begin level which acts as a gateway into and out of the program and the Processor level where several processors are available, each serving a specific purpose such as model generation, solution and post processing.

The ANSYS program works with one large database that stores all input and output data and results data in an organised manner.

Commands are the primary tool used to communicate with the ANSYS program each designed for a specific function. ANSYS program can be run either in interactive mode (issue a command then the program processes it, then another command is issued and so on) or batch mode (submit a complete file of commands) to the program.

The easiest way to communicate with the ANSYS program is via the menu system which is a shell built around the commands to make the program easier to use.

Every issued command is copied to a log file, creating a complete record of the ANSYS session for any further use.

FLOTRAN, a computational fluid dynamics (CFD) solver within the ANSYS program can be used for fluid flow analysis. It is a program based on finite element method and has the capabilities of laminar or turbulent flow; incompressible or compressible fluids; distributed flow resistance or porous media. The permeability of the rock can be modelled by using the Distributed Resistance feature which is available within the FLOTRAN solver.

The distributed resistance uses the concept of the medium resistance (C) to the flow of a certain fluid, the medium resistance (C) is equal to the inverse of the medium permeability (K).

The procedure for a typical analysis can be divided into three distinct steps:

i) Building the model (at the perprocessor).

ii) Obtain the solution (at the solution processor).

iii) Review the results (at the post processor).

A 2-dimensional model is assumed for illustrative purposes.

It uses the governing equations:

x-Momentum equation:

$$\rho u\frac{\partial u}{\partial x}+\rho v\frac{\partial u}{\partial y}=-\frac{\partial p}{\partial x}+\frac{\partial}{\partial x}(\mu_e\frac{\partial u}{\partial x})+\frac{\partial}{\partial y}(\mu_e\frac{\partial u}{\partial y})+f_x-R_x \qquad (4.8)$$

y-Momentum equation:

$$\rho u\frac{\partial v}{\partial x}+\rho v\frac{\partial v}{\partial y}=-\frac{\partial p}{\partial y}+\frac{\partial}{\partial x}(\mu_e\frac{\partial v}{\partial x})+\frac{\partial}{\partial y}(\mu_e\frac{\partial v}{\partial y})+f_y-R_y \qquad (4.9)$$

Continuity equation:

$$\frac{\partial(\rho u)}{\partial x}+\frac{\partial(\rho v)}{\partial y}=0 \qquad (4.10)$$

and solves them.

where R_x and R_y are the distributed resistance terms, μ_e is the effective viscosity and u and v are the flow velocity in the x and y direction respectively.

4.3.1 Building the model

(1) Specify the jobname and the analysis title by using the /FILNAME and the /TITLE commands.

(2) Define the Element type by using the /ET command. For 2-D fluid flow analysis, the Element Fluid 141 was used. It had four nodes with the velocity components in x and y direction, pressure and temperature as the degree of freedom. The output consists of pressure distribution and flow velocity distribution.

(3) Define Element Real constants by using the R command. The REAL attribute is used by FLOTRAN to flag elements which utilise the distributed resistance capability.

Distributed Resistance is a FLOTRAN feature which can be used to represent the resistance of the rock matrix to flow, as the Distributed Resistance Model adds losses to the flow field. Only elements with a real constant reference number (REAL) > 1 will be treated as distributed resistance element.

The basic form of the resistance terms is:

$$R = K\rho V|V| + (f / D)\rho V|V| + C\mu V \qquad (4.11)$$

Where K the loss coefficient (1/m)

C the permeability inverse ($1/m^2$)

f the friction factor (dimensionless)

D the hydraulic diameter (m)

These terms were included in the basic governing equations to give the effect of flow resistance by rock matrix for a 2-D model.

Then FLOTRAN solves the basic govering equations by assuming a laminar incompressible isothermal flow.

To simulate the flow through rock matrix, the permeability inverse term (C) was used by giving it a value while the other two terms were excluded by specifying them to be zero (by giving the friction factor (f) and the loss coefficient (K) zero values) in the R command.

(4) Model generation

A solid model of the structure is constructed allowing changes and modifications to be made. This is then passed to the finite element mesh generator which takes the coordianates of the individual structural components in the solid model and automatically constructs a network of nodes and elements.

Before issuing the mesh command (AMESH) the TYPE and REAL commands must be issued to define the active element type and the active Real constants set.

(5) Applying Boundary conditions: Boundary conditions are applied on nodes by using the D command with the appropriate label (Pressure or flow velocity).

The Inflow boundary conditions is the inlet velocity profile or the inlet pressure. Also the inlet temperature must be specified.

The Wall boundary conditions (zero tangent velocity) are applied by setting the velocity components at the wall to be zero and the pressure is unspecified.

The Outflow boundary conditions are applied by specifying only the outlet pressure and all other variables are left unspecified. Generally, a value of zero pressure is used at an outlet.

The Symmetry boundary conditions are applied by specifying the velocity component normal to the symmetry line as zero.

Since some of the flow boundary conditions can conflict, there is an optimum order (required by the FLOTRAN program) for setting the flow boundary conditions:

Symmetry boundaries (no flow in the direction perpendicular to the symmetry axis)

Inflow boundaries (flow velocity at the inlet)

Wall boundaries (no flow in the X and Y direction)

Outflow boundaries (pressure at the outlet)

(6) Define the Flotran CFD parameters: the fluid properties and flow analysis parameters are defined by using the FLDATA command. These parameters included the reference pressure, nominal temperature, type of analysis, fluid properties (constant or variable properties), number of iterations and flow system (turbulent or laminar).

4.3.2 Obtain the solution

The action command to initiate solution calculations is SOLVE. When this command is issued, the ANSYS program takes model and loading information from the data base and calculates the results. Output from the solver is written to the output file by using the /OUTPUT command. The solution output results are for each node and consist of the degree of freedom results such as the velocity components, velocity summation and pressure at each node in the model.

4.3.3 Review the results

This is done within the post processor which can be entered by issuing the command /POST1. The results can be viewed as either tables or as graphs. The graphs can be contoured to show gradation in, for example, pressure within the rock matrix.

The results can be reviewed in several ways such as:

(1) Displaying results graphically such as:

Boundary condition displays is performed by using the /PBC command.

Contour displays showed how a results item (such as pressure and velocity) varies over the model and performed by issuing the PLNSOL command.

Vector displays use arrows to show the variation of both the magnitude and direction of a vector quantity in the model, it is performed by issuing PLVECT command.

Path plots showed the variation of a quantity along a predefined path through the model, this is done by define a path using the LPATH command, map the desired quantity on to the path using the PDEF command and then use the PLPATH command to display the results.

Particle flow trace is a special form of graphics that show how a particle travels in a flowing fluid, performed by issuing the TRPOIN and the PLTRAC commands.

(2) Listing results in tabular form such as:

The PRNSOL command lists specified nodal solution data.

The PRRSOL command lists reactions at constrained nodes in the selected set of nodes.

The PRPATH calculate and then lists specified data along a predefined geometry path in the model.

4.4 The objectives of this chapter

In the experimental work, the results were the inlet pressure and the outlet flow velocity through side outlets and along the fracture. The pressure and fluid velocities were known at the ends of the fracture but the variation of pressure and fluid velocities within the fracture and within the rock matrix were unknown. To investigate these effects modelling techniques were examined. The flow geometry was such that no analytical solutions were applicable because the flow paths withins the rock and fracture were unknown. From other work done in the department by Zhang[108], network modelling was considered a possibility. This involves the establishment of a network of connections which represent the pore spaces in the rock. As Zhang showed the network is severely limited in size. Therefore the finite element method was chosen because it could represent the size of the experimental slab and the flow properties of the pore spaces. Once the small scale models of the fracture flow had been tested, the FEM program was used to scale up the flow to examine the effect of flow from a wellbore into a fracture.

The finite element program ANSYS was used to obtain a general pressure and flow velocity change with distance along the fracture. Several finite element fractured slab models, with the same dimensions as in the experiment, were designed and tested.

The pressure and velocity change with distance were obtained for different values of matrix permeability, fracture permeability, fracture length, fracture width and different inlet flow velocity.

For comparison a linear injection model was built and tested. The dimensions of this model were as in the linear injection experiments. A brief comparison between the results of the fracture model and the linear model was carried out.

As the fracture model had a flat fracture face, it will give a pressure drop which is lower than the actual pressure drop along rough fracture which may effect the pressure distribution along the fracture. So a rough fracture face model with different roughness factors was constructed and tested.

The large scale wellbore flow models examined six cases, a radial injection with and without near well bore damaged zone, radial injection with single fracture with or without near fracture damage zone, and radial injection with double fractures with or without near fracture damaged zone. Then a comparison study was performed between these cases.

4.5 ANSYS/FLOTRAN validation

To validate the ANSYS/FLOTRAN simulation program two flow geometries were built and run. These two geometrys have an analytical solution in the literature with which the FLOTRAN solution was compared for the flow geometry modelled.

The first flow geometry was chosen to be the flow of brine along a fracture.

The analytical solution for this case was expressed by *Reiss* as:

$$\Delta p = 10.65 \frac{QL\mu}{wbK}$$

where Q is the flow rate (bbl/day)
L is the length of the fracture (ft)
μ is the fluid viscosity (cp)
w is the width of the fracture face (ft)
b is the fracture aperture (inch)
Δp is the pressure drop along the fracture (psi)

The second flow geometry was chosen to be the flow of brine through a rock matrix block of a known permeability.

The analytical solution for this case was expressed by Darcy's law:

$$\Delta p = \frac{V\mu L}{K}$$

where V is the flow velocity

L is the flow path length

K is the rock matrix permeability

Concerning the first geometry, figure 4.3 shows the change in pressure drop versus fracture permeability taken from FLOTRAN and analytical solutions. There is a small difference between the two results. This difference increases from 2% (when the fracture permeability was 2000 Darcy) to 7% (when the fracture permeability was 6000 Darcy).

Concerning the second geometry, figure 4.4 shows the change in pressure drop versus matrix permeability taken from FLOTRAN and analytical solutions. The two results were identical.

4.6 Fractured slab simulation

To examine the pressure and flow velocity distribution along fracture and through rock matrix, the ANSYS / FLOTRAN finite element software was used to simulate the flow of brine along a fractured slab. The software used the distribution resistance technique (section 4.2.1) to simulate flow through a rock matrix.

4.6.1 Building the Fracture model

Element type FLUID 141 was used with two real constants sets, The first set was used to represent the rock matrix part of the model with a permeability inverse term (C) equal to $2x10^{12}$ m^{-2} (matrix permeability equal to 500 md), and the second set was used to represent the fracture part of the model with a permeability inverse term (C) equal to $2.5x10^{8}$ m^{-2} (fracture permeability equal to 4000 Darcy).

A symmetric 2-D model of the slab used in the experimental section was biult in ANSYS (Fig.4.5). The maximum number of elements avalabile in this ANSYS version (university version) was 8000, which limits the design to a 2-D model.

The length of the simulated slab was 0.4 m and its width was 0.03 m. The fracture half width was 0.0005 m (0.5 mm). The length of the model was divided into 400 divisions. The width of the matrix was divided into 10 divisions (with smaller divisions near the fracture) and the width of the fracture into 8 divisions. These allowed a mesh of 3200 elements to be constructed for

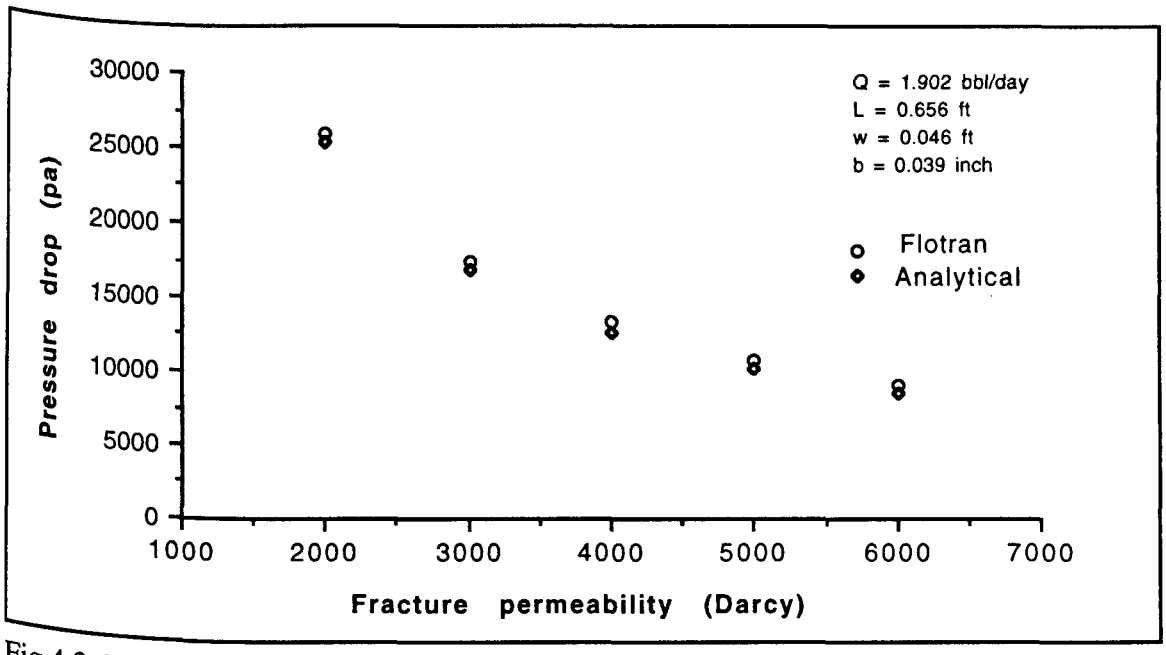

Fig.4.3: The FLOTRAN and the analytical results of the Pressure drop versus fracture permeability

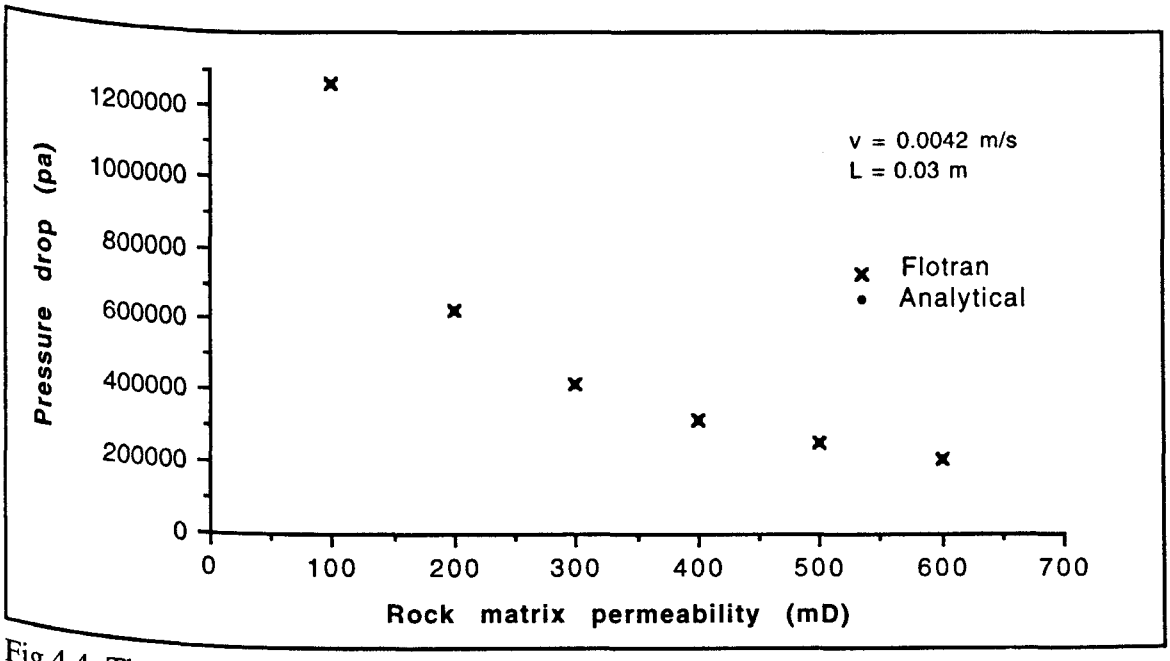

Fig.4.4: The FLOTRAN and the analytical results of the Pressure drop versus matrix permeability.

the fracture and the matrix part of the model was meshed into 4000 elements with small elements near the fracture (as the pressure gradient in the matrix near the fracture is higher than the pressure gradient in the rest of the matrix).

The fluid was allowed to enter only through the fracture inlet and to exit through the fracture outlet and through the upper side of the slab. The flow along the fracture was mainly in the x-direction and the flow through the rock matrix was mainly in the y-direction.

4.6.2 The boundary condition

The Boundary conditions were applied as follows:

(1) Symmetric boundary condition: the axis of symmetry was taken along the middle of the fracture in the direction of the x-axis.

$Vy = 0.0$ m/s at $y = 0.0$ m ;where V is the flow velocity.

(2) Inflow boundary condition: the flow velocity at the fracture inlet was in the x-direction only.

$Vx = 0.25$ m/s at $x = 0.0$ m and $0.0 < y < 0.0005$ (fracture half width)

$Vy = 0.0$ m/s

(3) Wall boundary condition: the flow veocity in the x and y directions at the wall boundary is equal to zero.

$Vx = 0.0$ m/s at $x = 0.0$ m and $0.0005 < y < 0.0305$

$Vy = 0.0$ m/s

(4) Outflow boundary conditions: the flow exit at the fracture outlet and at the side outlets. The flow velocity at these two locations is unknown, so the pressure was specified at the out flow boundary instead of the velocity.

fracture outlet:

$P = 0.0$ Pa at $x = 0.4$ m and $0.0 < y < 0.0005$

Side outlets:

$P = 0.0$ Pa at $0.0 < x < 0.4$ and $y = 0.0305$ m

4.6.3 Fluid Flow parameters

The FLOTRAN CFD parameters were defined as follows:

Constant fluid density equal to 1050 kg/m^3 (incompressible flow of brine).

Constant temperature equal to 300 K (isothermal flow).

Flow system is laminar.

Constant fluid vescocity of 0.001 kg/m.s.

At this stage the Solver was run and the results were stored for post-processing. A complete pressure and velocity distribution through the rock matrix and along the fracture was recorded. The results were presented as pressure and velocity variation with distance along the fracture and through matrix.

4.6.4 The results of the fracture models

The effects of the following factors on the pressure and the flow velocity distributions along a predefined path were investigated:

(1) The effect of Fracture permeability.

(2) The effect of Matrix permeability (incorporating some matrix damage by reducing the matrix permeability).

(3) The effect of flow velocity at the fracture inlet (by increasing or decreasing injection rate).

(4) The effect of fracture width.

(5) The effect of fracture length.

All the readings along the fracture were taken at 0.0625 mm distance from the fracture face i.e. the nodes within the fracture closest to the fracture face.

4.6.4.1 General case

A general case was studied to examine the capabilities of the Finite Element technique. The test was carried out with the variables defined in the above model which are:

Fracture length = 0.4 m (similar to the fractured slab length used in the experimental work)

Fracture permeability = 4000 Darcy or 4×10^{-9} m^2 (full open fracture)

Matrix permeability = 500 md or 5×10^{-13} m^2 (clean matrix)

Inlet flow velocity = 0.25 m/s

Fracture aperture = 0.001 m .

The results obtained for this case are shown in Figures 4.6 and 4.7. The pressure mapping along the fracture plot showed that the inlet pressure was 0.185 bar and decreased to 0.079 bar

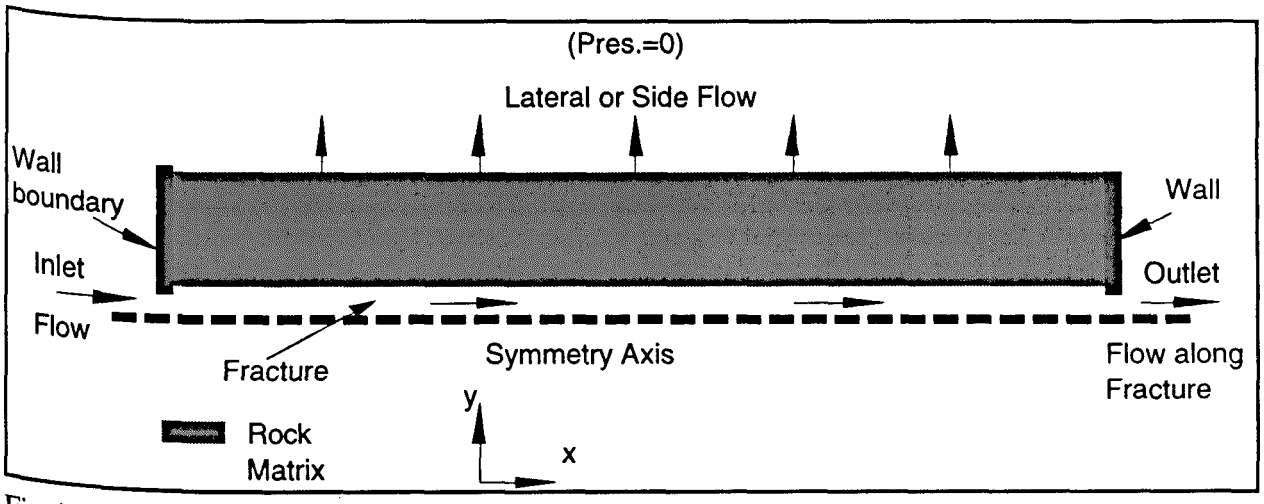

Fig.4.5: 2-D Linear Fracture model.

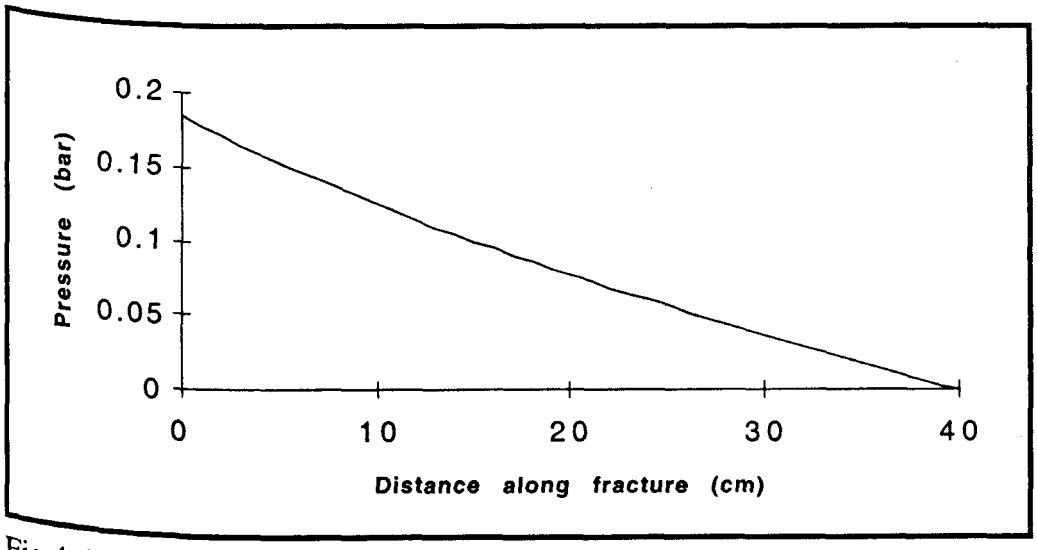

Fig.4.6: Pressure along the fracture (general case).

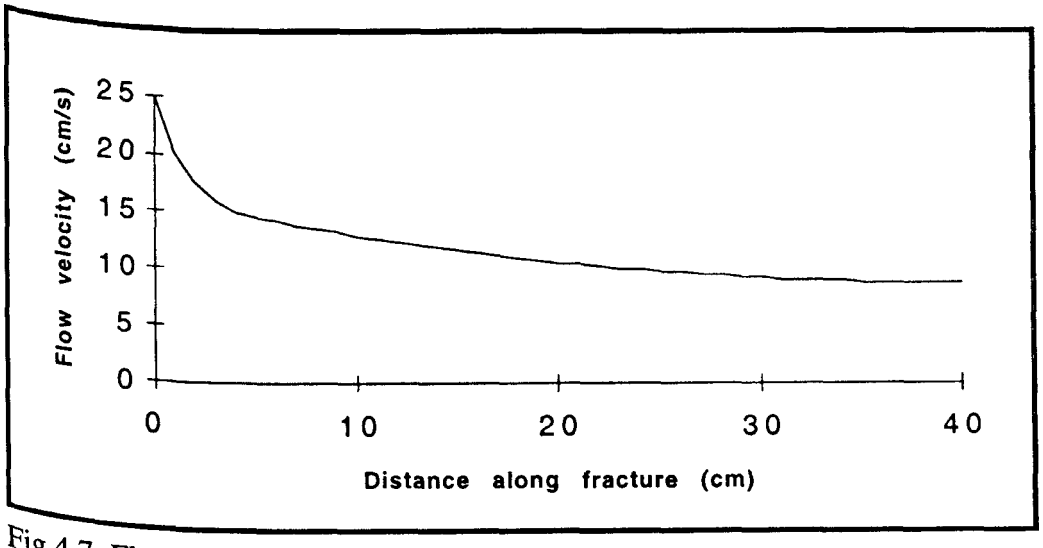

Fig.4.7: Flow velocity along the fracture (general case).

(which is 57% of the inlet pressure) half way along the fracture, so more than half of the pressure drop was lost in the first half of the fracture (Fig.4.6).

The flow velocity plot along the fracture plot showed that the flow velocity decreased sharply from 0.25 m/s (at the fracture inlet) to 0.15 m/s at 0.05 m along the fracture from the inlet. It then decreased smoothly to 0.107 m/s at half way along the fracture. The flow velocity along the fracture was 0.09 m/s near the fracture outlet. The total reduction in flow velocity along the fracture was 0.16 m/s. 62.5% of this reduction occured at 0.05 m from the inlet and 89% of this reduction in the first half of the fracture (Fig.4.7).

The mapping of pressure drop and flow velocity through side paths (in y-direction) showed that the side pressure drop with distance along the fracture had the same profile of the pressure change along the fracture because the side outlet pressure was set to zero along the slab length. The side flow velocity through the rock matrix at 10 cm from the inlet was 0.0208 cm/s and decreased to 0.0128 cm/s at 20 cm (a reduction rate of 3.8% per cm along the slab length) then decreased to 0.0062 cm/s at 30 cm distance from the fracture inlet (a lower reduction rate of 3.2% per cm along the slab length). As the flow approached the fracture outlet, the side flow rate was distributed on the fracture face more uniformly.

4.6.4.2 The Effect of fracture permeability on pressure and velocity distribution

The following variables were held constant :

Inlet velocity at 0.25 m/s.

Matrix permeability of 5×10^{-13} m^2 (equivalent to 500 md)

The fracture width was 0.001 m.

Fracture length was 0.4 m.

The fracture permeability was the only variable.

The plot of the pressure along the fracture showed that at high fracture permeability of 4000 Darcy (full open fracture) the pressure losses were distributed more uniformly along the fracture length.

As the fracture permeability was decreased most of the pressure started to be lost in the first half of the fracture (Fig.4.8). At a fracture permeability of 1000 Darcy the pressure loss at the first 0.2 m of the fracture was 72% of the total pressure loss.

The side pressure drop through rock matrix at 10 cm distance (Fig.4.9) from the fracture inlet (SPD1) is affected more by the fracture permeability than the side pressure drop at 20 and 30 cm distance (SPD2 and SPD3). The reduction in fracture permeability from 4000 to 1000 Darcy causes a 79% increase in SPD1 whereas it caused only 32% increase in SPD3 (Fig.4.10).

The 4000 Darcy fracture caused a higher reduction in flow velocity at 5 cm along the fracture than the 1000 Darcy fracture. For the high fracture permeability the velocity was uniformly distributed along the fracture (Fig.4.11) and as the fracture permeability decreased more and more of the flow velocity was lost in the first half along the fracture. This loss in flow velocity along fracture was reflected by an increase of side flow velocity (Fig.4.12). The side flow velocity at 10 cm distance along the slab (SFV1) was more sensitive to fracture permeability than the side flow velocity at 30 cm distance (SFV3).

4.6.4.3 The Effect of matrix permeability on pressure and velocity distribution

The fracture permeability was constant at 3000 Darcy with all other variables at the same values as in section 4.5.4.2 except the matrix permeability which was the only variable.

The matrix permeability variation had a little effect on the pressure drop along the fracture. By reducing matrix permeability from 500 md to 350 md (which makes the ratio of the two permeabilities PR = 0.7) the pressure drop increased by only 12% and increased by 34% when the matrix permeability was set to 150 md (PR = 0.3) and the pressure drop along the fracture became linear (Fig.4.13).

Decreasing the matrix permeability caused the side pressure drop at 30 cm distance from the fracture inlet SPD3 to increase by a higher rate than the side pressure drop at 10 cm distance from the fracture inlet SPD1 (Fig.4.14). By decreasing matrix permeability to 150 md, the SPD3 increased by 64% and the SPD1 increased by 47%.

Decreasing the matrix permeability resulted in a lower side flow (or a lower side flow velocity SFV) and more flow was directed along the fracture (or a higher flow velocity along fracture).

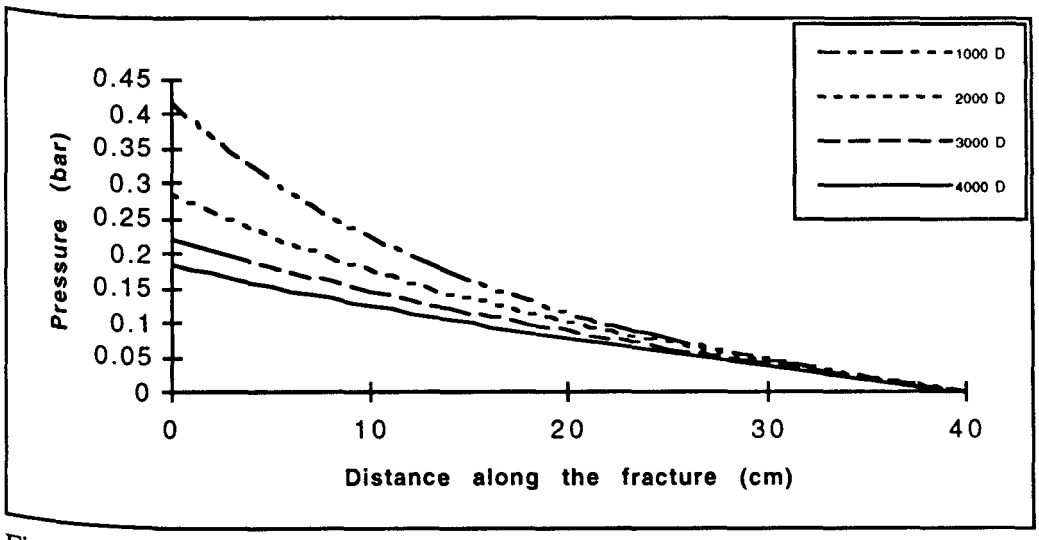

Fig.4.8: Pressure along the fracture as the fracture permeability varies.

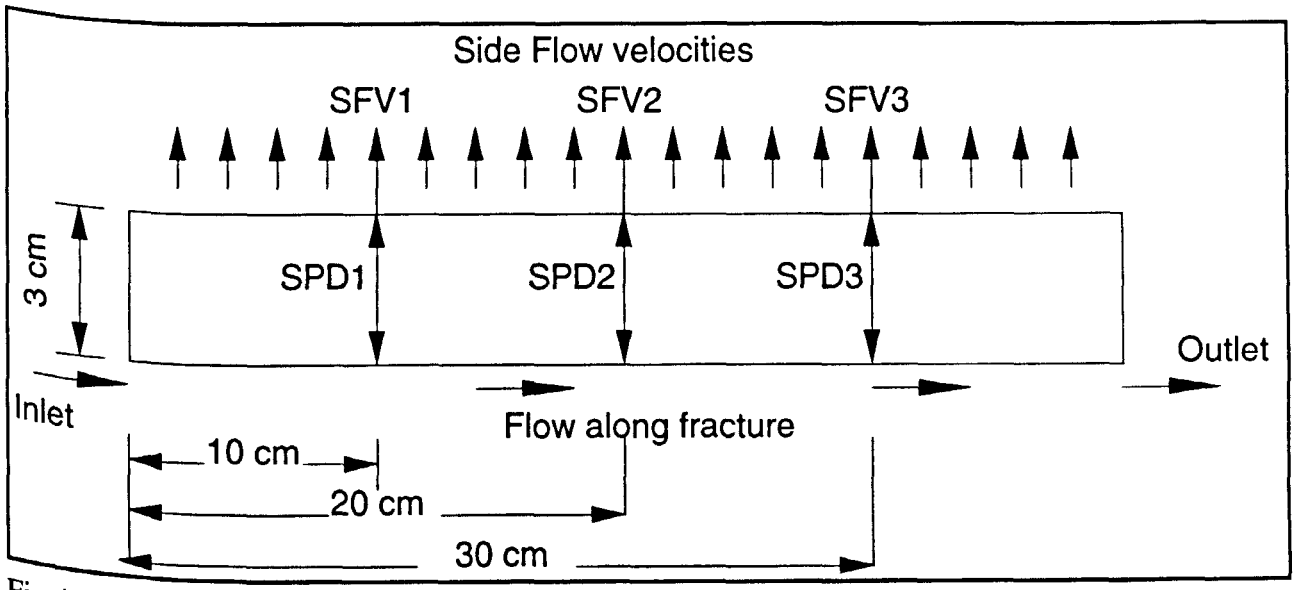

Fig.4.9: The side pressure drop and the side flow velocity along the slab.

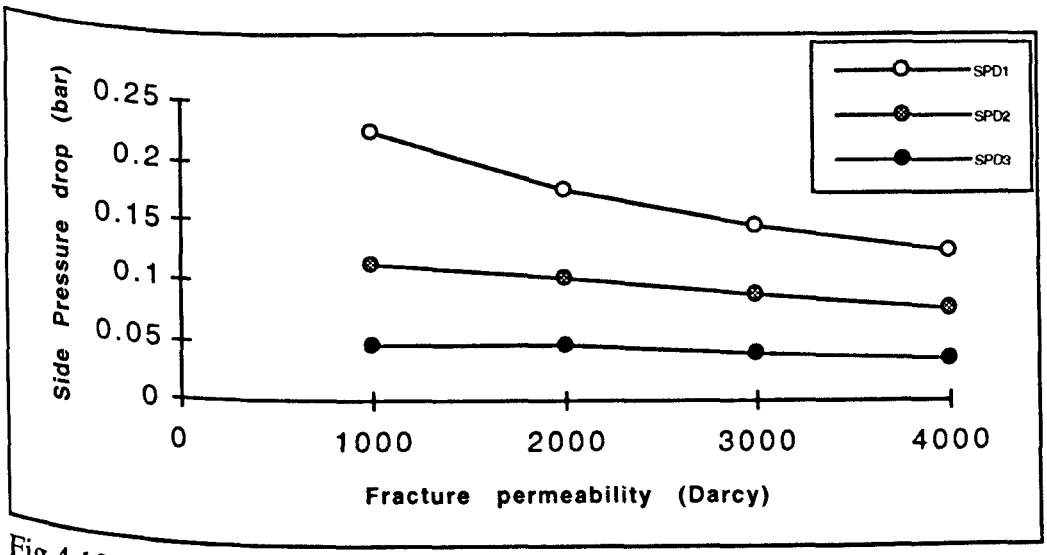

Fig.4.10: The change in side pressure drop as the fracture permeability varies.

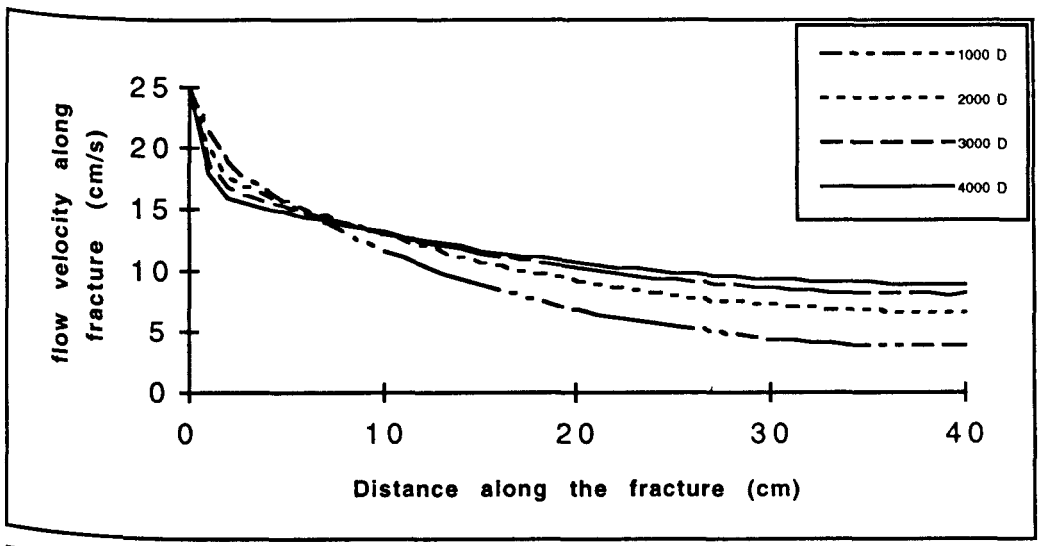

Fig.4.11: The change in flow velocity along fracture as the fracture permeability varies.

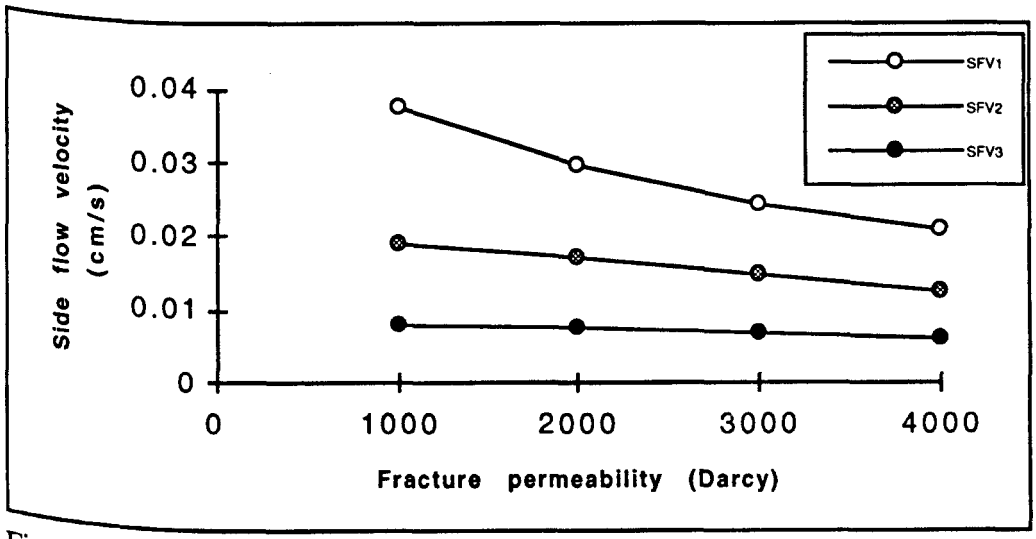

Fig.4.12: The change in side flow velocity as the fracture permeability varies.

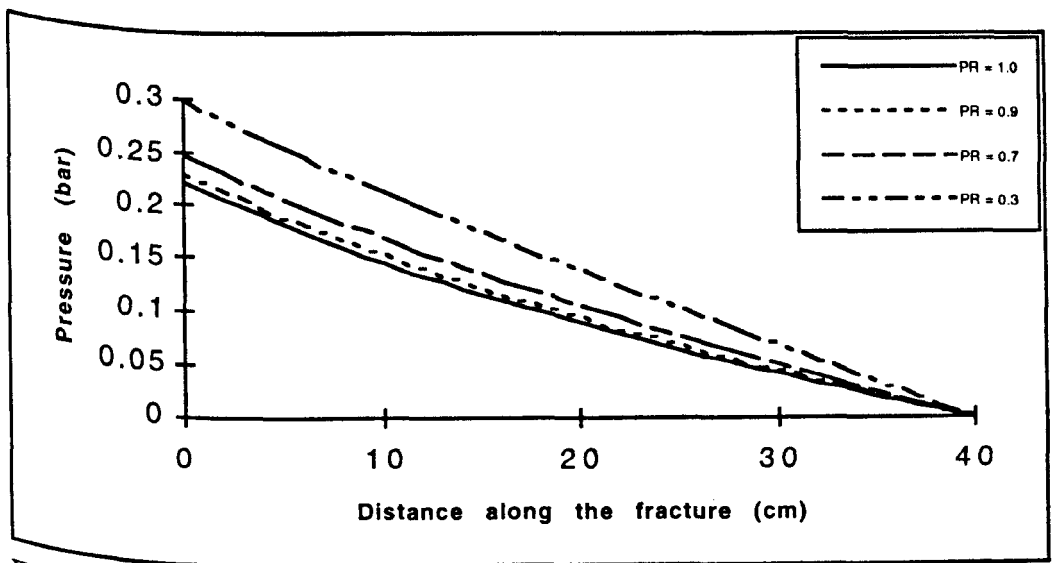

Fig.4.13: The change in pressure drop along the fracture as the matrix permeability varies.

The reduction in side flow through the rock matrix resulted in a lower reduction rate of flow velocity along fracture with distance (Fig.4.15). There is a sharp reduction in flow velocity along fracture at the first 5 cm to 0.15 m/s no mater what the matrix permeability was.
By decreasing matrix permeability to 150 md, the reduction of the side flow velocity at 10 cm distance from the fracture inlet SFV1 (56% reduction) was higher than the percentage reduction of the side flow velocity at 30 cm distance from the fracture inlet SFV3 (51% reduction) by 5% (Fig.4.16). This may be because the SPD3 increased by a higher rate than the SPD1.

4.6.4.4 The Effect of inlet flow velocity on pressure and velocity distribution

The following variables were held constant :

Fracture permeability was $3x10^{-9}$ m^2 (3000 D)

Matrix permeability was $5x10^{-13}$ m^2 (500 md)

The fracture width was 0.001 m.

Fracture length was 0.4 m.

The fracture inlet velocity was the only variable.

Increasing the inlet flow rate (or inlet velocity) by a certain fraction will cause an increase of the pressure drop by the same fraction as the flow rate and pressure drop were linearly related (as expected from Darcy's law). As the inlet flow velocity increased the difference between the side pressure drops SPD1 and SPD3 increased (Fig.4.17).

The same can be said for the side flow velocities SFV1 and SFV3.

4.6.4.5 The Effect of Fracture width on pressure and velocity distribution

The fracture width was varied from 0.6 to 1.2 mm while all other variables were held constant. The reduction of fracture width from 1.2 mm to 0.6 mm caused a 64% increase in pressure drop along the fracture (Fig.4.18). Reducing the fracture width affected the side pressure drop SPD1 more than it affected the side pressure drop SPD3 (Fig.4.19). Reducing fracture aperture from 1.2 to 0.6 mm caused a 47% increase in SPD1 but only 27% increase in SPD3.
As the fracture aperture decreased, the resistance to flow along the fracture increased which caused some of the flow along the fracture to be directed through the side outlets.

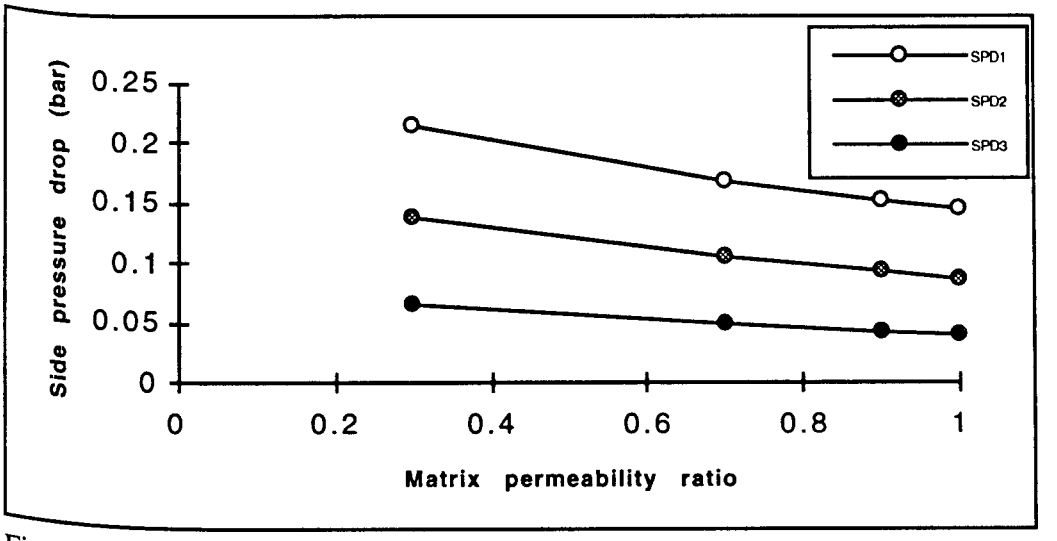

Fig.4.14: The change in side pressure drop as the matrix permeability varies.

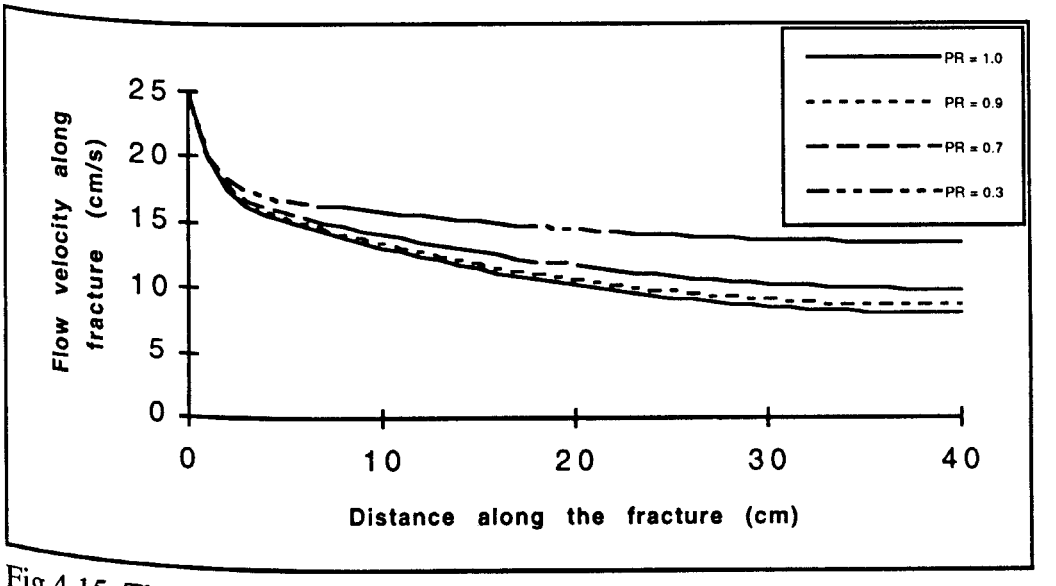

Fig.4.15: The change in flow velocity along fracture as the matrix permeability varies.

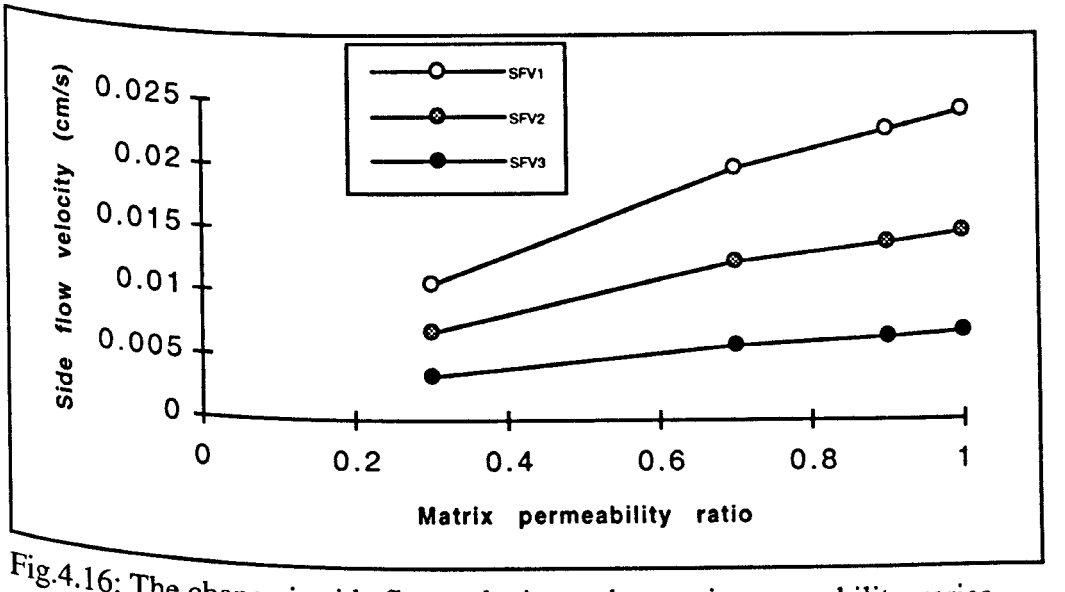

Fig.4.16: The change in side flow velocity as the matrix permeability varies.

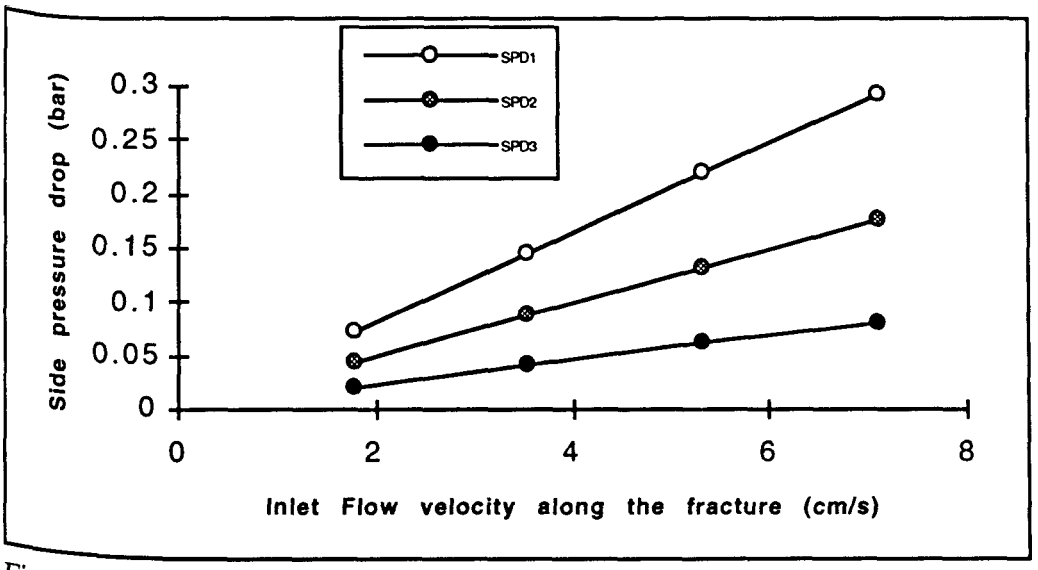

Fig.4.17: The change in side pressure drop as the inlet velocity varies.

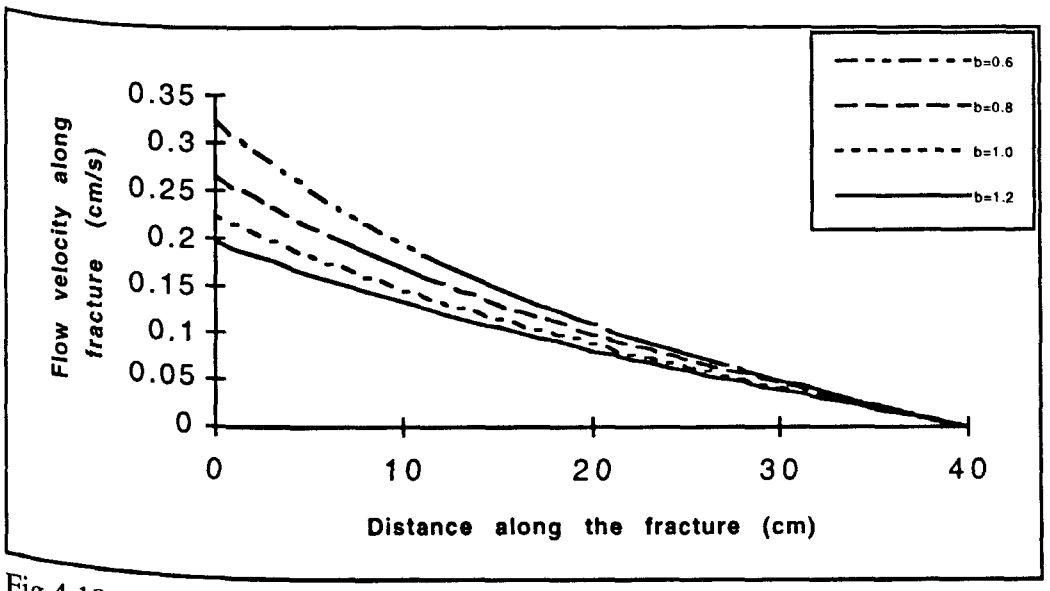

Fig.4.18: The change in pressure drop along the fracture as the fracture width (b) in mm varies.

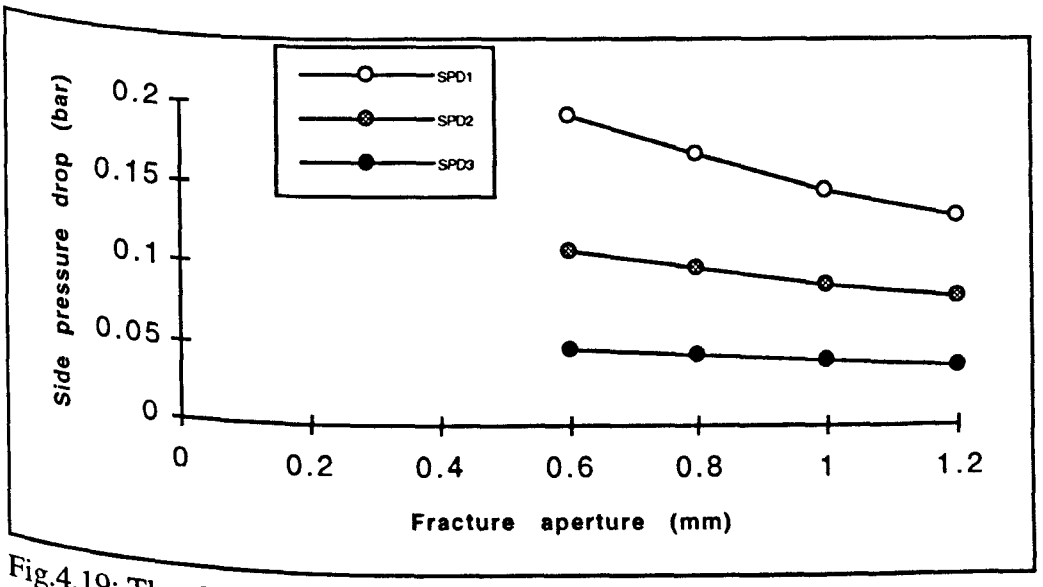

Fig.4.19: The change in side pressure drop as the fracture aperture varies.

The velocity SFV1 increased more than the velocity SFV3 as the resistance to flow was maximum in the first 10 cm along the fracture (Fig.4.20).

4.6.4.6 The Effect of Fracture length on pressure and velocity distribution

Two fracture lengths were used 40 and 80 cm with all other variables constant.

By increasing fracture length from 40 to 80 cm the pressure drop increased by only 12%. For the first half distance along the fracture, the pressure drop was 77% (of the total pressure drop) for the long fracture and 58% for the short fracture (Fig.4.21). The side pressure drop at 20 cm along the slab for the long fracture was higher than that of the short fracture by 38% (in spite of the pressure drop along the long fracture being higher than that of the short fracture by only 12%).

The reduction rate of the flow velocity along the fracture with distance was higher for the long fracture. At 30 cm distance along the fracture the flow velocity along fracture was reduced by 75% for the long fracture and by 65% for the short fracture (Fig.4.22). As the flow velocity along the 80 cm fracture was lower than that of the 40 cm fracture (the flow is more directed through side outlets in the long fracture), it was expected that the side flow velocity of the long fracture would be higher. When the fracture length increased from 40 to 80 cm, the side flow velocity at 20 cm distance along the slab increased by 36%.

4.7 Linear injection versus fracture injection:

A linear injection model was built and tested with the same element type and real constants as in the fracture injection model. The FLOTRAN CFD parameters were set to the same values as in the fracture injection model.

The linear injection model was 0.03 m long and 0.06 m width.

The boundary conditions for the linear injection model were as follows:

Inflow boundary conditions: inlet flow velocity (at the model inlet face) in the x-direction.

$Vx = 0.42$ cm/s at $x = 0.0$ and $0.0 < y < 0.06$ m (model width)

Wall boundary:

$Vx = 0.0$ and $Vy = 0.0$ at $0.0 < x < 0.03$ m (model length) and $y = 0.0$

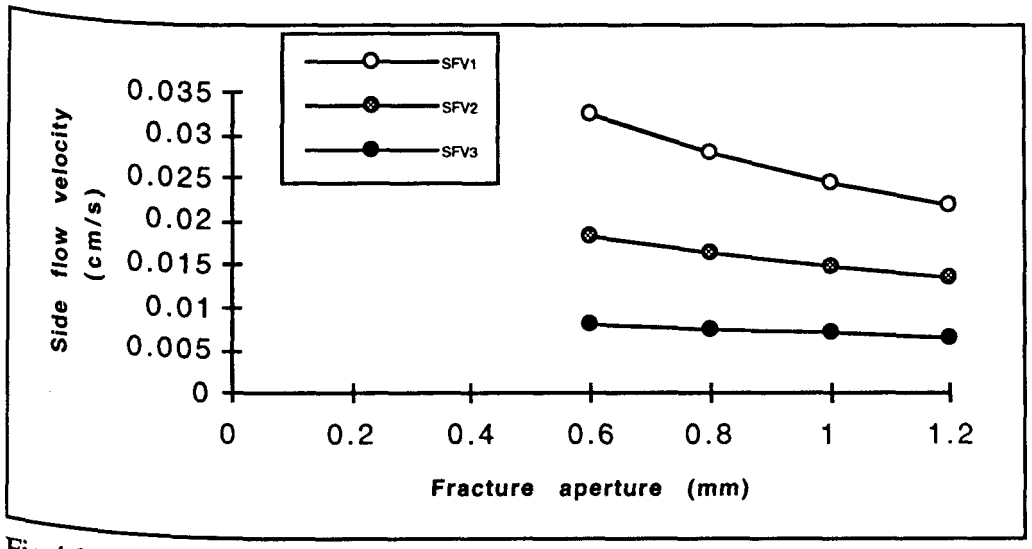

Fig.4.20: The change in side flow velocity as the fracture aperture varies.

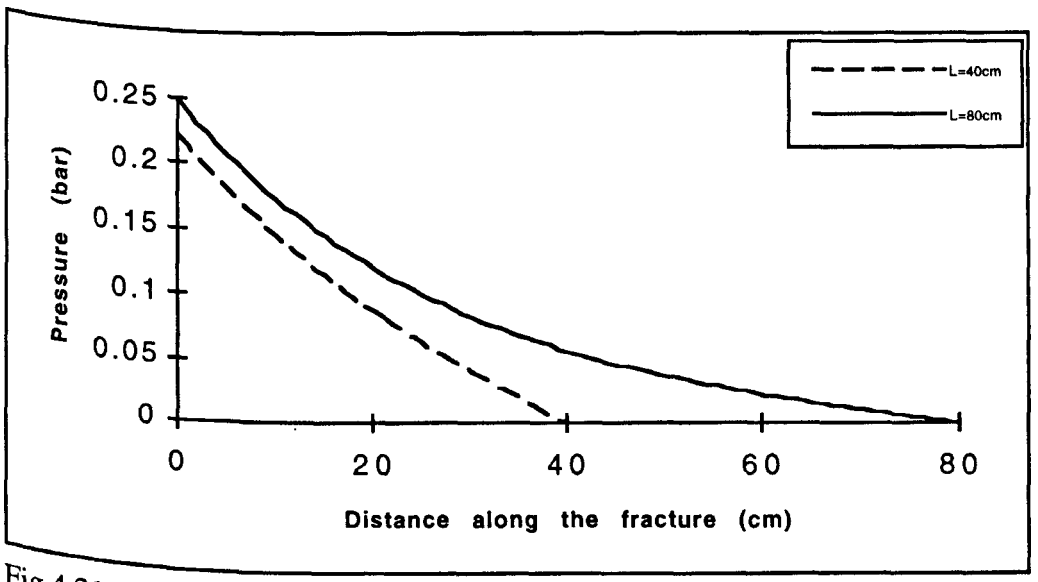

Fig.4.21: The change in pressure along the long and the short fractures.

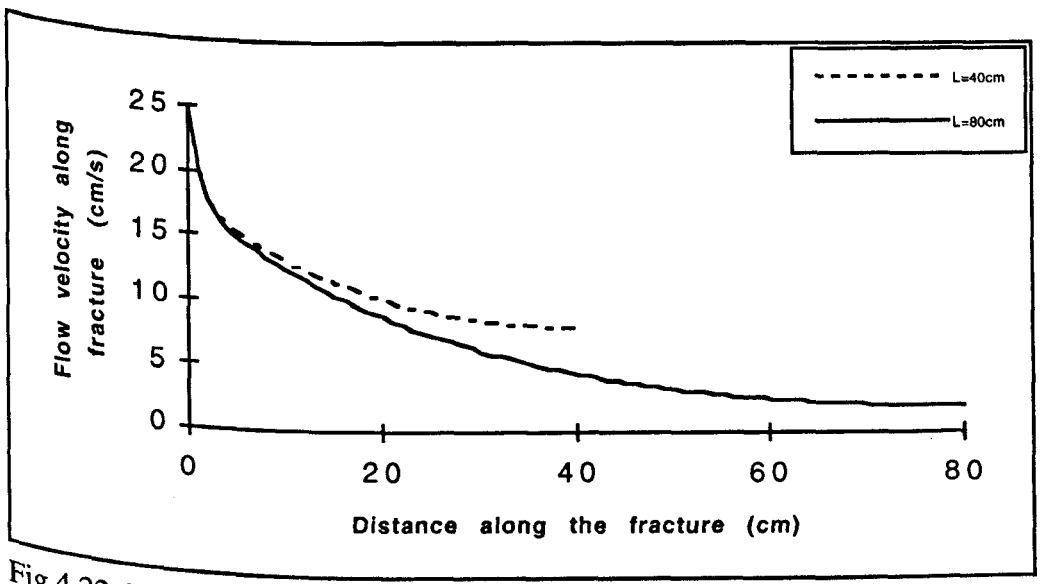

Fig.4.22: The change in flow velocity along the long and the short fractures.

$Vx = 0.0$ and $Vy = 0.0$ at $0.0 < x < 0.03$ m (model length) and $y = 0.06$ m

Outflow boundary was the outlet pressure (at the model outlet face):

$p = 0.0$ Pa at $x = 0.03$ m and $0.0 < y < 0.06$ m

The model was meshed with smaller elements at the inlet face.

A short comparison was made between the linear and fracture injection models (to indicate the effect of the geometry difference on pressure behaviour) at a constant inlet flow rate of 3.55 ml/s and constant model width of 0.06 m. The fracture was 0.4 m long with a permeability of 3000 Darcy and half width of 0.0005 m. The linear injection model was 0.03 m long. The inlet flow velocity along the fracture was 0.25 m/s and the flow velocity through the linear injection slab was 0.0042 m/s. The fracture face area was 13 times larger than the linear injection area. As the length of the side flow path in the fracture injection model was 0.03 m (which was equal to the linear injection model length), comparing the pressure drop through the linear injection model with the side pressure drop in the fracture injection model can be done (Fig.3.26).

4.7.1 The results of the comparison

At a matrix permeability of 500 md, the pressure drop through the linear injection model was 2.52 bar whereas in the fracture injection model the side pressure drops SPD1 and SPD3 were only 0.146 and 0.041 bar respectively. The pressure drop in the linear injection model was 27 times higher than the average side pressure drop in fracture injection model (Table 4.1).

This difference was due to a very small linear injection area compared with a much larger fracture face area. Also 32% of the flow was reaching the fracture outlet which makes the injected flow through the fracture face only 68% of the total inlet flow rate.

The same run was repeated with a 0.8 m long fracture. In this case only the first 0.4 m of the fracture was considered. The results showed that the pressure drop in the linear injection model was 20 times higher than the average side pressure drop in the first 0.4 m of the fracture. This reduction from 27 times to 20 times was because this time only 18% of the flow reaches the 0.4 m distance along the fracture and the injected flow through the fracture face was 82% of the total inlet flow rate (Table 4.2).

By decreasing the matrix permeability from 500 to 150 mD, the pressure drop along the 0.4 m fracture (FPD) increased by 34%. The side pressure drop SPD1 increased by 47%, the side pressure drop SPD2 increased by 57% and the side pressure drop SPD3 increased by 64%. But for the linear injection, the pressure drop through the rock matrix DP increased by 234%.
At a matrix permeability of 150 md the pressure drop in the linear injection model was 60 times higher than the average side pressure drop in the fracture injection and the injected flow through the fracture face was 46% of the total inlet flow rate.

For the case of the linear injection model, as the matrix permeability decreased, the resistance to flow increased which caused the pressure drop to increase sharply as the fluid was forced to flow through the rock matrix.
For the case of the fracture injection model, as the matrix permeability decreased, the resistance to flow through the side paths increasd but the fluid had another path with a lower resistance (along the fracture). As the resistance to flow through the side outlet increased, the flow was directed more and more along the fracture.

4.8 Fracture Roughness

To examine the effect of fracture roughness on the pressure and flow velocity profiles near the fracture face, rough fracture models incorporating fracture surface roughness were built and examined. The models were identical to those previously described but the fracture faces were not flat.

The fracture and the matrix permeabilities were set at constant values of 1000 Darcy and 500 md respectively. The roughness was simulated as triangles with a constant 1 mm base length and varying heights (Fig.4.23). The Spacing between each two triangles was zero and 1 mm. The height of the triangle represented the surface roughness (e). The pressure and the flow velocity were mapped along the fracture for different values of e/b ,where b is the fracture width.
In this model the friction loss was controlled by two factors which are the e/b value and the spacing between the triangles. Other models, where the roughness was simulated as squares, pyramids and circles, were examined also. By looking to the fracture face surface through a

microscope, it consists mainly of pyramids. So it was felt that it is more convenient to simulate roughness in the 2-D model as triangles than simulating it as squares, or half circles. Only the triangles roughness model is presented in this study.

4.8.1 The results of the fracture roughness model

For zero spacing between the roughness triangles, increasing the e/b value resulted in an increase in pressure loss along the fracture at the first 5 cm along the fracture. This was caused by the fracture width reduction due to roughness (resulted in smaller flow path) which resulted in higher flow velocity and eventually higher pressure drop (Fig.4.24 and 4.25). But as the flow continues along the fracture, the pressure loss profile for all the tested e/b values was nearly the same in the last 35 cm along the fracture. By increasing the e/b from 0.0625 to 0.25 the pressure loss along the fracture increased by 14 %.

Changing the e/b value (the area of the flow path was reduced as the value of e increased) had an effect on the flow velocity along the fracture only at the first 10 cm. At this first 10 cm, increasing the e/b value resulted in a higher flow velocity with nearly the same fluctuation. After the first 10 cm all the resultant velocities had nearly the same value and reduced at the same rate.

Then the spacing between the triangles was increased to 1mm. By increasing the e/b from 0.0625 to 0.25 (Fig.4.26) the pressure loss along the fracture increased by 8.5% (5.5% less than the case of zero spacing). Also the fluctuation in the flow velocity values increased (Fig.4.27).

The fracture roughness had no effect on the pressure loss profile after 5 cm distance along the fracture. At high values of e/b, fracture roughness caused a small increase in pressure drop along the fracture.

Flow velocity fluctuation may help in cleaning fracture face more efficiently.

The rough surface may be considered as a suitable place for particles and droplets to accumulate.

When the e/b increased from 0.0625 to 0.25, the accumulation effect would be higher than the cleaning effect as there was not much change in velocity fluctuation (also the chance of accumulation became higher as the triangle height increased).

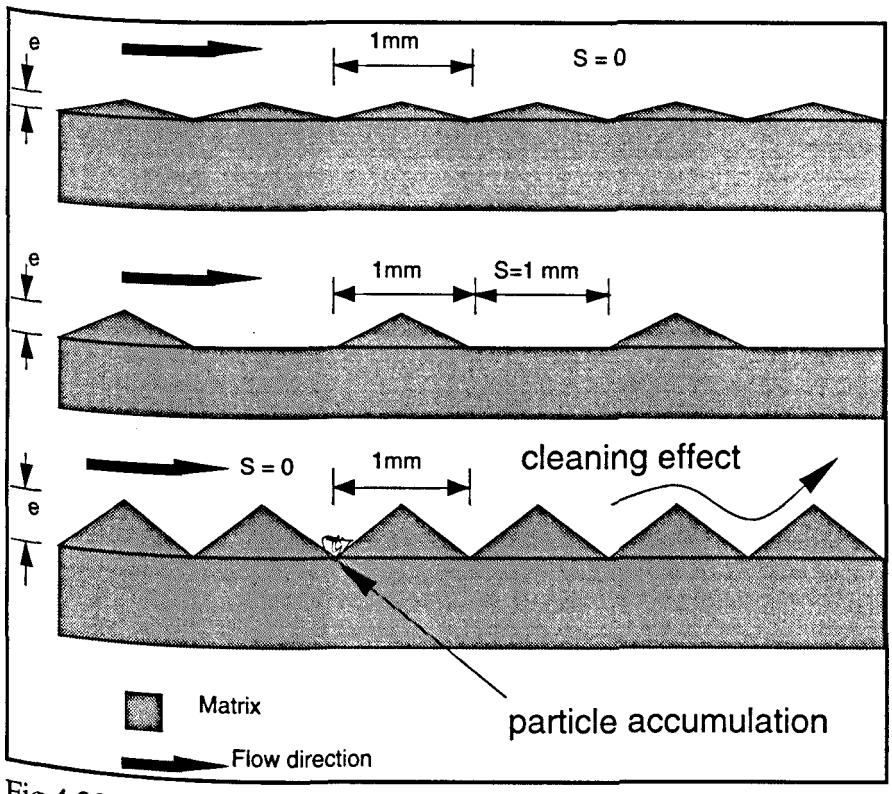

Fig.4.23: Rough surface simulation.

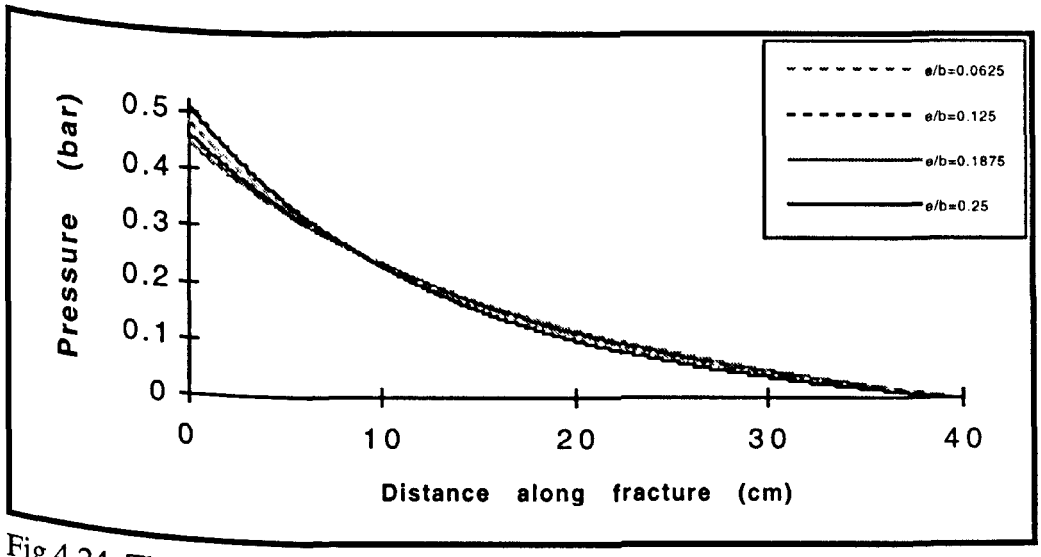

Fig.4.24: The change of pressure along rough fracture for zero spacing.

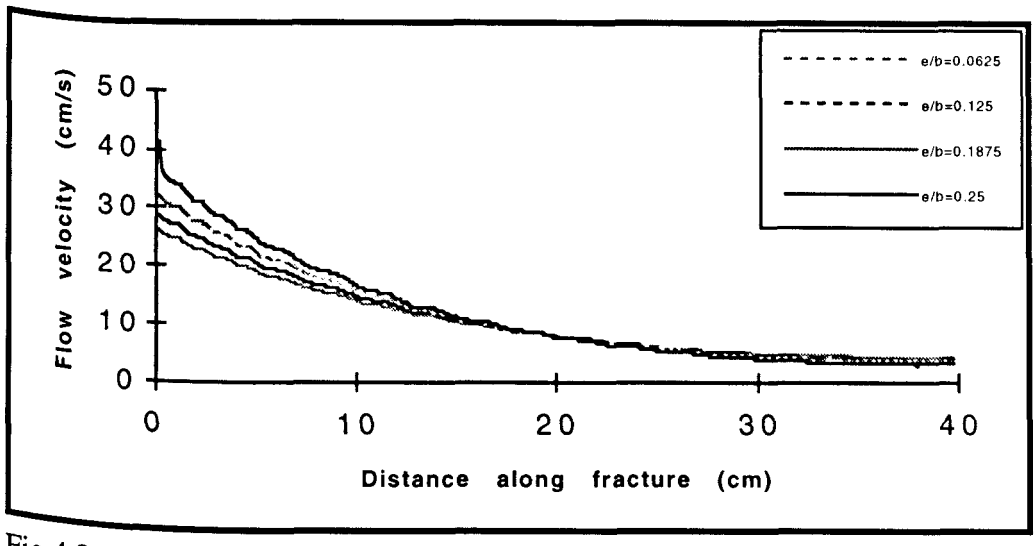

Fig.4.25: The change of flow velocity along rough fracture for zero spacing.

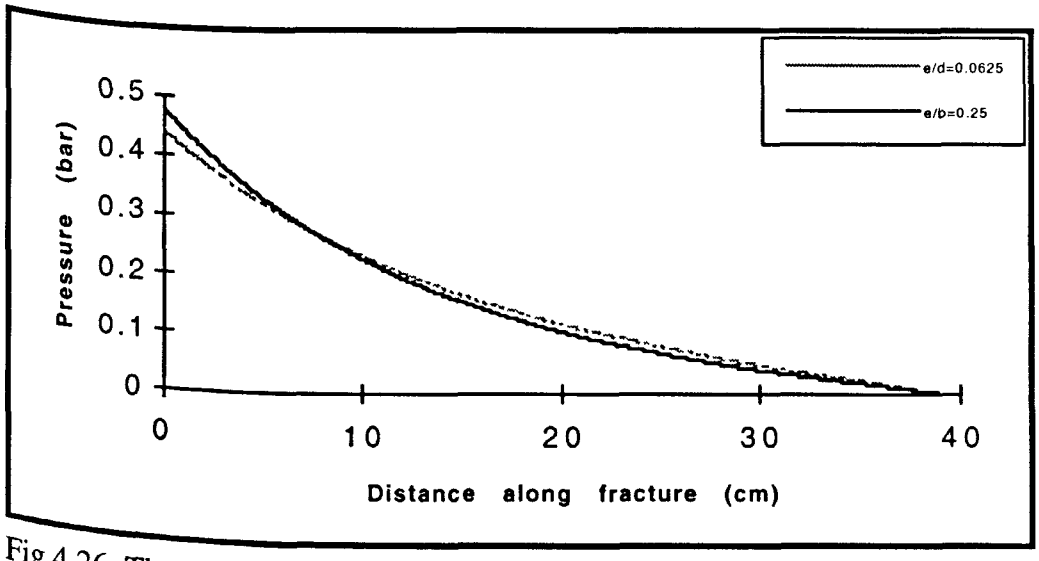

Fig.4.26: The change of pressure along rough fracture for 1 mm spacing.

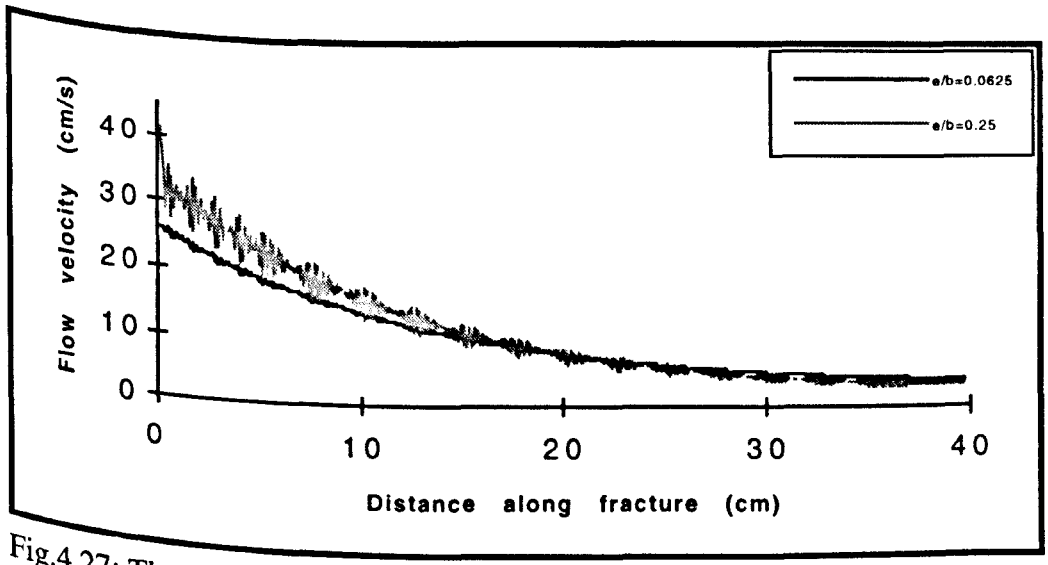

Fig.4.27: The change of flow velocity along rough fracture for 1 mm spacing.

When spacing increased from zero to 1 mm, the cleaning effect would be higher than the accumulation effect as the velocity fluctuation was higher for the 1 mm spacing (also the chance of accumulation became lower as the distance between the triangles increased).

4.9 Field Simulation

In this section an attempt was made to simulate a radial injection field operation for fracture and unfractured radial injection under laminar incompressible isothermal flow conditions. This was done to examine the pressure and flow velocity distribution along the fracture and through rock matrix (around the well bore) for an actual large scale operation. The factors most affecting pressure and velocity distribution were examined. The mean differences between the radial and the fracture injection systems were measured. Then the effect of the damaged zone around the well bore and near the fracture face on the pressure drop was also studed and evaluated. The complete simulation programs are listed in appendix A. They consist of building and meshing the model, applying the boundary condition, specify the operating constants, obtaining the solution and reviewing the results as detailed in previous sections. The simulation process was divided into six sections

4.9.1 Building the Models and applying boundary conditions

4.9.1.1 Radial injection with no fractures model

The model consisted of a quarter of a cylindrical reservoir with 10 m thickness (Fig.4.28). The well bore radius was 0.0635 m and the outer reservoir radius was 20.0635 m.

The total injection rate was 1037 m^3/day which made the flow velocity through the rock matrix equal to 0.003 m/s (Flow area was equal to 4.0 m^2).

The matrix permeability was set to 500, 300 and 100 md for each run.

The model was meshed into 7000 elements. A finer mesh was chosen near the well bore because the pressure drop near the well bore was very high compared with the rest of the formation.

Boundary conditions:

At the Symmetry boundary the flow velocity perpendicular to the symmetry line was set to zero.

$$Vx = 0.0 \qquad \text{at} \quad x = 0.0$$

$Vy = 0.0$ at $y = 0.0$

Inflow boundary was the inlet flow velocity perpendicular to the well bore injection face.

$V = 0.003$ m/s at $r = r_w = 0.0635$ m

Outflow boundary was the outlet pressure at the drainage radius because the outlet velocity was unknown.

$P = 0.0$ Pa at $r = r_e = 20$ m

Flotran CFD parameters were set to the same values of the prevous models.

4.9.1.2 Radial injection with a single vertical fracture model

The model was similar to the previous model but this time a single fracture parallel to the x-axis penetrated the reservoir to certain distance (Fig.4.29). Due to the limitation on the number of elements allowed, only a quarter of the reservoir was modelled. The flow was directed through the fracture inlet and no flow was allowed through the well bore face (to execlude the radial flow through well bore injection face) and the total flow rate was divided equally between the two fracture halves. So the flow rate through the fracture inlet was equal to one half the total flow rate.

The inlet flow velocity along the fracture was equal to the flow rate divided by the inlet flow area of the fracture. The fracture permeability was held constant at 3000 Darcy whereas the matrix permeability was set to 100, 300 and 500 md at each run.

Three fracture lengths were chosen:

5 m with a fracture width of 1mm and fracture inlet flow velocity of 0.6 m/s.

10 m with a fracture width of 2 mm and fracture inlet flow velocity of 0.3 m/s.

15 m with a fracture width of 3 mm and fracture inlet flow velocity of 0.2 m/sec.

The fracture length/fracture width ratio was always equal to a constant value of 5000.

The matrix was meshed into 7000 elements and the fracture was meshed into 280 elements.

In the matrix a finer mesh was chosen near the well bore and near the fracture face.

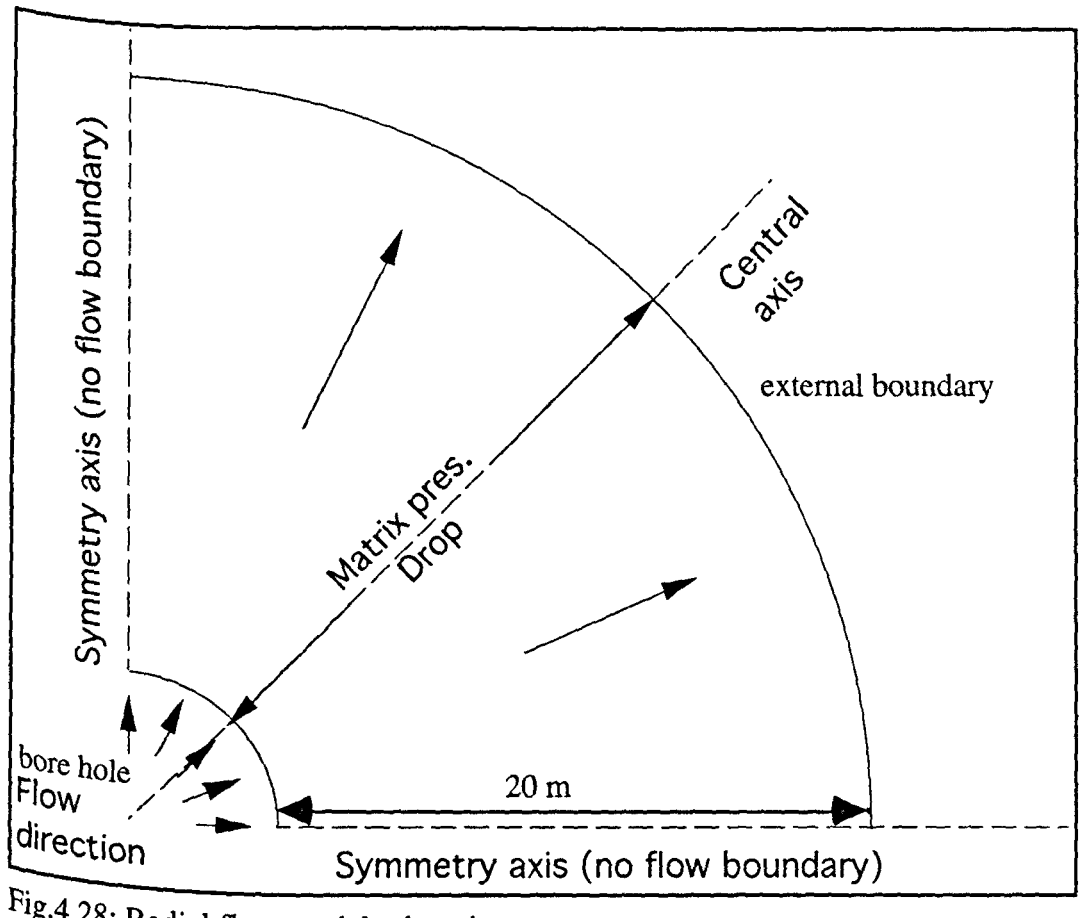

Fig.4.28: Radial flow model: plan view.

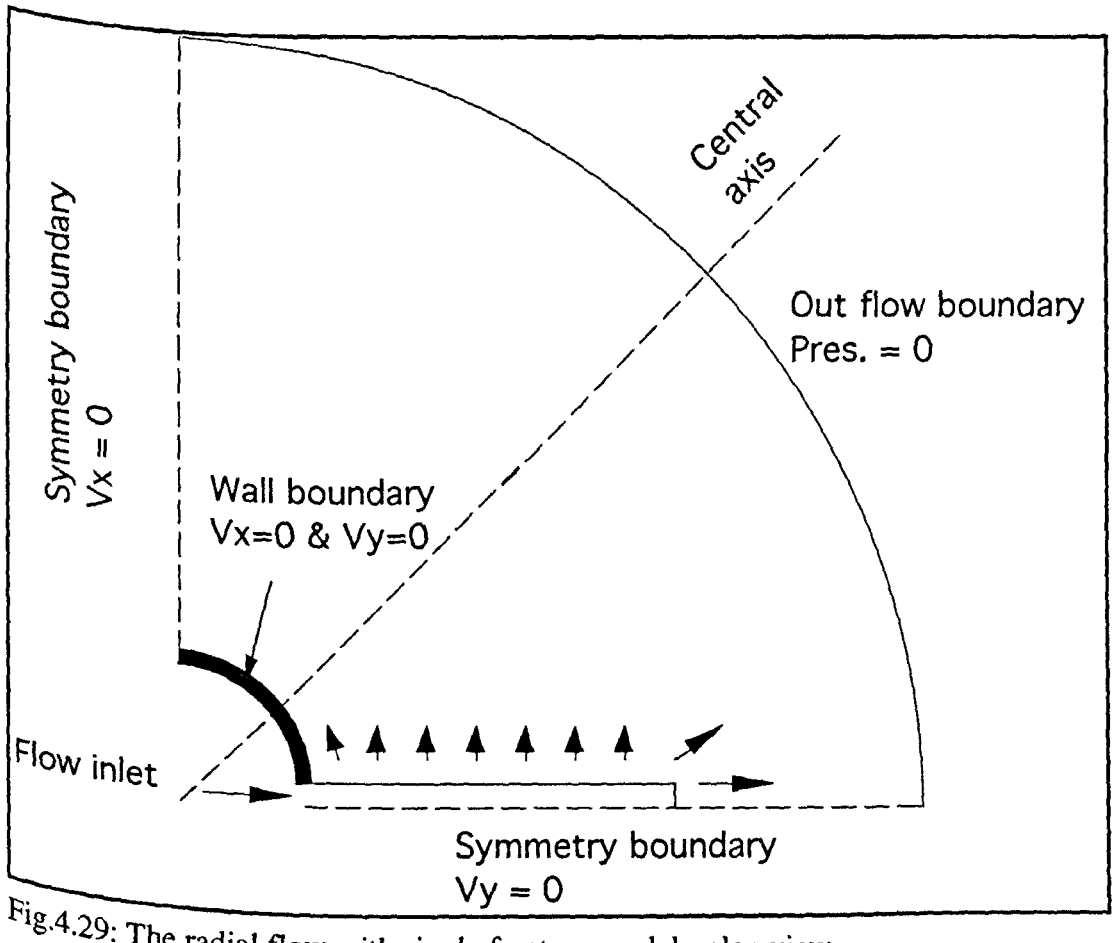

Fig.4.29: The radial flow with single fracture model : plan view.

Boundary conditions:

For the 5 m fracture

At symmetry boundary the flow velocity perpendicular to the symmetry line was set to zero.

$Vx = 0.0$ at $x = 0.0$

$Vy = 0.0$ at $y = -0.0005$ m

Inflow boundary was the fracture inlet flow velocity.

$V_f = 0.6$ m/s at $x = 0.0635$ m

and $-0.0005 < y < 0.0$ m

For the 10 m fracture

Symmetry boundary: $Vx = 0.0$ at $x = 0$

$Vy = 0.0$ at $y = -0.001$ m

Inflow boundary: $V_f = 0.3$ m/s at $x = 0.0635$ m

and $-0.001 < y < 0.0$ m

For the 15 m fracture

Symmetry boundary: $Vx = 0.0$ at $x = 0$

$Vy = 0.0$ at $y = -0.0015$ m

Inflow boundary: $V_f = Vx = 0.2$ m/s at $x = 0.0635$ m

and $-0.0015 < y < 0.0$ m

Outflow boundary was the pressure at the dranage radius.

$P = 0.0$ pa at $r = r_e = 20$ m

Wall boundary was applied at the well bore face where the velocity in the x and y-direction was set to zero.

$Vx = 0.0$ and $Vy = 0.0$ at $r = r_w = 0.0635$ m

and $y > 0.0$ m

The FLOTRAN CFD parameters were set to the same values of the prevous models.

4.9.1.3 Radial injection with two vertical fractures perpendicular to each other

The model was similar to the previous model but this time two fractures (of the same length) penetrated the reservoir to certain distance: one parallel to the x-axis and the other parallel to the y-axis (Fig.4.30). Again a quarter of the reservoir was modelled. The total flow rate was

divided equally between the four fractures halves. The flow rate through the each fracture inlet was equal to one fourth of the total flow rate (as each fracture had two inlets one each side).

Three fracture lengths were used.

Again in the matrix a finer mesh was chosen near the well bore and near the fracture face.

For the 5m double fractures the inlet flow velocity was 0.3 m/s.

For the 10m double fractures the inlet flow velocity was 0.15 m/s.

For the 15 m double fractures the inlet flow velocity was 0.1 m/s.

Boundary conditions:

For the 5 m double fractures:

At symmetry boundary the flow velocity perpendicular to the symmetry line was set to zero

$Vx = 0.0$ at $x = -0.0005$ m

$Vy = 0.0$ at $y = -0.0005$ m

Inflow boundary was the fracture inlet flow velocity.

$V_f = Vx = 0.3$ m/s at $x = 0.0635$ m and $-0.0005 < y < 0.0$ m

$V_f = Vy = 0.3$ m/s at $y = 0.0635$ m and $-0.0005 < x < 0.0$ m

For the 10 m double fractures

Symmetry boundary $Vx = 0.0$ at $x = -0.001$ m

$Vy = 0.0$ at $y = -0.001$ m

Inflow boundary: $V_f = Vx = 0.15$ m/s at $x = 0.0635$ m and $-0.001 < y < 0.0$ m

$V_f = Vy = 0.15$ m/s at $y = 0.0635$ m and $-0.001 < x < 0.0$ m

For the 15 m double fractures

Symmetry boundary $Vx = 0.0$ at $x = -0.0015$ m

$Vy = 0.0$ at $y = -0.0015$ m

Inflow boundary: $V_f = Vx = 0.1$ m/s at $x = 0.0635$ m and $-0.0015 < y < 0.0$ m

$V_f = Vy = 0.1$ m/s at $y = 0.0635$ m and $-0.0015 < x < 0.0$ m

Outflow boundary	P = 0.0 pa	at $r = r_e = 20$ m
Wall boundary	Vx = 0.0 and Vy = 0.0	at r = 0.0635 m
		and y > 0.0 and x > 0.0

Again, the Flotran CFD parameters were set to the same values of the prevous models.

4.9.1.4. Radial injection with a near well bore skin (damaged) zone model

The radial injection model was repeated (under the same boundary conditions) but this time a skin zone was created around the well bore (Fig.4.31). The matrix permeability was held constant at 300 md. The damaged zone thickness varied from 2 to 12 cm and the damaged zone permeability varied from 90 to 10 md.

4.9.1.5. Radial injection with a single vertical fracture and near fracture face skin (damaged) zone model

The radial injection with single vertical fracture model was repeated but this time a skin zone was created in the matrix near the fracture face along the whole fracture length (Fig.4.32). The matrix permeability was held constant at 300 md. The damaged zone thickness varied from 2 to 8 cm and the damaged zone permeability varied from 90 to 10 md. The fracture was chosen to be 10 m length with a 2 mm width. As the skin zone thickness increased the well bore radius was decreased to compensate.

At a skin thickness of 2 cm the well bore radius was reduced to 0.0435 m and at a skin thickness of 5 cm the well bore radius was further reduced to 0.0135 m. At a skin thickness of 8 cm the well bore radius was reduced to 0.0035 m.

The inlet flow velocity along the fracture was held constant at 0.3 m/s.

Boundary conditions:

Symmetry boundary	Vx = 0.0	at x = 0
	Vy = 0.0	at y = - 0.021 m

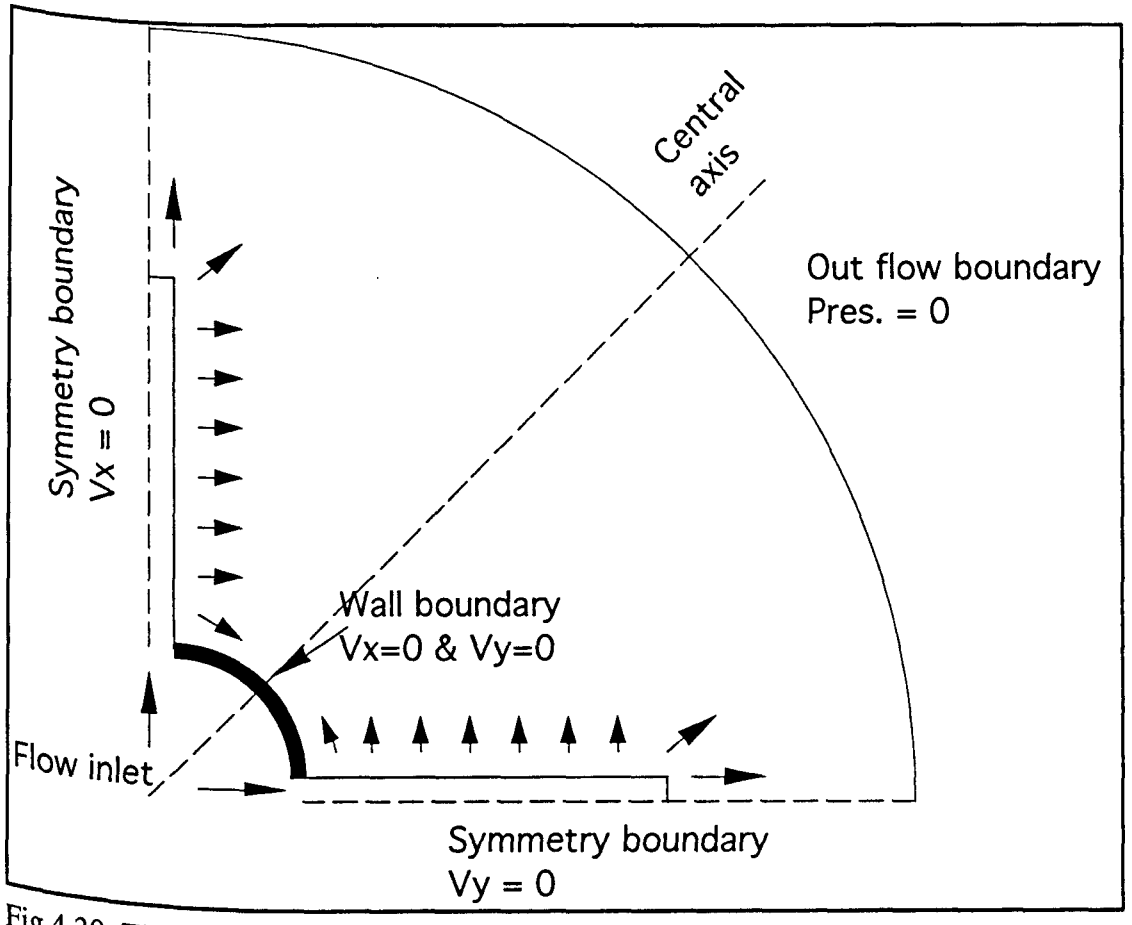

Fig.4.30: The radial flow with two fractures model : plan view.

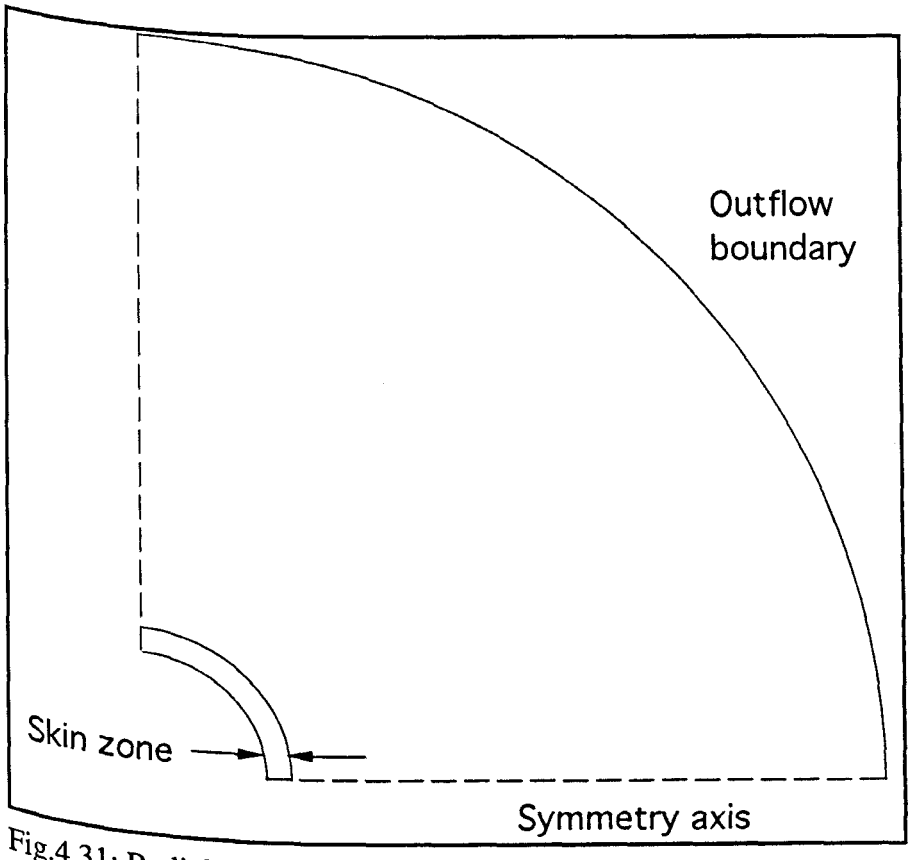

Fig.4.31: Radial flow with around well bore skin model : plan view.

Inflow boundary:

For the case of 2 cm skin:	$V_f = 0.3$ m/s	at $x = 0.0435$ m
		and $-0.021 < y < -0.02$ m
For the case of 5 cm skin:	$V_f = 0.3$ m/s	at $x = 0.0135$ m
		and $-0.021 < y < -0.02$ m
For the case of 8 cm skin:	$V_f = 0.3$ m/s	at $x = 0.0035$ m
		and $-0.021 < y < -0.02$ m
Outflow boundary:	$P = 0.0$ pa	at $r = r_e = 20$ m
Wall boundary:	$Vx = 0.0$ and $Vy = 0.0$	at $r = r_w$
		and $y > -0.02$

4.9.1.6. Radial injection with two vertical fractures and near fracture face skin zone:

The radial injection with two vertical fracture model was repeated but this time a skin zone was created in the matrix near the fracture face along the whole two fractures length (Fig.4.33). The same skin zone specifications and flow conditions as in section 4.9.1.5 were used. The inlet flow velocity along the fracture was held constant at 0.15 m/s.

Boundary conditions:

Symmetry boundary:	$Vx = 0.0$	at $x = -0.021$
	$Vy = 0.0$	at $y = -0.021$ m
Inflow boundary:		
For the case of 2 cm skin:	$V_f = 0.15$ m/s	at $x = 0.0435$ m
		and $-0.021 < y < -0.02$ m
	$V_f = 0.15$ m/s	at $y = 0.0435$ m
		and $-0.021 < x < -0.02$ m
For the case of 5 cm skin:	$V_f = 0.15$ m/s	at $x = 0.0135$ m
		and $-0.021 < y < -0.02$ m
	$V_f = 0.15$ m/s	at $y = 0.0135$ m
		and $-0.021 < x < -0.02$ m

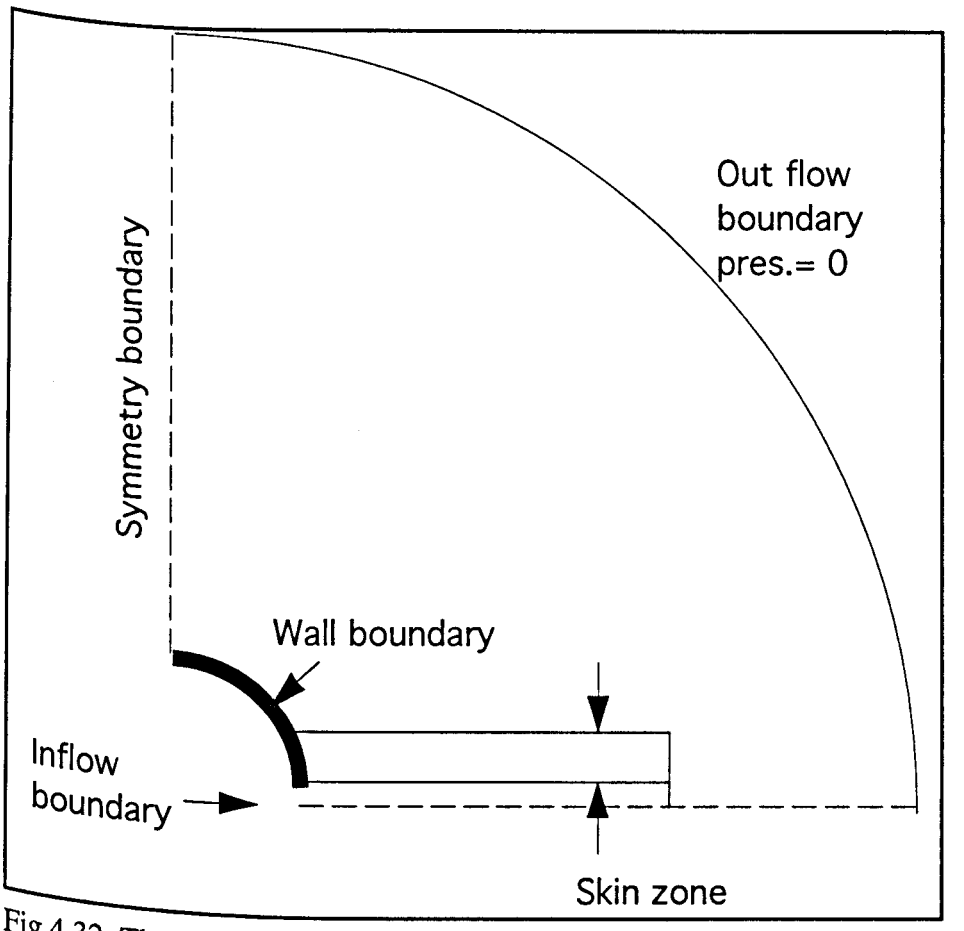

Fig.4.32: The radial fracture flow model with near fracture face skin : plan view.

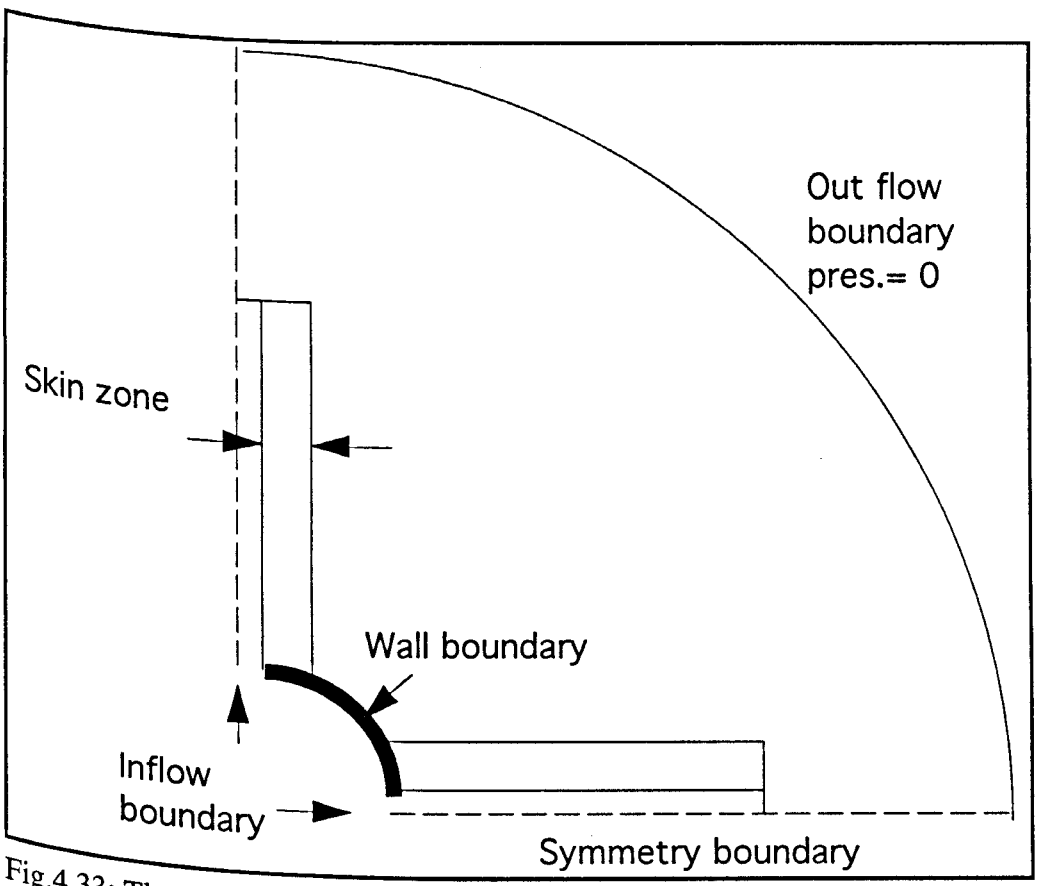

Fig.4.33: The radial double fractures flow model with near fracture face skin : plan view.

For the case of 8 cm skin:	$V_f = 0.15$ m/s	at $x = 0.0035$ m
		and $-0.021 < y < -0.02$ m
	$V_f = 0.15$ m/s	at $y = 0.0035$ m
		and $-0.021 < x < -0.02$ m
Outflow boundary:	$P = 0.0$ pa	at $r = r_e = 20$ m
Wall boundary:	$Vx = 0.0$ and $Vy = 0.0$	at $r = r_w$
		and $y > -0.02$ and $x > -0.02$

4.9.2. Field simulation Results

4.9.2.1. The Radial injection model results

Pressure drop was mapped on a radial path passing through the central axis of the model starting from the well bore face and ending at the outer boundary. The plot of the pressure change with radial distance for three different matrix permeabilities (Fig.4.34) showed the severe effect of the well bore flow area on the pressure drop curve. Due to the narrow area of the well bore compared with the outer flow area, 50% of the pressure drop occured in the first meter around the well bore. As the flow approached the outer boundary, and due to the enlargement of the radial flow area, the pressure drop in the last five meters was less than 5% of the total pressure drop.

The effect of the narrow well bore area can be seen more clearly in the flow velocity versus radial distance plot (Fig.4.35). The flow velocity decreased to 6% of the inlet flow velocity at the first meter.

4.9.2.2. The Radial injection with a single vertical fracture model results

(1) Matrix permeability effect:

For a constant fracture length of 10 m and varying matrix permeability, the pressure drop along the fracture and through the matrix along the central axis of the model were recorded and mapped with radial distance. The flow velocity through the same above two paths was also mapped.

The pressure drop distribution through the matrix (central axis path) became more uniform than it was in the radial injection case, especially at the first 10 m (Fig.4.36). The presence of the

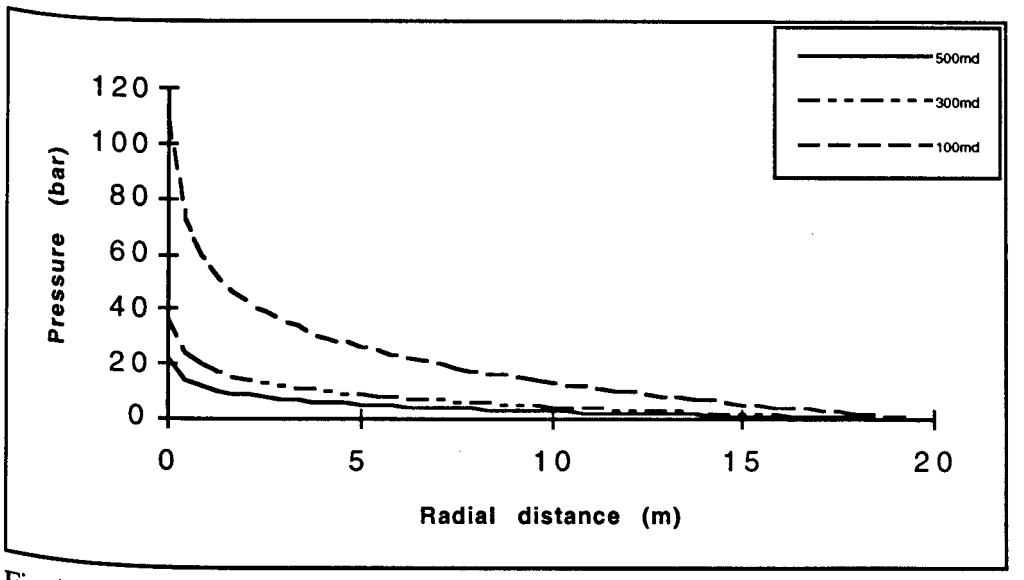

Fig.4.34: Pressure drop through matrix (along the central axis) for radial injection.

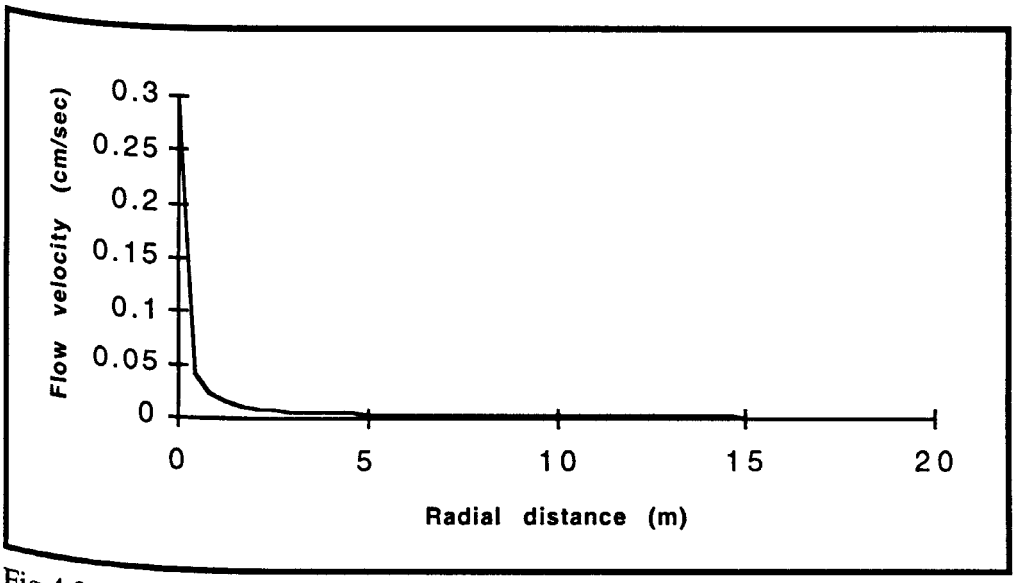

Fig.4.35: Flow velocity through matrix (along the central axis) for radial injection.

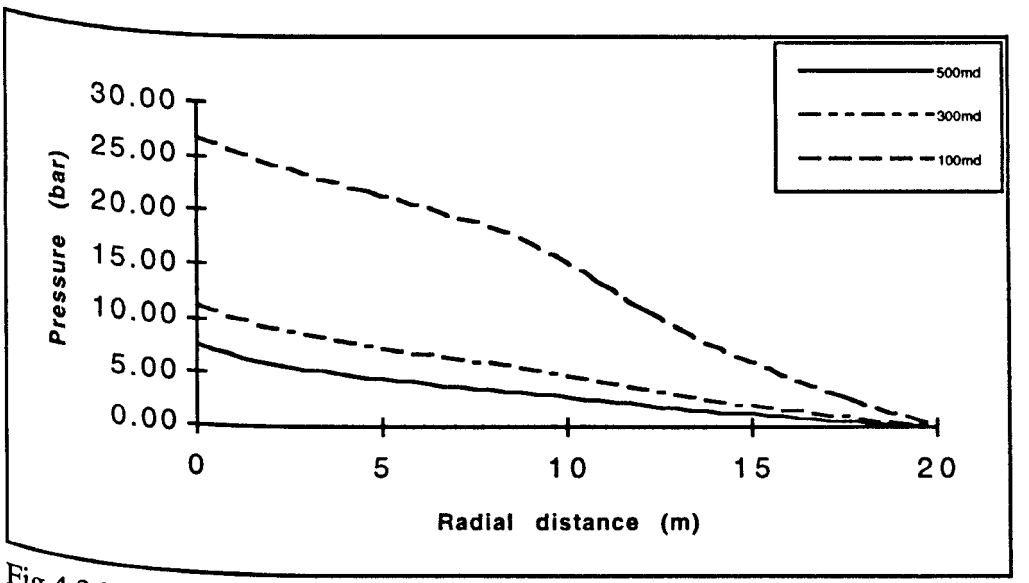

Fig.4.36: Pressure drop through matrix (along cenral axis) for radial injection with 10 m long single fracture.

fracture resulted in a gradual pressure loss through rock matrix with radial distance. This was due to the flow being distributed over a large flow area and it could reach a distance as far as 10 m with a low resistance.

The pressure drop distribution through the matrix became even more uniform as the matrix permeability decreased, with a lower pressure loss rate (for the case of low matrix permeability) at the first 10 m. For the case of 500 mD matrix permeability the pressure loss at the first 5 m was 40% of the total pressure drop but when the matrix permeability decreased to 100 the loss was reduced to only 20% (Fig.4.36).

The plot of the flow velocity through the matrix (along the central axis path) showed a much better distribution in flow velocity, especially for the case of low matrix permeability (Fig.4.37). There is a little increase in flow velocity at 10 m as the fluid was forced into the matrix at the end of the fracture (end effect). This end effect was reflected by a sharp reduction in flow velocity and pressure at the end of the fracture (fig.4.38 and 4.39).

The flow velocity contours for a 10 m single fracture injection for a 500 and 100 md matrix are given in Figures 4.40 and 4.41.

(2) Effect of fracture length:

Pressure and flow velocity were mapped for three different fracture lengths at a constant matrix permeability of 300 md. In the case of long fracture injection the pressure drop distribution through the matrix was more uniform than the pressure drop for the case of short fracture as the flow in the case of long fracture was distributed on a larger area (Fig.4.42).

Also the increase in fracture length enhanced the flow velocity distribution through the matrix along the central axis path (Fig.4.43) and the end effect reduced as the fracture length increased.

Longer fractures resulted in more uniform pressure drop and flow velocity along the fracture than the short fracture (Fig.4.44 and 4.45).

The flow velocity contours for the radial injection with 5 and 10 m fractures at constant matrix permeability of 300 md are given in Figures 4.46 and 4.47.

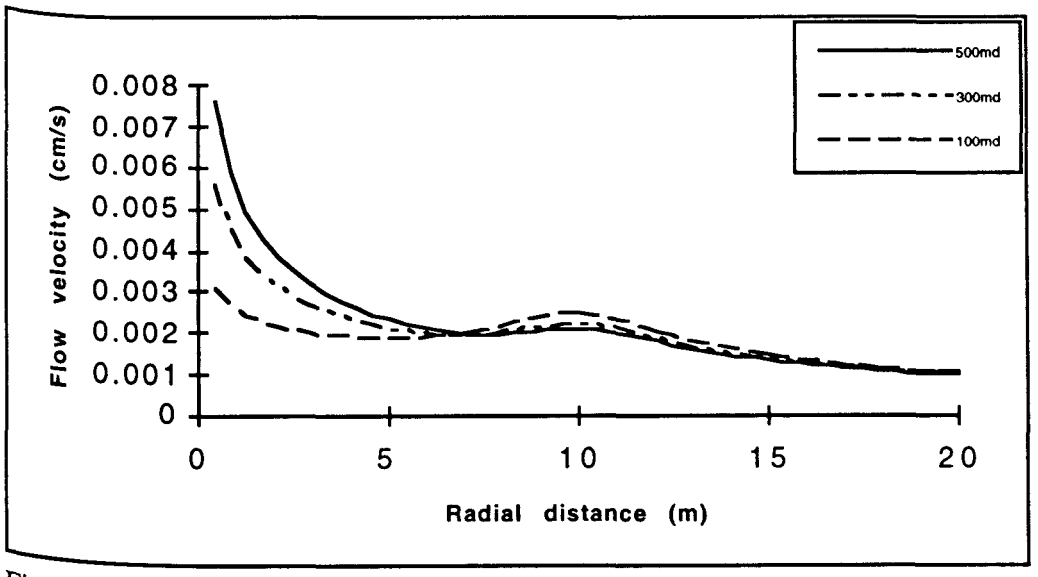

Fig.4.37: Flow velocity through matrix for radial injection with 10 m long single fracture.

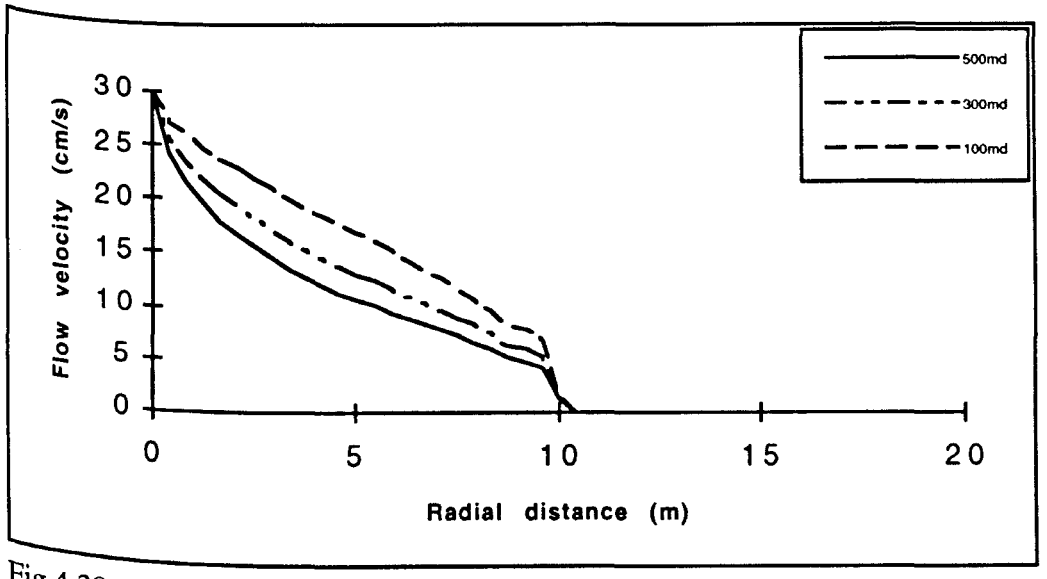

Fig.4.38: Flow velocity along fracture for radial injection with 10 m long single fracture.

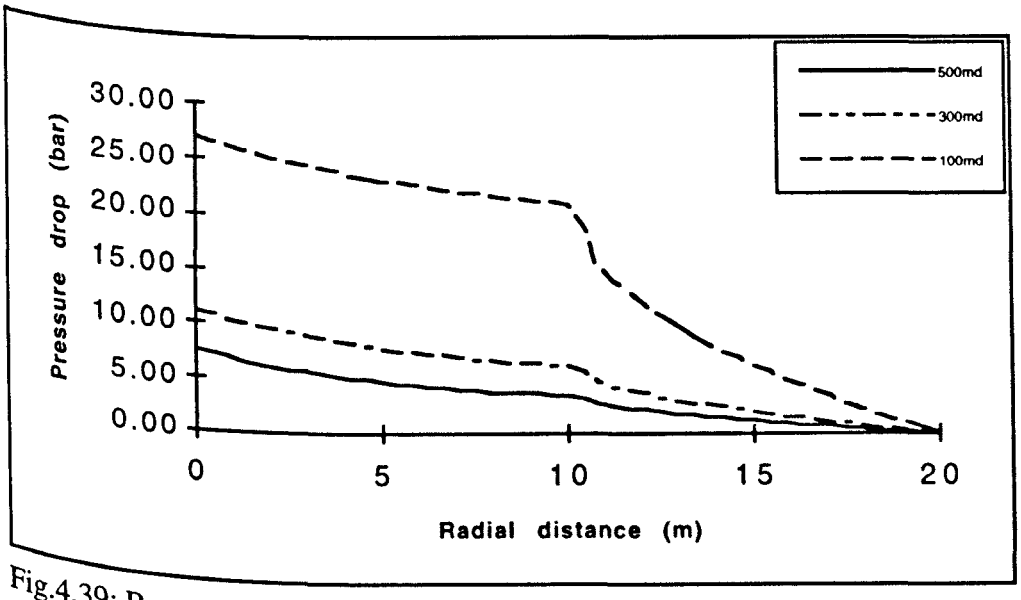

Fig.4.39: Pressure drop along fracture for radial injection with 10 m long single fracture.

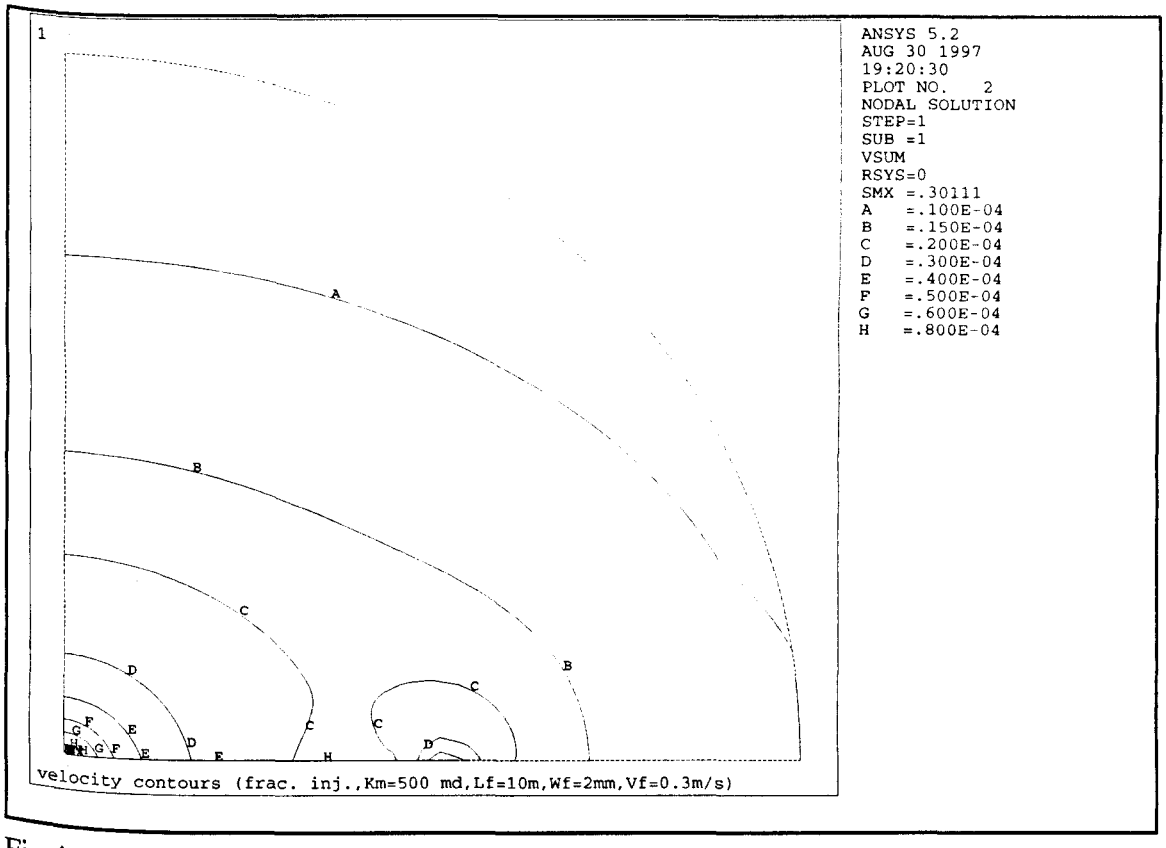

Fig.4.40: Flow velocity contours for radial injection with a 10 m single fracture (Km = 500 md).

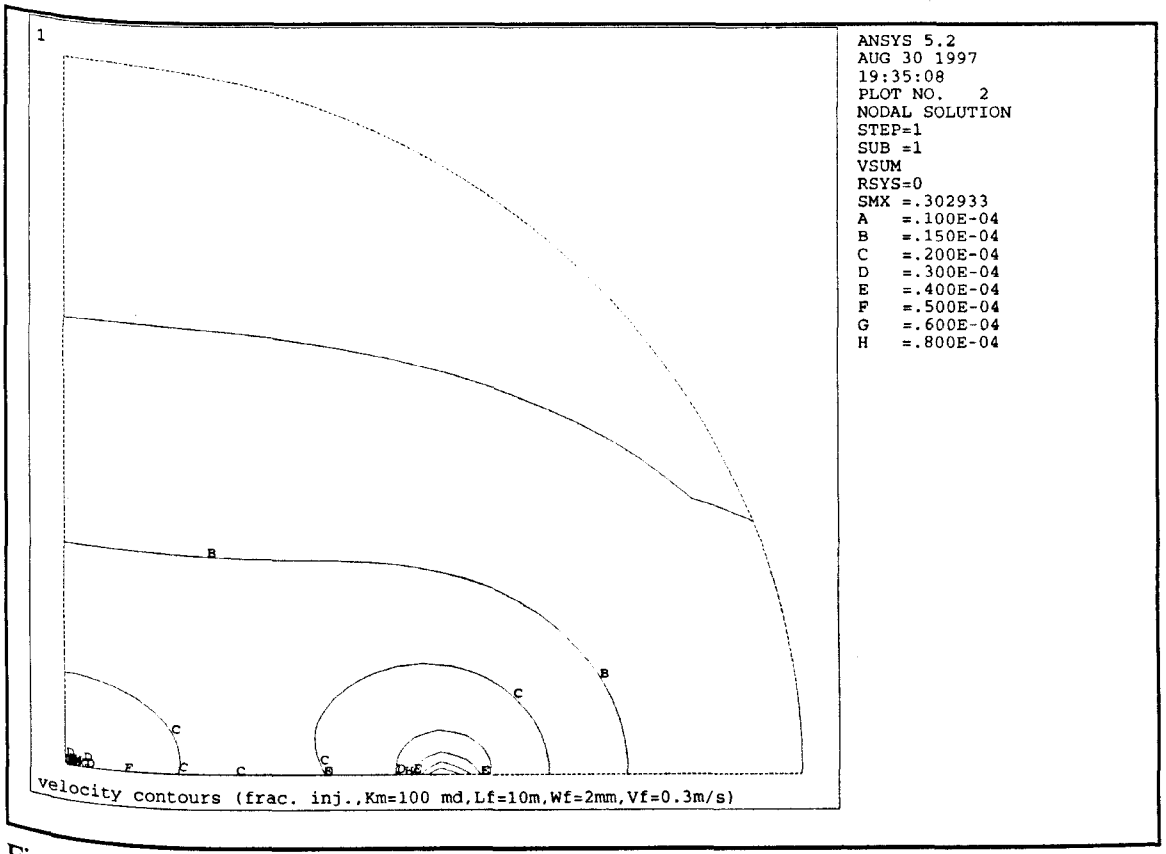

Fig.4.41: Flow velocity contours for radial injection with a 10 m single fracture (Km = 100 md).

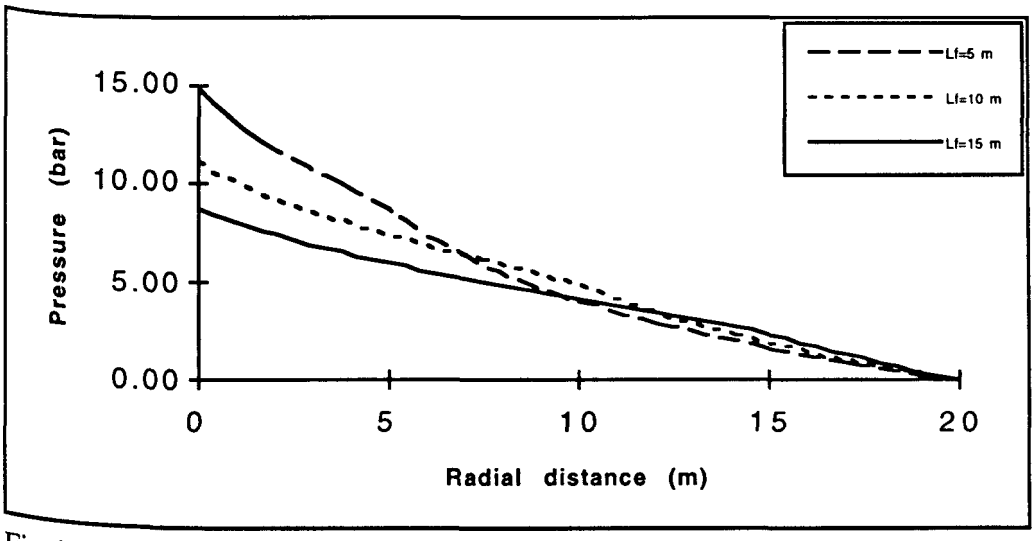

Fig.4.42: Pressure drop through matrix for radial injection with single fracture (Km = 300 md).

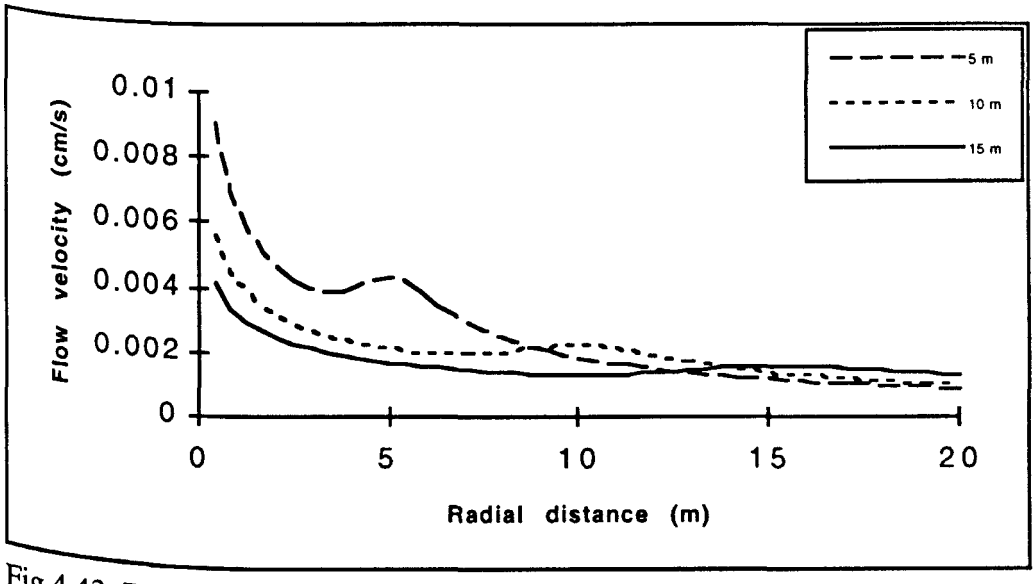

Fig.4.43: Flow velocity through matrix for radial injection with single fracture (Km = 300 md).

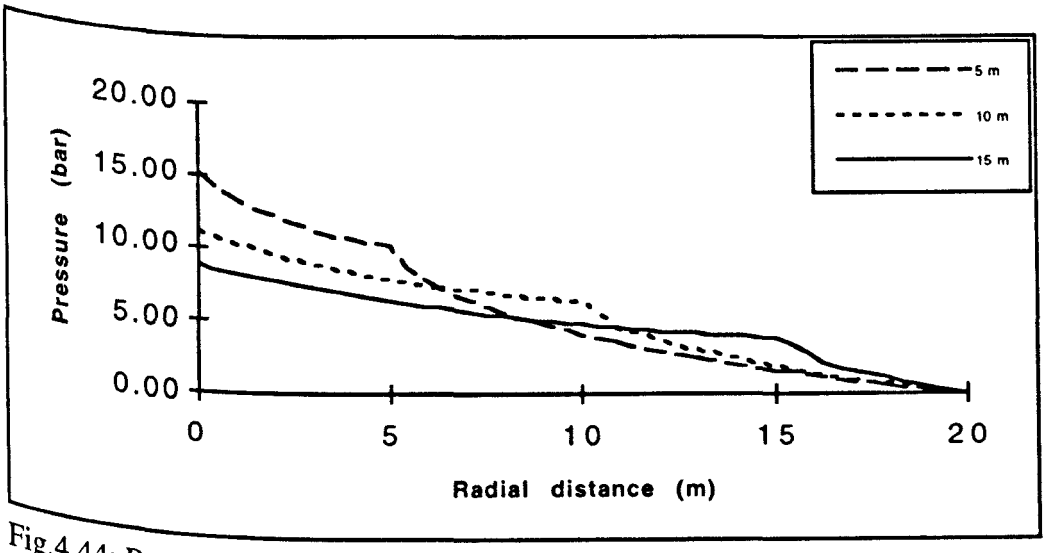

Fig.4.44: Pressure drop along fracture for radial injection with single fracture (Km = 300 md).

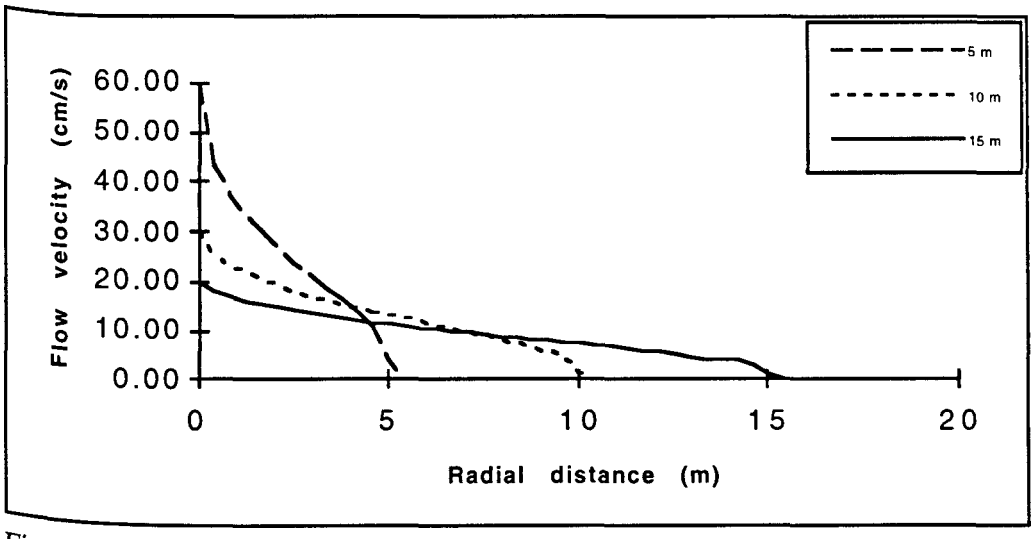

Fig.4.45: Flow velocity along fracture for radial injection with single fracture (Km = 300 md).

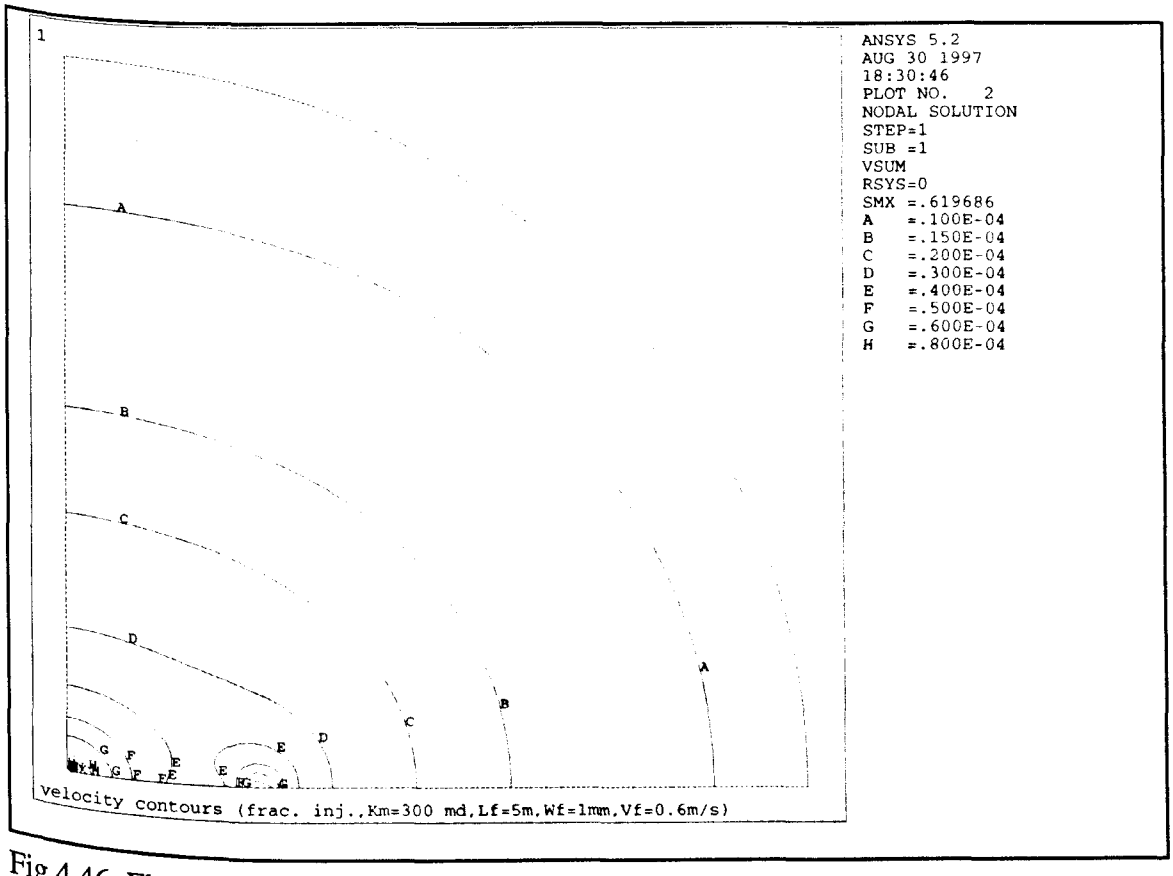

Fig.4.46: Flow velocity contours for radial injection with a single 5 m fracture (Km = 300 md).

4.9.2.3. Comparing radial injection with and without single fracture

In this section a comparison study was carried out with the matrix permeability and the fracture length held constant at 500 md and 10 m respectively.

The difference in flow velocity distribution through the matrix between the case of radial injection and the case of radial injection with a single fracture can be seen in Figure 4.48 especially in the region near to the well bore. The difference in pressure drop distribution through matrix of the two cases can be seen in Figure 4.49.

At a matrix permeability of 500 md the pressure drop at the first 10 m in the case of radial injection was 4 times the pressure drop in the case of radial injection with single fracture. By decreasing the matrix permeability from 500 to 100 md this difference increased to 8.34 times (Fig.4.50). The pressure drop in the case of radial injection increases with a higher rate as the matrix permeability decreased and this rate become very high for a matrix permeability lower than 300 md.

4.9.2.4. Radial injection with double fractures model

For a constant matrix permeability of 500 md and for a fracture length of 10 m, the double fracture injection results in a further improvement in flow velocity distribution (Fig.4.51).

The flow velocity contours for 10 m double fractures injection for a 500 and 100 md matrix are given in Figures 4.52 and 4.53.

The flow velocity contours for a 5 and 10 m double fractures injection at constant matrix permeability of 300 md are given in Figures 4.54 and 4.55.

4.9.2.5. Radial injection with a near well bore skin model

The clean (initial) matrix permeability was 300 md. The damaged zone permeability was reduced from 300 md (no damage) to 10 md and the damaged zone width was increased from 0 cm (no damage zone) to 12 cm.

The pressure drop was plotted versus damaged zone permeability for different damaged zone widths (Fig.4.56).

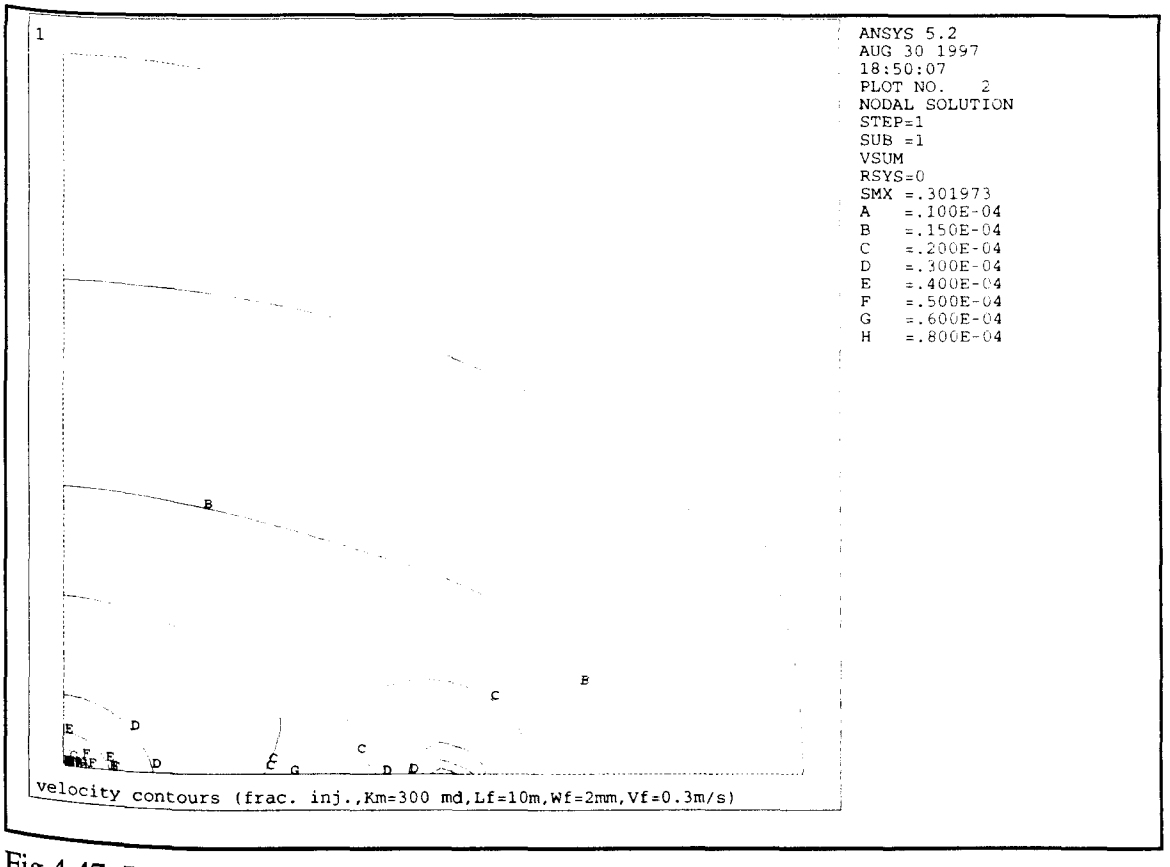

Fig.4.47: Flow velocity contours for radial injection with a single 10 m fracture (Km = 300 md).

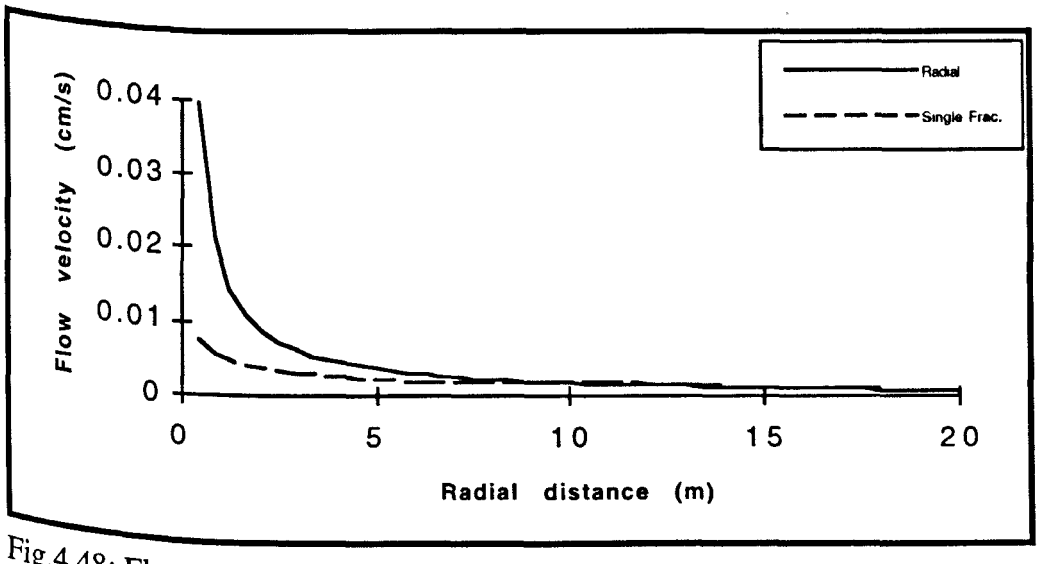

Fig.4.48: Flow velocity through matrix for radial flow with and without a 10 m fracture.

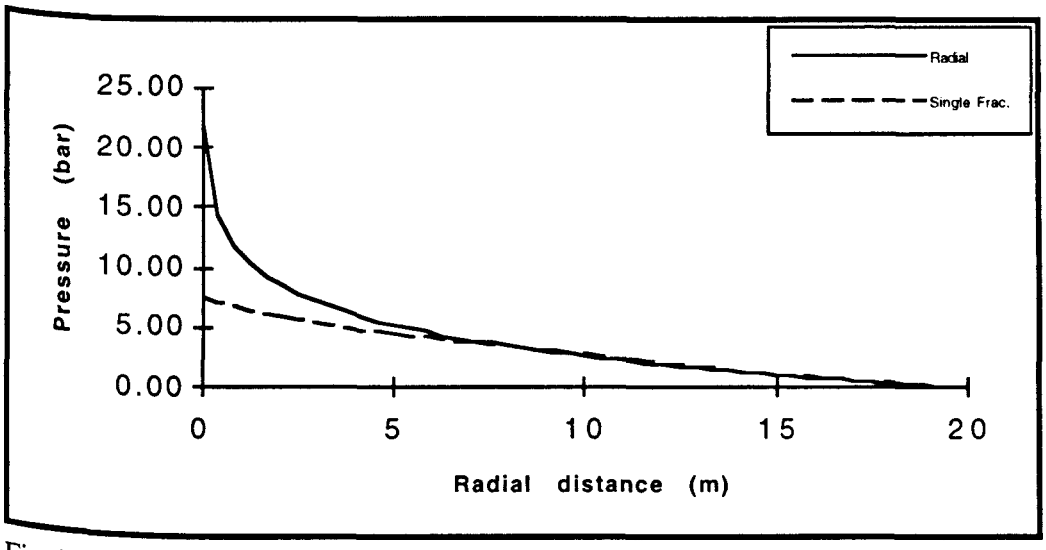

Fig.4.49: Pressure drop through matrix for radial flow with and without a 10 m fracture.

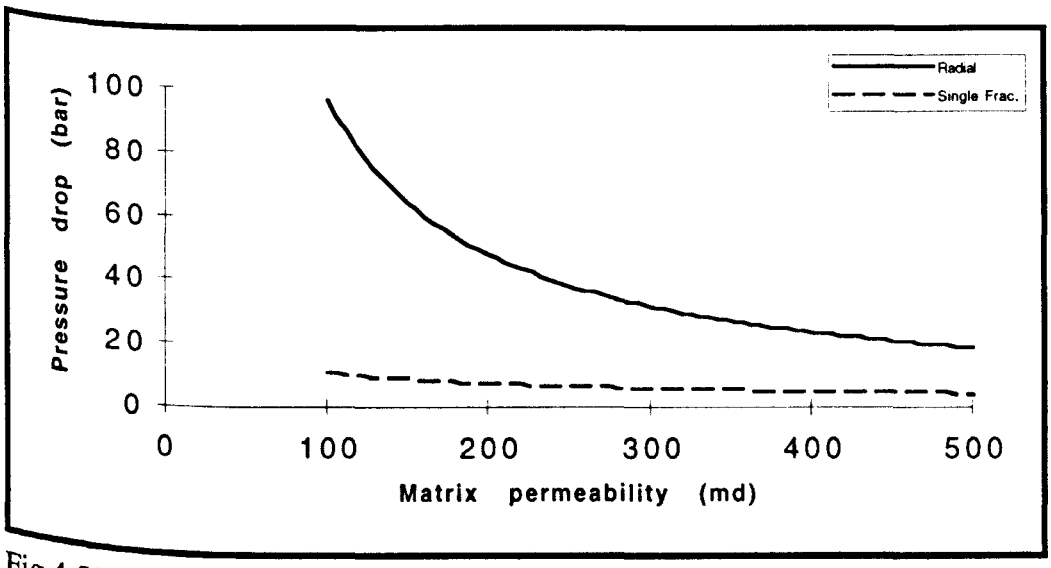

Fig.4.50: The change in pressure drop through the first 10 m of the matrix.

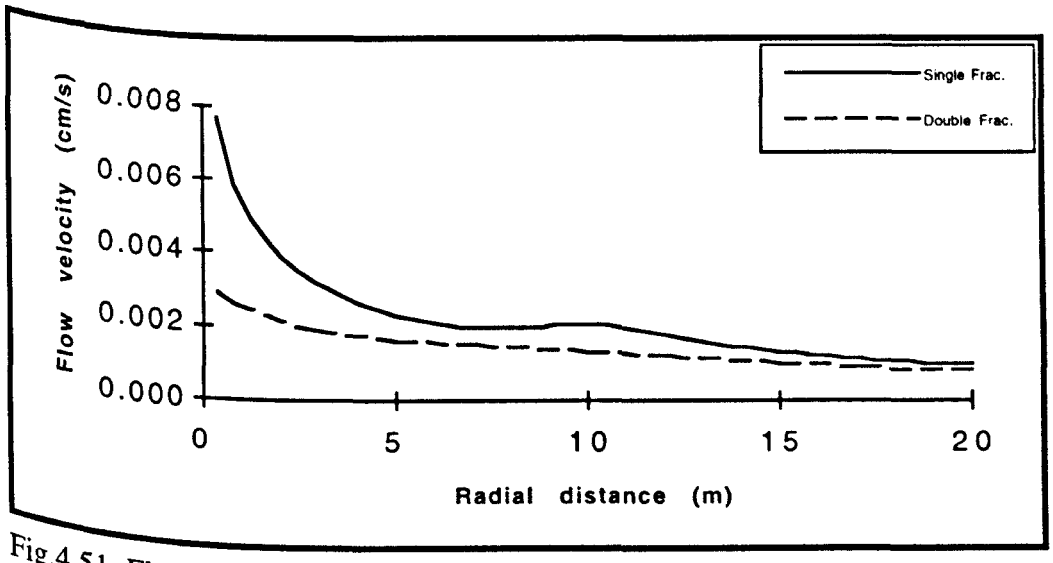

Fig.4.51: Flow velocity through matrix for radial flow with single fracture and a radial flow with two fractures (Km = 500 md, Lf = 10m).

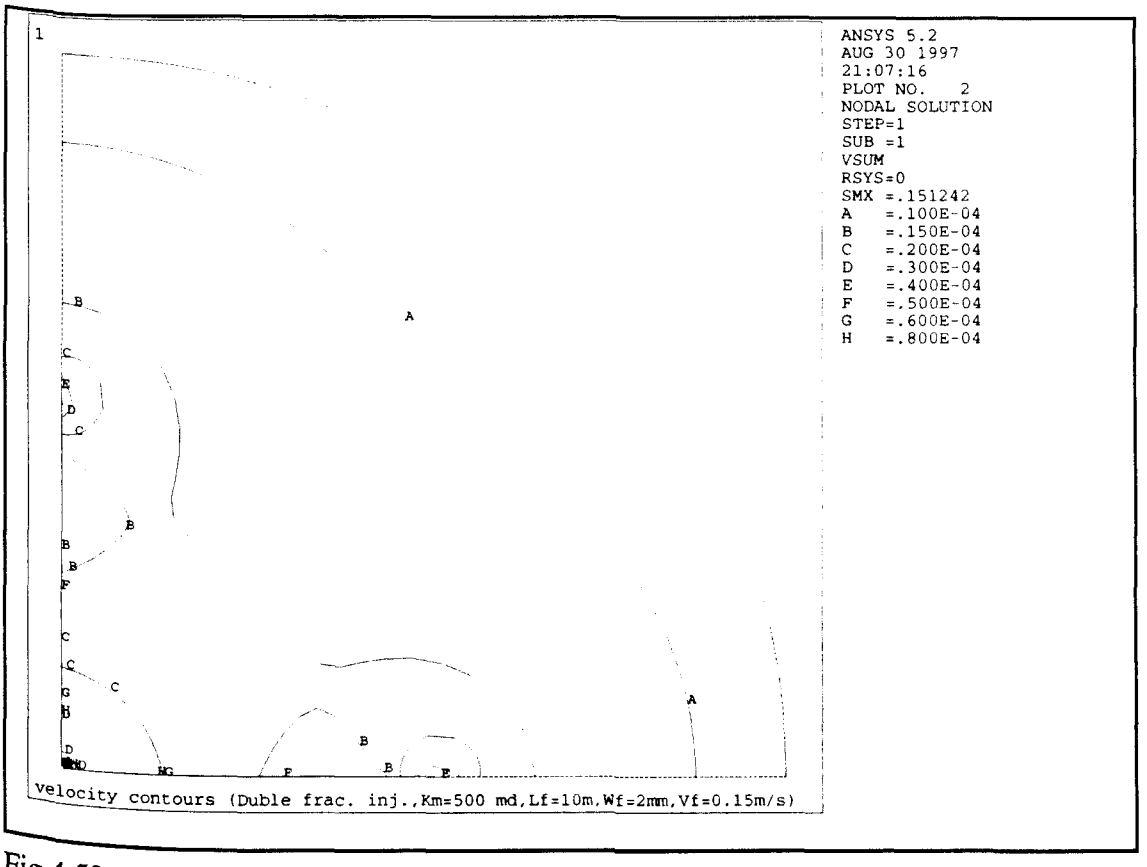

Fig.4.52:The flow velocity contours for a radial flow with two fractures (Km=500md, Lf=10m)

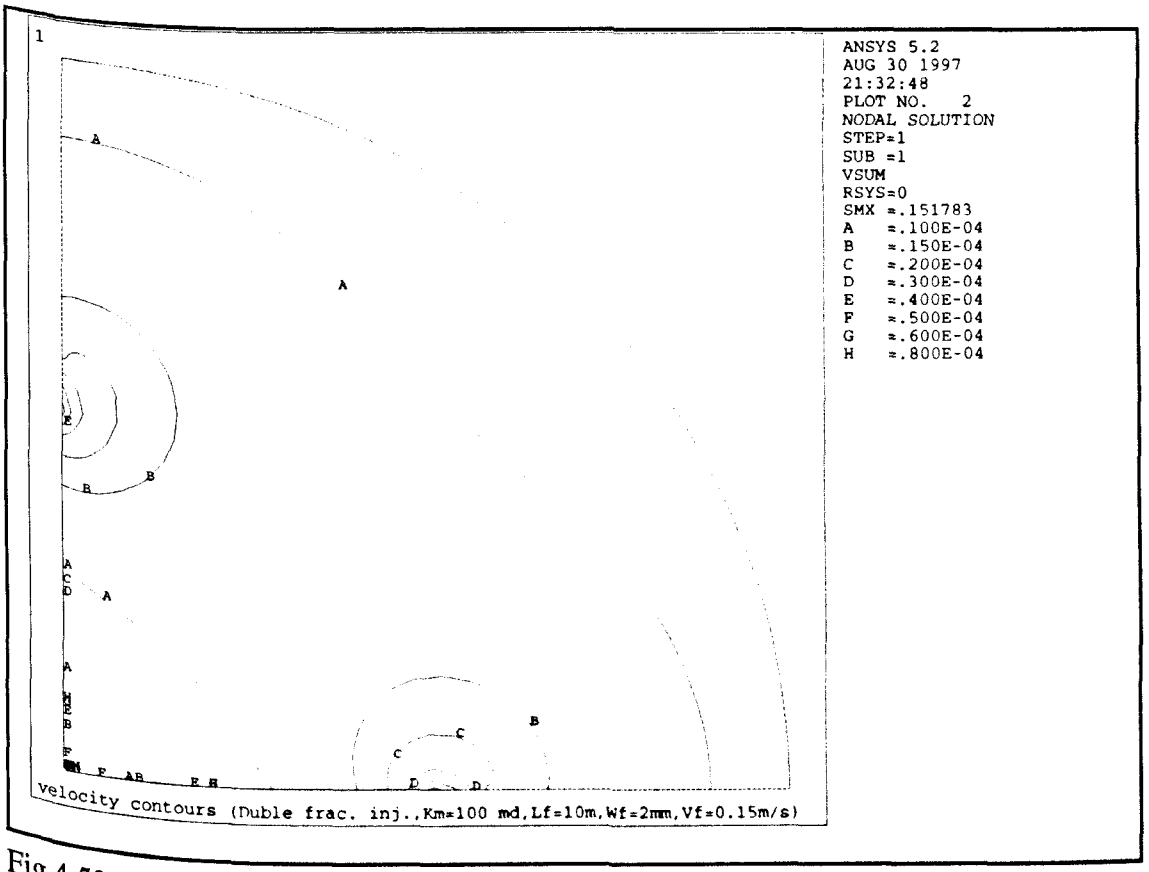

Fig.4.53:The flow velocity contours for a radial flow with two fractures (Km=100md, Lf=10m)

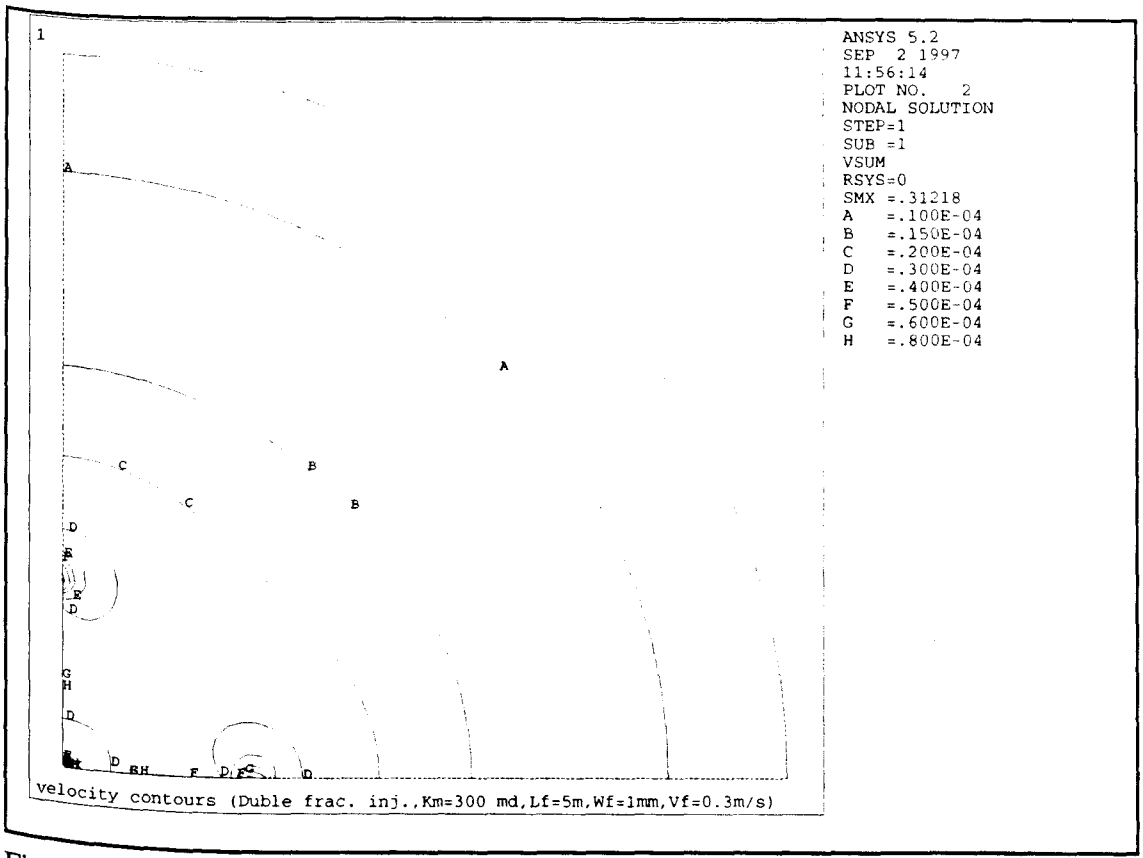

Fig.4.54:The flow velocity contours for radial flow with a two 5 m fractures (Km = 300 md).

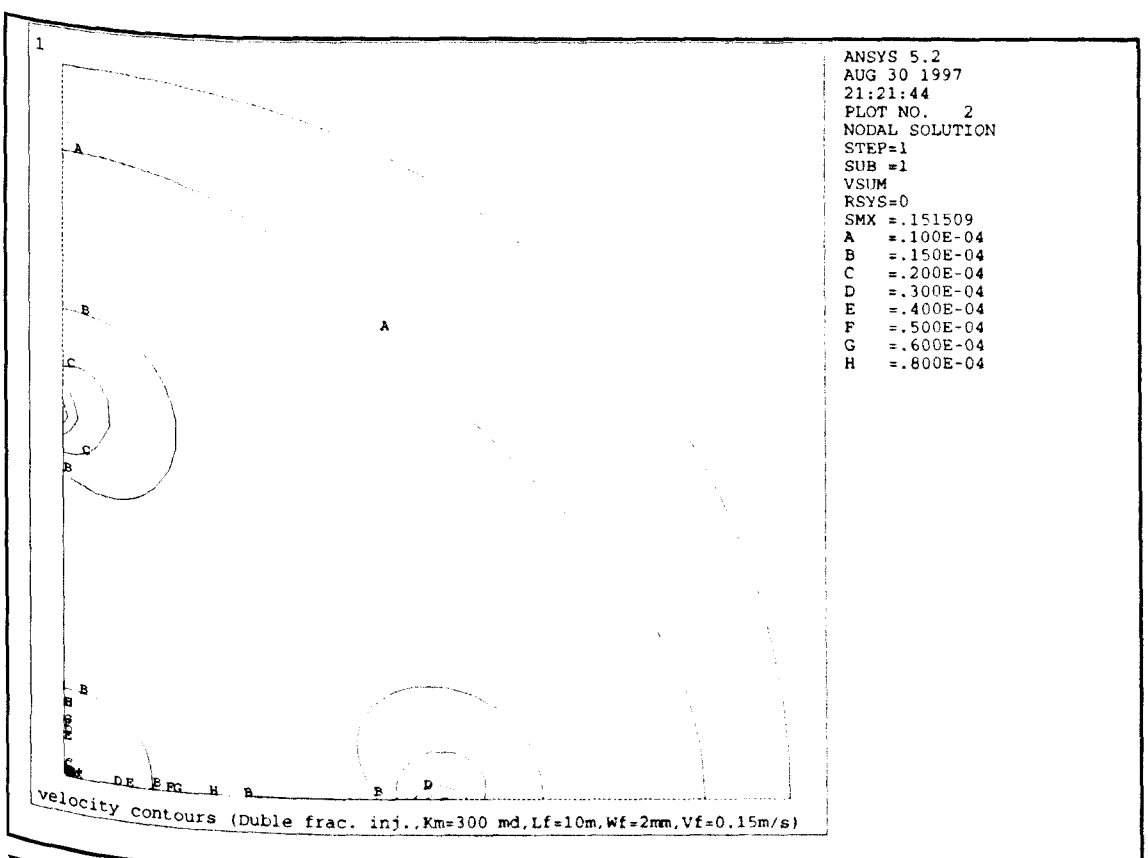

Fig.4.55:The flow velocity contours for radial flow with a two 10 m fractures (Km = 300 md).

As the damaged zone permeability decreased from 300 to 90 md the pressure drop increased for the case of 2 cm damaged zone width by a small rate of 0.02 bar per each 10 md reduction in damaged zone permeability. For the damaged zone of 12 cm width the pressure drop increases by a higher rate of 0.07 bar per each 10 md reduction in permeability (Table 4.3).

As the permeability of the damaged zone decreased to 30 md, the pressure drop rate increased to become 1.85 bar per 10 md reduction in damaged zone permeability for the case of 2 cm damaged zone and 7.22 for the case of 12 cm damaged zone (which is 100 times more than the rate of the 300 to 90 md change).

This rate became very high especially for the deeper damaged zone when the permeability of the damaged zone decreased to a value lower than 30 md. For this stage the pressure drop increase rate was 16.45 and 64.89 bar per 10 md reduction in damaged zone permeability (820 to 920 times higher than the starting rate).

To obtain more reliable results which can be useful in field application, the damaged zone permeability was related to the clean matrix permeability and the pressure drop after damage was related to the initial pressure drop (for clean matrix without damage).

As the injection rate is constant, the ratio of the initial pressure drop to the pressure drop after damage can be used as an indication of the total injectivity reduction caused by the damaged zone.

To perform this, the ratio of the initial pressure drop to the pressure drop after damage ($\Delta Pi/\Delta P$) was plotted versus the damaged zone width for different Kd/Km (damaged zone permeability / initial matrix permeability ratio) values (Fig.4.57 and Table 4.4).

It can be seen that the effect of damaged zone depth (for constant damaged zone permeability) on injectivity is very high at the first 2 cm. The effect of the following 3 cm (from 2 to 5 cm) on injectivity was less. The effect of the last 7 cm on injectivity was vary small compared with the effect of the first 2 cm.

Figure 4.58 shows the $\Delta Pi/\Delta P$ change versus Kd/Km with different values of damaged zone width.

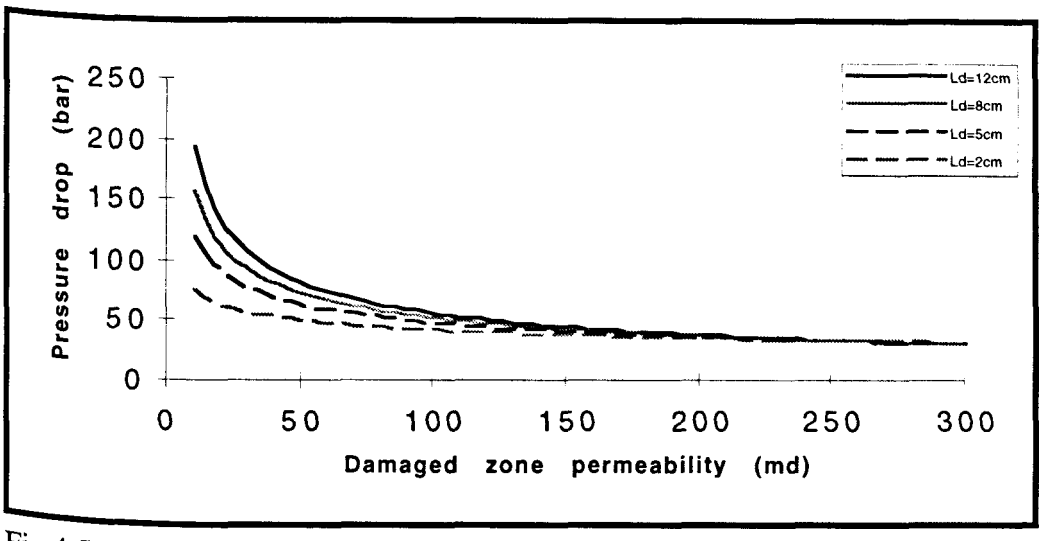

Fig.4.56:Pressure drop for radial injection for different damaged zone widths and permeabilities.

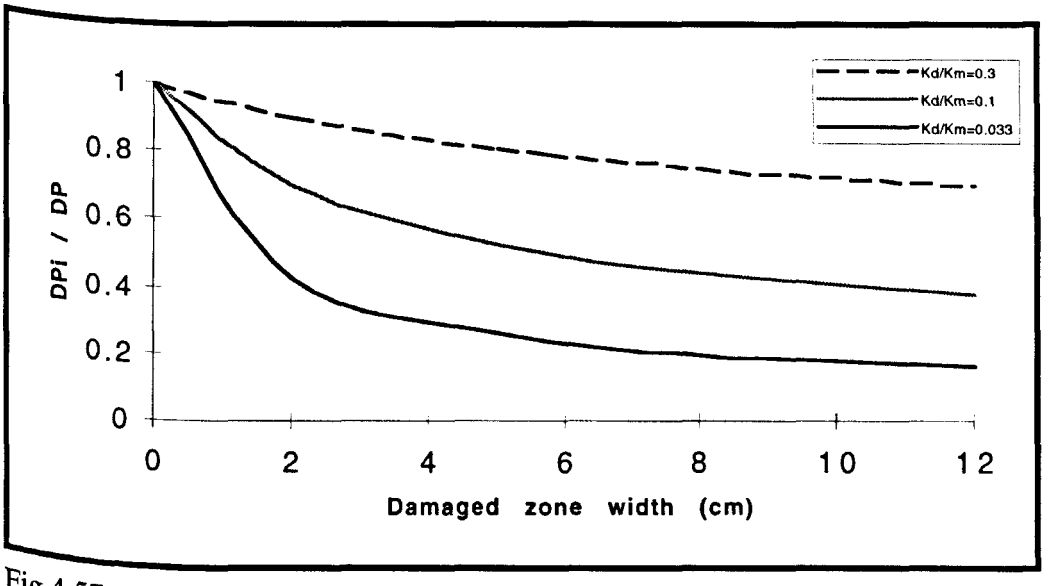

Fig.4.57: The change of ΔPi/ΔP for radial injection with damaged zone width at different Kd/Km values.

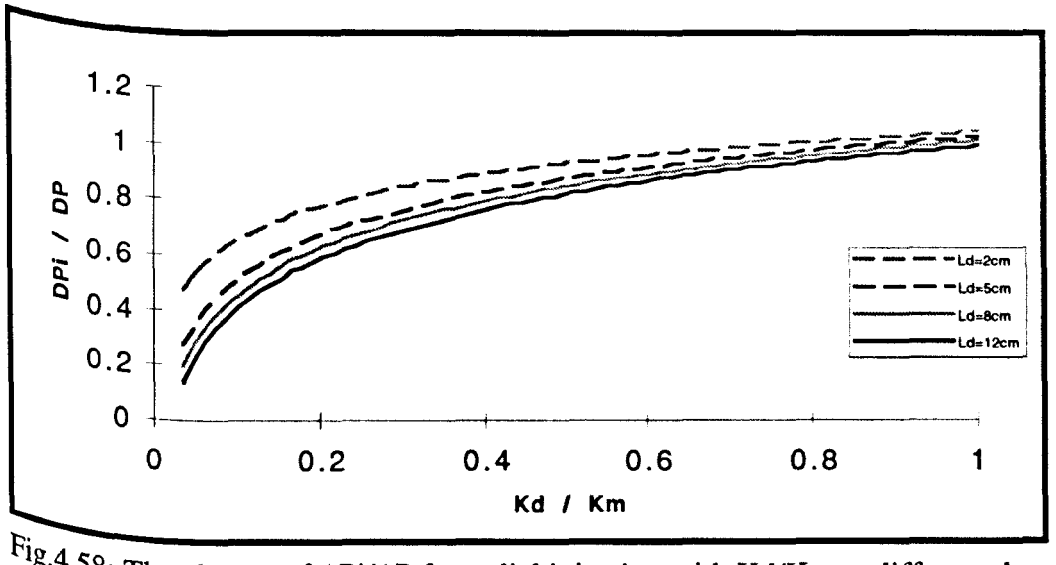

Fig.4.58: The change of ΔPi/ΔP for radial injection with Kd/Km at different damaged zone widths.

4.9.2.6. Radial injection with single fracture and a near fracture face skin model

All the results were obtained for a constant clean matrix permeability of 300 md and fracture length of 10 m. The damaged zone near the fracture face within the matrix had a varying permeability from 90 to 10 md and width from 2 to 8 cm.

For a constant damaged zone width of 8 cm, the reduction of the damaged zone permeability from 300 to 90 then to 10 md resulted in an improvement in flow velocity distribution through the matrix especially at the first 3 meters (Fig.4.59) (it resulted in the levelling of the flow velocity at 10 m and overcoming the end effect which was caused due to forcing fluid at the fracture end into the formation).

For a constant damaged zone permeability of 10 md, the increase of damaged zone width from 0 cm to 2 then to 8 cm resulted in a similar observations as above (Fig.4.60).

The pressure drop for the radial flow with single fracture injection (Fig.4.61 and Table 4.5) increased by a rate which was much lower than the rate of increase for the case of radial injection without fracture.

When the damaged zone permeability decreased from 300 to 90 md, the pressure drop increased by a rate of 0.0008 bar per each 10 md reduction in damaged zone permeability for a damaged zone width of 2 cm and by 0.0017 for a damaged zone width of 8 cm. These rates increased to 0.0217 and 0.08 for the damaged zone permeability change from 90 to 30 md (which was 27 and 47 times higher than the previous increase rate). When the damaged zone permeability decreased to lower than 30 md, the rates became 0.17 and 0.615 bar per each 10 md reduction in damaged zone permeability (which was 210 and 360 times higher than the starting rate).

Again the ratio of the initial pressure drop to the pressure drop after damage can be used as an indication for the total injectivity reduction caused by the damaged zone. The plot of $\Delta Pi/\Delta P$ versus damaged zone width for three different Kd/Km values can be seen in Figure 4.62. This plot showed that the effect of both damaged zone width and permeability on injectivity is very minimal even at both high damaged zone depth and very low damaged zone permeability (Table

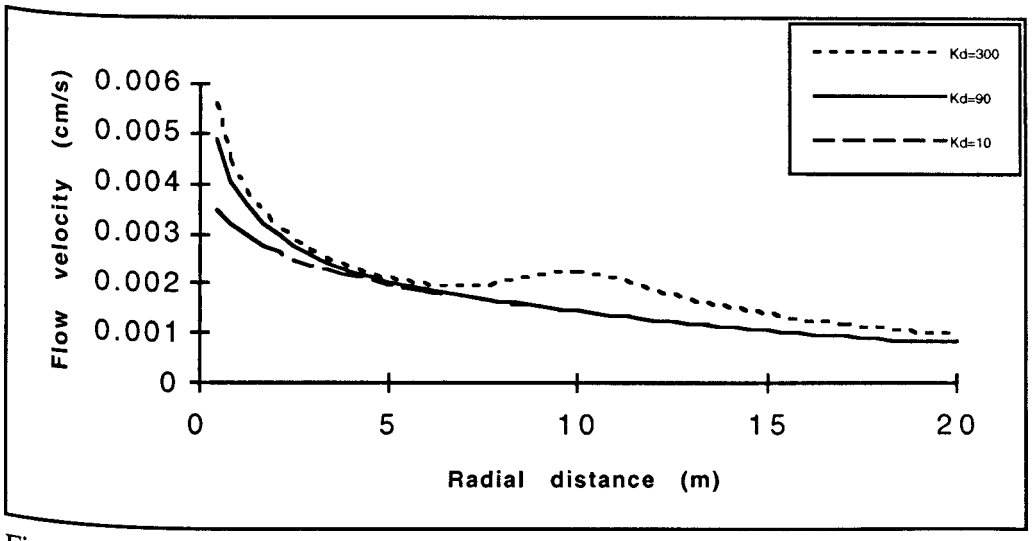

Fig.4.59: Flow velocity distribution through matrix of a radial-single fracture injection for different damaged zone permeabilities at a damaged zone width of 8 cm.

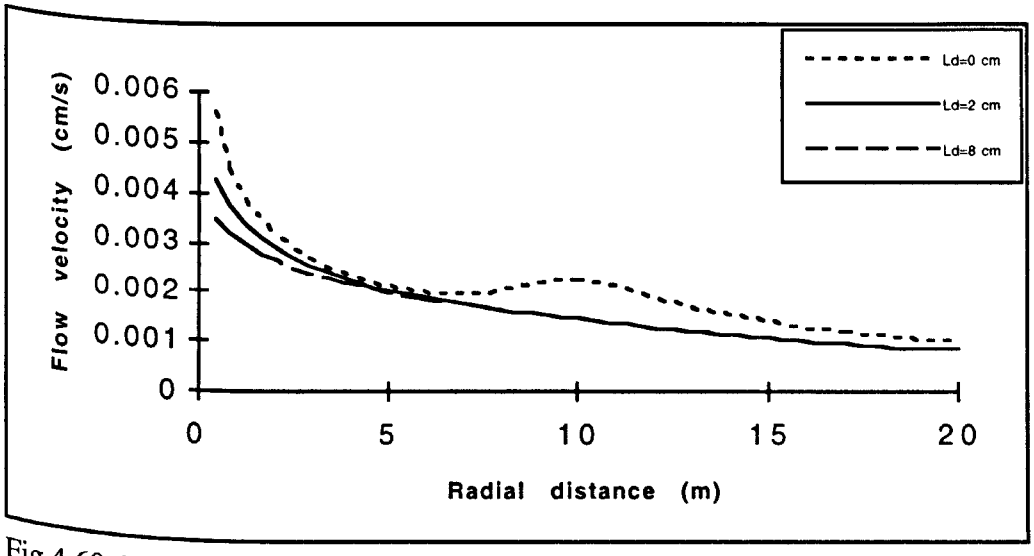

Fig.4.60: Flow velocity distribution through matrix of a radial-single fracture injection for different damaged zone widths at a damaged zone permeability of 10 md.

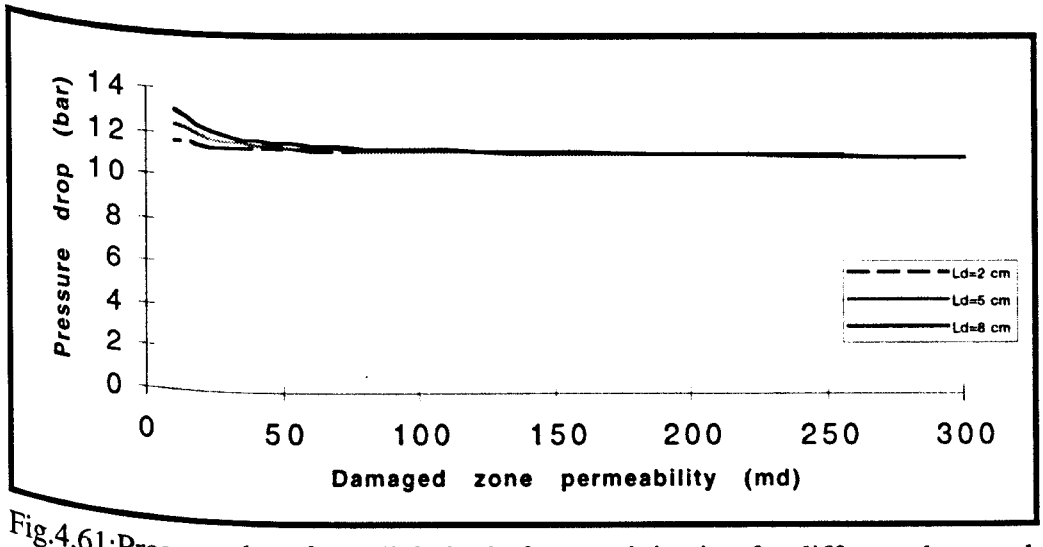

Fig.4.61:Pressure drop for radial-single fracture injection for different damaged zone widths and permeabilities.

4.6). The minimum ΔPi/ΔP value was 0.84 which was measured at a damaged zone width of 8 cm and damaged zone permeability of 10 md (Kd/Km = 0.033).

Figure 4.63 shows the difference between the injectivity in radial injection with near well bore skin and injectivity in radial injection with a near fracture face skin for a Kd/Km value of 0.033.

4.9.2.7. Radial injection with two fractures and a near fracture face skin model

For a constant fractures length of 10 m and a constant clean matrix permeability of 300 md, there was nearly no reduction in the injectivity when the damaged zone permeability was 90 md (Kd/Km = 0.3) even at a damaged zone width of 8 cm (Fig.4.64 and Table 4.7). The worst case of damage caused the ΔPi/ΔP value to decreased to 0.9 (Ld = 8 cm and Kd/Km = 0.033) recorded a 6% improvement over the single fracture case.

4.10 Conclusions of simulation study

For the linear and the 0.4 to 0.8 m fracture models:

(1) For the case of 0.4 m full open fracture with clean matrix, more than half of the pressure drop (57%) was lost in the first half of the fracture. The total reduction in flow velocity along the fracture was 0.16 m/s. 62.5% of this reduction occurred at 0.05 m from the inlet and 89% of this reduction in the first half of the fracture. The side pressure drop with distance along the fracture had the same profile of the pressure change along the fracture because the side outlet pressure was set to zero along the slab length. As the flow approached the fracture outlet, the side flow rate was distributed on the fracture face more uniformly.

(2) As the fracture permeability started to decrease (may be due filter cake formation) more pressure started to be lost in the first half of the fracture. At a fracture permeability of 1000 Darcy the pressure loss at the first half of the fracture was 72% of the total pressure loss. The reduction in fracture permeability from 4000 to 1000 Darcy causes a 79% increase in SPD1 whereas it causes only 32% increase in SPD3. As the fracture permeability decreased more and more of the flow velocity was lost in the first half along the fracture. This loss in flow velocity along fracture was reflected by an increase of side flow velocity.

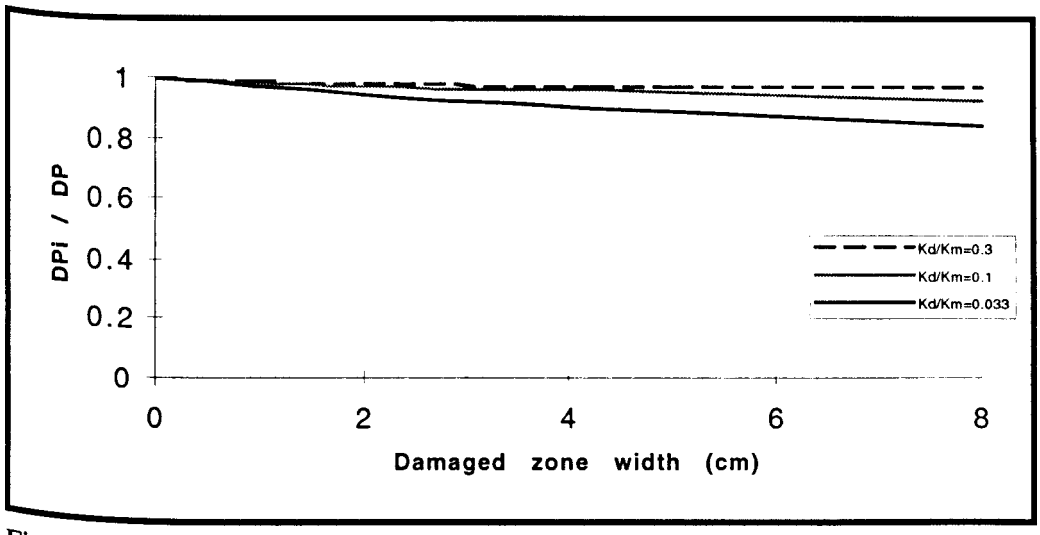

Fig.4.62: The change of ΔPi/ΔP for radial-single fracture injection with damaged zone width at different Kd/Km values.

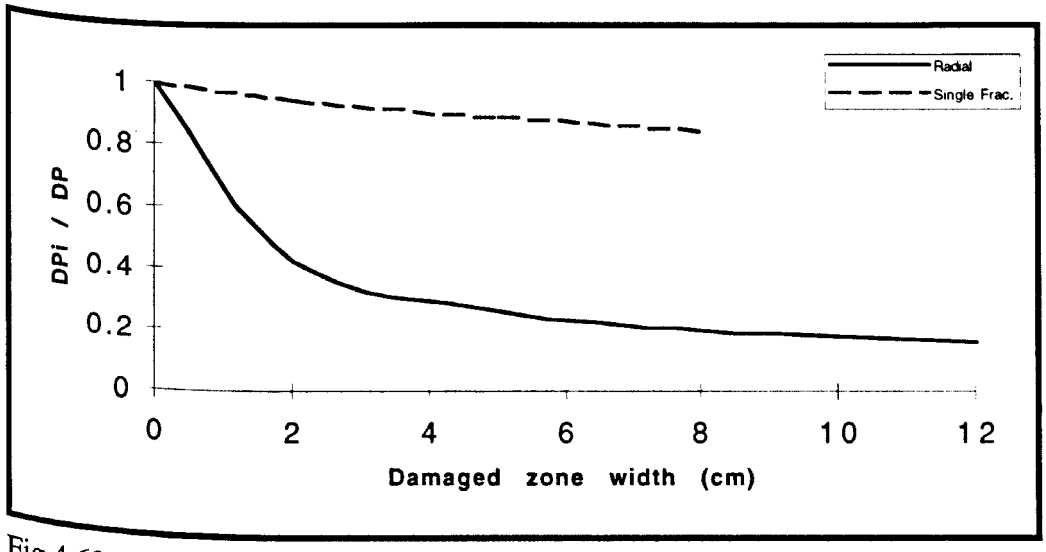

Fig.4.63: The change of ΔPi/ΔP for radial injection and radial-single fracture injection with damaged zone width at a damaged zone permeability of 10 md (Kd/Km = 0.033).

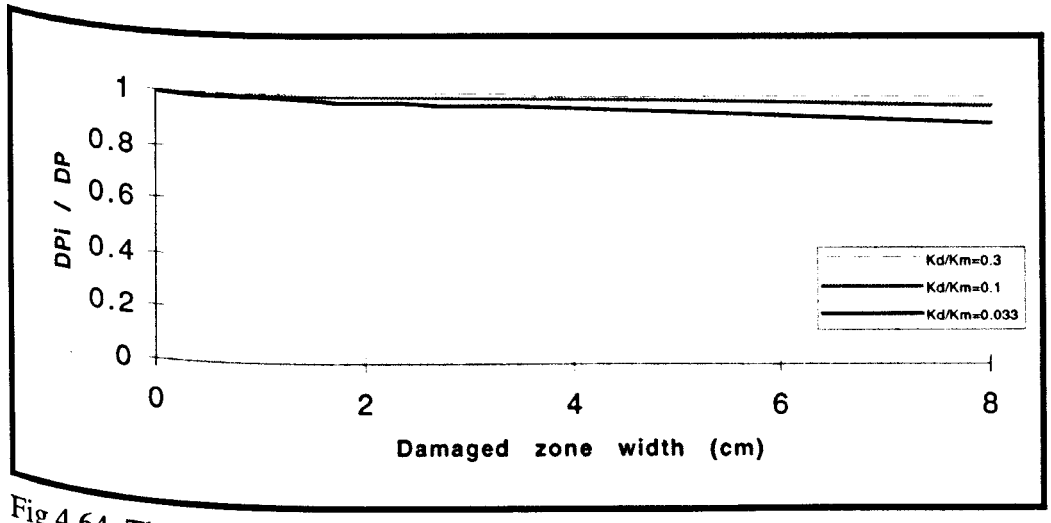

Fig.4.64: The change of ΔPi/ΔP for radial-double fractures injection with damaged zone width at different Kd/Km values.

(3) The matrix permeability variation had little effect on the pressure drop along the fracture. As the matrix permeability decreased, the pressure drop with distance along the fracture became more and more linear. Decreasing the matrix permeability caused the side pressure drop at 30 cm distance from the fracture inlet SPD3 to increase by a higher rate than the side pressure drop at 10 cm distance from the fracture inlet SPD1. As the matrix permeability decreased, the reduction of the side flow velocity at 10 cm distance from the fracture inlet SFV1was higher than the percentage reduction of the side flow velocity at 30 cm distance from the fracture inlet SFV3.

(4) As the inlet flow velocity increases the difference between the side pressure drops SPD1 and SPD3 increases. The same can be said for the side flow velocities SFV1 and SFV3.

(5) Reducing the fracture width affected the side pressure drop SPD1 more than it affected the side pressure drop SPD3. As the fracture aperture decreased, the resistance to flow along the fracture increased which caused some of the flow along the fracture to be directed through the side outlets.

(6) By increasing the fracture length from 40 to 80 cm the pressure drop increased by only 12%. For the first half distance along the fracture, the pressure drop was 77% (of the total pressure drop) for the long fracture and 58% for the short fracture. The reduction rate of the flow velocity along fracture with distance was higher for the long fracture. Consequently, the side flow velocity of the long fractured slab was higher.

(7) For the case of the linear injection model, as the matrix permeability decreased, the resistance to flow increased which caused the pressure drop to increase sharply as the fluid was forced to flow through the rock matrix.

For the case of the fracture injection model, as the matrix permeability decreases, the resistance to flow through the side paths increased but the fluid had another path with a lower resistance (along the fracture).

(8) In the rough fracture face model, increasing the e/b value resulted in an increase in pressure loss along the fracture for the first 5 cm along the fracture. The pressure loss profile for all the tested e/b values was nearly the same in the last 35 cm along the fracture. By increasing the e/b from 0.0625 to 0.25 the pressure loss along the fracture increased by 14 %.
Changing the e/b value had an effect on the flow velocity along the fracture only at the first 10 cm.

For field applications:

(1) In the radial injection model and due to the narrow area of the well bore compared with the outer flow area, 50% of the pressure drop occurred in the first meter around the well bore. As the flow approached the outer boundary, and due to the enlargement of the radial flow area, the pressure drop in the last five meters was less than 5% of the total pressure drop. The flow velocity at the first metre decreased to 6% of the inlet flow velocity.

(2) The presence of a 10 m fracture caused the pressure drop distribution through the matrix (central axis path) to be more uniform than it was in the radial injection case, especially at the first 10 m. The pressure drop distribution through the matrix became even more uniform as the matrix permeability decreased. The same can be said for the flow velocity distribution through the matrix. Increase the fracture length enhanced the flow velocity distribution and pressure drop through the matrix along the central axis path.
The double fracture injection model resulted in a further improvement in flow velocity distribution.

(3) In radial injection model with a near well bore skin, the ($\Delta P_i/\Delta P$) plot versus the damaged zone width for different K_d/K_m (damaged zone permeability / initial matrix permeability ratio) values (at constant flow rate) showed that the effect of damaged zone depth (for constant damaged zone permeability) on injectivity is very high at the first 2 cm. The effect of the following 3 cm (from 2 to 5 cm) on injectivity was less. And the effect of the last 7 cm on injectivity was vary small compared with the effect of the first 2 cm.

(4) For a radial model with a single 10 m fracture and a near fracture face skin, the ($\Delta P_i/\Delta P$) plot versus the damaged zone width for different K_d/K_m plot showed that the effect of both damaged zone width and permeability on injectivity is very minimal even at both high damaged zone depth and very low damaged zone permeability.

(5) For a radial model with a double 10 m fractures and a near fracture face skin, the was nearly no reduction in the injectivity when the damaged zone permeability was 90 md (Kd/Km = 0.3) even at a damaged zone width of 8 cm.

Matrix permeability mD	Pres. Drop Linear mode (bar)	Pres. Drop (along Frac.) (bar)	SPD1 (bar)	SPD2 (bar)	SPD3 (bar)
500	2.52	0.223	0.146	0.088	0.041
450	2.8	0.231	0.153	0.093	0.043
350	3.6	0.249	0.169	0.104	0.049
150	8.4	0.298	0.214	0.138	0.067

Table 4.1: Pressure drop in linear injection model and side pressure drop in fracture injection model.

	Pres.D rop (along a 0.4 m) (bar)	SPD1 (at 0.1 m) (bar)	SPD2 (at 0.2 m) (bar)	SPD3 (at 0.3 m) (bar)	Velocity (at 0.4 m) (bar)
The 0.4 m fracture	0.223	0.146	0.088	0.041	0.81
The 0.8 m fracture	0.193	0.174	0.121	0.083	0.45

Table 4.2: Side pressure drop and side flow velocity for the 0.4 m and the 0.8 m fractures injection models.

Kd	DP (Ld=2 cm)	DP (Ld=5 cm)	DP (Ld=8 cm)	DP(Ld=12cm)
300	36.466	36.466	36.466	36.466
90	40.543	44.97	48.30	51.656
30	51.65	68.74	81.72	94.98
10	84.555	139.69	181.73	224.77

Table 4.3: Pressure drop for radial injection with near well bore damage.

Wd (cm)	DPi/DP (Kd/Km=0.3)	DPi/DP (Kd/Km=0.1)	DPi/DP Kd/Km=0.033
0	1	1	1
2	0.90	0.71	0.43
5	0.81	0.53	0.26
8	0.76	0.45	0.20
12	0.71	0.38	0.16

Table 4.4: $\Delta Pi / \Delta P$ for radial injection with near well bore damage.

Kd	DP (Ld=2 cm)	DP (Ld=5 cm)	DP (Ld=8 cm)
300	11.07	11.07	11.07
90	11.24	11.35	11.43
30	11.37	11.65	11.91
10	11.711	12.45	13.14

Table 4.5: Pressure drop for radial-single 10 m fracture injection with near fracture face damage.

Wd (cm)	DPi/DP (Kd/Km=0.3)	DPi/DP (Kd/Km=0.1)	DPi/DP Kd/Km=0.033
0	1	1	1
2	0.98	0.97	0.95
5	0.98	0.95	0.89
8	0.97	0.93	0.84

Table 4.6: $\Delta Pi / \Delta P$ for radial-single 10 m fracture injection with near fracture face damage.

Wd (cm)	DPi/DP (Kd/Km=0.3)	DPi/DP (Kd/Km=0.1)	DPi/DP Kd/Km=0.033
0	1	1	1
2	1.00	0.99	0.97
5	0.99	0.97	0.93
8	0.99	0.96	0.90

Table 4.7: $\Delta Pi / \Delta P$ for radial-double 10 m fractures injection with near fracture face damage.

CHAPTER FIVE

DIMENSIONAL ANALYSIS OF MATRIX DAMAGE

5.1 Introduction

Dimensional analysis is a method by which information about a phenomenon is deduced, as long as the phenomenon can be described by a dimensionally correct equation among certain variables. By using this method a partial solution to nearly any problem is obtained. On the other hand, a complete solution is not obtained, nor is the inner mechanism of a phenomenon revealed, by dimensional reasoning alone.

The result of dimensional analysis of a problem is a reduction of the number of variables in the problem. In the experimental determination of a function, the number of variables determines how many experiments must be performed before obtaining an acceptable function. A reduction of the number of variables in a problem greatly amplifies the information that is obtained from a few experiments. Consequently, dimensional analysis is an important mathematical tool of experimenters.

The dimensional equation is assumed dimensionally homogeneous. However, it may not logically be assumed a prior that an unknown equation is dimensionally homogeneous, unless it is known that the equation contains all the variables that would appear in an analytical derivation of the equation.

The first step in the dimensional analysis of a problem is to decide what variables enter the problem. If variables are introduced that really do not affect the phenomenon, too many terms may appear in the final equation. Even though some variables are practically constants, they may be essential because they combine with other active variables to form dimensionless products. Therefore enough must be understood about a problem to explain why and how the variable influences the phenomenon [48].

The other steps are explained in section 5.4.

The equations which describe the matrix damage due to brine injection into a fractured formation is very complex. A simple practical equation (which is easy to use) to describe such a system is needed. This equation can be obtained by using dimensional analysis with the help of experimental results. If the obtained equation is not precise, it can give a correct indication about the pressure drop pattern.

5.2 The objectives of this chapter

The objective in this chapter is to represent the damage in the fracture system, caused by the presence of solid particles and/or oil droplets within the injected brine, by a mathematical formula using dimensional analysis. Since the degree of matrix damage was measured by the pressure drop through that matrix, then the best representation for such a case was to make pressure drop as a function of different variables and with time as the main variable.

This mathematical equation was used with the help of experimental results to evaluate the dimensional constant and exponent. The dimensional constant and exponent were evaluated for different simulated produced waters depending on particles mean size and concentration and oil droplets mean size and concentration. This enabled general equations (which can be applied in practical field injection) to predict the time needed for the injectivity ($q/\Delta p$) to decrease by 50% due to injection of produced water to be determined.

5.3 Dependent and independent variables

The degree of matrix damage was described by Darcy's law in which the pressure drop and flow rate were linked. The pressure drop was chosen as the dependent variable, with the following independent variables affecting the pressure drop:

b: fracture width.

ρ: fluid density.

μ: fluid viscosity.

K_f: fracture permeability.

Km: matrix permeability.

A: flow area.

q: flow rate through matrix.

D_{pore}: matrix pore throat diameter

D_p: Particle or droplet mean diameter.

C_p: Particle or droplet concentration.

L: length of the flow path.

t: injection time.

A relationship is assumed in which the pressure drop is a function of these variables:

$$\Delta p = f(b, \rho, \mu, K_f, Km, A, q, D_{pore}, D_P, C_P, L, t) \qquad (5.1)$$

a) Some of these variables will not be used in the dimensional analysis. Since the fracture aperture had an effect only on the initial pressure drop before damage takes place, then it was neglected. Also since the fracture permeability depends on the fracture width, it was also neglected.

The density for all the experiments conducted was similar and the tests were carried out under steady state laminar incompressible flow conditions, so the density was assumed constant and neglected in the analysis.

b) Some of the variables were combined together to form only one variable. The flow rate (q) through the matrix was divided by the flow area (A) to obtain one variable, flow velocity (v) through the matrix.

c) The particle mean diameter (D_P) was divided by the pore throat diameter (D_{pore}) to obtain one variable which is the D_P / D_{pore} ratio. Furthermore D_{pore} can be substituted by the square root of matrix permeability $\sqrt{Km}$ (from literature, D_{pore} was always assumed to be equal to $\sqrt{Km}$).

d) The particle concentration (C_P) was divided by fluid density (ρ) to obtain one variable which was the ratio of the mass of particles to the mass of fluid (particle concentration defined as grams of particles / each gram of fluid).

e) The pressure drop through matrix (Δp) was divided by the flow path length (L) to form one variable, the pressure gradient.

Substituting these in equation 5.1 gave:

$$\frac{\Delta p}{L} = f\left(\frac{C_p}{\rho}, \frac{D_p}{\sqrt{K_m}}, \frac{q}{A}, \mu, t, K_m\right) \qquad (5.2)$$

The variables C_P/ρ and $D_P/\sqrt{Km}$ are dimensionless.

5.4 Dimensional analysis procedure

The initial equation is:

$$\frac{\Delta p}{L} = C\left(\frac{C_p}{\rho}\right)^{\alpha}\left(\frac{D_p}{\sqrt{K_m}}\right)^{\beta}(v)^a(\mu)^b(K_m)^c(t)^d \qquad (5.3)$$

where C is the dimensional constant.

As the variables C_P/ρ and $D_P/\sqrt{Km}$ are dimensionless, they can be combined with the dimensional constant C to form one constant.

Therefore $$\frac{\Delta p}{L} = C_1(v)^a(\mu)^b(K_m)^c(t)^d \qquad (5.4)$$

Where $$C_1 = C\left(\frac{C_p}{\rho}\right)^{\alpha}\left(\frac{D_p}{\sqrt{K_m}}\right)^{\beta} \qquad (5.5)$$

Dimensions of the variables are:

	Length	Mass	Time
Δp/L	L^{-2}	M	T^{-2}
μ :	L^{-1}	M	T^{-1}
v :	L^{1}		T^{-1}
Km :	L^{2}		
t :			T^{1}

Replacing each variable with its dimensions resulted in:

$$L^{-2}\,M\,T^{-2} = (L^1\,T^{-1})^a\,(L^{-1}\,M\,T^{-1})^b\,(L^2)^c\,(T)^d$$

$$L^{-2}\,M\,T^{-2} = L^a\,T^{-a}\,L^{-b}\,M^b\,T^{-b}\,L^{2c}\,T^d \qquad (5.6)$$

Equating the exponents of the same dimensions on the two sides of the equation resulted in three equation with four unknowns:

$$-2 = a - b + 2c$$

$$1 = b$$

$$-2 = -a - b + d$$

Then $-2 = a - 1 + 2c \longrightarrow c = (-1 - a)/2$

$-2 = -a - 1 + d \longrightarrow a = d + 1$

Then $c = (-d - 2)/2$

Substituting for a, b and c give:

$$\frac{\Delta p}{L} = C_1(v)^{d+1}(\mu)^1(K_m)^{\frac{-d}{2}-1}(t)^d v$$

Or $$\frac{\Delta p}{L} = C_1\mu\left(\frac{v}{K_m}\right)\left(\frac{v*t}{\sqrt{K_m}}\right)^d \qquad (5.7)$$

For clean water injection, the exponent of the time (d) in the initial equation is equal to zero as the time had no effect on the pressure drop (no damaged would take place as time passes):

Then $d = 0$

And the above equation reduces to Darcy's law:

$$\frac{\Delta p_i}{L} = C_2 \frac{\mu * v}{K_m}$$

Where Δp_i is the initial pressure drop for clean salt water injection through clean matrix. Dividing $\frac{\Delta p}{L}$ by $\frac{\Delta p_i}{L}$ and assuming constant fluid viscosity μ resulted in the following equation:

$$\frac{\Delta p}{\Delta p_i} = C\left(\frac{v*t}{\sqrt{K_m}}\right)^d \qquad (5.8)$$

Where $\frac{\Delta p}{\Delta p_i}$ is the total pressure drop (pressure drop due to damage plus the pressure drop due to a clean matrix resistance) divided by the pressure drop through a clean matrix.

The above final equation contains the most important variables that affect the pressure drop value when damage takes place.

C is function of C_P and D_P variables: increasing the variables C_P and D_P resulted in higher pressure drop due to higher damage.

v is function of flow rate (q) and flow area A. For constant flow area (A), higher q means that more fluid volume per second (more solid and/or oil per second) is passing through the matrix which results in higher damage. For constant flow rate (q), higher A means that less fluid volume per second is passing through the matrix which results in less damage.

As time passes, more damage takes place within the matrix.

The pore throat diameter D_{pore} is a function of matrix permeability (Km) and as Km decreases, D_{pore} decreases which results in higher probability of pore throat bridging to take place in less time. For narrow pore throat, less fluid volume is needed to pass through it before bridging would take place. For constant flow rate this eventually means less time is needed for the bridging to take place.

5.5 Evaluation of constants

The constant C and the exponent d can be determined with the help of experimental results. First the equation was put in the following log-log form:

$$\log\left(\frac{\Delta p}{\Delta p_i}\right) = \log(C) + d\log\left(\frac{v*t}{\sqrt{K_m}}\right) \qquad (5.9)$$

For each experiment, the $\log\left(\frac{\Delta p}{\Delta p_i}\right)$ was plotted versus $\log\left(\frac{v*t}{\sqrt{K_m}}\right)$. The linear section represents the late injection time. The slope of this straight line is equal to d and the intersection of this line with the y-axis is equal to log(C).

Three examples are shown in Fig.5.1a - c for experiments 62, 52 and 75.

Table 5.1 shows the measured values of C and d for the linear injection (LI) experiments, short fracture injection (SFI) experiments and long fracture injection (LFI) experiments.

The flow area was 9 cm^2 for the LI, 59 cm^2 for the SFI and 112 cm^2 for the LFI.

For oil emulsion injection experiments (without any solids), the value of d was between 0.255 and 0.324 for the LI, between 0.15 and 0.18 for the SFI and around 0.11 for the LFI. The value of C was between 0.0036 and 0.013 for the LI, between 0.05 and 0.11 for the SFI and around 0.25 for the LFI.

Since the value of C and d are known, the injection time can be recalculated using the following equation:

$$t = \left(\frac{\Delta p}{\Delta p_i}\frac{1}{C}\right)^{\frac{1}{d}}\frac{\sqrt{K_m}}{v} \qquad (5.10)$$

The half injectivity time (HIT) (which is the time required for the injectivity ($q/\Delta p$) to decrease to half its initial value) was calculated by making $\frac{\Delta p}{\Delta p_i}$ equal to 2.0 and by assuming constant flow velocity. The results of the HIT are shown in Table 5.1.

For the case of oil emulsion injection (without any solid particle), the HIT of the LI experiments was 9 to 12 hours whereas the HIT of the SFI and LFI experiments was 140 to 275 hours.

When the injected suspension contained only 2.1 μm mean size particles (without any oil), the value of d for the LI experiments was around 0.51 and for the SFI and LFI experiments was between 0.17 and 0.2. The value of C was around 0.000156 for the LI and between 0.05 to 0.067 for the fracture injection experiments. The HIT for the LI was less than 4 hours and for the FI was from 90 to 300 hours. There was a large difference in HIT between the two injection systems (25 to 80 times) compared with the area difference which is only 6.5 to 13 times.

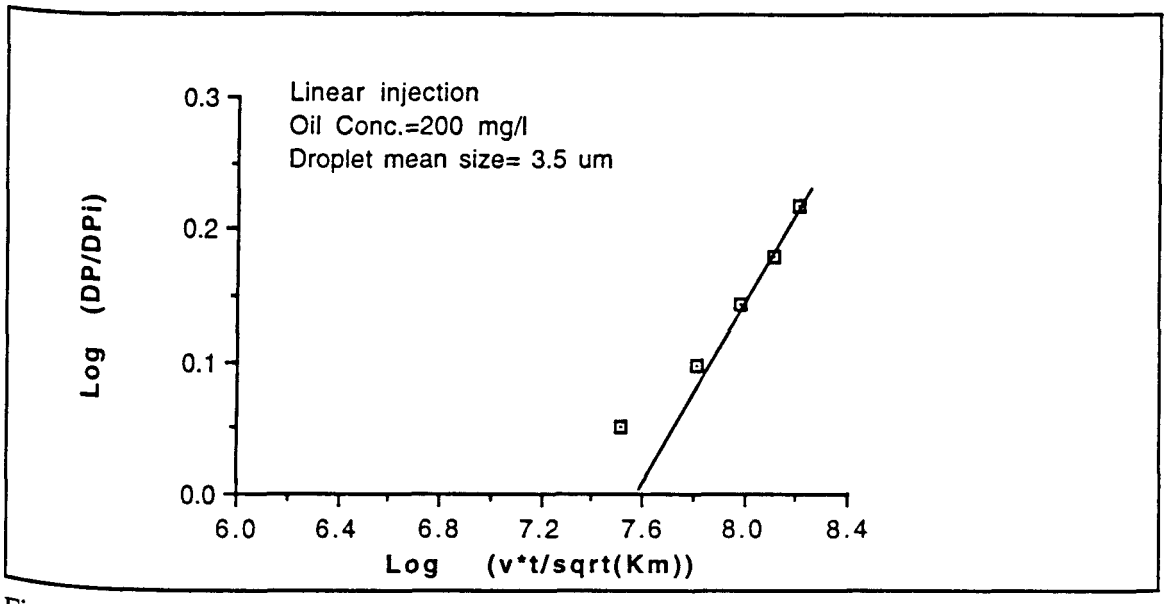

Fig.5.1a: Experiment 62 log-log data to measure d (the slope) and C (line intersect with y-axis).

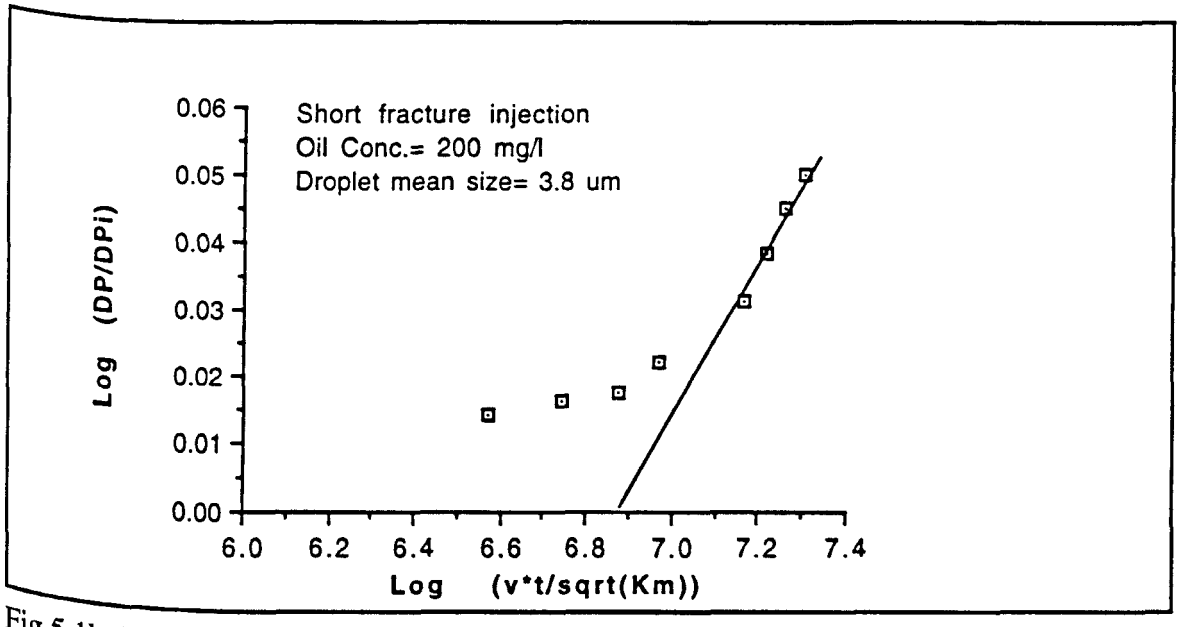

Fig.5.1b: Experiment 52 log-log data to measure d (the slope) and C (line intersect with y-axis).

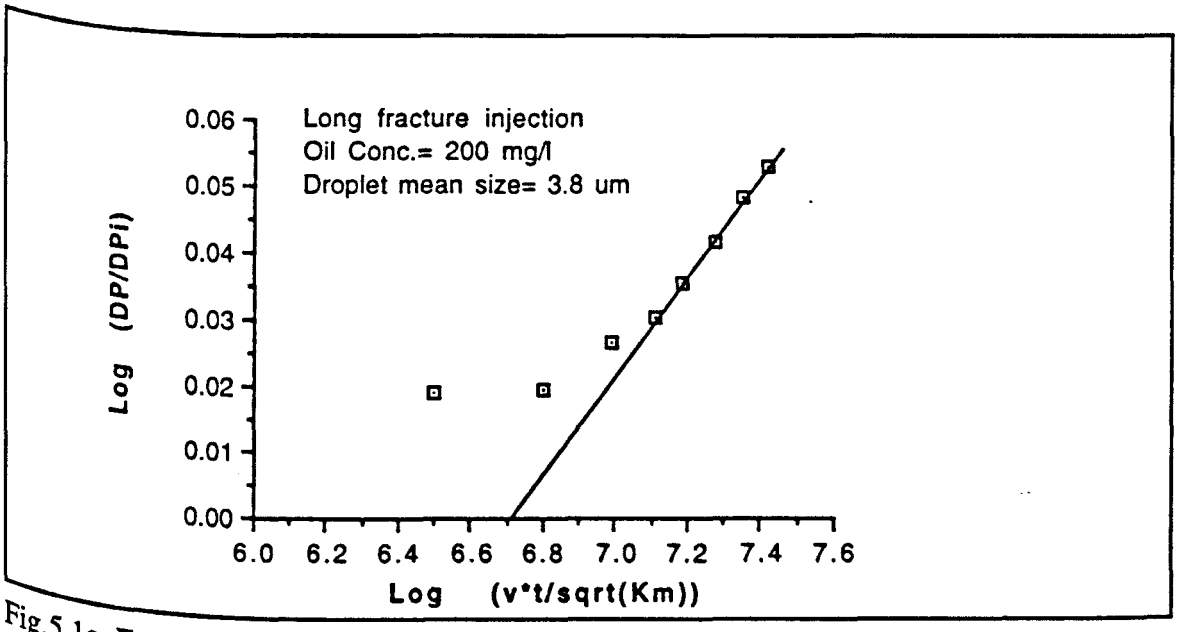

Fig.5.1c: Experiment 75 log-log data to measure d (the slope) and C_3 (line intersect with y-axis).

For the injection of the 4.7 μm mean size particle suspensions (without any oil), LI experiments resulted in a d value around 0.6 whereas the SFI and LFI experiments gave a value between 0.27 and 0.32. The value of C was between 0.000013 to 0.00085 for the LI and between 0.0075 to 0.013 for the FI. This time the difference in HIT between the LI and FI was only 7.5 to 14 times indicating that the FI was more sensitive to the 4.7 μm mean size particle suspensions thant it was to the 2.1 μm mean size particle suspensions.

For the injection of simulated produced water which contained 200 ppm oil and 10 mg/l of 2.1 μm mean size particles, the d value was 0.59 for the LI and between 0.26 to 0.3 for the FI. The C value was 0.000043 for the LI and from 0.008 to 0.015 for the FL. The HIT was 3.2 hours for the LI and 33 to 118 hours for the FI which made the difference between the two systems 10 to 37 time. The difference in HIT between the two injection systems when oil and particles are present was much lower than the difference when only oil (without any particles) or when only 2.1 μm particles (without any oil) were present.

The LI of simulated produced water which contains oil and 4.7 μm mean size particles gave a d value between 0.683 and 0.825. The FI results in d and HIT values which are nearly equal to the calculated d and HIT values when a 4.7 μm mean size particles suspension (without any oil) was injected, but with different values of C. The C for the LI was between 0.0000006 and 0.0000095 and the HIT was between 2.55 and 3.57 hours.

Some of the calculated values of d in the LI and FI experiments were gathered in Figure 5.2a and some of the calculated C values of the LI and FI experiments were gathered in Figure 5.2b. In these figures the d and C values where plotted as groups of points, each group of points consists of 3 values for d and 3 values for C (calculated for the same injected fluid composition), one for linear injection one for short fracture injection and one for the long fracture injection (Table 5.2).
All calculated HIT values of the LI and FI experiments were gathered in Figure 5.2c The fracture injection of oil emulsions experiments (without any solids) and the 10 mg/l 2.1 μm mean size particles suspension experiment (without any oil) had the best injectivity performance (points group 1 to 4) compared with the linear injection experiments. This performance was

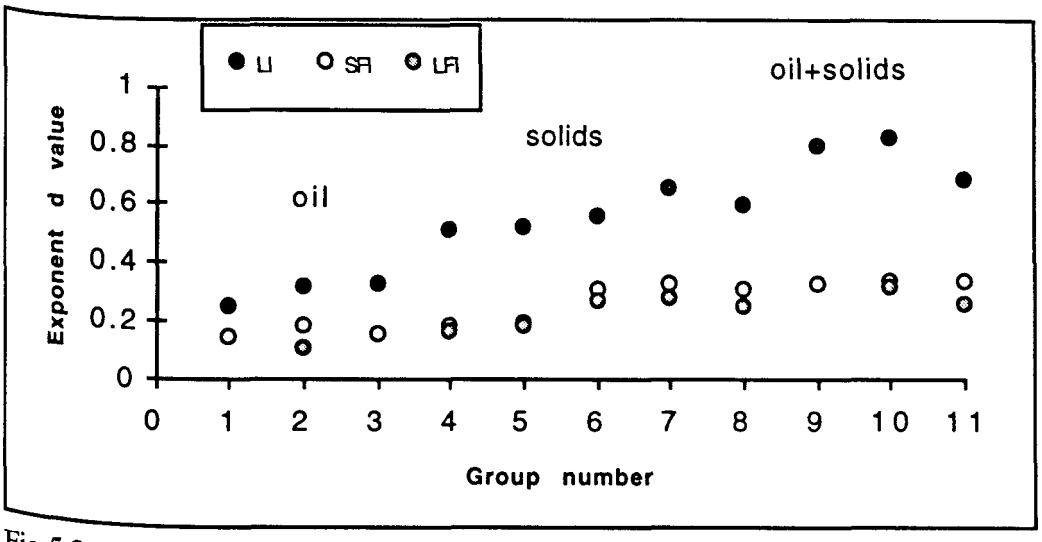

Fig.5.2a: The change in d value as the injection fluid composition and the injection system vary (the symbols LI, SFI and LFI refer to linear, short fracture and long fracture injection).

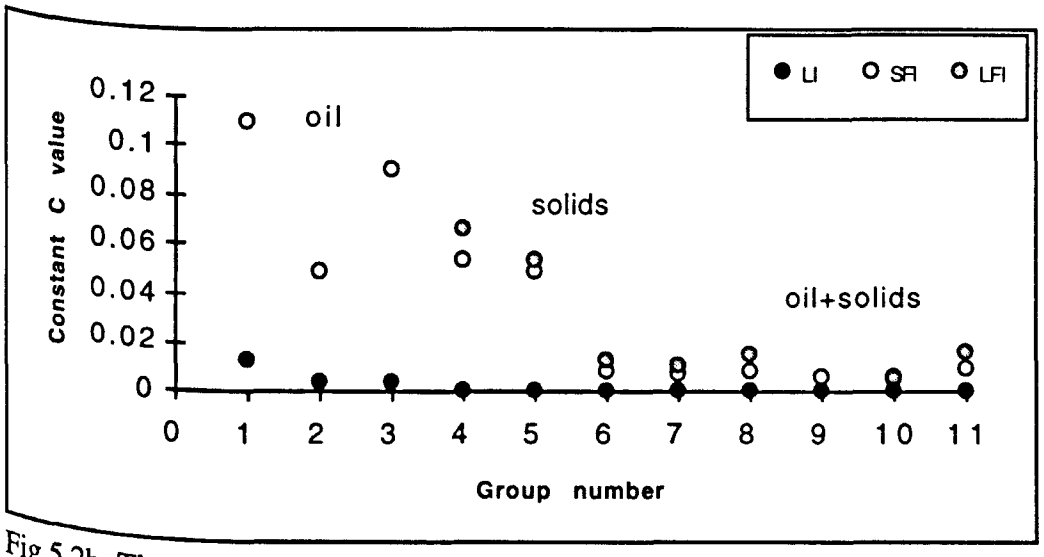

Fig.5.2b: The change in C_3 value as the injection fluid composition and the injection system vary (the symbols LI, SFI and LFI refer to linear, short fracture and long fracture injection).

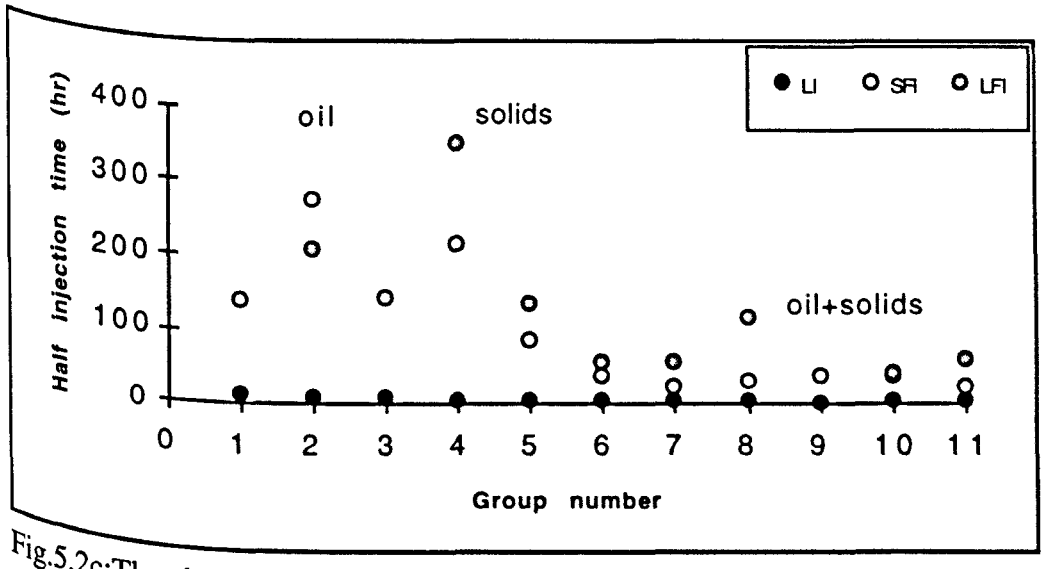

Fig.5.2c:The change in HIT value as the injection fluid composition and the injection system vary (the symbols LI, SFI and LFI refer to linear, short fracture and long fracture injection)

reduced to half when the particle concentration of the 2.1 μm suspension (without any oil) was increased to 15 mg/l (points group no. 5). The worst fracture injectivity performance was for the 4.7 μm mean size particles suspension experiments with or without oil (points group 6 to 7 and 9 to 11). The worst HIT calculated for the short fracture injection was 7 times higher than the HIT of the linear injection (experiments no. 70 and 47) and the worst HIT calculated for the long fracture injection was 13.5 times higher than the HIT of the linear injection (experiments no. 72 and 42).

5.6 Applications of dimensional analysis

In this section an attempt was made to find d and C values which can help in predicting the effect of produced water content on injectivity in real field fracture injection operations. These values were used to predict the change in pressure drop with time, matrix permeability and flow velocity.

5.6.1 The change of d and C values with flow velocity

The lab experiments were classified into six experimental groups; each one consisted of one linear injection experiment, one short fracture injection experiment and one long fracture injection experiment.

The three experiments were carried out nearly under the same conditions such as total flow rate, oil and solids concentrations and droplets and particles mean size. The initial matrix permeability of the three experiments was similar, which made the main variable (which determined the d and C values) is the flow velocity.

These groups are listed in Table 5.3 which contain the d and C values, the flow velocity through the matrix and the injected fluid composition for each group. Figures 5.3a -b show the change in d and C (for the LI and LFI experiments of each group) as the composition of the injected fluid varies. The value of C is very sensitive to the change in fluid composition. For oil emulsion injection C had a very high value compared with the C value for the particle suspensions or the simulated oily water. There is a huge difference between C values for LI and LFI. The d value for the particle suspensions was higher than the d value for the oil emulsion, and increased by a very small amount when oil was present with the particle suspensions (simulated oily water).

For each group log(d) and log(C) values were plotted versus the flow velocity through rock matrix. These plots of log(d) and log(C) versus flow velocity for experimental groups 2, 4 and 6 are shown in Figures. 5.4a - c and Figures 5.5a - c.

At very low flow velocities, the d and c values are very sensitive to any change in flow velocity and at high flow velocities the values of d and C start to level.

Figures 5.6 and 5.7 show the d and C values versus flow velocity for all the groups.

Interpolation of the plotted data can be used for injected fluids other than those used in the experiments (injected fluids with oil and solids concentration and droplet and particle mean size other than those used in the experiments in this work).

The plots were best fitted as:

For group 1 (oil Conc. of 200 ppm and droplet mean size of 3.7 μm)

$$\text{Log}(d) = 0.26036 + 0.31461\ \text{Log}(v)$$

$$\text{Log}(C) = -0.911 - 355.89\ v$$

For group 2 (particle Conc. of 10 mg/l and particle mean size of 2.1 μm)

$$\text{Log}(d) = 0.63127 + 0.38787\ \text{Log}(v)$$

$$\text{Log}(C) = -1.047 - 671.83\ v$$

For group 3 (particle Conc. of 15 mg/l and particle mean size of 2.1 μm)

$$\text{Log}(d) = 0.53404 + 0.34456\ \text{Log}(v)$$

$$\text{Log}(C) = -1.131 - 660.13\ v$$

For group 4 (particle Conc. of 10 mg/l and particle mean size of 4.7 μm)

$$\text{Log}(d) = 0.36649 + 0.25897\ \text{Log}(v)$$

$$\text{Log}(C) = -1.759 - 568.06\ v$$

For group 5 (particle Conc. of 15 mg/l and particle mean size of 4.7 μm)

$$\text{Log}(d) = 0.4906 + 0.28184\ \text{Log}(v)$$

$$\text{Log}(C) = -1.827 - 755.91\ v$$

For group 6 (oil Conc.= 200 ppm and particle Conc. of 10 mg/l at particle mean size of 2.1 μm)

$$\text{Log}(d) = 0.51649 + 0.30581\ \text{Log}(v)$$

$$\text{Log}(C) = -1.686 - 715.22\ v$$

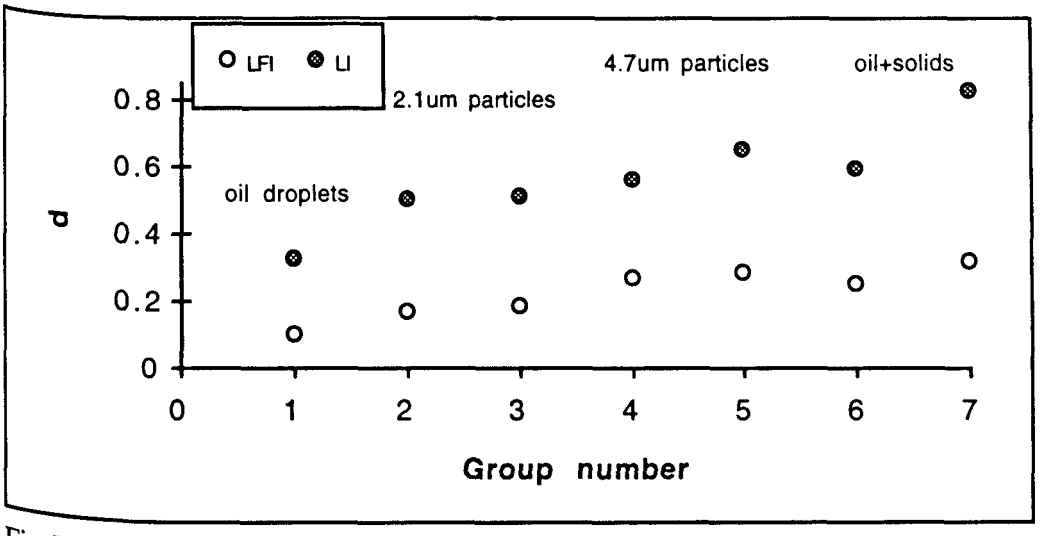

Fig.5.3a: The change in d of linear and fracture injection as the composition of the injected fluid vary (the symbols LI and LFI refer to linear and long fracture injection)

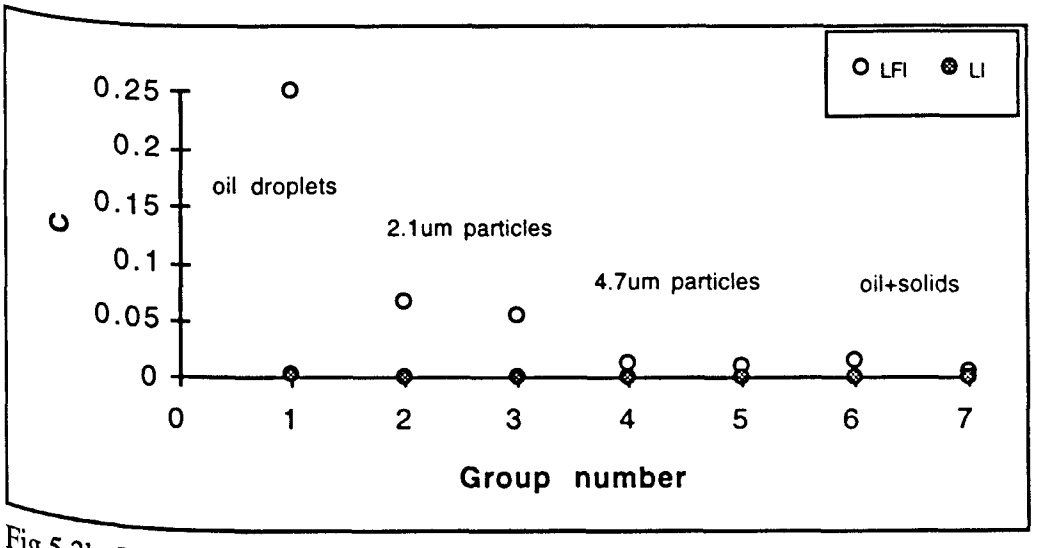

Fig.5.3b: The change in C for linear and fracture injection as the composition of the injected fluid vary (the symbols LI and LFI refer to linear and long fracture injection)

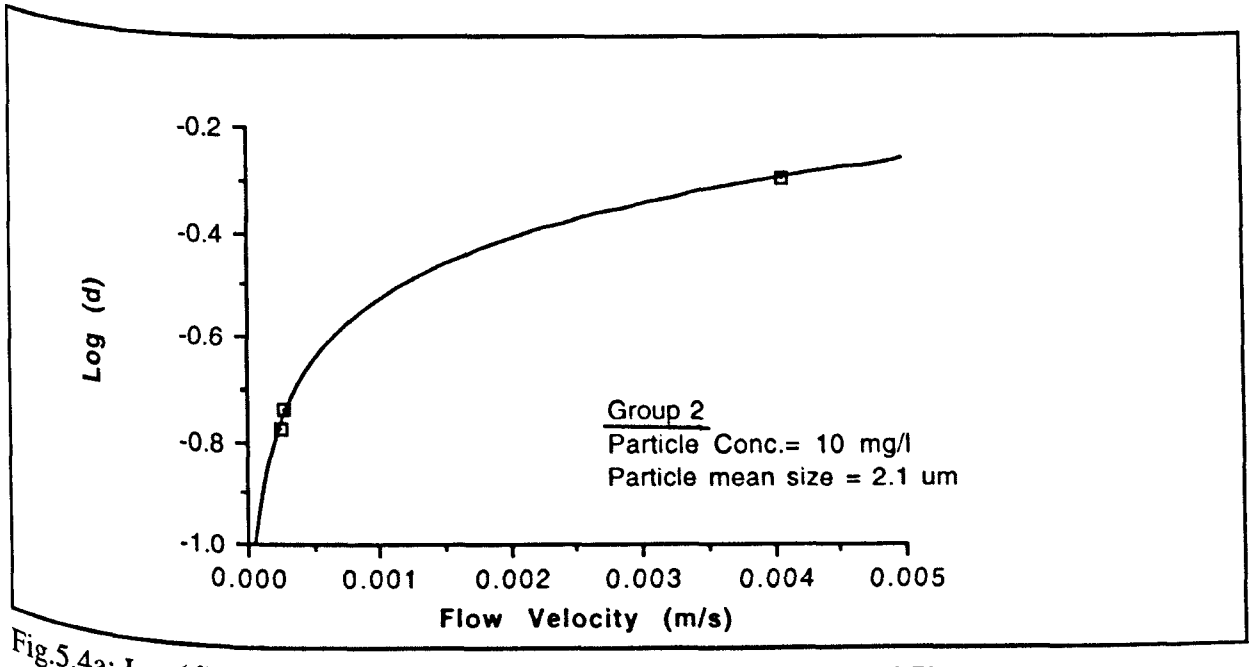

Fig.5.4a: Log(d) versus flow velocity for group 2 (Exps. 59, 56 and 77).

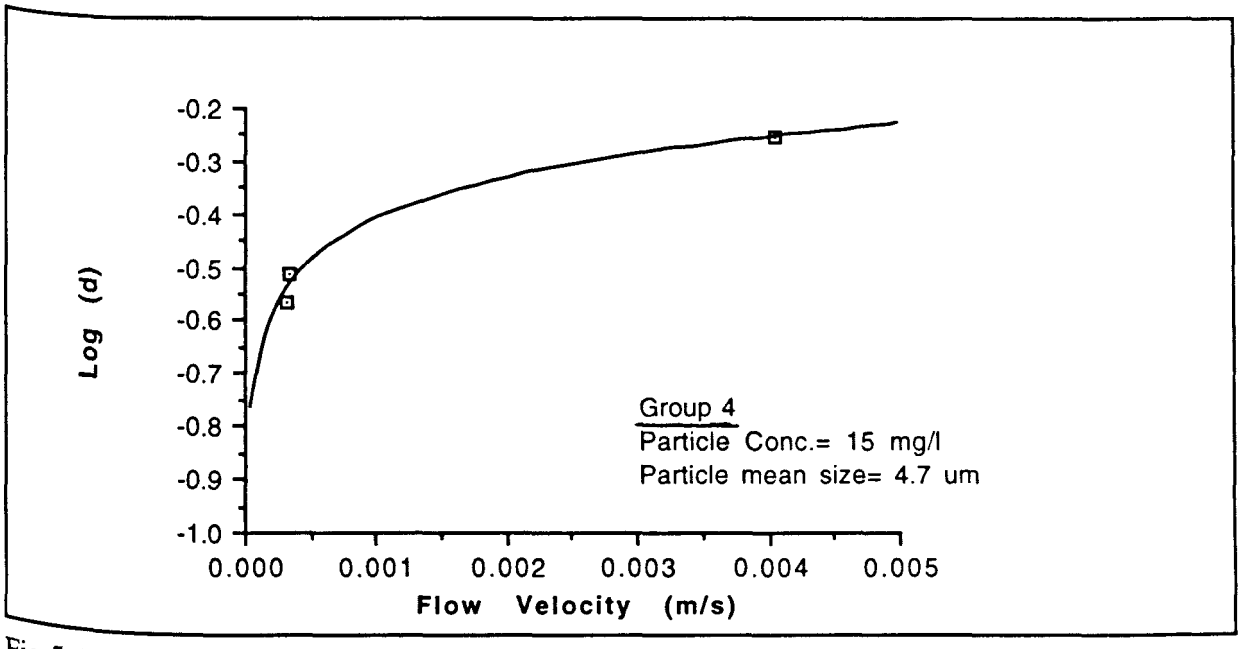

Fig.5.4b: The Log (d) versus flow velocity for group 4 (Exps. 65, 53 and 79).

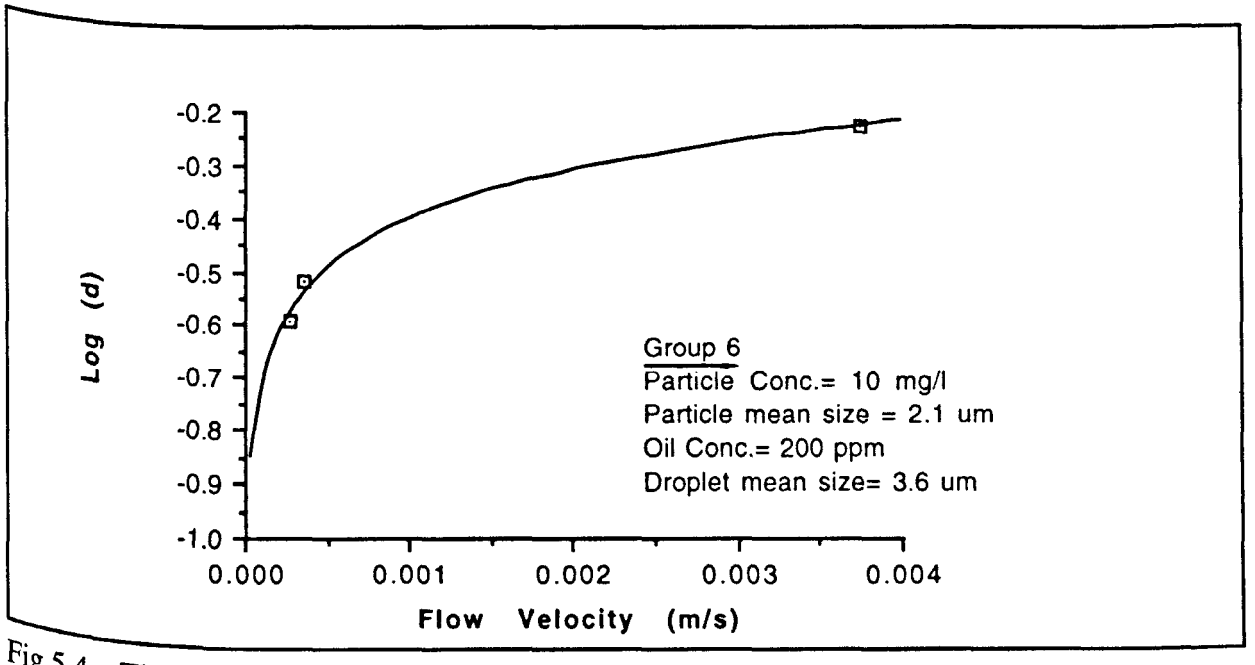

Fig.5.4c: The Log (d) versus flow velocity for group 6 (Exps. 74, 39 and 57).

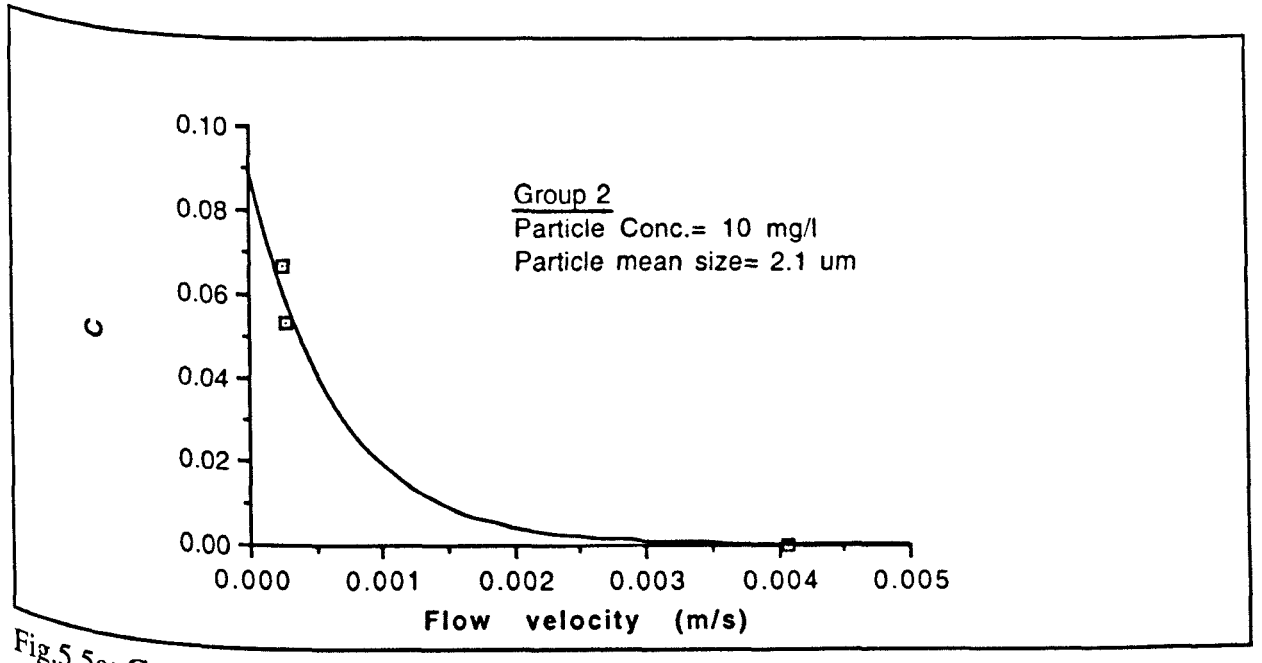

Fig.5.5a: C versus flow velocity for group 2 (Exps. 59, 56 and 77).

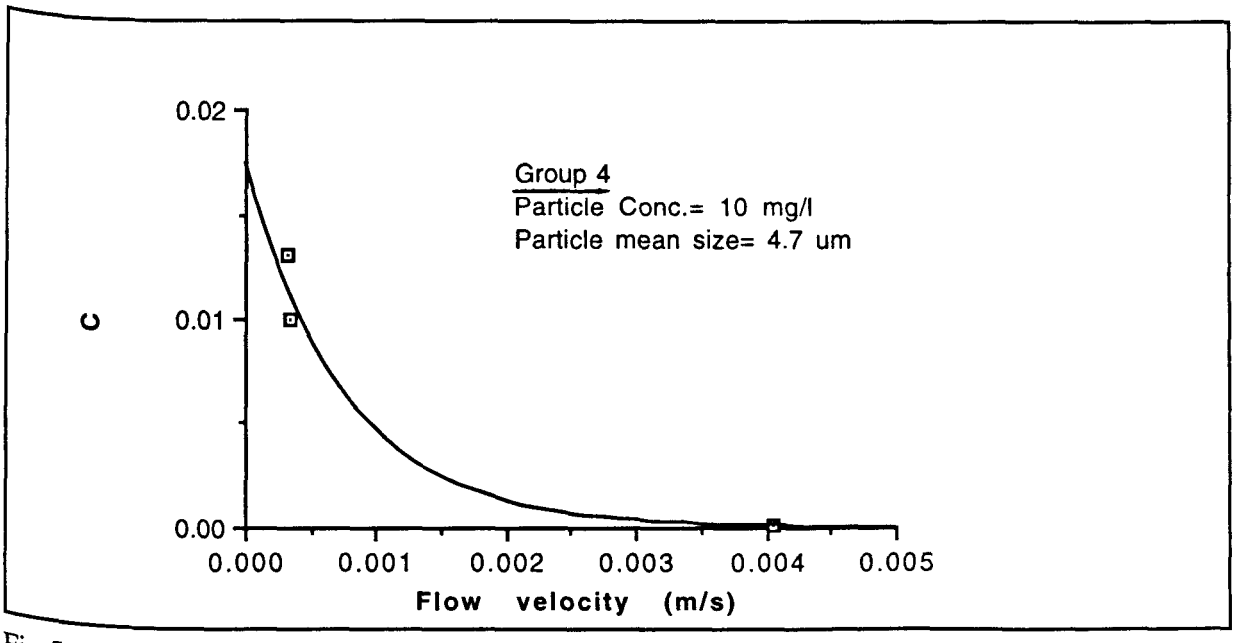

Fig.5.5b: C versus flow velocity for group 4 (Exps. 65, 53 and 79).

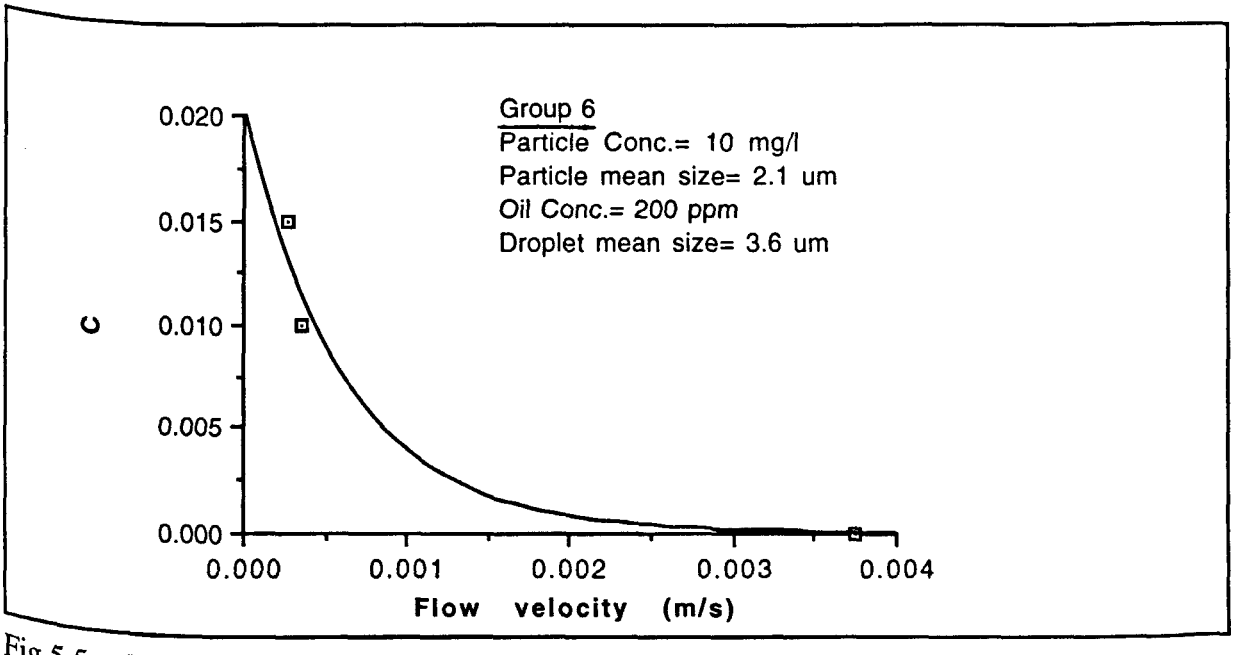

Fig.5.5c: C versus flow velocity for group 6 (Exps. 74, 39 and 57).

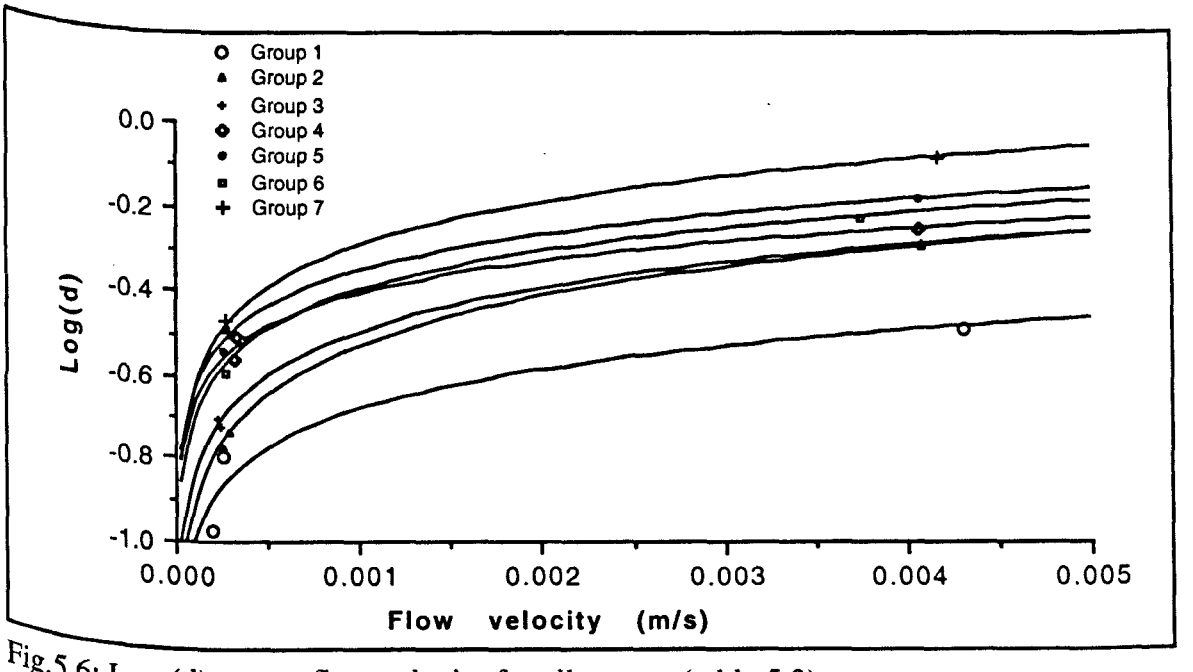

Fig.5.6: Log (d) versus flow velocity for all groups (table 5.3).

For group 7 (oil Conc.= 200 ppm and particle Conc. of 10 mg/l at particle mean size of 4.7 μm)

$$\text{Log}(d) = 0.7203 + 0.33817\ \text{Log}(v)$$

$$\text{Log}(C) = -2.005 - 1011.1\ v$$

The fitting was carried out with only three points, so the obtained fitting equations need further confirmation by carrying out more experiments in the future with varying flow velocities to obtain more values of d and C and eventually more points.

The d and C values can now be calculated, for a given injected fluid composition, at any flow velocity by using these equations.

d and C values were calculated at different flow velocities (flow rate per unit flow area) and at different injected fluid composition. The results can be seen in Table 5.4.

5.6.2 The change of pressure drop with time (Field case)

Two field cases were considered:

1) An injection well of a 7 inch bore diameter and 10 m formation thickness which makes the well bore flow area equal to 5.583 m^2. The initial matrix permeability was equal to 300 md.

2) An injection well with the same above condition but with a single vertical fracture. The average flow velocity through matrix near the fracture face was equal to total flow rate divided by the fracture face area.

When flow rate is constant, the pressure drop with time represents the injectivity ($q/\Delta p$) and the $\Delta pi/\Delta p$ represents the injectivity decline.

The following equation was used in calculating $\Delta p/\Delta pi$:

$$1/\text{injectivity} = \frac{\Delta p}{\Delta p_i} = \left(\frac{v*t}{\sqrt{K_m}}\right)^d \Big/ \left(\frac{v_i*t_i}{\sqrt{K_m}}\right)^d \qquad (5.11)$$

where Δp is the pressure drop through the invaded zone which is 3 cm as in the experiments. t_i is the initial time and t is the instantaneous time (at which the Δp was calculated). The viscosity was constant at 0.001 Pa.s.

Since the invaded zone is very small compared with the fracture length, then the flow in the invaded zone around the well bore will be assumed to be linear flow.

The flow velocity represents the effect of flow area at constant flow rate. At constant flow rate, the increase in flow area (such as the changing from linear injection to fracture injection) results in a lower flow velocity as the flow is distributed on a larger area which result in a lower matrix damage. So the effect of velocity is not for the velocity itself but as a result of distributing the dirty fluid flow on small or large flow area. For a large area, the dirty water is distributed on larger area (low flow velocity) which resulted in less matrix damage.

The matrix initial permeability represents the ability of the matrix pores to be bridged or/and blocked by a certain particle or/and droplet size (as $D_{pore} = \sqrt{K}$).

For constant flow velocity and matrix permeability, the change in pressure drop in the 3 cm invaded zone with time can be measured if the value of d and C are known.

Since d and C values were originally measured for the late injection time (the straight line section of the $\log(\Delta p/\Delta p_i)$ versus $\log(t)$ plot), then the Δp calculation will be started at an injection time of 8 hours for the fracture injection and at 3 hours for the linear injection. This time was assumed as the initial time, and the pressure drop at this initial time was the initial pressure drop Δp_i.

For an injection rate of 1037 m^3/day and fracture half length of 10 m, the average flow velocity through the rock matrix will be equal to 0.00003 m/s.

For the same injection rate, the flow velocity in the radial injection was 0.00215 m/s.

The values of d and C for the two cases can be found in Table 5.4.

Δp was calculated for the two injection systems (radial and fracture) at different injection times for different injected fluid composition. The $\Delta p/\Delta p_i$ was plotted versus injection time for radial injection (Fig.5.8) and for fracture injection (Fig.5.9).

The figures show that group 2 curve (10 mg/l 2.1 μm particles) for fracture injection become more close to group 1 curve (200 ppm 3.6 μm droplets) than it was in radial injection. Group 7 (10 mg/l 4.7 μm particles with 200 ppm oil) had a lower injectivity than groups 4 (10 mg/l 4.7 μm particles) and 5 (15 mg/l 4.7 μm particles) in radial injection, but in fracture injection it gave better injectivity than groups 4 and 5.

Group 6 (10 mg/l 2.1 μm particles with 200 ppm oil) gave much better results in fracture injection than groups 4, 5 and 7.

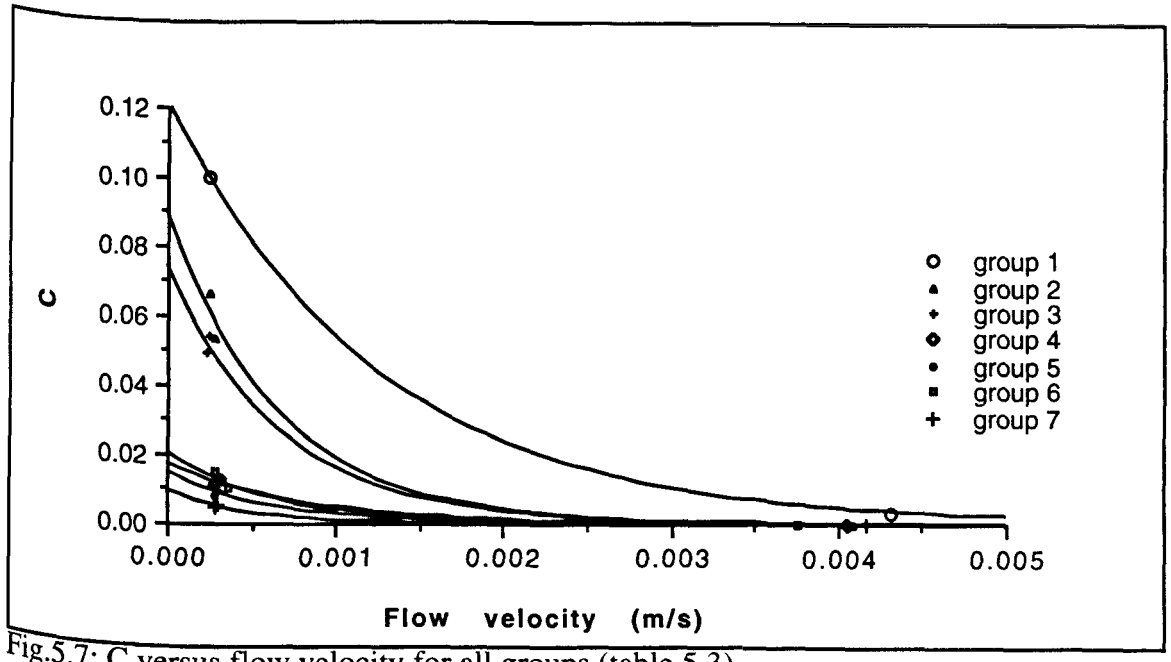

Fig.5.7: C versus flow velocity for all groups (table 5.3).

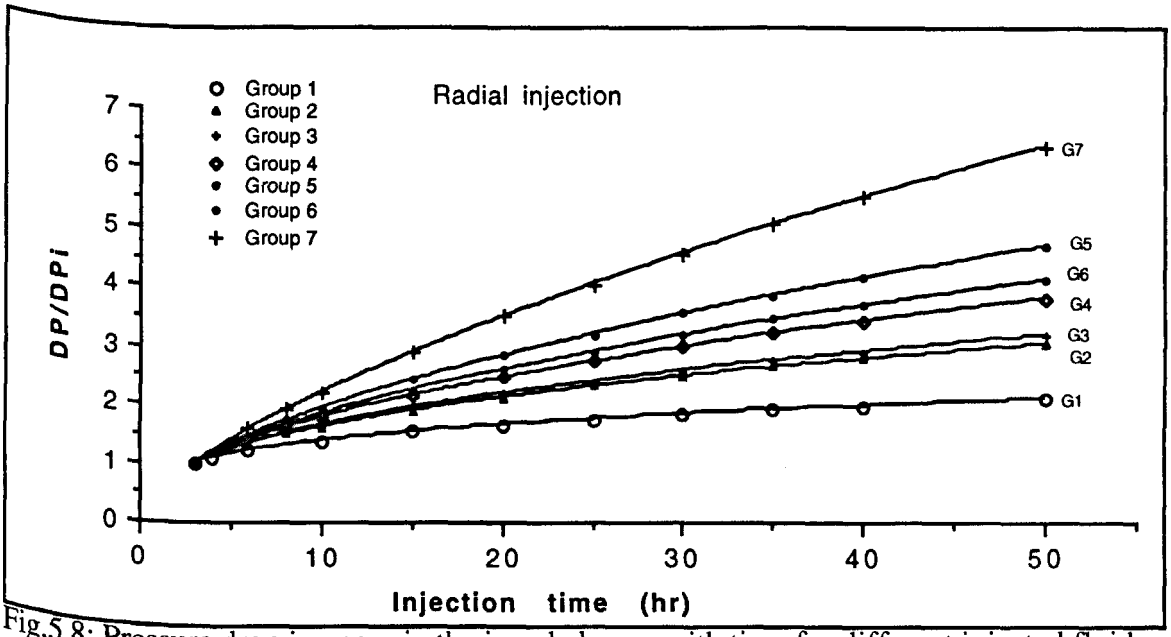

Fig.5.8: Pressure drop increase in the invaded zone with time for different injected fluids (table 5.5).

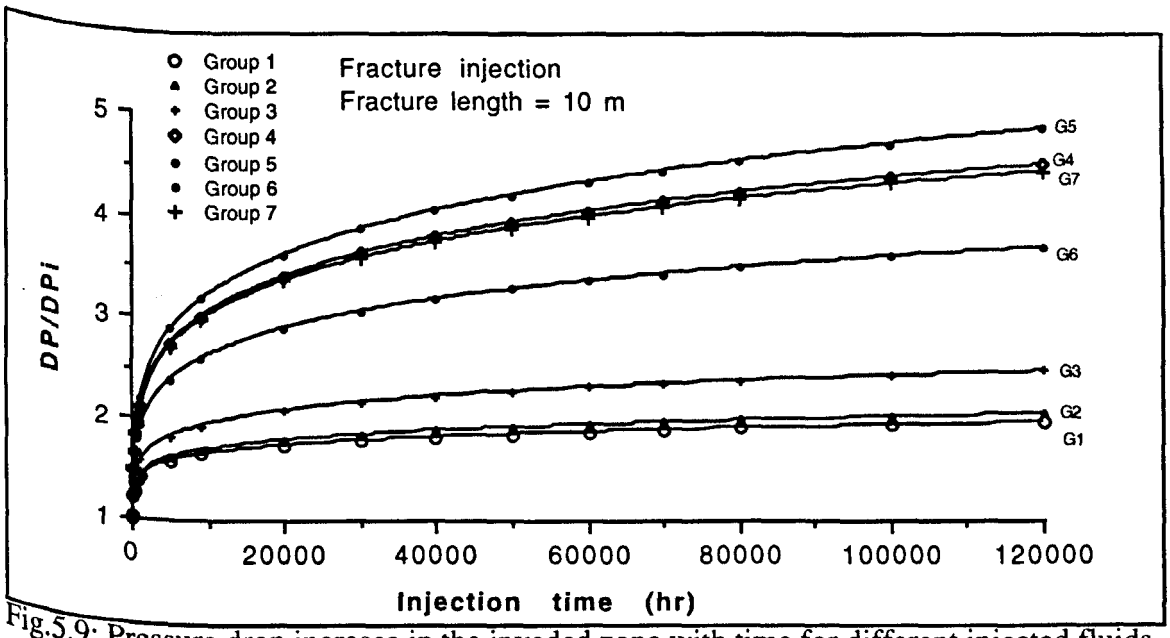

Fig.5.9: Pressure drop increase in the invaded zone with time for different injected fluids (table 5.6).

There was a large difference in injection time needed to increase the pressure drop to double its initial value (or reduce injectivity to the half HIT) between the two injection systems specially for group 1, 2 and 3. For the oil emulsion (without any particles) it takes 138,325 hours in the case of fracture injection for the pressure drop in the invaded zone to double whereas it takes only 42 hours in the case of radial injection (which is 3293 times higher in the case of fracture injection). This difference was 4526 times higher in the case of fracture injection of 10 mg/l 2.1 μm particle suspension (group 2) and reduced further to 764 for group 3 (15 mg/l 2.1 μm particle suspension). The lowest difference was recorded for the injection of 15 mg/l 4.7 μm particle suspension (group 5) which was 49 times. This showed again that the fracture injection is sensitive to the 4.7 μm particles. The HIT for the radial injection was between 8.5 and 17.5 hours, and 42 hours for the oil emulsion injection.

The HIT was calculated for different flow velocities and injected fluid compositions. The results are shown in Table 5.7 and Figures 5.10 and 5.11. In these figures the difference in HIT between the seven groups at different injected fluid composition is very clear. There is a sharp reduction in HIT when flow velocity increased from 0.00003 to 0.00006 m/s.

The sharpest reduction in HIT was for group 1 and 2 and the lowest reduction was for group 5. The reduction rate in HIT for flow velocity higher than 0.00006 m/s was less and started to level at a flow velocity higher than 0.00012 m/s.

Flow velocity lower than 0.00006 m/s (fracture injection) gave a very high HIT value compared with the HIT recorded for flow velocities higher than 0.00006 m/s.

5.7 Conclusions of dimensional analysis

Evaluating of the constants d and C in the equation $\log\left(\frac{\Delta p}{\Delta p_i}\right) = \log(C) + d\log\left(\frac{v*t}{\sqrt{K_m}}\right)$ gave:

(1) For oil emulsion injection experiments, the value of d was between 0.255 and 0.324 for the linear injection, between 0.15 and 0.18 for the short fracture injection (0.2 m) and around 0.11 for the long fracture injection (0.4 m). The value of C was between 0.0036 and 0.013 for the linear injection, between 0.05 and 0.11 for the short fracture injection and around 0.25 for the long fracture injection.

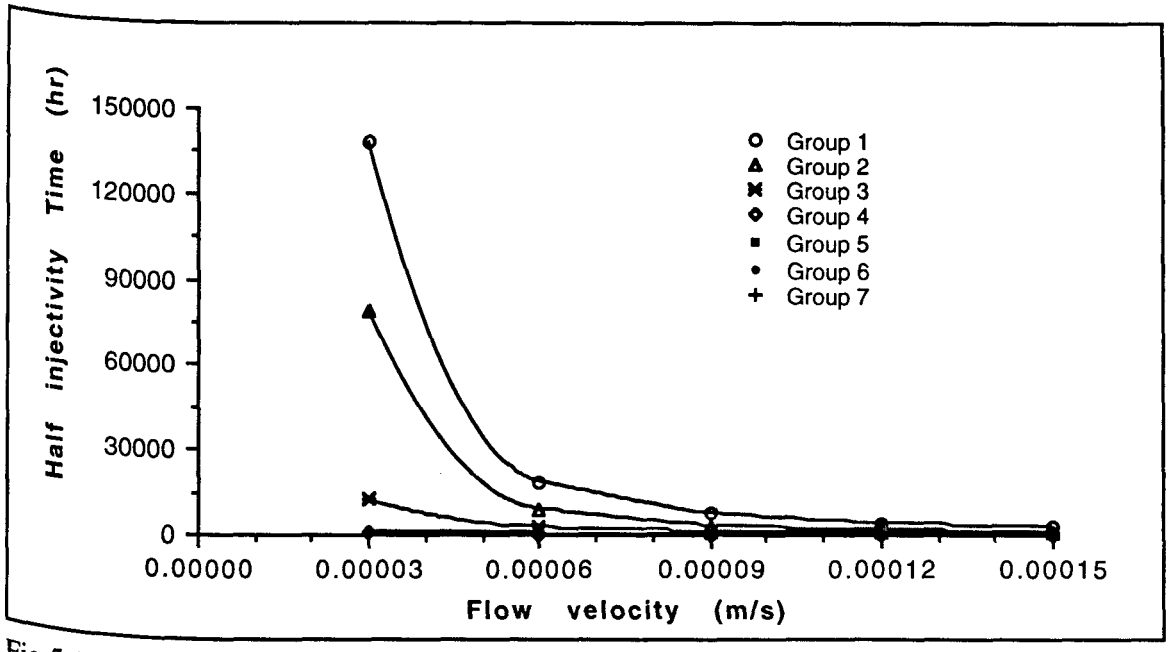

Fig.5.10: Half injectivity time (time needed to reduce $\Delta Pi/\Delta P$ to the half) versus flow velocity (table 5.7)

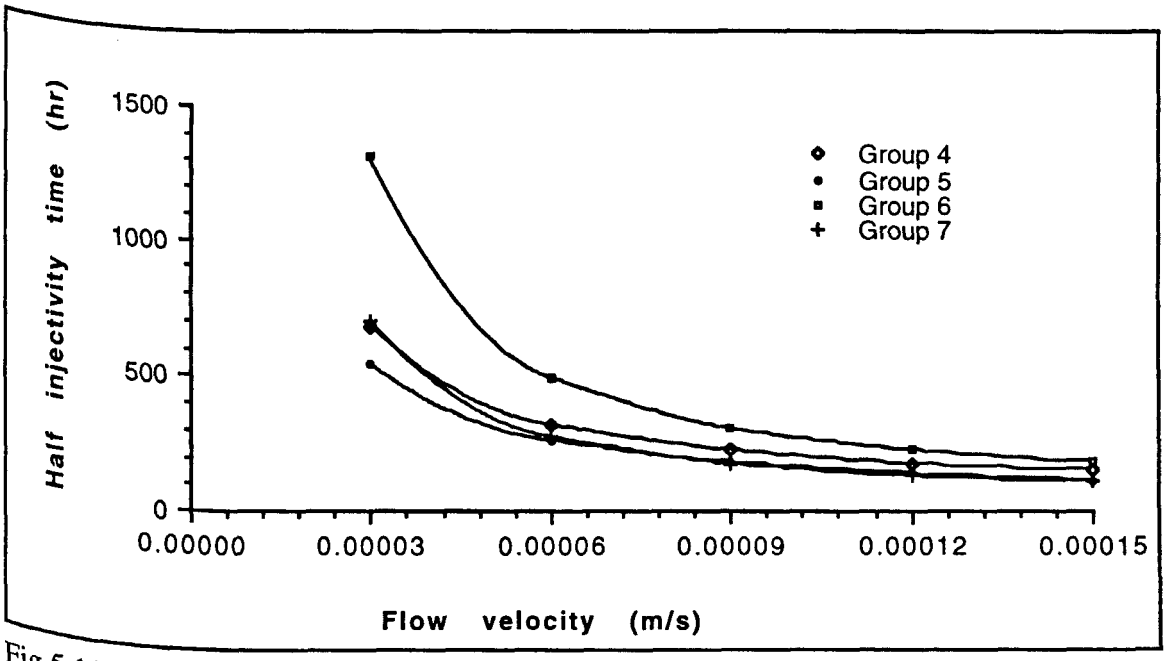

Fig.5.11: Half injectivity time versus flow velocity for groups 4, 5, 6 and 7 (table 5.7).

(2) For the 2.1 μm mean size particles suspension experiments, the value of d for the linear injection experiments was around 0.51 and for the fracture injection experiments was between 0.17 and 0.2. The value of C was around 0.000156 for the linear injection and between 0.05 to 0.067 for the fracture injection experiments.

(3) For the 4.7 μm mean size particle suspension experiments, linear injection experiments resulted in a d value around 0.6 whereas the fracture injection experiments gave a value between 0.27 and 0.32. The value of C was between 0.000013 to 0.00085 for the linear injection and between 0.0075 to 0.013 for the fracture injection.

(4) For the injection of fluid which contained 200 ppm oil and 10 mg/l of 2.1 μm mean size particles, the d value was 0.59 for the linear injection and between 0.26 to 0.3 for the fracture injection. The C value was 0.000043 for the linear injection and from 0.008 to 0.015 for the fracture injection.

(5) The linear injection of fluid which contains oil and 4.7 μm mean size particles gave a d value between 0.683 and 0.825, while the fracture injection resulted in d value which was nearly equal to the calculated d value when a 4.7 μm mean size particle suspension (without any oil) was injected, but with different values of C which is between 0.0000006 and 0.0000095.

(6) The worst half injectivity time calculated for the short fracture injection was 7 times higher than the half injectivity time of the linear injection and the worst half injectivity time calculated for the long fracture injection was 13.5 times higher than the half injectivity time of the linear injection.

(7) The value of C is very sensitive to the change in fluid composition. For oil emulsion injection C had a very high value compared with the C value for the particle suspensions or the simulated oily water. There is a huge difference between C values for linear injection and fracture injection.

(8) The plots of log(d) and log(C) versus flow velocity showed that at very low flow velocities, the d and c values are very sensitive to any change in flow velocity and at high flow velocities the values of d and C start to level.
Interpolation of the plotted data can be used for injected fluids other than those used in the experiments.

(9) These plots were best fitted as log-log equations, the d and C values can be calculated (for a given injected fluid composition) at any flow velocity by using these equations. The fitting was carried out with only three points, so the obtained fitting equations need further confirmation by carrying out more experiments in the future with varying flow velocities to obtain more values of d and C and eventually more points.

(10) The change in the injectivity with time was calculated for two field cases (unfractured and fractured well) with different injected fluid compositions The half injectivity time was calculated each time. There was a large difference in the half injectivity time between the two injection systems (unfractured and fractured well). For oil emulsion (without any particles) it takes 138325 hours in the case of fracture injection for the pressure drop (half injectivity time) in the invaded zone to double whereas it takes only 42 hours in the case of radial injection. Whereas for the case of 15 mg/l of 4.7 μm particle suspension, it was 540 hours for the fracture injection and 11 hours for the radial injection.

(11) There is a sharp reduction in the half injectivity time when flow velocity increased from 0.00003 to 0.00006 m/s. The reduction rate in half injectivity time for flow velocity higher than 0.00006 m/s was less and started to level at a flow velocity higher than 0.00012 m/s.

Experiment . no.	System type	Oil Conc. (ppm)	Particle Conc. (mg/l)	droplet mean size (um)	Particle mean size (um)	Initial permeability (md)	Flow velocity (m/s)	C	d	Half injectivity Time (hr)
Exp.61	Linear	100	None	3.5		234	0.00408	0.0131	0.255	12.1
Exp.63	Linear	100	None	6		269	0.0042	0.004	0.3205	9.1
Exp.62	Linear	200	None	3.5		230	0.00431	0.00359	0.324	9.2
Exp.59	Linear	None	10		2.1	240	0.00408	0.000163	0.506	4.0
Exp.60	Linear	None	15		2.1	248	0.00408	0.00015	0.514	3.6
Exp.65	Linear	None	10		4.7	493	0.00406	0.000086	0.558	4.1
Exp.64	Linear	None	15		4.7	488	0.00406	0.0000127	0.655	3.2
Exp.74	Linear	200	10	3.65	2.1	310	0.00375	0.000043	0.592	3.2
Exp.73	Linear	100	10	3.8	4.7	339	0.00396	0.0000038	0.734	2.6
Exp.71	Linear	100	10	6.2	4.7	340	0.00405	0.0000013	0.795	2.6
Exp.72	Linear	200	10	3.5	4.7	360	0.00417	0.0000006	0.825	3.2
Exp.70	Linear	100	15	3.6	4.7	500	0.00361	0.0000092	0.683	3.6
Exp.50	Short Frac.	100	None	3.5		251	0.00025	0.11	0.15	139.1
Exp.51	Short Frac.	100	None	5.7		281	0.00027	0.0495	0.1846	274.7
Exp52	Short Frac.	200	None	3.8		241	0.00025	0.09	0.16	142.6
Exp.56	Short Frac.	None	10		2.1	290	0.00028	0.0533	0.183	214.0
Exp.58	Short Frac.	None	15		2.1	228	0.00023	0.0497	0.1963	86.2
Exp.53	Short Frac.	None	10		4.7	473	0.00033	0.0079	0.307	39.0
Exp.49	Short Frac.	None	15		4.7	403	0.00024	0.0074	0.324	23.5
Exp.39	Short Frac.	200	10	3.6	2.1	344	0.00036	0.008	0.305	33.0
Exp.54	Short Frac.	100	10	3.6	4.7	325	0.00025	0.0219	0.25	44.1
Exp.46	Short Frac.	100	10	5.8	4.7	367	0.00025	0.00568	0.328	39.1
Exp.55	Short Frac.	200	10	3.8	4.7	348	0.00027	0.0045	0.34	37.2
Exp.47	Short Frac.	100	15	3.4	4.7	388	0.00028	0.00552	0.337	24.3
Exp.75	Long Frac.	200	None	3.8		207	0.0002	0.25	0.106	209.0
Exp.77	Long Frac.	None	10		2.1	252	0.00025	0.0665	0.168	351.0
Exp.76	Long Frac.	None	15		2.1	279	0.00024	0.054	0.188	135.0
Exp.79	Long Frac.	None	10		4.7	401	0.00031	0.0131	0.273	57.3
Exp.80	Long Frac.	None	15		4.7	387	0.00026	0.011	0.282	56.4
Exp.57	Long Frac.	200	10	3.5	2.1	286	0.00027	0.015	0.255	118.5
Exp.42	Long Frac.	200	10	3.4	4.7	317	0.00029	0.0059	0.32	43.5
Exp.82	Long Frac.	100	15	3.45	4.7	431	0.0003	0.0166	0.26	61.6

Table 5.1: The d, C and HIT value for the linear and fracture injection experiments.

Group number	d for linear injection	d for short fracture injection	d for long fracture injection	C for linear injection	C for short fracture injection	C for long fracture injection	HIT for linear injection (hr)	HIT for short fracture injection (hr)	HIT for long fracture injection (hr)
1	0.255	0.15		0.0131	0.11		12.06	139.05	
2	0.3205	0.1846	0.106	0.004	0.0495	0.25	9.05	274.71	209
3	0.324	0.16		0.00359	0.09		9.23	142.6	
4	0.506	0.183	0.168	0.000163	0.0533	0.0665	4.02	214	351
5	0.514	0.1963	0.188	0.00015	0.0497	0.054	3.6	86.21	135
6	0.558	0.307	0.273	0.000086	0.0079	0.0131	4.13	39	57.3
7	0.655	0.324	0.282	0.0000127	0.0074	0.011	3.2	23.5	56.4
8	0.592	0.305	0.255	0.000043	0.008	0.015	3.2	32.94	118.5
9	0.795	0.328		0.0000013	0.00568		2.55	39.12	
10	0.825	0.34	0.32	0.0000006	0.0045	0.0059	3.22	38.7	37
11	0.683	0.337	0.26	0.0000092	0.00552	0.0166	3.57	24.3	61.6

Table 5.2: The d, C and HIT value for 11 different groups points.

Exps. group 1	Droplet mean size= 3.7 um	Oil Conc.= 200 ppm	No solids	
Exp. no.	System type	Flow velocity (m/s)	C	d
Exp.62	LI	0.00431	0.00359	0.324
Exp52	SFI	0.00025	0.09	0.16
Exp.75	LFI	0.0002	0.25	0.106
Exps. group 2	particle mean size= 2.1 um	Particles Conc.= 10 mg/l	NO oil	
Exp. no.	System type	Flow velocity (m/s)	C	d
Exp.59	LI	0.00408	0.000163	0.506
Exp.56	SFI	0.00028	0.0533	0.183
Exp.77	LFI	0.00025	0.0665	0.168
Exps. group 3	particle mean size= 2.1 um	Particles Conc.= 15 mg/l	NO oil	
Exp. no.	System type	Flow velocity (m/s)	C	d
Exp.60	LI	0.00408	0.00015	0.514
Exp.58	SFI	0.00023	0.0497	0.1963
Exp.76	LFI	0.00024	0.054	0.188
Exps. group 4	Particle mean size= 4.7 um	Particles Conc.= 10 mg/l	No oil	
Exp. no.	System type	Flow velocity (m/s)	C	d
Exp.65	LI	0.00406	0.000086	0.558
Exp.53	SFI	0.00033	0.0079	0.307
Exp.79	LFI	0.00031	0.0131	0.273
Exps. group 5	Particle mean size= 4.7 um	Particles Conc.= 15 mg/l	No oil	
Exp. no.	System type	Flow velocity (m/s)	C	d
Exp.64	LI	0.00406	0.0000127	0.655
Exp.49	SFI	0.00024	0.0074	0.324
Exp.80	LFI	0.00026	0.011	0.285
Exps. group 6	Particle mean size= 2.1 um	Particle Conc.= 10 mg/l	Oil Con.= 200 ppm	
Exp. no.	System type	Flow velocity (m/s)	C	d
Exp.74	LI	0.00375	0.000043	0.592
Exp.39	SFI	0.00036	0.008	0.305
Exp.57	LFI	0.00027	0.015	0.255
Exps. group 7	Particle mean size = 4.7 um	Particles Conc.= 10 mg/l	Oil Conc.= 200 ppm	
Exp. no.	System type	Flow velocity (m/s)	C	d
Exp.72	LI	0.00417	0.0000006	0.825
Exp.55	SFI	0.00027	0.0045	0.34
Exp.42	LFI	0.00029	0.0059	0.32

Table 5.3: The values of d and C for different flow velocity and fluid compositions.

	Group1		Group 2		Group 3		Group 4		Group 5		Group 6		Group 7	
v	d	C	d	C	d	C	d	C	d	C	d	C	d	C
0.00003	0.069	0.1198	0.075	0.0857	0.095	0.0707	0.157	0.0167	0.164	0.0141	0.136	0.0196	0.155	0.00922
0.00006	0.086	0.1169	0.099	0.0818	0.120	0.0675	0.188	0.0161	0.200	0.0134	0.168	0.0187	0.196	0.00860
0.00009	0.097	0.1140	0.115	0.0781	0.138	0.0645	0.208	0.0155	0.224	0.0127	0.190	0.0178	0.225	0.00802
0.00012	0.106	0.1112	0.129	0.0745	0.152	0.0616	0.224	0.0149	0.243	0.0121	0.208	0.0169	0.248	0.00748
0.00015	0.114	0.1085	0.141	0.0712	0.165	0.0589	0.238	0.0143	0.259	0.0115	0.222	0.0161	0.267	0.00697
0.00215	0.264	0.0211	0.395	0.00323	0.412	0.00282	0.474	0.00105	0.548	0.000353	0.502	0.000597	0.658	0.000066
0.0043	0.328	0.00362	0.517	0.00016	0.523	0.00015	0.567	0.00009	0.666	0.000013	0.592	0.000043	0.832	0.000001

Table 5.4: The calculated values of d and C at different flow velocities.

	DP/DPi						
Injection time (hr)	Group 1	Group 2	Group 3	Group 4	Group 5	Group 6	Group 7
3.00	1.00	1.00	1.00	1.00	1.00	1.00	1.00
4.00	1.08						
6.00	1.20	1.31	1.33	1.39	1.46	1.42	1.58
8.00		1.47	1.50	1.59	1.71	1.64	1.91
10.00	1.37	1.61	1.64	1.77	1.93	1.83	2.21
15.00	1.53	1.89	1.94	2.14	2.42	2.24	2.88
20.00	1.65	2.12	2.18	2.46	2.83	2.59	3.48
25.00	1.75	2.31	2.40	2.73	3.20	2.90	4.04
30.00	1.84	2.48	2.58	2.98	3.53	3.18	4.55
35.00	1.91	2.64	2.75	3.20	3.84	3.43	5.04
40.00	1.98	2.78	2.91	3.41	4.13	3.67	5.50
50.00	2.10	3.04	3.19	3.79	4.67	4.11	6.37
60.00	2.20	3.27	3.44	4.14	5.16	4.50	7.18
70.00	2.29	3.47	3.66	4.45	5.62	4.86	7.95

Table 5.5: The ΔP/ΔPi change with time for Radial injection at flow velocity of 0.00215 m/s.

	DP/DPi						
Injection time (hr)	Group 1	Group 2	Group 3	Group 4	Group 5	Group 6	Group 7
3							
6	1.00						
8		1.00	1.00	1.00	1.00	1.00	1.00
10	1.04	1.02	1.02	1.04	1.04	1.03	1.04
100	1.21	1.21	1.27	1.49	1.51	1.41	1.48
200	1.27	1.27	1.36	1.66	1.70	1.55	1.65
400	1.34	1.34	1.45	1.85	1.90	1.70	1.83
600	1.37	1.38	1.50	1.97	2.03	1.80	1.95
1000	1.42	1.44	1.58	2.13	2.21	1.93	2.11
5000	1.59	1.62	1.84	2.74	2.88	2.40	2.71
9000	1.66	1.70	1.94	3.01	3.17	2.60	2.97
20000	1.75	1.80	2.10	3.41	3.62	2.90	3.37
30000	1.80	1.86	2.18	3.63	3.87	3.06	3.59
40000	1.84	1.90	2.24	3.80	4.06	3.18	3.75
50000	1.86	1.93	2.28	3.94	4.21	3.28	3.88
60000	1.89	1.96	2.32	4.05	4.34	3.37	3.99
70000	1.91	1.98	2.36	4.15	4.45	3.44	4.09
80000	1.93	2.00	2.39	4.24	4.55	3.50	4.18
100000	1.96	2.04	2.44	4.39	4.72	3.61	4.32
120000	1.98	2.06	2.48	4.51	4.86	3.70	4.45
130000	1.99	2.08					
139000	2.00						

Table 5.6: The ΔP/ΔPi change with time for Fracture injection at flow velocity of 0.00003 m/s.

	Half injectivity time (hr)						
Flow velocity (m/s)	Group 1	Group 2	Group 3	Group 4	Group 5	Group 6	Group 7
0.00003	138325	79200	12225	680	540	1310	700
0.00006	18990	9060	2620	320	260	495	275
0.00009	7625	3280	1215	225	180	305	175
0.00012	4055	1730	755	175	140	225	130
0.00015	2650	1106	540	150	115	180	108
0.00215	42	17.5	16	13	11	12	8.5
0.0043	25	11.5	11	10	8.5	9.7	7

Table 5.7: The half injectivity time for different injection flow velocities.

CHAPTER SIX
APPLICATION OF THE DAMAGE MODELS TO THE EXPERIMENTAL RESULTS

6.1 Introduction

The main differences between the injection along fracture and linear or radial injection can be summarised as follows:

(a) The fracture had a very large flow area compared with the linear or radial injection geometries which made the flow velocity through the fracture face into the rock matrix (for constant flow rate) very low compared with the linear or radial flow velocity. The large flow area of the fracture face improved the injectivity and maintained it for a longer period (for the case of produced water injection) than the linear or radial injection does. But the very low flow velocity through the rock matrix, in the case of fracture injection (as a result of larger flow area), especially through the rock matrix at the fracture end, had an opposite effect on the injectivity of produced water. The capture probability of solid particles and oil droplets would be higher in the case of very low flow velocity (especially for lower than 0.035 cm/s, which is close to the flow velocity through matrix in fracture injection). Kumar (1988) and Van Velzen (1992) demonstrated the effect of flow velocity through rock matrix on the matrix impairment.

(b) At a constant flow rate, the initial injection pressure in the case of fracture injection (due to the large flow area) is much lower than the initial injection pressure for the case of linear or radial injection. The pressure in the linear and radial injection is uniformly distributed on the inflow face. Whereas in the fracture injection, the pressure on the fracture face is maximum at the fracture inlet and decreases along the fracture to its minimum value at the fracture end (this difference is equal to the pressure drop along the fracture).

(c) The very high flow velocity along the fracture delayed the accumulation of external filter cake due the shear force created by this high flow velocity. The accumulation of the external filter cake started at the fracture end where the flow velocity along the fracture is minimum. Even after the external cake was formed, it can be eroded when the flow velocity along the fracture became high enough (as more flow is directed along the fracture and as the flow path along the fracture become smaller due to the presence of external cake) to do so.

6.2 The objectives of this chapter

The objective was to compare the experimental results generated by this thesis with the predictions of formation damage models reported in the literature.

The linear injection formation damage models were applied on the linear and the fracture injection experiments to investigate the change of injectivity with time as matrix damage took place and to measure the difference in the injectivity (due to matrix damage) between the two injection systems.

The geometric skins to convert from linear to radial system and to convert from radial to fracture system were defined and calculated. Also the skin to account for the difference in the matrix damage extent between the radial and fracture systems was defined then measured and calculated.

6.3 Formation damage models

In this chapter the linear injection formation damage models will be applied to the fracture injection experiments, but before that some assumptions (concerning the fracture injection variables) must be made:

(a) The flow through the fracture face into the rock matrix was assumed to be linear.

(b) The pressure is the same all over the fracture face and equal to the pressure at the fracture inlet minus half the pressure drop along the fracture (the pressure was averaged to be equal to the pressure at half distance along the fracture).

(c) The flow velocity through the matrix is equal to the total side flow rate divided by the total fracture face area.

Most of the linear or radial injection formation damage models derivation in the literature started with three basic equations which are:

(1) Darcy's law was applied by assuming that the rock matrix consisted of two separate zones, an invaded zone with a damaged permeability and a clean undamaged zone with a permeability equal to the initial matrix permeability. The Darcy's law was derived for two separate zones in series.

(2) The deep bed filtration equation which defined the deep bed filtration process whereby particles and/or droplets penetrating the pores of a porous medium are trapped, thereby

increasing the resistance to injected fluid flow (the degree of particle and/or droplet filtration and removal from the flowing stream, as the particles and/or droplets are captured within the rock matrix pores). Deep bed filtration was described by the following basic equation [95]:

$$\frac{dC}{dL} = -\lambda C_o \exp(-\lambda L) \qquad (6.1)$$

where C_0 is the influent concentration.

λ is the filtration coefficient.

L is the length of porous medium.

(3) The material balance equation between the influent and effluent solid particle and/or oil droplet concentration. This equation calculated the reduction in matrix porosity due to particle and/or droplets accumulation within the rock matrix pores. This reduction in the porosity decreased the matrix permeability by a certain factor.

The equation was derived by the author as follows:

Initial pore volume - accumulated particles volume = Final pore volume

$$\phi_i AL - \frac{(C_i - C)V}{\rho_{os}} = \phi_f AL \qquad (6.2)$$

where C_i is the influent concentration

C is the effluent concentration

V is the cumulative injection volume

A is the inflow area

L is the porous medium length

AL is the bulk volume of the rock matrix

$\phi_i and \phi_f$ are the initial and final porous medium porosity.

ρ_{os} is the particle or droplet density or the particle and droplet equivalent density

Rearranging eqs. 6.2, multiplying and dividing by ϕ_i results in:

$$\phi_f = \phi_i - \frac{(C_i - C)V\phi_i}{\rho_{os} AL\phi_i}$$

As the deposited particles and/or droplets volume is very small compared with the porous pore volume, then

$$\phi_f = \phi_i - \frac{(C_i - C)\phi_i N_{PV}}{\rho_{os}} \qquad (6.3)$$

where N_{PV} is the number of pore volume injected.

Two linear damage models will be applied to the fracture and linear injection experiments which were carried out in the present study.

(1) Eylander (1988) model was modified by Zhang (1994) to include the case of oil and solids combined damaging effect by using the concept of equivalent oil/solids concentration and the weight mean density of oil and solids. The equivalent oil/solids concentration is the concentration of oil and solids combined together. This model uses Darcy's law and the material balance equation between the solids in the injection water and the solids deposited within the porous medium. It was assumed that the injection fluid is Newtonian and incompressible and the flow is laminar flow. Also it is assumed that the volume of injected fluid is equal to the filtrate fluid volume (as the particle and/or droplets volume is negligible compared with the injection fluid volume).

The model consisted of a severe impaired zone of permeability K_d and a clean matrix zone of a permeability equal to the initial permeability K_i. The total pressure drop is equal to the sum of the pressure drop through the impaired zone and the pressure drop in the clean zone.

The relation between the impaired zone length and the injected fluid volume was obtained by making a material balance between the solids in the injection water and the solids deposited within the porous medium.

The final equation derived by Zhang (1994) was:

$$\frac{\Delta p}{v} = \theta \mu L N_{PV} + \mu \frac{L}{K_i} \qquad (6.4)$$

where v is the flow velocity

K_i is the initial matrix permeability

L is the total porous medium length

Δp is the total pressure drop through the whole porous medium.

μ is the injected fluid viscosity

N_{PV} is the number of pore volume injected

$$\theta = \left(\frac{1}{K_d} - \frac{1}{K_i}\right)\left(\frac{C_{os}\rho_l}{(1-\phi_d)\rho_{os} + C_{os}\phi_d(\rho_{os} - \rho_l)}\right)$$

where K_d is the impaired zone permeability

$\phi_i and \phi_d$ are the initial matrix porosity and the impaired zone porosity

C_{os} is the equivalent influent concentration of particles and droplets

$\rho_l and \rho_{os}$ are the injected fluid density and the weight mean density of oil and solids

Eq. 6.4 was modified by the author to be suitable for experimental applications as follows:

From Darcy's law

$$\frac{\Delta p}{v} = \frac{\mu L}{K} \qquad (6.5)$$

By substituting Eq. 6.5 into Eq. 6.4

$$\frac{\mu L}{K} = \theta \mu L N_{PV} + \mu \frac{L}{K_i}$$

Or

$$\frac{1}{K} = \theta N_{PV} + \frac{1}{K_i} \qquad (6.6)$$

where K is the total permeability of the impaired and the clean zones.

Rearranging Equ. 6.6

$$\frac{K_i}{K} = 1 + \theta K_i N_{PV} \qquad (6.7)$$

K_i / K is equal to the injectivity inverse $\frac{1}{\alpha}$

$$N_{PV} = \frac{Q}{AL\phi_i} t \qquad (6.8)$$

where Q is the injection flow rate through the rock matrix

t is the injection time.

Substituting Eq. 6.8 into Eq. 6.7, then:

$$\frac{1}{\alpha} = \frac{K_i}{K} = 1 + \theta \frac{K_i Q}{AL\phi_i} t \qquad (6.9)$$

Which is the injectivity inverse function of injection time.

Only the effect of the particle and/or droplet concentration was included in Eylander / Zhang model, while the particle and/or droplet sizes effect was not considered in their models. To include the particle and/or droplet sizes effect, the deep filtration equation (which contains the filtration coefficient) must be included in the formulation of the model.

(2) Van Velzen's[95] model is a mathematical model that described the reduction in injectivity from internal filter cake formation. The model used Darcy's law for linear flow to define

pressure drop through the invaded and the clean matrix. Then the material balance equation was used to obtain the relation between the change in the invaded zone length and the change in particle and/or droplet concentration with distance. Then the deep filtration equation was used to define the change of concentration with distance as a function of volume filter coefficient. So the particle and/or droplet concentration and size effects were included in this model. The flow is assumed to be laminar and the injection fluid is assumed to be Newtonian and incompressible.

The Final equation for linear injection case was:

$$\left(\frac{1}{\alpha}-1\right)L=\frac{\delta C_o}{A\phi_i}\left[1-\exp(-\frac{\lambda AL}{Q_o})\right]V \qquad (6.10)$$

where Q_o is the initial injection rate.

δ is the damage factor $=\left(\frac{K_i}{K_d}-1\right)\frac{1}{(1-\phi_d)}$ (6.11)

λ is the volume filter coefficient

C_o is the volume fraction of solids in suspension at injection surface.

Eq. 6.10 was rearranged by the author to be suitable for experimental applications as follows:

$$\frac{1}{\alpha}=1+\frac{\delta C_o V}{AL\phi_i}\left[1-\exp(-\frac{\lambda AL}{Q_o})\right]$$

The equation was re-written by the author in the form of injectivity inverse as a function of injection time and the damage factor was substituted by its value from Eq. 6.11.

$$\frac{1}{\alpha}=\frac{K_i}{K}=1+\frac{C_oQ}{AL\phi_i}\left(\frac{K_i}{K_d}-1\right)\left(\frac{1}{1-\phi_d}\right)\left[1-\exp(-\frac{\lambda AL}{Q_o})\right]t$$

Multiplying and dividing the left hand side of the equation with K_i

$$\frac{K_i}{K}=1+\frac{K_iQ}{AL\phi_i}\left(\frac{1}{K_d}-\frac{1}{K_i}\right)\left(\frac{C_o}{1-\phi_d}\right)\left[1-\exp(-\frac{\lambda AL}{Q_o})\right]t$$

Or

$$\frac{K_i}{K}=1+\beta\frac{K_iQ}{AL\phi_i}t \qquad (6.12)$$

where

$$\beta=\left(\frac{1}{K_d}-\frac{1}{K_i}\right)\left(\frac{C_o}{1-\phi_d}\right)\left[1-\exp(-\frac{\lambda AL}{Q_o})\right]$$

Eq. 6.9 had the same form as Eq. 6.12, but the factor θ has a physical meaning which is different from the physical meaning of the factor β.

The increase in θ or β value (for a constant matrix permeability, matrix porosity, injection rate and flow path length) indicated a higher permeability damage.

Before applying the experimental work on these equations to investigate the effect of the different factors on the permeability alteration, the dominant capture mechanism for the fracture and the linear injection experiments will be specified.

6.4 The capture mechanisms in fracture and linear injection experiments

Wojtanowicz *et al.* (1987) summarise the particle capture mechanisms into three mechanisms (Fig.1.67) depending on the plot of K/K_i versus pore volume injected. Gradual pore blocking which is associated with a continuous capture of fines at the rock walls due to retention forces and the rate of capture is directly proportional to the solids concentration in the flow stream. Single pore blocking (screening) which occurs when single particles of size close to the pore size blocks an individual pores. Internal or external cake formation (straining) caused by particles greater than pore size and/or by high solids concentration.

Pang *et al.* (1994) collected and analysed water core flow test data available in the literature. He re-plotted the data as the inverse of the injectivity decline (K_i/K) versus pore volume injected. A straight line was observed when an incompressible external filter cake (Fig.1.37) or a pure internal filter cake (Fig.1.38) was formed. Curves with increasing slope were obtained when compressible external cake (Fig.1.39) or internal filter cake (Fig.1.40) are formed. In some experiments with no external filter cake formation the slope of the curve decreases with time as in Figure 1.41 (smaller injected particle size).

Depending on these observations the dominant capture mechanism within the rock matrix in the fracture and linear injection experiments (which were carried out in the present study) can be detected.

First the experimentally measured K/K_i and K_i/K values were plotted against pore volume injected or time for the fracture and linear injection experiments.

When the particle concentration was less than 15mg/l, no external cake was formed on the inflow face in all the experiments. This observation excluded the probability of external cake formation from the expected capture mechanisms; this left the internal blocking

and the internal filter cake formation as the only expected mechanisms which would reduce the permeability of the rock matrix.

Depending on Wojtanowicz and Pang observations, the capture mechanisms of the linear and the fracture injection experiments were examined and defined by the author. The linear injection plots of K/Ki versus pore volume injected (Fig.6.1) indicated a clear internal cake formation or straining mechanism for the 15 mg/l of a 2.1 μm particle mean size suspension and for the injection fluid which contained 100 mg/l oil of 5.8 μm droplet mean size and 10 mg/l solids of 4.7 μm particle mean size. For the case of 200 mg/l of 3.8 μm mean size droplet oil emulsion and for the case of injection fluid which contained 100 mg/l oil of 3.8 μm droplet mean size and 10 mg/l solids of 2.1 μm particle mean size, the plots show less straining mechanism which can be said to be in-between a clear straining mechanism and gradual pore blocking mechanism.

The linear injection plots of Ki/K versus pore volume injected (Fig.6.2) indicated a low resistance internal filter cake mechanism similar to that in figure 1.38 (after Pang et al.) when the injection fluid was 200 mg/l of 3.8 μm droplet mean size oil emulsion or when the injection fluid contains a 100 mg/l oil of 3.8 μm droplet mean size and 10 mg/l solids of 2.1 μm particle mean size. When the injection fluid was a 15 mg/l of 2.1 μm particle mean size suspension and when the injection fluid contains 100 mg/l oil of 5.8 μm droplet mean size and 10 mg/l solids of 4.7 μm particle mean size, the plots showed an internal cake mechanism similar to that in figure 1.40 (after Pang et al.)

The fracture injection plots of K/Ki versus pore volume injected (Figs.6.3 and 6.4) indicated a gradual pore blocking mechanism in all the fracture injection experiments (depending on Wojtanowicz observations) with some injected fluids causing higher blocking than the others, such as in the case of injected fluid which contains a 4.7 μm mean size particles.

The fracture injection plots of Ki/K (injectivity inverse) versus pore volume injected (Figs.6.5 and 6.6) for all the fracture injection experiments indicated a permeable internal filter cake (depending on Pang observations) especially in the case of long fracture injection experiments.

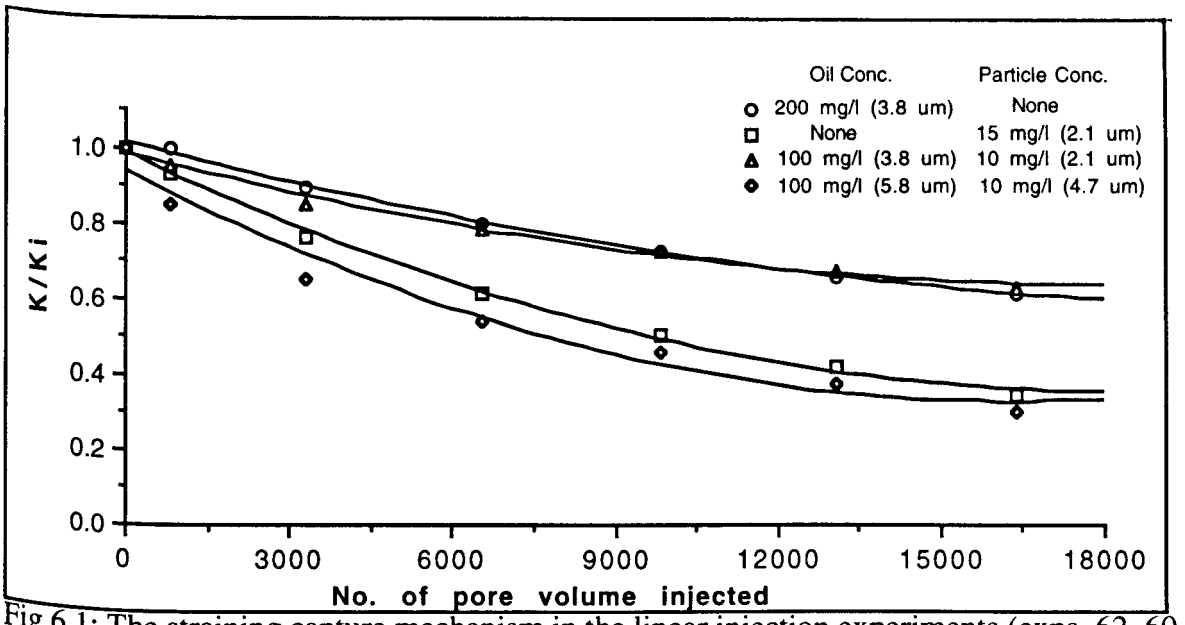

Fig.6.1: The straining capture mechanism in the linear injection experiments (exps. 62, 60, 69, and 73).

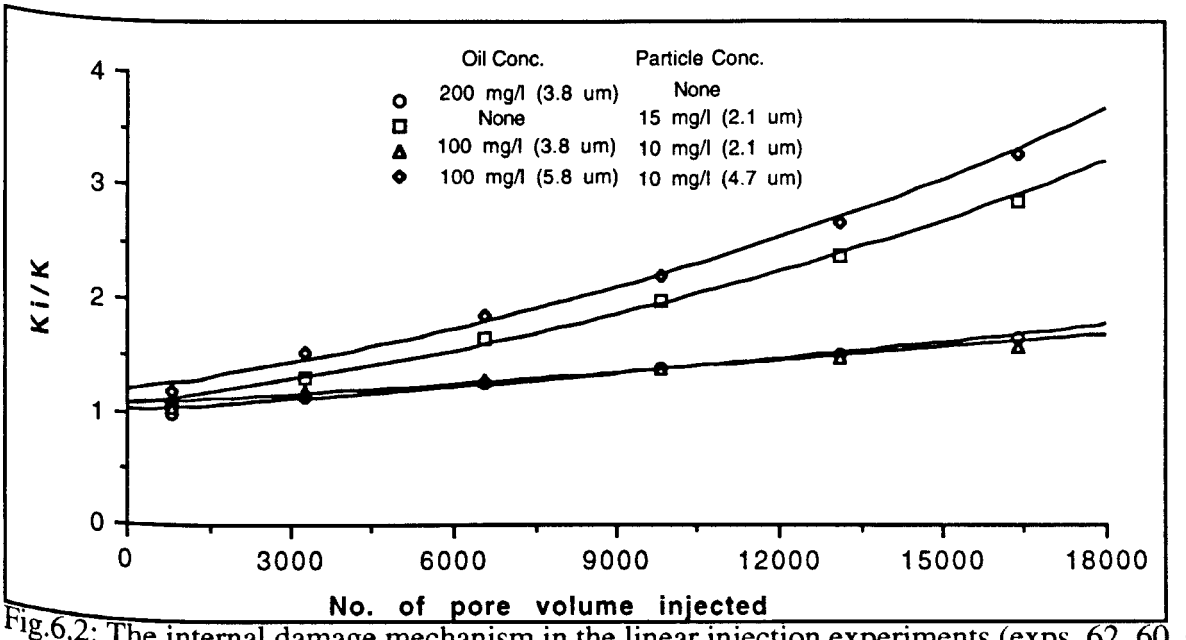

Fig.6.2: The internal damage mechanism in the linear injection experiments (exps. 62, 60, 69, and 73)..

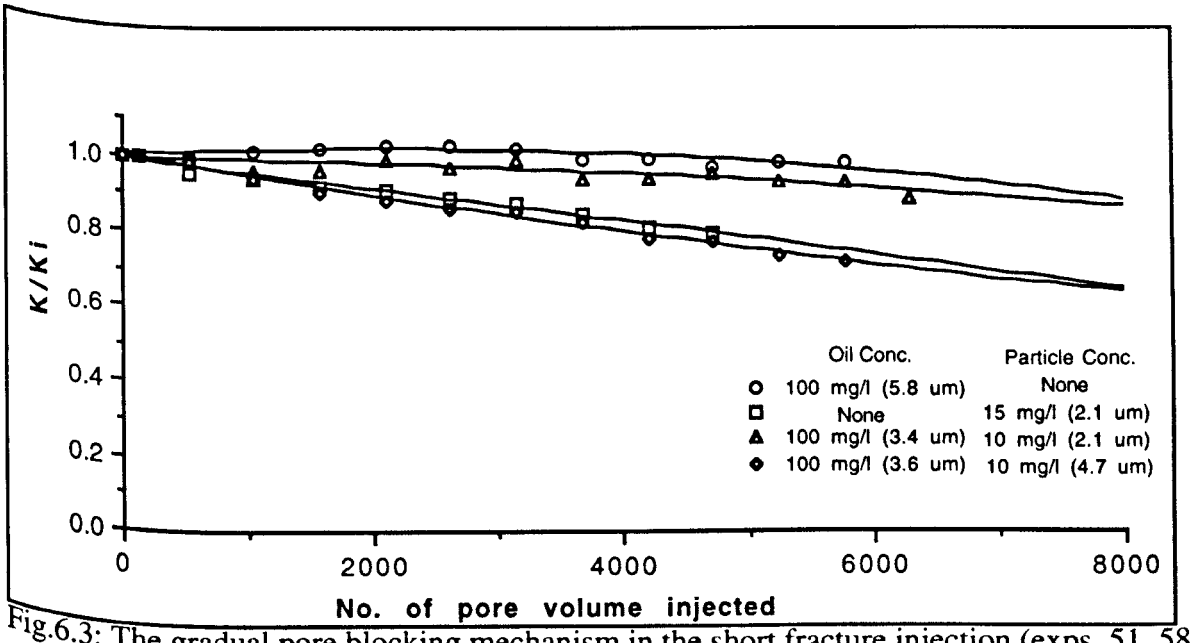

Fig.6.3: The gradual pore blocking mechanism in the short fracture injection (exps. 51, 58, 25, and 54).

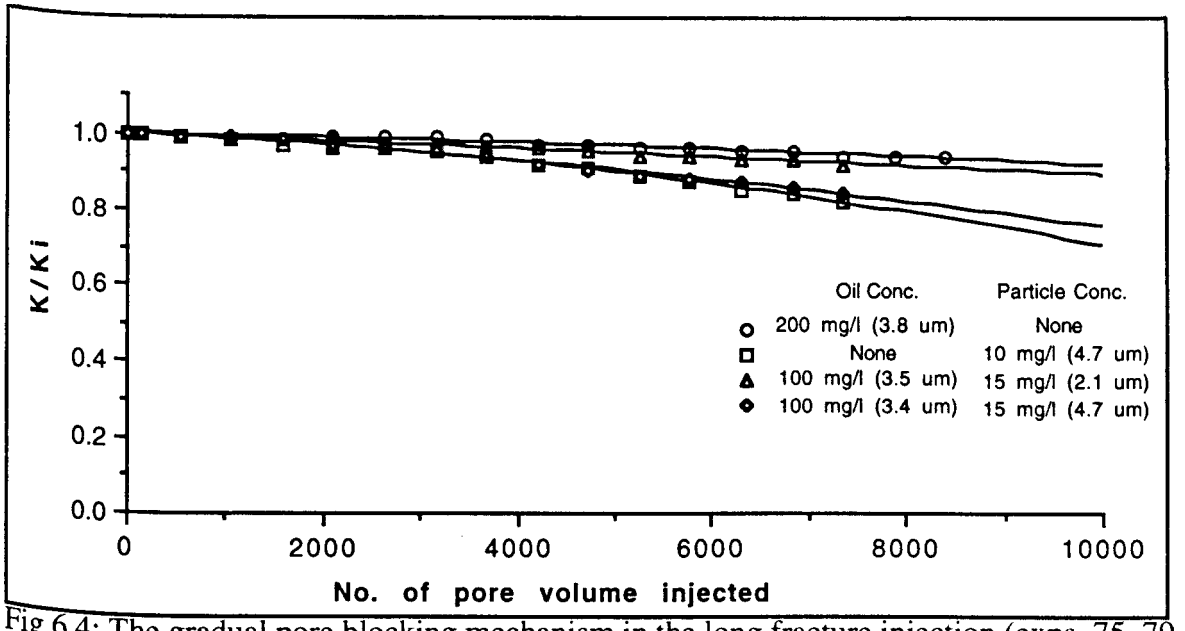

Fig.6.4: The gradual pore blocking mechanism in the long fracture injection (exps. 75, 79, 81, and 82).

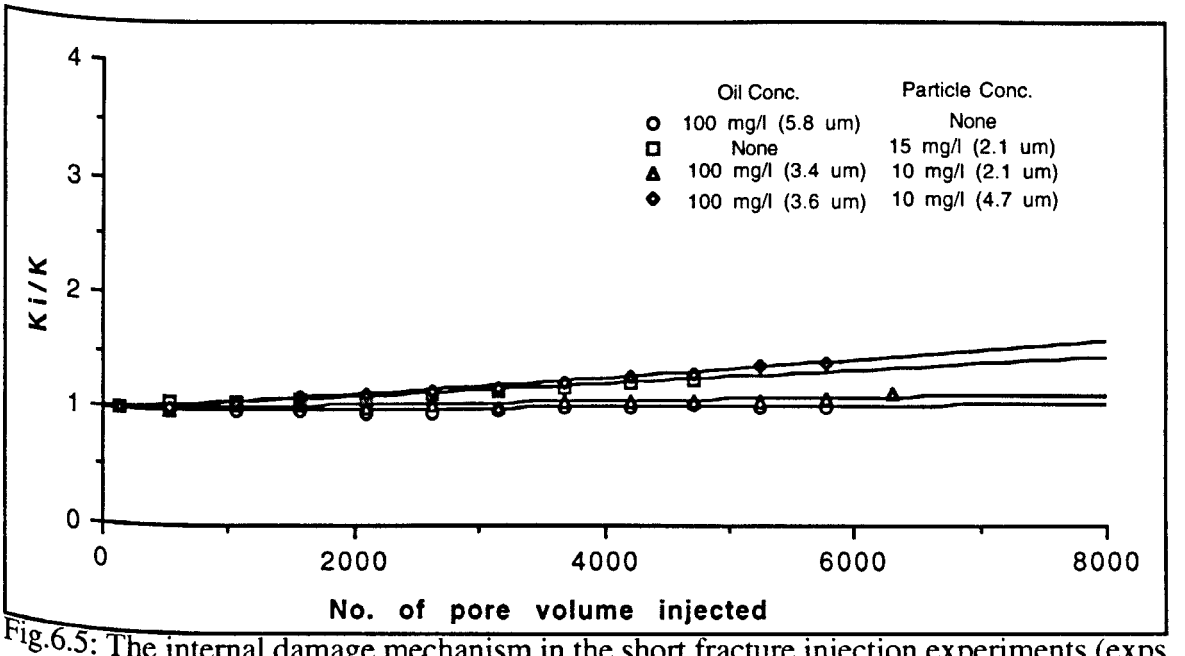

Fig.6.5: The internal damage mechanism in the short fracture injection experiments (exps. 51, 58, 25, and 54).

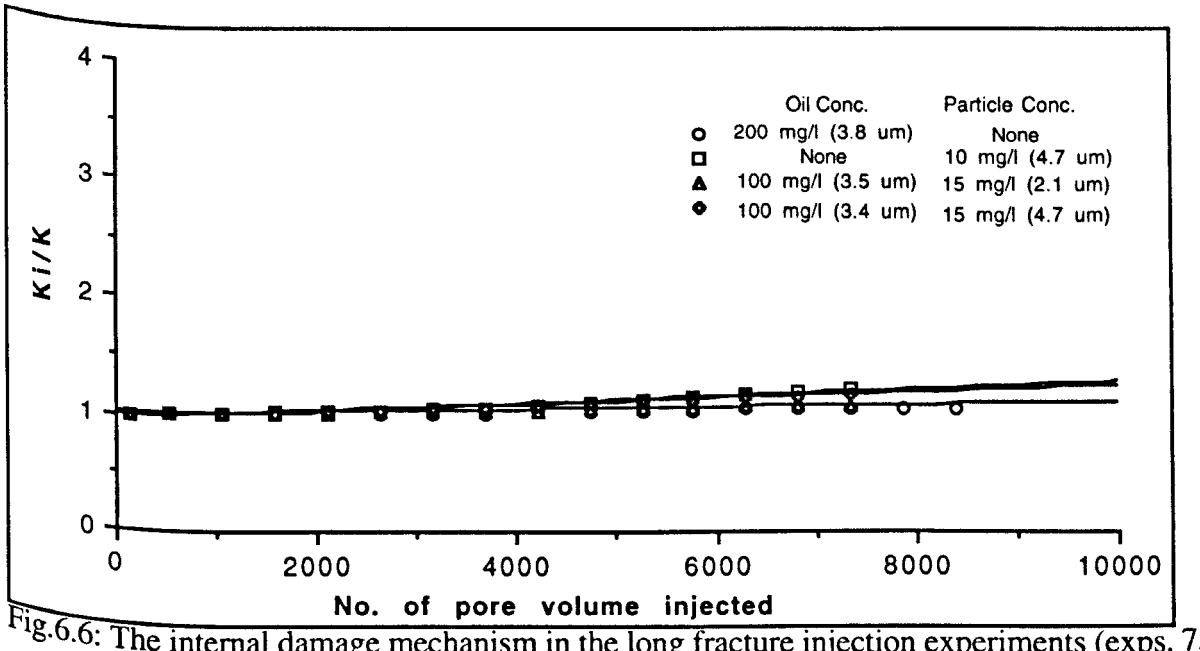

Fig.6.6: The internal damage mechanism in the long fracture injection experiments (exps. 75, 79, 81, and 82)..

6.5 Application of formation damage models to linear and fracture injection systems

For a constant flow rate, initial permeability, initial porosity and flow path length, the main factors affecting the matrix permeability alteration are the oil and/or solids concentration contained in the injected fluid, droplet and/or droplet mean size, the flow area, the flow velocity and the initial injection pressure. The first three factors were studied by using the experimental results in conjunction with Eqs. 6.9 and 6.12 and the last two factors were studied by using experimental observations only.

6.5.1 Concentration and mean size effect

The initial matrix permeability to the damaged matrix permeability ratio K_i/K values, obtained from fracture and linear experiments, were plotted against $[(K_i\ Q\ t) / (A\ L\ \emptyset)]$. The slope was equal to θ or β which only represent the degree of permeability alteration due to oil and/or solid concentration and droplet and/or particle mean size without taking in account the area difference between the fracture and the linear injection experiments.

These plots show the difference in slope (θ or β) for the fracture and the linear injection experiments. For the case of the 200 mg/l oil emulsion injection (Fig.6.7), changing from linear to fracture injection reduced the slope to 63 % of the linear injection slope. For the 10 mg/l suspension of 2.1 μm mean size particles (Fig.6.8), the same slope difference between the fracture and linear experiments (as in the 200 mg/l oil emulsion) was obtained.

The slope of the 10 mg/l suspension of the 2.1 μm mean size particles experiment, in the case of fracture injection, was higher than the slope of the 200 mg/l oil emulsion experiment by 81%. For the case of linear injection experiments nearly the same difference was obtained. It seams that the 3.8 μm mean size oil droplets at a concentration of 200 mg/l had the same permeability damage effect as the 2.1 μm particles at a concentration of 10 mg/l what ever the injection system was (fracture or linear system). The change from linear to fracture injection reduces the permeability damage by one third.

For the case of increasing the particle mean size from 2.1 μm to 4.7 μm at a constant particle concentration of 10 mg/l, changing from linear to fracture injection reduced the slope to 80 % of the linear injection slope (Fig.6.9). This percentage became 83% when particle concentration increased from 10 to 15 mg/l at a constant particle mean size of 2.1 μm (Fig.6.10), and increased further to 92% as the particle mean size increased from 2.1 μm to 4.7 μm at constant particle concentration of 15 mg/l (Fig.6.11).

Increasing the particle size and/or the particle concentration narrowed the difference between the matrix permeability damage caused by the linear injection and that caused by fracture injection. The improvement in permeability damage, caused by changing the injection system from linear injection to fracture injection, decreased from 37% (for the injection of 10 mg/l suspension of 2.1 μm mean size particles) to less than 8% (when the injection fluid was a 15 mg/l suspension of 4.7 μm mean size particles).

As the initial matrix permeability of the 4.7 μm particles suspension experiments was nearly double the initial matrix permeability of the 2.1 μm particles suspension experiments, this caused the calculated slope of the linear and the fracture injection experiments for the case of the 4.7 μm particles suspensions to be lower than that of the 2.1 μm particles suspension experiments.

For the case of injection fluid which contained a 200 mg/l oil concentration and 10 mg/l solid concentration of 2.1 μm particle mean size (Fig.6.12), the change from linear to fracture injection reduced the permeability damage (the slope) to 32% of the linear injection slope (which is 68% improvement is permeability damage), whereas the addition of oil at a 100 mg/l to the 15 mg/l particle suspension of 2.1 μm particle mean size (Fig.6.13) reduced the slope to 93% (which is only 7% improvement in permeability damage).

When oil was added at a 100 or 200 mg/l concentration and 3.8 μm droplet mean size to the 2.1 μm mean size particle suspension, changing the injection system from linear to fracture injection can greatly reduce the permeability damage effect if the particle concentration was kept less than 10 mg/l.

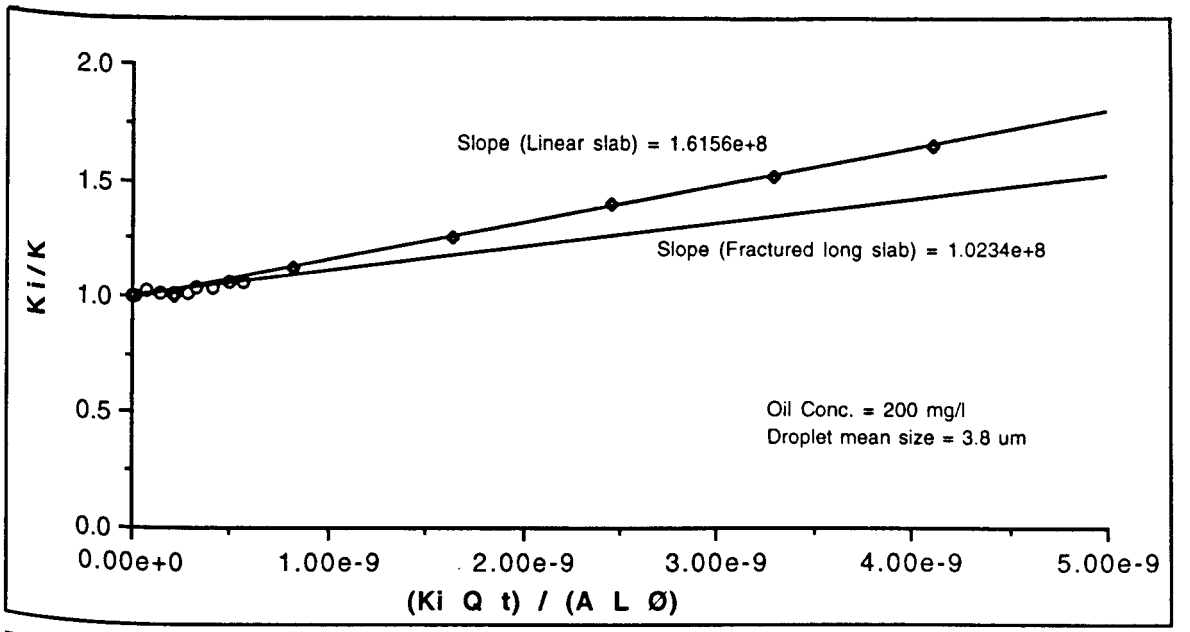

Fig.6.7: The effect of oil droplets on the injectivity inverse (Exps. 62 and 75).

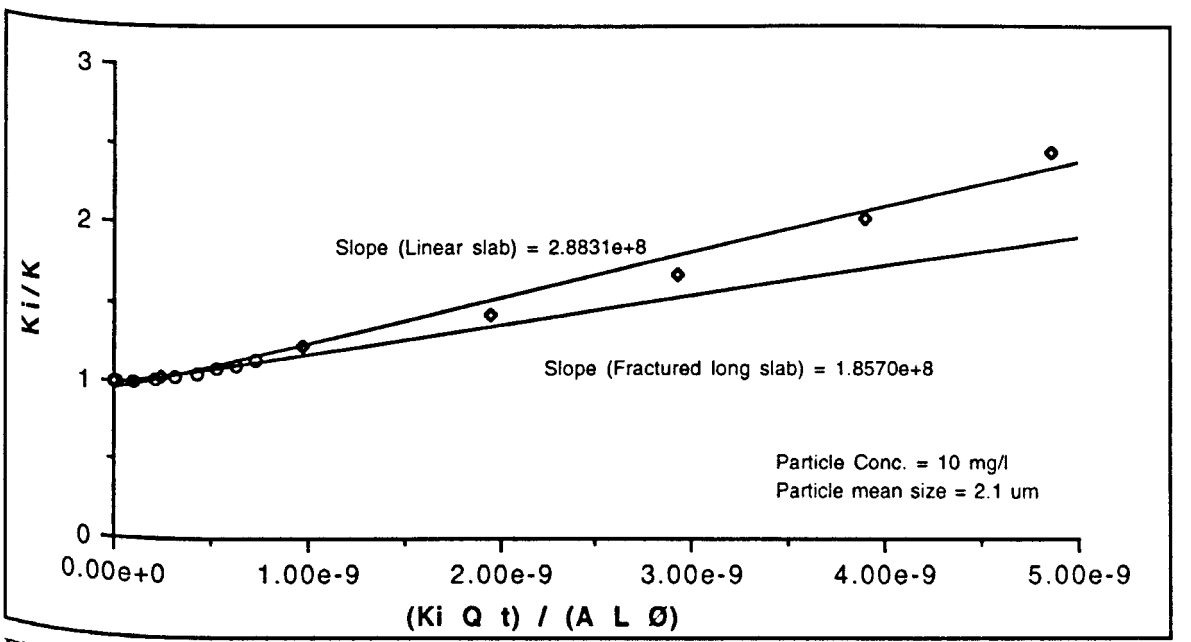

Fig.6.8: The effect of the 2.1 μm particles on the injectivity inverse (Exps. 59 and 77).

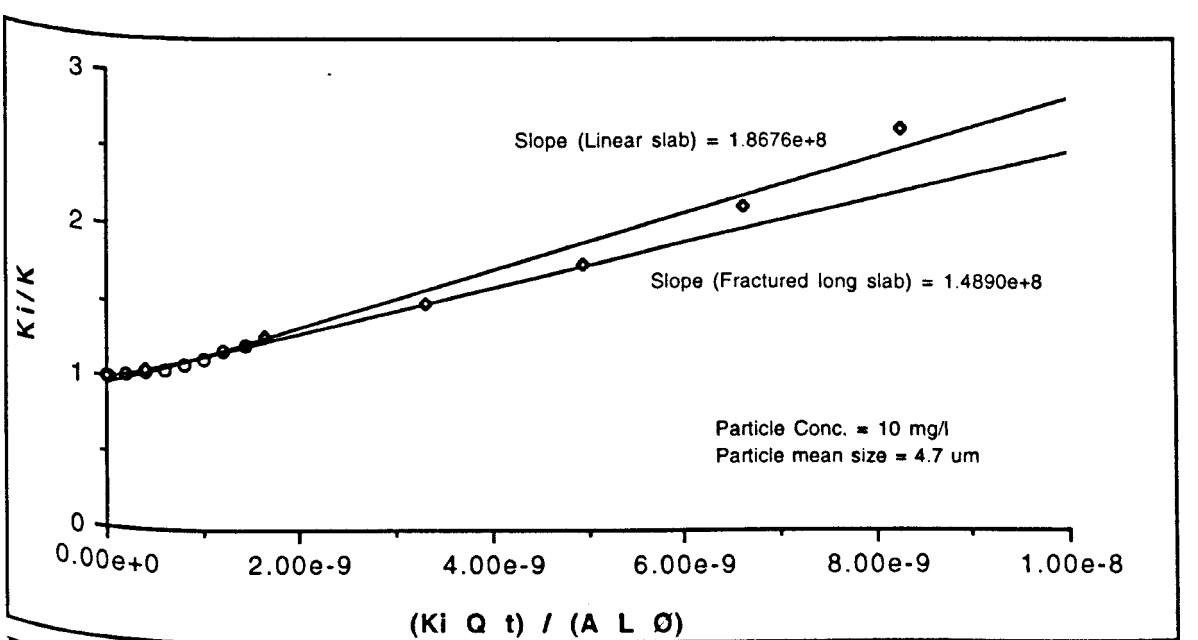

Fig.6.9: The effect of the 4.7 μm particles on the injectivity inverse (Exps. 65 and 79).

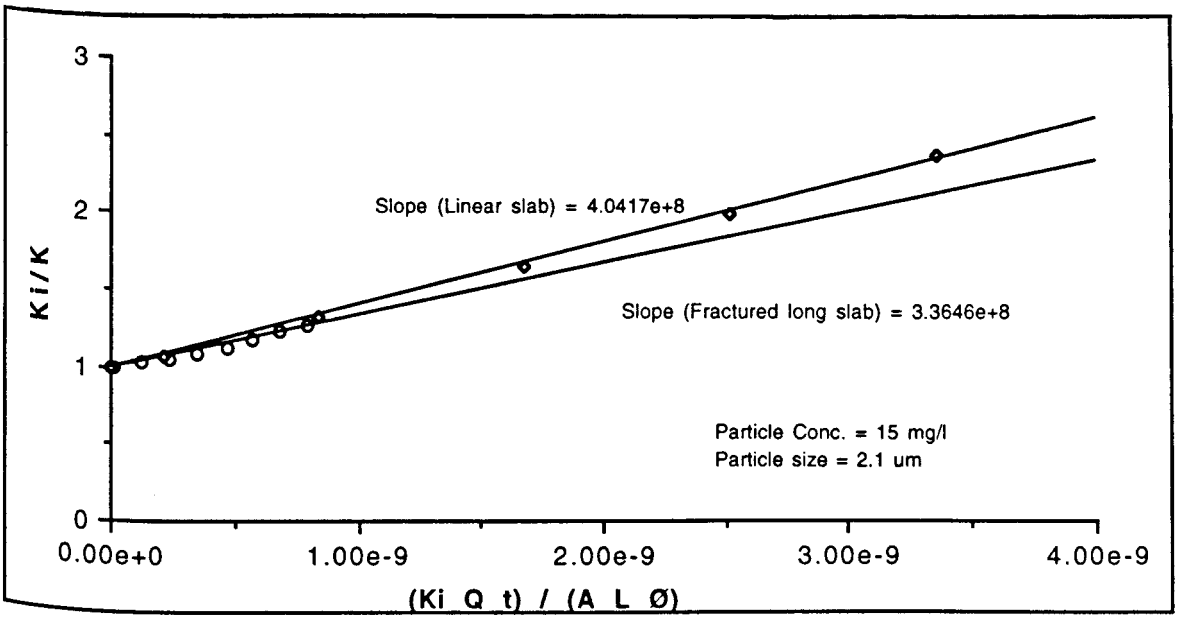

Fig.6.10: The effect of the 2.1 μm particles at a concentration of 15 mg/l on the injectivity inverse (Exps.60 and 76).

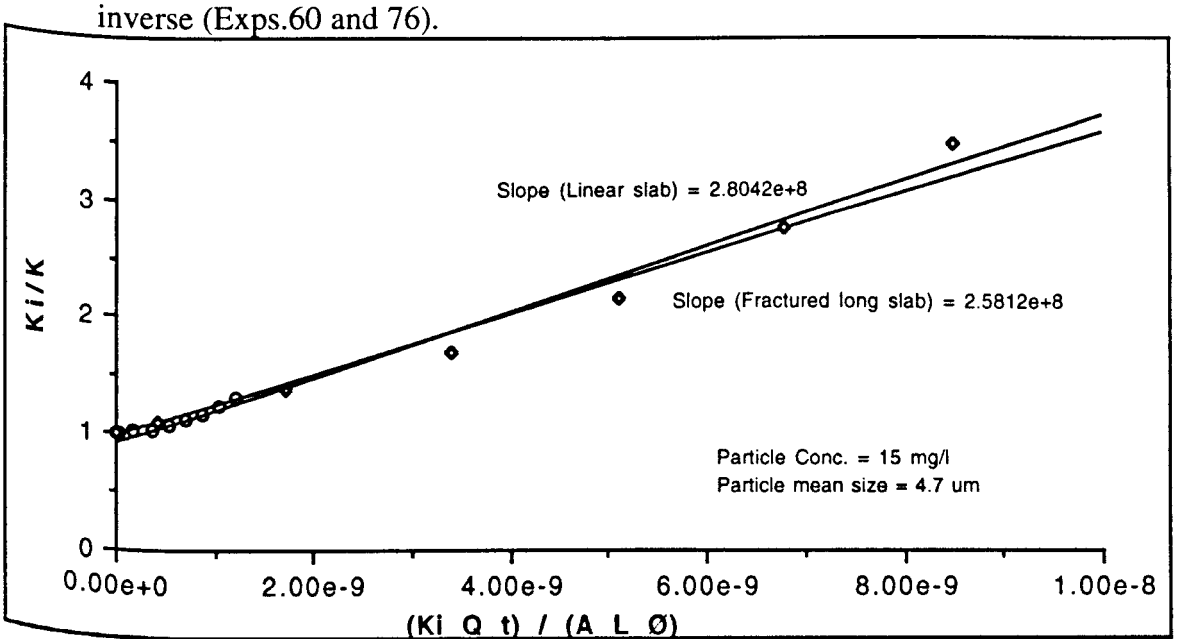

Fig.6.11: The effect of the 4.7 μm particles at a concentration of 15 mg/l on the injectivity inverse (Exps. 64 and 80).

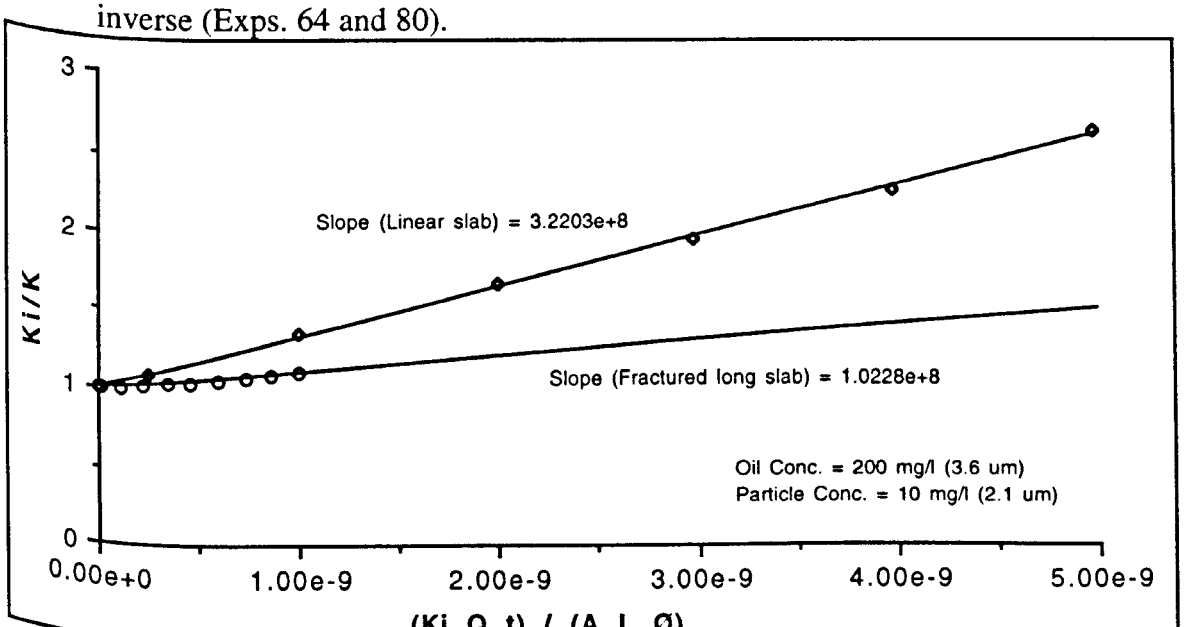

Fig.6.12: The effect of the 2.1 μm particles at a concentration of 10 mg/l and oil at concentration of 200 mg/l on the injectivity inverse (Exps. 74 and 57).

The addition of oil at 100 and 200 mg/l to the 4.7 μm particle suspensions gave unclear permeability damage results.

6.5.2 Concentration, mean size and flow area combined effect

The initial matrix permeability to the damaged matrix permeability ratio K_i/K values, obtained from fracture and linear experiments, were plotted against injection time t. The slope will be equal to $\theta\frac{K_iQ}{AL\phi_i}$ or $\beta\frac{K_iQ}{AL\phi_i}$. This time the slope represents the degree of permeability alteration due to the area difference between the fracture and the linear injection experiments as well as the alteration due to oil and/or solid concentration and droplet and/or particle mean size.

For the 200 mg/l oil emulsion injection experiments and the 10 mg/l of 2.1 μm particle suspension injection experiments, changing the injection system from linear to fracture injection reduced the slope and, apparently, the permeability damage effect to 3% of the permeability damage caused by the linear injection experiment (Figs.6.14 and 6.15).

For the 15 mg/l of 2.1 μm mean size particle suspension, the 10 mg/l of 4.7 μm mean size particle suspension and the 15 mg/l of 4.7 μm mean size particle suspension injection experiments, the change from linear to fracture injection reduced the slope to 5% (Figs.6.16 - 6.18).

For the case of the injection fluid which contained a 200 mg/l oil concentration of 3.5 μm mean size droplets and 10 mg/l solids concentration of 2.1 μm mean size particles, changing from linear to fracture injection reduced the slope to 2% (Fig.6.19).
For the other experiments with an injection fluids which contained oil and solids, the slope was reduced to 5% in average (Figs.6.20 - 6.22).

By combining the effect of droplets and particles concentration and mean size with the effect of area difference, changing of the injection system from linear to fracture injection reduced the slope (in average) to 4 % of the linear injection experiments slope (this is true for all the carried out experiments). This means a 25 times increase in the injectivity.

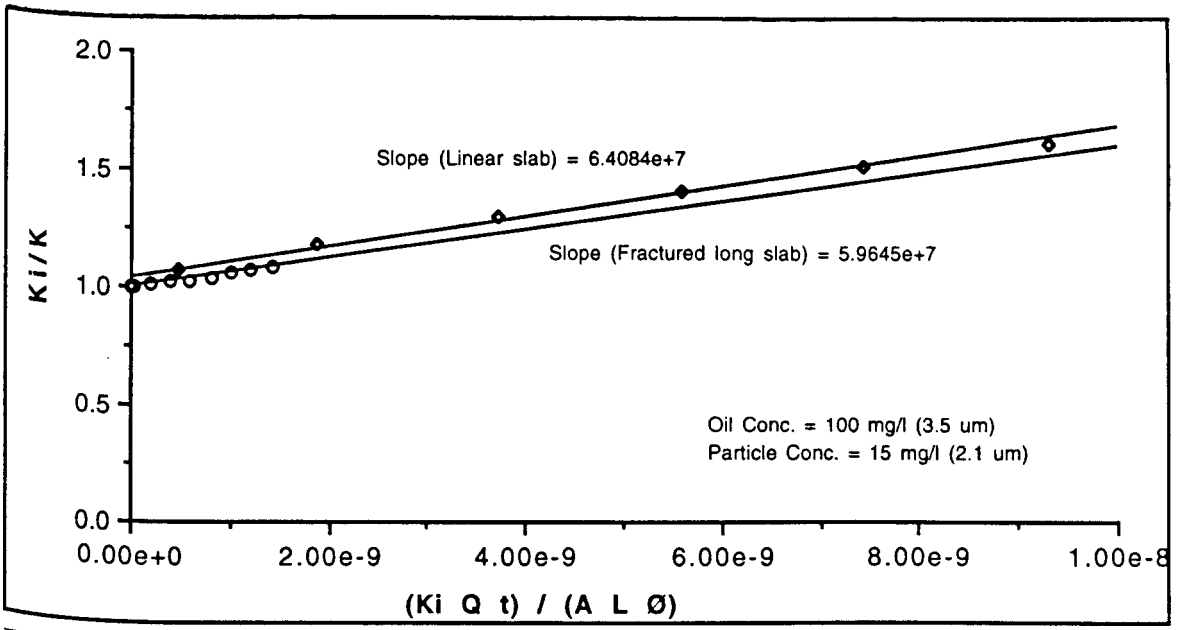

Fig.6.13: The effect of the 2.1 μm particles at a concentration of 15 mg/l and oil at concentration of 100 mg/l on the injectivity inverse (Exps. 67 and 81).

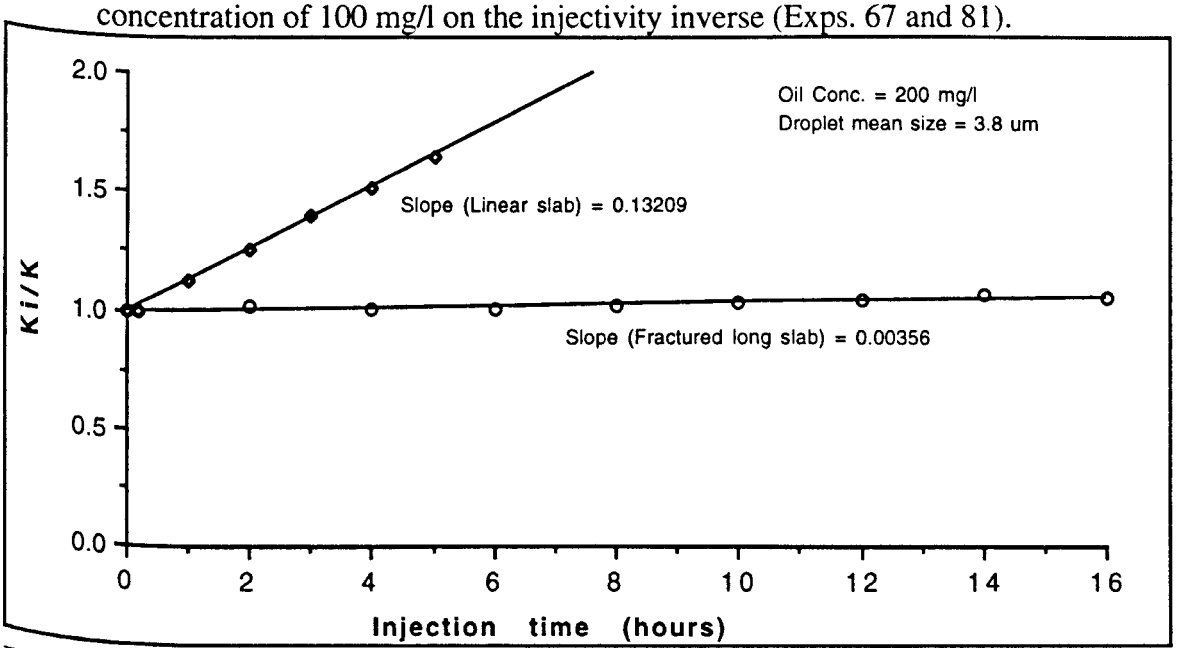

Fig.6.14: The combined effect of oil droplets and flow area on the injectivity inverse (Exps.62 and 75).

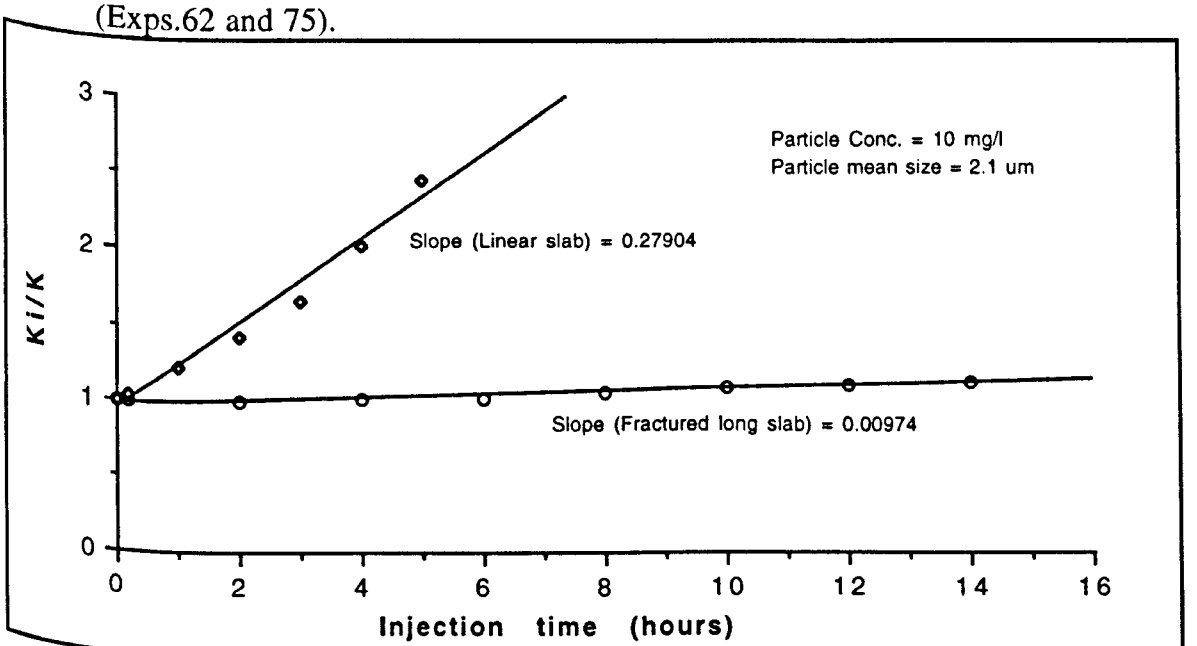

Fig.6.15: The combined effect of the 2.1 μm particles at 10 mg/l concentration and the flow area on the injectivity inverse (Exps.59 and 77).

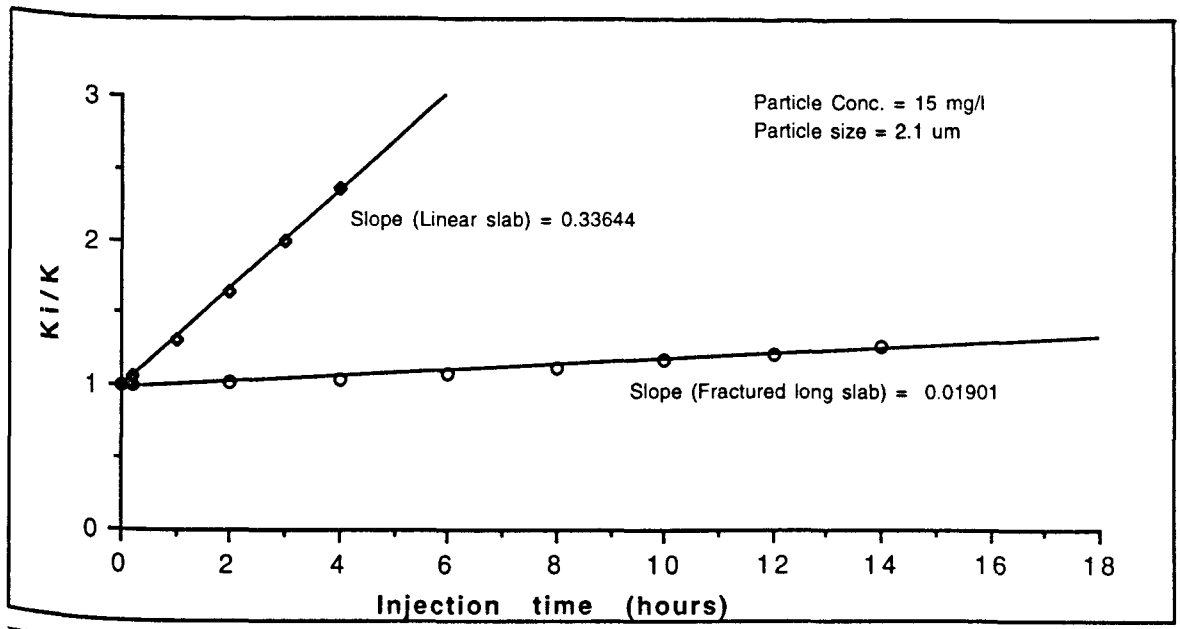

Fig.6.16: The combined effect of the 2.1 μm particles at 15 mg/l concentration and the flow area on the injectivity inverse (Exps.60 and 76).

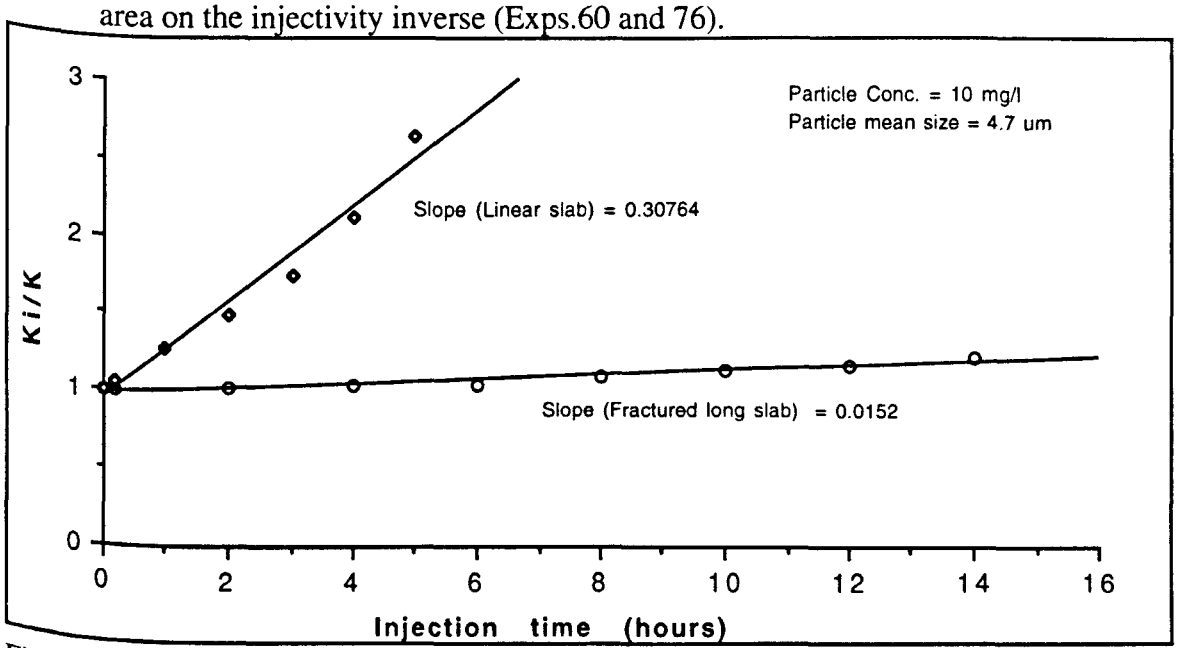

Fig.6.17: The combined effect of the 4.7 μm particles at 10 mg/l concentration and the flow area on the injectivity inverse (Exps.65 and 79).

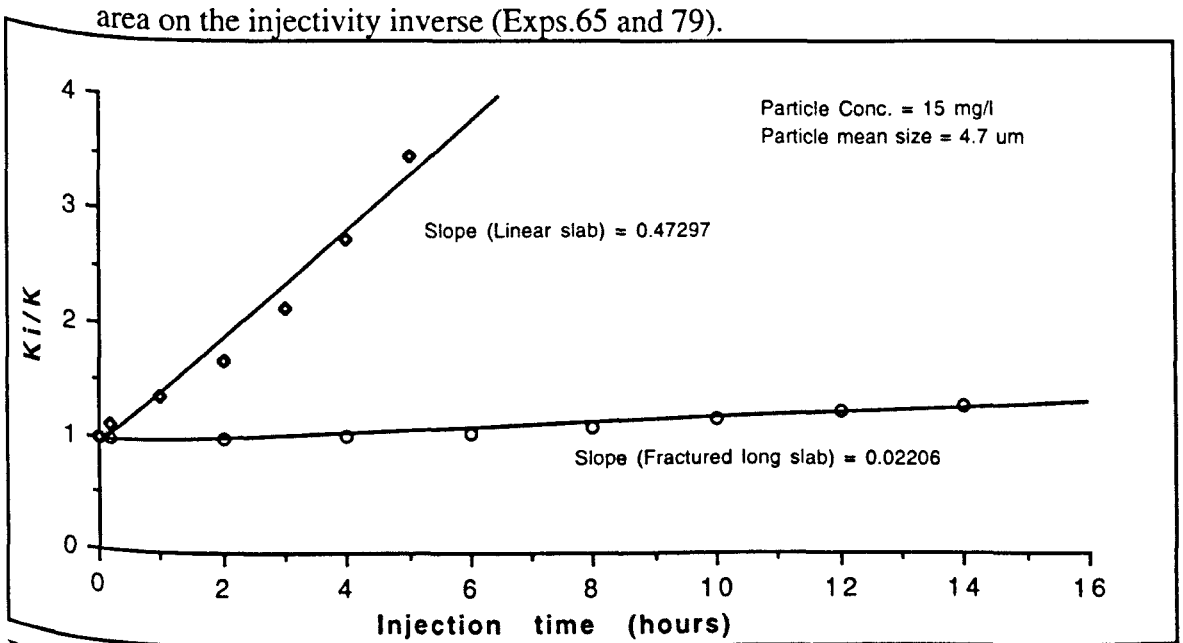

Fig.6.18: The combined effect of the 4.7 μm particles at 15 mg/l concentration and the flow area on the injectivity inverse (Exps.64 and 80).

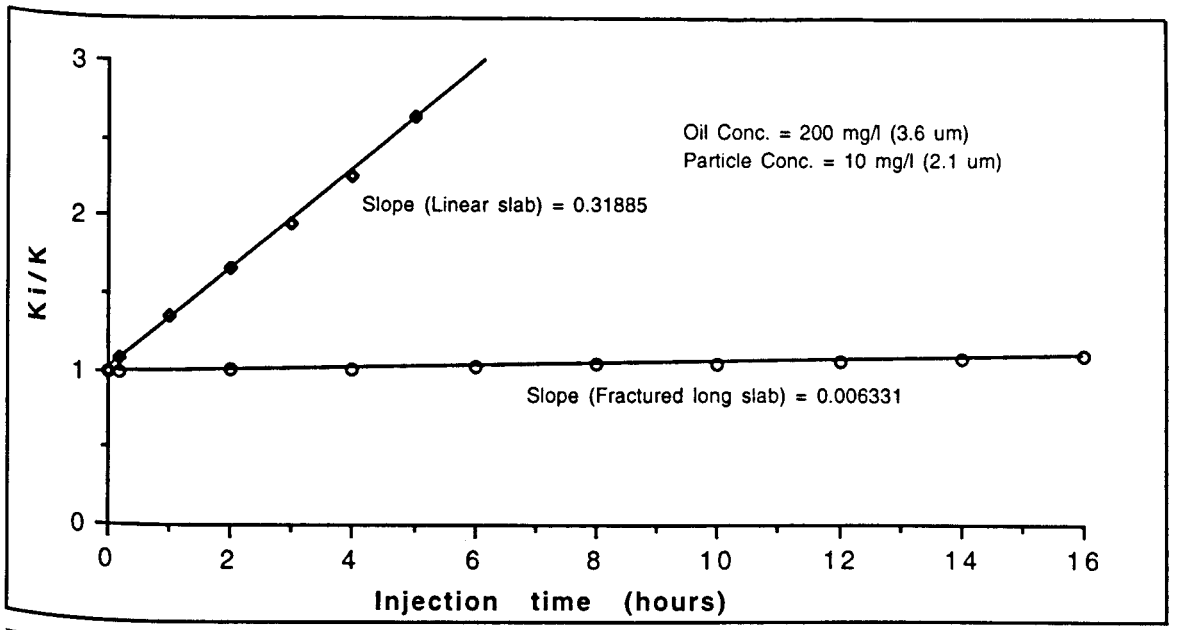

Fig.6.19: The combined effect of the 2.1 μm particles at 10 mg/l concentration, the oil droplets and the flow area on the injectivity inverse (Exps.74 and 57).

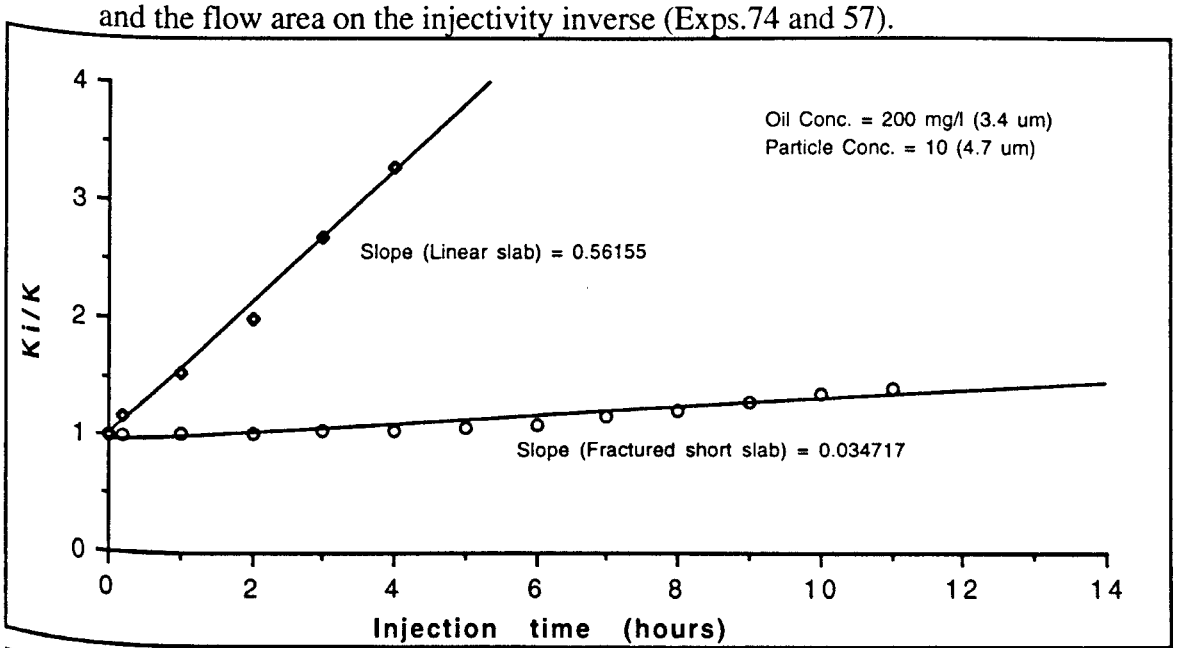

Fig.6.20: The combined effect of the 4.7 μm particles at 10 mg/l concentration, the oil droplets and the flow area on the injectivity inverse (Exps.72 and 55).

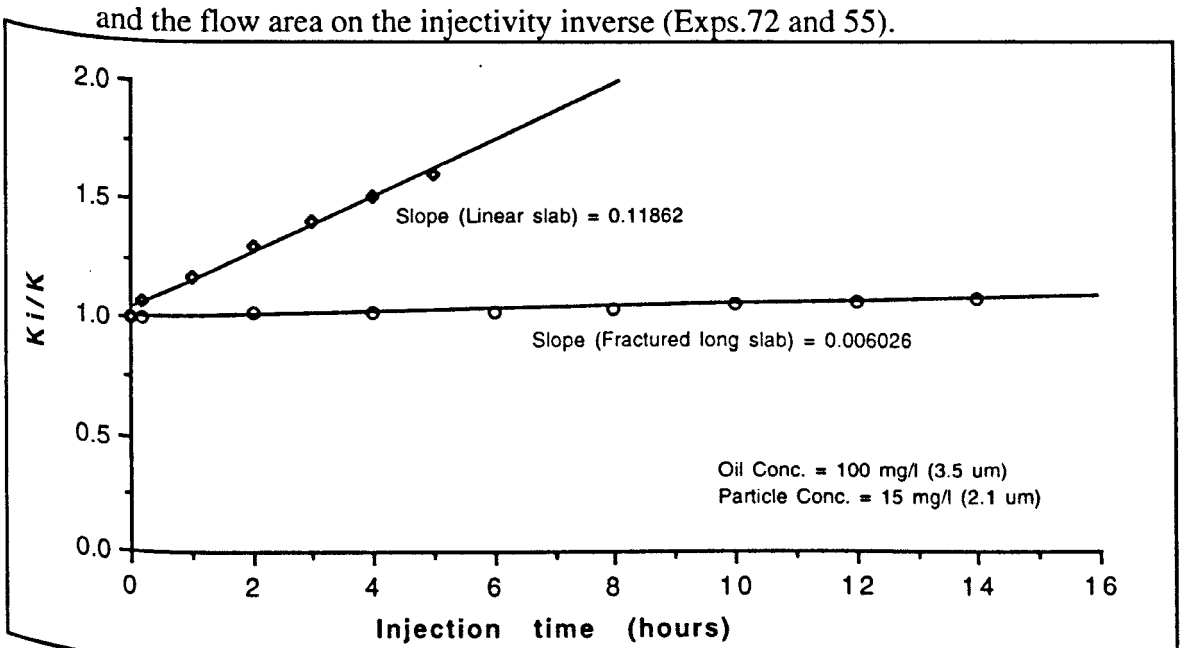

Fig.6.21: The combined effect of the 2.1 μm particles at 15 mg/l concentration, the oil droplets and the flow area on the injectivity inverse (Exps.67 and 81).

The injectivity inverse can be represented by the equation:

$$\frac{K_i}{K} = 1 + m*t$$

Where m has a value from 0.12 to 0.65 for the linear injection

And m has a value from 0.0036 to 0.035 for the fracture injection

6.5.3 Flow velocity and pressure drop effect

The flow velocity through rock matrix in the linear injection experiments was between 0.36 and 0.43 cm/s and in the fracture injection experiment was between 0.022 and 0.036 cm/s.

The pressure drop through rock matrix in the linear injection experiment was between 2.2 and 11.5 bar and in the fracture injection experiments was between 0.22 and 0.44 bar. This huge difference in the flow velocity and pressure drop between linear and fracture injection experiments may have had some effect on the capture and release mechanism of droplets and particles within the rock matrix.

The effect of these two factors can be deduced by studying the concentration ratio (CR) of the effluent (the ratio of effluent concentration to the influent concentration) of the linear and the fracture injection experiments.

When the injection fluid was particle suspension only without any oil being added, the CR of the side outlets effluent in the fracture injection was between zero and 0.3 which meant that more than 70% of the particles were captured within the rock matrix. On the other hand the CR of effluent in the linear injection was between 0.25 and 0.8 which mean that 20 to 75% of the particles were captured within the rock matrix.

This difference in the percentage of the captured particles can be related to the huge difference in flow velocity and pressure drop between the two injection systems (linear and fracture injection). The high flow velocity in linear injection can effectively prevent the precipitation or the capture of particles, whereas the very low flow velocity through matrix in the fracture injection encouraged more precipitation and capture of particles. Also the high pressure drop in the linear injection tended to force the particles through the matrix pores and to break the pre-formed particle bridges at the pore throats which enabled the particles to travel deep into the matrix before being captured which resulted in more particles reaching the outlet.

On the other hand in the case of fracture injection, the pressure drop was not high enough to force the particles through pore throat or to break the pre-formed particle bridges and most of the particles were captured after travelling a very short distance into the matrix which resulted in less particles reaching the side outlets.
As a result, it can be expected that the invasion depth of particles in the linear injection would be higher than the invasion depth in the fracture injection.

When the injection fluid was oil emulsion only without any solids being added, the difference in flow velocity and pressure drop between the linear and fracture injection had less effect on the effluent CR. The CR of the effluent in the linear injection was between 0.92 and 1.0 and the CR of side effluent in the fracture injection was between 0.84 and 1.0.

The close CR values of the two systems in the case of oil emulsion experiments, contrarily to the case of particle suspension experiments, can be explained by the deforming nature of the oil droplets. The 3.8 μm oil droplets do not need a high pressure to be forced through the small pore throat, also the oil droplets do not form bridges at the pore entry. The oil droplet density is less than the brine density which prevented its precipitation within the rock matrix. The small difference in CR between the two systems (in the case of oil emulsion experiments) may be due to the high flow velocity (as in the linear injection system) forcing pre-captured oil droplets into the flow stream (due to higher shear force) more efficiently than the low flow velocity (as in the fracture injection system).

So the flow velocity and pressure drop are very important factors which must be carefully studied to measure their effect on the matrix permeability damage in the fracture injection system.

6.6 Damage effect in radial and fracture injection

In this section the linear injection system was converted to a radial injection system. Then all the linear injection experimental results were re-calculated as if they were radial geometries results. Also a comparison study between linear and radial injection systems is presented in this section.

Further more, the radial injection system was converted to a fracture injection system. Then the relation between the damage effect in the radial and the fracture injection systems was investigated. The difference in damage effect between the radial and the fracture injection systems was calculated (by using the converting equation from radial to fracture system) and experimentally measured.

6.6.1 Converting from linear to radial injection

The difference between the linear injection system and the radial injection system is the enlargement of flow area in the direction of radius in the case of radial injection compared with constant flow area in the case of linear injection. Due to this difference in geometry, the radial system caused a lower pressure drop than linear system.

Thus, for a clean brine injection: pressure drop in radial system = pressure drop in linear system - pressure drop difference due to the geometry effect

$$\Delta P_R = \Delta P_L - \Delta P_{Gr} \qquad (6.13)$$

And

$$\Delta P_{Gr} = \Delta P_L - \Delta P_R$$

$$\Delta p_{Gr} = \frac{q\mu L}{K_i A_L} - \frac{q\mu Ln(r_o/r_w)}{2\pi K_i h}$$

Figure 6.23 shows the linear and the radial systems.

Multiplying and dividing the radial pressure drop term by r_w gave:

$$\Delta p_{Gr} = \frac{q\mu L}{K_i A_L} - \frac{r_w q\mu Ln(r_o/r_w)}{r_w 2\pi K_i h}$$

The inlet flow area of the radial system $2\pi r_w h = A$ (the inflow area of the linear system).

Thus

$$\Delta p_{Gr} = \frac{q\mu L}{K_i A_L} - \frac{r_w q\mu Ln(r_o/r_w)}{A_L K_i}$$

And

$$\Delta p_{Gr} = \frac{q\mu L}{K_i A_L}\left(1 - \frac{r_w}{L} Ln\left(\frac{r_o}{r_w}\right)\right)$$

Where $r_o = L + r_w$

Thus

$$\Delta p_{Gr} = \Delta p_L\left(1 - \frac{r_w}{L} Ln\left(\frac{r_o}{r_w}\right)\right)$$

Or

$$\Delta P_R = \Delta P_L (1 + S_{Gr}) \qquad (6.14)$$

where $S_{Gr} = -\left(1 - \frac{r_w}{L} Ln\left(\frac{r_o}{r_w}\right)\right)$ is the geometry skin

For a the following variables:

$L = 0.03$ m

$r_w = A / 2\pi h = 0.01$ m

$r_o = L + r_w = 0.04$ m

The calculated geometry skin S_{Gr} was - 0.538.

When the dirty water injection started, the pressure drop in the radial injection can be assumed to be equal to the pressure drop in the linear injection matrix minus the pressure drop difference due to geometry skin.

$$\Delta Pd_R = \Delta Pd_L - \Delta P_{Gr} \quad \text{or} \quad \Delta Pd_R = \Delta Pd_L (1 + S_{Gr}) \qquad (6.15)$$

This is true if it is assumed that the geometry difference between the two systems had no effect on the degree of permeability damage.

The pressure drop due to matrix damage for the radial injection ΔPd_R was calculated by using the linear injection results and by applying Eq.6.15.

6.6.2 Converting from radial to fracture injection

The main difference between the radial injection system and the fracture injection system is in the inflow area and the pressure distribution on the inflow surface area. The high inflow area in fracture injection causes a very low flow velocity through the rock matrix. The pressure exerted on the fracture face decreased with distance along the fracture. Due to this difference in geometry, the radial system caused a higher pressure drop than the fracture system.

Thus, for a clean brine injection: pressure drop in fractured system = pressure drop in radial system - pressure drop difference due to geometry effect

$$\Delta P_{Fi} = \Delta P_{Ri} - \Delta P_{Gf} \qquad (6.16)$$

And $$\Delta P_{Gf} = \Delta P_{Ri} - \Delta P_{Fi}$$

where ΔP_{Ri} and ΔP_{Fi} are the initial injection pressure drop.

$$\Delta p_{Gf} = \frac{q_R \mu L Ln(r_o / r_w)}{2\pi K_{Ri} h} - \frac{q_F \mu L}{A_F K_{Fi}}$$

where K_{Ri} and K_{Fi} are the initial matrix permeability in the case of the radial and the fracture systems respectively.

q_S is the side flow rate in the case of fracture system.

Multiplying and dividing the right hand side by the radial pressure drop term gives:

$$\Delta p_{Gf} = \frac{q_R \mu Ln(r_o/r_w)}{2\pi K_{Ri} h}\left(1-\left(\frac{q_S \mu L}{A_F K_{Fi}}\frac{2\pi K_{Ri} h}{q_R \mu Ln(r_o/r_w)}\right)\right)$$

Or

$$\Delta p_{Gf} = \Delta p_R\left(1-\frac{v_F L K_{Ri}}{r_w v_R K_{Fi} Ln(r_o/r_w)}\right)$$

where v_F (flow velocity through matrix in fracture system) = q_s / A_F

v_R (flow velocity at the inflow face in the radial system) = q / $2\pi r_w h$

q_s is the total side outlets flow rate.

And $$\Delta P_{Fi} = \Delta P_{Ri}\,(1 + S_{Gf}) \qquad (6.17)$$

where $S_{Gf} = -\left(1-\frac{v_F L K_{Ri}}{r_w v_R K_{Fi} Ln(r_o/r_w)}\right)$ is the geometry skin.

For constant radial and fracture systems (L, r_w and r_o are constants), S_{Gf} is a function of ($v_F K_{Ri}$ / $v_R K_{Fi}$). If the K_{Ri} equal K_{Fi}, then S_{Gf} is a function only of v_F.

The calculated S_{Gf} values are presented in Table 6.1 and plotted versus ($v_F K_{Ri}$ / $v_R K_{Fi}$) in Figure 6.24. The $|S_{Gf}|$ value increased as the initial matrix permeability (K_{Ri} and K_{Fi}) increased and as the flow velocity through the rock matrix in the fracture system (v_F) decreased. The value of S_{Gf} was between - 0.80 and - 0.89.

When the dirty water injection started, the large flow area of the fracture system resulted in less matrix damage than the small flow area of the radial system. This difference in matrix damage extent between the two systems resulted in a higher pressure drop in the case of the radial system. Thus, the difference in pressure drop between the two systems (ΔPd_R - ΔPd_F) consists of:

Pressure drop difference due to geometry (ΔP_{Gf})

Pressure drop difference due to the difference in matrix damage extent (ΔPd).

$$\Delta Pd_F = \Delta Pd_R - \Delta P_{Gf} - \Delta Pd \qquad (6.18)$$

Or

$$\Delta Pd = \Delta Pd_R - \Delta P_{Gf} - \Delta Pd_F$$

The change in ΔPd with time can experimentally measured or numerically calculated.

The change in ΔPd with time can be experimentally measured by calculating the change in ΔPd_R with time from Eq.6.15 (ΔPd_L is the experimental value of the pressure drop change with time for the linear system after damage took place) and ΔP_{Gf} from Eq.6.16, while ΔPd_F is the

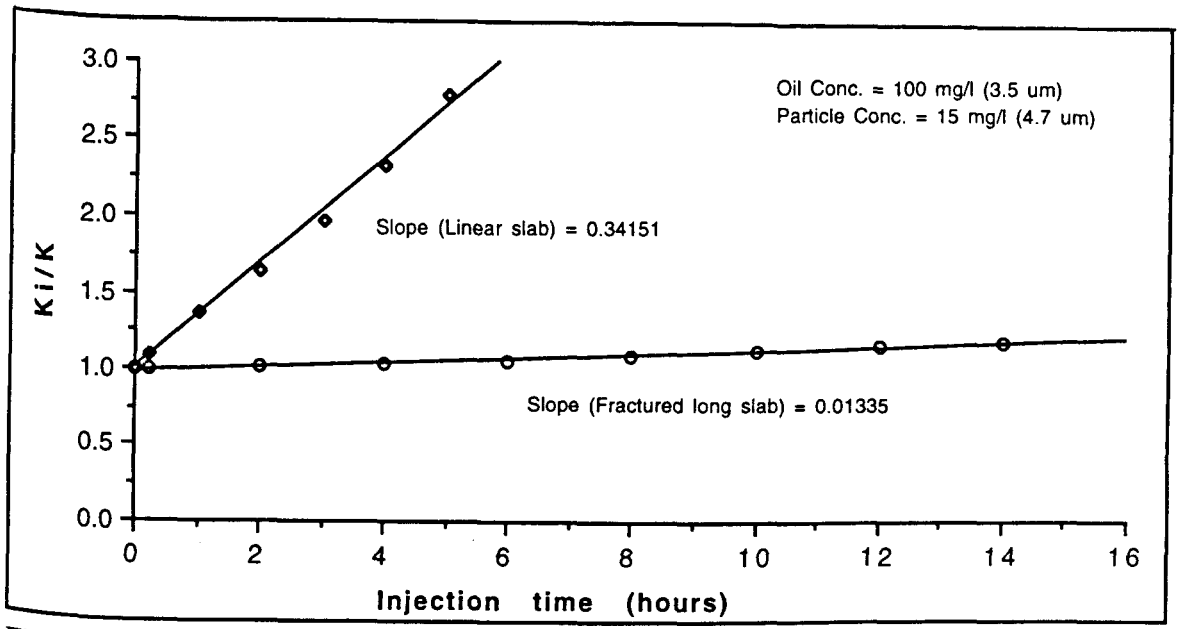

Fig.6.22: The combined effect of the 4.7 μm particles at 15 mg/l concentration, the oil droplets and the flow area on the injectivity inverse (Exps.70 and 82).

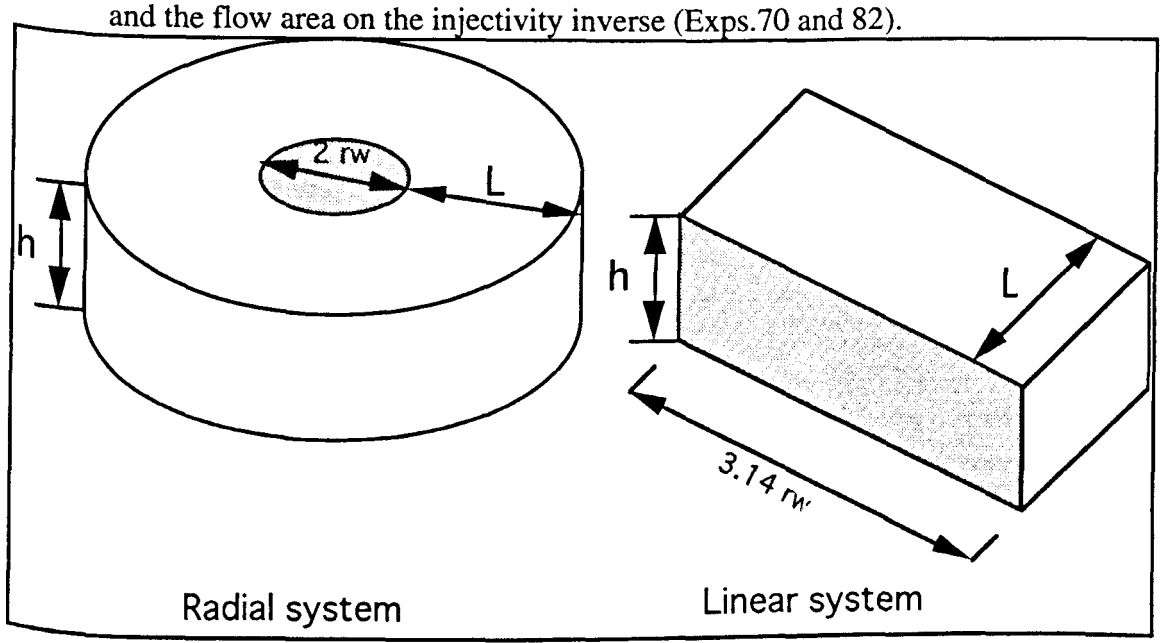

Fig.6.23: The linear and the radial injection systems.

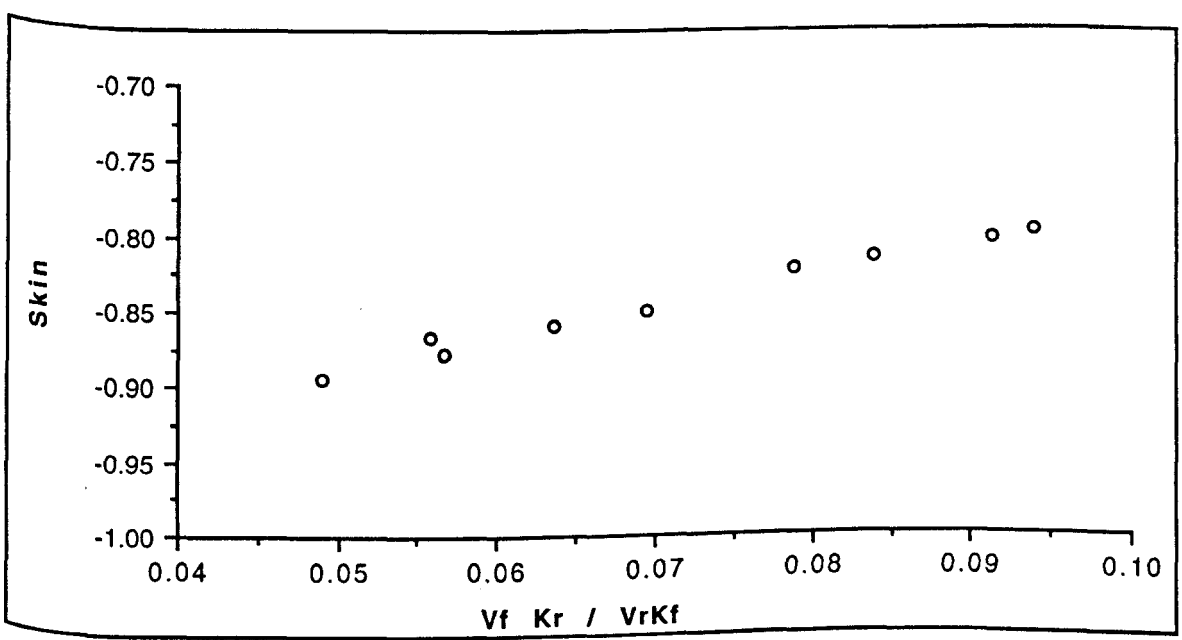

Fig.6.24: The change in geometric skin value with ($v_F K_{Ri} / v_R K_{Fi}$), for converting from radial to fracture system.

corrected experimental pressure drop (average pressure drop through the side flow path) change with time of the fracture system after damage took place.

The ΔPd_F was corrected as follows:

ΔPd_F (corrected) = ΔPd_F (experimentally measured) - (ΔP_{Fi} (experimentally measured) - ΔP_{Fi} (calculated))

Also the change in ΔPd with time can be numerically calculated as follows:

At any time during the injection of simulated produced water:

$$\Delta Pd_F = \Delta P_{Fi} (1 + S_{Fd})$$

$$\Delta Pd_R = \Delta P_{Ri} (1 + S_{Rd})$$

$$\Delta P_{Gf} = \Delta P_{Ri} S_{Gf}$$

$$\Delta Pd = \Delta P_{Ri} S_d$$

Where S_{Fd} is the skin due to matrix damage in the fracture system and S_{Rd} is the skin due to matrix damage in the radial system. The S_{Gf} is the skin due to geometry difference between radial and fracture systems. The S_d is the skin due to the difference in matrix damage extent between the two systems.

Substituting in Eq.6.18:

Then $$\Delta P_{Fi} (1 + S_{Fd}) = \Delta P_{Ri} (1 + S_{Rd}) + \Delta P_{Ri} S_{Gf} + \Delta P_{Ri} S_d \qquad (6.19)$$

where S_{Gf} and S_d have a negative sign.

But $$\Delta P_{Fi} = \Delta P_{Ri} (1 + S_{Gf})$$

Substituting in Eq.6.19, thus:

$$\Delta P_{Ri} (1 + S_{Gf}) (1 + S_{Fd}) = \Delta P_{Ri} (1 + S_{Rd}) + \Delta P_{Ri} S_{Gf} + \Delta P_{Ri} S_d$$

Or $$(1 + S_{Gf}) (1 + S_{Fd}) = (1 + S_{Rd}) + S_{Gf} + S_d$$

$$1 + S_{Fd} + S_{Gf} + S_{Gf} S_{Fd} = 1 + S_{Rd} + S_{Gf} + S_d$$

$$S_{Fd} + S_{Gf} S_{Fd} = S_{Rd} + S_d$$

$$S_{Fd} (1 + S_{Gf}) = S_{Rd} + S_d \qquad (6.20)$$

But $$S_{Fd} = (\Delta Pd_F - \Delta P_{Fi}) / \Delta P_{Fi} = (K_{Fi} / K_{Fd}) - 1$$

$$S_{Rd} = (\Delta Pd_R - \Delta P_{Ri}) / \Delta P_{Ri} = (K_{Ri} / K_{Rd}) - 1$$

Substituting in Eq.6.20, thus:

$$\left(\frac{K_{Fi}}{K_{Fd}} - 1\right)(1 + S_{Gf}) = \left(\frac{K_{Ri}}{K_{Rd}} - 1\right) + S_d$$

And $$S_d = -\left(\left(\frac{K_{Ri}}{K_{Rd}} - 1\right) - \left(\frac{K_{Fi}}{K_{Fd}} - 1\right)(1 + S_{Gf})\right)$$

Or $$S_d = -\left(\left(\frac{1}{\alpha_{Rd}} - 1\right) - \left(\frac{1}{\alpha_{Fd}} - 1\right)(1 + S_{Gf})\right) \qquad (6.21)$$

where $$S_{Gf} = -\left(1 - \frac{v_F L K_{Ri}}{r_w v_R K_{Fi} Ln(r_o/r_w)}\right)$$

$\frac{1}{\alpha_{Rd}}$ *and* $\frac{1}{\alpha_{Fd}}$ are the injectivity inverse for the radial and the fracture systems after matrix damage took place and were calculated as follows:

$$\frac{1}{\alpha_{Rd}} = \frac{\Delta p_{Rd}/q}{\Delta p_{Ri}/q} \qquad (6.22)$$

$$\frac{1}{\alpha_{Fd}} = \frac{\Delta p_{Fd}/q_F}{\Delta p_{Fi}/q_{Fi}} \qquad (6.23)$$

where q_{Fi} is the initial side flow rate in the fracture system.

The measured and the calculated S_d values are presented in Tables 6.2 - 6.10. Also the value of ΔPd_R, ΔPd_F and ΔPd (measured and calculated) are presented in the same tables. There is a very good agreement between the measured and the calculated values of ΔPd (Fig.6.25).

The change in ΔPd_R and ΔPd_F with time is shown in Figures 6.26 - 6.32. The change in the summation of S_d plus S_{Gf} with time is shown in Figure 6.33 for different injected fluid compositions.

For all the experiments carried out, the geometry skin is less than |–0.9|. For the oil emulsion injection, the $|S_d|$ value increased gently with time, while the 2.1 μm particle suspension at a concentration of 10 mg/l caused a higher increases in the $|S_d|$ value with time. The increase in particle concentration and particle mean size resulted in further increase in the $|S_d|$ value with time.

When the injection fluid was 200 mg/l oil emulsion, the increase rate of $|S_d|$ with time was 0.28 per hour. This rate was increased to the double when the injected fluid was 10 mg/l of 2.1 μm mean size particle suspension, and increases by nearly 4 times when the injected fluid was 15 mg/l of 4.7 μm mean size particle suspension.

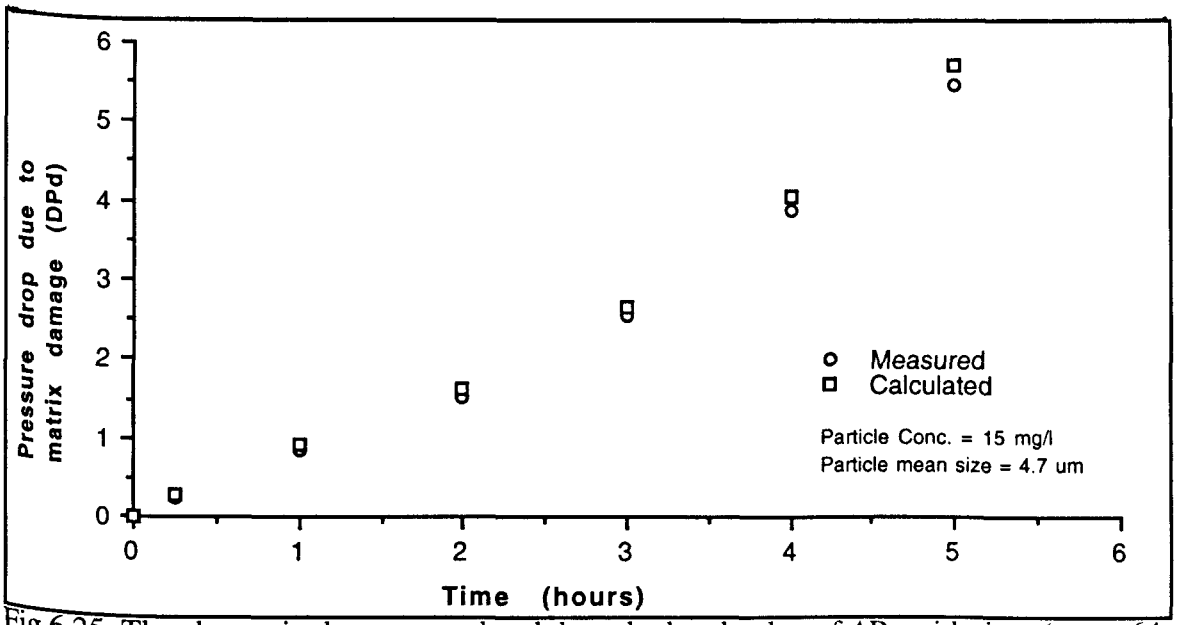

Fig.6.25: The change in the measured and the calculated value of ΔP_d with time (exps. 64 and 80).

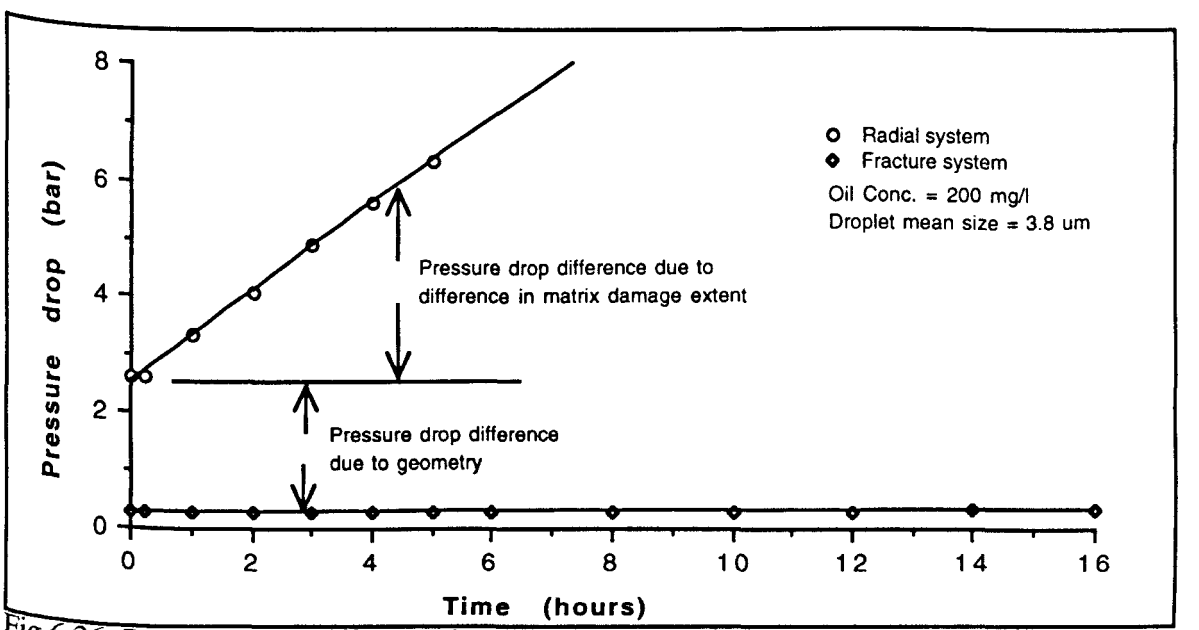

Fig.6.26: Pressure drop difference between radial and fracture systems for the case of oil emulsion injection (exps. 62 and 75).

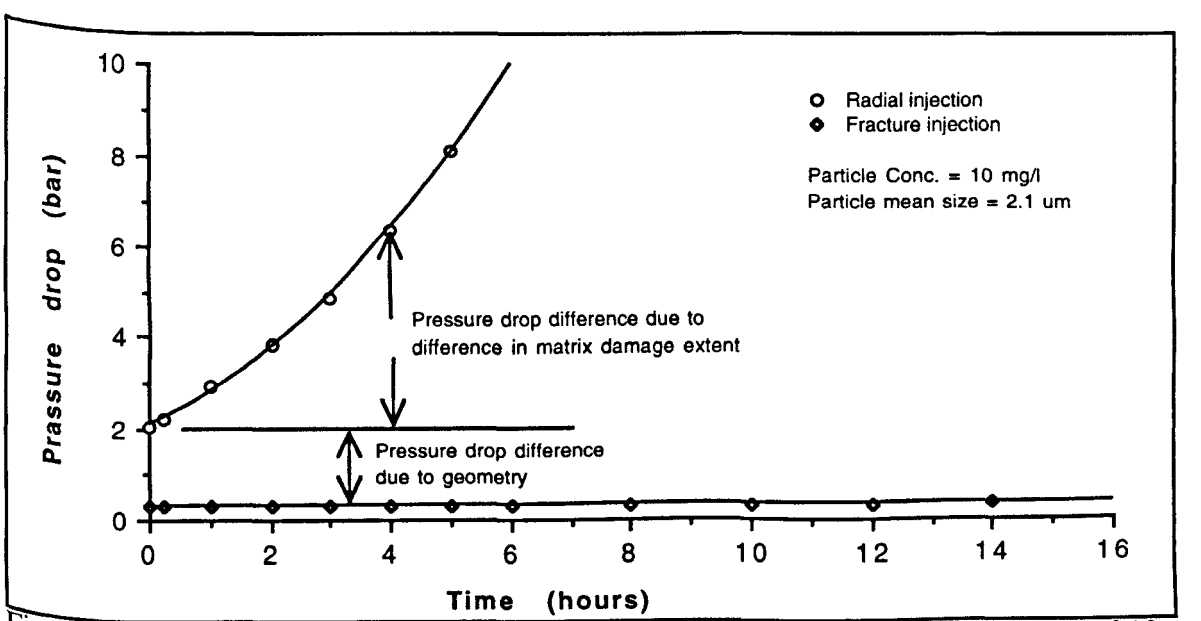

Fig.6.27: Pressure drop difference between radial and fracture systems for the case of 10 mg/l of 2.1 μm mean size particle suspension (exps. 59 and 77).

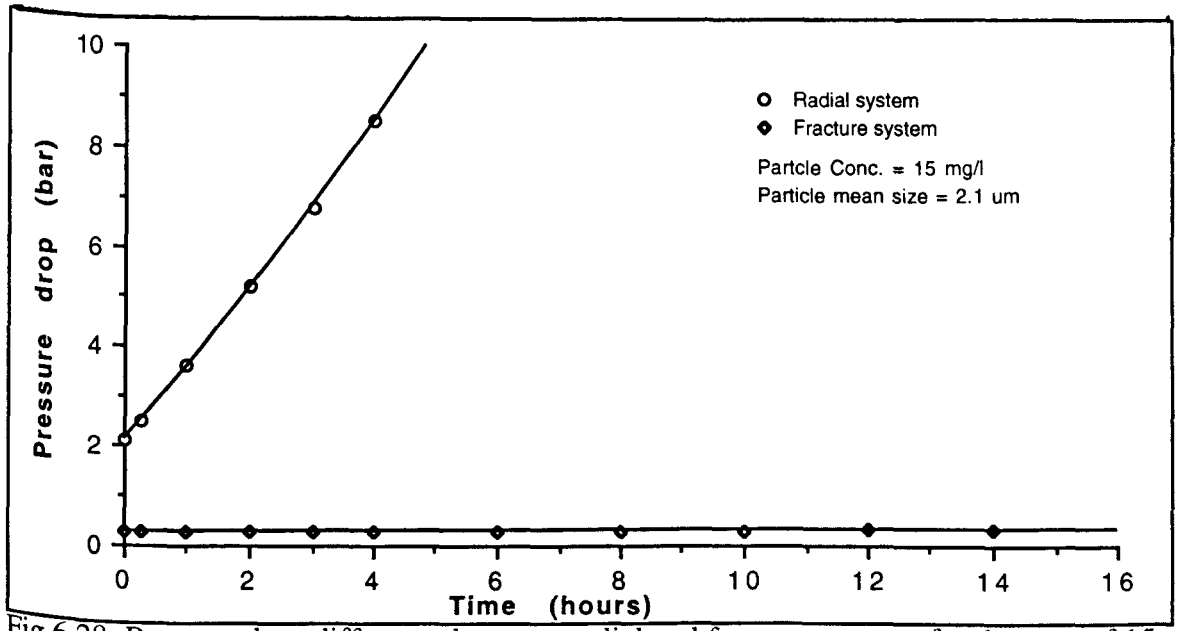

Fig.6.28: Pressure drop difference between radial and fracture systems for the case of 15 mg/l of 2.1 μm mean size particle suspension (exps. 60 and 76).

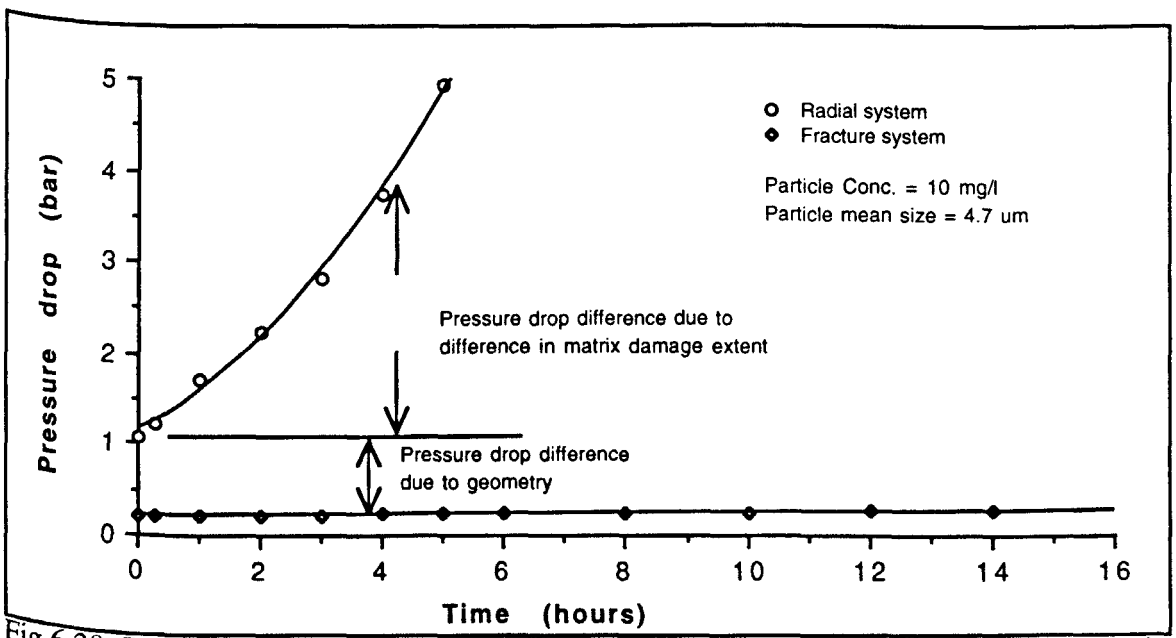

Fig.6.29: Pressure drop difference between radial and fracture systems for the case of 10 mg/l of 4.7 μm mean size particle suspension (exps. 65 and 79).

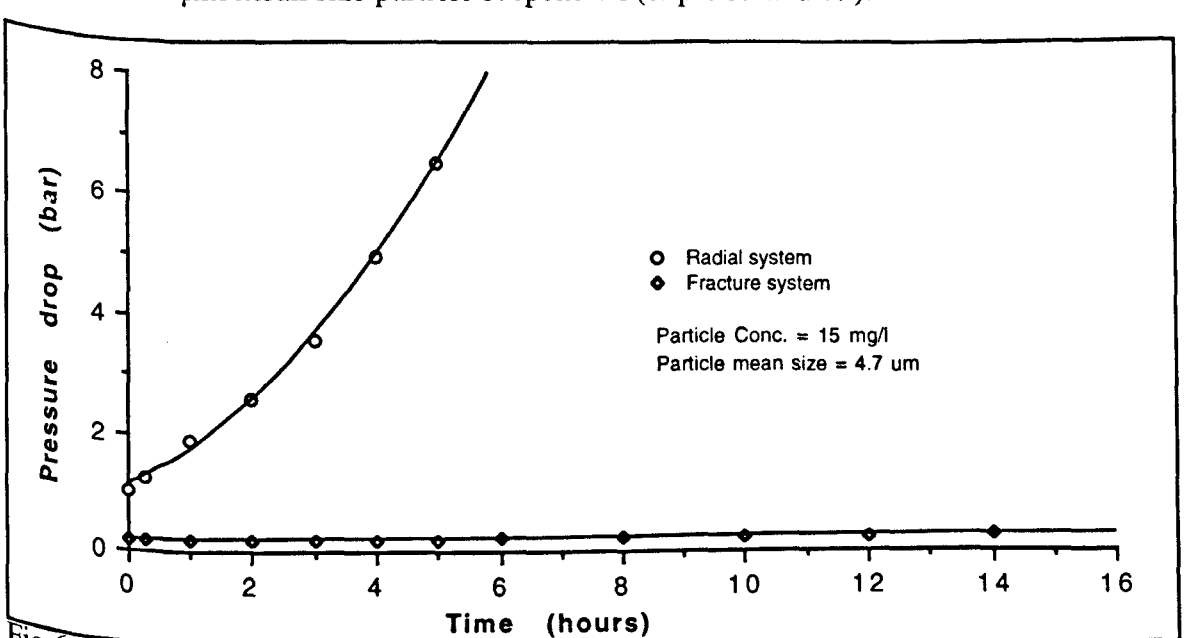

Fig.6.30: Pressure drop difference between radial and fracture systems for the case of 15 mg/l of 4.7 μm mean size particle suspension (exps. 64 and 80).

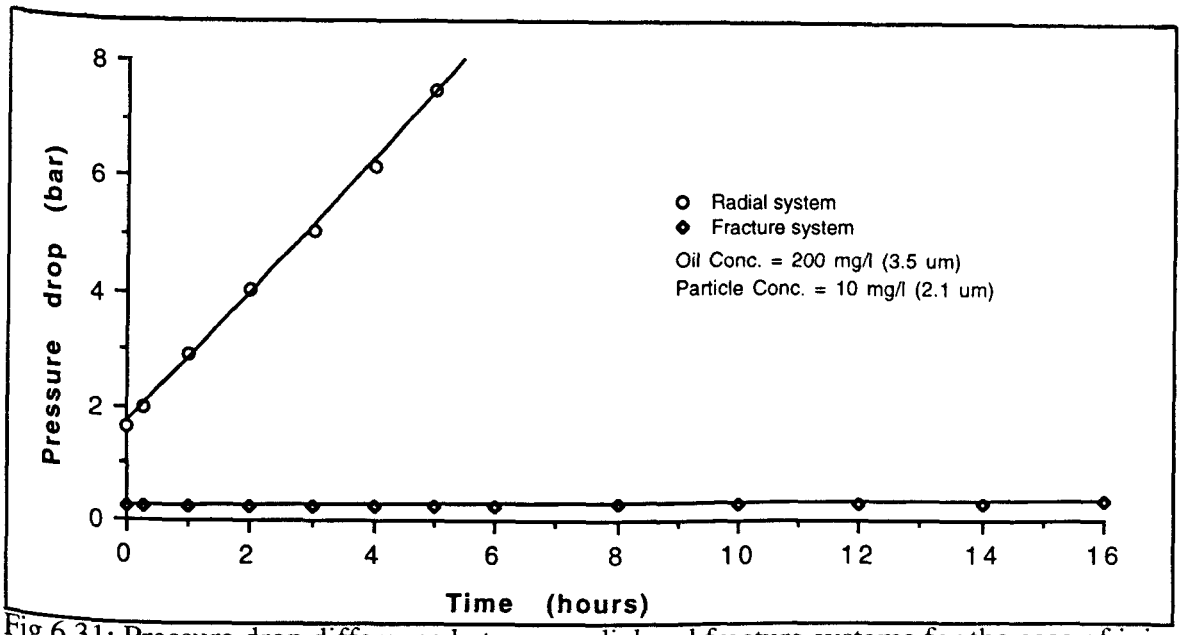

Fig.6.31: Pressure drop difference between radial and fracture systems for the case of injection fluid which contains 10 mg/l of 2.1 μm particles size and 200 mg/l oil (exps. 74 and 57).

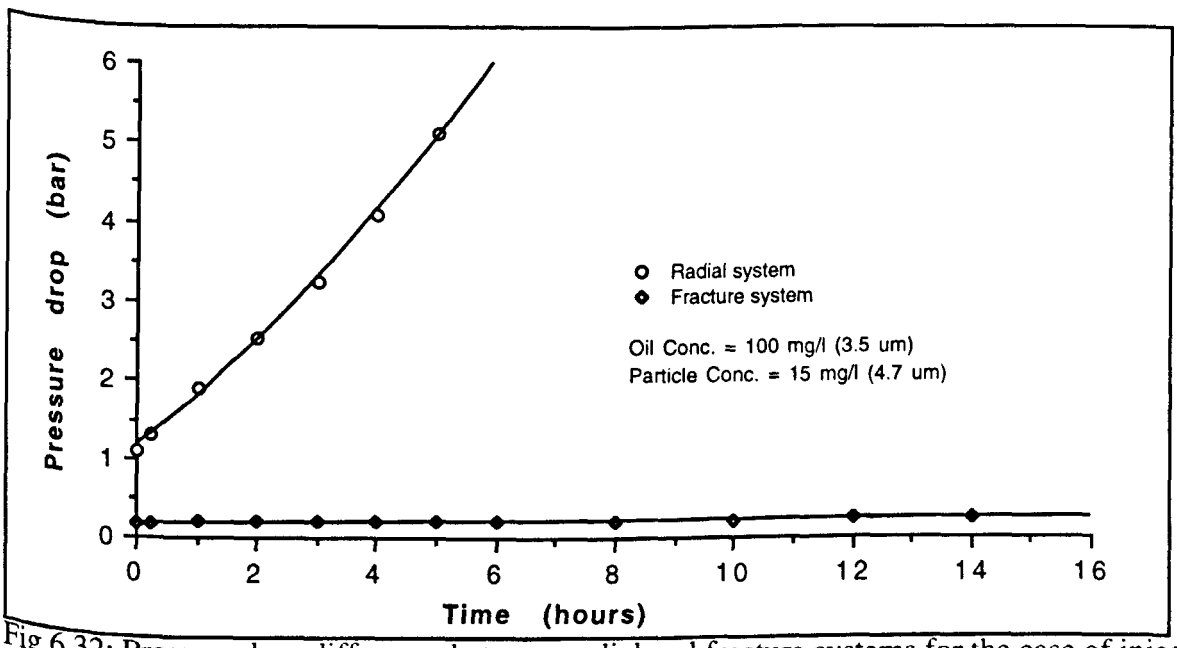

Fig.6.32: Pressure drop difference between radial and fracture systems for the case of injection fluid which contains 15 mg/l of 4.7 μm particles size and 100 mg/l oil (exps. 70 and 82).

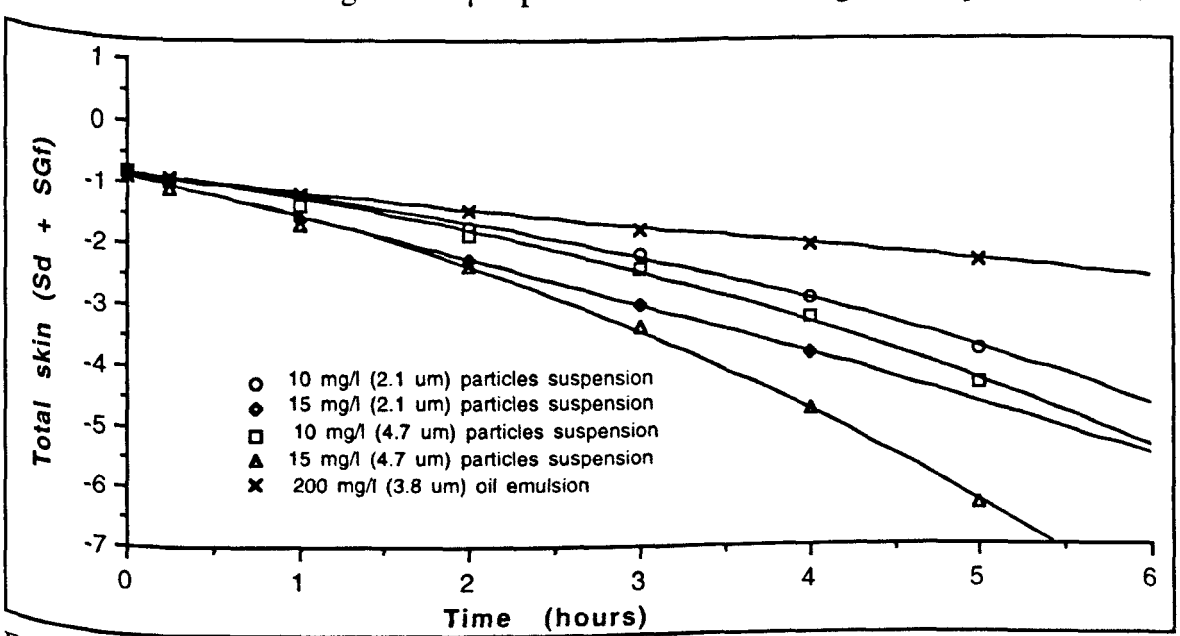

Fig.6.33: The change in total skin ($S_d + S_{Gf}$) with time.

6.7 Conclusions of the linear model applications

I- The linear injection plots of K/K_i versus pore volume injected indicated a clear internal cake formation (straining mechanism) or in-between a clear straining mechanism and gradual pore blocking mechanism (depending on Wojtanowicz theory).

The linear injection plots of K_i/K versus pore volume injected indicated a low resistance or high resistance internal filter cake mechanism (depending on Pang observations).

The fracture injection plots of K/K_i versus pore volume injected indicated a gradual pore blocking mechanism in all the fracture injection experiments (depending on Wojtanowicz theory) with some injected fluids causing higher blocking than the others.

The fracture injection plots of K_i/K (injectivity inverse) versus pore volume injected for all the fracture injection experiments indicated a permeable internal filter cake (depending on Pang observations) especially in the case of long fracture injection experiments.

II- The K_i/K versus time equation was re-arranged in the form $\frac{K_i}{K} = 1 + n\frac{K_i Q}{AL\phi_i}t$

When the K_i/K values obtained from fracture and linear experiments were plotted against [(K_i Q t) / (A L Ø)], the slope n only represents the degree of permeability alteration due to oil and/or solid concentration and droplet and/or particle mean size without taking in account the effect of flow difference between the fracture and the linear injection experiments.

(1) For the case of the 200 mg/l oil emulsion injection, changing from linear to fracture injection reduced the slope m to 63 %. And for the 10 mg/l suspension of 2.1 μm mean size particles, the same slope difference was obtained.

(2) Increasing the particle size and/or the particle concentration narrowed the difference between the matrix permeability damage (or the slope n) caused by the linear injection and that caused by fracture injection. The improvement in permeability damage (or the reduction of the slope n), caused by changing the injection system from linear injection to fracture injection, decreased from 37% (for the injection of 10 mg/l suspension of 2.1 μm mean size particles) to less than 8% (when the injection fluid was a 15 mg/l suspension of 4.7 μm mean size particles).

(3) When oil was added at a 100 or 200 mg/l concentration and 3.8 μm droplet mean size to the 2.1 μm mean size particle suspension, changing the injection system from linear to fracture injection can greatly reduce the permeability damage effect (or decreases the slope n) if the particle concentration was kept less than 10 mg/l.

III- The K_i/K versus time equation was re-arranged in the form $\frac{K_i}{K} = 1 + mt$

When the K_i/K values obtained from fracture and linear experiments were plotted against the time t, the slope represents the degree of permeability alteration due to the area difference between the fracture and the linear injection experiments as well as the alteration due to oil and/or solid concentration and droplet and/or particle mean size.

(1) By combining the effect of droplets and particles concentration and mean size with the effect of area difference, changing of the injection system from linear to fracture injection reduced the slope m (on average) to less than 5% of the linear injection experiments slope (this is true for all the carried out experiments). This means a 25 times increase in the injectivity.

(2) The slope m has a value from 0.12 to 0.65 for the linear injection and has a value from 0.0036 to 0.035 for the fracture injection.

V- The huge difference in the flow velocity and pressure drop between linear and fracture injection experiments may have had some effect on the capture and release mechanism of droplets and particles within the rock matrix. The effect of these two factors was deduced by studying the concentration ratio of the effluent (the ratio of effluent concentration to the influent concentration) of the linear and the fracture injection experiments.

(1) When the injected fluid was particle suspension only without any oil being added, the CR of the side outlets effluent in the fracture injection was between zero and 0.3. On the other hand the CR of effluent in the linear injection was between 0.25 and 0.8.

(2) The high flow velocity in linear injection can effectively prevent the precipitation or the capture of particles, whereas the very low flow velocity through matrix in the fracture injection encouraged more precipitation and capture of particles.

(3) The high pressure drop in the linear injection tended to force the particles through the matrix pores and to break the pre-formed particle bridges at the pore throats which enabled the particles to travel deep into the matrix before being captured which resulted in more particles reaching the outlet. On the other hand in the case of fracture injection, the pressure drop was not high enough to force the particles through pore throat or to break the pre-formed particle bridges and most of the particles were captured after travelling a very short distance into the matrix which resulted in less particles reaching the side outlets.

(4) As a result, it can be expected that the invasion depth in the linear injection was higher than the invasion depth in the fracture injection.

(5) When the injection fluid was oil emulsion only without any solids being added, the CR of the effluent in the linear injection was between 0.92 and 1.0, and the CR of side effluent in the fracture injection was between 0.84 and 1.0.

(6) The close concentration ratio (CR) values of the two systems in the case of oil emulsion experiments, contrary to the case of particle suspension experiments, can be explained by the deforming nature of the oil droplets. The 3.8 μm oil droplets do not need a high pressure to be forced through the small pore throat, also the oil droplets do not form bridges at the pore entry. The oil droplet density is less than the brine density which prevents its precipitation within the rock matrix.

(7) The difference in the effluent CR between the linear and the fracture systems (in the case of oil emulsion experiments) could be due to the difference in flow velocity through matrix between the two systems. The high flow velocity (as in the linear injection system) can return the pre-captured oil droplet into the flow stream (by shear force) more efficiently than the low flow velocity (as in the fracture injection system).

The flow velocity and pressure drop are very important factors which must be carefully studied to measure their effect on the matrix permeability damage in the fracture injection system.

IV- The calculated geometry skin (S_{Gr}) to convert from linear to radial system, depending on the dimensions of slabs which was used in the experiments, was - 0.538.

Due to difference in geometry, the radial system caused a higher pressure drop than the fracture system. The geometry skin to convert from radial to fracture system (S_{Gf}) is a function of (v_F K_{Ri} / v_R K_{Fi}). And if K_{Ri} was equal to K_{Fi}, then S_{Gf} is only a function of v_F.

The $|S_{Gf}|$ value increased as the initial matrix permeability (K_{Ri} and K_{Fi}) increased and as the side flow velocity through the rock matrix in the fracture system (v_F) decreased. The calculated value of S_{Gf} was between - 0.80 and - 0.89.

When the dirty water injection started, the large flow area of the fracture system resulted in less matrix damage than the small flow area of the radial system. Thus, the difference in pressure drop between the two systems consists of the pressure drop difference due to geometry (ΔP_{Gf}) plus the pressure drop difference due to the difference in matrix damage extent (ΔPd).
The total Skin is equal to the geometry skin (S_{Gf}) plus the skin due to the difference in matrix damage extent (S_d).
The S_d was experimentally measured and calculated, there was a very good agreement between the measured and the calculated values of S_d.

For the oil emulsion injection, the $|S_d|$ value increased gently with time with a rate of 0.28 per hour. This rate was increased to the double when the injected fluid was 10 mg/l of 2.1 μm mean size particle suspension, and increases by nearly 4 times when the injected fluid was 15 mg/l of 4.7 μm mean size particle suspension.

Matrix flow velocity in the fracture system (V_F)(cm/s)	Flow velocity at inflow face in the radial system (V_{Ri})(cm/s)	Initial Matrix permeability in fracture system (K_{Fi})(mD)	Initial Matrix permeability in radial system (K_{Ri})(mD)	$V_F K_{Ri} / V_R K_{Fi}$	Skin
0.024	0.410	252	240	0.056	-0.867
0.026	0.408	279	248	0.057	-0.877
0.031	0.406	401	493	0.094	-0.797
0.027	0.406	387	488	0.084	-0.815
0.019	0.431	207	230	0.049	-0.894
0.022	0.375	286	310	0.064	-0.860
0.028	0.417	348	360	0.069	-0.850
0.028	0.403	424	557	0.091	-0.803
0.030	0.441	431	500	0.079	-0.823

Table 6.1: The calculated skin factor for changing from radial to fracture system at initial conditions of clean salt water injection.

Time (hours)	DP_L	ΔP_{Gr} (bar)	ΔP_{Ri} (bar)	ΔPd_R (bar)	ΔP_{Fi} (bar)	ΔPd_F (bar) (corrected)	S_{Gf}	ΔP_{Gf} (bar)	ΔPd (bar) (measured)	S_d	ΔPd (bar) Calculated	Total skin S_d+S_{Gf}
0	4.15	2.07	2.08	2.08	0.278	0.278	-0.8665	1.8	0	0	0	-0.8665
0.25	4.30			2.23		0.278			0.15	-0.0705	0.15	-0.937
1	5.05			2.98		0.281			0.89	-0.4309	0.9	-1.2974
2	5.90			3.83		0.284			1.74	-0.8393	1.75	-1.7058
3	6.90			4.83		0.287			2.74	-1.3208	2.75	-2.1873
4	8.40			6.33		0.289			4.24	-2.0421	4.25	-2.9086
5	10.20			8.13		0.294			6.03	-2.9037	6.04	-3.7702

Table 6.2: The measured and the calculated skin values for an oil emulsion (exps. 62 and 75).

Time (hours)	DP_L	ΔP_{Gr} (bar)	ΔP_{Ri} (bar)	ΔPd_R (bar)	ΔP_{Fi} (bar)	ΔPd_F (bar) (corrected)	S_{Gf}	ΔP_{Gf} (bar)	ΔPd (bar) (measured)	S_d	ΔPd (bar) Calculated	Total skin S_d+S_{Gf}
0	4.15	2.07	2.08	2.08	0.278	0.278	-0.8665	1.8	0	0	0	-0.8665
0.25	4.30			2.23		0.278			0.15	-0.0705	0.15	-0.937
1	5.05			2.98		0.281			0.89	-0.4309	0.9	-1.2974
2	5.90			3.83		0.284			1.74	-0.8393	1.75	-1.7058
3	6.90			4.83		0.287			2.74	-1.3208	2.75	-2.1873
4	8.40			6.33		0.289			4.24	-2.0421	4.25	-2.9086
5	10.20			8.13		0.294			6.03	-2.9037	6.04	-3.7702

Table 6.3: The measured and the calculated skin values for the 10 mg/l of 2.1 μm mean size particle suspension (exps. 59 and 77).

Time (hours)	DP_L	ΔP_{Gr} (bar)	ΔP_{Ri} (bar)	ΔPd_R (bar)	ΔP_{Fi} (bar)	ΔPd_F (bar) (corrected)	S_{Gf}	ΔP_{Gf} (bar)	ΔPd (bar) (measured)	S_d	ΔPd (bar) Calculated	Total skin S_d+S_{Gf}
0	4.65	2.5	2.15	2.15	0.263	0.263	-0.8774	1.89	0	0	0	-0.8774
0.25	5			2.5		0.263			0.35	-0.163	0.35	-1.0404
1	6.14			3.64		0.267			1.49	-0.6914	1.49	-1.5688
2	7.67			5.17		0.271			3.01	-1.4013	3.01	-2.2787
3	9.26			6.76		0.275			4.6	-2.1399	4.6	-3.0173
4	11			8.5		0.278			6.34	-2.9481	6.33	-3.8255

Table 6.4: The measured and the calculated skin values for the 15 mg/l of 2.1 μm mean size particle suspension (exps. 60 and 76).

Time (hours)	DP_L	ΔP_{Gr} (bar)	ΔP_{Ri} (bar)	ΔPd_R (bar)	ΔP_{Fi} (bar)	ΔPd_F (bar) (corrected)	S_{Gf}	ΔP_{Gf} (bar)	ΔPd (bar) (measured)	S_d	ΔPd (bar) Calculated	Total skin S_d+S_{Gf}
0	2.35	1.26	1.09	1.09	0.221	2.21	-0.7969	0.87	0	0	0	-0.7969
0.25	2.5			1.24		0.221			0.15	-0.138	0.15	-0.9349
1	2.98			1.72		0.223			0.63	-0.5777	0.63	-1.3746
2	3.5			2.24		0.226			1.14	-1.0542	1.14	-1.8511
3	4.1			2.84		0.228			1.74	-1.6044	1.74	-2.4013
4	5			3.74		0.231			2.64	-2.4308	2.64	-3.2277
5	6.2			4.94		0.233			3.84	-3.5343	3.84	-4.3312

Table 6.5: The measured and the calculated skin values for the 10 mg/l of 4.7 μm mean size particle suspension (exps. 65 and 79).

Time (hours)	DP_L	ΔP_{Gr} (bar)	ΔP_{Ri} (bar)	ΔPd_R (bar)	ΔP_{Fi} (bar)	ΔPd_F (bar) (corrected)	S_{Gf}	ΔP_{Gf} (bar)	ΔPd (bar) (measured)	S_d	ΔPd (bar) Calculated	Total skin S_d+S_{Gf}
0	2.21	1.17	1.04	1.04	0.192	0.192	-0.8152	0.84	0	0	0	-0.8152
0.25	2.44			1.27		0.192			0.23	-0.2657	0.28	-1.0809
1	3.05			1.88		0.195			0.84	-0.8718	0.9	-1.687
2	3.75			2.58		0.199			1.53	-1.5677	1.62	-2.3829
3	4.75			3.58		0.201			2.53	-2.5635	2.66	-3.3787
4	6.1			4.93		0.204			3.88	-3.9088	4.05	-4.724
5	7.7			6.53		0.207			5.48	-5.5025	5.7	-6.3177

Table 6.6: The measured and the calculated skin values for the 15 mg/l of 4.7 μm mean size particle suspension (exps. 64 and 80).

Time (hours)	DP_L	ΔP_{Gr} (bar)	ΔP_{Ri} (bar)	ΔPd_R (bar)	ΔP_{Fi} (bar)	ΔPd_F (bar) (corrected)	S_{Gf}	ΔP_{Gf} (bar)	ΔPd (bar) (measured)	S_d	ΔPd (bar) Calculated	Total skin S_d+S_{Gf}
0	3.55	1.88	1.66	1.66	0.233	0.233	-0.8598	1.43	0	0	0	-0.8598
0.25	3.85			1.97		0.233			0.3	-0.2239	0.37	-1.0837
1	4.8			2.92		0.24			1.25	-0.8136	1.35	-1.6734
2	5.9			4.02		0.247			2.34	-1.4966	2.49	-2.3564
3	6.9			5.02		0.251			3.34	-2.1176	3.52	-2.9774
4	8.05			6.17		0.256			4.48	-2.8317	4.71	-3.6915
5	9.35			7.47		0.26			5.78	-3.6399	6.06	-4.4997

Table 6.7: The measured and the calculated skin values for the injected fluid which contains a 10 mg/l of 2.1 μm mean size particles and 200 mg/l oil (exps. 74 and 57).

Time (hours)	DP_L	ΔP_{Gr} (bar)	ΔP_{Ri} (bar)	ΔPd_R (bar)	ΔP_{Fi} (bar)	ΔPd_F (bar) (corrected)	S_{Gf}	ΔP_{Gf} (bar)	ΔPd (bar) (measured)	S_d	ΔPd (bar) Calculated	Total skin S_d+S_{Gf}
0	3.52	1.89	1.63	1.63	0.245	0.245	-0.8497	1.38	0	0	0	-0.8497
0.25	4.1			2.21		0.245			0.58	-0.3565	0.58	-1.2062
1	5.45			3.56		0.252			1.92	-1.1837	1.93	-2.0334
2	7.05			5.16		0.258			3.52	-2.1647	3.52	-3.0144
3	9.45			7.56		0.266			5.91	-3.6366	5.92	-4.4863
4	11.6			9.71		0.272			8.05	-4.9577	8.06	-5.8074

Table 6.8: The measured and the calculated skin values for the injected fluid which contains a 10 mg/l of 4.7 μm mean size particles and 200 mg/l oil (exps. 72 and 42).

Time (hours)	DP_L	ΔP_{Gr} (bar)	ΔP_{Ri} (bar)	ΔPd_R (bar)	ΔP_{Fi} (bar)	ΔPd_F (bar) (corrected)	S_{Gf}	ΔP_{Gf} (bar)	ΔPd (bar) (measured)	S_d	ΔPd (bar) Calculated	Total skin S_d+S_{Gf}
0	2.05	1.1	0.95	0.95	0.187	0.187	-0.8025	0.76	0	0	0	-0.8025
0.25	2.2			1.1		0.187			0.15	-0.1584	0.15	-0.9609
1	2.41			1.31		0.19			0.36	-0.3776	0.36	-1.1801
2	2.67			1.57		0.194			0.61	-0.6496	0.62	-1.4521
3	2.89			1.79		0.195			8.33	-0.8815	0.84	-1.684
4	3.11			2.01		0.196			1.05	-1.1133	1.05	-1.9158
5	3.31			2.21		0.198			1.25	-1.3233	1.25	-2.1258

Table 6.9: The measured and the calculated skin values for the injected fluid which contains a 15 mg/l of 2.1 μm mean size particles and 100 mg/l oil (exps. 67 and 81).

Time (hours)	DP_L	ΔP_{Gr} (bar)	ΔP_{Ri} (bar)	ΔPd_R (bar)	ΔP_{Fi} (bar)	ΔPd_F (bar) (corrected)	S_{Gf}	ΔP_{Gf} (bar)	ΔPd (bar) (measured)	S_d	ΔPd (bar) Calculated	Total skin S_d+S_{Gf}
0	2.27	1.19	1.08	1.08	0.192	0.192	-0.8227	0.89	0	0	0	-0.8227
0.25	2.5			1.31		0.192			0.23	-0.2999	0.32	-1.1226
1	3.1			1.91		0.194			0.83	-0.8926	0.97	-1.7153
2	3.72			2.53		0.197			1.45	-1.505	1.63	-2.3277
3	4.45			3.26		0.199			2.17	-2.2257	2.41	-3.0484
4	5.29			4.1		0.202			3.01	-3.0552	3.31	-3.8779
5	6.32			5.13		0.204			4.04	-4.0727	4.41	-4.8954

Table 6.10: The measured and the calculated skin values for the injected fluid which contains a 15 mg/l of 4.7 μm mean size particles and 100 mg/l oil (exps. 70 and 82).

CONCLUSIONS AND RECOMMENDATIONS

7.1 Conclusions

This study was conducted to investigate the matrix damage caused by the injection of simulated produced water along a fractured slab. The extent of matrix damage in the fracture system was compared with the extent of matrix damaged in the linear injection system. The difference between the two systems was shown experimentally and calculated numerically. A simple practical model was developed by using a dimensional analysis method. The linear system matrix damage results were converted to a radial system matrix damage, then a comparison study was performed between the radial and the fracture system by using the skin factor as the comparison criteria.

The following conclusions were reached:

(I) The experimental studies showed that:

(1) For the flow of clean brine, the pressure drop along the fracture affected the flow distribution through the fracture face. At low fracture pressure drop along the fracture, the flow through all 3 side outlets was similar, as the fracture pressure drop increased the flow through the side outlets varied. Increasing the matrix permeability resulted in a similar effect.

(2) For the case of fracture experiments, the injection of an emulsion of less than 200 mg/l oil concentration with a droplet mean size of less than 6 μm caused a very small reduction in matrix permeability with time (0.4 % per hour) compared with the linear injection of the same dispersion.(7.8 % per hour).

The flow in the fracture injection is distributed on a much larger area which will reduce the damage effect of the injected emulsion.

The fracture side effluent concentration ratio (CR) took some time (4 hours) before reaching the value of 1.0 whereas the CR of the linear injection effluent reached the value of 1.0 at the start of the experiment due to the flushing effect of the high flow velocity in the linear injection.

In the first 4 hours the mean diameter ratio of the effluent of the linear injection was higher than that of the side effluent of the fracture injection by only 0.04 because of the higher flow velocity of the linear injection which tends to flush the droplets deeper into the matrix to reach the slab outlet. As the permeability damage was taking place at a higher rate in the case of linear injection, more large droplets were captured within the matrix and the mean diameter ratio of the linear injection effluent started to decrease after 3 hours of injection (Fig.3.28). The mean diameter ratio of the fracture injection ended at a value of 0.9 after 14 hours of injection which means that the large droplets were still managing to get through and reaching the side outlets after a long injection time.

The linear injection effluent properties (the mean diameter ratio and the concentration ratio) had nearly the same values of the fracture injection side effluent properties (in spite of the difference in flow velocity), which indicate that oil droplets do not need a high driving flow (in the case of fracture injection) to pass through rock matrix.

In spite of the variations in flow velocity and pressure drop through the 3 side outlets, the location of the side outlet (close to or far from fracture inlet) had no effect on the droplet size or the oil concentration of its effluent. This mean that oil droplets capture at outlet A1 is similar to droplets capture at A3.

(3) The distribution of the particle suspension on the large fracture face area in the case of fracture injection resulted in a very low reduction rate in matrix permeability with time (0.9 to 1.7 % per hour). On the other hand the passing of particles through a very small flow area in the case of linear injection resulted in a much higher reduction rate in matrix permeability with time (12 to 14 % per hour). The flux density through matrix in the fracture system is distributed on a larger area which resulted in a lower damage with time. As the particle size or/and concentration increased, the difference in the damage rate between the two systems was decreased.

At early injection time the difference between the two reduction rates is higher than would be expected compared with the flow area difference (geometry difference between the two systems) between the linear and fracture experiments.

In the fracture injection process the reduction in matrix permeability is not sensitive to the variation in particle mean size and concentration or to the variation in droplet mean size and concentration if the injection time was short.
On the other hand, the matrix permeability reduction in the linear injection test was very sensitive to the variation in particle mean size and concentration.

For the case of fractured slabs, the 4.7 μm particle suspension caused a reduction in matrix permeability which is two to three times higher than the reduction caused by the 2.1 μm particle suspension injection. Thus to maximise the injectivity, particles higher than 2.1 μm should be filtered out before injecting the produced water into the fractured formation.

The particle concentration ratio of the linear injection effluent (from 0 to 0.3) was higher than the concentration ratio of the fracture injection side effluent (from 0.4 to 0.8).
This is due to the difference in the driving force (flow velocity and pressure drop) between the two systems, which is higher in the case of linear injection than it is in the fracture injection. The very low flow velocity through the rock matrix in the case of fracture injection will encourage the particle capture within the matrix pores near the fracture face while in the case of linear injection the high flow velocity flushed the particles deeper into the rock matrix.

From this it can be concluded that the particle invasion in the case of linear injection would be greater than in the case of fracture injection.

In the fracture injection, the concentration ratio of the side outlets effluent decreased as the particle concentration of the influent fluid increased from 10 to 15 mg/l, which indicated more capture of particles within the matrix. The particle concentration of the effluent of the outlet A1 was always equal or higher than the particle concentration of the outlet A3 which indicated that

the capture of particles is higher at A3 than it is at A1 (because the flow velocity through outlet A1 is higher than it is through A3).
As the influent particle concentration increased from 10 to 15 mg/l, the difference between the effluent particle concentration of the side outlets A1 and A3 increased.
The outlet A1 effluent had a mean size which was higher than the influent particle mean size of the outlet A3 which means that large particles is captured at A3 more efficiently that it is at A1.

(4) The presence of oil at a concentration of 100 mg/l and at 3.6 μm droplet mean size reduced the damage effect (on matrix permeability) caused by the presence of particle.

Oil has the property of lubrication which may reduces the friction between the solid particles and the rock matrix grains and reduces the contact between them.
The presence of oil in much higher concentration than the solids gives the oil droplets a control on most of the flow paths which reduces the total particle blocking probability due to the small number of paths available for particles. Oil droplets blocks the small pore throats and the particles is directed to the larger pore throats where the chance of particle capture is less, this mechanism resulted in less pore throat blocking, and as oil droplet can deform and passes through the small pores, this leads to less permeability damage.

As the oil droplets concentration (in the experiments where the injected fluid contains oil and solids) was far higher than the solid particles concentration, it was believed that the mean diameter ratio and concentration ratio results represent the oil droplet mean diameter ratio and concentration ratio more than they represented the particle mean diameter ratio and concentration ratio.

The addition of oil at a concentration of 200 mg/l with 3.6 μm droplet mean size to the solid particle suspension resulted in further reduction in matrix permeability.

(5) The pressure - flow rate distribution showed that there is selective unblocking and blocking of sections of matrix, rather than a section being blocked and remaining blocked.

The reduction in flow rate through a certain side outlet due to matrix blocking may cause an increase in flow rate of a nearby side outlet which has less permeability impairment and higher differential pressure (instead of directing the flow along the fracture to cover a new less damaged fresh matrix).

As the fracture length increased a wider range of matrix heterogeneity will exist, which will lead to more variation in the degrees of matrix blocking from location to location. The random variation in matrix permeability along the fracture will result in a random degree of matrix blocking which may not be dependent on the distance from the fracture inlet.

(6) In the experiments which were designed to simulate the external filter cake accumulation on the fracture face and its erosion, as the permeability of the filter cake decreased, the flow was directed more and more along the fracture which caused the erosion of the filter cake as the flow forced its way along the fracture. This resulted in an increase in the CR of the effluent along the fracture to a value which is double the influent particle concentration due to the erosion of the filter cake.

When the slab was cut open along the fracture length, a very thick external filter cake all the way along the fracture was observed. Within the cake a thin and long channel (connecting the inlet and the outlet of the fracture) could be seen.

(II) The computer simulation study showed that:

For the small scale models:

(1) For a 40 cm long full open fractured slab injection model with a clean matrix, more than half of the pressure drop was lost in the first half of the fracture, as the flow velocity along the fracture in the first half of the fracture is much higher than it is in the second

(2) As the matrix permeability decreased, the pressure drop with distance along the fracture became more and more linear (as the flow velocity reduction along the fracture become more uniform).

(3) By increasing fracture length from 40 to 80 cm (while the flow velocity at the fracture inlet is constant) the pressure drop along the fracture increased by only 12%, but still most of the pressure drop and flow velocity along the fracture is lost in the first 20 cm along the fracture.

This indicated the major effect of the first section of the fracture in the damage process, as most of the fluid is directed through the fracture face in this section.

(4) The rough fracture face model showed that the effect of fracture face surface roughness was negligible along the fracture, except at the high flow region at the fracture inlet.

For the field application:

(1) The presence of a fracture changes the flow pattern around the wellbore considerably. It can significantly improved the pressure drop and flow velocity distribution through formation matrix. The presence of two fractures resulted in further improvement in the flow pattern.

(2) For a field radial injection model with a single fracture and a near fracture face skin, the effect of both damaged zone width and permeability on the injectivity is very minimal even at both high damaged zone depth and very low damaged zone permeability.
The huge length of the fracture compared with the small width of the damaged zone reduced the effect of the damaged zone permeability on the injectivity, and maintain it for a much longer time.

(III) The dimensional analysis study resulted in:

(1) A simple model was developed by using dimensional analysis method with the experimental results: Injectivity inverse $II = C\left(\frac{v*t}{\sqrt{K_m}}\right)^d$

The above final equation contains the most important variables that affect the pressure drop value when matrix damage takes place.
C is function of droplets and particles concentartion and size (C_P and D_P) variables: increasing the variables C_P and D_P resulted in higher pressure drop due to higher damage.
Flow velocity through matrix (v) is function of flow rate (q) and flow area A. For constant flow rate (q), larger flow area (A) means that less fluid volume per unit area per second (more solid and/or oil per second) is passing through the matrix which results in less matrix damage.
As time passes, more damage takes place within the matrix.

The pore throat diameter D_{pore} is a function of matrix permeability (Km) and as Km decreases, D_{pore} decreases which results in higher probability of pore throat bridging to take place in less time. For narrow pore throat, less fluid volume is needed to pass through it before bridging would take place. For constant flow rate this eventually means less time is needed for the bridging to take place.

(2) The C and the d were evaluated by using the experimental results.
Each time the linear and the fracture injection experiments were carried out nearly under the same conditions such as total flow rate, oil and solids concentrations, and droplets and particles mean size. The initial matrix permeability of the two experiments was similar, which made the main variable (which determined the d and C values) is the flow velocity through matrix. Thus the C and d values were potted versus flow velocity and best fitted.

(3) For the fracture injection experiments the value of C is very sensitive to the change in fluid composition. For oil emulsion injection C had a very high value (0.05 - 0.25) compared with the C value for the particle suspensions injection (0.0075 - 0.067), which shows the higher ability of particles to block the matrix pores than the oil droplets does.
There is a huge difference between C values for linear injection (0.000013 - 0.013) and fracture injection (0.0075 - 0.25), which indicated the difference in the blocking extent of droplets and particles of the rock matrix pores between the fracture and the linear injection experiments.

(4) The d value for the particle suspensions was higher than the d value for the oil emulsion, which indicated that the effect of flow velocity, injection time, and matrix permeability in the case of particle suspension injection is greater than their effect in the case of oil emulsion injection.

For the oil emulsion injection, exponent d for the linear injection experiments had a value which is double the d value of the fracture injection experiments. And for the particle suspension experiments this difference was treble. These d values indicated that the effect of flow velocity, injection time, and matrix permeability in the case of linear injection is 2 to 3 time greater than their effect in the case of fracture injection.

(5) At very low flow velocities, the d and C values are very sensitive to any change in flow velocity and at high flow velocities the values of d and C tend to constant values.

Interpolation of the plotted data of C and d versus flow velocity can be used for injected fluids other than those used in the experiments.

(6) The HIT (time needed to reduce the injectivity to half) for the injection experiments were calculated by using the C and d values which were evaluated by using the experimental results. For the case of oil emulsion injection experiments and the 2.1 μm particle suspension injection experiments, there was a large difference in the calculated HIT between the two injection systems (80 times) compared with the area difference between the two systems (linear and long fracture) which is only to 13 times.

For the injection of the 4.7 μm mean size particle suspensions, the difference in the calculated HIT between the linear injection and long fracture experiments was 14 times indicating that the fracture injection was more sensitive to the 4.7 μm mean size particle suspensions than it was to the 2.1 μm mean size particle suspensions.

(7) The C and d values can be calculated, for a given injected fluid composition, at any flow velocity by using the C and d versus flow velocity fitting equations. The calculated C and d values were used to measure the change in the injectivity with time for two field cases (unfractured and fractured wells) with different injected fluid compositions.

There was a large difference in the half injectivity time between the two injection systems (unfractured and fractured wells). For the 200 mg/l oil emulsion injection the half injectivity time was 3293 times higher in the case of fractured well (with single 10 m long fracture) than it was in the unfractured well. Whereas for the case of 15 mg/l of 4.7 μm particle suspension injection (worst case) it was 50 times higher.

There was a sharp reduction in the half injectivity time when flow velocity increased from 0.00003 to 0.00006 m/s. The reduction rate in half injectivity time for flow velocity higher than 0.00006 m/s was less and started to level at a flow velocity higher than 0.00012 m/s.

(IV) The application of formation damage models showed that:

(1) The fracture injection plots of K/K_i versus pore volume injected indicated a gradual pore blocking mechanism in all the fracture injection experiments. The fracture injection plots of K_i/K (injectivity inverse) versus pore volume injected for all the fracture injection experiments indicated a permeable internal filter cake was formed.

(2) The K_i/K versus time equation was re-arranged in the form $\frac{K_i}{K} = 1 + n\frac{K_i Q}{AL\phi_i}t$

The K_i/K values obtained from fracture and linear experiments were plotted against [(K_i Q t) / (A L Ø)], the slope n only represents the degree of permeability alteration due to oil and/or solid concentration and droplet and/or particle mean size and does not represents the effect of flow area difference between the fracture and the linear injection experiments, as the flow area (A) was not included in the mathematical presentation of the slope n.

The improvement in the injectivity (or the reduction of the slope n), caused by changing the injection system from linear injection to fracture injection was between 8% and 37%.

(3) Again the K_i/K versus time equation was re-arranged in the form $\frac{K_i}{K} = 1 + mt$

The slope (this time) represents the degree of permeability alteration due to the area difference between the fracture and the linear injection experiments as well as the alteration due to oil droplets and/or solid particle, as this time the flow area (A) was included in the mathematical presentation of the slope m .

Changing of the injection system from linear to fracture injection reduced the slope m (in average) to less than 5% of the linear injection experiments slope (this is true for all the experiments). This means a large improvement in the injectivity (nearly 25 times improvement in the injectivity).

(4) For the clean salt water injection, the calculated geometry skin to convert from radial to fracture system, $|S_{Gf}|$ value, increased as the initial matrix permeability increased, and as the side flow velocity through the rock matrix in the fracture system (v_F) decreased. The calculated value of S_{Gf} was between - 0.80 and - 0.89.

(5) When the dirty produced water injection started, the total skin is equal to the geometry skin (S_{Gf}) plus the skin due to the difference in matrix damage extent between the radial and the fracture system (S_d). The S_d was experimentally measured and calculated with very good agreement between the measured and the calculated values of S_d.

(6) For the oil dispersion injection, the $|S_d|$ value increased with time with a rate of 0.28 per hour. This rate was doubled when the injected fluid was 10 mg/l of 2.1 μm mean size particle suspension, and increases by nearly 4 times when the injected fluid was 15 mg/l of 4.7 μm mean size particle suspension, which indicated that the difference in matrix damage extent between the two systems is increasing with time.

7.2 Recommendations For Future Work

(1) This study was conducted for a matrix permeabilities of 240 to 550 md. The variation in the initial matrix permeability requires investigation to ensure that the relationships developed are applicable to other ranges of permeabilities.

(2) To obtain a clearer relation between the flow geometry and the injectivity reduction with time, experiments using longer fractured slabs with higher flow rates need to be undertaken.

(3) The variation of damage with flow velocity through matrix requires further investigation to ensure that the plots of C and d versus flow velocity are correct. It is also important to directly measure the pressure distribution along the fracture.

(4) As the droplet and particle concentrations differ from field to field, it is important to extend this work to investigate the injection of particle suspensions of less than 10 mg/l and the injection of oil dispersions of higher than 200 mg/l and their effect on the injectivity.

(5) To be more close to the actual field case, a radial flow cell with a single vertical fracture is recommended to be designed and tested under different injection conditions and different injection fluid compositions.

(6) The injection process should be continuous, especially for the high solid concentration suspension experiments.

(7) It is recommended to investigate the effect of pressure pulsation on the injectivity improvement in the fractured systems (as the case in the field injection operations).

(8) For the case of low solids concentration, as the case in the true field injection, it is recommended to measure the injection time needed for the external filter cake to start to accumulate on the fracture face, and the dependence of this time on the injection conditions and the injected fluid composition should be investigated.

(9) The relationship between the damage skin (S_d) and the composition of the injected fluid should be further investigated to define the exact relation between them.

REFERENCES

(1)
Ahmed Hussain H.: "Perforation Screen-Out During Hydraulic Fracturing," PhD Heriot-Watt University, Dept. of Petroleum Engineering, June 1993.

(2)
Anderson William G.: "Wettability Literature Survey-Part1: Rock/Oil/Brine Interactions and the effects of core handling on Wettability," Journal of Petroleum Technology, October 1986.

(3)
Arcia Einstein Millan, Civan Faruk: "Characterisation of Formation Damage by Particulate Processes," Journal of Canadian Petroleum Technology, March 1992, vol 31, No.3.

(4)
Bennion, D.B., Bennion, D.W., Thomas, F.B., Bietz, R.F.: "Injection Water Quality-A Key Factor to Successful Waterflooding," Petroleum Society of CIM & AOSTRA. 45th annual technical meeting of the Petroleum Society of CIM, Calgary, Canada, June 12-15, 1994.

(5)
Berkowitz Brian.: "Boundary Conditions along Permeable Fracture Walls: Influence on Flow and Conductivity," Water Resources Research. Vol.25. No.8.Pages 1919-1922. Aug 1989.

(6)
Burnett David S,: "Finite Element Analysis. From Concepts to Applications," Addison -Wesley Publishing Company 1987.

(7)
Chamoun, H., Schechter, R.S., Sharma, M.: "The Hydrodynamic Forces necessary to release Non-Brownian Particles Attached to a Surface," Syposium on Advances in Oil Field Chemistry. American Chemical Society, Toronto meeting, June 5-11 1988.

(8)
Charles Dawari D., Xiaopeng Xie,: "Effectiveness of Fluid Loss Additives in Laboratory Dynamic Fluid Loss Experiments," SPE 29498. Production Operations Symposium, Oklahoma City. OK 2-4 April 1995.

(9)
Cinco Heber L., Samaniego, F.V., Dominguez, N.A.: "Transient Pressure Behaviour for a Well with a finite-conductivity Vertical Fracture," SPE-AIME 51st Anuual Fall Technical Conference and Exhibition, New Orleans, Oct 3-6 1976.

(10)
Cinco-Ley Heber, Samaniego Fernando V.: "Effect of Wellbore Storage and Damage on the transient Pressure Behaviour of Vertically Fractured Wells," SPE 6752. 52nd Annual Fall Technical Conference and Exhibition of the SPE of AIME, Denver, Colorado. Oct 9-12 1977.

(11)
Cinco-Ley Heber, Samaniego Fernando V.: "Transient Pressure Analysis: Finite Conductivity Fracture Case Versus Damaged Fracture Case," SPE 10179. 56th Annual Fall Technical Conference and Exhibition of the SPE of AIME, San Antonio, TX OCt 5-7 1981.

(12)
Civan Faruk, Kapp Roy M., Ohen Henry A. : "Alteration of permeability by fine particle processes" Journal of Petroleum Science and Engineering, 3 (1989) 65 - 79.

(13)
Clark Kenneth K., Somerton Wilbur H.: "Laboratory Investigation of Reuction of Fracture Pressures of Rocks by Intensive Borehole heating," SPE 1055. Conference on Drilling and Rock Mechanics, Austin, TX, Jan 20-21 1965.

(14)
Clifford, P.J., Mellor, D.W., Jones, T.J.: "Water Quality Requirements for Fractured injection Wells," SPE 21439. SPE Middle East Oil Show, Bahrain, Nov.16-19 1991.

(15)
Craft, B.C., Hawkins, M.F, Revised by Terry, Ronald E.: "Applied Petroleum Reservoir Engineering Second Edition," Prentice Hall, N.J.1991.

(16)
Crawford Paul B, Collins, R.E.: "Estimated Effect of Vertical Fractures on Secondary Recovery," T.P.3879. Petroleum Transactions, AIME, 1953.

(17)
Davidson Donald H.: "Invasion and Impairment of Formations by Particulates," SPE 8210. 54th Annual Fall Conference and Exhibition of the SPE of AIME, Las Vegas, Nevada, Sept 23-26 1979.

(18)
Detienne, J.L., Creusot, M., Kessler, N., Sahuquet, B., Bergerot, J.L.: "Thermally Induced Fractures: A Field Proven Analytical Model," SPE 30777. SPE Annual Technical Conference and Exhibition, Dallas, TX 22-25 Oct. 1995.
(19)
Dixon Bryan P., Newton Jr, L.E.: "Reinjection of Large Volumes of Produced Water in Secondary Operations," SPE 1147. SPE Permian Basin Oil Recovery Symposium, Midland, TX May 10-11, 1965.
(20)
Donaldson Erle C., Baker Byron A., Carroll Herbert B.: "Particle Transport in Sandstones," SPE 6905. 52nd Anual Fall Technical Conference and Exhinbition of the SPE of AIME, Denver, Colorado, Oct 9-12, 1977.
(21)
Donaldson Erle C., Thomas Rex D.: "Microscopic Observations of Oil Displacement in Water-Wet and Oil-Wet Systems," SPE 3555. 46th Annual Fall Meeting of the SPE of AIME, New Orleans, La., Oct.3-6, 1971.
(22)
Eleri, O.O, Ursin, J.R.: "Physical Aspects of Formation Damage in Linear Flooding Experiments," SPE 23784. SPE Intl. Symposium on Formation Damage Control., Lafayette, Louisiana, Feb.26-27 1992.
(23)
Ershaghi, I., Hashemi, R., Caothien, S.C., Abdassah, D.: "Injectivity Losses Under Particle Cake Buildup and Particle Invasion," SPE 15073. 56th California Regional Meeting of the SPE, Oakland, CA, April 2-4, 1986.
(24)
Eylander, J.G.R.: "Suspended Solids Specifications for Water Injection from Coreflood Tests," SPE Resevoir Engineering, Nov. 1988.
(25)
Garon, A.M., Lin, C.Y., Dunayevsky, V.A.: "Simulation of Thermally Induced Waterflood Fracturing in Prudhoe Bay," SPE 17417. SPE California Regional Meeting, Long Beach, California, March 23-25, 1988.
(26)
Gidley John L., Holditch Stephen A, Nierode Dale E, Veatch Jr.: "Recent Advances in Hydraulic Fracturing," Henry L. Doherty Memorial Fund of AIME. SPE, Richardson, TX 1989.
(27)
Graciaa Alain, Fortney Lester, N., Schechter Robert S., Wade William H., Yiv Seang.: " Criteria for Structuring Surfactants to Maximize Solubilization of Oil and Water: Part1 - Commercial Nonionics," SPE 9815. SPE/DOE Enhanced Oil Recovery Symposium, Tulsa, April 5-8, 1981.
(28)
Gringaten, A.C., Ramey Jr, H.J., Raghaven, R.: "Applied Pressure Analysis for Fractured Wells," JPT July 1975.
(29)
Gruesbeck Clay, Collins, R.E.: "Entrainment and Deposition of fine Particles in Porous Media," SPE 8430, JPT Dec. 1982.
(30)
Hagoort Jacques, Weatherill Brian D., Settari Antonin.: "Modeling the Propagation of Waterflood-Induced Hydraulic Fractures," JPT Aug.1980.
(31)
Herzig, J.P., Leclerc, D.M., Le Goff, P.: "Flow of Suspensions through Porous Media-Application to Deep Filtration," Flow Through Porous Media Symposium. Industrial and Engineering Chemistry, Vol.62, No.5, May 1979.
(32)
Hofman, J.A.M.H., Stein, H.N.: "Permeability reduction of porous media on transport of emulsions through them," Colloids and Surfaces, 61 (1991) 317-329, Elsevier Science Publishers B.V., Amsterdam.
(33)
Holzhausen, G.R., Egan, H.N.: "Detection and Control of Hydraulic Fractures in Water Injection Wells," SPE 16362. SPE California Regional Meeting, Ventura, California, April 8-10, 1987.
(34)
Howard, G.C., Fast, C.R.: "Hydraulic Fracturing," Henry L. Doherty Memorial Fund of AIME. SPE of AIME, New York & Dallas 1970.

(35)
Hsi, C.D., Dudzik, D.S., Lane, R.H., Buettner, J.W., Neira, R.D.: "Formation Injectivity Damage Due to Produced Water Reinjection," SPE 27395. SPE Intl. Symposium on Formation Damage Control, Lafayette, Louisiana, 7-10Feb. 1994.

(36)
Hsi, C.D., Strassner, J.E., Tucker, H.E., Townsend, M.A.: "Prudhow Bay Field, Alaska, Waterflood Injection Water Quality and Remedial Treatment Study," SPE 20689. 65th Annual Technical Conference and exhibition of the SPE, New Orleans, La., September 23-26, 1990.

(37)
Huntley, H.E.: "Dimensional Analysis," Constable and Company Ltd, London, 1967.

(38)
"Hydraulic Fracturing-1," SPE Reprint series no.28. 1990 Edition, SPE, Richardson, TX.

(39)
"Hydraulic Fracturing-2," SPE Reprint series no.28. 1990 Edition, SPE, Richardson, TX.

(40)
Ismail Abdul R., Peden James M., Arshad Azmi M.: "The effects of Solids Concentration and Formation Characteristics on Formation Damage and Permeability Recovery," SPE 28762. SPE Asia Pacific Oil and Gas Conference, Melbourne, Australia, Nov 7-10 1994.

(41)
Jiao Di, Sharma Mukul M.: "Mud Induced Formation Damage in Fractured Reservoirs," SPE 30107. European Formation Damage Conference, The Hague, Netherlands May 15-16 1995.

(42)
Jiao, D., Sharma Mukul M.: "Mechanism of Cake Buildup in Crossflow Filtration of Colloidal Suspensions," Journal of Colloid and Interface Science 162, 454-462 (1994).

(43)
Johnson, M.H., Ashton, J.P., Nguyen Hang: "The effects of Erosion Velocity on Filter-Cake Stability during Gravel Placement of Openhole Horizontal Gravel-Pack Completions," SPE 23773. SPE Intl. Symposium on Formation Damage Control, Lafayette, Louisiana, Feb 26-27 1992.

(44)
Jones, T.A., Wooten, S.O., Kaluza, T.J.: "Single-Phase Flow through Natural Fractures," SPE 18175. 63rd Annual Technical Conference and Exhibition of the SPE, Houston, TX, Oct. 2-5 1988.

(45)
Khatib, Z.I.: "Prediction of Formation Damage Due to Suspended SOlids: Modeling Approach of Filter Cake Buildup in Injectors," SPE 28488. SPE 69th Annual Technical Conference and Exhibition, New Orleans, La., 25-28 Sept.1994.

(46)
King, R.E.: "Maureen produced Water Injection," SPE 26703. Offshore European Conference, Aberdeen, 7-10 Sept.1993.

(47)
Kumar Tarkeshwar.: "Modelling of Formation Damage due to Particle Invasion in relation to Water Injection Schemes," PhD, Heriot-Watt University, Dept. of Petroleum Engineering, Aug. 1988.

(48)
Langhaar Henry L.: "Dimensional Analysis and Theory of Models," John Wiley & Sons, New York: Chapman & Hall, London 1951.

(49)
Lee Sheng-Tai, Brockenbrough John R.: "A new Approximate Analytic Solution for Finite-Conductivity Vertical Fractures," SPE Formation Evaluation Feb. 1986.

(50)
Martins, J.P., Murray, L.R., Clifford, P.J.G., McLelland Gregory, Hanna, M.F., Sharp Jr, J.W.: "Long-Term Performance of Injection Wells at Prudhoe Bay: The Observed Effects of Thermal Fracturing and Produced Water Re-Injection," SPE 28936. SPE 69th Annual Technical Conference and Exhibition, New Orleans, La, Sept 25-28 1994.

(51)
Massey, B.S.: "Units, Dimensional Analysis and Physical Similarity," Van Nostrand Reinhold Company, London, 1971.

(52)
Morales,R.H., Abou-Sayed, A.S., Jones, A.H.: "Detection of Formation Fracture in a Waterflooding Experiment," SPE 13747. SPE Middle East Oil Technical Conference and Exhibition, Bahrain, March 11-14 1985.
(53)
Muecke, T.W.: "Formation Fines and Factors Controlling their Movement in Porous Media," SPE7007. Journal of Petroleum Technology, 1978.
(54)
Muskat, M.: "The Flow of Homogeneous Fluids Through Porous Media," International Human Resources Develoment Corporation, Boston, 1982.
(55)
Navarette, R.C., Cawiezel, K.E., Constien, V.G.: "Dynamic Fluid Loss in Hydraulic Fracturing Under Realistic Shear Conditions in High-Permeability Rocks," SPE 28529. SPE 69th Annual technical Conference and Exhibition, New Orleans, La. 25-28 Sept. 1994.
(56)
Nielson Derek A.: "Injection Well Fracture Propogation Study," MEng. Project Report. 1983/84.
(57)
Olarewaju, J.S., Holditch, S.A., Lee, W.J.: "A new Analytical Model of Finite-Conductivity Hydraulic fracture in a Finite Resevoir," SPE 19093. SPE Gas Technology Symposium, Dallas, TX June 7-9 1989.
(58)
Palacios, J.: "Dimensional Analysis," MacMillan & Co. Ltd, London, 1964

(59)
Pang Shutong, Sharma Mukul M.: "Evaluating the Performance of Open-Hole, Perforated and Fractured Water Injection Wells," SPE 30127. European Formation Damage Conference, The Hague, Netherlands, 15-16 May, 1995.
(60)
Pang Shutong, Sharma, M. M.: " A Model for Predicting Injectivity Decline in Water Injection Wells," SPE 28489. SPE 69th Annual Conference and Exhibition, New Orleans, La, Sept. 25-28, 1994.
(61)
Parsons, R.W." "Permeability of Idealized Fractured Rock," SPE 1289. SPE ANnual Fall Meeting, Denver Colorado, Oct.3-6, 1965.
(62)
Pautz, J.F., Crocker, M.E., Walton, C.G.: "Relating Water Quality and Formation Permeability to Loss of Injectivity," SPE 18888. SPE Production Operations Symposium, Oklahoma City, Oklahoma, March 13-14 1989.
(63)
Peden James M.: "The Filtration and Associated Permeability Impairment Characteristics of Drilling and Completion Fluids," PhD Heriot-Watt University, Dept. Of Petroleum Engineering, Sept.1983
(64)
Peng Shuang Jiu, Peden, J.M.: "Prediction of Filtration Under Dynamic Conditions," SPE 23824. SPE Intl. Symposium on Formation Damage Control, Lafayette, La, Feb. 26-27, 1992.
(65)
Penny Glenn S, Conway Michael W.: "Control and Modeling of Fluid Leakoff during Hydraulic Fracturing," JPT June 1985.
(66)
Poulsen, D.K.: "A Comprehensive Theoretical Treatment of Fracturing Fluid Loss," SPE 18262. 63rd Annual Technical Conference and Exhibition of the SPE, Houston, TX, Oct.2-5, 1988.
(67)
Prats, M.: "Effect of Vertical Fractures on Reservoir Behavior Incompressible Fluid Case," 35th Annual Fall Meeting of the SPE, Oct.2-5, Denver, 1960.
(68)
Pucknell, J.K., Clifford, P.J.: "Calculation of Total Skin Factors," SPE 23100. Offshore Europe Conference, Aberdeen, 3-6 Sept. 1991.
(69)
Rein Jr, R.G., Lord, D.L., Shah, S.N.: "Description of a large, High-Pressure Slot Flow Apparatus for Characterizing Fracturing Fluids," SPE 26524. 68th Annual Technical Conference and Exhibition of the SPE, Houston, TX, 3-6 Oct. 1993

(70)
Rickford, R.L., Finney, T.P.: "Formation Damage from fine Particulate Invasion: An Example from the Lost Soldier Tensleep Formation," SPE 18886. SPE Production Operations Symposium, Oklahoma City, Oklahoma, March 13-14, 1989.
(71)
Rochon, J., Creusot, M.R., Rivet, P., Roque, C., Renard, M.: "Water Quality for Water Injection Wells," SPE 31122. SPE Formation Damage Control Symposium, Lafayette, USA, 14-15 Feb. 1996.
(72)
Roque, C., Chauveteau, G., Renard, M., Thibault, G., Bouteca, M., Rochon, J.: "Mechanisms of Formation Damage by Retention of Particles Suspended in Injection Water," SPE 30110. European Formation Damage Conference, The Hague, Netherlands, 15-16 May 1995.
(73)
Scott Graham C.: "Methods of predicting permeability impairment and injectivity decline for homogeneous sandstone reservoirs," MEng project report, Petroleum Engineering Department, Heriot-Watt University, 1983-84.
(74)
Selmeczi Joseph G.: "Capture Mechanisms in Deep-Bed Filtration," Industial Water Engineering, June/July 1971.
(75)
Settari, A. & Warren, G.M. : "Simulation and field analysis of waterflood induced fracturing," Eurock '94, 1994 Balkema, Rotterdam.
(76)
Settari, A.: "General Model of Fluid Flow (Leakoff) from Fractures Induced in Injection Operations," SPE 18197, 63rd Annual Technical Conference and Exhibition of the Society of Petroleum Engineers held in Houston, TX, October 2-5, 1988.
(77)
Sharma Mukul M., Chamoun Habib, Sarma, D.S.H. Sita Rama, Schechter Robert S.: "Factors Controlling the Hydrodynamic Detachment of Particles from Surfaces," Journal of Celloid and Interface Science Vol. 149 No.1, March 1992.
(78)
Sharma Mukul. M., Pang Shutong, Wennberg Kjell Erik, Morgenhalter Lee.: "Injectivity Decline in Water Injection Wells: An offshore Gulf of Mexico Case Study," SPE 38180. SPE European Formation Damage Conference, The Hague, Netherlands, 2-3 June 1997.
(79)
Simpson, A.J., Paige, R.W.: "Advances in Forties Field Water Injection," SPE 23140. Offshore Europe Conference, Aberdeen, 3-6 Sept. 1991.
(80)
Soo Hwalli, Radke Clayton J.: "The Flow Mechansim of Dilute, Stable Emulsions in Porous Media," Ind. Eng. Chem. Fundam. 1984, 23, 342-347.
(81)
Soo, H., Radke, C.J.: "A Filtration Model for the Flow of Dilute, Stable Emulsions in Porous Media-I. Theory," Chemical Engineering Science. Vol. 41, No.2. pp.263-272, 1986.
(82)
Soo, H., Radke, C.J.: "Flow of Dilute, Stable Liquid and Solid Dispersions in Underground Porous Media," AIChE Journal (Vol. 31, No.11) Page 1926, November 1985.
(83)
Soo, H., Williams, M.C., Radke, C.J.: "A Filtration Model for the Flow of Dilute, Stable Emulsions in Porous Media-II. Parameter Evaluation and Estimation," Chemical Engineering Science. Vol. 41. No.2, pp.273-281, 1986.
(84)
Spielman Lloyd, A.: "Particle Capture from Low-Speed Laminar Flows," Ann.Rev. Fluid Mech. 1977. 9: 297-319.
(85)
Sprow, F.B.: "Distribution of Drop Sizes Produced in Turbulent Liquid-Liquid Dispersion," Chemical Engineering Science, 1967 Vol. 22, pp.435-442.
(86)
Stasa Frank L.: "Applied Finite Element Analysis for Engineers," Holt, Rinehart and Winston, London 1985.
(87)
Tang, J.: "Injectivity Damage Caused by Reinjection of Oily Produced Water," Petroleum Society of CIM, Paper No. 82-33-55.

(88)
Taylor Edward S.: "Dimensional Analysis for Engineers," Clarendon Press, Oxford 1974.

(89)
Todd Adrian C., Brown, J., Noorkami, M., Tweedie, J.A.: "Review of Permeability Damage Studies and related North Sea Water Injection," SPE 7883. The 1979 SPE of AIME International Symposium on Oilfield and Geothermal Chemistry, Houston, Texas, Jan. 22-24, 1979.

(90)
Todd, A.C., Kumar, T., Mohammadi, S.: "The Value and Analysis of Core-Based Water Quality Experiments as Related to Water Injection Schemes," SPE 17148. SPE Formation Damage Control Symposium, Bakersfield, California, February 8-9, 1988.

(91)
Todd, A.C., Somerville, J.E., Scott Graham: "The Application of Depth of Formation Damage Measurements in Predicting Water Injectivity Decline," SPE 12498. Formation Damage Control Symposium, Bakersfield, CA, Feb.13-14, 1984.

(92)
Toran Laura, Palumbo, A.V.: "Colloid transport through fractured and unfractured laboratory sand columns," Journal of Contaminant Hydrology, 9 (1992) 289-303.

(93)
Turnbull, R.W., Johnston, C.S., Yang Ming.: "Treatment of Water Offshore. Quarterly" Institute of Offshore Engineering, Heriot-Watt University, Dec.1993.

(94)
Turnbull, R.W., Yang, M.: "Produced Water Reinjection: Lessons learnt from Extended Core Testing.," Inst. of Offshore Engineering, Heriot-Watt University, October 1993.

(95)
Van Velzen, J.F.G., Leerlooijer Klass.: "Impairment of a Water Injection Well by Suspended Solids: Testing and Prediction," SPE 23822. SPE Intl. Symposium on Formation Damage Control, Lafayette, Louisiana, Feb. 26-27, 1992.

(96)
Vetter, O.J., Kandarpa, V., Stratton, M., Veith, E.: "Particle Invasion into Porous Medium and Related Injectivity Problems," SPE 16255. SPE International Symposium on Oilfield Chemistry, San Antonio, Texas, Feb. 4-6 1987.

(97)
Weinstein Herbert G.: "Cold Waterflooding a Warm Reservoir," SPE 5083. 49th Annual Fall Meeting of the SPE of AIME, Houston, TX, Oct 6-9, 1974.

(98)
Wennberg, K.E., Sharma, M.M.:"Determination of the Filtration Coefficient and the Transition Time for Water Injection Wells," SPE 38181. SPE European Formation Damage Conference, The Hague, Netherlands, 2-3 June 1997.

(99)
Wheeler Douglas W., Weinbrandt Richard M.: "Secondary and Tertiary Recovery with Sea Water and Produced Water in the Huntington Beach Field," SPE 7464. 53rd Annual Fall Technical Conference and Exhibition of the SPE of AIME, Houston, TX, Oct 1-3 1978.

(100)
Williams Milton., Junior Member A.I.M.E.: "Radial Filtration of Drilling Muds".T.P.1112, Petroleum Technology, Nov.1939.

(101)
Williams, D. Brian, Sherrard David W., Lin, C.Y.: "Impact of Inducing Fractures at Prudhow Bay," JPT Oct.1989.

(102)
Williams, D.B., Sherrard, D.W., Lin, C.Y.: "The Impacts on Waterflood Management of Inducing Fractures in Injection Wells in the Prudhoe Bay Oil Field," SPE 16358. SPE Californian Regional Meeting, Ventura, California, April 8-10, 1987.

(103)
Wojitanowicz, A.K., Krilov, Z., Langlinais, J.P.: " Study on the Effect of Pore Blocking Mechanisms on Formation Damage," SPE 16233. SPE Production Operations Symposium, Oklahoma City, Oklahoma, March 8-10, 1987.

(104)
Wright, M.S., Svendsen, A.P., Norway, B.P, Clifford.: "Thermally Induced Fracturing of Ula Water Injectors (NOCS)," SPE 20898. Europec 90, The Hague, Netherlands, 22-24 Oct. 1990.

(105)
Wyer R. H.: "Evaluation of waste water treatment technology for offshore oil production facilities". SPE 5475P, 1975.
(106)
Yan Yuhua, Pal Rajinder, Masliyah Jacob.: "Rheology of Oil-In -Water Emulsions with Added Solids," Chemical Engineering Science Vol. 46 No.4 pp.985-994, 1991.
(107)
Yi Tongchun : "Numerical simulation of fluid loss in hydraulic fracturing treatments" PhD, Heriot-Watt University, Department of Petroleum Engineering, March 1992.

(108)
Zhang Ningsheng.: "Study of Permeability Alteration associated with the Invasion of Oil Droplets and Solid Particles in Produced Oily Water into Porous Media," PhD, Heriot-Watt University, Department of Petroleum Engineering, April 1994.
(109)
Zhang, N.S., Somerville, J.M., Todd, A.C.: "An experimental Investigation of the Formation Damage caused by Produced Oily Water Injection," SPE 26702. Offshore European Conference, Aberdeen, Sept 7-10, 1993.

Appendix I

Short fractured slab experimental data

Time (hr)	Side pres. Drop (atm)	Pres Drop along Frac. (atm)	Permeability ratio	Mean dia. ratio	Conc. ratio	Side Flow Rate ml/s	Side velocity cm/s
0.25	0.296	0.217	1.00	0.62	0.90	1.82	0.033
1	0.301	0.227	1.00	0.91	0.92	1.85	0.033
2	0.316	0.237	0.96	0.80	1.03	1.86	0.033
3	0.331	0.227	0.96	0.90	0.89	1.94	0.035
4	0.336	0.237	0.99	0.91	0.93	2.04	0.036
5	0.341	0.247	0.97	0.80	0.95	2.02	0.036
6	0.341	0.247	0.99	0.81	0.84	2.07	0.037
7	0.360	0.247	0.94	0.80	0.92	2.09	0.037
8	0.380	0.207	0.94	0.87	0.74	2.19	0.039
9	0.395	0.197	0.95	0.84	0.88	2.31	0.041
10	0.400	0.207	0.93	0.90	0.75	2.29	0.041
11	0.400	0.207	0.93	1.02	0.80	2.28	0.041
12	0.429	0.207	0.89	0.80	0.74	2.34	0.042

Table (I.1) The experimental data for fracture injection of a simulated produced water contains 100 mg/l of 3.4 μm oil droplets and 10 mg/l of 2.1 μm solid particles (exp. 25).

Time (hr)	Side pres. Drop (atm)	Pres Drop along Frac. (atm)	Permeability ratio	Mean dia. ratio	Conc. ratio	Side Flow Rate ml/s	Side velocity cm/s
0.25	0.222	0.207	1.00	0.95	0.80	2.42	0.043
1	0.232	0.207	0.95	1.08	0.84	2.4	0.043
2	0.232	0.207	0.97	1.18	0.94	2.44	0.044
3	0.227	0.197	1.00	1.23	0.94	2.47	0.044
4	0.227	0.197	1.03	1.23	0.92	2.54	0.045
5	0.222	0.188	1.04	1.04	0.87	2.52	0.045
6	0.227	0.178	1.01	0.91	0.87	2.51	0.045
7	0.247	0.197	0.95	0.95	0.78	2.55	0.046
8	0.252	0.188	0.92	1.06	0.78	2.53	0.045
9	0.257	0.197	0.84	0.99	0.75	2.34	0.044
10	0.267	0.197	0.89	0.98	0.76	2.59	0.046
11	0.276	0.197	0.85	0.85	0.71	2.55	0.046
12	0.311	0.188	0.86	0.96	0.77	2.9	0.052

Table (I.2) The experimental data for fracture injection of a simulated produced water contains 100 mg/l of 6.7 μm oil droplets and 10 mg/l of 2.1 μm solid particles (exp. 33).

Time (hr)	Side pres. Drop (atm)	Pres Drop along Frac. (atm)	Permeability ratio	Mean dia. ratio	Conc. ratio	Side Flow Rate ml/s	Side velocity cm/s
.25	0.296	0.168	1.00	0.97	0.78	1.57	0.028
1	0.306	0.168	0.98	1.01	0.86	1.59	0.028
2	0.315	0.168	0.94	1.03	0.87	1.57	0.028
3	0.321	0.168	0.90	1.06	0.85	1.53	0.027
4	0.331	0.168	0.88	1.03	0.85	1.54	0.028
5	0.337	0.165	0.86	0.99	0.78	1.54	0.028
6	0.341	0.165	0.85	0.89	0.80	1.54	0.028
7	0.348	0.163	0.82	1.00	0.90	1.51	0.027
8	0.355	0.163	0.78	1.00	0.88	1.47	0.026
9	0.362	0.161	0.77	1.00	0.85	1.47	0.026
10	0.369	0.161	0.73	0.98	0.82	1.43	0.026
11	0.376	0.160	0.72	1.00	0.83	1.43	0.026

Table (I.3) The experimental data for fracture injection of a simulated produced water contains 100 mg/l of 3.6 μm oil droplets and 10 mg/l of 4.7 μm solid particles (exp. 54).

Time (hr)	Side pres. Drop (atm)	Pres Drop along Frac. (atm)	Permeability ratio	Mean dia. ratio	Conc. ratio	Side Flow Rate ml/s	Side velocity cm/s
0.25	0.242	0.148	1.00	0.97	0.85	1.45	0.026
1	0.244	0.143	0.98	0.89	0.76	1.43	0.026
2	0.252	0.138	0.95	1.05	0.91	1.43	0.026
3	0.259	0.133	0.93	1.05	0.86	1.45	0.026
4	0.262	0.128	0.92	0.97	0.76	1.45	0.026
5	0.271	0.128	0.90	0.95	0.75	1.46	0.026
6	0.279	0.123	0.87	0.90	0.79	1.45	0.026
7	0.276	0.138	0.88	0.99	0.84	1.45	0.026
8	0.286	0.128	0.84	1.02	0.85	1.44	0.026
9	0.301	0.128	0.80	1.01	0.80	1.44	0.026
10	0.311	0.128	0.77	0.97	0.75	1.43	0.026
11	0.321	0.128	0.74	0.91	0.74	1.43	0.026

Table (I.4) The experimental data for fracture injection of a simulated produced water contains 100 mg/l of 6 μm oil droplets and 10 mg/l of 4.7 μm solid particles (exp. 46).

Time (hr)	Side pres. Drop (atm)	Pres Drop along Frac. (atm)	Permeability ratio	Mean dia. ratio	Conc. ratio	Side Flow Rate ml/s	Side velocity cm/s
0.25	0.326	0.237	1.00	0.75	0.84	1.83	0.033
1	0.321	0.227	1.05	0.70	0.83	1.89	0.034
2	0.326	0.217	1.07	0.83	0.91	1.95	0.035
3	0.355	0.217	1.06	0.86	0.93	2.11	0.038
4	0.346	0.217	1.07	0.95	0.95	2.08	0.037
5	0.350	0.207	1.06	0.93	0.85	2.09	0.037
6	0.355	0.197	1.06	0.99	0.86	2.11	0.038
7	0.375	0.217	0.96	1.01	0.80	2.03	0.036
8	0.400	0.227	0.93	1.00	0.79	2.1	0.038
9	0.410	0.227	0.91	0.99	0.84	2.09	0.037
10	0.420	0.227	0.90	1.02	0.85	2.13	0.038
11	0.434	0.217	0.89	1.06	0.85	2.18	0.039
12	0.454	0.217	0.86	1.04	0.92	2.19	0.039
13	0.459	0.227	0.79	1.01	0.82	2.03	0.036
14	0.484	0.217	0.76	0.99	0.80	2.06	0.037
15	0.503	0.217	0.73	0.95	0.81	2.06	0.037
16	0.513	0.217	0.72	0.94	0.81	2.08	0.037
17	0.523	0.217	0.69	1.00	0.85	2.03	0.036

Table (I.5) The experimental data for fracture injection of a simulated produced water contains 200 mg/l of 3.6 μm oil droplets and 10 mg/l of 2.1 μm solid particles (exp. 39).

Time (hr)	Side pres. Drop (atm)	Pres Drop along Frac. (atm)	Permeability ratio	Mean dia. ratio	Conc. ratio	Side Flow Rate ml/s	Side velocity cm/s
0.25	0.273	0.125	1.00	0.96	0.90	1.55	0.028
1	0.280	0.120	0.99	1.01	0.97	1.57	0.028
2	0.286	0.118	0.97	1.06	0.99	1.58	0.028
3	0.294	0.115	0.95	1.06	0.99	1.59	0.028
4	0.300	0.112	0.95	1.06	0.99	1.62	0.029
5	0.306	0.111	0.93	1.01	0.97	1.62	0.029
6	0.311	0.109	0.91	0.97	0.95	1.61	0.029
7	0.321	0.109	0.86	0.91	0.93	1.56	0.028
8	0.331	0.109	0.82	0.94	0.95	1.55	0.028
9	0.341	0.109	0.77	0.93	0.89	1.5	0.027
10	0.350	0.109	0.74	0.94	0.88	1.48	0.026
11	0.360	0.109	0.72	0.97	0.90	1.47	0.026

Table (I.6) The experimental data for fracture injection of a simulated produced water contains 200 mg/l of 3.8 μm oil droplets and 10 mg/l of 4.7 μm solid particles (exp. 55).

Time (hr)	Side pres. Drop (atm)	Pres Drop along Frac. (atm)	Permeability ratio	Mean dia. ratio	Conc. ratio	Side Flow Rate ml/s	Side velocity cm/s
0.25	0.267	0.237	1.00	0.95	0.72	2.15	0.038
1	0.267	0.237	0.97	1.05	0.82	2.09	0.037
2	0.257	0.217	0.98	1.09	0.84	2.02	0.036
3	0.257	0.217	0.98	1.07	0.82	2.02	0.036
4	0.257	0.217	0.97	1.08	0.81	2.01	0.036
5	0.252	0.207	1.02	0.98	0.79	2.07	0.037
6	0.257	0.197	1.01	0.91	0.80	2.09	0.037
7	0.276	0.197	1.00	1.02	0.66	2.23	0.040
8	0.286	0.197	0.97	1.10	0.75	2.23	0.040
9	0.286	0.197	0.94	1.03	0.70	2.18	0.039
10	0.296	0.197	0.92	1.00	0.70	2.19	0.039
11	0.296	0.197	0.93	0.99	0.71	2.23	0.040

Table (I.7) The experimental data for fracture injection of a simulated produced water contains 100 mg/l of 3.6 μm oil droplets and 15 mg/l of 2.1 μm solid particles (exp. 40).

Time (hr)	Side pres. Drop (atm)	Pres Drop along Frac. (atm)	Permeability ratio	Mean dia. ratio	Conc. ratio	Side Flow Rate ml/s	Side velocity cm/s
0.25	0.231	0.141	1.00	0.93	0.75	1.46	0.026
1	0.235	0.142	0.98	0.92	0.83	1.46	0.026
2	0.252	0.138	0.92	0.94	0.85	1.47	0.026
3	0.259	0.133	0.91	0.82	0.74	1.5	0.027
4	0.271	0.128	0.88	0.82	0.77	1.52	0.027
5	0.276	0.118	0.87	0.77	0.73	1.53	0.027
6	0.294	0.114	0.84	0.84	0.78	1.56	0.028
7	0.300	0.130	0.80	0.97	0.79	1.53	0.027
8	0.313	0.133	0.77	1.00	0.83	1.52	0.027
9	0.326	0.128	0.72	1.00	0.81	1.49	0.027
10	0.338	0.133	0.69	0.88	0.75	1.47	0.026
11	0.350	0.138	0.66	0.87	0.72	1.46	0.026

Table (I.8) The experimental data for fracture injection of a simulated produced water contains 100 mg/l of 3.4 μm oil droplets and 15 mg/l of 4.7 μm solid particles (exp. 47).

Time (hr)	Side pres. Drop (atm)	Pres Drop along Frac. (atm)	Permeability ratio	Mean dia. ratio	Conc. ratio	Side Flow Rate ml/s	Side velocity cm/s
0.25	0.308	0.155	1.00	1.06	0.79	1.26	0.023
1	0.314	0.149	1.06	1.00	1.05	1.36	0.024
2	0.312	0.146	1.07	0.81	1.15	1.37	0.024
3	0.314	0.142	1.08	0.97	1.10	1.39	0.025
4	0.316	0.138	1.08	1.03	1.05	1.4	0.025
5	0.325	0.130	1.10	0.99	0.98	1.46	0.026
6	0.330	0.124	1.09	1.02	0.94	1.48	0.026
7	0.324	0.152	1.04	0.89	0.97	1.38	0.025
8	0.331	0.148	1.03	0.92	1.08	1.4	0.025
9	0.331	0.138	1.05	0.99	1.01	1.42	0.025
10	0.332	0.138	1.04	0.95	0.95	1.41	0.025
11	0.334	0.135	1.05	1.02	0.93	1.44	0.026

Table (I.9) The experimental data for fracture injection of an oil emulsion contains 100 mg/l of 3.5 μm oil droplets (exp. 50).

Time (hr)	Side pres. Drop (atm)	Pres Drop along Frac. (atm)	Permeability ratio	Mean dia. ratio	Conc. ratio	Side Flow Rate ml/s	Side velocity cm/s
0.25	0.316	0.178	1.00	0.98	0.94	1.45	0.026
1	0.317	0.172	1.00	1.01	0.95	1.46	0.026
2	0.316	0.168	1.01	1.05	0.98	1.47	0.026
3	0.316	0.158	1.02	1.04	0.91	1.48	0.026
4	0.316	0.158	1.03	1.02	0.88	1.49	0.027
5	0.314	0.152	1.03	1.01	0.87	1.49	0.027
6	0.317	0.145	1.06	0.92	0.91	1.54	0.028
7	0.318	0.173	0.99	0.97	1.00	1.45	0.026
8	0.327	0.166	0.99	1.01	1.05	1.48	0.026
9	0.331	0.167	0.97	1.03	1.03	1.48	0.026
10	0.337	0.166	0.98	1.01	0.96	1.51	0.027
11	0.337	0.163	0.98	0.97	0.95	1.52	0.027

Table (I.10) The experimental data for fracture injection of an oil emulsion contains 100 mg/l of 6 μm oil droplets (exp. 51).

Time (hr)	Side pres. Drop (atm)	Pres Drop along Frac. (atm)	Permeability ratio	Mean dia. ratio	Conc. ratio	Side Flow Rate ml/s	Side velocity cm/s
0.25	0.338	0.148	1.00	0.99	0.88	1.33	0.024
1	0.347	0.144	1.03	1.00	0.96	1.41	0.025
2	0.349	0.141	1.03	1.02	0.98	1.41	0.025
3	0.350	0.138	1.02	1.04	1.00	1.41	0.025
4	0.351	0.134	1.03	1.01	0.94	1.42	0.025
5	0.355	0.132	1.02	1.00	0.97	1.43	0.026
6	0.355	0.130	1.04	0.98	0.96	1.45	0.026
7	0.353	0.153	1.01	0.95	1.01	1.4	0.025
8	0.363	0.153	0.98	0.98	1.01	1.4	0.025
9	0.369	0.151	0.96	0.99	0.97	1.4	0.025
10	0.373	0.152	0.95	0.99	0.95	1.4	0.025
11	0.378	0.152	0.94			1.4	0.025

Table (I.11) The experimental data for fracture injection of an oil emulsion contains 200 mg/l of 3.8 μm oil droplets (exp. 52).

Time (hr)	Side pres. Drop (atm)	Pres Drop along Frac. (atm)	Permeability ratio	Mean dia. ratio	Conc. ratio	Side Flow Rate ml/s	Side velocity cm/s
0.25	0.325	0.151	1.00	0.00	0.11	1.54	0.028
1	0.331	0.148	0.98	0.05	0.10	1.54	0.028
2	0.336	0.147	0.95	0.10	0.10	1.52	0.027
3	0.342	0.145	0.93	0.25	0.19	1.5	0.027
4	0.346	0.148	0.90	0.84	0.20	1.47	0.026
5	0.328	0.143	0.93	0.38	0.15	1.44	0.026
6	0.333	0.143	0.91	0.00	0.00	1.43	0.026
7	0.338	0.143	0.88	0.00	0.00	1.41	0.025
8	0.343	0.143	0.86	0.00	0.00	1.4	0.025
9	0.346	0.142	0.84	0.10	0.01	1.38	0.025

Table (I.12) The experimental data for fracture injection of a solid suspension contains 10 mg/l of 2.1 μm particles (exp. 56).

Time (hr)	Side pres. Drop (atm)	Pres Drop along Frac. (atm)	Permeability ratio	Mean dia. ratio	Conc. ratio	Side Flow Rate ml/s	Side velocity cm/s
0.25	0.343	0.133	1.00	0.75	0.08	1.28	0.023
1	0.353	0.133	0.95	1.18	0.11	1.25	0.022
2	0.363	0.133	0.94	0.67	0.04	1.27	0.023
3	0.368	0.133	0.92	0.21	0.04	1.26	0.023
4	0.394	0.140	0.91	0.00	0.00	1.11	0.024
5	0.404	0.140	0.89	0.00	0.07	1.11	0.024
6	0.414	0.140	0.87			1.11	0.024
7	0.422	0.143	0.84			1.1	0.024
8	0.432	0.143	0.81			1.08	0.023
9	0.442	0.143	0.79			1.08	0.023

Table (I.13) The experimental data for fracture injection of a solid suspension contains 15 mg/l of 2.1 μm particles (exp. 58).

Time (hr)	Side pres. Drop (atm)	Pres Drop along Frac. (atm)	Permeability ratio	Mean dia. ratio	Conc. ratio	Side Flow Rate ml/s	Side velocity cm/s
0.25	0.224	0.125	1.00	0.62	0.00	1.47	0.026
1	0.234	0.133	0.93	0.62	0.00	1.44	0.026
2	0.242	0.128	0.87	0.55	0.00	1.39	0.025
3	0.252	0.128	0.82	0.43	0.00	1.36	0.024
4	0.262	0.128	0.78	0.46	0.00	1.35	0.024
5	0.271	0.128	0.74	0.39	0.00	1.32	0.024
6	0.281	0.128	0.70	0.37	0.00	1.29	0.023
7	0.291	0.128	0.65			1.25	0.022
8	0.301	0.128	0.61			1.21	0.022
9	0.311	0.128	0.57			1.17	0.021

Table (I.14) The experimental data for fracture injection of a solid suspension contains 15 mg/l of 4.7 μm particles (exp. 49).

Time (hr)	Side pres. Drop (atm)	Pres Drop along Frac. (atm)	Permeability ratio	Mean dia. ratio	Conc. ratio	Side Flow Rate ml/s	Side velocity cm/s
0.25	0.241	0.180	1.00	0.97	0.42	1.86	0.033
1	0.245	0.181	0.97	0.81	0.37	1.84	0.033
2	0.252	0.177	0.94	0.92	0.22	1.83	0.033
3	0.255	0.175	0.92	0.89	0.23	1.81	0.032
4	0.259	0.174	0.90	0.86	0.25	1.79	0.032
5	0.263	0.172	0.87	0.83	0.05	1.76	0.031
6	0.269	0.173	0.82	0.84	0.05	1.71	0.031
7	0.276	0.172	0.80	0.91	0.02	1.7	0.030
8	0.286	0.173	0.77	1.00	0.00	1.69	0.030
9	0.295	0.173	0.73			1.66	0.030

Table (I.15) The experimental data for fracture injection of a solid suspension contains 10 mg/l of 4.7 μm particles (exp. 53).

Appendix II

SIMULATION PROGRAMS

Simulate the 40 cm fractured model
Injection through a 40 cm long fracture

```
/BATCH
/filn,LLFF
/titel,fracture injection (2D)
/units,si
/prep7
et,1,fluid141
c***Distributed resistance specifications
r,2,1,,0,2e+12,1,0
rmore,1
r,3,1,,0,1e+09,1,0
rmore,1
c***Variables
c***Frcature length = 40 cm
len=0.4
c***Slab width = 3 cm
wid=0.03
c***Fracture half aperture = 0.5 mm
fl=0.0005
fw=wid+fl
c***Building the model
k,1
k,2,len,0
k,3,len,fl
k,4,len,fw
k,5,0,fw
k,6,0,fl
a,1,2,3,6
a,6,3,4,5
/triad,lbot
nummrg,node
nummrg,kp
/pnum,line,1
lplot
lsel,s,line,,1
lsel,a,line,,3
lsel,a,line,,6
lesize,all,,,398
lsel,s,line,,5
lesize,all,,,10,4
lsel,s,line,,7
lesize,all,,,10,0.25
lsel,s,line,,2
lsel,a,line,,4
lesize,all,,,8
nummrg,kp
!save
real,2
amesh,2
real,3
amesh,1
c***Apply boundary conditions
c***Symmetry boundary
nsel,s,loc,y,0
d,all,vy,0
d,all,vz,0
c***Inflow boundary
nsel,s,loc,x,0
nsel,r,loc,y,0,fl
d,all,vx,0.25
d,all,vy,0.0
d,all,vz,0.0
c***Wall boundary
nsel,s,loc,x,0
nsel,r,loc,y,fl,fw
d,all,vx,0
d,all,vy,0
d,all,vz,0
nsel,s,loc,x,len
nsel,r,loc,y,fl,fw
d,all,vx,0
d,all,vy,0
d,all,vz,0
c***Outflow boundary
nsel,s,loc,x,len
nsel,r,loc,y,0,fl
d,all,pres,0.0
nsel,s,loc,y,fw
d,all,pres,0.0
allsel
!Define the Flotran CFD parameters
fldata,term,pres,1e-08
fldata,solu,flow,t
fldata,iter,exec,50
fldata,solu,turb,f
fldata,temp,nomi,300.0
fldata,nomi,dens,1050.0
fldata,nomi,visc,0.001
finish
c***Solution
/solu
solve
finish
c***post precessing
/post1
c***Specify disply file
/show,ELF4R1,grph
set
!Map pressure along longe fracture
lpath,4796,4795
pdef,pressure,pres
/plopts,info,off
c***Spacify the output file
/output,PDLFAF5R2
/title,Pressure change along 40 cm longe fracture
prpath,pressure
/output
pdef,save
!Map flow velocity along longe fracture
lpath,4796,4795
pdef,velocity,v,sum
pdef,Vx,v,x
pdef,Vy,v,y
/plopts,info,off
/output,VDLFAF5R2
/title,Flow velocity change along 40 cm longe fracture
prpath,velocity,Vx,Vy
/output
pdef,save
!Map pressure through matrix to side outlet 1
lpath,300,708
pdef,pressure,pres
/plopts,info,off
/output,PDLFM5R2T1
/title,Pressure change through matrix (side outlet 1)
prpath,pressure
/output
pdef,save
!Map flow velocity through matrix to side outlet 1
lpath,300,708
pdef,velocity,v,sum
pdef,Vx,v,x
pdef,Vy,v,y
/plopts,info,off
/output,VDLFM5R2T1
/title, Flow velocity change through matrix (side outlet 1)
prpath,velocity,Vx,Vy
/output
pdef,save
```

```
!Map pressure through matrix to side outlet 2
lpath,200,608
pdef,pressure,pres
/plopts,info,off
/output,PDLFM5R2T2
/title,Pressure change through matrix (side outlet 2)
prpath,pressure
/output
pdef,save
!Map flow velocity through matrix to side outlet 2
lpath,200,608
pdef,velocity,v,sum
pdef,Vx,v,x
pdef,Vy,v,y
/plopts,info,off
/output,VDLFM5R2T2
/title, Flow velocity change through matrix (side outlet 2)
prpath,velocity,Vx,Vy
/output
pdef,save
!Map pressure through matrix to side outlet 3
lpath,100,508
pdef,pressure,pres
/plopts,info,off
/output,PDLFM5R2T3
/title,Pressure change through matrix (side outlet 3)
prpath,pressure
/output
pdef,save
!Map flow velocity through matrix to side outlet 3
lpath,100,508
pdef,velocity,v,sum
pdef,Vx,v,x
pdef,Vy,v,y
/plopts,info,off
/output,VDLFM5R2T3
/title, Flow velocity change through matrix (side outlet 3)
prpath,velocity,Vx,Vy
/output
pdef,save
finish
```

Roughness simulation
Injection along rough fracture

```
/BATCH
/filn,LFricME
/titel,Rough fracture injection (2D)
/units,si
/prep7
et,1,fluid141
c*** Distributed resistance specifications
r,2,1,,0,2e+12,1,0
rmore,1
r,3,1,,0,1e+09,1,0
rmore,1
c***Variables
c***Roughness (Rgh) = 0.0625 - 0.375 mm
c***Spacing between each two roughness (S) = 0 - 5 mm
c***Fracture length = 40 cm
len=0.4
c***Slabe width = 3 cm
wid=0.03
c***Fracture half aperture (Wf) = 0.5 mm
fl=0.0005
fw=wid+fl
c***Building the model
k,1
k,2,len,0
!k,3,len,0.000375
!k,3,len,0.0003125
!k,3,len,0.00025
!k,3,len,0.0001875
k,3,len,0.000125
!k,4,len,0.0004375
!k,4,len,0.000375
!k,4,len,0.0003125
!k,4,len,0.00025
k,4,len,0.0001875
k,5,len,0.0005
k,6,len,fw
k,7,0,fw
k,8,0,0.0005
!k,9,0,0.0004375
!k,9,0,0.000375
!k,9,0,0.0003125
!k,9,0,0.00025
k,9,0,0.0001875
!k,10,0,0.000375
!k,10,0,0.0003125
!k,10,0,0.00025
!k,10,0,0.0001875
k,10,0,0.000125
a,1,2,3,10
a,10,3,4,9
a,9,4,5,8
a,8,5,6,7
nummrg,kp
nummrg,node
lsel,s,line,,1,3,2
lsel,a,line,,6
lesize,all,,,800
lsel,s,line,,9,12,3
lesize,all,,,400
lsel,s,line,,2,4,2
lesize,all,,,3
lsel,s,line,,5,7,2
lesize,all,,,1
lsel,s,line,,8,10,2
lesize,all,,,2
lsel,s,line,,11
lesize,all,,,8,4
lsel,s,line,,13
lesize,all,,,8,0.25
nummrg,kp
nummrg,node
real,3
amesh,1,2,1
real,2
amesh,4
real,3
eshape,1
amesh,3
save
esel,s,elem,,6406,7597,18
emodif,all,real,2
allsel
c***Apply boundary conditions
c***Symmetry boundary
nsel,s,loc,y,0
d,all,vy,0
d,all,vz,0
c***Inflow boundary
nsel,s,loc,x,0
nsel,r,loc,y,0,fl
d,all,vx,0.25
d,all,vy,0.0
d,all,vz,0.0
c***Wall boundary
nsel,s,loc,x,0
nsel,r,loc,y,fl,fw
d,all,vx,0
d,all,vy,0
d,all,vz,0
nsel,s,loc,x,len
nsel,r,loc,y,fl,fw
d,all,vx,0
d,all,vy,0
d,all,vz,0
c***Outflow boundary
```

```
nsel,s,loc,x,len
nsel,r,loc,y,0,fl
d,all,pres,0.0
nsel,s,loc,y,fw
d,all,pres,0.0
allsel
!Define the Flotran CFD parameters
fldata,term,pres,1e-06
fldata,conv,pres,1e-06
fldata,maxi,pres,1500
fldata,solu,flow,t
fldata,iter,exec,30
fldata,solu,turb,f
fldata,temp,nomi,300.0
fldata,nomi,dens,1050.0
fldata,nomi,visc,0.001
finish
c***solution
/solu
solve
finish
c***Post processing
/post1
/show,LFricME515,grph
set
/edge
!Map pressure along rough longe fracture
lpath,805,1500,1400,1300,1200,1100,1000,900,802
pdef,pressure,pres
/plopts,info,off
/axlab,y,pressure (pa)
/axlab,x,distance from the inlet (m)
/title,Pressure change along rough fracture
(Rgh=0.125,Wf=0.5,S=1)
/yrange,0,70000
/color,curve,black
/color,grbak,lgra
plpath,pressure
/output,PalnE515Fric
/title,Pressure change along rough fracture
(Rgh=0.125,Wf=0.5,S=1)
prpath,pressure
/output
pdef,save
/axlab,y
/axlab,x
!Map flow velocity along rough longe fracture
lpath,805,1500,1400,1300,1200,1100,1000,900,802
pdef,velocity,v,sum
pdef,Vx,v,x
pdef,Vy,v,y
/plopts,info,off
/axlab,y,velocity (m/s)
/axlab,x,distance from the inlet (m)
/title,Flow velocity change along rough fracture
(Rgh=0.125,Wf=0.5,S=1)
/yrange,0,0.4
plpath,velocity,Vx,Vy
/output,ValnE515Fric
/title,Flow velocity change along rough fracture
(Rgh=0.125,Wf=0.5,S=1)
prpath,velocity,Vx,Vy
/output
pdef,save
/axlab,y
/axlab,x
!Map pressure through matrix to side outlet 1
lpath,4300,4708
pdef,pressure,pres
/plopts,info,off
/axlab,y,pressure (pa)
/axlab,x,distance from fracture face (m)
/title,Pressure change through matrix (outlet 1,
Rgh=0.125,Wf=0.5,S=1)
/yrange,0,70000
plpath,pressure
/output,PthME515Fric1
/title,Pressure change through matrix (outlet 1,
Rgh=0.125,Wf=0.5,S=1)
prpath,pressure
/output
pdef,save
/axlab,y
/axlab,x
!Map flow velocity through matrix to side outlet 1
lpath,4300,4708
pdef,velocity,v,sum
pdef,Vx,v,x
pdef,Vy,v,y
/plopts,info,off
/axlab,y,velocity (m/s)
/axlab,x,distanc from fractur face (m)
/title, Flow velocity change through matrix (outlet 1,
Rgh=0.125,Wf=0.5,S=1)
/yrange,0,0.001
plpath,Vx,Vy
/output,VthME515Fric1
/title, Flow velocity change through matrix (outlet 1,
Rgh=0.125,Wf=0.5,S=1)
prpath,velocity,Vx,Vy
/output
pdef,save
/axlab,y
/axlab,x
!Map pressure through matrix to side outlet 2
lpath,4200,4608
pdef,pressure,pres
/plopts,info,off
/axlab,y,pressure (pa)
/axlab,x,distance from fracture face (m)
/title,Pressure change through matrix (outlet 2,
Rgh=0.125,Wf=0.5,S=1)
/yrange,0,70000
plpath,pressure
/output,PthME515Fric2
/title,Pressure change through matrix (outlet 2,
Rgh=0.125,Wf=0.5,S=1)
prpath,pressure
/output
pdef,save
/axlab,y
/axlab,x
!Map flow velocity through matrix to side outlet 2
lpath,4200,4608
pdef,velocity,v,sum
pdef,Vx,v,x
pdef,Vy,v,y
/plopts,info,off
/axlab,y,velocity (m/s)
/axlab,x,distanc from fractur face (m)
/title, Flow velocity change through matrix (outlet 2,
Rgh=0.125,Wf=0.5,S=1)
/yrange,0,0.001
plpath,velocity,Vx,Vy
/output,VthME515Fric2
/title, Flow velocity change through matrix (outlet 2,
Rgh=0.125,Wf=0.5,S=1)
prpath,velocity,Vx,Vy
/output
pdef,save
/axlab,y
/axlab,x
!Map pressure through matrix to side outlet 3
lpath,4100,4508
pdef,pressure,pres
/plopts,info,off
/axlab,y,pressure (pa)
/axlab,x,distance from fracture face (m)
/title,Pressure change through matrix (outlet 3,
Rgh=0.125,Wf=0.5,S=1)
```

```
/yrange,0,70000
plpath,pressure
/output,PthME515Fric3
/title,Pressure change through matrix (outlet 3,
Rgh=0.125,Wf=0.5,S=1)
prpath,pressure
/output
pdef,save
/axlab,y
/axlab,x
!Map flow velocity through matrix to side outlet 3
lpath,4100,4508
pdef,velocity,v,sum
pdef,Vx,v,x
pdef,Vy,v,y
/plopts,info,off
/axlab,y,velocity (m/s)
/axlab,x,distanc from fractur face (m)
/title, Flow velocity change through matrix (outlet 3,
Rgh=0.125,Wf=0.5,S=1)
/yrange,0,0.001
plpath,velocity,Vx,Vy
/output,VthME515Fric3
/title, Flow velocity change through matrix (outlet 3,
Rgh=0.125,Wf=0.5,S=1)
prpath,velocity,Vx,Vy
/output
pdef,save
/axlab,y
/axlab,x
finish
```

Radial injection Simulation (Field case)

```
/BATCH
/filn,NR
/titel,Radial injection (2D)
/units,si
/prep7
et,1,fluid141
c***Distributed resistance specifications
r,2,1,,0,2e+12,1,0
rmore,1
c***Variables
!Radial injection:
!Injection zone thickness h = 10 m
!Injection area or inlet flow area = 4 sqm
!Injection rate = 1037 M3/day
!Flow velocity through rock matrix V = 0.003 m/s
!Only a quarter of the linear system will be simulated.
!Matrix initial permeability = 500 md (5e-13 sqm)
!vsum=(vx**2+vy**2)**0.5
!vx(radial)=v cos(Theta)
!vy(radial)=v sin(Theta)
!Theta is from 0 to 90 in steps of 0.9.
!Well radius = 0.0635 m
!Drainage radius = 20 m
c***Building the model
pcirc,0.0635,20.0635,0,90
nummrg,kp
lsel,s,line,,1,3,2
lesize,all,,,100
lsel,s,line,,2
lesize,all,,,70,0.01
lsel,s,line,,4
lesize,all,,,70,0.01
real,2
amesh,1
allsel
c***Apply boundary conditions
c***symmetry boundary
nsel,s,loc,x,0
d,all,vx,0
d,all,vz,0
nsel,s,loc,y,0
d,all,vy,0
d,all,vz,0
c***Inflow boundary
nsel,s,node,,172,271,1
nsel,a,node,,102
d,172,vx,0.003
d,172,vy,0
d,173,vx,0.00299963
d,173,vy,0.000047141
d,174,vx,0.00299852
d,174,vy,0.00009427
d,175,vx,0.00299667
d,175,vy,0.00014138
d,176,vx,0.00299408
d,176,vy,0.00018845
d,177,vx,0.00299074
d,177,vy,0.00023547
d,178,vx,0.00298668
d,178,vy,0.00028244
d,179,vx,0.00298187
d,179,vy,0.00032933
d,180,vx,0.00297633
d,180,vy,0.00037615
d,181,vx,0.00297005
d,181,vy,0.00042287
d,182,vx,0.00296304
d,182,vy,0.00046949
d,183,vx,0.00295529
d,183,vy,0.00051599
d,184,vx,0.00294682
d,184,vy,0.00056236
d,185,vx,0.00293762
d,185,vy,0.0006086
d,186,vx,0.00292769
d,186,vy,0.00065469
d,187,vx,0.00291704
d,187,vy,0.00070061
d,188,vx,0.00290568
d,188,vy,0.00074636
d,189,vx,0.00289359
d,189,vy,0.00079193
d,190,vx,0.00288079
d,190,vy,0.0008373
d,191,vx,0.00286727
d,191,vy,0.00088246
d,192,vx,0.00285305
d,192,vy,0.00092741
d,193,vx,0.00283813
d,193,vy,0.00097212
d,194,vx,0.0028225
d,194,vy,0.0010166
d,195,vx,0.00280618
d,195,vy,0.00106083
d,196,vx,0.00278916
d,196,vy,0.00110479
d,197,vx,0.00277146
d,197,vy,0.00114848
d,198,vx,0.00275307
d,198,vy,0.00119189
d,199,vx,0.002734
d,199,vy,0.001235
d,200,vx,0.00271426
d,200,vy,0.00127781
d,201,vx,0.00269384
d,201,vy,0.0013203
d,202,vx,0.00267276
d,202,vy,0.00136247
d,203,vx,0.00265103
d,203,vy,0.0014043
d,204,vx,0.00262863
d,204,vy,0.00144579
d,205,vx,0.00260559
d,205,vy,0.00148691
d,206,vx,0.0025819
```

```
d,206,vy,0.00152767
d,207,vx,0.00255758
d,207,vy,0.00156805
d,208,vx,0.00253262
d,208,vy,0.00160805
d,209,vx,0.00250704
d,209,vy,0.00164765
d,210,vx,0.00248084
d,210,vy,0.00168684
d,211,vx,0.00245403
d,211,vy,0.00172561
d,212,vx,0.00242661
d,212,vy,0.00176396
d,213,vx,0.00239859
d,213,vy,0.00180187
d,214,vx,0.00236998
d,214,vy,0.00183934
d,215,vx,0.00234079
d,215,vy,0.00187636
d,216,vx,0.00231101
d,216,vy,0.00191291
d,217,vx,0.00228067
d,217,vy,0.00194898
d,218,vx,0.00224976
d,218,vy,0.00198458
d,219,vx,0.0022183
d,219,vy,0.00201969
d,220,vx,0.00218629
d,220,vy,0.0020543
d,221,vx,0.00215374
d,221,vy,0.0020884
d,222,vx,0.00212066
d,222,vy,0.00212198
d,223,vx,0.00208705
d,223,vy,0.00215504
d,224,vx,0.00205293
d,224,vy,0.00218757
d,225,vx,0.0020183
d,225,vy,0.00221956
d,226,vx,0.00198318
d,226,vy,0.002251
d,227,vx,0.00194756
d,227,vy,0.00228189
d,228,vx,0.00191146
d,228,vy,0.00231221
d,229,vx,0.0018749
d,229,vy,0.00234196
d,230,vx,0.00183786
d,230,vy,0.00237113
d,231,vx,0.00180038
d,231,vy,0.00239972
d,232,vx,0.00176245
d,232,vy,0.00242771
d,233,vx,0.00172408
d,233,vy,0.00245511
d,234,vx,0.00168529
d,234,vy,0.00248189
d,235,vx,0.00164608
d,235,vy,0.00250807
d,236,vx,0.00160647
d,236,vy,0.00253363
d,237,vx,0.00156646
d,237,vy,0.00255856
d,238,vx,0.00152606
d,238,vy,0.00258285
d,239,vx,0.00148529
d,239,vy,0.00260652
d,240,vx,0.00144415
d,240,vy,0.00262953
d,241,vx,0.00140265
d,241,vy,0.0026519
d,242,vx,0.0013608
d,242,vy,0.00267361
d,243,vx,0.00131862
d,243,vy,0.00269467
d,244,vx,0.00127612
d,244,vy,0.00271505
d,245,vx,0.0012333
d,245,vy,0.00273477
d,246,vx,0.00119017
d,246,vy,0.00275381
d,247,vx,0.00114675
d,247,vy,0.00277218
d,248,vx,0.00110305
d,248,vy,0.00278985
d,249,vx,0.00105908
d,249,vy,0.00280684
d,250,vx,0.00101484
d,250,vy,0.00282314
d,251,vx,0.00097035
d,251,vy,0.00283873
d,252,vx,0.00092563
d,252,vy,0.00285363
d,253,vx,0.00088067
d,253,vy,0.00286782
d,254,vx,0.0008355
d,254,vy,0.00288131
d,255,vx,0.00079012
d,255,vy,0.00289408
d,256,vx,0.00074455
d,256,vy,0.00290614
d,257,vx,0.00069879
d,257,vy,0.00291748
d,258,vx,0.00065286
d,258,vy,0.0029281
d,259,vx,0.00060677
d,259,vy,0.002938
d,260,vx,0.00056053
d,260,vy,0.00294717
d,261,vx,0.00051415
d,261,vy,0.00295561
d,262,vx,0.00046764
d,262,vy,0.00296333
d,263,vx,0.00042102
d,263,vy,0.00297031
d,264,vx,0.00037429
d,264,vy,0.00297656
d,265,vx,0.00032747
d,265,vy,0.00298207
d,266,vx,0.00028057
d,266,vy,0.00298685
d,267,vx,0.00023361
d,267,vy,0.00299089
d,268,vx,0.00018658
d,268,vy,0.00299419
d,269,vx,0.00013951
d,269,vy,0.00299675
d,270,vx,0.0000924
d,270,vy,0.00299858
d,271,vx,0.0000452
d,271,vy,0.00299966
d,102,vx,0.0
d,102,vy,0.003
c***Outflow boundary
nsel,s,node,,1,101,1
d,all,pres,0.0
allsel
!Define the Flotran CFD parameters
fldata,term,pres,1e-08
fldata,solu,flow,t
fldata,iter,exec,50
fldata,solu,turb,f
fldata,temp,nomi,300.0
fldata,nomi,dens,1050.0
fldata,nomi,visc,0.001
finish
c***Solution
/solu
solve
finish
```

```
c***Post processing
/post1
set
/show,ENRR1,grph
/triad,off
/edge,1,1
/device,vector,on
/plopts,info,1
!Disply Pressure and Velocity contours
/title,Pressure contours (Radial injection Km = 500
md,Vm=0.003 m/s)
/clabel,1,50
!/cval,1
plnsol,pres
/plopts,info,1
/title,velocity contours (Radial injection Km = 500
md,Vm=0.003 m/s)
/cval,1,0.00002,0.00004,0.00006,0.00008,0.0001,0.00
012,0.00025,0.0005
plnsol,v,sum
!Mapping pressure change through matrix
lpath,222,52
pdef,pressure,pres
/plopts,info,off
/output,PmNRR1
/title,Pressure change through matrix (Radial inj. Km =
500 md,Vm=0.003 m/s)
prpath,pressure
/output
pdef,save
!Mapping flow velocity change through matrix
lpath,222,52
pdef,velocity,v,sum
pdef,Vx,v,x
pdef,Vy,v,y
/plopts,info,off
/output,VmNRR1
/title,Flow velocity through matrix (Radial inj. Km = 500
md,Vm=0.003 m/s)
prpath,velocity,Vx,Vy
/output
pdef,save
finish
```

Frcature injection simulation (Field case) Radial injection with single fracture

```
/BATCH
/filn,NSRF
/titel,Radial injection with single fracture (2D)
/units,si
/prep7
et,1,fluid141
c***Specify the distributed resistance specifications
r,2,1,,0,3.333e+12,1,0
rmore,1
r,3,1,,0,3.333e+08,1,0
rmore,1
c***Variables
!Radial injection with single fracture:
!Injection zone thickness h = 10 m
!Injection area or inlet flow area = 4 sqm
!Injection rate = 1036 M3/day
!Only a quarter of the system will be simulated.
!So the flow rate will be 1/4th of the total flow rate (259
M3/day).
!All the flow will be directed through the fracture inlet.
!Flow velocity at the fracture inlet Vf = 0.6 - 0.2 m/s
!Fracture aperture = 1 - 3 mm
!Fracture inlet area = 0.01 - 0.03 m
!Fracture length = 5 - 15 m
!Fracture permeability = 3000 Darcy
!Matrix initial permeability = 300 md (3e-13 sqm)
!Well radius = 0.0635 m
!Drainage radius = 20.0635 m
c***Building the model
k,1,0.0635,-0.001
k,2,20.0635,-0.001
k,3,20.0635,0
k,4,0.0635,0
a,1,2,3,4
pcirc,0.0635,20.0635,0,90
nummrg,kp
lsel,s,line,,5,7,2
lesize,all,,,100,50
lsel,s,line,,3
lesize,all,,,70,0.01
lsel,s,line,,6
lesize,all,,,70,0.01
lsel,s,line,,1
lesize,all,,,70,100
lsel,s,line,,2,4,2
lesize,all,,,4
nummrg,kp
real,2
amesh,2
real,2
amesh,1
allsel
c***Creating the fracture
esel,s,elem,,7001,7060,1
esel,a,elem,,7071,7130,1
esel,a,elem,,7141,7200,1
esel,a,elem,,7211,7270,1
emodif,all,real,3
c***Apply boundary conditions
c***symmetry boundary
nsel,s,loc,y,-0.001
d,all,vy,0
d,all,vz,0
nsel,s,loc,x,0
d,all,vx,0
d,all,vz,0
c***Inflow boundary
nsel,s,node,,7246,7248,1
nsel,a,node,,7172
d,all,vx,0.6
d,all,vy,0
c***wall boumdary
nsel,s,node,,172,271,1
nsel,a,node,,102
d,all,vx,0
d,all,vy,0
c***Outflow boundary
nsel,s,node,,1,101,1
d,all,pres,0.0
nsel,s,node,,7243,7245,1
nsel,a,node,,7173
d,all,pres,0.0
allsel
c***Define the Flotran CFD parameters
fldata,term,pres,1e-08
fldata,solu,flow,t
!fldata,meth,pres,1
fldata,iter,exec,50
fldata,solu,turb,f
fldata,temp,nomi,300.0
fldata,nomi,dens,1050.0
fldata,nomi,visc,0.001
finish
c***Solusion
/solu
solve
finish
c***Post processing the results
/post1
set
/triad,off
/show,ENRSFR31,grph
/edge,1,1
/device,vector,on
```

```
/plopts,info,1
!Disply Pressure and Velocity contours
/title,Pressure contours (frac. inj.,Km=300
md,Lf=10m,Wf=2mm,Vf=0.6m/s)
/clabel,1,50
plnsol,pres
/plopts,info,1
/title,velocity contours (frac. inj.,Km=300
md,Lf=10m,Wf=2mm,Vf=0.6m/s)
/cval,1,0.00001,0.000015,0.00002,0.00003,0.00004,0.
00005,0.00006,0.00008
plnsol,v,sum
!Mapping pressure along the fracture
lpath,7246,7245
pdef,pressure,pres
/plopts,info,off
/axlab,y,pressure (pa)
/axlab,x,Radial distance (m)
plpath,pressure
/output,PASRFR31
/title,Pressure along the fracture path(Km=300
md,Lf=10m,Wf=2mm,Vf=0.6m/s)
prpath,pressure
/output
pdef,save
/axlab,y
/axlab,x
!Mapping flow velocity along the fracture
lpath,7246,7245
pdef,velocity,v,sum
pdef,Vx,v,x
pdef,Vy,v,y
/plopts,info,off
/axlab,y,velocity (m/s)
/axlab,x,Radial distance (m)
plpath,velocity,Vx,Vy
/output,VASRFR31
/title,Flow velocity along the fracture path(Km=300
md,Lf=10m,Wf=2mm,Vf=0.6m/s)
prpath,velocity,Vx,Vy
/output
pdef,save
/axlab,y
/axlab,x
!Mapping pressure through matrix
lpath,222,52
pdef,pressure,pres
/plopts,info,off
/axlab,y,pressure (pa)
/axlab,x,Radial distance (m)
plpath,pressure
/output,PmSRFR31
/title,Pressure through matrix(frac. inj.,Km=300
md,Lf=10m,Wf=2mm,Vf=0.6m/s)
prpath,pressure
/output
pdef,save
/axlab,y
/axlab,x
!Mapping flow velocity through matrix
lpath,222,52
pdef,velocity,v,sum
pdef,Vx,v,x
pdef,Vy,v,y
/plopts,info,off
/axlab,y,velocity (m/s)
/axlab,x,Radial distance (m)
plpath,velocity,Vx,Vy
/output,VmSRFR31
/title,Flow velocity through matrix(frac. inj.,Km=300
md,Lf=10m,Wf=2mm,Vf=0.6m/s)
prpath,velocity,Vx,Vy
/output
pdef,save
/axlab,y
/axlab,x
Finish
```

Frcature injection simulation (Field case) Radial injection with Two fractures

```
/BATCH
/filn,NDRF
/titel,Radial injection with two fractures (2D)
/units,si
/prep7
et,1,fluid141
c***Specify the distributed resistance specifications
r,2,1,,0,3.333e+12,1,0
rmore,1
r,3,1,,0,3.333e+08,1,0
rmore,1
c***Variables
!Radial injection with Double fractures:
!Injection zone thickness h = 10 m
!Injection area or inlet flow area = 4 sqm
!Injection rate = 1037 M3/day
!Only a quarter of the system will be simulated.
!So the flow rate will be 1/4th of the total flow rate (259
M3/day).
!All the flow will be directed through the fractures inlet.
!Flow velocity at the fractures inlet Vf = 0.3 - 0.1 m/s
!Fracture aperture = 1- 3 mm
!Fracture inlet area = 0.01 - 0.03 m
!Fracture length = 5 - 15 m
!Fracture permeability = 3000 Darcy
!Matrix initial permeability = 300 md (3e-13 sqm)
!Well radius = 0.0635 m
!Drainage radius = 20.0635 m
c***Building the model
k,1,0.0635,-0.001
k,2,20.0635,-0.001
k,3,20.0635,0
k,4,0.0635,0
K,5,0,0.0635
k,6,0,20.0635
k,7,-0.001,20.0635
k,8,-0.001,0.0635
a,1,2,3,4
pcirc,0.0635,20.0635,0,90
a,5,6,7,8
nummrg,kp
lsel,s,line,,5,7,2
lesize,all,,,100,-50
lsel,s,line,,3
lesize,all,,,70,0.01
lsel,s,line,,6
lesize,all,,,70,0.01
lsel,s,line,,1
lesize,all,,,70,100
lsel,s,line,,11
lesize,all,,,70,0.01
lsel,s,line,,2,4,2
lsel,a,line,,10,12,2
lesize,all,,,4
real,2
amesh,2
real,2
amesh,1
real,2
amesh,3
allsel
c***Creating the two fractures
esel,s,elem,,7001,7060,1
esel,a,elem,,7071,7130,1
esel,a,elem,,7141,7200,1
esel,a,elem,,7211,7270,1
emodif,all,real,3
esel,s,elem,,7281,7340,1
esel,a,elem,,7351,7410,1
esel,a,elem,,7421,7480,1
```

```
esel,a,elem,,7491,7550,1
emodif,all,real,3
c***Apply boundary conditions
c***symmetry boundary
nsel,s,loc,x,-0.001
d,all,vx,0
d,all,vz,0
nsel,s,loc,y,-0.001
d,all,vy,0
d,all,vz,0
c***Inflow boundary
nsel,s,node,,7246,7248,1
nsel,a,node,,7172
d,all,vx,0.3
d,all,vy,0
nsel,s,node,,7530,7532,1
nsel,a,node,,7460
d,all,vx,0
d,all,vy,0.3
c***wall boundary
nsel,s,node,,172,271,1
nsel,a,node,,102
d,all,vx,0
d,all,vy,0
c***Outflow boundary
nsel,s,node,,1,101,1
d,all,pres,0.0
nsel,s,node,,7243,7245,1
nsel,a,node,,7173
nsel,a,node,,7457,7459,1
nsel,a,node,,7456
d,all,pres,0.0
allsel
c***Define the Flotran CFD parameters
fldata,term,pres,1e-08
fldata,solu,flow,t
!fldata,meth,pres,1
fldata,iter,exec,50
fldata,solu,turb,f
fldata,temp,nomi,300.0
fldata,nomi,dens,1050.0
fldata,nomi,visc,0.001
finish
c***Solution
/solu
solve
finish
c***Post processing the results
/post1
set
/triad,off
c***Specify the display file
/show,ENDRFR31,grph
/edge,1,1
/device,vector,on
/plopts,info,1
!Disply Pressure and Velocity contours
/title,Pressure contours (Duble frac. inj.,Km=300
md,Lf=10m,Wf=2mm,Vf=0.3m/s)
/clabel,1,50
plnsol,pres
/plopts,info,1
/title,velocity contours (Duble frac. inj.,Km=300
md,Lf=10m,Wf=2mm,Vf=0.3m/s)
/cval,1,0.00001,0.000015,0.00002,0.00003,0.00004,0.
00005,0.00006,0.00008
plnsol,v,sum
!Mapping pressure along the fracture
lpath,7246,7245
pdef,pressure,pres
/plopts,info,off
/axlab,y,pressure (pa)
/axlab,x,Radial distance (m)
plpath,pressure
/output,PADRFR31
/title,Pressure along fracture(Duble frac.,Km=300
md,Lf=10m,Wf=2mm,Vf=0.3m/s)
prpath,pressure
/output
pdef,save
/axlab,y
/axlab,x
!Mapping flow velocity along the fracture
lpath,7246,7245
pdef,velocity,v,sum
pdef,Vx,v,x
pdef,Vy,v,y
/plopts,info,off
/axlab,y,velocity (m/s)
/axlab,x,Radial distance (m)
plpath,velocity,Vx,Vy
/output,VADRFR31
/title,Flow velocity along fracture(Duble frac.,Km=300
md,Lf=10m,Wf=2mm,Vf=0.3m/s)
prpath,velocity,Vx,Vy
/output
pdef,save
/axlab,y
/axlab,x
!Mapping pressure through matrix
lpath,222,52
pdef,pressure,pres
/plopts,info,off
/axlab,y,pressure (pa)
/axlab,x,Radial distance (m)
plpath,pressure
/output,PmDRFR31
/title,Pressure through matrix(Duble frac.,Km=300
md,Lf=10m,Wf=2mm,Vf=0.3m/s)
prpath,pressure
/output
pdef,save
/axlab,y
/axlab,x
!Mapping flow velocity through matrix
lpath,222,52
pdef,velocity,v,sum
pdef,Vx,v,x
pdef,Vy,v,y
/plopts,info,off
/axlab,y,velocity (m/s)
/axlab,x,Radial distance (m)
plpath,velocity,Vx,Vy
/output,VmDRFR31
/title,Flow velocity through matrix(Duble frac.,Km=300
md,Lf=10m,Wf=2mm,Vf=0.3m/s)
prpath,velocity,Vx,Vy
/output
pdef,save
/axlab,y
/axlab,x
Finish
```

Radial injection with near well bore damage (Field case)

```
/BATCH
/filn,NRSkin
/titel,Radial injection with near well bore skin zone (2D)
/units,si
/prep7
et,1,fluid141
c***Distributed resistance specifications
r,2,1,,0,3.333e+12,1,0
rmore,1
r,3,1,,0,1.111e+13,1,0
rmore,1
c***Variables
!Radial injection with skin:
!Injection zone thickness h = 10 m
!Injection area or inlet flow area = 4 sqm
```

```
!Injection rate = 1036 M3/day
!Flow velocity through rock matrix V = 0.003 m/s
!Only a quarter of the linear system will be simulated.
!Matrix initial permeability = 300 md (3e-13 sqm)
!Skin zone thickness (Ld) = 2 - 12 cm
!Skin zone permeability (Kd) = 10 - 90 md
!vsum=(vx**2+vy**2)**0.5
!vx(radial)=v cos(Theta)
!vy(radial)=v sin(Theta)
!Theta is from 0 to 90 in steps of 0.9.
!Well radius = 0.0635 m
!Drainage radius = 20 m
c***Building the model
pcirc,0.1135,20.0635,0,90
pcirc,0.0635,0.1135,0,90
nummrg,kp
lsel,s,line,,1,3,2
lsel,a,line,,7
lesize,all,,,100
lsel,s,line,,2
lesize,all,,,70,0.01
lsel,s,line,,4
lesize,all,,,70,0.01
lsel,s,line,,6,8,2
lesize,all,,,8
real,2
amesh,1
real,3
amesh,2
allsel
c***Apply boundary conditions
c***symmetry boundary
nsel,s,loc,x,0
d,all,vx,0
d,all,vz,0
nsel,s,loc,y,0
d,all,vy,0
d,all,vz,0
c***Inflow boundary
nsel,s,node,,7180,7279,1
nsel,a,node,,7172
d,7180,vx,0.003
d,7180,vy,0
d,7181,vx,0.00299963
d,7181,vy,0.000047141
d,7182,vx,0.00299852
d,7182,vy,0.00009427
d,7183,vx,0.00299667
d,7183,vy,0.00014138
d,7184,vx,0.00299408
d,7184,vy,0.00018845
d,7185,vx,0.00299074
d,7185,vy,0.00023547
d,7186,vx,0.00298668
d,7186,vy,0.00028244
d,7187,vx,0.00298187
d,7187,vy,0.00032933
d,7188,vx,0.00297633
d,7188,vy,0.00037615
d,7189,vx,0.00297005
d,7189,vy,0.00042287
d,7190,vx,0.00296304
d,7190,vy,0.00046949
d,7191,vx,0.00295529
d,7191,vy,0.00051599
d,7192,vx,0.00294682
d,7192,vy,0.00056236
d,7193,vx,0.00293762
d,7193,vy,0.0006086
d,7194,vx,0.00292769
d,7194,vy,0.00065469
d,7195,vx,0.00291704
d,7195,vy,0.00070061
d,7196,vx,0.00290568
d,7196,vy,0.00074636
d,7197,vx,0.00289359
d,7197,vy,0.00079193
d,7198,vx,0.00288079
d,7198,vy,0.0008373
d,7199,vx,0.00286727
d,7199,vy,0.00088246
d,7200,vx,0.00285305
d,7200,vy,0.00092741
d,7201,vx,0.00283813
d,7201,vy,0.00097212
d,7202,vx,0.0028225
d,7202,vy,0.0010166
d,7203,vx,0.00280618
d,7203,vy,0.00106083
d,7204,vx,0.00278916
d,7204,vy,0.00110479
d,7205,vx,0.00277146
d,7205,vy,0.00114848
d,7206,vx,0.00275307
d,7206,vy,0.00119189
d,7207,vx,0.002734
d,7207,vy,0.001235
d,7208,vx,0.00271426
d,7208,vy,0.00127781
d,7209,vx,0.00269384
d,7209,vy,0.0013203
d,7210,vx,0.00267276
d,7210,vy,0.00136247
d,7211,vx,0.00265103
d,7211,vy,0.0014043
d,7212,vx,0.00262863
d,7212,vy,0.00144579
d,7213,vx,0.00260559
d,7213,vy,0.00148691
d,7214,vx,0.0025819
d,7214,vy,0.00152767
d,7215,vx,0.00255758
d,7215,vy,0.00156805
d,7216,vx,0.00253262
d,7216,vy,0.00160805
d,7217,vx,0.00250704
d,7217,vy,0.00164765
d,7218,vx,0.00248084
d,7218,vy,0.00168684
d,7219,vx,0.00245403
d,7219,vy,0.00172561
d,7220,vx,0.00242661
d,7220,vy,0.00176396
d,7221,vx,0.00239859
d,7221,vy,0.00180187
d,7222,vx,0.00236998
d,7222,vy,0.00183934
d,7223,vx,0.00234079
d,7223,vy,0.00187636
d,7224,vx,0.00231101
d,7224,vy,0.00191291
d,7225,vx,0.00228067
d,7225,vy,0.00194898
d,7226,vx,0.00224976
d,7226,vy,0.00198458
d,7227,vx,0.0022183
d,7227,vy,0.00201969
d,7228,vx,0.00218629
d,7228,vy,0.0020543
d,7229,vx,0.00215374
d,7229,vy,0.0020884
d,7230,vx,0.00212066
d,7230,vy,0.00212198
d,7231,vx,0.00208705
d,7231,vy,0.00215504
d,7232,vx,0.00205293
d,7232,vy,0.00218757
d,7233,vx,0.0020183
d,7233,vy,0.00221956
d,7234,vx,0.00198318
```

```
d,7234,vy,0.002251
d,7235,vx,0.00194756
d,7235,vy,0.00228189
d,7236,vx,0.00191146
d,7236,vy,0.00231221
d,7237,vx,0.0018749
d,7237,vy,0.00234196
d,7238,vx,0.00183786
d,7238,vy,0.00237113
d,7239,vx,0.00180038
d,7239,vy,0.00239972
d,7240,vx,0.00176245
d,7240,vy,0.00242771
d,7241,vx,0.00172408
d,7241,vy,0.00245511
d,7242,vx,0.00168529
d,7242,vy,0.00248189
d,7243,vx,0.00164608
d,7243,vy,0.00250807
d,7244,vx,0.00160647
d,7244,vy,0.00253363
d,7245,vx,0.00156646
d,7245,vy,0.00255856
d,7246,vx,0.00152606
d,7246,vy,0.00258285
d,7247,vx,0.00148529
d,7247,vy,0.00260652
d,7248,vx,0.00144415
d,7248,vy,0.00262953
d,7249,vx,0.00140265
d,7249,vy,0.0026519
d,7250,vx,0.0013608
d,7250,vy,0.00267361
d,7251,vx,0.00131862
d,7251,vy,0.00269467
d,7252,vx,0.00127612
d,7252,vy,0.00271505
d,7253,vx,0.0012333
d,7253,vy,0.00273477
d,7254,vx,0.00119017
d,7254,vy,0.00275381
d,7255,vx,0.00114675
d,7255,vy,0.00277218
d,7256,vx,0.00110305
d,7256,vy,0.00278985
d,7257,vx,0.00105908
d,7257,vy,0.00280684
d,7258,vx,0.00101484
d,7258,vy,0.00282314
d,7259,vx,0.00097035
d,7259,vy,0.00283873
d,7260,vx,0.00092563
d,7260,vy,0.00285363
d,7261,vx,0.00088067
d,7261,vy,0.00286782
d,7262,vx,0.0008355
d,7262,vy,0.00288131
d,7263,vx,0.00079012
d,7263,vy,0.00289408
d,7264,vx,0.00074455
d,7264,vy,0.00290614
d,7265,vx,0.00069879
d,7265,vy,0.00291748
d,7266,vx,0.00065286
d,7266,vy,0.0029281
d,7267,vx,0.00060677
d,7267,vy,0.002938
d,7268,vx,0.00056053
d,7268,vy,0.00294717
d,7269,vx,0.00051415
d,7269,vy,0.00295561
d,7270,vx,0.00046764
d,7270,vy,0.00296333
d,7271,vx,0.00042102
d,7271,vy,0.00297031
d,7272,vx,0.00037429
d,7272,vy,0.00297656
d,7273,vx,0.00032747
d,7273,vy,0.00298207
d,7274,vx,0.00028057
d,7274,vy,0.00298685
d,7275,vx,0.00023361
d,7275,vy,0.00299089
d,7276,vx,0.00018658
d,7276,vy,0.00299419
d,7277,vx,0.00013951
d,7277,vy,0.00299675
d,7278,vx,0.0000924
d,7278,vy,0.00299858
d,7279,vx,0.0000452
d,7279,vy,0.00299966
d,7172,vx,0.0
d,7172,vy,0.003
c***Outflow boundary
nsel,s,node,,1,101,1
d,all,pres,0.0
allsel
!Define the Flotran CFD parameters
fldata,term,pres,1e-08
fldata,solu,flow,t
fldata,iter,exec,50
fldata,solu,turb,f
fldata,temp,nomi,300.0
fldata,nomi,dens,1050.0
fldata,nomi,visc,0.001
finish
c***Solution
/solu
solve
finish
c***Post processing
/post1
set
/show,ENRSR21,grph
/triad,off
/edge,1,1
/device,vector,on
/plopts,info,1
!Disply Pressure and Velocity contours
/title,Pressure contours (Rad. inj. with skin,Km
=300md,Ld=5cm,Kd=90md)
/clabel,1,50
!/cval,1
plnsol,pres
/plopts,info,1
/title,velocity contours (Rad. inj. with skin,Km
=300md,Ld=5cm,Kd=90md)
/cval,1,0.00002,0.00004,0.00006,0.00008,0.0001,0.00
012,0.00025,0.0005
plnsol,v,sum
!Mapping pressure change through matrix
lpath,7230,52
pdef,pressure,pres
/plopts,info,off
/output,PmNRSR21
/title,Pressure change through matrix (Rad. inj. with
skin,Km =300md,Ld=5cm,Kd=90md)
prpath,pressure
/output
pdef,save
!Mapping flow velocity change through matrix
lpath,7230,52
pdef,velocity,v,sum
pdef,Vx,v,x
pdef,Vy,v,y
/plopts,info,off
/output,VmNRSR21
/title,Flow velocity through matrix (Rad. inj. with
skin,Km =300md,Ld=5cm,Kd=90md)
prpath,velocity,Vx,Vy
```

```
/output
pdef,save
finish
```

Frcature injection simulation with damaged zone (Field case)
Radial injection with single fracture and a near fracture damage

```
/BATCH
/filn,NSRFSkin
/titel,Radial injection with single fracture and a near
fracture skin zone (2D)
/units,si
/prep7
et,1,fluid141
c***distributed resistane specifictions
r,2,1,,0,3.333e+12,1,0
rmore,1
r,3,1,,0,3.333e+08,1,0
rmore,1
r,4,1,,0,1.111e+13,1,0
rmore,1
c***Variables
!Radial injection with single fracture and skin zone:
!Injection zone thickness h = 10 m
!Injection area or inlet flow area = 4 sqm
!Injection rate = 1037 M3/day
!Only a quarter of the system will be simulated.
!So the flow rate will be 1/4th of the total flow rate (259
M3/day).
!All the flow will be directed through the fracture inlet.
!Flow velocity at the fracture inlet (Vf) = 0.3 m/s
!Fracture aperture = 2 mm
!Fracture inlet area = 0.02 m
!Fracture length (Lf) = 10 m
!Fracture permeability (Km) = 3000 Darcy
!Matrix initial permeability = 300 md (3e-13 sqm)
!Well radius = 0.0035  - 0.0435 m
!Drainage radius = 20.0035 - 20.0435 m
!Skin width (Ld) = 2 - 8 cm
!Damaged zone permeability (Kd) = 90 - 10 md
c***Building the model
k,1,0.0135,-0.051
k,2,20.0135,-0.051
k,3,20.0135,-0.05
k,4,0.0135,-0.05
a,1,2,3,4
pcirc,0.0135,20.0135,0,90
k,10,0.0135,-0.05
k,11,20.0135,-0.05
k,12,20.0135,0
k,13,0.0135,0
a,10,11,12,13
nummrg,kp
lsel,s,line,,5,7,2
lesize,all,,,100
lsel,s,line,,3,8,5
lesize,all,,,70,0.01
lsel,s,line,,6
lesize,all,,,70,0.01
lsel,s,line,,1
lesize,all,,,70,100
lsel,s,line,,2,4,2
lesize,all,,,4
lsel,s,line,,10,12,2
lesize,all,,,10
nummrg,kp
real,2
amesh,2
real,2
amesh,1
real,2
amesh,3
allsel
c***Creating the fracture
esel,s,elem,,7001,7060,1
esel,a,elem,,7071,7130,1
esel,a,elem,,7141,7200,1
esel,a,elem,,7211,7270,1
emodif,all,real,3
c***Creating the damaged zone
esel,s,elem,,7281,7340,1
esel,a,elem,,7351,7410,1
esel,a,elem,,7421,7480,1
esel,a,elem,,7491,7550,1
esel,a,elem,,7561,7620,1
esel,a,elem,,7631,7690,1
esel,a,elem,,7701,7760,1
esel,a,elem,,7771,7830,1
esel,a,elem,,7841,7900,1
esel,a,elem,,7911,7970,1
emodif,all,real,4
c***Apply boundary conditions
c***symmetry boundary
nsel,s,node,,7172,7242,1
d,all,vy,0
d,all,vz,0
!nsel,s,loc,y,-0.051
!d,all,vy,0
!d,all,vz,0
nsel,s,loc,x,0
d,all,vx,0
d,all,vz,0
c***Inflow boundary
nsel,s,node,,7317,7319,1
nsel,a,node,,7172,7247,75
d,all,vx,0.3
d,all,vy,0
c***wall boumdary
nsel,s,node,,172,271,1
nsel,a,node,,102
d,all,vx,0
d,all,vy,0
nsel,s,node,,7536,7544,1
nsel,a,node,,7247
d,all,vx,0
d,all,vy,0
c***Outflow boundary
nsel,s,node,,1,101,1
d,all,pres,0.0
nsel,s,node,,7243,7246,1
nsel,a,node,,7173
d,all,pres,0.0
nsel,s,node,,7527,7535,1
d,all,pres,0.0
allsel
!Define the Flotran CFD parameters
fldata,term,pres,1e-08
fldata,solu,flow,t
!fldata,meth,pres,1
fldata,iter,exec,50
fldata,solu,turb,f
fldata,temp,nomi,300.0
fldata,nomi,dens,1050.0
fldata,nomi,visc,0.001
finish
c***Solution
/solu
solve
finish
c***Post processing the results
/post1
set
/triad,off
/show,ENRSFSR21,grph
/edge,1,1
/device,vector,on
/plopts,info,1
!Disply Pressure and Velocity contours
```

```
/title,Pressure contours
(Km=300md,Lf=10m,Wf=2mm,Vf=0.3m/s,Kd=90md,Ld=5
cm)
/clabel,1,50
plnsol,pres
/plopts,info,1
/title,velocity contours
(Km=300md,Lf=10m,Wf=2mm,Vf=0.3m/s,Kd=90md,Ld=5
cm)
/cval,1,0.00001,0.000015,0.00002,0.00003,0.00004,0.
00005,0.00006,0.00008
plnsol,v,sum
!Mapping pressure along the fracture
lpath,7317,7246
pdef,pressure,pres
/plopts,info,off
/axlab,y,pressure (pa)
/axlab,x,Radial distance (m)
plpath,pressure
/output,PASRFSR21
/title,Pressure along the
fracture(Km=300md,Lf=10m,Wf=2mm,Vf=0.3m/s,Kd=90
md,Ld=5cm)
prpath,pressure
/output
pdef,save
/axlab,y
/axlab,x
!Mapping flow velocity along the fracture
lpath,7317,7246
pdef,velocity,v,sum
pdef,Vx,v,x
pdef,Vy,v,y
/plopts,info,off
/axlab,y,velocity (m/s)
/axlab,x,Radial distance (m)
plpath,velocity,Vx,Vy
/output,VASRFSR21
/title,Velocity along the
fracture(Km=300md,Lf=10m,Wf=2mm,Vf=0.3m/s,Kd=90
md,Ld=5cm)
prpath,velocity,Vx,Vy
/output
pdef,save
/axlab,y
/axlab,x
!Mapping pressure through matrix
lpath,222,52
pdef,pressure,pres
/plopts,info,off
/axlab,y,pressure (pa)
/axlab,x,Radial distance (m)
plpath,pressure
/output,PmSRFSR21
/title,Pressure through
matrix(Km=300md,Lf=10m,Wf=2mm,Vf=0.3m/s,Kd=90m
d,Ld=5cm)
prpath,pressure
/output
pdef,save
/axlab,y
/axlab,x
!Mapping flow velocity through matrix
lpath,222,52
pdef,velocity,v,sum
pdef,Vx,v,x
pdef,Vy,v,y
/plopts,info,off
/axlab,y,velocity (m/s)
/axlab,x,Radial distance (m)
plpath,velocity,Vx,Vy
/output,VmSRFSR21
/title,Flow velocity through
matrix(Km=300md,Lf=10m,Wf=2mm,Vf=0.3m/s,Kd=90m
d,Ld=5cm)
prpath,velocity,Vx,Vy
/output
pdef,save
/axlab,y
/axlab,x
finish
```

Frcature injection simulation with damaged zone (Field case)

Radial injection with Two fracture and a near fracture damage

```
/BATCH
/filn,NDRFSkin
/titel,Radial injection with two fractures and a near fracture
skin (2D)
/units,si
/prep7
et,1,fluid141
c***Distributed resistance specifications
r,2,1,,0,3.333e+12,1,0
rmore,1
r,3,1,,0,3.333e+08,1,0
rmore,1
r,4,1,,0,1.111e+13,1,0
rmore,1
c***Variables
!Radial injection with Duble fracture and skin zone:
!Injection zone thickness h = 10 m
!Injection area or inlet flow area = 4 sqm
!Injection rate = 1036 M3/day
!Only a quarter of the system will be simulated.
!So the flow rate will be 1/4th of the total flow rate (259
M3/day).
!All the flow will be directed through the fracture inlet.
!Flow velocity at the fracture inlet Vf = 0.15 m/s
!Fracture aperture = 2 mm
!Fracture inlet area = 0.02 m
!Fracture length (Lf) = 10 m
!Fracture permeability = 3000 Darcy
!Matrix initial permeability (Km) = 300 md (3e-13 sqm)
!Well radius = 0.0035 - 0.0435 m
!Drainage radius = 20.0035 - 20.0435 m
!Skin width (Ld) = 2 - 8 cm
!Damaged zone permeability (Kd) = 90 -10 md
c***Building the model
k,1,0.0135,-0.051
k,2,20.0135,-0.051
k,3,20.0135,-0.05
k,4,0.0135,-0.05
K,5,-0.05,0.0135
k,6,-0.05,20.0135
k,7,-0.051,20.0135
k,8,-0.051,0.0135
a,1,2,3,4
pcirc,0.0135,20.0135,0,90
a,5,6,7,8
k,13,0.0135,-0.05
k,14,20.0135,-0.05
k,15,20.0135,0
k,16,0.0135,0
a,13,14,15,16
k,17,-0.05,0.0135
k,18,-0.05,20.0135
k,19,0,20.0135
k,20,0,0.0135
a,17,18,19,20
nummrg,kp
lsel,s,line,,5,7,2
lesize,all,,,80
lsel,s,line,,3,8,5
lesize,all,,,70,0.01
lsel,s,line,,6
lesize,all,,,70,0.01
lsel,s,line,,1
lesize,all,,,70,100
```

```
lsel,s,line,,11,
lesize,all,,,70,0.01
lsel,s,line,,9,
lesize,all,,,70,100
lsel,s,line,,2,4,2
lsel,a,line,,10,12,2
lesize,all,,,4
lsel,s,line,,14,20,2
lesize,all,,,10
real,2
amesh,2
real,2
amesh,4
real,2
amesh,5
real,2
amesh,1
real,2
amesh,3
allsel
c***Creating the two fractures
esel,s,elem,,7001,7060,1
esel,a,elem,,7071,7130,1
esel,a,elem,,7141,7200,1
esel,a,elem,,7211,7270,1
emodif,all,real,3
esel,s,elem,,7281,7340,1
esel,a,elem,,7351,7410,1
esel,a,elem,,7421,7480,1
esel,a,elem,,7491,7550,1
emodif,all,real,3
c***Creating the damaged zone
esel,s,elem,,5601,5660,1
esel,a,elem,,5671,5730,1
esel,a,elem,,5741,5800,1
esel,a,elem,,5811,5870,1
esel,a,elem,,5881,5940,1
esel,a,elem,,5951,6010,1
esel,a,elem,,6021,6080,1
esel,a,elem,,6091,6150,1
esel,a,elem,,6161,6220,1
esel,a,elem,,6231,6290,1
emodif,all,real,4
esel,s,elem,,6301,6891,1
esel,a,elem,,6302,6892,1
esel,a,elem,,6303,6893,1
esel,a,elem,,6304,6894,1
esel,a,elem,,6305,6895,1
esel,a,elem,,6306,6896,1
esel,a,elem,,6307,6897,1
esel,a,elem,,6308,6898,1
esel,a,elem,,6309,6899,1
esel,a,elem,,6310,6900,1
emodif,all,real,4
c***Apply boundary conditions
c***symmetry boundary
nsel,s,node,,7172,7242,1
d,all,vy,0
d,all,vz,0
nsel,s,node,,7461,7529,1
nsel,a,node,,7456,7460,4
d,all,vx,0
d,all,vz,0
!nsel,s,loc,x,-0.051
!d,all,vx,0
!d,all,vz,0
!nsel,s,loc,y,-0.051
!d,all,vy,0
!d,all,vz,0
c***Inflow boundary
nsel,s,node,,7246,7248,1
nsel,a,node,,7172
nsel,a,node,,5753
d,all,vx,0.15
d,all,vy,0
nsel,s,node,,7530,7532,1
nsel,a,node,,7460
nsel,a,node,,6462
d,all,vx,0
d,all,vy,0.15
c***wall boundary
nsel,s,node,,5832,5840,1
nsel,a,node,,5753
d,all,vx,0
d,all,vy,0
nsel,s,node,,6542,6550,1
nsel,a,node,,6462
d,all,vx,0
d,all,vy,0
nsel,s,node,,152,231,1
nsel,a,node,,82
d,all,vx,0
d,all,vy,0
c***Outflow boundary
nsel,s,node,,1,81,1
d,all,pres,0.0
nsel,s,node,,5823,5831,1
nsel,a,node,,5752
nsel,a,node,,7243,7245,1
nsel,a,node,,7173
d,all,pres,0.0
nsel,s,node,,6533,6541,1
nsel,a,node,,6463
nsel,a,node,,7456,7459,1
d,all,pres,0.0
allsel
!Define the Flotran CFD parameters
fldata,term,pres,1e-08
fldata,solu,flow,t
!fldata,meth,pres,1
fldata,iter,exec,50
fldata,solu,turb,f
fldata,temp,nomi,300.0
fldata,nomi,dens,1050.0
fldata,nomi,visc,0.001
finish
c***Solution
/solu
solve
finish
c***Post processing the results
/post1
set
/triad,off
/show,ENDRFSR21,grph
/edge,1,1
/device,vector,on
/plopts,info,1
!Disply Pressure and Velocity contours
/title,Pressure contours (Duble
frac.,Km=300md,Lf=10m,Wf=2mm,Vf=0.15m/s,Kd=90md
,Ld=5cm)
/clabel,1,50
plnsol,pres
/plopts,info,1
/title,velocity contours (Duble
frac.,Km=300md,Lf=10m,Wf=2mm,Vf=0.15m/s,Kd=90md
,Ld=5cm)
/cval,1,0.00001,0.000015,0.00002,0.00003,0.00004,0.
00005,0.00006,0.00008
plnsol,v,sum
!Mapping pressure along the fracture
lpath,7246,7245
pdef,pressure,pres
/plopts,info,off
/axlab,y,pressure (pa)
/axlab,x,Radial distance (m)
plpath,pressure
/output,PADRFSR21
```

```
/title,Pressure along
fracture(Dub.frac.,Km=300md,Lf=10m,Wf=2mm,Vf=0.15
m/s,Kd=90md,Ld=5cm)
prpath,pressure
/output
pdef,save
/axlab,y
/axlab,x
!Mapping flow velocity along the fracture
lpath,7246,7245
pdef,velocity,v,sum
pdef,Vx,v,x
pdef,Vy,v,y
/plopts,info,off
/axlab,y,velocity (m/s)
/axlab,x,Radial distance (m)
plpath,velocity,Vx,Vy
/output,VADRFSR21
/title,Velocity along
fracture(Dub.frac.,Km=300md,Lf=10m,Wf=2mm,Vf=0.15
m/s,Kd=90md,Ld=5cm)
prpath,velocity,Vx,Vy
/output
pdef,save
/axlab,y
/axlab,x
!Mapping pressure through matrix
lpath,192,42
pdef,pressure,pres
/plopts,info,off
/axlab,y,pressure (pa)
/axlab,x,Radial distance (m)
plpath,pressure
/output,PmDRFSR21
/title,Pressure through
matrix(Dub.frac.,Km=300md,Lf=10m,Wf=2mm,Vf=0.15m
/s,Kd=90md,Ld=5cm)
prpath,pressure
/output
pdef,save
/axlab,y
/axlab,x
!Mapping flow velocity through matrix
lpath,192,42
pdef,velocity,v,sum
pdef,Vx,v,x
pdef,Vy,v,y
/plopts,info,off
/axlab,y,velocity (m/s)
/axlab,x,Radial distance (m)
plpath,velocity,Vx,Vy
/output,VmDRFSR21
/title,Velocity through
matrix(Dub.frac.,Km=300md,Lf=10m,Wf=2mm,Vf=0.15m
/s,Kd=90md,Ld=5cm)
prpath,velocity,Vx,Vy
/output
pdef,save
/axlab,y
/axlab,x
Finish
```

Appendix III

Malvern master sizer distribution samples.

MALVERN Instruments SB.89 Tue 19 Mar 1996 Time 10:53 am

Experiment no.33 : Sample from sample line.

High Size	In %	High Size	In %	High Size	In %	High Size	In %	High Size	In %	High Size	In %	Span 1.82
80.0	0.0	24.9	0.1	7.75	6.1	2.41	1.7	0.75	1.4	0.23	0.4	D[4,3] 6.14µm
71.9	0.0	22.4	0.2	6.97	5.0	2.17	1.7	0.68	1.4	0.21	0.3	
64.7	0.0	20.1	0.4	6.27	4.1	1.95	1.8	0.61	1.3	0.19	0.2	
58.2	0.0	18.1	0.8	5.64	3.2	1.75	1.9	0.55	1.2	0.17	0.2	D[3,2] 1.76µm
52.3	0.0	16.3	1.6	5.07	2.5	1.58	1.9	0.49	1.1	0.15	0.1	
47.1	0.0	14.6	2.8	4.56	2.1	1.42	1.8	0.44	1.0	0.14	0.1	
42.3	0.0	13.2	4.3	4.10	1.9	1.28	1.7	0.40	0.8	0.12	0.1	D[v,0.9] 11.91µm
38.1	0.0	11.8	5.8	3.69	1.7	1.15	1.6	0.36	0.7	0.11	0.0	
34.2	0.0	10.7	7.1	3.32	1.5	1.03	1.6	0.32	0.6	0.10	0.0	
30.8	0.0	9.58	7.8	2.98	1.5	0.93	1.5	0.29	0.5			D[v,0.1] 0.65µm
27.7	0.0	8.62	7.3	2.68	1.6	0.83	1.5	0.26	0.4			

Source = :Sample	Beam length = 2.2 mm	Model indp	D[v,0.5] 6.19µm
	Residual = 1.187 %		
Focal length = 45 mm	Obscuration = 0.0567	Volume Conc. = 0.0023%	
Presentation = stnd	Volume distribution	Sp.S.A 1.2861 m²/gm.	

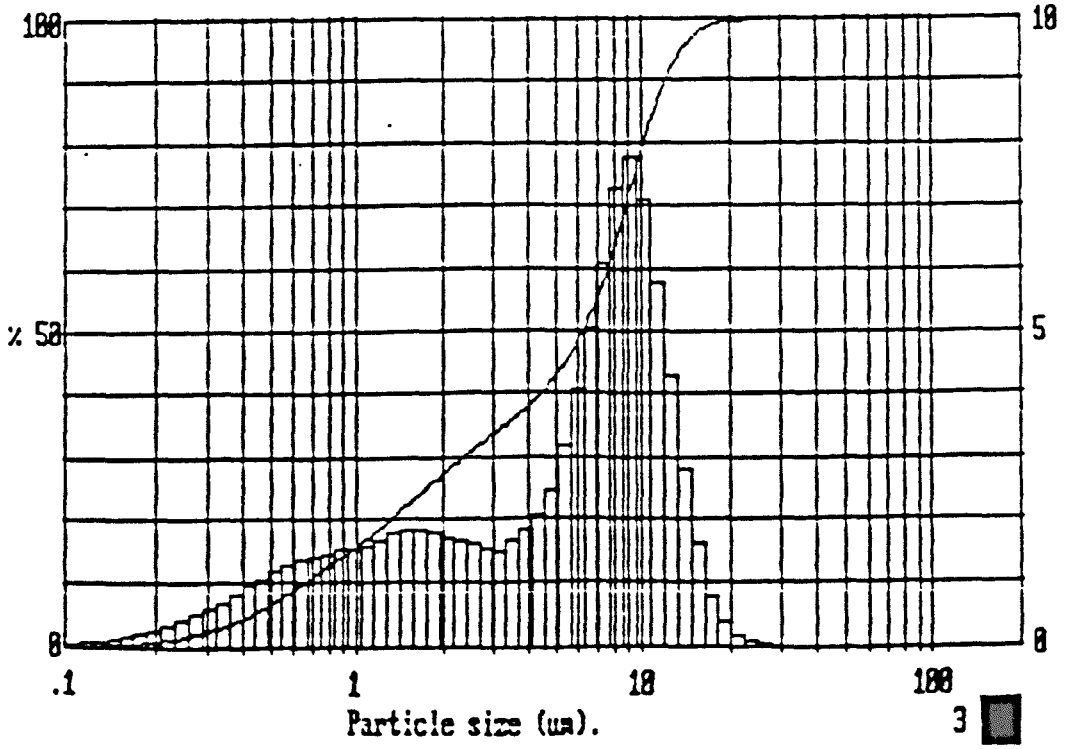

MALVERN Instruments SB.09 Wed 26 Jun 1996 Time 10:03 am

Experiment No.42: Testing droplet size.

High Size	In %	High Size	In %	High Size	In %	High Size	In %	High Size	In %	High Size	In %	Span 1.63
80.0	0.0	24.9	0.0	7.75	2.4	2.41	2.7	0.75	2.0	0.23	0.1	D[4,3] 3.34µm
71.9	0.0	22.4	0.0	6.97	4.2	2.17	2.6	0.68	1.8	0.21	0.1	
64.7	0.0	20.1	0.0	6.27	6.2	1.95	2.6	0.61	1.5	0.19	0.0	D[3,2] 1.71µm
58.2	0.0	18.1	0.0	5.64	7.5	1.75	2.8	0.55	1.3	0.17	0.0	
52.3	0.0	16.3	0.0	5.07	8.0	1.58	2.9	0.49	1.0	0.15	0.0	
47.1	0.0	14.6	0.0	4.56	7.5	1.42	2.9	0.44	0.8	0.14	0.0	D[v,0.9] 6.11µm
42.3	0.0	13.2	0.0	4.10	6.5	1.28	2.8	0.40	0.6	0.12	0.0	
38.1	0.0	11.8	0.1	3.69	5.3	1.15	2.7	0.36	0.4	0.11	0.0	
34.2	0.0	10.7	0.2	3.32	4.2	1.03	2.6	0.32	0.3	0.10	0.0	
30.8	0.0	9.58	0.5	2.98	3.5	0.93	2.4	0.29	0.2			D[v,0.1] 0.74µm
27.7	0.0	8.62	1.2	2.68	3.0	0.83	2.2	0.26	0.2			

Source = :Sample	Beam length = 2.2 mm	Model indp	D[v,0.5] 3.29µm
	Residual = 1.515 %		
Focal length = 45 mm	Obscuration = 0.3117	Volume Conc. = 0.0114%	
Presentation = stnd	Volume distribution	Sp.S.A 1.3206 m²/gm.	

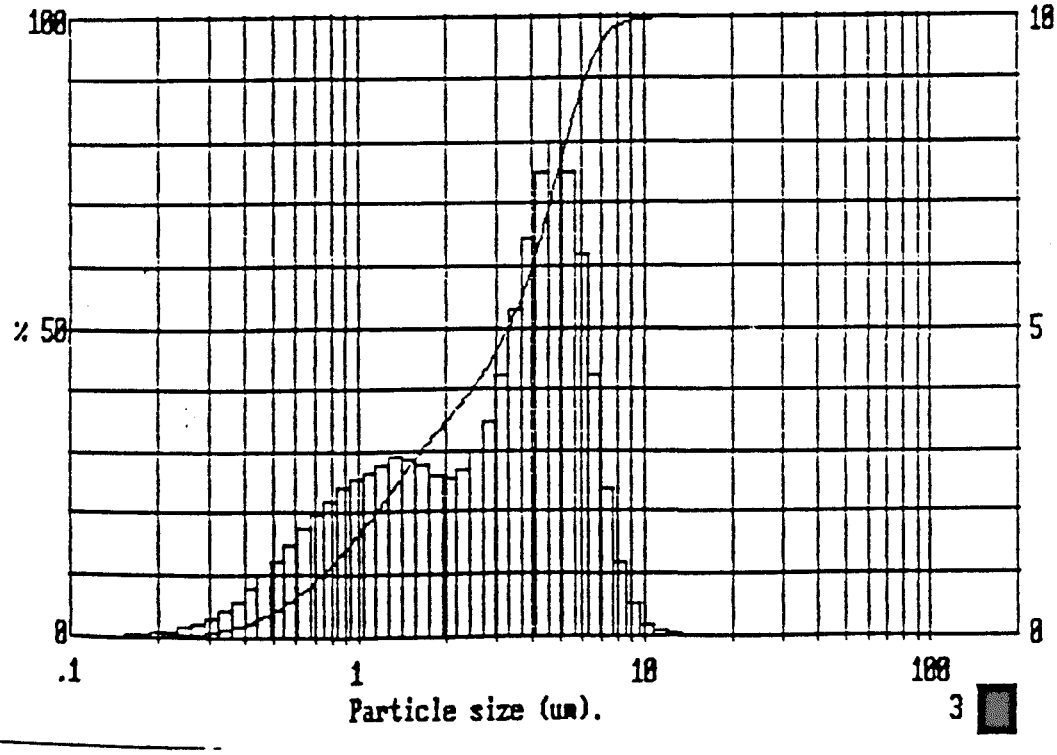

Appendix IV

The injection Rig and the testing cell